# DEVELOPMENTAL BIOLOGY AND REGULATION OF OSTEOCLASTS

EDITED BY: Yankel Gabet, Drorit Neumann, Ari Elson, Noam Levaot and Natalie A. Sims

PUBLISHED IN: Frontiers in Cell and Developmental Biology and Frontiers in Molecular Biosciences

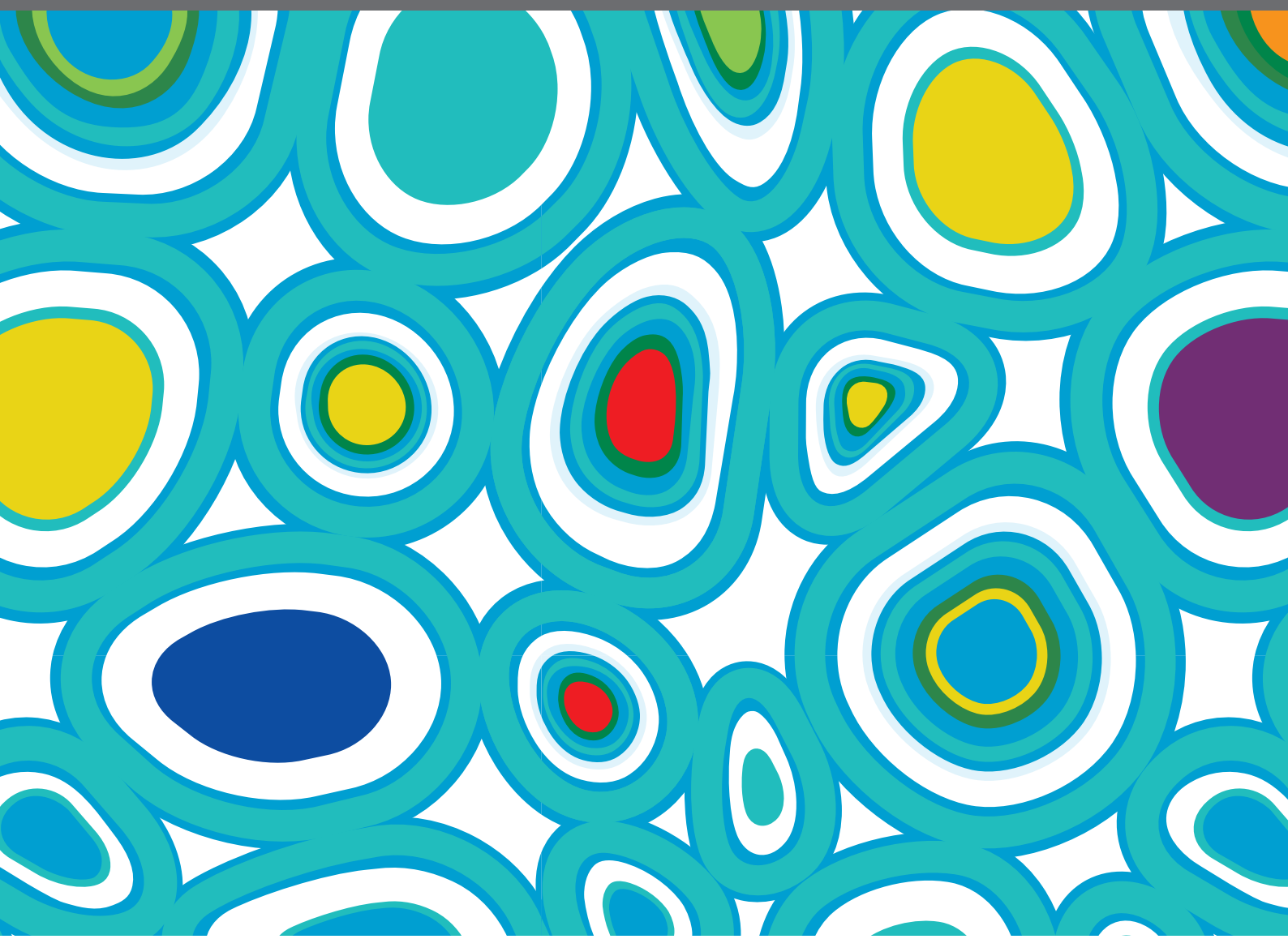

frontiers Research Topics

ISSN 1664-8714
ISBN 978-2-88971-867-2
DOI 10.3389/978-2-88971-867-2

## About Frontiers

Frontiers is more than just an open-access publisher of scholarly articles: it is a pioneering approach to the world of academia, radically improving the way scholarly research is managed. The grand vision of Frontiers is a world where all people have an equal opportunity to seek, share and generate knowledge. Frontiers provides immediate and permanent online open access to all its publications, but this alone is not enough to realize our grand goals.

## Frontiers Journal Series

The Frontiers Journal Series is a multi-tier and interdisciplinary set of open-access, online journals, promising a paradigm shift from the current review, selection and dissemination processes in academic publishing. All Frontiers journals are driven by researchers for researchers; therefore, they constitute a service to the scholarly community. At the same time, the Frontiers Journal Series operates on a revolutionary invention, the tiered publishing system, initially addressing specific communities of scholars, and gradually climbing up to broader public understanding, thus serving the interests of the lay society, too.

## Dedication to Quality

Each Frontiers article is a landmark of the highest quality, thanks to genuinely collaborative interactions between authors and review editors, who include some of the world's best academicians. Research must be certified by peers before entering a stream of knowledge that may eventually reach the public - and shape society; therefore, Frontiers only applies the most rigorous and unbiased reviews.
Frontiers revolutionizes research publishing by freely delivering the most outstanding research, evaluated with no bias from both the academic and social point of view. By applying the most advanced information technologies, Frontiers is catapulting scholarly publishing into a new generation.

## What are Frontiers Research Topics?

Frontiers Research Topics are very popular trademarks of the Frontiers Journals Series: they are collections of at least ten articles, all centered on a particular subject. With their unique mix of varied contributions from Original Research to Review Articles, Frontiers Research Topics unify the most influential researchers, the latest key findings and historical advances in a hot research area! Find out more on how to host your own Frontiers Research Topic or contribute to one as an author by contacting the Frontiers Editorial Office: frontiersin.org/about/contact

# DEVELOPMENTAL BIOLOGY AND REGULATION OF OSTEOCLASTS

Topic Editors:
**Yankel Gabet,** Tel Aviv University, Israel
**Drorit Neumann,** Tel Aviv University, Israel
**Ari Elson,** Weizmann Institute of Science, Israel
**Noam Levaot,** Ben-Gurion University of the Negev, Israel
**Natalie A. Sims,** University of Melbourne, Australia

**Citation:** Gabet, Y., Neumann, D., Elson, A., Levaot, N., Sims, N. A., eds. (2021). Developmental Biology and Regulation of Osteoclasts. Lausanne: Frontiers Media SA. doi: 10.3389/978-2-88971-867-2

# Table of Contents


**05** ***Editorial: Developmental Biology and Regulation of Osteoclasts***
Yankel Gabet, Drorit Neumann, Noam Levaot, Ari Elson and Natalie A. Sims

**08** ***Synonymous Mutations of Porcine* Igf1r *Extracellular Domain Affect Differentiation and Mineralization in MC3T3-E1 Cells***
Chunli Wang, Siyao Wang, Songcai Liu, Yunyun Cheng, Hongwei Geng, Rui Yang, Tianqi Feng, Guanhong Lu, Xiaotong Sun, Jie Song and Linlin Hao

**26** ***The Bone Morphogenetic Protein Pathway: The Osteoclastic Perspective***
Franziska Lademann, Lorenz C. Hofbauer and Martina Rauner

**34** ***Effects of Erythropoietin in White Adipose Tissue and Bone Microenvironment***
Sukanya Suresh, Jeeyoung Lee and Constance Tom Noguchi

**44** ***Osteoblast and Osteoclast Activity Affect Bone Remodeling Upon Regulation by Mechanical Loading-Induced Leukemia Inhibitory Factor Expression in Osteocytes***
Jingke Du, Jiancheng Yang, Zihao He, Junqi Cui, Yiqi Yang, Mingming Xu, Xinhua Qu, Ning Zhao, Mengning Yan, Hanjun Li and Zhifeng Yu

**54** ***Membrane Transport Proteins in Osteoclasts: The Ins and Outs***
Amy B. P. Ribet, Pei Ying Ng and Nathan J. Pavlos

**75** ***Hypoxia-Inducible Factors Regulate Osteoclasts in Health and Disease***
Xianyi Meng, Ben Wielockx, Martina Rauner and Aline Bozec

**84** ***Sestrin2 Regulates Osteoclastogenesis via the p62-TRAF6 Interaction***
Sue Young Oh, Namju Kang, Jung Yun Kang, Ki Woo Kim, Jong-Hoon Choi, Yu-Mi Yang and Dong Min Shin

**96** ***The Mechanism Switching the Osteoclast From Short to Long Duration Bone Resorption***
Jean-Marie Delaisse, Kent Søe, Thomas Levin Andersen, Aleksandra Maria Rojek and Niels Marcussen

**113** ***Lack of Adiponectin Drives Hyperosteoclastogenesis in Lipoatrophic Mice***
Maria-Bernadette Madel, He Fu, Dominique D. Pierroz, Mariano Schiffrin, Carine Winkler, Anne Wilson, Cécile Pochon, Barbara Toffoli, Mahdia Taïeb, Jean-Yves Jouzeau, Federica Gilardi, Serge Ferrari, Nicolas Bonnet, Claudine Blin-Wakkach, Béatrice Desvergne and David Moulin

**129** ***Role of OSCAR Signaling in Osteoclastogenesis and Bone Disease***
Iva R. Nedeva, Mattia Vitale, Ari Elson, Judith A. Hoyland and Jordi Bella

**148** ***Sorting Nexin 10 as a Key Regulator of Membrane Trafficking in Bone-Resorbing Osteoclasts: Lessons Learned From Osteopetrosis***
Ari Elson, Merle Stein, Grace Rabie, Maayan Barnea-Zohar, Sabina Winograd-Katz, Nina Reuven, Moran Shalev, Juraj Sekeres, Moien Kanaan, Jan Tuckermann and Benjamin Geiger

**165** ***Quantification of Osteoclasts in Culture, Powered by Machine Learning***
Edo Cohen-Karlik, Zamzam Awida, Ayelet Bergman, Shahar Eshed, Omer Nestor, Michelle Kadashev, Sapir Ben Yosef, Hussam Saed, Yishay Mansour, Amir Globerson, Drorit Neumann and Yankel Gabet

176 ***Regulation of Osteoclastogenesis and Bone Resorption by miRNAs***
Kazuki Inoue, Courtney Ng, Yuhan Xia and Baohong Zhao

187 ***The Effects of Receptor Activator of NF-κB Ligand-Binding Peptides on Bone Resorption and Bone Formation***
Fatma Rashed, Shingo Kamijyo, Yuri Shimizu, Yuna Hirohashi, Masud Khan, Yasutaka Sugamori, Ramachandran Murali and Kazuhiro Aoki

194 ***Fluorescence-Based Real-Time Analysis of Osteoclast Development***
Áron Pánczél, Simon P. Nagy, János Farkas, Zoltán Jakus, Dávid S. Győri and Attila Mócsai

frontiers in Cell and Developmental Biology

EDITORIAL
published: 22 October 2021
doi: 10.3389/fcell.2021.769320

# Editorial: Developmental Biology and Regulation of Osteoclasts

*Yankel Gabet*[1]*, *Drorit Neumann*[2], *Noam Levaot*[3], *Ari Elson*[4] and *Natalie A. Sims*[5,6]

[1] Department of Anatomy and Anthropology, Sackler Faculty of Medicine, Tel Aviv University, Tel Aviv, Israel, [2] Department of Cell and Developmental Biology, Sackler Faculty of Medicine, Tel Aviv University, Tel Aviv, Israel, [3] Department of Physiology and Cell Biology, Faculty of Health Sciences, Ben-Gurion University of the Negev, Beersheba, Israel, [4] Department of Molecular Genetics, The Weizmann Institute of Science, Rehovot, Israel, [5] St. Vincent's Institute of Medical Research, Melbourne, VIC, Australia, [6] Department of Medicine at St. Vincent's Hospital, The University of Melbourne, Melbourne, VIC, Australia

**Keywords: osteoclast, osteoclastogenesis, coupling, osteopetrosis, bone disease, imaging, bone resorption**

## Editorial on the Research Topic

## Developmental Biology and Regulation of Osteoclasts

The proper structure and function of the skeleton is critical for the health and well-being of vertebrates. Bone structures enable growth, posture, movement, protect the internal organs, regulate calcium levels, and provide the proper environment for production and maturation of several types of hematopoietic cells. Bone is reshaped and renewed throughout life by the processes of bone modeling and remodeling, respectively (Sims and Vrahnas, 2014). These processes depend on the coordinated actions of mesenchymal-derived osteoblasts, which form new bone matrix, and hematopoietic-derived osteoclasts, which remove it (Sims and Vrahnas, 2014). Osteocytes, which are osteoblast lineage cells that reside within the bone matrix, and regulate the opposing activities of osteoblasts and osteoclasts in response to physiological and pathological cues (Schaffler et al., 2014).

Haemopoietic-derived osteoclasts are large, multi-nucleated phagocytic cells that are formed through fusion of monocyte/macrophage precursors. These cells are unique in the sense that they are the only cells that can resorb bone matrix. The essential nature of their activity is best demonstrated by the consequences of their absence or inactivity, which occur in various diseases. In such cases significant changes in the quality and mass of bone may ensue, severely reducing the quality of life of patients and in some cases, leading to their demise. During the process of bone remodeling, osteoclasts also produce "coupling factors," which provide the necessary message to osteoblasts to form new bone matrix in order to replace the degraded bone and thereby maintain the structural integrity of the skeleton (Sims and Martin, 2020).

This series of articles, which we outline here, explores the development and function of osteoclasts, and examines the molecular, genetic, and environmental cues directed at these cells in order to deepen our understanding of their involvement in health and disease.

Osteoclast differentiation involves multiple steps prior to bone resorption, including induction of osteoclast-specific gene expression patterns, cell fusion, and bone surface attachment; these are highlighted in the review of Nedeva et al., which focuses on the interaction of ITAM Adaptor FcRγ with the osteoclast-associated receptor (OSCAR) in bone health and disease. This special issue also includes a review of the role of bone morphogenetic proteins (BMPs) in the interaction between osteoblasts and osteoclasts (Lademann et al.). While the roles of BMPs

OPEN ACCESS

***Edited and reviewed by:***
*Cecilia Giulivi,*
*University of California, Davis,*
*United States*

***Correspondence:**
*Yankel Gabet*
*yankel@tau.ac.il*

***Specialty section:***
*This article was submitted to Cellular Biochemistry, a section of the journal Frontiers in Cell and Developmental Biology*

***Received:*** *01 September 2021*
***Accepted:*** *28 September 2021*
***Published:*** *22 October 2021*

***Citation:***
*Gabet Y, Neumann D, Levaot N, Elson A and Sims NA (2021) Editorial: Developmental Biology and Regulation of Osteoclasts. Front. Cell Dev. Biol. 9:769320. doi: 10.3389/fcell.2021.769320*

in promoting bone formation are well-established (Sampath and Reddi, 2020), this review stresses that BMPs also have direct and indirect actions on the osteoclast lineage to stimulate osteoclast formation, bone resorption and osteoclast-derived coupling signals that promote bone formation. The review also considers the impact of this novel aspect of BMP2 function when using recombinant BMP in the clinic for bone repair and regeneration. In parallel, Rashed et al. review the literature demonstrating that the cytokine RANKL, the key regulator of osteoclast differentiation, also promotes bone formation through "outside-in" signaling within the osteoblast. Their work indicates that this pathway can be activated via RANKL-binding proteins and suggests a novel approach to stimulating bone formation. An additional review by Inoue et al. summarizes the field of miRNA regulation of both bone resorption and coupling factor activity.

Osteoclastogenesis is critical for maintaining bone architecture and integrity. While excessive bone resorption by osteoclasts is associated with osteoporosis and rheumatoid arthritis, impaired osteoclast differentiation and activity lead to osteopetrosis, a severe and often fatal condition (Sobacchi et al., 2013). Mutations in Sorting Nexin 10 (SNX10) were recently identified in patients with malignant infantile osteopetrosis. Elson et al. provide an in-depth discussion of SNX10 and its roles in intracellular membrane trafficking and link these roles to vital processes controlling osteoclast functions. They also point to a link between membrane trafficking in osteoclasts with the majority of genes associated with recessive osteopetrosis. Together with a review by Ribet et al. on the function of a range of membrane transport proteins, these articles stress the critical importance of membrane trafficking and membrane transport proteins to osteoclast function, and provide an update on the wide range of membrane transport proteins now known to regulate osteoclast activity. Further emphasizing the importance of cytoskeletal mobility in osteoclasts, Delaisse et al. review studies that demonstrate the dynamics of osteoclasts that "glide" over the resorbed bone by continuous reorganization of their ruffled border and associated enzymes, while maintaining a tightly sealed resorption compartment.

Pertaining to the controversial skeletal role(s) of erythropoietin (EPO) in bone (Hiram-Bab et al., 2017), Suresh et al. now add a novel aspect to resolve this conflict at least partially. Their work distinguishes between physiological levels of EPO, which maintain bone homeostasis by regulating the balance between bone formation and adipogenesis in bone marrow stromal cells, and pharmacological administration of exogenous EPO at higher levels, which decreases bone marrow adipogenesis, stimulates osteoclast activity and induces bone loss. Hypoxia inducible factors (HIFs), which also control EPO production, are important determinants of bone homeostasis via direct and indirect effects on osteoclasts (Meng et al.) in the hypoxic bone environment. HIF inhibitors may thus present clinical relevance as they may target osteoclast activation and secondary bone loss in numerous diseases. Future studies on HIF signaling and its role in osteoclastogenesis will likely lead to effective treatments for human diseases involving disruption of bone homeostasis. In line with the importance of oxidative stress in osteoclast development, Oh et al. present original data on Sestrin2, an antioxidant that regulates reactive oxygen species, autophagy, and inflammation. Interestingly, these authors show that Sestrin2 has an oxidative stress-independent role in bone homeostasis by facilitating protein-protein interaction between TRAF6 and p62 and induction of NFATc1 expression during osteoclast differentiation.

While the link between osteoblast differentiation and bone marrow adipogenesis is well established (Pierce et al., 2019), the connection between marrow adipogenesis and osteoclast formation has been more controversial. In this issue, Madel et al. show that loss of adipocytes results in increased osteoclast activity that links adipocytes to osteoclasts in mice and humans. Using three different models, the authors elegantly establish a mechanism in which adiponectin signaling inhibits osteoclastogenesis *in vivo*.

Du et al. suggest that the loss of trabecular bone in a mouse tail-suspension model may be caused by reduced leukemia inhibitory factor (LIF) expression by osteocytes and loss of its known actions to stimulate bone formation. Tail suspension also results in increased osteoclast numbers, and Du et al. show that LIF directly stimulates osteoclastogenesis *in vitro*. A direct effect of LIF on osteoclast differentiation is surprising, as it contradicts earlier work that reported the absence of LIF receptor expression on osteoclasts (Allan et al., 1990).

Two original studies present novel imaging and analytical tools relevant for osteoclast research. Pánczél et al. present two elegant fluorescence-based real-time imaging and analytical assays to monitor osteoclast development *in vitro* by replacing membrane-targeted tdTomato with eGFP, under control of the osteoclast-specific cathepsin K promoter linked to the Cre recombinase gene (Ctsk-Cre). A somewhat similar approach has been used by others for intravital imaging of osteoclasts (McDonald et al., 2021). Cohen-Karlik et al. use artificial intelligence and the power of machine learning to establish an unbiased, automatic method for evaluating osteoclast number and surface in cultures.

Collectively, this series of manuscripts provides a wealth of knowledge about this unique and intriguing cell type, including new developments in understanding their formation and function. We hope it will provide a useful resource both for researchers well-versed in osteoclasts and those who are new to the field, and will stimulate new interdisciplinary research in this field.

## AUTHOR CONTRIBUTIONS

NL and YG wrote the first draft of the manuscript. All authors contributed to manuscript revision, read, and approved the submitted version.

## REFERENCES


Allan, E. H., Hilton, D. J., Brown, M. A., Evely, R. S., Yumita, S., Metcalf, D., et al. (1990). Osteoblasts display receptors for and responses to leukemia-inhibitory factor. *J. Cell. Physiol.* 145, 110–119. doi: 10.1002/jcp.1041450116

Hiram-Bab, S., Neumann, D., and Gabet, Y. (2017). Erythropoietin in bone - controversies and consensus. *Cytokine* 89, 155–159. doi: 10.1016/j.cyto.2016.01.008

McDonald, M. M., Khoo, W. H., Ng, P. Y., Xiao, Y., Zamerli, J., Thatcher, P., et al. (2021). Osteoclasts recycle via osteomorphs during RANKL-stimulated bone resorption. *Cell* 184, 1330–1347.e1313. doi: 10.1016/j.cell.2021.02.002

Pierce, J. L., Begun, D. L., Westendorf, J. J., and McGee-Lawrence, M. E. (2019). Defining osteoblast and adipocyte lineages in the bone marrow. *Bone* 118, 2–7. doi: 10.1016/j.bone.2018.05.019

Sampath, T. K., and Reddi, A. H. (2020). Discovery of bone morphogenetic proteins - a historical perspective. *Bone* 140, 115548. doi: 10.1016/j.bone.2020.115548

Schaffler, M. B., Cheung, W. Y., Majeska, R., and Kennedy, O. (2014). Osteocytes: master orchestrators of bone. *Calcif. Tissue Int.* 94, 5–24. doi: 10.1007/s00223-013-9790-y

Sims, N. A., and Martin, T. J. (2020). Osteoclasts provide coupling signals to osteoblast lineage cells through multiple mechanisms. *Ann. Rev. Physiol.* 82, 507–529. doi: 10.1146/annurev-physiol-021119-034425

Sims, N. A., and Vrahnas, C. (2014). Regulation of cortical and trabecular bone mass by communication between osteoblasts, osteocytes and osteoclasts. *Arch. Biochem. Biophys.* 561, 22–28. doi: 10.1016/j.abb.2014.05.015

Sobacchi, C., Schulz, A., Coxon, F. P., Villa, A., and Helfrich, M. H. (2013). Osteopetrosis: genetics, treatment and new insights into osteoclast function. *Nat. Rev. Endocrinol.* 9, 522–536. doi: 10.1038/nrendo.2013.137


**Conflict of Interest:** The authors declare that the research was conducted in the absence of any commercial or financial relationships that could be construed as a potential conflict of interest.

frontiers in Cell and Developmental Biology

ORIGINAL RESEARCH
published: 09 July 2020
doi: 10.3389/fcell.2020.00623

# Synonymous Mutations of Porcine *Igf1r* Extracellular Domain Affect Differentiation and Mineralization in MC3T3-E1 Cells

*Chunli Wang†, Siyao Wang†, Songcai Liu, Yunyun Cheng, Hongwei Geng, Rui Yang, Tianqi Feng, Guanhong Lu, Xiaotong Sun, Jie Song and Linlin Hao**

*College of Animal Sciences, Jilin University, Changchun, China*

OPEN ACCESS

**Edited by:**
*Drorit Neumann,*
*Tel Aviv University, Israel*

**Reviewed by:**
*Teresita Padilla-Benavides,*
*University of Massachusetts Medical School, United States*
*Zhong Yao,*
*University of Toronto, Canada*

***Correspondence:**
*Linlin Hao*
*haolinlin@jlu.edu.cn*

*† These authors have contributed equally to this work*

**Specialty section:**
*This article was submitted to Cellular Biochemistry, a section of the journal Frontiers in Cell and Developmental Biology*

**Received:** *30 March 2020*
**Accepted:** *22 June 2020*
**Published:** *09 July 2020*

**Citation:**
*Wang C, Wang S, Liu S, Cheng Y, Geng H, Yang R, Feng T, Lu G, Sun X, Song J and Hao L (2020) Synonymous Mutations of Porcine Igf1r Extracellular Domain Affect Differentiation and Mineralization in MC3T3-E1 Cells. Front. Cell Dev. Biol. 8:623. doi: 10.3389/fcell.2020.00623*

Owing to the wide application of miniature pigs in biomedicine, the formation mechanism of its short stature must be elucidated. The insulin-like growth factor 1 receptor (IGF-1R), which receives signals through the extracellular domain (ECD) binding with ligands, is crucial in regulating cell growth and bone matrix mineralization. In this study, two haplotypes of *Igf1r* with four synonymous mutations in the coding sequences of IGF-1R ECD between large pigs (LP) and Bama pigs (BM) were stably expressed in the *Igf1r*-knockout MC3T3-E1 cells and named as MC3T3-LP cells (LP group) and MC3T3-BM cells (BM group), respectively. IGF-1R expression was lower in the BM group than in the LP group both in terms of transcription and translation levels, and IGF-1R expression inhibited cell proliferation. In addition, IGF-1R expression in the BM group promoted early-stage differentiation but delayed late-stage differentiation, which not only suppressed the expression of bone-related factors but also reduced alkaline phosphatase activity and calcium deposition. Moreover, different haplotypes of *Igf1r* changed the stability and conformation of the protein, further affecting the binding with IGF-1. Our data indicated that the four synonymous mutations of IGF1R ECD encoded by affect gene transcription and translation, thereby further leading to differences in the downstream pathways and functional changes of osteoblasts.

**Keywords: synonymous mutations, IGF-1R, cell differentiation, osteoblast mineralization, protein conformation**

## INTRODUCTION

Miniature pigs possess many similarities with humans in terms of anatomical, morphological, and physiological characteristics. Hence, miniature pigs have invaluable advantages as biomedical animal models (Liu et al., 2010). With the development and utilization of miniature pig models, current studies focus on xenotransplantation and model construction. However, a systematic study on the formation mechanism of miniature pig dwarfism is lacking (Cheng et al., 2018; Cao et al., 2019). The genetic background of miniature pigs and the mechanism of dwarfism are the prerequisites of scientific research using miniature pig models. Therefore, the formation mechanism of miniature pigs must be elucidated. In China, the Bama Xiang pig is a well-known miniature pig breed from Guangxi Zhuang Autonomous Region. It is characterized by highly

inbred, stable heredity and mini-body size (the mean body weight of adults is nearly 40 kg) (Cheng et al., 2016; Yang et al., 2018). The Large White pig also called Yorkshire pigs, is considered the most representative of large pigs because of its large body size and high growth rate (mean body weight of adults is almost 250 kg) and is considered as the most typical representative of large pigs. The contrast in the size and bodyweight of these two breeds makes them an ideal model for comparing the differences in body size between miniature and large pigs. Moreover, bone size (bone mass, volume) and bone growth are regarded as important indicator of body size in mammals (Ruff, 2003; Nieves et al., 2005; Schlecht et al., 2015). Cellular signaling pathways controlled by growth factors and hormones are also believed to influence bone size and bone growth (Efstratiadis, 1998).

The insulin-like growth factor-1 receptor (IGF-1R) is a typical receptor tyrosine kinase that regulates embryonic and postnatal growth (Efstratiadis, 1998; Siddle, 2011). An intragenic IGF-1R deletion that was identified in a patient presented short stature (Harmel et al., 2013). IGF-1R signaling, which is activated by IGF-1, plays an essential role in cell growth and development, as well as in bone formation via osteoblast-mediated bone mineralization (Fang et al., 2019). IGF-1R is also involved in bone matrix mineralization. Studies using osteoblast culture systems have shown that IGF-1R, by binding to IGF-1, enhances bone matrix production and stimulates the proliferation and differentiation of osteoblasts (Canalis, 1993; Birnbaum et al., 1995; Wang et al., 2015). IGF-1R signaling activates autophagy, which is necessary for stimulating early osteoblast differentiation, at the early stage of differentiation by activating AMPK (Xi et al., 2016).

IGF-1R exhibits different protein expression levels in the liver and muscle tissues of large and miniature pigs (Cheng et al., 2016). A previous study screened nine strong linkage synonymous mutations in the coding sequence (CDS) of IGF-1R between large and miniature pigs, four of which were found in the extracellular domain (ECD), whereas five were located in the intracellular domain (ICD) (Changhong et al., 2018). As a ligand-dependent receptor, mutations in IGF-1R ECD can potentially affect its biological function. A clinical research indicated that mutations in *Egfr* are associated with *Igf1r* variants in female patients with lung adenocarcinoma (Liu et al., 2016). A study showed that the mutant of V599E-IGF-1R ECD interferes with the receptor's transport processes, thereby eliminating the processing of pro-receptors and localization of the plasma membrane (Wallborn et al., 2010). However, most studies presently focus on the missense mutations of *Igf1r* (Wallborn et al., 2010; Liu et al., 2016). A systematic functional research on synonymous mutations is lacking.

Changes in synonymous codons that do not alter the final protein sequence were previously regarded as silent mutations without any functional consequences. Most recent evidence shows that synonymous mutations are shaped by evolutionary selection and affects other aspects of protein biogenesis (Chaney and Clark, 2015). Advances in synthetic biology have provided researchers with new methods for understanding the diverse roles of synonymous variations (Hunt et al., 2014). Synonymous codon usage affects multiple steps of transcription and translation processes, including regulation of speed and accuracy of the translation, co-translational folding, protein post-translational modifications, secretion, and expression levels (Plotkin and Kudla, 2011). Therefore, exploring the functions of synonymous mutations may be the key to uncovering the influence mechanism of the correlation between gene polymorphisms and phenotypes.

Although the growth-related traits of Angus cattle have been proved to be related to a synonymous mutation of *Igf1r* (Szewczuk et al., 2013), the question of whether the synonymous mutations in *Igf1r* can affect the body size traits in pigs remains unclear. Moreover, the potential functions of these synonymous mutations have yet to be recognized. In the present study, we focused on four single nucleotide polymorphisms (SNPs) of IGF-1R ECD previously screened from pigs of different body size traits (**Figure 1A** and **Table 1**) to confirm the effects of synonymous mutations on the differentiation and mineralization of osteoblasts. We further clarified the molecular mechanism of bone development to determine the effects of *Igf1r* synonymous mutations on the formation of body shape traits. We expected to provide new evidence clarifying the roles of IGF-1R in the formation mechanism of miniature pigs.

The linkage effects of these synonymous mutations may be involved in the formation of body size in miniature pigs. The present study explored the functions of potentially valuable synonymous mutations and provided a theoretical basis for the formation of body size in miniature pigs. According to the results, we indeed observed differences of IGF-1R at both mRNA and protein levels between the two haplotypes of IGF-1R from large and miniature pigs. Furthermore, these cellular and biochemical alterations affected the stability of IGF-1R and its ability to bind its ligand. Importantly, our results reveal that four synonymous mutations of IGF-1R contribute to the consequent changes in IGF-1R signaling and cellular functions observed in the proliferation, differentiation, and mineralization of osteoblasts.

# MATERIALS AND METHODS

## Construction of sgRNA and PiggyBac Vectors

The sgRNA vector was constructed as follows: One sgRNA of *Igf1r* in exon 4 was designed by the Crispr/cas9 sgRNA prediction website[1], and the PX458 knockout vectors containing the sgRNA were constructed (Zafra et al., 2018). The sgRNA forward primer was 5′-CACCGCAATCTGCTTATTAACATC-3′, whereas the reverse primer was 5′-AAACGATGTTAATAAGCAGATTGC-3′. The PiggyBac vector was constructed as follows: Two fusion genes were made using the CDS of *Igf1r* ICD to splice the ECD of the Large White pig and Bama Xiang pig. Two fusion genes contained the FLAG tag sequence and enzyme recognition sequences, which were then synthesized by Jilin Comate Bioscience Co., Ltd (China), and the FLAG tag sequence was added to C-terminal tail of IGF-1R (**Figures 1A,B** and **Table 1**). The fusion genes were successfully connected to the pB513B-Puro vector (MiaoLingBio, China). These genes were

[1]https://zlab.bio/guide-design-resources

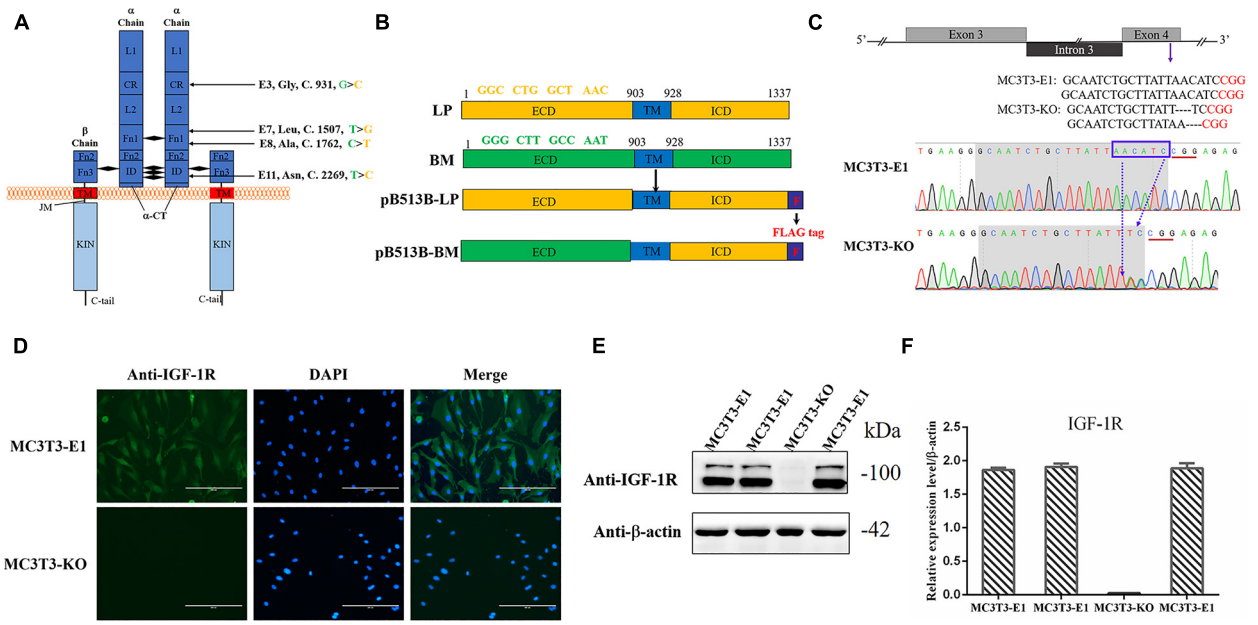


**FIGURE 1 |** Generating *Igf1r*-Knockout MC3T3-E1 Clones. **(A)** Four SNPs were located in the coding sequence of the *Igf1r* gene ECD between miniature (green) and large (yellow) pigs. **(B)** The full-length *Igf1r* of large pigs (LP) and Bama Xiang pigs (BM) were shown in the top line. The sequences were inserted into the pB513 vector between the *Eco*RI and *Xho*I sites and respectively named as pB513B-LP (with the CDS of full *Igf1r* of Large White pigs) and pB513B-BM (with the CDS of IGF-1R ECD of Bama Xiang pigs and IGF-1R ICD of Large White pigs). TM: transmembrane region (blue), F: FLAG tag (purple). **(C)** Schematic illustration and DNA sequence map showing the position of sgRNA target site. The target sequence and PAM sequence were highlighted by the gray background and red underline, respectively. **(D)** Immunostaining of IGF-1R (Green) and DAPI (Cyan) in MC3T3-E1 and MC3T3-KO cells. **(E)** The protein expression levels of IGF-1R in MC3T3-E1 and MC3T3-KO cells were analyzed by western blot. **(F)** Quantification of the **(E)** western blot results.

named pB513B -LP (with the CDS of full *Igf1r* of Large White pigs) and pB513B-BM (with the CDS of *Igf1r* ECD of Bama Xiang pigs and *Igf1r* ICD of Large White pigs) (**Figure 1B**).

## Cell Culture

Given that the osteoblast cell lines of pigs are difficult to obtain, a mouse osteoblast cell line (MC3T3-E1 cells), which was obtained from the Hospital of Stomatology Jilin University, was selected. The IGF-1R amino acid sequences in mice (NP_034643.2) were found to be 95% similar to those in humans (NP_000866.1) and pigs (NP_999337.1) according to NCBI[2]. Moreover, a certain amount of IGF-1R was detected in MC3T3-E1 cells (Joung et al., 2013). The cells were cultured in Dulbecco's minimal essential medium (DMEM) (Hyclone, United States) supplemented with 10% heat-inactivated fetal bovine serum and 1% streptomycin/penicillin (Gibco, United States) in an incubator with 5% $CO_2$ at 37°C. At 80% cell confluence, the culture medium was changed to a differentiation medium that contained 50 mg/mL ascorbic acid (Sigma, United States) and 10 mmol/L β-glycerophosphate (Sigma, United States) (Zheng et al., 2018).

[2]https://blast.ncbi.nlm.nih.gov/Blast.cgi

**TABLE 1 |** SNPs parameters of IGF-1R gene ECD in Bama Xiang pigs and large pigs.

| SNP number | Gene | | mRNA | Protein |
|---|---|---|---|---|
| | Position | Exon | Allele change | Position |
| rs338724264 | g.267380 | 3 | G/C | 301 |
| rs325909655 | g.286723 | 7 | T/G | 493 |
| rs337838116 | g.288540 | 8 | C/T | 578 |
| rs326728191 | g.296721 | 11 | T/C | 747 |

## *Igf1r* Knockout in MC3T3-E1 Cell Lines

Exactly 30 μg of PX458-sgRNA vectors were transfected into MC3T3-E1 cells by using the BTX-ECM 2001 Electroporation system (United States). Two days after electroporation, the cells expressing the GFP fluorescent protein were separated via flow cytometry for further culture. A few days later, the monoclonal cells were selected and seeded in 24-well plates. When the cells became confluent, NP40 lysis buffer was used to lyse a few cells. The lysate was used as the PCR template for genotyping to identify the knockout activity, and IGF-1R antibody was used for Western blot and immunofluorescence assays further to verify the expression of IGF-1R in MC3T3-E1 cells.

## Generation of Two Recombinant Cell Lines

Exactly 30 μg of pB513B-LP and pB513B-BM vectors and 12 μg PiggyBac transposase vector were successively co-transfected into MC3T3-KO cells using the BTX-ECM 2001 electroporation

system. Two days after electroporation, the cells transfected with pB513B-puro vectors were screened with puromycin (3 μg/ml). After 9 days, individual cell clones were selected and seeded in 24-well plates. When the cells became confluent, NP40 lysis buffer was used to lyse a few cells. Genotyping was performed using lysate as the PCR template. The integrated *Igf1r* gene copy number per genome was determined via quantitative real-time PCR (q-PCR). q-PCR was performed using SYBR Select Master Mix (Roche). The primers used are listed in **Table 2**. For each sample, 100 ng of the DNA template was amplified in PCR reactions on an ABI PRISM 7900HT thermocycler (Applied Biosystems, United States). All samples were performed in triplicate, and each quantification data represented an average of at least three measurements. A standard curve for the *Igf1r* gene copy number was generated according to the continuous dilution of pB513B genetic recombination vector. The transgene *Igf1r* copy number per diploid cell was then calculated as described previously (Joshi et al., 2008; Wang et al., 2013). Finally, the expression of IGF-1R in MC3T3-KO was verified by FLAG antibody. The positive clones were named as MC3T3-LP and MC3T3-BM.

## Immunofluorescence Assay

Paraformaldehyde (4%) was used to fix cells for 20 min, and 0.5% Triton X-100 in PBS was utilized to permeabilize the cells for 10 min. Subsequently, 10% fetal bovine serum was used to block the cells for 1 h. Finally, the cells were incubated with IGF-1R antibody (Abcam, United States) at 4°C overnight. On the following day, FITC-labeled immunofluorescence secondary antibody (Bioworld, United States) was added to plates of cells for incubation for 1 h in the dark. Then, 4-6-diamino-2-phenindole (Bioworld, United States) was used to visualize the nucleus. Images were captured using a fluorescence microscope (Leica, Frankfurt, Germany).

## RNA Extraction and qRT-PCR

The RNAiso Plus reagent (Takara, United States) was used to extract total RNA from the cells according to the manufacturer's instructions. Reverse transcription was performed to generate cDNA using a reverse transcription kit. SYBR Select Master Mix (Roche) was used for Quantitative Real-time PCR (qRT-PCR). The primers used are listed in **Table 3**. The PCR reactions were performed on an ABI PRISM 7900HT thermocycler (Applied Biosystems, United States), and 10 ng of the cDNA template was amplified for each sample. All samples were repeated three times, and each mRNA quantification data represented the average of these three measurements. The Ct values of the target genes were normalized by the Ct value of the β-actin gene. The $2^{-\Delta Ct}$ method was employed to quantify and normalize the expression data (Cheng et al., 2020).

**TABLE 2 |** Primer information for qPCR analysis of copy number.

| Gene | Sequences (5′-3′) | Product lengths (bp) | Tm (°C) |
|---|---|---|---|
| PB | F: TCACGCGGTCGTTATAGTTCAA<br>R: CCGTGAGGCGTGCTTGTC | 62 | 58.5 |
| β-actin | F: TTCAACACCCCAGCCATGTA<br>R: TGTGGTACGACCAGAGGCATAC | 69 | 58.5 |

## Immunoblotting Assay

Protein content was quantified using a BCA protein assay kit (Beyotime, China) following the manufacturer's protocols. About 40 μg of the total proteins of each sample were separated using 12 or 8% SDS-PAGE gels. The total proteins were transferred to polyvinylidene difluoride membranes. Afterward, 10% non-fat dry milk dissolved in TBST buffer was used to block the membranes for 1.5 h at 37°C. Thereafter, the primary antibodies were used to incubate with the membranes overnight at 4°C, followed by incubation with horseradish peroxidase-labeled anti-mouse IgG or anti-rabbit IgG (Bioworld, United States) for 1.5 h at room temperature. Finally, the proteins were detected using the enhanced chemiluminescence plus Western blot detection system (Amersham Biosciences). The primary antibodies used in this study were as follows: phospho-AKT (S473), AKT, and phospho-ULK-1 (S555) (Cell Signaling, Beverly, MA, United States); phosphor-mTOR (S2448), phospho-AMPK (T172 and S485), AMPK, FLAG, and IGF-1R (Abcam, United Kingdom); Beclin-1, ULK1, mTOR, OPN, and collagen I (WanLeiBio, China); and β-actin (BBI, China). Protein quantifications were analyzed using the GenoSens gel analysis software.

## Cell Proliferation

Cell proliferation assays were performed using Cell Counting Kit-8 (CCK-8, Dojindo, Japan). MC3T3-KO, MC3T3-LP, and MC3T3-BM cells were inoculated in 96-well plates at an initial density of $6.0 \times 10^3$ cells/well in 100 μL of culture medium.

At 0, 24, 48, and 72 h, 10 μL of the CCK-8 reagent was added to each well and reacted at 37°C for 1 h. Absorbance was detected using a microplate reader (TECAN, Switzerland) at a wavelength of 450 nm.

**TABLE 3 |** Primer information for RT-qPCR analysis of expression of target genes.

| Gene | Sequences (5′-3′) | Product lengths (bp) | Tm (°C) |
|---|---|---|---|
| *Col-1* | F: CCAGCCGCAAAGAGTCTACA<br>R: TTCCACGTCTCACCATTGGG | 170 | 58.5 |
| *Opn* | F: ACACTTTCACTCCAATCGTCC<br>R: TGCCCTTTCCGTTGTTGTCC | 240 | 58.5 |
| *Ocn* | F: AGACTCCGGCGCTACCTT<br>R: CTCGTCACAAGCAGGGTTAG | 203 | 58.5 |
| *Runx2* | F: GAGGGACTATGGCGTCAAACA<br>R: GGATCCCAAAAGAAGCTTTGC | 70 | 58.5 |
| *Osterix* | F: TCAGCCGCCCCGATCTTCCA<br>R: CAATGGGTCCACCGCGCCAAG | 157 | 58.5 |
| *Alp* | F: CAACAGGGTAGATTCTCTTGG<br>R: GGTCAGATCCAGAATGTTCC | 135 | 58.5 |
| *Igf1r* | F: CAAGGCTGAGAACGGCCC<br>R: TCACTTGTCATCGTCGTCCTTG | 160 | 58.5 |
| *β-actin* | F: GGCTGTATTCCCCTCCATCG<br>R: CCAGTTGGTAACAATGCCATGT | 154 | 58.5 |

## Measurement of Alkaline Phosphatase (ALP) Activity

MC3T3-LP, MC3T3-BM, and MC3T3-KO cells with a density of $2.0 \times 10^4$ cells/well were inoculated in 24-well plates and cultured in differentiation media. The cells were eventually harvested after 3, 5, 7, 9, 14, 18, and 21 days. Alkaline phosphatase (ALP) activities were determined using an ALP kit (Nanjing Jiancheng, China) in accordance with the manufacturer's instructions. Protein concentrations were measured using a BCA protein assay kit (KeyGEN BioTECH, China). Enzyme activity was quantified via absorbance measurements at 520 nm using a 96-well microplate reader (TECAN, China) and calculated according to protein concentrations. Total protein content was used to normalize ALP activity, and all assays were repeated at least three times.

## Alizarin Red Staining (ARS)

Mineralization is considered the last stage of osteogenic differentiation, and the formation of mineralized nodules is a definitive marker of osteoblast mineralization. Alizarin Red (AR) chelates with calcium ions are usually used to form orange-red depositions (mineralized nodules) to determine the osteogenic mineralization ability in tissues or cells (Puchtler et al., 1969; Xi et al., 2016; Zheng et al., 2018). MC3T3-LP, MC3T3-BM, and MC3T3-KO cells with a density of $2.0 \times 10^4$ cells/well were inoculated in 24-well plates and cultured in differentiation media for 7, 14, and 21 days. PBS was used to wash the cells twice before they were fixed with 70% ethanol for 1 h and stained with 1% AR (pH 7.2) for 10 min at room temperature. Afterward, the cells were washed with $ddH_2O$ twice and dried. The images were captured at 10 × magnification on the inverted phase-contrast microscope (Nikon, Japan) (Bae et al., 2017). The stained nodules were dissolved with 10% cetylpyridinium chloride to quantify the degree of staining, and the absorbance at 562 nm (Jiang et al., 2019) was measured using a microplate reader (TECAN, China). The results were replicated in at least three independent experiments.

## Stability Assay

MC3T3-LP and MC3T3-BM cells with a density of $3.0 \times 10^5$ cells/well were inoculated in 6-well plates. Actinomycin D (ActD, 5 μg/mL) and cycloheximide (CHX, 50 μg/mL) were added to the medium and used to block mRNA transcription and protein synthesis respectively. The cells were collected at 0, 1, 2, 3, and 4 h after culture, and the total RNAs and proteins were extracted. The stability of the mRNAs and proteins was detected from the collected RNAs and proteins, respectively.

## Co-immunoprecipitation Analysis (Co-IP)

Exactly 500 nM IGF-1 was added to the medium because previous studies reported that 500 nM IGF-1 reaches the maximum binding concentration when IGF-1R is combined with IGF-1 (Jansson et al., 1997; Whitten et al., 2009). The MC3T3-LP, MC3T3-BM and MC3T3-KO cells were incubated in the medium containing IGF-1 for 6 h. Subsequently, the cells were collected and lysed. Co-IP incubation was performed using Pierce™ protein A/G magnetic beads (Thermo, United States). The lysate was centrifuged at 13,000 × *g* for 15 min, and the supernatant was immunoprecipitated overnight with IGF-1R antibody or IgG antibody (control). On the following day, the magnetic beads and the antigen-antibody complex was incubated for 2 h at 4°C. The collected protein and magnetic bead complexes were washed five times with a wash buffer and eluted with an elution buffer. Finally, the eluents were neutralized with a neutralization buffer and boiled in a protein sample buffer under reducing conditions. The sample proteins were resolved and analyzed via SDS-PAGE analysis and Western blot, respectively.

## Flow Cytometry Analysis

The MC3T3-LP, MC3T3-BM and MC3T3-KO cells were incubated with 4% paraformaldehyde alone or incubated with 4% paraformaldehyde and permeabilized with 0.1% Triton X100 to evaluate the cell surface expression of IGF-1R in the cells (Rezgui et al., 2009). The cells were stained with FITC-conjugated anti-FLAG antibody (1:400, Abcam, United States) and analyzed via flow cytometry (BD FACSAriaII) (Ip et al., 2018).

The MC3T3-LP, MC3T3-BM and MC3T3-KO cells were incubated in 4% paraformaldehyde for 20 min and permeabilized with 0.5% Triton X-100 in PBS for 10 min for IGF-1R staining to evaluate the differences in protein conformations of IGF-1R. Subsequently, 5% goat serum was used to block the cells for 1 h, and the primary antibody against IGF-1R (1:80, Abcam, United States) was used to incubate the cells overnight at 4°C. On the following day, an FITC-labeled secondary antibody (1:100, Bioworld, United States) was used to incubate the cells for 1 h in the dark. The fluorescence intensity of a population of 10,000 cells was measured with the fluorescence associated with the FITC. IgG-treated cells were used as negative controls (Fung et al., 2014).

Subsequently, 5% goat serum was used to block the cells for 1 h, and the primary antibody against IGF-1R (1:80, Abcam, United States) was used to incubate the cells overnight at 4°C. On the following day, an FITC-labeled secondary antibody (1:100, Bioworld, United States) was used to incubate the cells for 1 h in the dark. The fluorescence intensity of a population of 10,000 cells was measured with the fluorescence associated with FITC. IgG-treated cells were used as negative controls.

## Statistics Analysis

All experimental results are presented as the mean ± SEM of at least three independent experiments. One-way or two-way ANOVA was used to test statistical differences among groups. All statistical analyses were performed using GraphPad Prism 6.0. Differences were considered significant at $p < 0.05$ ($^*p < 0.05$, $^{**}p < 0.01$).

# RESULTS

## Generation of *Igf1r*-Knockout MC3T3-E1 Clones

Four homozygous mutations (c.931G > C, c.1507T > G, c.1762C > T, and c.2269 T > C) in the CDS of IGF-1R ECD from

pigs of different body size traits were all synonymous mutations (**Figure 1A**). Two haplotypes, of which GTCT is the haplotype of BM pigs and CGTC is that of large pigs, were formed (**Figure 1B**).

To investigate the role of different *Igf1r* haplotypes in bone development and avoid endogenous *Igf1r* interference in osteoblasts, we first constructed *Igf1r*-knockout in MC3T3-E1 cells by using the CRISPR/cas9 system. To ensure complete *Igf1r* knockout, we designed one target site on the exon 4 of *Igf1r* sequences to target the common sequences contained in all the alternative splicing isoforms. The position of the target site was relatively close to the beginning of the sequence (**Figure 1C**). sgRNA sequences were then connected to plasmid PX458 and transfected into MC3T3-E1 cells. Fluorescence-activated cell sorting was implemented to select the cells expressing GFP fluorescence to improve the efficiency of positive cloning screening. The presence of IGF-1R mutations in genomic DNA was identified via DNA sequencing. Most cell clones showed frameshift mutation, and one cell clone had a nucleotide deletion near the protospacer adjacent motif (**Figure 1C**). To assess knockout efficiency, we performed immunofluorescence staining on the $Igf1r^{Knockout}$ cell clones by using the IGF-1R antibody. The MC3T3-E1 cells exhibited strong IGF-1R signals, whereas the $Igf1r^{Knockout}$ cell clones lost the IGF-1R signal (**Figure 1D**). Meanwhile, the IGF-1R protein levels in different mutant clones were measured via immunoblotting. The $Igf1r^{Knockout}$ cell clones lost the IGF-1R protein expression as indicated by the Western blot results (**Figures 1E,F**). We selected a clone with sufficient *Igf1r* knockout and named MC3T3-knockout cell.

## Stable Expression of Two Haplotypes of *Igf1r* in MC3T3-KO Cells

The pB513B-LP and pB513B-BM vectors were co-transfected with the PB transposase expression plasmid into MC3T3-KO cells, respectively, and normal MC3T3-KO cells were used as a control. The co-transfected cells were selected by puromycin for 10 days to obtain puromycin-resistant cell clones. About 50 cell clones per well were left after the co-transfection of the screened PB dual vector system. Almost no cell clones survived in the control group, indicating that the cell clones that survived puromycin selection were positively transposed cell clones.

Genomic DNA was extracted from transposed MC3T3-KO cells and MC3T3-KO control cells to evaluate whether exogenous genes had been stably integrated into the genome. The expression level of exogenous genes was then detected. Specific PCR products corresponding to the two haplotypes of *Igf1r* sequences were observed from the transposed cells, whereas no PCR products were found from the control cells without transposed cells. qPCR was performed to detect the two integrated haplotypes of *Igf1r* gene copy number and analyze 10 clonal cell lines for each haplotype. The cell clones had 3–13 copies with an average of five copies per clone. We finally selected two cell clones with haplotypes of five copies each. The copy number of our clones was similar to that reported by previous studies in which mammalian cells were transfected with the PB transposon system (Ding et al., 2005; Grabundzija et al., 2010). Finally, puromycin-resistant cell clones with two different strong IGF-1R signals were observed via immunofluorescence staining (**Figure 2A**). These cell clones were named as MC3T3-LP cells (LP group) and MC3T3-BM cells (BM group).

## Effects of Two Haplotypes of *Igf1r* on the IGF-1R mRNA and Protein Expression Level

The expression levels of IGF-1R in MC3T3-LP cells containing the CGTC haplotype and MC3T3-BM cells containing the GTCT haplotype were detected to clarify the biological effects of these haplotypes. A reverse primer was designed on the FLAG tag sequences to avoid the interference of intracellular IGF-1R in detecting the mRNA expression level (**Figure 2B**). The mRNA expression levels were significantly lower in the BM group than in the LP group (**Figure 2C**) ($P < 0.01$). The protein expression level of each group was detected using an anti-IGF-1R antibody (**Figures 2D,E**) ($P < 0.01$) and anti-FLAG tag antibody (**Figures 2F,G**) ($P < 0.01$). Results consistently showed that the mRNA and protein expression levels of the BM group were lower than those of the LP group. Given that changes in expression levels can affect the biological effects of genes, we speculated that different haplotypes of *Igf1r* may also affect its function based on the observed differences in expression levels.

## Effect of Two Haplotypes of *Igf1r* on Cell Proliferation

To verify the functions of IGF-1R ECD encoded by the haplotypes in Bama Xiang and large pigs, we investigated the cell proliferation abilities of MC3T3-LP and MC3T3-BM cells and compared them with that of MC3T3-KO cells. CCK-8 assay revealed that the cell proliferation ability of the LP group was more substantial than that of the BM and KO groups from 0 to 72 h (**Figure 3**) ($p < 0.01$), suggesting that the cells of the BM group had a lower growth potential than the cells of the LP groups.

## Effect of Two Haplotypes of *Igf1r* on the ALP Activity of Osteoblasts

The proliferation and differentiation of osteoblasts are essential factors in bone growth. On the basis of our observations of the effects of cell proliferation, we further detected the effects of different haplotypes of *Igf1r* on osteoblast differentiation. ALP activity is a marker of early osteogenic differentiation that is used to evaluate the effects of different *Igf1r* haplotypes on cell differentiation (Golub et al., 1992; Bancroft et al., 2002; Hosseini et al., 2019). The MC3T3-LP, MC3T3-BM, and MC3T3-KO cells were maintained in a differentiation medium. The ALP activities of the LP, BM, and KO groups were separately measured on days 3, 5, 7, 9, 14, and 21. As shown in **Figure 4A**, the ALP activities of all three groups fluctuated: the trend initially fell and then rose from day 3 to day 21. Meanwhile, the ALP activity of the BM group was significantly higher than that of the LP and KO groups from day 3 to day 7 ($P < 0.01$). Thereafter, the ALP activity of the LP group was significantly higher than that of the MC3T3-BM and MC3T3-KO groups ($P < 0.01$). Compared with the LP group, the BM group promoted ALP activity at the early stage of

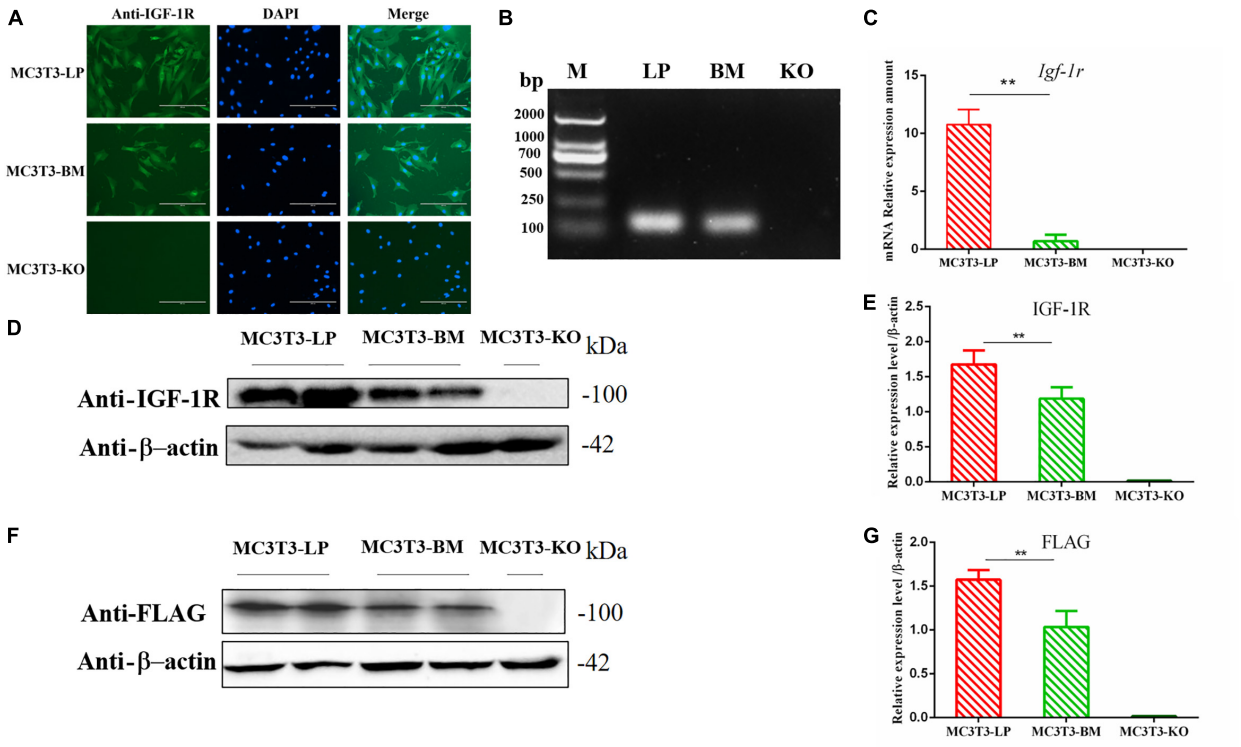


**FIGURE 2 |** Generation of recombinant cell lines of two haplotypes of *Igf1r* and effect of the haplotypes of *Igf1r* on gene transcription, translation. **(A)** Immunostaining of IGF-1R (Green) and DAPI (Cyan) in MC3T3-LP and MC3T3-BM cells. **(B)** PCR results of the MC3T3-LP (LP), MC3T3-BM(BM) and MC3T3-KO (KO)cells. **(C)** RT-qPCR analysis of IGF-1R expression in MC3T3-LP, MC3T3-BM and MC3T3-KO cells. **(D,F)** Western blot analysis of the IGF-1R and FLAG expression in MC3T3-LP, MC3T3-BM and MC3T3-KO cells and identified with anti-IGF-1R and anti-FLAG antibodies, respectively. **(E,G)** Quantification of the **(D,F)** western blot results, respectively (**$p < 0.01$).

differentiation but significantly inhibited ALP activity at the late stage of differentiation. However, the detection of ALP activity alone was insufficient to prove that the different haplotypes of *Igf1r* affected osteoblast differentiation as this process is regulated by numerous genes and transcription factors. We speculated that the haplotypes of *Igf1r* may affect the expression of genes related to bone differentiation.

## Effect of the Two Haplotypes of *Igf1r* on the Expression of Genes Related to Osteogenic Differentiation

We explored how the genotypes of *Igf1r* affect osteogenic differentiation. We investigated the expression of the genes related to osteogenic differentiation in the BM, LP, and KO groups. The expression levels of collagen-1 (*Col-1*), osteocalcin (*Ocn*), osterix (*Osx*), osteopontin (*Opn*), runt-related transcription factor 2 (*Runx2*), and *Alp* were significantly different in the cells carrying the two haplotypes of *Igf1r*. On the 7th day of differentiation, the mRNA expression level of *Col-1* and ALP was lower in the KO and LP groups than that in the LP group (**Figures 4B,C**) ($P < 0.01$). However, the mRNA expression level of *Opn*, *Ocn*, *Runx2*, and *Osx* were higher in the LP group than that in the KO and BM groups on days 7, 14, and 21 (**Figures 4D–G**) ($P < 0.01$).

*Col-1* induces extracellular matrix formation at the early stages of osteocyte differentiation, whereas *Opn* acts as a mediator of mineralization (Chai et al., 2019; Hosseini et al., 2019). The expression levels of these two genes play a crucial role in osteoblast differentiation. Western blot revealed that the expression level of Col-1 was higher in the BM group than that in

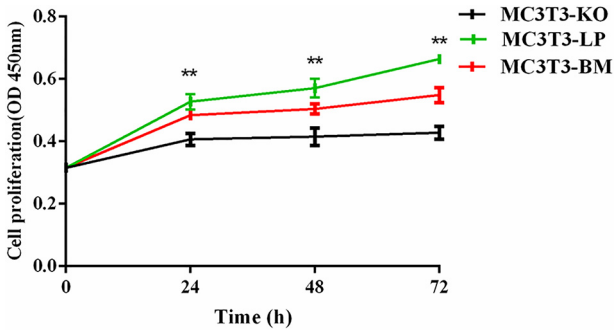


**FIGURE 3 |** Effect of two haplotypes of *Igf1r* on cell proliferation in MC3T3-LP, MC3T3-BM and MC3T3-KO cells, CCK-8 proliferation assay of MC3T3-LP, MC3T3-BM and MC3T3-KO cells after starved in DMEM containing 3% FBS for 3 h at 0, 24, 48, and 72 h (**$P < 0.01$).

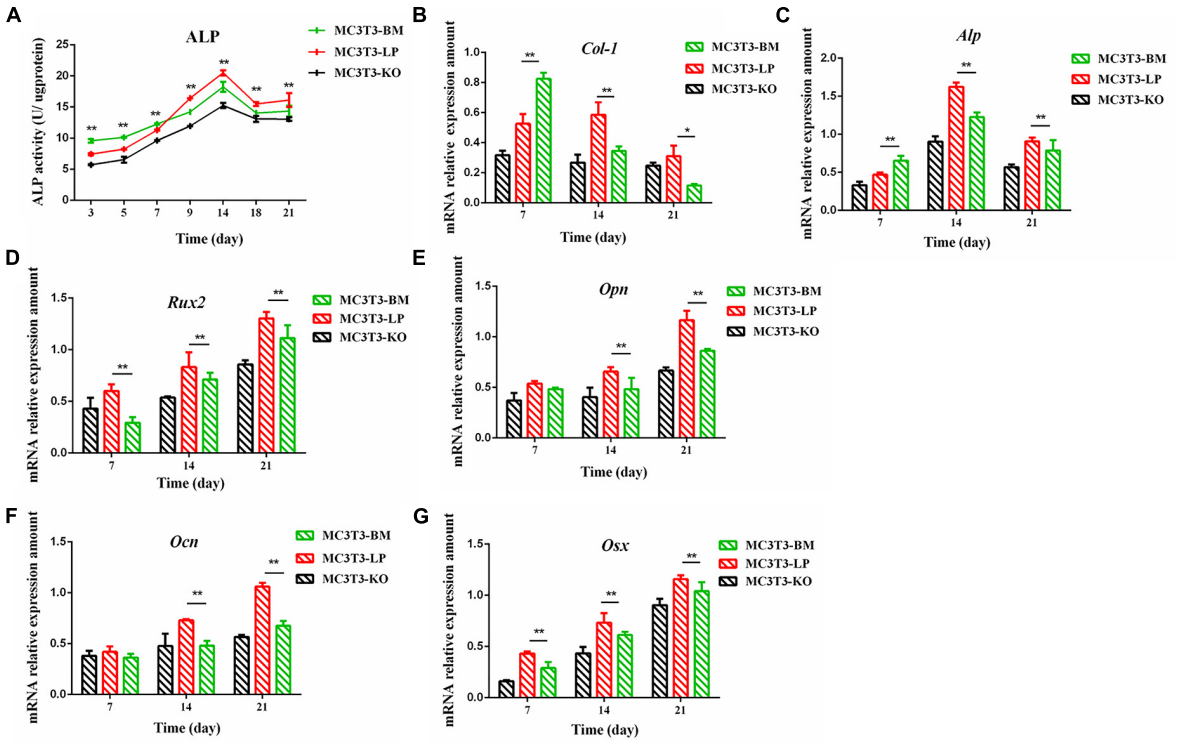


**FIGURE 4 |** Effect of two haplotypes of *Igf1r* on ALP activity and the mRNA amount of differentiation related gene in MC3T3-LP, MC3T3-BM and MC3T3-KO cells. **(A)** ALP activity assay of MC3T3-LP, MC3T3-BM and MC3T3-KO cells on days 7, 14 and 21, respectively. **(B–G)** RT-qPCR analysis of *Col-1*, *ALP*, *Runx2, Opn*, *Ocn* and *Osx* expression levels in MC3T3-LP, MC3T3-BM and MC3T3-KO cells on days 7, 14, and 21, respectively (**$P < 0.01$).

the LP group on days 1 and 2 but lower from days 3 to 6 ($P < 0.01$) (**Figures 5A,C**). Furthermore, the protein expression level of OPN was markedly attenuated in the BM group compared with that in the LP group from days 3 to 21 (**Figures 5B,D**) ($P < 0.01$). These results were consistent with the results described in the preceding section.

## Effects of the Two Haplotypes of *Igf1r* on Mineralized Nodules

Calcium deposition is an important indicator of matrix mineralization in bone differentiation. AR, which preferentially chelates with calcium ions, is widely used to identify matrix mineralization (Puchtler et al., 1969). A previous study indicated that the mineralization of MC3T3-E1 cells occurs in a time-dependent manner and can be examined during osteoblast differentiation for up to 21 days (Xi et al., 2016). The initial formation of mineralized nodules was observed on day 7. The mineralized nodules gradually increased with the extension of culture time and degree of differentiation. After induction of osteoblast mineralization, ARS revealed that the BM group had slightly less mineralized nodules compared with the LP and KO groups on day 7. The modules were remarkably larger in the LP group than those in the BM and KO groups on days 14 and 21 (**Figures 6A,B**) ($P < 0.01$). The results suggested that the BM group promoted the early stage of osteogenic mineralization, whereas the LP group promoted the late stage of osteogenic mineralization. Both groups exhibited similar trend in terms of the expression levels of genes related to osteogenic differentiation. On the basis of osteogenic differentiation, we observed that the regulation of the haplotypes of *Igf1r* were different at various stages of differentiation. We speculated that the haplotypes of *Igf1r* may affect the expression of genes related to bone development by affecting the signaling pathways associated with intracellular osteogenic differentiation.

## Effects of the Two Haplotypes of *Igf1r* on the Signal Output of Osteogenic Differentiation

Induction of autophagy is required in early differentiation, and the binding of IGF-IR with IGF-1 can activate different AMPK phosphorylation sites at different stages of cell differentiation to regulate autophagy stimulation or inhibition (Xi et al., 2016). Given that phosphorylation of AMPK-T172 directly phosphorylates unc-51-like autophagy-activating kinase-1 S555 (ULK-1 S555), we compared the phosphorylation of AMPK-T172 and ULK-1 S555 and the expression level of Beclin-1 (another critical component of autophagosomes) at the early stage of differentiation. Given that the late activation of mTOR S2448/AKT S473/AMPK S485 occurs in the osteogenic differentiation of human mesenchymal stem cells and MC3T3-E1 cells (Pantovic et al., 2013; Xi et al., 2016), we then detected

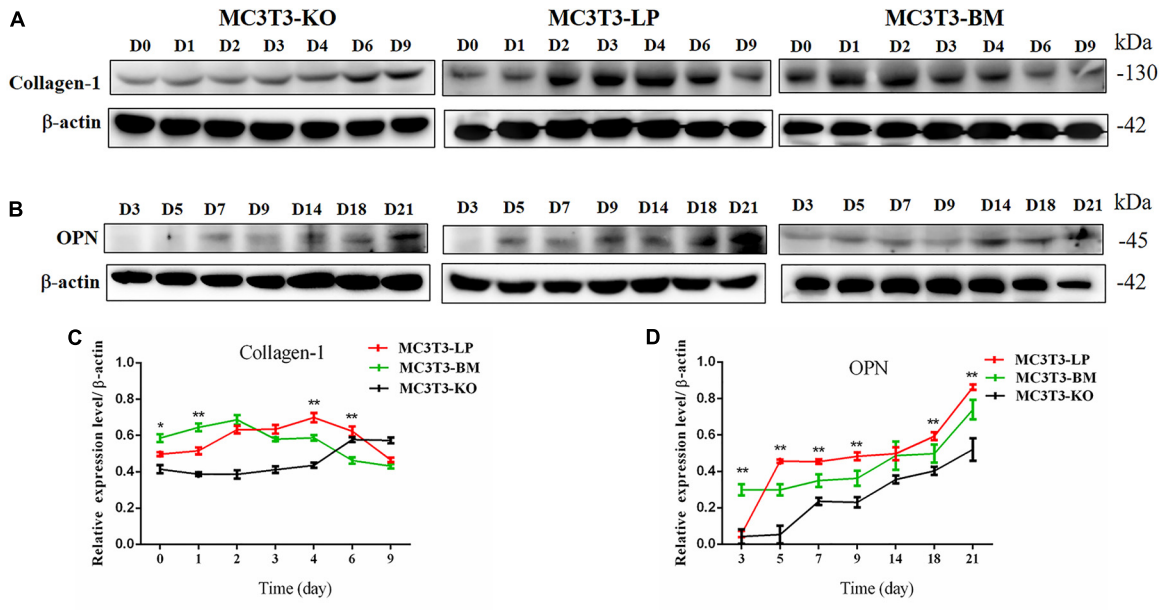


**FIGURE 5 |** Effect of two haplotypes of *Igf1r* on the protein amount Col-1 and OPN. **(A)** Western blot analysis of Col-1 expression in MC3T3-LP, MC3T3-BM and MC3T3-KO cells on days 0, 1, 2, 3, 4, 6, and 9. **(B)** Western blot analysis of OPN expression in MC3T3-LP, MC3T3-BM and MC3T3-KO cells on days 3, 5, 7, 9, 14, 18 and 21. **(C)** The line chart of the **(A)** after a gray scale analysis. **(D)** The line chart of the **(B)** after a gray scale analysis (*$P < 0.05$, **$P < 0.01$).

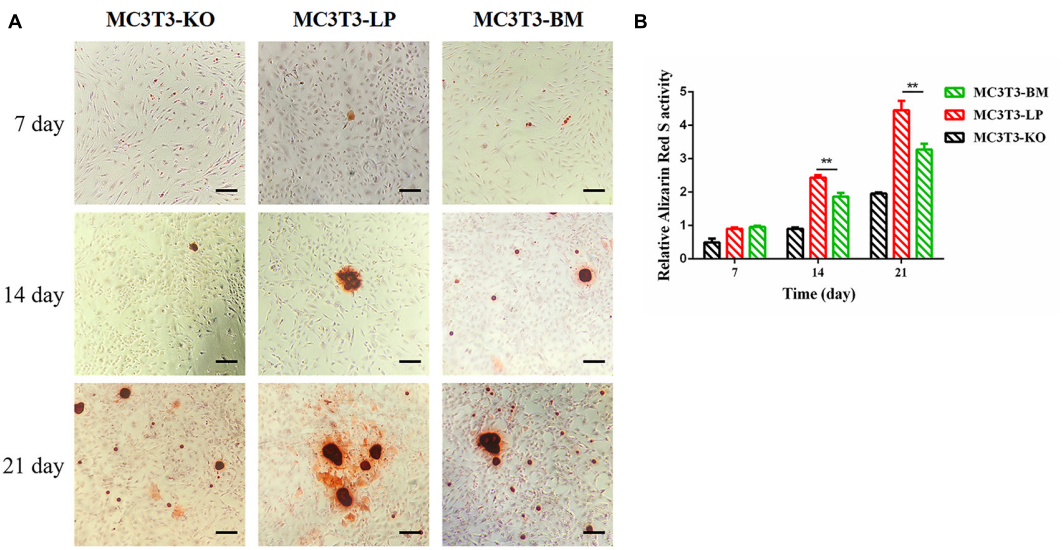


**FIGURE 6 |** Effect of two haplotypes of *Igf1r* on cell mineralization in MC3T3-LP, MC3T3-BM and MC3T3-KO cells. **(A)** Mineralized nodules of MC3T3-LP, MC3T3-BM and MC3T3-KO cells on days 7, 14, and 21. The images were captured on the inverted phase microscope (scale bar, 200 μm). **(B)** The quantified result of mineralization by 10% cetylpyridinium chloride (**$P < 0.01$).

the phosphorylation levels of mTOR S2448, AKT S473, and AMPK S485 at the late stage of differentiation. AMPK-T172 phosphorylation level and Beclin-1 expression level initially increased in the BM group from day 0 to 2, but the phosphorylation level of ULK-1 S555 was not significantly different. Moreover, Beclin-1 expression level and AMPK-T172 and ULK-1 S555 phosphorylation levels evidently decreased in the BM group compared with those in the LP group from day 3 to 9 (**Figure 7**). However, at the relatively late stage of differentiation, mTOR S2448, AKT S473, and AMPK S485 phosphorylation levels in the BM group continued to decrease from day 3 to 21 (**Figure 8**).

These results suggested that the two haplotypes of *Igf1r* play different roles in regulating the downstream signaling pathway of osteoblast differentiation. The osteoblasts in the BM group had a higher AMPK phosphorylation level and Beclin-1

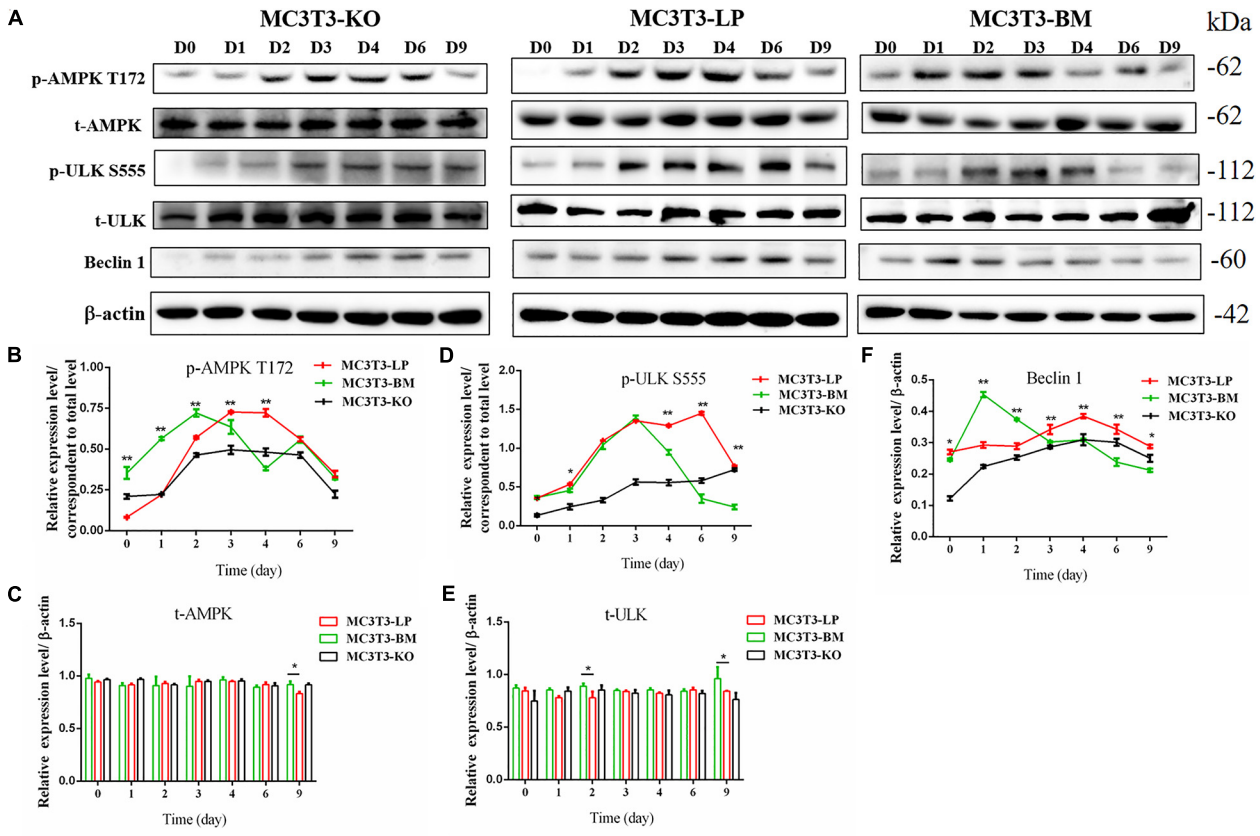


**FIGURE 7 |** Effect of two haplotypes of *Igf1r* on the signal output of early-stage osteogenic differentiation. **(A)** Western blot evaluation results of AMPK-T172, T-AMPK, ULKS55, T-ULK, and Beclin-1 protein expression in MC3T3-LP, MC3T3-BM and MC3T3-KO cells, respectively on days 0, 1, 2, 3, 4, 6, and 9. **(B–F)** Quantification of the **(A)** western blot results (*$P < 0.05$, **$P < 0.01$).

expression level compared with the LP group at the early stage of differentiation, and the osteoblasts inhibited autophagy from the third day of differentiation.

## Effects of the Two Haplotypes of *Igf1r* on mRNA and Protein Stability

Synonymous mutations can affect gene expressions by affecting gene stability and translation folding (Hunt et al., 2014; Cheng et al., 2018). We speculated that the haplotypes of *Igf1r* may be influenced by differences in mRNA and protein stability. On the basis of the differences in the expression level of *Igf1r* in the BM and LP groups at the transcription and translation levels (**Figures 2D,E,G**), we evaluated the differences in mRNA and protein structural stabilities between the two haplotypes of *Igf1r*. The secondary mRNA structures and minimum free energies of the two haplotypes of *Igf1r* ECD were predicted through the bioinformatics website RNAfold web server. Results showed that the secondary mRNA structures of the two haplotypes of *Igf1r* ECD were different, and the minimum free energy increased by 6.8 kcal when the GTCT haplotype carried by the BM group was converted to the CGTC haplotype carried by the LP group (**Figures 9A,B**). In combination with these results and the differences in the expression levels of the two haplotypes of *Igf1r* previously detected, we speculated that these haplotypes may regulate gene expression levels on the basis of theory of codon translation efficiency. In other words, the translation rates of individual codons might vary by 5- to 25-fold (Curran and Yarus, 1989; Srensen and Pedersen, 1991). Another study reported that stabilization by a mutation of the initiator helix by -3.6 kcal/mol resulted a 500-fold drop in expression (Smit and Duin, 1990).

We examined the mRNA stability of the two haplotypes. The MC3T3-LP and MC3T3-BM cells were treated with the mRNA transcription inhibitor ActD, respectively. Results showed that the mRNA stability of *Igf1r* in the MC3T3-BM cells was higher than that in the MC3T3-LP cells ($P < 0.01$) (**Figure 9C**). This result was consistent with the prediction outcomes of mRNA secondary structures. Meanwhile, the protein stability test results showed that the IGF-1R protein degradation in MC3T3-BM cells was more slowly than that in MC3T3-LP cells ($P < 0.01$) (**Figures 9D,E**).

## Different *Igf1r* Haplotypes Alter Binding Affinity With IGF-1

Considering that the four synonymous mutations on IGF-1R ECD are located near the binding site with the ligand IGF-1, we detected the interactions between IGF-1 and IGF-1R

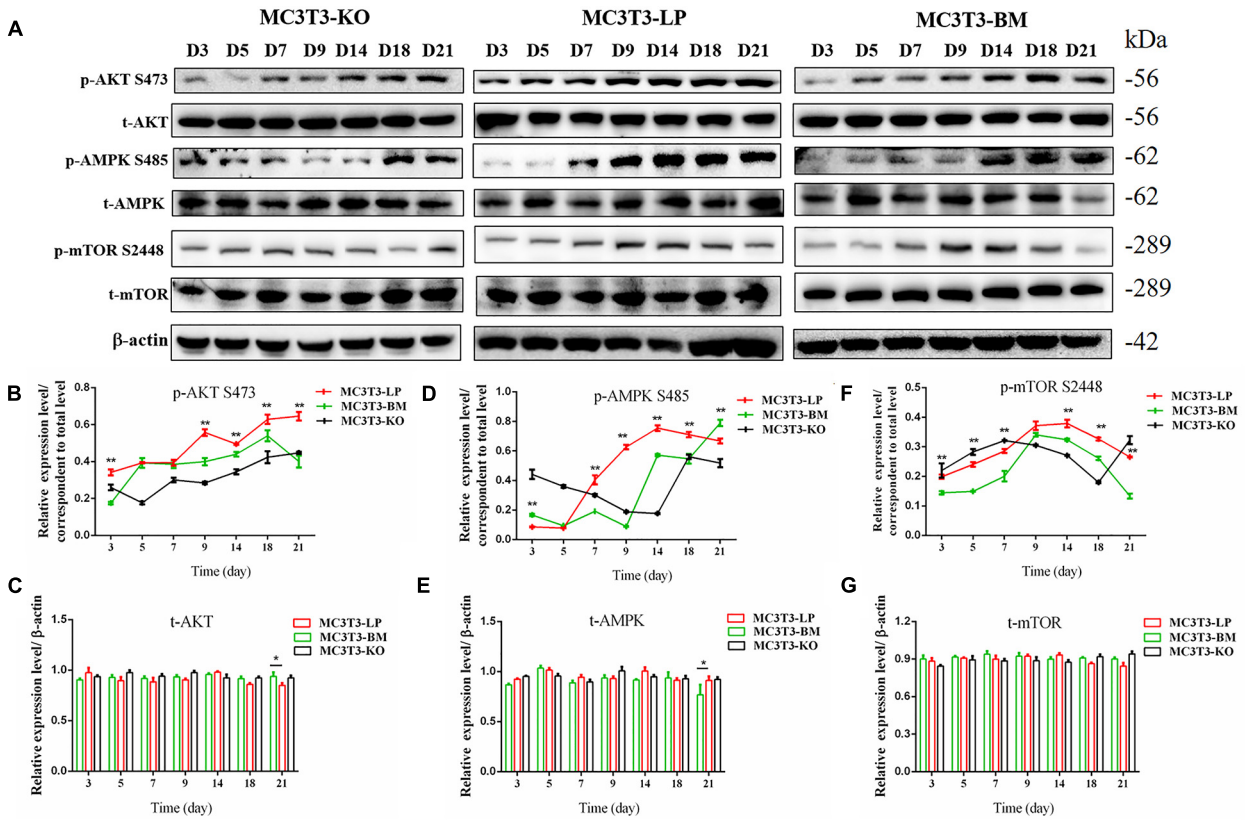


**FIGURE 8 |** Effects of two haplotypes of *Igf1r* on the signal output of late stage of differentiation. **(A)** Western blot evaluation results of P-AKT (473), T-AKT, P-AMPK S485, T-AMPK, mTOR S 2448 and mTOR protein expression in MC3T3-LP, MC3T3-BM and MC3T3-KO cells, respectively, on days 3, 5, 7, 9, 14, 18, and 21. **(B–G)** Quantification of the **(A)** western blot results (*$P < 0.05$, **$P < 0.01$).

in MC3T3-LP, MC3T3-BM, and MC3T3-KO cells via co-immunoprecipitation assay. As shown in **Figure 10**, except that IGF1R was not expressed in MC3T3KO cells, different amounts of IGF-1 and IGF-1R were the inputs of MC3T3-LP, MC3T3-BM and MC3T3-KO cells (**Figures 10A,B**) ($P < 0.01$). Additionally, IGF-1 was co-immunoprecipitated with IGF-1R when it was immunoprecipitated by the IGF-1R antibody (**Figure 10A**). No binding was detected between IGF-1 and IGF-1R in MC3T3-KO cells, excluding the interference of non-specific binding, and compared with IGF-1 in the input, the amount of IGF-1 that bound with IGF-1R in the MC3T3-LP cells was higher than that in the MC3T3-BM cells (**Figure 10C**) ($P < 0.01$). The difference in the binding rate between IGF-1R and IGF-1 can be influenced by several factors, such as the expression of IGF-1R on cell surfaces and the conformation of IGF-1R proteins. Thus, we detected the expression level of IGF-1R on the surface of cell membranes and the conformation of IGF-1R proteins.

## Effect of the Two Haplotypes of *Igf1r* on Membrane Surface Expression and Protein Conformation

To determine the reasons for the decrease in affinity of the two haplotypes of *Igf1r* with IGF-1, we detected IGF-1R distributions across the MC3T3-LP, MC3T3-BM and MC3T3-KO cell membranes by using the anti-FLAG antibody. The expression of IGF-1R on cell membrane surface in fixed and non-permeabilized cells and the expression of total IGF-1R in fixed and permeabilized cells were quantitatively detected via flow cytometry. Almost no fluorescence was detected in MC3T3-KO cells. Excluding the interference of non-specific binding, the total protein and IGF-1R expression levels on the surfaces of cell membranes were lower in the BM group than those in the LP group (**Figures 11A–C**) ($p < 0.01$). Moreover, the relative membranal expression level of IGF-1R was lower in the BM group than that in the LP group (**Figure 11D**) ($p < 0.01$).

Monitoring the antigen-antibody interaction of a protein in an intact cell by using flow cytometry has the considerable advantage of allowing a conformation-sensitive antibody to explore the tertiary structure of a functional protein in its native environment (Sauna et al., 2009). To determine whether the four synonymous mutations of *Igf1r* in ECD changed their protein conformations, we incubated the MC3T3-LP and MC3T3-BM and MC3T3-KO cells with the IGF-1R antibody, the KO group as a negative control group. We detected the fluorescence intensity of each haplotype by using a flow cytometer to reflect the binding rate between IGF-1R and its antibody. The distribution

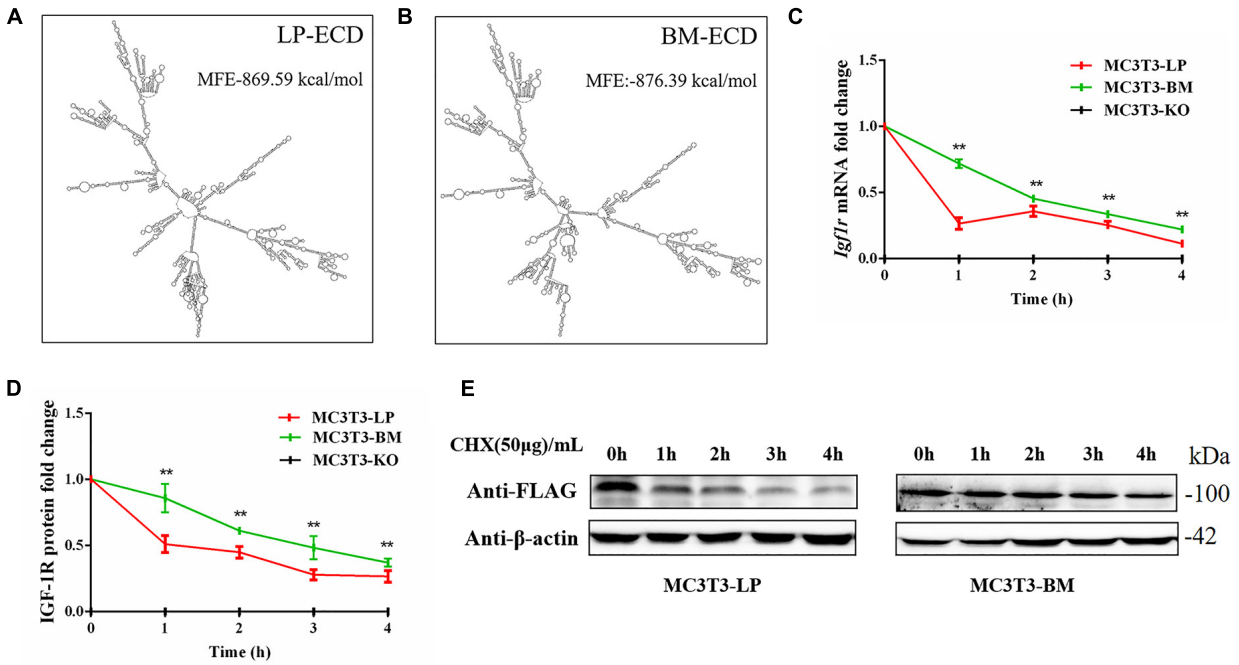


**FIGURE 9 |** The effect of two haplotypes of *Igf1r* on the stability of mRNA and protein **(A, B)** mRNA secondary structure and minimum free energy of two haplotypes of *Igf1r* ECD cDNA sequence from large pig and Bama Xiang pig. **(C)** MC3T3-LP and MC3T3-BM cells were treated with ActD for 0–4 h. The level of IGF-1R was analyzed. **(D)** MC3T3-LP and MC3T3-BM cells were treated CHX for 0–4 h. The level of IGF-1R was analyzed by western blot and β-actin was used as a loading control. **(E)** Line chart of the **(D)** after the gray scale analysis (**$P < 0.01$).

of fluorescence intensity in a population of 10,000 cells is shown in **Figure 10E**. The cells treated with the IgG antibody established a baseline with a low level of fluorescence that intuitively represented non-specific interactions and interactions with the secondary antibody alone. The fluorescence intensity of the binding of MC3T3-KO cells to the antibody was similar to that of IgG antibody, which could exclude the endogenous interference of MC3T3-KO cells. In addition, the MC3T3-LP and MC3T3-BM cells exhibited specific binding to the *Igf1r* antibody. The MC3T3-LP cells showed a higher increase in fluorescence than the MC3T3-BM cells, indicating that the *Igf1r* haplotypes of large pigs have a more remarkable affinity with the antibody than the *Igf1r* haplotypes of Bama Xiang pigs. Thus, the two haplotypes of *Igf1r* generated by the four synonymous mutations affected the membrane surface expression and protein conformation of IGF-1R.

## DISCUSSION

Miniature pigs have likely become important laboratory animals and xenotransplantation donors in biomedical research (Prather et al., 2013). However, the formation of miniature pigs remains unclear. IGF-1R is composed of seven extracellular domains, namely, L1, CR, L2, Fn1, Fn2, ID, and Fn3, as well as a transmembrane (TM) region and an intracellular domain (Baxter, 2015). The L1, ID, and Fn3 domains are the key regions where IGF-1R binds with IGF-1 (Adams et al., 2000). A previous study demonstrated that the five synonymous mutations of IGF-1R ICD affect cell proliferation and alter kinase activity (Wang et al., 2020). By contrast, in the present study, we discussed the four synonymous mutations identified in the IGF-1R ECD of large and miniature pigs. These mutations were located at the CR, Fn1, and ID structural domains of IGF-1R, as well as near the IGF-1 binding domains. IGF-1R, activated by IGF-1, mediates a conserved signaling pathway necessary for stimulating osteoblast proliferation (LeRoith et al., 1995), thereby accelerating their differentiation and enhancing bone matrix production (Xi et al., 2016). Loss of IGF-1R leads to severe growth deficiency and developmental delays in ossification (Baker et al., 1993). Mice with targeted IGF-1R overexpression in osteoblasts exhibit an increased bone formation rate and an enhanced trabecular and cortical bone volume (Zhao et al., 2000). Numerous studies demonstrated that synonymous mutations have considerable biological effects on various processes, such as gene expression, gene stability, and protein conformation (Fung et al., 2014; Chaney and Clark, 2015; Cheng et al., 2018). As a ligand-dependent receptor, stability and conformational changes in IGF-1R regulate IGF-1R activity and lead to differences in downstream functions. Moreover, previous studies corroborated the relationship between gene SNPs and bone phenotypes in animals (Horvath et al., 2016; Bin et al., 2017; Gaffney-Stomberg et al., 2017). Therefore, we suspected that these synonymous mutations of porcine IGF-1R ECD most likely play a vital role in regulating IGF-1R expression, as well as in the regulation of the proliferation, differentiation, and mineralization of osteoblasts.

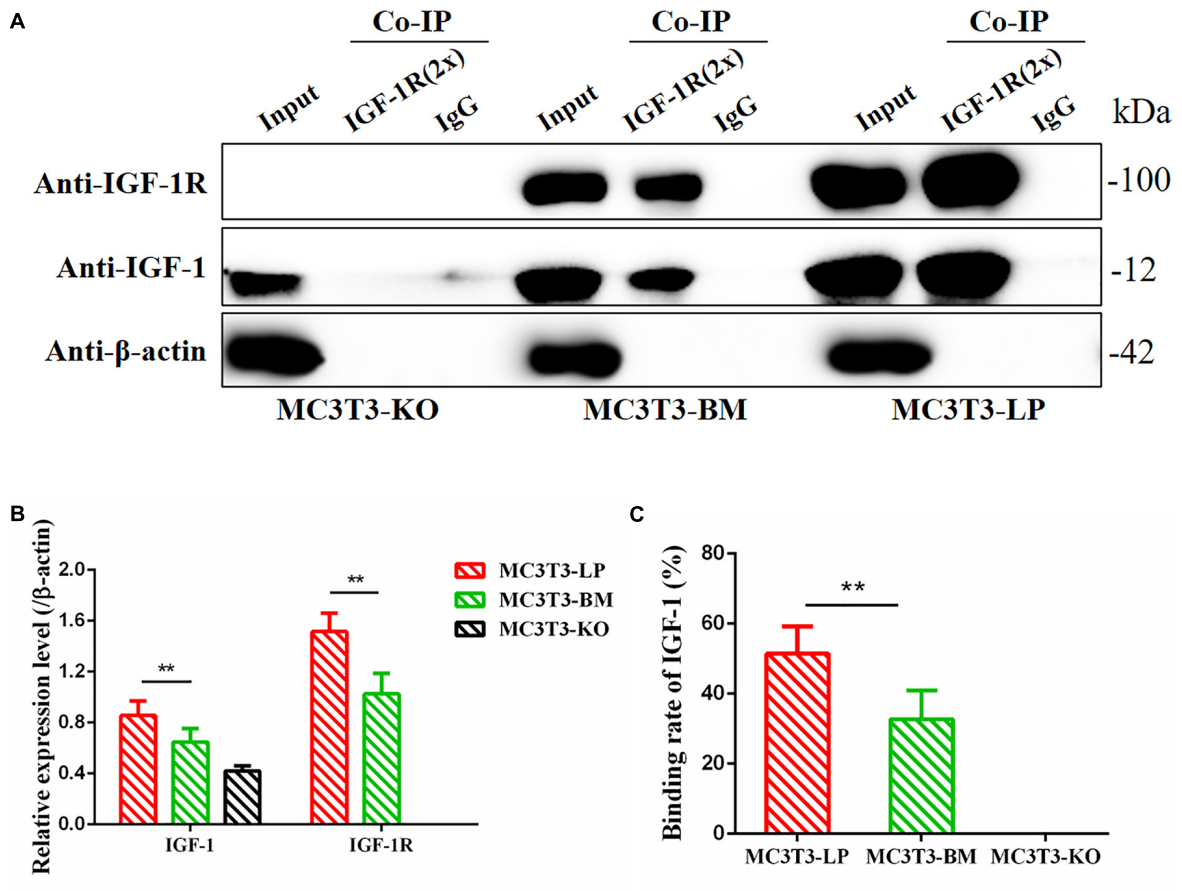


**FIGURE 10 |** Binding affinity analysis of the IGF-1 with IGF-1R in MC3T3-KO, MC3T3-BM and MC3T3-LP cells **(A)** MC3T3-KO cells (the KO group), MC3T3-BM cells (GTCT haplotype of BM group) and MC3T3-LP cells (CGTC haplotype of LP group) were lysed, IGF-1R was immunoprecipitated and IgG served as a negative control, IGF-1 and IGF-1R were then examined by western blot. **(B)** Quantification of IGF-1 and IGF-1R levels in the immunoprecipitated complex. **(C)** Quantification of the related binding rate with IGF-1 (**$P < 0.01$).

We first investigated the effects of two *Igf1r* haplotypes formed by four linkage synonymous mutations on gene expression. The results were consistent with our expectations, indicating that the expression levels in the BM group were lower than those in the LP group at both the transcription and translation levels. We observed different effects of the two *Igf1r* haplotypes on promoting cell proliferation. The KO group had the lowest proliferation capacity, thus indirectly indicating that IGF-1R plays an important role in cell proliferation. Furthermore, the LP group had a better effect on promoting cell proliferation than the BM group. These results suggested that the preferred codons in large pigs are more conducive to cell proliferation and survival. Moreover, the four synonymous mutations of porcine *Igf1r* ECD may contribute to the formation of body size in animals.

We also found that IGF-1R is involved in the regulation of osteoblast differentiation and mineralization. Among the indicators of cell differentiation, ALP activity is considered one of the most essential factors affecting osteoblast differentiation (Whyte, 1994). ALP generates calcium phosphate to be deposited in mature osteoblasts and contributes to bone mineralization (Orimo and Shimada, 2008; Hosseini et al., 2019). Aside from ALP activity, the expression levels of genes related to osteogenic differentiation (*Col-1*, *Alp*, *Opn*, *Ocn*, *Rux2*, and *Osx*) were also found to be important factors for evaluating cell differentiation. *Col-1* and *Alp* induce the formation of the primary extracellular matrix (ECM) at the early stage of differentiation (Hosseini et al., 2019). The early differentiation of pre-osteoblasts is regulated by *Runx2* (Ducy et al., 1997). *Runx2* and *Osx* play a regulative role in regulating osteoblast differentiation and bone formation in growing bones (Baek et al., 2009). *Ocn* is a marker at the late stage of osteoblast differentiation (Hosseini et al., 2019). *Opn* is a highly phosphorylated glycoprotein secreted during osteoblast differentiation and differentiation, the expression level of which gradually increases from days 7 to 21 (Letzring et al., 2010; Wei et al., 2020). Hence, *Opn* can be used as an indicator of the intermediate and late stages of differentiation. These genes play an essential role in regulating osteoblast differentiation and bone formation in growing bones. A previous study reported that the expression of *Col-1* increases at the early stage and then decreases at the later stage of differentiation (Hosseini et al., 2019; Wei et al., 2020). The expression level of *Opn* continues to increase on the 7th day of differentiation (Wei et al., 2020).

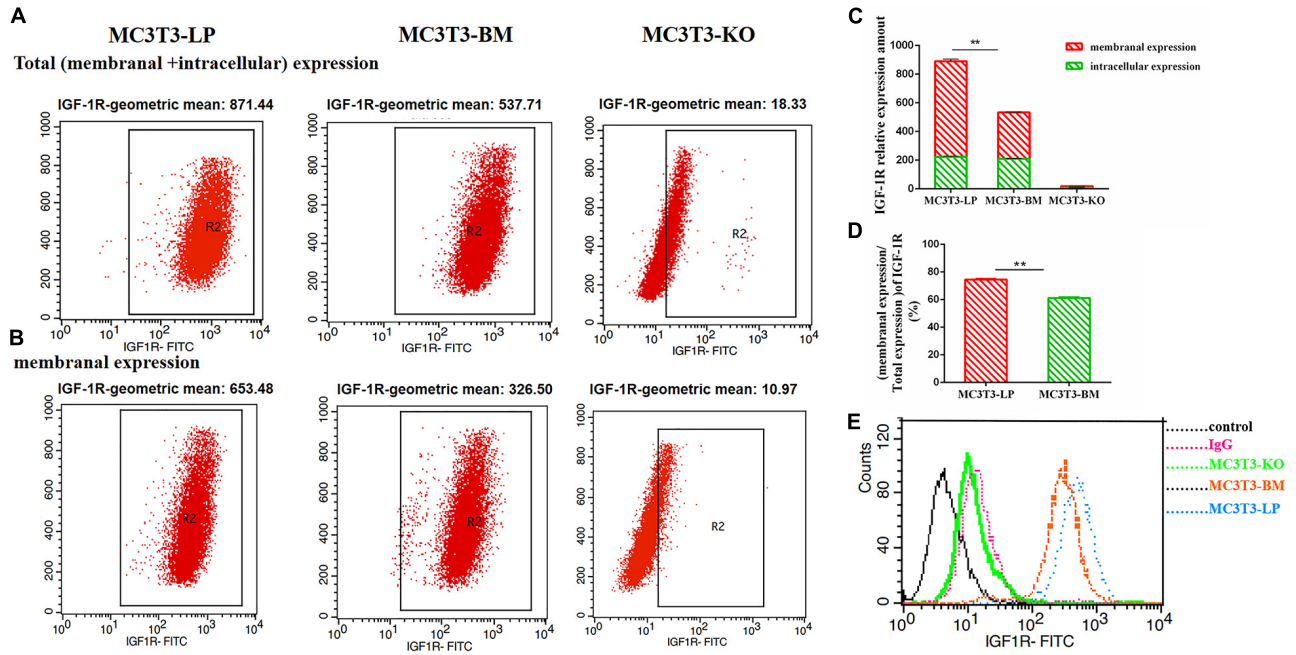


**FIGURE 11 |** The effect of two haplotypes of *Igf1r* on membrane bound expression and conformation of IGF-1R. **(A,B)** Flow cytometry of IGF-1R membrane bound expression with anti-FLAG antibody in MC3T3-LP, MC3T3-BM and MC3T3-KO cells. **(C)** Quantification of IGF-1R membranal expression and intracellular expression levels in MC3T3-LP, MC3T3-BM and MC3T3-KO cells. **(D)** Quantification of the related membranal expression rate in MC3T3-LP, MC3T3-BM cells (**$P < 0.01$). **(E)** Flow cytometry assay to detect the conformation of IGF-1R of MC3T3-BM cells (GTCT haplotype of BM group, yellow line), MC3T3-LP cells (CGTC haplotype of LP group, blue line) and MC3T3-KO cells (green line).

On the basis of these reports, we selected *Col-1* and *Opn* as the indicators of early and late differentiation stages, respectively, for follow-up studies.

The ALP activity of the LP and BM groups was substantially higher than that of the KO. The BM group promoted the early stage of osteogenic differentiation, whereas the LP group promoted the late stage of osteogenic differentiation. This observation was further confirmed by the detection of the expression levels of genes related to osteogenic differentiation. Matrix mineralization is the final step in osteoblast differentiation. It marks osteogenic maturation ability and plays a crucial role in regulating bone size (i.e., bone mass and volume). AR stains are widely used to detect mineral deposition (Puchtler et al., 1969). In this study, the number of mineralized nodules was substantially greater in the LP and BMs than in the KO group. Moreover, the nodules in the BM group decreased compared with in the LP group. This trend was consistent with ALP activity. Similar to the findings of previous studies, the present results confirmed that IGF-1R regulates osteoblast differentiation and mineralization. Furthermore, codon preference plays a role in regulating gene functions to a certain extent.

Like most receptors, IGF-1R is involved in or cross-talk with various signal pathways (Larsson et al., 2005; Tandon et al., 2016). Autophagy is a phenomenon that cannot be ignored during cell differentiation. It is regulated by multiple cellular pathways. Stimulation of autophagy is necessary for early osteoblast differentiation, which requires biphasic regulation of AMPK. IGF-1R signaling stimulates AMPK activation, thereby resulting in autophagy activation at the early stage of differentiation (Xi et al., 2016). Alternatively, AKT activation stimulates AMPK S485 phosphorylation (Sarbassov et al., 2005), thus leading to the suppression of AMPK activation (reduction of T172 phosphorylation) and the termination of autophagy between days 9 and 15 (Xi et al., 2016). Therefore, we detected the related downstream signaling pathways of IGF-1R via Western blot. In contrast to the LP group, the BM group first upregulated the phosphorylation of AMPK and the expression of autophagosome components at the early stage of osteoblast differentiation. Thereafter, the LP group remained suppressed at the late stage of differentiation. These results suggested that the two haplotypes of IGF-1R may affect their differentiation patterns by changing the phosphorylation levels of downstream pathways during the period of AMPK induction. We further indicated that the haplotype of the BM group can promote early stage differentiation and delay the late stage differentiation. Furthermore, the haplotype of the BM group inhibits the expression of bone-related genes (*Rux2*, *Alp*, *Ocn*, *Opn*, and *Osx*) and decreases ALP activity and calcium deposition. Prior studies confirmed the positive selection of early maturation in the development of Bama Xiang pigs. Functional enrichment analysis indicated that autophagy regulation is one of the most important biological processes (Yang et al., 2018). From day 0 to day 160, the growth curve of miniature pigs is approximately linear. By contrast, normal, fattening pigs have low average daily gain during the early growth stage, and it gradually increases

after day 50 (Kohn et al., 2007). The results of previous studies were consistent with our findings that osteoblast differentiation in miniature pigs is more active during the early stage of growth and development than during the other growth stages. Therefore, we speculated that the polymorphisms of IGF-1R play a specific role in regulating the unique growth characteristics of miniature pigs. Further research is warranted to verify this hypothesis.

mRNA and protein stabilities can be affected by a synonymous codon change (Pedersen, 1984; Letzring et al., 2010). Chaney et al. demonstrated that the temporal coordination of co-translational folding is an additional mechanism of synonymous mutation in regulating translation dynamics (Chaney and Clark, 2015). Moreover, stable mRNA structures can lead to translational pauses (Tu et al., 1992). Thus, the issue of whether the difference in functions between two haplotypes is due to stability changes remains uncertain. In this study, a significant difference was predicted between the mRNA secondary structures of the two different sequences of IGF-1R ECD. When the GTCT haplotype of the BM group changed to the CGTC haplotype of the LP group, the minimum free energy increased by 6.8 kcal. In addition, the mRNA stability of IGF-1R with the BM haplotype was higher than that of the LP haplotype, which was consisted with the prediction result of mRNA secondary structures and the minimum free energy for two haplotypes. A number of studies have shown that protein synthesis is affected by many factors, such as mRNA expression level, mRNA secondary structure, mRNA stability and so on (Mitsuo, 1999; Tsai et al., 2008; Hunt et al., 2014). Our results showed that the protein level of BM group was lower than that of LP group.

On the one hand, the mRNA expression level and mRNA stability of BM group were higher and the mRNA secondary structure was more stable than that of the LP group, which may affect the initiation of IGF-1R protein translation and protein synthesis. Meanwhile, there is a strong heterogeneity between different haplotypes caused by synonymous mutations. For example, in the synonymous mutations found by Cheng et al. (2018) the group with high mRNA stability and protein stability may have a low expression level. But Capon et al. (2004) described that synonymous mutations with high mRNA stability showed high protein expression. On the other hand, IGF-1R proteins in LP group have low stability, and the half-life is shorter than that in BM group. However, this possible effect is not enough to offset the higher IGF1R synthesis in LP group based on our detection results. In addition, the process of protein synthesis is also affected by other factors and these influence needs to be further studied.

On the basis of the four synonymous mutations of IGF-1R ECD near the location of the IGF-1 binding domain, we speculated that the two haplotypes may have different binding affinities with IGF-1. The Co-IP experiment proved our conjecture that the relative binding rate of IGF-1 and IGF-1R significantly changed between the LP and BM groups. Moreover, the mechanisms underlying the relative difference in binding rates must be discussed. We considered that the number of receptors on the cell membrane surface changed. Previous studies found that the mutations in the extracellular domain of receptors can change their expression on the cell membrane surface (Ip et al., 2018). This change may be the reason for the difference in the ligand-binding rates of the different haplotypes of *Igf1r*. We detected a significant difference in the relative membranal expression rates of the two haplotypes *Igf1r*. We speculated further that the subtle changes in protein conformation of IGF-1R may affect transport, thereby decreasing the expression of receptors on the cell membrane. Numerous studies reported that genetic mutations can affect the changes in protein conformation. Atomic-level techniques, such as nuclear magnetic resonance or X-ray crystallography, can detect protein conformations. However, a study utilizing such techniques for detecting synonymous mutations has not been conducted yet. Subtle differences in protein conformations can also be inferred via differential immunodetection (Hunt et al., 2014). Proteins of different conformations have different binding efficiencies with a specific conformational sensitivity antibody. Thus, detecting conformation differences of proteins caused by synonymous mutations is a feasible method. In this study, conformation detection revealed that the synonymous mutation of IGF-1R changed the receptor's binding affinity with the IGF-1R antibody. We speculated that it might be the synonymous mutation that affected the conformation of IGF-1R protein. The difference in conformations of the two haplotypes of *Igf1r* confirmed our prediction. We considered the difference as one of the reasons for the observed difference in binding capacity with IGF-1. These differences directly change the binding rates of IGF-1R and IGF-1. Moreover, these differences affect the transduction of intracellular signaling pathways and the differentiation of osteoblasts.

Owing to the extensive mechanisms of synonymous mutations and their random degrees of influence, several uncertainties and contingencies in the study of synonymous mutations remain. Therefore, the effects of synonymous mutations on the functions of specific genes must be explored. On the basis of the theory of codon preference, we observed that large pigs preferred to use common codons, whereas small pigs preferred rare codons. In combination with these results and the findings of previous studies, rare codons may lead to extreme translational pauses, provoke protein co-translation folding mechanisms, and change protein conformations and binding capacity (Tsai et al., 2008; Nissley et al., 2016). Synthesis of the receptor caused by synonymous mutations in the human dopamine receptor D2 (*Drd2*) alters mRNA stability (Duan et al., 2003). In turn, this alteration may affect the continuity of translation and even cause translational pause (Mitsuo, 1999). Synonymous mutations and ribosome stalling may lead to altered folding pathways. Although the conformational and functional differences between native and alternative states may be minor, subtle differences in conformations caused by synonymous mutations in *Mdr1* (*P*-glycoprotein) alter the structure of the substrate and inhibitor interaction sites (Tsai et al., 2008; Fung et al., 2014). Thus, even slight differences caused by synonymous mutations may affect physiological functions. In this study, we found that the difference in binding affinity with IGF-1 caused by the four *Igf1r* synonymous mutations. Another study showed that a

synonymous mutation of its ligand IGF-1 has similar effects (Cheng et al., 2018), suggesting that these findings are not isolated cases. Meanwhile, the codon preference differences between the large and miniature pigs we observed suggested that codon usage may be a factor regulating body size. Further studies are warranted to prove or falsify this hypothesis.

## CONCLUSION

We detected two haplotypes formed by four synonymous mutations in IGF-1R ECD from pigs with different body size traits. These haplotypes may affect *Igf1r* transcription and translation, IGF-1R protein conformation, and IGF-1 interactions, resulting in differences in osteoblast differentiation and mineralization. Furthermore, the linkage effects of these synonymous mutations may be involved in the formation of body size in miniature pigs. We explored the functions of potentially valuable synonymous mutations. Our results provide a theoretical basis for the formation of body size in miniature pigs.

## DATA AVAILABILITY STATEMENT

The original contributions presented in the study are included in the article/supplementary material, further inquiries can be directed to the corresponding author.

## AUTHOR CONTRIBUTIONS

LH, CW, and SW conceived and designed the experiments. CW and SW performed the experiments. LH, CW, SW, SL, YC, HG, RY, TF, GL, XS, and JS assessed the experiments and provided the data analysis. CW and SW wrote the manuscript. All the authors read and approved the manuscript.

## FUNDING

This work was supported by the National Natural Science Foundation of China (31772699 and 31672514) and the Natural Science Foundation of Jilin Province (20200201119JC).

## REFERENCES

Adams, T. E., Epa, V. C., Garrett, T. P., and Ward, C. W. (2000). Structure and function of the type 1 insulin-like growth factor receptor. *Cell Mol. Life. Sci.* 57, 1050–1093. doi: 10.1007/PL00000744

Bae, S. J., Kim, H. J., Won, H. Y., Min, Y. K., and Hwang, E. S. (2017). Acceleration of osteoblast differentiation by a novel osteogenic compound, DMP-PYT, through activation of both the BMP and Wnt pathways. *Sci. Rep.* 7:8455. doi: 10.1038/s41598-017-08190-9

Baek, W. Y., Lee, M. A., Jung, J. W., Kim, S. Y., Akiyama, H., de Crombrugghe, B., et al. (2009). Positive regulation of adult bone formation by osteoblast-specific transcription factor osterix. *J. Bone Miner. Res.* 24, 1055–1065. doi: 10.1359/jbmr.081248

Baker, J., Liu, J. P., Robertson, E. J., and Efstratiadis, A. (1993). Role of insulin-like growth factors in embryonic and postnatal growth. *Cell* 75, 73–82. doi: 10.1016/s0092-8674(05)80085-6

Bancroft, G. N., Sikavitsas, V. I., van den Dolder, J., Sheffield, T. L., Ambrose, C. G., Jansen, J. A., et al. (2002). Fluid flow increases mineralized matrix deposition in 3D perfusion culture of marrow stromal osteoblasts in a dose-dependent manner. *Proc. Natl. Acad. Sci. U.S.A.* 99, 12600–12605. doi: 10.1073/pnas.202296599

Baxter, R. C. (2015). How IGF-1 activates its receptor. *J. Cell. Commun. Signal.* 9:87. doi: 10.1007/s12079-015-0276-8

Bin, X., Lin, C., Huang, X., Zhou, Q., Wang, L., and Xian, C. J. (2017). FGF-2 gene polymorphism in osteoporosis among Guangxi's Zhuang Chinese. *Int. J. Mol. Sci.* 18:E1358. doi: 10.3390/ijms18071358

Birnbaum, R. S., Bowsher, R. R., and Wiren, K. M. (1995). Changes in IGF-I and -II expression and secretion during the proliferation and differentiation of normal rat osteoblasts. *J. Endocrinol.* 144, 251–259. doi: 10.1677/joe.0.1440251

Canalis, E. (1993). Insulin like growth factors and the local regulation of bone formation. *Bone* 14, 273–276. doi: 10.1016/8756-3282(93)90151-y

Cao, C., Zhang, Y., Jia, Q., Wang, X., Zheng, Q., Zhang, H., et al. (2019). An exonic splicing enhancer mutation in DUOX2 causes aberrant alternative splicing and severe congenital hypothyroidism in Bama pigs. *Dis. Model. Mech.* 12:dmm036616. doi: 10.1242/dmm.036616

Capon, F., Allen, M. H., Ameen, M., Burden, A. D., Tillman, D., Barker, J. N., et al. (2004). A synonymous SNP of the corneodesmosin gene leads to increased mRNA stability and demonstrates association with psoriasis across diverse ethnic groups. *Hum. Mol. Genet.* 13, 2361–2368. doi: 10.1093/hmg/ddh273

Chai, X., Zhang, W., Chang, B., Feng, X., Song, J., Li, L., et al. (2019). GPR39 agonist TC-G 1008 promotes osteoblast differentiation and mineralization in MC3T3-E1 cells. *Artif. Cells Nanomed. Biotechnol.* 47, 3569–3576. doi: 10.1080/21691401.2019.1649270

Chaney, J. L., and Clark, P. L. (2015). Roles for synonymous codon usage in protein biogenesis. *Annu. Rev. Biophys.* 44, 143–166. doi: 10.1146/annurev-biophys-060414-034333

Changhong, L., Mingguo, Z., Weiyi, H., Wenzhen, W., Rui, Y., and Linlin, H. (2018). Study on amplification of IGF1R gene and SNPs screening in different pig breeds. *J. Jilin Agric. Univ.* 40, 734–739. doi: 10.13327/j.jjlau.2018.4639

Cheng, Y., Chen, T., Song, J., Qi, Q., Wang, C., Xi, Q., et al. (2020). miR-709 inhibits GHRP6 induced GH synthesis by targeting PRKCA in pituitary. *Mol. Cell. Endocrinol.* 506:110763. doi: 10.1016/j.mce.2020.110763

Cheng, Y., Liu, S., Wang, G., Wei, W., Huang, S., Yang, R., et al. (2018). Porcine IGF1 synonymous mutation alter gene expression and protein binding affinity with IGF1R. *Int. J. Biol. Macromol.* 116, 23–30. doi: 10.1016/j.ijbiomac.2018.05.022

Cheng, Y., Liu, S., Zhang, X., Wu, Q., Li, S., Fu, H., et al. (2016). Expression profiles of IGF-1R gene and polymorphisms of its regulatory regions in different pig breeds. *Protein J.* 35, 231–236. doi: 10.1007/s10930-016-9666-x

Curran, J. F., and Yarus, M. (1989). Rates of aminoacyl-tRNA selection at 29 sense codons in vivo. *J. Mol. Biol.* 209, 65–77. doi: 10.1016/0022-2836(89)90170-8

Ding, S., Wu, X., Li, G., Han, M., Zhuang, Y., and Xu, T. (2005). Efficient transposition of the piggyBac (PB) transposon in mammalian cells and mice. *Cell* 122, 473–483. doi: 10.1016/j.cell.2005.07.013

Duan, J., Wainwright, M. S., Comeron, J. M., Naruya, S., Sanders, A. R., Joel, G., et al. (2003). Synonymous mutations in the human dopamine receptor D2 (DRD2) affect mRNA stability and synthesis of the receptor. *Hum. Mol. Genet.* 12, 205–216. doi: 10.1093/hmg/ddg055

Ducy, P., Rui, Z., Geoffroy, V., Ridall, A. L., and Karsenty, G. (1997). Osf2/Cbfa1: a transcriptional activator of osteoblast differentiation. *Cell* 89, 747–754. doi: 10.1016/s0092-8674(00)80257-3

Efstratiadis, A. (1998). Genetics of mouse growth. *Int. J. Dev. Biol.* 42, 955–976.

Fang, Y., Xue, Z., Zhao, L., Yang, X., Yang, Y., Zhou, X., et al. (2019). Calycosin stimulates the osteogenic differentiation of rat calvarial osteoblasts by activating the IGF1R/PI3K/Akt signaling pathway. *Cell Biol. Int.* 43, 323–332. doi: 10.1002/cbin.11102

Fung, K. L., Pan, J., Ohnuma, S., Lund, P. E., Pixley, J. N., Kimchi-Sarfaty, C., et al. (2014). MDR1 synonymous polymorphisms alter transporter specificity and protein stability in a stable epithelial monolayer. *Cancer Res.* 74, 598–608. doi: 10.1158/0008-5472.CAN-13-2064

Gaffney-Stomberg, E., Lutz, L. J., Shcherbina, A., Ricke, D. O., Petrovick, M., Cropper, T. L., et al. (2017). Association between single gene polymorphisms

and bone biomarkers and response to calcium and vitamin D supplementation in young adults undergoing military training. *J. Bone. Miner. Res.* 32, 498–507. doi: 10.1002/jbmr.3008

Golub, E. E., Harrison, G., Taylor, A. G., Camper, S., and Shapiro, I. M. (1992). The role of alkaline phosphatase in cartilage mineralization. *Bone Miner.* 17, 273–278. doi: 10.1016/0169-6009(92)90750-8

Grabundzija, I., Irgang, M., Mátés, L., Belay, E., Matrai, J., Gogol-DRing, A., et al. (2010). Comparative analysis of transposable element vector systems in human cells. *Mol. Ther. J. Am. Soc. Gene Ther.* 18, 1200–1209. doi: 10.1038/mt.2010.47

Harmel, E. M., Binder, G., Barnikol-Oettler, A., Caliebe, J., Kiess, W., Losekoot, M., et al. (2013). Alu-mediated recombination defect in IGF1R: haploinsufficiency in a patient with short stature. *Horm. Res. Paediatr.* 80, 431–442. doi: 10.1159/000355410

Horvath, P., Balla, B., Kosa, J. P., Tobias, B., Szili, B., Kirschner, G., et al. (2016). Strong effect of SNP rs4988300 of the LRP5 gene on bone phenotype of Caucasian postmenopausal women. *J. Bone Miner. Metab.* 34, 79–85. doi: 10.1007/s00774-014-0645-z

Hosseini, S., Naderi-Manesh, H., Vali, H., Baghaban Eslaminejad, M., Azam Sayahpour, F., Sheibani, S., et al. (2019). Contribution of osteocalcin-mimetic peptide enhances osteogenic activity and extracellular matrix mineralization of human osteoblast-like cells. *Coll. Surf. B Biointerfaces* 173, 662–671. doi: 10.1016/j.colsurfb.2018.10.035

Hunt, R. C., Simhadri, V. L., Iandoli, M., Sauna, Z. E., and Kimchi-Sarfaty, C. (2014). Exposing synonymous mutations. *Trends Genet.* 30, 308–321. doi: 10.1016/j.tig.2014.04.006

Ip, C. K. M., Ng, P. K. S., Jeong, K. J., Shao, S. H., Ju, Z., Leonard, P. G., et al. (2018). Neomorphic PDGFRA extracellular domain driver mutations are resistant to PDGFRA targeted therapies. *Nat. Commun.* 9:4583. doi: 10.1038/s41467-018-06949-w

Jansson, M., Hallen, D., Koho, H., Andersson, G., Berghard, L., Heidrich, J., et al. (1997). Characterization of ligand binding of a soluble human insulin-like growth factor I receptor variant suggests a ligand-induced conformational change. *J. Biol. Chem.* 272, 8189–8197. doi: 10.1074/jbc.272.13.8189

Jiang, H. T., Ran, C. C., Liao, Y. P., Zhu, J. H., Wang, H., Deng, R., et al. (2019). IGF-1 reverses the osteogenic inhibitory effect of dexamethasone on BMP9-induced osteogenic differentiation in mouse embryonic fi broblasts via PI3K/AKT/COX-2 pathway. *J. Steroid Biochem. Mol. Biol.* 191:105363. doi: 10.1016/j.jsbmb.2019.04.012

Joshi, M. U., Pittman, H. K., Haisch, C. E., and Verbanac, K. M. (2008). Real-time PCR to determine transgene copy number and to quantitate the biolocalization of adoptively transferred cells from EGFP-transgenic mice. *Biotechniques* 45, 247–258. doi: 10.2144/000112913

Joung, Y. H., Lim, E. J., Darvin, P., Jang, J. W., Park, K. D., Lee, H. K., et al. (2013). Hwanggeumchal sorghum extract enhances BMP7 and GH signaling through the activation of Jak2/STAT5B in MC3T3E1 osteoblastic cells. *Mol. Med. Rep.* 8, 891–896. doi: 10.3892/mmr.2013.1593

Kohn, F., Sharifi, A. R., and Simianer, H. (2007). Modeling the growth of the Goettingen minipig. *J. Anim. Sci.* 85, 84–92. doi: 10.2527/jas.2006-271

Larsson, O., Girnita, A., and Girnita, L. (2005). Role of insulin-like growth factor 1 receptor signalling in cancer. *Br. J. Cancer* 92, 2097–2101. doi: 10.1038/sj.bjc.6602627

LeRoith, D., Werner, H., Beitner-Johnson, D., and Roberts, C. T. Jr. (1995). Molecular and cellular aspects of the insulin-like growth factor I receptor. *Endocr. Rev.* 16, 143–163. doi: 10.1210/edrv-16-2-143

Letzring, D. P., Dean, K. M., and Grayhack, E. J. (2010). Control of translation efficiency in yeast by codon-anticodon interactions. *RNA* 16, 2516–2528. doi: 10.1261/rna.2411710

Liu, H. B., Lv, P. R., He, R. G., Yang, X. G., Qin, X. E., Pan, T. B., et al. (2010). Cloned Guangxi Bama minipig (*Sus scrofa*) and its offspring have normal reproductive performance. *Cell Reprogram* 12, 543–550. doi: 10.1089/cell.2009.0094

Liu, T. C., Hsieh, M. J., Liu, M. C., Chiang, W. L., Tsao, T. C., and Yang, S. F. (2016). The clinical significance of the insulin-like growth factor-1 receptor polymorphism in non-small-cell lung cancer with epidermal growth factor receptor mutation. *Int. J. Mol. Sci.* 17:763. doi: 10.3390/ijms17050763

Mitsuo, Z. (1999). Correlation between mRNA structure of the coding region and translational pauses. *Nucleic Acids Symp.* 42, 81–82. doi: 10.1093/nass/42.1.81

Nieves, J. W., Formica, C., Ruffing, J., Zion, M., Garrett, P., Lindsay, R., et al. (2005). Males have larger skeletal size and bone mass than females, despite comparable body size. *J. Bone Miner. Res.* 20, 529–535. doi: 10.1359/JBMR.041005

Nissley, D. A., Sharma, A. K., Ahmed, N., Friedrich, U. A., Kramer, G., Bukau, B., et al. (2016). Accurate prediction of cellular co-translational folding indicates proteins can switch from post- to co-translational folding. *Nat. Commun.* 7:10341. doi: 10.1038/ncomms10341

Orimo, H., and Shimada, T. (2008). The role of tissue-nonspecific alkaline phosphatase in the phosphate-induced activation of alkaline phosphatase and mineralization in SaOS-2 human osteoblast-like cells. *Mol. Cell. Biochem.* 315, 51–60. doi: 10.1007/s11010-008-9788-3

Pantovic, A., Krstic, A., Janjetovic, K., Kocic, J., Harhaji-Trajkovic, L., Bugarski, D., et al. (2013). Coordinated time-dependent modulation of AMPK/Akt/mTOR signaling and autophagy controls osteogenic differentiation of human mesenchymal stem cells. *Bone* 52, 524–531. doi: 10.1016/j.bone.2012.10.024

Pedersen, S. (1984). *Escherichia coli* ribosomes translate in vivo with variable rate. *EMBO J.* 3, 2895–2898. doi: 10.1002/j.1460-2075.1984.tb02227.x

Plotkin, J. B., and Kudla, G. (2011). Synonymous but not the same: the causes and consequences of codon bias. *Nat. Rev. Genet.* 12, 32–42. doi: 10.1038/nrg2899

Prather, R. S., Lorson, M., Ross, J. W., Whyte, J. J., and Walters, E. (2013). Genetically engineered pig models for human diseases. *Annu. Rev. Anim. Biosci.* 1, 203–219. doi: 10.1146/annurev-animal-031412-103715

Puchtler, H., Meloan, S. N., and Terry, M. S. (1969). On the history and mechanism of alizarin and alizarin red S stains for calcium. *J. Histochem. Cytochem.* 17, 110–124. doi: 10.1177/17.2.110

Rezgui, D., Williams, C., Savage, S. A., Prince, S. N., Zaccheo, O. J., Jones, E. Y., et al. (2009). Structure and function of the human Gly1619Arg polymorphism of M6P/IGF2R domain 11 implicated in IGF2 dependent growth. *J. Mol. Endocrinol.* 42, 341–356. doi: 10.1677/JME-08-0154

Ruff, C. (2003). Growth in bone strength, body size, and muscle size in a juvenile longitudinal sample. *Bone* 33, 317–329. doi: 10.1016/s8756-3282(03)00161-3

Sarbassov, D. D., Guertin, D. A., Ali, S. M., and Sabatini, D. M. (2005). Phosphorylation and regulation of Akt/PKB by the rictor-mTOR complex. *Science* 307, 1098–1101. doi: 10.1126/science.1106148

Sauna, Z. E., Okunji, C., Hunt, R. C., Gupta, T., Allen, C. E., Plum, E., et al. (2009). Characterization of conformation-sensitive antibodies to ADAMTS13, the von Willebrand cleavage protease. *PLoS One* 4:e6506. doi: 10.1371/journal.pone.0006506

Schlecht, S. H., Bigelow, E. M., and Jepsen, K. J. (2015). How does bone strength compare across sex, site, and ethnicity? *Clin. Orthop. Relat. Res.* 473, 2540–2547. doi: 10.1007/s11999-015-4229-6

Siddle, K. (2011). Signalling by insulin and IGF receptors: supporting acts and new players. *J. Mol. Endocrinol.* 47, R1–R10. doi: 10.1530/JME-11-0022

Smit, M. H. D., and Duin, J. V. (1990). Secondary structure of the ribosome binding site determines translational efficiency: a quantitative analysis. *Proc. Natl. Acad. Sci. U.S.A.* 87, 7668–7672. doi: 10.1073/pnas.87.19.7668

Srensen, M., and Pedersen, S. (1991). Absolute in vivo translation rates of individual codons in *Escherichia coli*. The two glutamic acid codons GAA and GAG are translated with a threefold difference in rate. *J. Mol. Biol.* 222, 265–280. doi: 10.1016/0022-2836(91)90211-n

Szewczuk, M., Zych, S., Wojcik, J., and Czerniawska-Piatkowska, E. (2013). Association of two SNPs in the coding region of the insulin-like growth factor 1 receptor (IGF1R) gene with growth-related traits in Angus cattle. *J. Appl. Genet.* 54, 305–308. doi: 10.1007/s13353-013-0155-z

Tandon, M., Chen, Z., Othman, A. H., and Pratap, J. (2016). Role of Runx2 in IGF-1Rbeta/Akt- and AMPK/Erk-dependent growth, survival and sensitivity towards metformin in breast cancer bone metastasis. *Oncogene* 35, 4730–4740. doi: 10.1038/onc.2015.518

Tsai, C. J., Sauna, Z. E., Kimchi-Sarfaty, C., Ambudkar, S. V., Gottesman, M. M., and Nussinov, R. (2008). Synonymous mutations and ribosome stalling can lead to altered folding pathways and distinct minima. *J. Mol. Biol.* 383, 281–291. doi: 10.1016/j.jmb.2008.08.012

Tu, C., Tzeng, T. H., and Bruenn, J. A. (1992). Ribosomal movement impeded at a pseudoknot required for frameshifting. *Proc. Natl. Acad. Sci. U.S.A.* 89, 8636–8640. doi: 10.1073/pnas.89.18.8636

Wallborn, T., Wuller, S., Klammt, J., Kruis, T., Kratzsch, J., Schmidt, G., et al. (2010). A heterozygous mutation of the insulin-like growth factor-I receptor causes retention of the nascent protein in the endoplasmic reticulum and results in intrauterine and postnatal growth retardation. *J. Clin. Endocrinol. Metab.* 95, 2316–2324. doi: 10.1210/jc.2009-2404

Wang, C., Liu, S., Wu, Q., Cheng, Y., Feng, T., Song, J., et al. (2020). Porcine IGF-1R synonymous mutations in the intracellular domain affect cell proliferation and alter kinase activity. *Int. J. Biol. Macromol.* 152, 147–153. doi: 10.1016/j.ijbiomac.2020.02.281

Wang, T., Wang, Y., Menendez, A., Fong, C., Babey, M., Tahimic, C. G., et al. (2015). Osteoblast-specific loss of IGF1R signaling results in impaired endochondral bone formation during fracture healing. *J. Bone. Miner. Res.* 30, 1572–1584. doi: 10.1002/jbmr.2510

Wang, X., Wei, R., Li, Q., Liu, H., Huang, B., Gao, J., et al. (2013). PK-15cells transfected with porcine CD163 by PiggyBac transposon system are susceptible to porcine reproductive and respiratory syndrome virus. *J. Virol. Methods* 193, 383–390. doi: 10.1016/j.jviromet.2013.06.035

Wei, W., Liu, S., Song, J., Feng, T., Yang, R., Cheng, Y., et al. (2020). MGF-19E peptide promoted proliferation, differentiation and mineralization of MC3T3-E1 cell and promoted bone defect healing. *Gene* 749:144703. doi: 10.1016/j.gene.2020.144703

Whitten, A. E., Smith, B. J., Menting, J. G., Mai, B. M., Mckern, N. M., Lovrecz, G. O., et al. (2009). Solution structure of ectodomains of the insulin receptor family: the ectodomain of the type 1 insulin-like growth factor receptor displays asymmetry of ligand binding accompanied by limited conformational change. *J. Mol. Biol.* 394, 878–892. doi: 10.1016/j.jmb.2009.10.011

Whyte, M. P. (1994). Hypophosphatasia and the role of alkaline phosphatase in skeletal mineralization. *Endocr. Rev.* 15, 439–461. doi: 10.1210/edrv-15-4-439

Xi, G., Rosen, C. J., and Clemmons, D. R. (2016). IGF-I and IGFBP-2 stimulate AMPK activation and autophagy, which are required for osteoblast differentiation. *Endocrinology* 157, 268–281. doi: 10.1210/en.2015-1690

Yang, Y., Adeola, A. C., Xie, H. B., and Zhang, Y. P. (2018). Genomic and transcriptomic analyses reveal selection of genes for puberty in Bama Xiang pigs. *Zool. Res.* 39, 424–430. doi: 10.24272/j.issn.2095-8137.2018.068

Zafra, M. P., Schatoff, E. M., Katti, A., Foronda, M., Breinig, M., Schweitzer, A. Y., et al. (2018). Optimized base editors enable efficient editing in cells, organoids and mice. *Nat. Biotechnol.* 36, 888–893. doi: 10.1038/nbt.4194

Zhao, G., Monier-Faugere, M. C., Langub, M. C., Geng, Z., Nakayama, T., Pike, J. W., et al. (2000). Targeted overexpression of insulin-like growth factor I to osteoblasts of transgenic mice: increased trabecular bone volume without increased osteoblast proliferation. *Endocrinology* 141, 2674–2682. doi: 10.1210/endo.141.7.7585

Zheng, X., Dai, J., Zhang, H., and Ge, Z. (2018). MicroRNA-221 promotes cell proliferation, migration, and differentiation by regulation of ZFPM2 in osteoblasts. *Braz. J. Med. Biol. Res.* 51:e7574. doi: 10.1590/1414-431X20187574

**Conflict of Interest:** The authors declare that the research was conducted in the absence of any commercial or financial relationships that could be construed as a potential conflict of interest.

frontiers in Cell and Developmental Biology

MINI REVIEW
published: 16 October 2020
doi: 10.3389/fcell.2020.586031

# The Bone Morphogenetic Protein Pathway: The Osteoclastic Perspective

*Franziska Lademann[1,2], Lorenz C. Hofbauer[1,2] and Martina Rauner[1,2]**

[1] Department of Medicine III, Technische Universität Dresden, Dresden, Germany, [2] Center for Healthy Aging, Technische Universität Dresden, Dresden, Germany

Bone health crucially relies on constant bone remodeling and bone regeneration, both tightly controlled processes requiring bone formation and bone resorption. Plenty of evidence identifies bone morphogenetic proteins (BMP) as major players in osteoblast differentiation and thus, bone formation. However, in recent past years, researchers also increasingly reported on the pivotal role of these multi-functional growth factors in osteoclast formation and activity. This review aims to summarize the current knowledge of BMP signaling within the osteoclast lineage, its role in bone resorption, and osteoblast–osteoclast coupling. Furthermore, subsequent clinical implications for recombinant BMP therapy will be discussed in view of recent preclinical and clinical studies.

**Keywords: bone morphogenetic proteins, osteoclasts, bone resorption, osteoblast-osteoclast coupling, bone fracture healing, recombinant BMP therapy**

OPEN ACCESS

***Edited by:***
*Ari Elson,*
*Weizmann Institute of Science, Israel*

***Reviewed by:***
*Eleni Douni,*
*Agricultural University of Athens, Greece*
*Kent Søe,*
*University of Southern Denmark, Denmark*

***Correspondence:**
*Martina Rauner*
*martina.rauner@ukdd.de*

***Specialty section:***
*This article was submitted to Cellular Biochemistry, a section of the journal Frontiers in Cell and Developmental Biology*

***Received:*** *22 July 2020*
***Accepted:*** *29 September 2020*
***Published:*** *16 October 2020*

***Citation:***
*Lademann F, Hofbauer LC and Rauner M (2020) The Bone Morphogenetic Protein Pathway: The Osteoclastic Perspective. Front. Cell Dev. Biol. 8:586031. doi: 10.3389/fcell.2020.586031*

## INTRODUCTION

Bone is a dynamic tissue that is maintained by continuous destruction and reformation. Within the bone remodeling cycle, osteoclasts, which derive from hematopoietic precursors, are responsible for removing old or destructed bone, while mesenchymal-derived osteoblasts synthesize and mineralize new bone matrix. The proper balance of osteoclasts and osteoblasts ensures intact bone microarchitecture, mass and function throughout life. Given that pathological osteoclast activation can lead to serious health conditions such as postmenopausal osteoporosis (Eastell et al., 2016), understanding the molecular mechanisms of osteoclast development and activity is indispensable. Latest research on the *in vivo* origin of osteoclasts identified embryonic erythro-myeloid progenitors, independent of the hematopoietic stem cell (HSC) lineage, as precursors of fetal osteoclasts crucially contributing to bone development during embryogenesis. In adult and aging mice, however, HSC-derived precursors are indispensable for postnatal osteoclast homeostasis and bone remodeling (Jacome-Galarza et al., 2019; Yahara et al., 2020). Essential cytokines involved in osteoclastogenesis are receptor activator of nuclear factor kappa-B ligand (RANKL) and macrophage colony-stimulating factor (M-CSF). M-CSF governs the survival and proliferation of osteoclast precursors by binding to its receptor c-Fms (Yoshida et al., 1990). For differentiation, RANKL is particularly important as it regulates osteoclast commitment and formation by either activating the receptor activator of nuclear factor κ B (RANK) or binding to its decoy receptor osteoprotegerin (OPG). The RANKL/RANK/OPG system controls downstream signaling such as nuclear factor κB (NF- κB), mitogen-activated protein kinase (MAPK), and c-Fos pathways as well as the master transcription factor nuclear factor of activated T-cells, cytoplasmic

1 (NFATc1) (Hofbauer et al., 2004; Takayanagi, 2007). During terminal differentiation, several osteoclast precursors fuse iteratively to become large-sized, multinuclear cells and must attach to the bone surface for bone resorption to begin (Jacome-Galarza et al., 2019). Integrins, especially integrin αvβ3, play important roles during attachment and act jointly with F-actin and actin binding proteins to form podosomes, the structural prerequisites for bone resorption. After the formation of a sealing zone, $H^+$ and $Cl^-$ as well as proteases such as cathepsin K are secreted into the resorption pit to dissolve the mineralized and organic structures of the underlying bone (Teitelbaum, 2000).

During this process, growth factors embedded in the bone matrix are released and help to recruit osteoblasts to the resorption area and stimulate their activity (Charles and Aliprantis, 2014). Among them, bone morphogenetic proteins (BMP) that belong to the transforming growth factor beta (TGFβ) superfamily are well-studied and vital signaling molecules controlling osteoblastogenesis and thus, bone formation. To date, 12 different BMP ligands have been identified in humans (Lowery and Rosen, 2018) and researchers accomplished to produce recombinant human BMPs (rhBMP) for research purposes, and later clinical use (Wang et al., 1990; Bessho et al., 1999). BMP signaling starts upon BMP ligand binding to a transmembranous, heterotetrameric receptor complex composed of type I BMP receptors (BMPR) (ACVR1/ALK2, BMPR1A/ALK3, BMPR1B/ALK6) and type II BMPR (BMPR2, ActR-2A, ActR-2B). Canonical BMP signaling comprises the SMAD-dependent pathway involving three types of SMADs: receptor-SMADs (R-SMADs) transducing signals, common-SMADs (Co-SMADs) supporting gene transcription activation and inhibitory-SMADs negatively regulating BMP signaling. Activated type I receptors phosphorylate R-SMADs 1, 5 and 8 enabling them to form a heterotrimeric complex with Co-SMAD4. In the nucleus, this complex acts as a transcription factor to induce the expression BMP target genes. SMAD-independent, non-canonical BMP signaling may involve MAPK, such as extracellular signal-regulated kinases (ERK) and P38, or the phosphoinositide 3-kinase (PI3K)/AKT pathway (Beederman et al., 2013; Wu et al., 2016).

## BMP SIGNALING IN OSTEOCLASTS: WHAT CELL STUDIES AND MOUSE MODELS TELL US

Despite the comprehensive knowledge about BMP signaling in osteoblasts, its role in osteoclast formation has long been underrated. Several studies report on the endogenous expression of several BMP ligands (BMP1, BMP2, BMP4, BMP6, BMP7), SMAD proteins (SMAD1/5, SMAD4), and BMP receptors (BMPR1A, BMPR1B, BMPR2) in osteoclasts or osteoclast-like cell lines (Anderson et al., 2000; Garimella et al., 2008; Jensen et al., 2010; Broege et al., 2013; Tasca et al., 2015, 2018).

BMP2 and BMP4, both ligands with high osteogenic potential, have also been shown to stimulate bone resorption of isolated rat osteoclasts in a dose-dependent manner (Kaneko et al., 2000). In line with this, BMP2 directly increased RANKL-mediated survival, proliferation and differentiation of murine osteoclast precursor cells (Itoh et al., 2001; Jensen et al., 2010). Interestingly, BMP2 distinctly induced canonical versus non-canonical signaling depending on the stage of osteoclast differentiation. P38 phosphorylation was increased by BMP2 only in pre-fusion osteoclasts while BMP2-mediated SMAD-activation occurred around fusion of osteoclast precursors (Broege et al., 2013). In a controversy study, RANKL and M-CSF mediated osteoclast differentiation of non-adherent human bone marrow mononuclear cells and resorption capacity were inhibited by the presence of rhBMP2 (Wan et al., 2006). BMP4 promoted osteoclast formation *in vitro* and BMP4 overexpression in osteoblasts (Col1a-Bmp4 transgenic mice) or liver (AAV8-BMP4 mice) led to elevated osteoclast numbers resulting in bone loss (Okamoto et al., 2006; Holien et al., 2018). In contrast to BMP2, BMP5 and BMP6 are less potent and enhanced osteoclast formation in a biphasic curve: at high doses (>300 mg/dl) BMP5 and BMP6 decreased and in lower doses (10–100 mg/dl) increased murine osteoclast formation (Wutzl et al., 2006). BMP7 was shown to prevent human cord blood CD14+ monocytes from differentiating into osteoclasts due to impaired persistence of important osteoclast transcription factors (Maurer et al., 2012). In contrast, a recent study demonstrated BMP7 enhanced RANKL-induced osteoclastogenesis of bone marrow derived precursors and elevated bone-resorbing activity of osteoclasts being as potent as BMP2 (Omi et al., 2019). BMP9 is able to stimulate osteoclast activity and survival through activated SMAD and ERK1/2 signaling of human cord blood monocytes-derived osteoclasts (Fong et al., 2013). All in all, the majority of studies suggest that BMP ligands increase osteoclast formation and activity while impeding osteoclast apoptosis (**Table 1**).

With regards to BMP receptors, mechanisms regulating their expression during osteoclast development remain elusive. However, studies analyzing transgenic mouse models and thereof derived osteoclasts or precursors have implicated distinct roles of type I and type II BMP receptors in osteoclast formation and bone resorption (**Table 2**). Recently, ACVR1-induced SMAD-dependent BMP signaling was shown to support RANKL-induced osteoclastogenesis by activating the osteoclast master regulator NFATc1 (Omi et al., 2019). Global *Bmpr1b* knockout resulted in a transient and gender-specific osteopenia in 8-week-old male *Bmpr1b* null mice, however, *in vivo* bone turnover analysis did not detect changes in either bone formation or bone resorption (Shi et al., 2016). In contrast, *in vitro Bmpr1b*-deficient osteoclast precursors showed enhanced differentiation and survival, but decreased resorption activity (Shi et al., 2016). Deletion of *Bmpr1a* in mature osteoclasts ($Bmpr1a^{fl/fl}$;Ctsk-Cre mice, 8-weeks-old, sex not specified) and myeloid, osteoclast precursor cells ($Bmpr1a^{fl/fl}$;LysM-Cre mice, 8- to 10-weeks-old, male) led to trabecular bone gain due to decreased bone resorption suggesting that BMPR1A positively regulates terminal osteoclast formation and activity (Okamoto et al., 2011; Li et al., 2017). At the cellular level, osteoclast formation was impaired with *Bmpr1a*-deficiency *in vitro* (Li et al., 2017). Pharmacological blockade of type I receptors in fusion-staged osteoclasts

**TABLE 1 |** Cell studies investigating the effects of BMP ligands on osteoclast physiology.

| Cell studies | | | |
|---|---|---|---|
| **Ligand** | **Species** | ***In vitro* osteoclast physiology** | **References** |
| BMP2 | Rat | ⇑ Resorptive activity | Kaneko et al., 2000 |
| | Mouse | ⇑ Survival, proliferation and differentiation | Itoh et al., 2001; Jensen et al., 2010 |
| | Mouse | ⇑ Induces canonical versus non-canonical signaling depending on the stage of osteoclast differentiation | Broege et al., 2013 |
| | Human | ⇓ Differentiation and resorptive activity | Wan et al., 2006 |
| BMP4 | Rat | ⇑ Resorptive activity | Kaneko et al., 2000 |
| | Mouse | ⇑ Osteoclast formation | Okamoto et al., 2006; Holien et al., 2018 |
| BMP5 | Mouse | Effect depends on concentration<br>⇑ Osteoclast formation with 10-100 mg/dl<br>⇓ Osteoclast formation with > 300 mg/dl | Wutzl et al., 2006 |
| BMP6 | Mouse | Effect depends on concentration<br>⇑ Osteoclast formation with 10–100 mg/dl<br>⇓ Osteoclast formation with > 300 mg/dl | Wutzl et al., 2006 |
| BMP7 | Human | ⇓ Differentiation | Maurer et al., 2012 |
| | Mouse | ⇑ Differentiation | Omi et al., 2019 |
| BMP9 | Human | ⇑ Resorptive activity and survival | Fong et al., 2013 |

using dorsomorphin inhibited intracellular SMAD-signaling and further osteoclast differentiation and thus, highlights the importance of canonical BMP signaling during the time of osteoclast fusion (Jensen et al., 2010; Broege et al., 2013). Conditional knockout of *BMPR2* in myeloid osteoclast precursors ($BMPRII^{fl/fl}$;LysM-Cre mice, 12-weeks-old, male) caused trabecular bone gain due to defective osteoclast formation and activity (Broege et al., 2013). Accordingly, bone marrow derived *Bmpr2*-deficient osteoclasts showed impaired differentiation and resorptive activity indicating that BMPR2 plays an important role in osteoclastogenesis (Broege et al., 2013). Thus, both type I and type II BMP receptors are vital for proper osteoclast formation and bone resorption (**Table 2**), however, only during bone remodeling but not early skeletal development as bone changes are only seen in 8 to 12-week-old mice as compared to younger cohorts. Downstream of receptors, *in vitro* genetic ablation of SMAD1/5 or SMAD4 in osteoclast precursors led to the formation of fewer and smaller multinucleated osteoclasts and to a reduction of resorption pits and resorbed areas (Tasca et al., 2015). Correspondingly, mice with a conditional *Smad1/5* knockout in osteoclast precursors ($Smad1^{fl/fl}$;$Smad5^{fl/fl}$;c-Fms-Cre mice, 12-week-old, male) showed mild bone gain due to reduced bone resorption and stimulated bone formation (Tasca et al., 2018). In contrast, *Smad4* deletion in mature osteoclasts ($Smad4^{fl/fl}$;Ctsk-Cre mice, 8-week-old, female) increased osteoclast formation and bone resorption leading to an osteopenic phenotype, however, caused by disrupted TGFβ signaling and independent of the BMP pathway (Morita et al., 2016). Several extracellular proteins tightly regulate BMP signaling by restricting local BMP availability and thus, may also act on the skeleton (Lowery and Rosen, 2018). Global deletion of BMP antagonist twisted gastrulation ($Twsg1^{-/-}$ mice, 12-week-old, female) in mice induced osteopenia with increased osteoclast formation and activity caused by activated SMAD1/5 signaling in osteoclasts (Sotillo Rodriguez et al., 2009). Vice versa, *Twsg1* overexpression inhibited osteoclastogenesis (Pham et al., 2011) with BMP ligand binding being an indispensable requirement (Huntley et al., 2015). Overexpression of noggin, a prominent BMP2 and BMP4 ligand scavenger, resulted in increased bone volume due to both reduced bone formation and resorption (Okamoto et al., 2006). Accordingly, noggin restricted BMP signaling in osteoclasts and thus, osteoclast formation *in vitro* (Okamoto et al., 2006; Abe et al., 2010), however, only when administered to osteoclast precursors until day 3 of differentiation (Jensen et al., 2010). In sum, activation of BMP signaling supports osteoclastogenesis and osteoclast activity, while BMP blockade through specific inhibitors restrains proper osteoclast formation (**Figure 1**).

## BMPs AS MEDIATORS BETWEEN BONE RESORPTION AND BONE FORMATION

Initially, BMPs were reported to augment osteoclast development and activity solely indirectly through actions of other skeletal cells (Kanatani et al., 1995). Earlier studies demonstrate enhanced RANKL expression by bone marrow stromal cells, chondrocytes, osteoblasts, and osteocytes after stimulation with BMP ligands (Hentunen et al., 1995; Usui et al., 2008; Tachi et al., 2010; Granholm et al., 2013). Further, BMP2 is able to downregulate *Opg* mRNA levels in osteoblasts (Hofbauer et al., 1998). Eventually, an increased RANKL/OPG ratio promotes osteoclastogenesis and osteoclast function (Hofbauer et al., 2004). According to this, the BMP antagonist noggin ameliorated osteoclast formation through its effects on stromal cell/osteoblast differentiation (Abe et al., 2010). Recently, we demonstrated reduced osteoclast numbers in mice treated over 4 weeks with ALK3-Fc, a recombinant fusion protein that specifically scavenges BMPR1A/ALK3-activating BMP ligands (Lademann et al., 2020). However, due to systemic drug application it is unclear whether osteoclasts are affected in a direct or indirect manner as ALK3-Fc is reported to enhance OPG and reduce RANKL levels in serum of treated mice as well as in SaOS2 cells (Baud'huin et al., 2012). In line with this, transgenic mouse models with deleted *Bmpr1a* in either osteoblasts ($Bmpr1a^{fl/fl}$;Col1-Cre) or osteocytes ($Bmpr1a^{fl/fl}$;Dmp1-Cre) show enhanced bone volume not only caused by increased bone formation but also mitigated bone resorption (Kamiya et al., 2008, 2016). These effects were mediated by a decreased RANKL/OPG ratio that negatively affected osteoclast formation and function and thus, bone resorption (Kamiya et al., 2008,

**TABLE 2 |** Conditional overexpression (OE) and knockout (KO) mouse models for the analysis of BMP signaling in osteoclasts.

| | | Mouse models | | | |
|---|---|---|---|---|---|
| **Gene** | **OE/KO** | **Target** | **Bone mass** | **Osteoclast formation and/or activity** | **References** |
| *Bmp4* | OE | Osteoblasts (Col1a promotor) | ⇓ | ⇑ | Okamoto et al.; 2006 |
| | OE | Liver (hAAT1 promotor) | ⇓ | ⇑ | Holien et al., 2018 |
| *Bmpr1a* | KO | Osteoclasts (Ctsk-Cre) | ⇑ | (⇑) | Okamoto et al., 2011 |
| *Bmpr1a* | KO | Osteoclast precursors (LysM-Cre) | ⇑ | ⇓ | Li et al., 2017 |
| *Bmpr1a* | KO | Osteoblasts (Col1-Cre) | ⇑ | ⇓ | Kamiya et al., 2008 |
| *Bmpr1a* | KO | Osteocytes (Dmp1-Cre) | ⇑ | ⇓ | Kamiya et al., 2016 |
| *Bmpr2* | KO | Osteoclast precursors (LysM-Cre) | ⇑ | ⇓ | Broege et al., 2013 |
| *Smad1, Smad5* | KO | Osteoclasts (c-Fms-Cre) | ⇑ | ⇓ | Tasca et al., 2018 |
| *Smad4* | KO | Osteoclasts (Ctsk-Cre) | ⇓ | ⇑, TGFβ-mediated | Morita et al., 2016 |

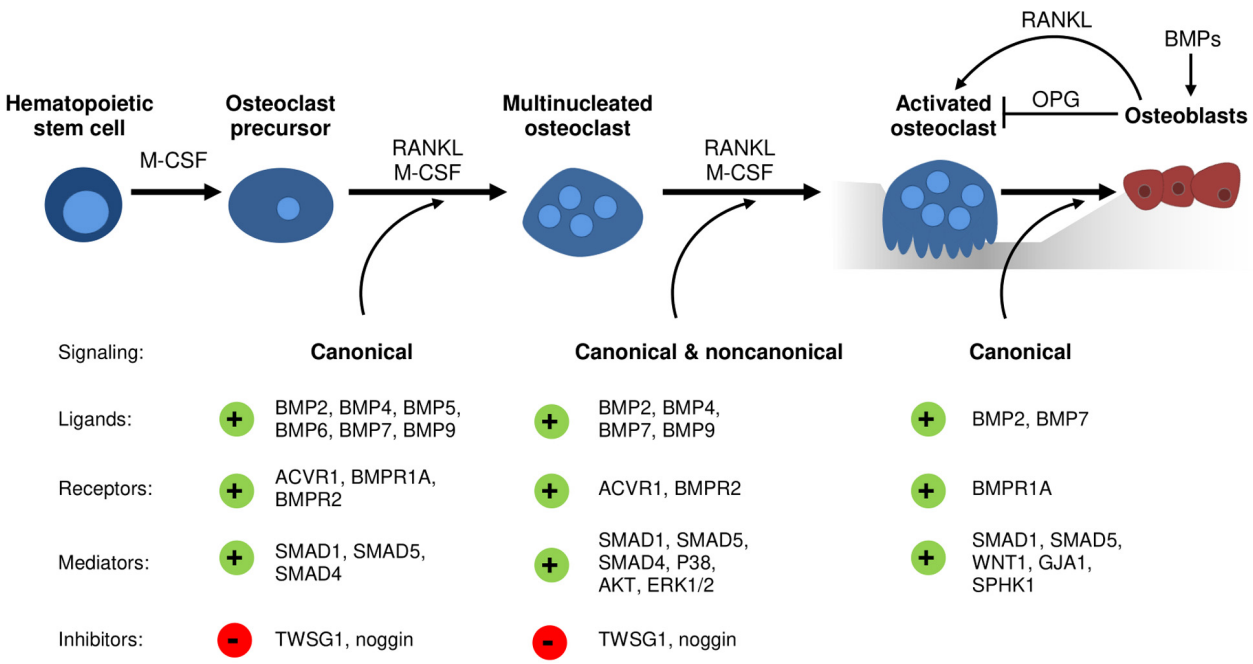


**FIGURE 1 |** The emerging role of BMP signaling during osteoclastogenesis and osteoblast-osteoclast coupling. Conditional knockout models and cell culture studies indicate a vital role of canonical and non-canonical BMP signaling in osteoclastogenesis. Several distinct BMP ligands, BMP receptors, BMP inhibitors and downstream mediators regulate osteoclast differentiation, fusion, and resorption activity as well as osteoblast-osteoclast coupling.

2016). Vice versa, osteoclast-specific *Bmpr1a* knockout enhanced bone formation suggesting an important role of BMPR1A within osteoblast and osteoclast coupling (Okamoto et al., 2011). Furthermore, osteoblasts can be recruited by osteoclasts to sites of active bone remodeling, mediated through coupling factors such as WNT1 (Weivoda et al., 2016; Tasca et al., 2018), Gap junction alpha-1 protein (GJA1) (Tasca et al., 2018), and sphingosine kinase 1 (SPHK1) (Ryu et al., 2006; Pederson et al., 2008; Tasca et al., 2018). A recent study proposed that especially SMAD1/5-dependent signaling in osteoclasts might regulate bone formation since mRNA levels of aforementioned coupling factors were upregulated in osteoclasts with deleted SMAD1/5 (Tasca et al., 2018). In conclusion, there is manifest evidence that BMPs and their antagonists can act as mediators in osteoblast–osteoclast coupling (**Figure 1**) and therefore display critical determinants that dictate the rate of bone remodeling (Abe et al., 2010). Thus, time-sensitive processes such as bone healing after fracture incidences might benefit from novel therapies with targeted BMP pathway manipulation.

## RECOMBINANT BMP THERAPY AND OSTEOCLASTS: CLINICAL IMPLICATIONS

Bone has a large self-healing capacity and during fracture repair ontological events of embryonic skeletal development are recapitulated to restore the damaged skeletal tissue. This regenerative process is driven by a complex interplay of various cells, multiple growth factors and extracellular matrix, involving both anabolic and catabolic actions. Following the initial fracture, inflammatory cells invade the disrupted tissue

and a hematoma is built. Subsequently, mesenchymal stem cells, the precursors of chondrocytes and osteoblasts, are recruited mainly from the periosteum and a soft, cartilaginous callus is formed by chondrocytes providing a mechanical support of the fractured area. During the following process of endochondral ossification, osteoclasts gradually resorb the soft callus matrix and highly active osteoblasts replace it by an irregularly woven and mineralized (hard) bone matrix. The final stage of remodeling involves multiple cycles of coupled bone resorption and formation as well as vascularization and reestablishes the former bone structure, strength and function (Schindeler et al., 2008; Einhorn and Gerstenfeld, 2015). Given that inadequate healing occurs in 10% of the cases, new, well-tolerated therapeutic options are needed to improve poor bone healing (Schindeler et al., 2008; Einhorn and Gerstenfeld, 2015). BMP ligands 2, 4, 6, 7, and 9 show a high osteoinductive potential as needed in case of fracture repair (Beederman et al., 2013; Wu et al., 2016). Interestingly, BMP2, BMP4, and BMP7 expression by osteoclasts is highly elevated within fracture sites of membranous fracture healing (Spector et al., 2001), In the clinics, rhBMP2 and rhBMP7 are reported to support fracture healing (Govender et al., 2002; Dumic-Cule et al., 2014), however, only in a limited subset of fractures (i.e., open tibial fractures), and in some cases are associated with side effects such as inflammation and heterotopic ossification (Fu et al., 2012; Simmonds et al., 2013; Vukicevic et al., 2014). Comprehensive reviews on fracture repair and recombinant BMPs therapy, its advantages and disadvantages can be found elsewhere (Einhorn and Gerstenfeld, 2015; Dumic-Cule et al., 2018).

As BMPs stimulate osteoclasts directly as well as indirectly via the RANKL/OPG ratio, also adverse effects of rhBMP therapy through enhanced bone resorption should be considered. In non-human primates, treatment of metaphyseal core defects with rhBMP2 delivered in an absorbable collagen sponge (ACS) resulted in transient bone resorption followed by bone formation. Animals treated with rhBMP2/ACS showed increased size of the proximal and distal core defects compared with animals treated with ACS alone. Histological analysis revealed bone resorption of the rhBMP2/ACS-treated limbs that started at 1 week and peaked at 2 weeks. Bone formation was observed at 2 weeks and was ongoing at 24 weeks (Seeherman et al., 2010). Also in patients with unstable thoracolumbar fractures, spinal fusion treatment with BMP7 as a bone graft substitute resulted in severe bone resorption as a primary event and segmental collapse (Laursen et al., 1999). This was due to a pronounced effect of high dosed rhBMP on osteoclasts and thus, enhanced substantial bone resorption at trabecular surfaces, the major part of vertebrae (Dumic-Cule et al., 2018). In retrospective analyses, initial rhBMP-stimulated bone resorption was found to be transient and followed by subsequent bone formation and repair (Fu et al., 2012; Simmonds et al., 2013). At the bone-titanium implant interface, biological response to wear particles displays the prevalent cause of aseptic loosening and osteolysis (Jacobs et al., 2001) through stimulated bone resorption (Haynes et al., 2001). A recent *in vitro* study shows that BMP2 synergizes with titanium particles to enhance RANKL-mediated osteoclast formation in osteoclast-like RAW 264.7 cells and enhanced their resorptive activity, and that at low concentrations (Sun et al., 2014). In the clinics, rhBMP2-coated devices led to early osteolysis causing implant shifts and subsequent fracture instability (Ekrol et al., 2008). To contain adverse effects of rhBMP therapy on osteoclasts while retaining the anabolic effect, several preclinical studies investigated the benefit of blocking osteoclast differentiation and activity with drugs. As such, bisphosphonates can inactivate osteoclasts by inducing apoptosis and thus, impair bone resorption (Rogers et al., 2011). Importantly, in healthy rats treated with bisphosphonates remodeling of hard fracture callus was delayed but not stopped, ensuring sufficient endochondral fracture repair (McDonald et al., 2008). In rat models with a cancellous allograft that remodels *in vivo* in a bone conduction chamber, BMPs increased the rate of bone remodeling and the volume of the remodeled graft, however, most of the newly formed bone was resorbed (Harding et al., 2008; Belfrage et al., 2011). A higher amount of newly formed bone was retained by adding bisphosphonates either locally (Belfrage et al., 2011) or systemically (Harding et al., 2008). The synergistic efficiency of combined rhBMP and bisphosphonate therapy was also shown in a critical femoral defect model (Little et al., 2005), carrier-based femoral open-fracture model (Doi et al., 2011) and femoral open-fracture models that are prone to non-union and were treated with autografts (Bosemark et al., 2013) or allografts (Mathavan et al., 2013).

Taken together, rhBMP therapy can negatively affect clinical results due to adverse effects such as simultaneously stimulation of bone resorption. Preclinical studies indicate that additionally blocking osteoclasts with bisphosphonates benefits rhBMP therapy by restricting catabolic actions while retaining anabolic effects. Still, further research is needed to fully understand the therapeutic potential and restrictions of rhBMPs in fracture repair, in particular, focusing on their effects in human osteoclasts and considering the genetic heterogeneity of patients.

## CONCLUSION

Bone morphogenetic proteins are multi-functional cytokines that are involved in a multitude of molecular cascades and signaling pathways. In bone remodeling, besides their essential role within bone formation, BMPs also influence osteoclast homeostasis. In this review, we show that both canonical and non-canonical BMP signaling promotes osteoclast formation and activity. In particular, BMPs support distinct steps of osteoclast differentiation and activation in a direct manner and via BMP-stimulated surrounding skeletal cells via the RANK/RANKL/OPG system. Thus, BMP signaling acts as a mediator in osteoblast-osteoclast coupling and critically affects the rate of bone remodeling. The ability of BMPs to improve poor bone healing by stimulation of osteoblasts has been reported in several clinical studies. However, rhBMP therapy can negatively affect clinical results due to adverse effects such as enhanced bone resorption. Thus, uncoupling bone formation from bone resorption through pharmacological osteoclast blockade or other

approaches might be the critical step to advance rhBMP-mediated fracture repair.

## AUTHOR CONTRIBUTIONS

FL, LH, and MR contributed to the literature research, discussion, and interpretation. FL and MR drafted the manuscript. All the authors critically read, revised, and approved the final version of the manuscript.

## FUNDING

This work was supported by the Deutsche Forschungsgemeinschaft Schwerpunktprogramm μBone (to LH and MR).

## REFERENCES

Abe, E., Yamamoto, M., Taguchi, Y., Lecka-Czernik, B., O'Brien, C. A., Economides, A. N., et al. (2010). Essential requirement of BMPs-2/4 for both osteoblast and osteoclast formation in murine bone marrow cultures from adult mice: antagonism by noggin. *J. Bone Miner. Res.* 15, 663–673. doi: 10.1359/jbmr.2000.15.4.663

Anderson, H. C., Hodges, P. T., Aguilera, X. M., Missana, L., and Moylan, P. E. (2000). Bone morphogenetic protein (BMP) localization in developing human and rat growth plate, metaphysis, epiphysis, and articular cartilage. *J. Histochem. Cytochem.* 48, 1493–1502. doi: 10.1177/002215540004801106

Baud'huin, M., Solban, N., Cornwall-Brady, M., Sako, D., Kawamoto, Y., Liharska, K., et al. (2012). A soluble bone morphogenetic protein type IA receptor increases bone mass and bone strength. *Proc. Natl. Acad. Sci. U.S.A.* 109, 12207–12212. doi: 10.1073/pnas.1204929109

Beederman, M., Lamplot, J. D., Nan, G., Wang, J., Liu, X., Yin, L., et al. (2013). BMP signaling in mesenchymal stem cell differentiation and bone formation. *J. Biomed. Sci. Eng.* 6, 32–52. doi: 10.4236/jbise.2013.68A1004

Belfrage, O., Flivik, G., Sundberg, M., Kesteris, U., and Tägil, M. (2011). Local treatment of cancellous bone grafts with BMP-7 and zoledronate increases both the bone formation rate and bone density. *Acta Orthop.* 82, 228–233. doi: 10.3109/17453674.2011.566138

Bessho, K., Kusumoto, K., Fujimura, K., Konishi, Y., Ogawa, Y., Tani, Y., et al. (1999). Comparison of recombinant and purified human bone morphogenetic protein. *Br. J. Oral Maxillofac. Surg.* 37, 2–5. doi: 10.1054/bjom.1998.0379

Bosemark, P., Isaksson, H., McDonald, M. M., Little, D. G., and Tägil, M. (2013). Augmentation of autologous bone graft by a combination of bone morphogenic protein and bisphosphonate increased both callus volume and strength. *Acta Orthop.* 84, 106–111. doi: 10.3109/17453674.2013.773123

Broege, A., Pham, L., Jensen, E. D., Emery, A., Huang, T. H., Stemig, M., et al. (2013). Bone morphogenetic proteins signal via SMAD and mitogen activated protein (MAP) kinase pathways at distinct times during osteoclastogenesis. *J. Biol. Chem.* 288, 37230–37240. doi: 10.1074/jbc.M113.496950

Charles, J. F., and Aliprantis, A. O. (2014). Osteoclasts: more than "bone eaters.". *Trends Mol. Med.* 20, 449–459. doi: 10.1016/j.molmed.2014.06.001

Doi, Y., Miyazaki, M., Yoshiiwa, T., Hara, K., Kataoka, M., and Tsumura, H. (2011). Manipulation of the anabolic and catabolic responses with BMP-2 and zoledronic acid in a rat femoral fracture model. *Bone* 49, 777–782. doi: 10.1016/j.bone.2011.07.005

Dumic-Cule, I., Brkljacic, J., Rogic, D., Bordukalo Niksic, T., Tikvica Luetic, A., Draca, N., et al. (2014). Systemically available bone morphogenetic protein two and seven affect bone metabolism. *Int. Orthop.* 38, 1979–1985. doi: 10.1007/s00264-014-2425-8

Dumic-Cule, I., Peric, M., Kucko, L., Grgurevic, L., Pecina, M., and Vukicevic, S. (2018). Bone morphogenetic proteins in fracture repair. *Int. Orthop.* 42, 2619–2626. doi: 10.1007/s00264-018-4153-y

Eastell, R., O'Neill, T. W., Hofbauer, L. C., Langdahl, B., Reid, I. R., Gold, D. T., et al. (2016). Postmenopausal osteoporosis. *Nat. Rev. Dis. Prim.* 2:16069. doi: 10.1038/nrdp.2016.69

Einhorn, T. A., and Gerstenfeld, L. C. (2015). Fracture healing: mechanisms and interventions. *Nat. Rev. Rheumatol.* 11, 45–54. doi: 10.1038/nrrheum.2014.164

Ekrol, I., Hajducka, C., Court-Brown, C., and McQueen, M. M. (2008). A comparison of RhBMP-7 (OP-1) and autogenous graft for metaphyseal defects after osteotomy of the distal radius. *Injury* 39, S73–S82. doi: 10.1016/S0020-1383(08)70018-4

Fong, D., Bisson, M., Laberge, G., McManus, S., Grenier, G., Faucheux, N., et al. (2013). Bone morphogenetic protein-9 activates Smad and ERK pathways and supports human osteoclast function and survival in vitro. *Cell. Signal.* 25, 717–728. doi: 10.1016/j.cellsig.2012.12.003

Fu, R., Selph, S., Mcdonagh, M., Peterson, K., Tiwari, A., Chou, R., et al. (2012). Effectiveness and Harms of Recombinant Human Bone Morphogenetic. *Ann. Intern. Med.* 158, 890–902. doi: 10.7326/0003-4819-158-12-201306180-00006

Garimella, R., Tague, S. E., Zhang, J., Belibi, F., Nahar, N., Sun, B. H., et al. (2008). Expression and synthesis of bone morphogenetic proteins by osteoclasts: a possible path to anabolic bone remodeling. *J. Histochem. Cytochem.* 56, 569–577. doi: 10.1369/jhc.2008.950394

Govender, S., Csimma, C., Genant, H. K., Valentin-Opran, A., Amit, Y., Arbel, R., et al. (2002). Recombinant human bone morphogenetic protein-2 for treatment of open tibial fractures: a prospective, controlled, randomized study of four hundred and fifty patients. *J. Bone Joint Surg. Am.* 84A, 2123–2134. doi: 10.2106/00004623-200212000-00001

Granholm, S., Henning, P., Lindholm, C., and Lerner, U. H. (2013). Osteoclast progenitor cells present in significant amounts in mouse calvarial osteoblast isolations and osteoclastogenesis increased by BMP-2. *Bone* 52, 83–92. doi: 10.1016/j.bone.2012.09.019

Harding, A. K., Aspenberg, P., Kataoka, M., Bylski, D., and Tägil, M. (2008). Manipulating the anabolic and catabolic response in bone graft remodeling: synergism by a combination of local BMP-7 and a single systemic dosis of zoledronate. *J. Orthop. Res.* 26, 1245–1249. doi: 10.1002/jor.20625

Haynes, D. R., Crotti, T. N., Potter, A. E., Loric, M., Atkins, G. J., Howie, D. W., et al. (2001). The osteoclastogenic molecules RANKL and RANK are associated with periprosthetic osteolysis. *J. Bone Jt. Surg. Ser. B* 83, 902–911. doi: 10.1302/0301-620X.83B6.10905

Hentunen, T. A., Lakkakorpi, P. T., Tuukkanen, J., Lehenkari, P. P., Sampath, T. K., and Väänänen, H. K. (1995). Effects of recombinant human osteogenic protein-1 on the differentiation of osteoclast-like cells and bone resorption. *Biochem. Biophys. Res. Commun.* 209, 433–443. doi: 10.1006/bbrc.1995.1521

Hofbauer, L. C., Dunstan, C. R., Spelsberg, T. C., Riggs, B. L., and Khosla, S. (1998). Osteoprotegerin production by human osteoblast lineage cells is stimulated by vitamin D, bone morphogenetic protein-2, and cytokines. *Biochem. Biophys. Res. Commun.* 250, 776–781. doi: 10.1006/bbrc.1998.9394

Hofbauer, L. C., Kühne, C. A., and Viereck, V. (2004). The OPG/RANKL/RANK system in metabolic bone diseases. *J. Musculoskelet. Neuronal Interact.* 4, 268–275.

Holien, T., Westhrin, M., Moen, S. H., Zahoor, M., Buene, G., Størdal, B., et al. (2018). BMP4 gene therapy inhibits myeloma tumor growth, but has a negative impact on bone. *Blood* 132, 1928–1928. doi: 10.1182/blood-2018-99-112429

Huntley, R., Davydova, J., Petryk, A., Billington, C. J., Jensen, E. D., Mansky, K. C., et al. (2015). The function of twisted gastrulation in regulating osteoclast differentiation is dependent on BMP binding. *J. Cell. Biochem.* 116, 2239–2246. doi: 10.1002/jcb.25174

Itoh, K., Udagawa, N., Katagiri, T., Iemura, S., Ueno, N., Yasuda, H., et al. (2001). Bone morphogenetic protein 2 stimulates osteoclast differentiation and survival supported by receptor activator of nuclear factor-κB ligand. *Endocrinology* 142, 3656–3662. doi: 10.1210/endo.142.8.8300

Jacobs, J. J., Roebuck, K. A., Archibeck, M., Hallab, N. J., and Glant, T. T. (2001). Osteolysis: basic science. *Clin. Orthop. Relat. Res.* 393, 71–77. doi: 10.1097/00003086-200112000-00008

Jacome-Galarza, C. E., Percin, G. I., Muller, J. T., Mass, E., Lazarov, T., Eitler, J., et al. (2019). Developmental origin, functional maintenance and genetic rescue of osteoclasts. *Nature* 568, 541–545. doi: 10.1038/s41586-019-1105-7

Jensen, E. D., Pham, L., Billington, C. J., Espe, K., Carlson, A. E., Westendorf, J. J., et al. (2010). Bone morphogenic protein 2 directly enhances differentiation of

murine osteoclast precursors. *J. Cell. Biochem.* 109, 672–682. doi: 10.1002/jcb.22462

Kamiya, N., Shuxian, L., Yamaguchi, R., Phipps, M., Aruwajoye, O., Adapala, N. S., et al. (2016). Targeted disruption of BMP signaling through type IA receptor (BMPR1A) in osteocyte suppresses SOST and RANKL, leading to dramatic increase in bone mass, bone mineral density and mechanical strength. *Bone* 91, 53–63. doi: 10.1016/j.bone.2016.07.002

Kamiya, N., Ye, L., Kobayashi, T., Lucas, D. J., Mochida, Y., Yamauchi, M., et al. (2008). Disruption of BMP signaling in osteoblasts through type IA receptor (BMPRIA) increases bone mass. *J. Bone Miner. Res.* 23, 2007–2017. doi: 10.1359/jbmr.080809

Kanatani, M., Sugimoto, T., Kaji, H., Kobayashi, T., Nishiyama, K., Fukase, M., et al. (1995). Stimulatory effect of bone morphogenetic protein-2 on osteoclast-like cell formation and bone-resorbing activity. *J. Bone Miner. Res.* 10, 1681–1690. doi: 10.1002/jbmr.5650101110

Kaneko, H., Arakawa, T., Mano, H., Kaneda, T., Ogasawara, A., Nakagawa, M., et al. (2000). Direct stimulation of osteoclastic bone resorption by bone morphogenetic protein (BMP)-2 and expression of BMP receptors in mature osteoclasts. *Bone* 27, 479–486. doi: 10.1016/S8756-3282(00)00358-6

Lademann, F., Weidner, H., Tsourdi, E., Kumar, R., Rijntjes, E., Köhrle, J., et al. (2020). Disruption of BMP signaling prevents hyperthyroidism-induced bone loss in male mice. *J. Bone Miner. Res.* doi: 10.1002/jbmr.4092 [Epub ahead of print].

Laursen, M., Høy, K., Hansen, E. S., Gelineck, J., Christensen, F. B., and Bünger, C. E. (1999). Recombinant bone morphogenetic protein-7 as an intracorporal bone growth stimulator in unstable thoracolumbar burst fractures in humans: preliminary results. *Eur. Spine J.* 8, 485–490. doi: 10.1007/s005860050210

Li, A., Cong, Q., Xia, X., Leong, W. F., Yeh, J., Miao, D., et al. (2017). Pharmacologic calcitriol inhibits osteoclast lineage commitment via the BMP-Smad1 and IκB-NF-κB pathways. *J. Bone Miner. Res.* 32, 1406–1420. doi: 10.1002/jbmr.3146

Little, D. G., McDonald, M., Bransford, R., Godfrey, C. B., and Amanat, N. (2005). Manipulation of the anabolic and catabolic responses with OP-1 and zoledronic acid in a rat critical defect model. *J. Bone Miner. Res.* 20, 2044–2052. doi: 10.1359/JBMR.050712

Lowery, J. W., and Rosen, V. (2018). The BMP pathway and its inhibitors in the skeleton. *Physiol. Rev.* 98, 2431–2452. doi: 10.1152/physrev.00028.2017

Mathavan, N., Bosemark, P., Isaksson, H., and Tägil, M. (2013). Investigating the synergistic efficacy of BMP-7 and zoledronate on bone allografts using an open rat osteotomy model. *Bone* 56, 440–448. doi: 10.1016/j.bone.2013.06.030

Maurer, T., Zimmermann, G., Maurer, S., Stegmaier, S., Wagner, C., and Hänsch, G. M. (2012). Inhibition of osteoclast generation: a novel function of the bone morphogenetic protein 7/osteogenic protein 1. *Mediat. Inflamm.* 2012:171209. doi: 10.1155/2012/171209

McDonald, M. M., Dulai, S., Godfrey, C., Amanat, N., Sztynda, T., and Little, D. G. (2008). Bolus or weekly zoledronic acid administration does not delay endochondral fracture repair but weekly dosing enhances delays in hard callus remodeling. *Bone* 43, 653–662. doi: 10.1016/j.bone.2008.05.019

Morita, M., Yoshida, S., Iwasaki, R., Yasui, T., Sato, Y., Kobayashi, T., et al. (2016). Smad4 is required to inhibit osteoclastogenesis and maintain bone mass. *Sci. Rep.* 6, 1–11. doi: 10.1038/srep35221

Okamoto, M., Murai, J., Imai, Y., Ikegami, D., Kamiya, N., Kato, S., et al. (2011). Conditional deletion of Bmpr1a in differentiated osteoclasts increases osteoblastic bone formation, increasing volume of remodeling bone in mice. *J. Bone Miner. Res.* 26, 2511–2522. doi: 10.1002/jbmr.477

Okamoto, M., Murai, J., Yoshikawa, H., and Tsumaki, N. (2006). Bone morphogenetic proteins in bone stimulate osteoclasts and osteoblasts during bone development. *J. Bone Miner. Res.* 21, 1022–1033. doi: 10.1359/jbmr.060411

Omi, M., Kaartinen, V., and Mishina, Y. (2019). Activin A receptor type 1-mediated BMP signaling regulates RANKL-induced osteoclastogenesis via canonical SMADsignaling pathway. *J. Biol. Chem.* 294, 17818–17836. doi: 10.1074/jbc.RA119.009521

Pederson, L., Ruan, M., Westendorf, J. J., Khosla, S., and Oursler, M. J. (2008). Regulation of bone formation by osteoclasts involves Wnt/BMP signaling and the chemokine sphingosine-1-phosphate. *Proc. Natl. Acad. Sci. U.S.A.* 105, 20764–20769. doi: 10.1073/pnas.0805133106

Pham, L., Beyer, K., Jensen, E. D., Rodriguez, J. S., Davydova, J., Yamamoto, M., et al. (2011). Bone morphogenetic protein 2 signaling in osteoclasts is negatively regulated by the BMP antagonist, twisted gastrulation. *J. Cell. Biochem.* 112, 793–803. doi: 10.1002/jcb.23003

Rogers, M. J., Crockett, J. C., Coxon, F. P., and Mönkkönen, J. (2011). Biochemical and molecular mechanisms of action of bisphosphonates. *Bone* 49, 34–41. doi: 10.1016/j.bone.2010.11.008

Ryu, J., Kim, H. J., Chang, E.-J., Huang, H., Banno, Y., and Kim, H.-H. (2006). Sphingosine 1-phosphate as a regulator of osteoclast differentiation and osteoclast-osteoblast coupling. *EMBO J.* 25, 5840–5851. doi: 10.1038/sj.emboj.7601430

Schindeler, A., McDonald, M. M., Bokko, P., and Little, D. G. (2008). Bone remodeling during fracture repair: the cellular picture. *Semin. Cell Dev. Biol.* 19, 459–466. doi: 10.1016/j.semcdb.2008.07.004

Seeherman, H. J., Li, X. J., Bouxsein, M. L., and Wozney, J. M. (2010). rhBMP-2 induces transient bone resorption followed by bone formation in a nonhuman primate core-defect model. *J. Bone Jt. Surg. Ser. A* 92, 411–426. doi: 10.2106/JBJS.H.01732

Shi, C., Iura, A., Terajima, M., Liu, F., Lyons, K., Pan, H., et al. (2016). Deletion of BMP receptor type IB decreased bone mass in association with compromised osteoblastic differentiation of bone marrow mesenchymal progenitors. *Sci. Rep.* 6, 1–13. doi: 10.1038/srep24256

Simmonds, M. C., Brown, J. V. E., Heirs, M. K., Higgins, J. P. T., Mannion, R. J., Rodgers, M. A., et al. (2013). Safety and effectiveness of recombinant human bone morphogenetic protein-2 for spinal fusion: a meta-analysis of individual-participant data. *Ann. Intern. Med.* 158, 877–889. doi: 10.7326/0003-4819-158-12-201306180-00005

Sotillo Rodriguez, J. E., Mansky, K. C., Jensen, E. D., Carlson, A. E., Schwarz, T., Pham, L., et al. (2009). Enhanced osteoclastogenesis causes osteopenia in twisted gastrulation-deficient mice through increased BMP signaling. *J. Bone Miner. Res.* 24, 1917–1926. doi: 10.1359/jbmr.090507

Spector, J. A., Luchs, J. S., Mehrara, B. J., Greenwald, J. A., Smith, L. P., and Longaker, M. T. (2001). Expression of bone morphogenetic proteins during membranous bone healing. *Plast. Reconstr. Surg.* 107, 124–134. doi: 10.1097/00006534-200101000-00018

Sun, S. X., Guo, H. H., Zhang, J., Yu, B., Sun, K. N., and Jin, Q. H. (2014). BMP-2 and titanium particles synergistically activate osteoclast formation. *Braz. J. Med. Biol. Res.* 47, 461–469. doi: 10.1590/1414-431X20132966

Tachi, K., Takami, M., Zhao, B., Mochizuki, A., Yamada, A., Miyamoto, Y., et al. (2010). Bone morphogenetic protein 2 enhances mouse osteoclast differentiation via increased levels of receptor activator of NF-κB ligand expression in osteoblasts. *Cell Tissue Res.* 342, 213–220. doi: 10.1007/s00441-010-1052-y

Takayanagi, H. (2007). The role of NFAT in osteoclast formation. *Ann. N.Y. Acad. Sci.* 1116, 227–237. doi: 10.1196/annals.1402.071

Tasca, A., Astleford, K., Blixt, N. C., Jensen, E. D., Gopalakrishnan, R., and Mansky, K. C. (2018). SMAD1/5 signaling in osteoclasts regulates bone formation via coupling factors. *PLoS One* 13:e0203404. doi: 10.1371/journal.pone.0203404

Tasca, A., Stemig, M., Broege, A., Huang, B., Davydova, J., Zwijsen, A., et al. (2015). Smad1/5 and Smad4 expression are important for osteoclast differentiation. *J. Cell. Biochem.* 116, 1350–1360. doi: 10.1002/jcb.25092

Teitelbaum, S. L. (2000). Bone resorption by osteoclasts. *Science* 289, 1504–1508. doi: 10.1126/SCIENCE.289.5484.1504

Usui, M., Xing, L., Drissi, H., Zuscik, M., O'Keefe, R., Chen, D., et al. (2008). Murine and chicken chondrocytes regulate osteoclastogenesis by producing RANKL in response to BMP2. *J. Bone Miner. Res.* 23, 314–325. doi: 10.1359/jbmr.071025

Vukicevic, S., Oppermann, H., Verbanac, D., Jankolija, M., Popek, I., Curak, J., et al. (2014). The clinical use of bone morphogenetic proteins revisited: a novel biocompatible carrier device OSTEOGROW for bone healing. *Int. Orthop.* 38, 635–647. doi: 10.1007/s00264-013-2201-1

Wan, C., He, Q., and Li, G. (2006). Osteoclastogenesis in the nonadherent cell population of human bone marrow is inhibited by rhBMP-2 alone or together with rhVEGF. *J. Orthop. Res.* 24, 29–36. doi: 10.1002/jor.20010

Wang, E. A., Rosen, V., D'Alessandro, J. S., Bauduy, M., Cordes, P., Harada, T., et al. (1990). Recombinant human bone morphogenetic protein induces bone formation. *Proc. Natl. Acad. Sci. U.S.A.* 87, 2220–2224.

Weivoda, M. M., Ruan, M., Pederson, L., Hachfeld, C., Davey, R. A., Zajac, J. D., et al. (2016). Osteoclast TGF-β receptor signaling induces Wnt1 secretion and couples bone resorption to bone formation. *J. Bone Miner. Res.* 31, 76–85. doi: 10.1002/jbmr.2586

Wu, M., Chen, G., and Li, Y. P. (2016). TGF-β and BMP signaling in osteoblast, skeletal development, and bone formation, homeostasis and disease. *Bone Res.* 4:16009. doi: 10.1038/boneres.2016.9

Wutzl, A., Brozek, W., Lernbass, I., Rauner, M., Hofbauer, G., Schopper, C., et al. (2006). Bone morphogenetic proteins 5 and 6 stimulate osteoclast generation. *J. Biomed. Mater. Res. A* 77, 75–83. doi: 10.1002/jbm.a.30615

Yahara, Y., Barrientos, T., Tang, Y. J., Puviindran, V., Nadesan, P., Zhang, H., et al. (2020). Erythromyeloid progenitors give rise to a population of osteoclasts that contribute to bone homeostasis and repair. *Nat. Cell Biol.* 22, 49–59. doi: 10.1038/s41556-019-0437-8

Yoshida, H., Hayashi, S. I., Kunisada, T., Ogawa, M., Nishikawa, S., Okamura, H., et al. (1990). The murine mutation osteopetrosis is in the coding region of the macrophage colony stimulating factor gene. *Nature* 345, 442–444. doi: 10.1038/345442a0

**Conflict of Interest:** MR reports honoraria for lectures from Amgen. LH reports honoraria for advisory boards from Alexion, Amgen, Merck, Radius, Roche, Shire, and UCB to his institution and himself.

The remaining author declares that the research was conducted in the absence of any commercial or financial relationships that could be construed as a potential conflict of interest.

frontiers in Cell and Developmental Biology

MINI REVIEW
published: 24 November 2020
doi: 10.3389/fcell.2020.584696

# Effects of Erythropoietin in White Adipose Tissue and Bone Microenvironment

*Sukanya Suresh, Jeeyoung Lee and Constance Tom Noguchi**

*Molecular Medicine Branch, National Institute of Diabetes and Digestive and Kidney Diseases, National Institutes of Health, Bethesda, MD, United States*

Erythropoietin (EPO) is expressed primarily in fetal liver and adult kidney to stimulate red blood cell production. Erythropoietin receptor expression is not restricted to erythroid progenitor cells, and non-erythroid EPO activity includes immune response and bone remodeling. In bone fracture models, EPO administration promotes bone formation and accelerates bone healing. In contrast, in healthy adult mice, exogenous EPO-stimulated erythropoiesis has been concomitant with bone loss, particularly at high EPO, that may be accompanied by increased osteoclast activation. Other EPO-associated responses include reduced inflammation and loss of fat mass with high-fat diet feeding, especially in male mice. While EPO exhibited a sex-dimorphic response in regulation of fat mass and inflammation in obese mice, EPO-stimulated erythropoiesis as well as EPO-associated bone loss was comparable in males and females. EPO administration in young mice and in obese mice resulted in bone loss without increasing osteoclasts, suggesting an osteoclast-independent mechanism, while loss of endogenous EPO decreased bone development and maintenance. Ossicle formation of bone marrow stromal cell transplants showed that EPO directly regulates the balance between osteogenesis and adipogenesis. Therefore, during development, endogenous EPO contributes to normal bone development and in maintaining the balance between osteogenesis and adipogenesis in bone marrow stromal cells, while EPO treatment in mice increased erythropoiesis, promoted bone loss, decreased bone marrow adipogenesis, and increased osteoclast activity. These observations in mouse models suggest that the most prevalent use of EPO to treat anemia associated with chronic kidney disease may compromise bone health and increase fracture risk, especially at a high dose.

**Keywords: brain, fat, macrophage, osteoclast, osteoblast, bone, erythropoietin, microglial**

OPEN ACCESS

***Edited by:***
*Natalie A. Sims,*
*The University of Melbourne, Australia*

***Reviewed by:***
*Martina Rauner,*
*Dresden University of Technology, Germany*
*Robert F. Paulson,*
*The Pennsylvania State University, United States*

***Correspondence:**
*Constance Tom Noguchi*
*connien@niddk.nih.gov*

***Specialty section:***
*This article was submitted to Cellular Biochemistry, a section of the journal Frontiers in Cell and Developmental Biology*

***Received:*** *17 July 2020*
***Accepted:*** *20 October 2020*
***Published:*** *24 November 2020*

***Citation:***
*Suresh S, Lee J and Noguchi CT (2020) Effects of Erythropoietin in White Adipose Tissue and Bone Microenvironment. Front. Cell Dev. Biol. 8:584696. doi: 10.3389/fcell.2020.584696*

## INTRODUCTION

Erythropoietin (EPO) regulates red blood cell production, and recombinant EPO is used primarily to treat anemia in chronic kidney disease. EPO can stimulate additional non-erythroid cell response mediated by erythropoietin receptor (EPOR) expression in other hematopoietic cells and non-hematopoietic tissues including white adipose tissue (WAT), brain, and bone (Suresh et al., 2019b). In mice, EPO treatment is associated with anti-inflammatory activity, neuroprotection, cardioprotection, skeletal muscle wound healing, protection against diet-induced obesity

(Zhang et al., 2014; Suresh et al., 2019b), and bone loss accompanying EPO-stimulated erythropoiesis (Hiram-Bab et al., 2015; Suresh et al., 2019a). Hormones, cytokines, and growth factors can influence osteoblast and osteoclast differentiation, bone remodeling, and macrophage immune response, and the resultant production of inflammatory cytokines can modulate osteoclast differentiation and bone resorption activity (Sinder et al., 2015; Adamopoulos, 2018; Kubatzky et al., 2018). Here we describe the EPO response of cells derived from the monocyte–macrophage lineage such as the anti-inflammatory EPO response during diet-induced obesity in white adipose tissue and brain and the osteoclasts associated with EPO-stimulated bone loss. We also include a discussion of EPO effects on fat accumulation during diet-induced obesity and on bone marrow stromal cells associated with EPO-stimulated bone loss.

## SEX-SPECIFIC EPO REGULATION AND DIET-INDUCED OBESITY

The estrogen-dependent EPO activity was first identified with EPO angiogenic response in the uterus during the mouse estrus cycle (Yasuda et al., 1998). Among non-hematopoietic tissues, EPOR has a relatively high expression in brain and adipose tissue. The EPO-stimulated hypoxic ventilatory response in brain and carotid body is also sex dimorphic and is increased in females compared with males in human and mouse (Soliz et al., 2012). With respect to adipose tissue, mice with erythroid-restricted EPOR expression show a disproportionate accumulation of fat mass that is greater in females that develop obesity and insulin resistance at a younger age compared with their male counterpart (Teng et al., 2011).

### EPO Protection in Mouse Adipose Tissue Inflammation

C57BL/6 mice fed a high-fat diet develop an obese phenotype and inflammation in WAT. With obesity, the macrophages in WAT stromal vascular fraction shift from an anti-inflammatory toward a pro-inflammatory phenotype, decrease the secretion of the anti-inflammatory cytokine IL-10 that enhances adipocyte insulin sensitivity, and increase the expression of inflammatory cytokines, TNFα, and IL-6, contributing to insulin resistance (Lumeng et al., 2007; Lauterbach and Wunderlich, 2017). The increased WAT inflammation and macrophage infiltration result in crown-like structures, which are macrophages surrounding necrotic or dying adipocytes, indicating the proinflammatory state of adipose tissue.

In mice, EPO contributes directly to metabolic homeostasis by maintenance of WAT. During high-fat-diet feeding, EPO treatment protects against glucose intolerance, insulin resistance, WAT inflammation, and fat mass accumulation, particularly in male mice (Wang et al., 2014; Zhang et al., 2014; Alnaeeli and Noguchi, 2015). In WAT, EPOR is highly expressed in adipocytes and primarily in macrophages in the stromal vascular fraction (Alnaeeli et al., 2014; Alnaeeli and Noguchi, 2015). EPO treatment significantly reduced the inflammation in WAT, macrophage infiltration, and crown-like structures and promoted an anti-inflammatory phenotype (Alnaeeli et al., 2014). EPO directly stimulated EPOR-expressing macrophages by activating STAT3, reducing proinflammatory gene expression and increasing IL-10 expression. The protective effect of endogenous EPO in metabolic control was demonstrated in mice with EPOR restricted to erythroid tissue (Suzuki et al., 2002). Subjected to high-fat-diet-induced obesity, these mice with similar body weight and fat mass as wild-type mice had greater glucose intolerance and insulin resistance, increased WAT inflammation and macrophage infiltration, enhanced crown-like structures, and increased inflammatory cytokine production (Alnaeeli et al., 2014). In the liver, EPO inhibited gluconeogenesis, attenuated obesity-related inflammatory cytokine expression and production of TNF-α and IL-6, reduced the activation of NFκB and inflammatory signaling, and enhanced insulin-related PI3K signaling (Meng et al., 2013). In the pancreas, EPO exerted JAK2-dependent protective effects in pancreatic β-cells and induced proliferative, anti-inflammatory, and angiogenic activity within the islets in diabetic mouse models (Choi et al., 2010).

The expansion of adipose tissue requires increased adipose tissue vasculature to maintain appropriate blood flow to supply oxygen and nutrients. A deficit in adipose tissue angiogenesis may contribute to insulin resistance and metabolic disease (Corvera and Gealekman, 2014). It has been suggested that vascular dysfunction resulting in adipose tissue hypoxia may lead to obesity-associated inflammation and occur before insulin resistance (Ye, 2011). Adipose tissue vasculature has been considered as a potential target for type 2 diabetes (Corvera and Gealekman, 2014). In retinoic acid treatment, activation of the brown fat-associated program in white adipocytes was mediated by vascular endothelial growth factor-stimulated angiogenesis (Wang et al., 2017). With exercise, vascularization in subcutaneous WAT is increased and may mediate an improved metabolic response (Min et al., 2019). EPO exhibits angiogenic and neovascularization activity in animal models (Yasuda et al., 1998; Ribatti et al., 1999; Kertesz et al., 2004; Wang et al., 2004; Li et al., 2007). EPO treatment in patients with Friedreich ataxia suggested the possibility for EPO to increase capillary density in skeletal muscle (Nachbauer et al., 2012). Further investigation is warranted to determine whether EPO treatment promotes vascularization, particularly in white adipose tissue, to contribute to a potentially beneficial metabolic response.

### Sex-Specific EPO Regulation of Fat Mass and Inflammation

Exogenous EPO treatment for 3 to 4 weeks in male, but not female, C57BL/6 mice reduced fat mass accumulation (Zhang et al., 2017). EPO treatment during high-fat-diet feeding in male mice increased the expression of genes PRDM16 and UCP1 associated with brown adipocyte differentiation in both brown fat and white fat (Wang et al., 2013; Kodo et al., 2017). This sex-dimorphic activity of EPO fat mass regulation is attributed to the anti-obesity effect of estrogen that interferes with EPO regulation of fat mass. In contrast to acute EPO treatment, long-term EPO treatment is able to regulate fat mass and body weight in both genders. Male and female transgenic mice with chronically

increased EPO production have decreased body weight (Katz et al., 2010). Increased EPO expression by gene electrotransfer in skeletal muscle resulted in a 100-fold increase in serum EPO. By 12 weeks after the electrotransfer in female obese mice, fat mass was reduced by 28% (Hojman et al., 2009). The transfected muscle showed increased muscle volume and vascularization. However, in mice with mixed strain background, the absence of EPO receptor expression in WAT did not have any effect on adipocyte regulation (Luk et al., 2013).

The interference of estrogen with EPO regulation of fat mass was demonstrated by acute EPO treatment in ovariectomized female mice on high-fat diet that decreased fat mass accumulation, but not when combined with estradiol supplementation (Zhang et al., 2017). EPO regulation of fat mass is associated with increased activity and decreased food intake mediated by EPOR expression in non-hematopoietic tissue, especially in WAT adipocytes and in the brain (Zhang et al., 2017; Dey et al., 2020). EPOR expression in the hypothalamus arcuate nucleus localizes with proopiomelanocortin (POMC) neurons that, when stimulated, produces POMC to suppress appetite (Teng et al., 2011). EPO administration increases POMC expression in the hypothalamus and in POMC neural cell cultures (Teng et al., 2011; Dey et al., 2016). Male mice with EPOR restricted to erythroid cells exhibit increased hematocrit and reduced POMC expression, and EPO administration in these mice does not alter fat mass or POMC expression (Teng et al., 2011).

Erythropoietin is produced in the brain by astrocytes and neurons contributing to intrinsic hypoxic response (Marti et al., 1997; Bernaudin et al., 2000; Shingo et al., 2001). In animal models, a neuroprotective effect is associated with EPO activity in the brain, and EPO reduces neuronal cell death and inflammation associated with brain ischemia, with a decrease in astrocyte activation, recruitment of microglia, and proinflammatory cytokine production (Villa et al., 2003). High-fat-diet-induced obesity in mice also increases inflammation in the hypothalamus, activation of microglial cells, and inflammatory cytokine production. Hypothalamus inflammation is linked to a disruption of energy homeostasis and contributes to obesity, insulin resistance, and glucose intolerance (Jais and Bruning, 2017). Increased EPO in the brain, either by cerebral transgenic EPO expression (Tg21-mice) or by implanted EPO secreting intracerebral ventricular pump in mice, reduced fat mass accumulation during high-fat-diet feeding, reduced hypothalamus inflammation, and prevented myeloid cell recruitment to the hypothalamus in males. The unchanged hematocrit in these mice suggested an insufficient transport of EPO across the blood–brain barrier to affect EPO-stimulated erythropoiesis and showed that cerebral EPO regulation of fat mass and hypothalamus inflammation is independent of EPO-stimulated erythropoiesis (Dey et al., 2020). In contrast, deletion of *EPOR* in neural cells using the *Nestin-Cre* transgenic model showed increased weight gain, hypothalamus inflammation, and inflammatory cytokine expression in male mice, indicating that endogenous cerebral EPO also contributes to the protection against weight gain and hypothalamus inflammation during diet-induced obesity (Dey et al., 2020).

A sex-dimorphic response of cerebral EPO regulation during diet-induced obesity resulted from estrogen blocking the protective effects of EPO signaling in the brain on fat mass accumulation and hypothalamus inflammation during high-fat-diet feeding in female mice. In female ovariectomized Tg21-mice, increased EPO levels in the brain regulated body weight and hypothalamus inflammation during high-fat diet, while no such changes were evident in female non-ovariectomized Tg21-mice or in female mice with *Nestin-Cre* deletion of *EPOR* in neural cells (Dey et al., 2020). While elevated EPO improves glucose tolerance in both male and female mice, EPO regulation of fat mass accumulation and inflammation during diet-induced obesity, mediated in part *via* activity in WAT and the hypothalamus, appears to be sex specific.

## ENDOGENOUS EPO IS REQUIRED FOR BONE DEVELOPMENT

Lineage tracing studies for EPOR expression using the Epo-R-Cre and yellow fluorescent protein reporter mice showed 75% labeling efficiency of Ter119+ cells. This suggested erythroid specificity for EPOR expression in the bone marrow microenvironment, with no yellow fluorescent protein expression in hematopoietic stem cells, B-lymphoid or myeloid lineages, or mesenchymal- and osteoblastic-enriched populations (Singbrant et al., 2011). However, other reports showed that bone marrow stromal cells (BMSCs) expressed *EPOR* mRNA and EPOR protein by flow cytometry and were EPO responsive in culture, resulting in induced osteoblastic differentiation with increased mineral deposition and alkaline phosphatase activity. EPO also stimulated osteoclastogenesis of preosteoclasts in culture (Shiozawa et al., 2010; Hiram-Bab et al., 2015). EPOR expression on BMSCs, osteoblasts, and osteoclasts thus adds to the increasing select non-erythroid cells that respond to EPO, mediated *via* EPOR cell surface expression (Shiozawa et al., 2010; Hiram-Bab et al., 2015; Suresh et al., 2019a, 2020b).

Mice with EPOR restricted to erythroid tissue ($\Delta EpoR_E$), generated by rescuing the *EPOR* knockout mouse with an erythroid *EPOR* transgene driven by the *GATA1* locus hematopoietic regulatory domain, demonstrated the requirement for EPO/EPOR signaling in normal bone development (Suresh et al., 2019a). These $\Delta EpoR_E$-mice lacked EPOR expression in BMSCs and osteoblasts, and in cultures, these osteoblasts had reduced differentiation and mineralization. $\Delta EpoR_E$-mice had reduced trabecular bone and no significant changes in cortical bone, suggesting that endogenous EPO–EPOR signaling is essential for proper bone development (**Table 1**). The $\Delta EpoR_E$-mice showed excessive marrow adiposity (Suresh et al., 2019a). Enhanced marrow adipogenesis is often observed with reduced osteogenesis, suggesting an imbalance in the differentiation of BMSCs (Muruganandan et al., 2018). Ectopic ossification assays in immunodeficient mice using wild-type BMSCs with intact EPO–EPOR signaling formed ossicles with a defined outer cortical bone, interspersed with trabeculae and marrow containing hematopoietic cells and adipocytes. $\Delta EpoR_E$-BMSCs formed ossicles with a cortical bone similar to control cells but

**TABLE 1 |** Effects of erythropoietin in the bone *in vivo*.

| Type | Genetic background | Bone phenotype | Mechanism | References |
|---|---|---|---|---|
| **Transgenic animal models of EPO signaling** | | | | |
| Tg6 | Overexpression of human EPO driven by PDGF-β promoter, males and females | Trabecular bone loss, thin cortical bone, decreased marrow adiposity – femora | Increased bone resorption and reduced bone formation rate | Hiram-Bab et al., 2015; Suresh et al., 2019a |
| $\Delta EpoR_E$ | Epor−/− mice rescued by erythroid restricted EPOR transgene (GATA-1 locus hematopoietic regulatory domain driving mouse EPOR cDNA), males and females | Reduced trabecular bone, cortical bone unaffected, increased marrow adiposity – femora | Increased bone resorption with age; reduced osteogenic potential of osteoblasts | Suresh et al., 2019a |
| Mice with EPOR deletion in osteoblasts | Mice generated by crossing Osteocalcin (Bglap)-Cre mice with $Epor^{floxp/floxp}$ mice, males and females | Reduced trabecular bone, cortical bone, and marrow adiposity unaffected – femora | No change in bone resorption; reduced osteogenic potential of osteoblasts; reduced osteocytes and increased empty lacunae | Suresh et al., 2020b |
| **EPO administration in healthy animals** | | | | |
| Wild-type mice | C57BL6 strain, female | Trabecular bone loss – femora | Increased bone resorption | Hiram-Bab et al., 2015; Suresh et al., 2019a |
| Wild-type mice | C57BL6 strain, male | Trabecular bone loss – tibiae | Increase in both bone resorption and bone formation | Singbrant et al., 2011 |
| Wild-type mice | C57BL6 strain, gender unknown | Increased bone mineral density and bone volume – vertebrae | Increased osteoblasts on bone surface | Shiozawa et al., 2010 |
| $\Delta EpoR_E$ | C57BL6 background, females | No changes in trabecular or cortical bone – femora | No changes in osteoblasts or osteoclasts | Suresh et al., 2019a |
| Mice with EPOR deletion in osteoblasts | C57BL6 background, males and females | Non-significant reduction in trabecular bone in males, intact trabecular bone in females, cortical bone unaffected in both males and females – femora | No changes in osteoblasts or osteoclasts | Suresh et al., 2020b |

with reduced trabecular bone and increased marrow adipocytes. These studies conclusively showed that endogenous EPO–EPOR signaling is essential in regulating normal differentiation and the lineage commitment of BMSCs, with a specific role in the development and the maintenance of the trabecular bone.

Mice with *EPOR* deletion, specifically in mature osteoblasts, using the *Osteocalcin-Cre* system demonstrated the contribution of osteoblast direct response to EPO in bone development and remodeling (Suresh et al., 2020b). Both male and female mice had normal hematocrits and a significant reduction in trabecular bone volume, with the cortical bone unaffected (**Table 1**). The osteoprogenitors derived from calvaria had reduced differentiation and mineralization potential in cultures similar to the $\Delta EpoR_E$-mice. This study showed endogenous EPO–EPOR signaling in osteoblasts as an essential mechanism integral for the development of the trabecular bone (**Figure 1**).

## Elevated EPO in Mice Promotes Bone Remodeling Independent of EPO-Stimulated Erythropoiesis

Studies focusing on the role of EPO in bone have utilized mouse models treated with recombinant human EPO either at physiological or elevated doses for acute EPO effects or the transgenic mouse model Tg6 with constitutive overexpression of human EPO to explore the chronic effects of elevated EPO (Singbrant et al., 2011; Hiram-Bab et al., 2015; Suresh et al., 2019a). Modulation of endogenous EPO signaling in mice with Von Hippel–Lindau (VHL) mutation in osteoblasts caused an increase in hypoxia inducible factor-1/2 (HIF), resulting in elevated EPO production in osteoblasts and polycythemia (Rankin et al., 2012). In these mice, even with significant expansion of erythropoiesis, trabecular bone volume was increased. The targeted deletion of prolyl hydroxylase (PHD) in osteoblasts also induced osteoblast production of EPO and increased hematocrit, demonstrating that manipulation of the PHD/VHL/HIF pathway in osteoblasts in mice alters endogenous EPO production, elevates hematocrit, and affects bone formation. In contrast, mice with deletion of VHL, HIF-1, and HIF-2 in osteoblasts exhibited reduced EPO levels and low trabecular bone volume, with HIF-2 being the critical HIF-regulating EPO in bone (Rankin et al., 2012). In mice with PHD2 deletion in renal cells, macrophages, neural cells, and astrocytes, there was a significant reduction of bone volume due to reduced bone formation (Rauner et al., 2016). Increased EPO levels were observed in mice with PHD2 deletion, and the conditional deletion of HIF-2α in this model rescued the loss of bone. These mice exhibit increased hematocrits and elevated EPO; however, the high levels of EPO did not increase osteoclast differentiation or drive bone resorption as seen in the Tg6 mouse model, which also has chronically elevated EPO (Hiram-Bab et al., 2015). PHD2 deletion specifically in osteoblasts, however, increased bone density by reducing osteoclasts, showing that the loss of PHD2 in osteoblasts is not essential for bone reduction (Rauner et al., 2016).

The effects of elevated EPO in bone metabolism appear controversial as EPO treatment has resulted in a gain in bone density and volume in some models while reducing bone in others, suggesting a context-dependent role for EPO in bone remodeling (Hiram-Bab et al., 2017; Suresh et al., 2019b).

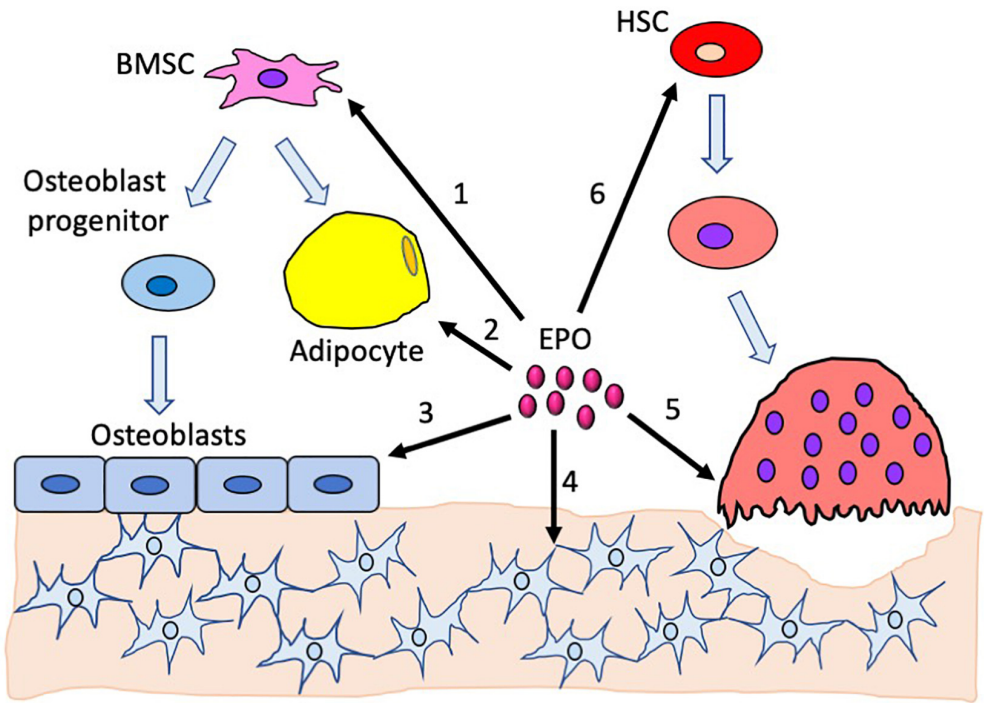


**FIGURE 1 |** Effects of erythropoietin in the bone and the bone marrow compartment. 1. Endogenous EPO regulates bone marrow stromal cell differentiation to adipocytes and osteoblasts. 2. Increased EPO decreases bone marrow adipocytes. 3. EPO directly regulates osteoblast differentiation; the absence of EPO signaling in osteoblasts reduces their differentiation potential. Elevated EPO has a dose-dependent effect on osteoblasts, with low-dose EPO reducing differentiation and high-dose EPO increasing differentiation. 4. Absence of EPO signaling in mature osteoblasts reduces osteocytes, resulting in empty lacunae. 5. High EPO stimulates differentiation of preosteoclasts into osteoclasts. 6. EPO stimulates hematopoietic stem cells which, in turn, promotes both osteoblast and osteoclast differentiation.

In animal models of bone fracture, EPO treatment significantly accelerated bone healing (Holstein et al., 2007; Mihmanli et al., 2009; Rolfing et al., 2014b; Omlor et al., 2016). The process of new bone formation occurs in two ways: by endochondral ossification, where cartilage is replaced by bone tissue as seen in long bones, or by intramembranous ossification, where mesenchyme is converted to osteoblasts as seen in the formation of flat bones like the skull and the clavicle (Breeland et al., 2019). Studies done in murine fracture models showed that EPO administration promotes endochondral ossification and aids in the healing process. In cranial bone fracture models where the bone is usually repaired by intramembranous ossification, EPO administration along with bone morphogenetic protein 2 (BMP2) resulted in new bone formation by endochondral process along with increased angiogenesis possibly mediated by EPO (Sun et al., 2012). The HIF signaling pathway has also been shown to be important in EPO-stimulated repair of osteonecrosis in rat models, as EPO administration increased the expression of alkaline phosphatase, HIF-1α, runt-related transcription factor 2, and vascular endothelial growth factor (Li et al., 2018).

While EPO primarily regulates red blood cell production, most of the studies with EPO administration in healthy mouse models of different ages show a reduction in bone volume accompanying the increase in hematocrit (Singbrant et al., 2011; Hiram-Bab et al., 2015; Suresh et al., 2019a). However, in contrast to these reports, another study reported an increase in bone formation in the vertebrae of both newborn and 4–6-week-old mice receiving supraphysiological doses of EPO with a modest increase in hematocrits (Shiozawa et al., 2010; **Table 1**). Unlike EPO regulation of fat mass and inflammation associated with diet-induced obesity, EPO-stimulated bone loss in mice does not appear to exhibit gender bias. Chronic exposure of EPO severely disrupts bone microarchitecture as demonstrated by Tg6-mice expressing a high level of transgenic human EPO (Hiram-Bab et al., 2015). Tg6-mice show reduced trabecular bone, cortical bone mineral density, cortical bone volume (Oikonomidou et al., 2016; Suresh et al., 2019a), and thickness (Hiram-Bab et al., 2015; **Table 1**). Excess EPO in these mice reduces osteoblast-dependent mineral apposition and bone formation rate while simultaneously increasing the osteoclast numbers (Hiram-Bab et al., 2015). BMSCs from Tg6-mice had high EPO expression and, in ectopic ossification assays in immunodeficient mice, formed markedly reduced ossicles without a defined structure or significant bone or adipocytes (Suresh et al., 2019a). The direct effects of EPO on BMSCs were shown using culture studies, where adding EPO less than 5 U/ml to primary mouse BMSC cultures inhibited osteogenic differentiation, while elevated doses of EPO between 50 and 250 U/ml increased their osteogenic differentiation potential (Rauner et al., 2016). Osteogenic differentiation assays of BMSCs in the presence of EPO have been reported to activate EphrinB2/EphrinB4 (Li et al., 2015) mTOR (Kim et al., 2012) and JAK2/PI3K pathways (Rolfing et al., 2014a). In BMSC cultures

and *in vivo*, the administration of EPO increased BMP2 expression in hematopoietic stem cells, which have been suggested to increase osteoclasts initially, followed by a rise in osteoblast numbers (Shiozawa et al., 2010). Wnt signaling has been proposed to mediate EPO effects in non-hematopoietic cells. Endothelial cell cultures exposed to elevated glucose suggested that EPO cytoprotection was mediated *via* Wnt1 and inhibition of glycogen synthase kinase activity (Chong et al., 2007). This led to the suggestion of potential application of EPO and Wnt signaling for the prevention of neurovascular injury associated with diabetes mellitus (Maiese, 2008). In human bone marrow-derived mesenchymal stem cell cultures, EPO induced neurogenic differentiation, especially at reduced oxygen, and stimulated increased Wnt3a- and Wnt3a-mediated EPO neuroprotection against glutamate toxicity (Danielyan et al., 2009). Wnt signaling was also shown to mediate the EPO-stimulated differentiation of mesenchymal stromal cells to osteoblasts. In cultures of human bone marrow mesenchymal stromal cells from young donors, EPO stimulated osteoblast-specific gene expression and osteoblast mineralization, but not in cultures from patients with myelodysplastic syndromes and old healthy donors that exhibited a reduced expression of genes associated with the canonical Wnt pathway. Activation of the Wnt pathway in these cells restored EPO-associated osteoblast differentiation (Balaian et al., 2018).

The polycythemia mouse model with JAK2 V617F mutation in hematopoietic cells gives rise to constitutively active EPOR, low EPO concentrations in the serum, low trabecular bone volume, and reduced osteoblast number (Oikonomidou et al., 2016). Thus, both low and elevated EPO or EPOR activation impaired osteoblast differentiation and function. In patients with thalassemia, low bone mass developing into osteoporosis is a common complication due to a myriad of factors like excess ineffective erythropoiesis, iron overload, or endocrine dysfunction seen during the disease (Wong et al., 2016). A mouse model of β-thalassemia major *th3* has high serum EPO levels (Rivella et al., 2003), reduced trabecular bone volume, and thin cortical bone (Vogiatzi et al., 2010). These mice provide examples of increased EPO or EPOR signaling, resulting in increased erythropoiesis and decreased bone formation or bone loss. However, while exogenous EPO administration increased hematocrit in $\Delta EpoR_E$-mice, there was no accompanying reduction in trabecular bone (Suresh et al., 2019a), suggesting that EPO-stimulated bone loss is mediated by non-hematopoietic response and independent of increased erythropoiesis. In female mice lacking EPOR signaling in osteoblasts, exogenous EPO administration did not reduce trabecular bone volume, while in male mice a similar treatment resulted in only a trend for reduced trabeculae (Suresh et al., 2020b; **Table 1**). These findings show that bone loss during EPO-stimulated erythropoiesis is mediated in part by direct EPO–EPOR signaling in osteoblasts.

## EPO-Mediated Bone Remodeling *Via* Osteoclast-Dependent Mechanisms

In cocultures of bone marrow monocytes and calvarial osteoblasts, addition of both EPO and erythroblasts did not stimulate osteoclast differentiation (Singbrant et al., 2011). However, in bone marrow-derived cultures, EPO did not affect preosteoclast proliferation but increased osteoclast differentiation *via* JAK2 and PI3K pathways (Hiram-Bab et al., 2015). EPO stimulated osteoclastogenesis in culture even at a low dose (Hiram-Bab et al., 2017). Other studies using bone marrow-derived cultures showed that EPO increased the osteoclast numbers, but not activity (Shiozawa et al., 2010). An osteoclast differentiation assay of RAW264.7 mouse monocyte/macrophage cell line similarly shows that EPO increased the osteoclast numbers, but not osteoclast activity (Li et al., 2015). It was suggested that EPO contributes to the communication between differentiation of osteoclasts and osteoblasts through the EphrinB2/EphrinB4 signaling pathway and increases the number of EphrinB2-expressing osteoclasts and EphrinB4 expression in ST2 stromal cells to promote osteoblastic differentiation that may play a role in bone formation (Li et al., 2015). EPO-stimulated osteoclastogenesis in bone marrow mononuclear cell cultures and RAW264.7 cells was mTOR signaling dependent, but the increased expression of the master transcription regulator of osteoclast differentiation NFATC1 in EPO-treated osteoclasts was independent of mTOR signaling in RAW264.7 cells (Kim et al., 2012; Kim and Kim, 2014).

Bone loss with elevated EPO has been associated with EPO-stimulated osteoclastogenesis (Hiram-Bab et al., 2015). Tg6-mice with elevated EPO have an increased bone marrow preosteoclast number, with 25% more osteoclasts per bone surface, and increased serum levels of bone resorption marker TRAP5b. Increased preosteoclast and osteoclast numbers and TRAP5b serum levels were also observed with EPO treatment in wild-type mice (Singbrant et al., 2011; Hiram-Bab et al., 2015). The increase in osteoclasts in mice with EPO stimulation has been reported to be dependent on the duration of EPO exposure, as a 2-week EPO administration increased the osteoclasts which appeared to decline with two more weeks of EPO treatment (Shiozawa et al., 2010). HIF signaling has also been shown to be important in osteoclast function. Inactivation of PHD in osteoblasts, leading to the specific activation of HIF-1α, has been associated with an increased production of osteoprotegerin, which blocks RANKL and RANK interaction to limit osteoclast differentiation (Shao et al., 2015), and increased interleukin-33 to reduce bone marrow-derived monocyte osteoclastic differentiation (Kang et al., 2017). Since PHD inactivation in osteoblasts increased HIF-2α and EPO (Rankin et al., 2012), these observations suggest that hypoxia induction of EPO may also restrict the expansion of osteoclastogenesis in support of other osteoclast-independent mechanisms contributing to EPO-stimulated bone loss.

## EPO-Mediated Bone Loss *Via* Osteoclast-Independent Mechanisms

Studies on the role of EPO signaling in osteoclasts showed elevated EPO directly stimulating osteoclasts in C57BL6/J mice treated with EPO and in Tg6-mice with chronically elevated EPO resulting in bone loss (Hiram-Bab et al., 2015). However, other studies observed reduction in bone volume but without an increase in osteoclast activity in C57BL/6 mice given exogenous EPO (Suresh et al., 2019a) or in C57BL/6 mice transplanted with bone marrow from Tg6-mice to induce

polycythemia (Oikonomidou et al., 2016). The polycythemia $JAK2^{V617F}$ mouse model with constitutively active EPOR has reduced bone and normal osteoclast numbers (Oikonomidou et al., 2016). β-Thalassemia major *th3* mouse model with high serum EPO and reduced bone exhibits decreased bone formation and resorption, suggesting overall reduction in bone remodeling (Rivella et al., 2003). The reduced osteoclast numbers in these mice show that elevated EPO stimulating osteoclasts is not always required for bone loss.

$\Delta EpoR_E$-mice were developed for erythroid-restricted expression of EPOR (Suzuki et al., 2002), but the presence of *GATA1* hematopoietic regulatory domain in the preosteoclasts results in EPOR expression in these cells (Suresh et al., 2019a). The presence of EPO–EPOR signaling in osteoclasts and its absence in other key bone regulatory cells like BMSCs and osteoblasts led to some interesting observations of endogenous EPO signaling in osteoclasts depending on the age of the mice. As $\Delta EpoR_E$-mice age, accumulation of excess fat mass due to the absence of endogenous EPO signaling in WAT results in increased systemic inflammation (Teng et al., 2011). The body weight of young $\Delta EpoR_E$-mice (8 weeks) was comparable to that of wild-type mice, and these young $\Delta EpoR_E$-mice did not have any increase in osteoclasts on their bone surface. However, at this age, these mice have a reduced trabecular number with increased spacing, indicating an early disruption of trabecular microarchitecture, but bone mineral density and volume were unaffected (Suresh et al., 2019a). By 11 weeks of age, $\Delta EpoR_E$-mice gain substantial body weight due to increased body fat mass and have about 40% reduction in trabecular bone volume and increased osteoclasts, in both male and female mice. Thus, in young $\Delta EpoR_E$-mice, reduction in bone is an osteoclast-independent mechanism. This study shows that dysregulation of WAT stemming from lack of EPO signaling results in inflammation and increased osteoclastogenesis with age, which adversely affects the bone.

## EPO Administration and Bone Remodeling in Mice on High-Fat Diet

In mice, the effects of EPO signaling in the bone have been largely studied in the trabecular bone compartment which comprises 20% of bone mass and is interspersed with bone marrow and adipocytes, with a higher remodeling rate than the cortical bone (Singbrant et al., 2011; Hiram-Bab et al., 2015; Suresh et al., 2019a). The cortical bone is stiffer but brittle and is essential for maintaining structure and mechanical loading (Ott, 2018). In C57BL/6J mice fed a high-fat diet, EPO administration showed distinct effects in trabecular and cortical bone compartments (Suresh et al., 2020a). On regular chow diet, daily EPO administration for 10 days reduced the trabecular bone and the cortical bone volumes, with a reduction of cortical bone osteocytes and periosteal osteoblasts surrounding the cortical bone (Suresh et al., 2019a). In contrast, the cortical bone in mice on high-fat diet was unaffected by EPO administration, but excessive marrow fat accumulation in these mice was completely abrogated by EPO administration. High-fat-diet feeding increased the osteoclast numbers but was not further increased with EPO treatment (Suresh et al., 2020a). Therefore, EPO-induced reduction of bone can affect various types of cells in the bone and marrow compartment under different dietary conditions.

# CONCLUSION

Studies in animal models show that, beyond stimulating erythropoiesis, EPO can also regulate fat mass and monocyte–macrophage-derived cell response in obesity-associated inflammation and bone remodeling. The potential for EPO to regulate fat mass and the increase in EPO production at high altitude may contribute to the lower obesity rate observed in humans residing at a high altitude (Voss et al., 2014; Diaz-Gutierrez et al., 2016). Sex-dimorphic EPO response is related to estrogen in female mice, which interferes with EPO protective activity in fat mass regulation and obesity-related inflammation. The relationship between EPO and body weight in humans is suggested in a subset analysis of full-heritage Pima Indians with a high prevalence of obesity and type 2 diabetes. This study showed that endogenous plasma EPO negatively associated with percent weight change per year in males, while the females exhibited a positive association (Reinhardt et al., 2016). In the bone, EPO activity is mediated *via* osteoclast-dependent and osteoclast-independent mechanisms and can affect bone healing or stimulate bone loss with increased erythropoiesis (**Figure 1**). Wild-type mice with EPO administration exhibit both increased erythropoiesis and bone loss, while mouse models with EPOR deletion, either in non-hematopoietic cells or specifically in osteoblasts, have increased erythropoiesis but no accompanying bone loss. Consistent with EPO promoting bone healing in animal models of fracture, a pilot study in 60 patients with tibiofibular factures who received either EPO or saline showed patients in the EPO receiving arm having faster union rates by a couple of weeks and reduced nonunion fracture (Bakhshi et al., 2013). However, in a recent study, high EPO level was also associated with higher fracture risk independent of hemoglobin and age in elderly Swedish men (Kristjansdottir et al., 2020), suggesting that, as observed in mice, EPO may also affect bone homeostasis, and chronic EPO treatment may impact on bone health. EPO stimulated FGF23 production in mouse and human, increasing serum FGF23 and reducing serum phosphate, and may contribute to elevated FGF23 in chronic kidney disease patients receiving EPO (Clinkenbeard et al., 2017). Increased FGF23 in response to EPO administration has been suggested as a possible mechanism of EPO-induced bone reduction associated with disrupted mineralization (Clinkenbeard et al., 2017). EPOR expression in non-erythroid tissues, including BMSCs, adipocytes, osteoblasts and osteoclasts, contributes to EPO activity independent of erythropoiesis that regulates bone formation and bone marrow microenvironment (Suresh et al., 2019a, 2020b). These activities demonstrated in animal models suggest that, while some non-hematopoietic EPO responses may be protective, bone health may be adversely affected with chronic EPO treatment such as that associated with chronic kidney disease.

## AUTHOR CONTRIBUTIONS

SS, JL, and CN contributed to the planning, writing, and editing of this manuscript. All authors contributed to the article and approved the submitted version.

## FUNDING

This work was supported by the Intramural Research Program of the National Institute of Diabetes and Digestive and Kidney Diseases at the National Institutes of Health.

## REFERENCES

Adamopoulos, I. E. (2018). Inflammation in bone physiology and pathology. *Curr. Opin. Rheumatol.* 30, 59–64. doi: 10.1097/bor.0000000000000449

Alnaeeli, M., and Noguchi, C. T. (2015). Erythropoietin and obesity-induced white adipose tissue inflammation: redefining the boundaries of the immunometabolism territory. *Adipocyte* 4, 153–157. doi: 10.4161/21623945.2014.978654

Alnaeeli, M., Raaka, B. M., Gavrilova, O., Teng, R., Chanturiya, T., and Noguchi, C. T. (2014). Erythropoietin signaling: a novel regulator of white adipose tissue inflammation during diet-induced obesity. *Diabetes* 63, 2415–2431. doi: 10.2337/db13-0883

Bakhshi, H., Kazemian, G., Emami, M., Nemati, A., Karimi Yarandi, H., and Safdari, F. (2013). Local erythropoietin injection in tibiofibular fracture healing. *Trauma. Mon.* 17, 386–388. doi: 10.5812/traumamon.7099

Balaian, E., Wobus, M., Weidner, H., Baschant, U., Stiehler, M., and Ehninger, G. (2018). Erythropoietin inhibits osteoblast function in myelodysplastic syndromes via the canonical Wnt pathway. *Haematologica* 103, 61–68. doi: 10.3324/haematol.2017.172726

Bernaudin, M., Bellail, A., Marti, H. H., Yvon, A., Vivien, D., Duchatelle, I., et al. (2000). Neurons and astrocytes express EPO mRNA: oxygen-sensing mechanisms that involve the redox-state of the brain. *Glia* 30, 271–278. doi: 10.1002/(sici)1098-1136(200005)30:3<271::aid-glia6>3.0.co;2-h

Breeland, G., Sinkler, M. A., and Menezes, R. G. (2019). *Embryology, Bone Ossification*. Treasure Island, FL: StatPearls Publishing.

Choi, D., Schroer, S. A., Lu, S. Y., Wang, L., Wu, X., Liu, Y., et al. (2010). Erythropoietin protects against diabetes through direct effects on pancreatic beta cells. *J. Exp. Med.* 207, 2831–2842. doi: 10.1084/jem.20100665

Chong, Z. Z., Shang, Y. C., and Maiese, K. (2007). Vascular injury during elevated glucose can be mitigated by erythropoietin and Wnt signaling. *Curr. Neurovasc. Res.* 4, 194–204. doi: 10.2174/156720207781387150

Clinkenbeard, E. L., Hanudel, M. R., Stayrook, K. R., Appaiah, H. N., Farrow, E. G., and Cass, T. A. (2017). Erythropoietin stimulates murine and human fibroblast growth factor-23, revealing novel roles for bone and bone marrow. *Haematologica* 102, 427–430e.

Corvera, S., and Gealekman, O. (2014). Adipose tissue angiogenesis: impact on obesity and type-2 diabetes. *Biochim. Biophys. Acta* 1842, 463–472. doi: 10.1016/j.bbadis.2013.06.003

Danielyan, L., Schafer, R., Schulz, A., Ladewig, T., Lourhmati, A., and Buadze, M. (2009). Survival, neuron-like differentiation and functionality of mesenchymal stem cells in neurotoxic environment: the critical role of erythropoietin. *Cell Death Differ.* 16, 1599–1614. doi: 10.1038/cdd.2009.95

Dey, S., Cui, Z., Gavrilova, O., Zhang, X., Gassmann, M., and Noguchi, C. T. (2020). Sex-specific brain erythropoietin regulation of mouse metabolism and hypothalamic inflammation. *JCI Insight* 5:e134061.

Dey, S., Li, X., Teng, R., Alnaeeli, M., Chen, Z., Rogers, H., et al. (2016). Erythropoietin regulates POMC expression via STAT3 and potentiates leptin response. *J. Mol. Endocrinol.* 56, 55–67. doi: 10.1530/jme-15-0171

Diaz-Gutierrez, J., Martinez-Gonzalez, M. A., Pons Izquierdo, J. J., Gonzalez-Muniesa, P., Martinez, J. A., and Bes-Rastrollo, M. (2016). Living at Higher Altitude and Incidence of Overweight/Obesity: Prospective Analysis of the SUN Cohort. *PLoS One* 11:e0164483. doi: 10.1371/journal.pone.0164483

Hiram-Bab, S., Liron, T., Deshet-Unger, N., Mittelman, M., Gassmann, M., Rauner, M., et al. (2015). Erythropoietin directly stimulates osteoclast precursors and induces bone loss. *FASEB J.* 29, 1890–1900. doi: 10.1096/fj.14-259085

Hiram-Bab, S., Neumann, D., and Gabet, Y. (2017). Context-Dependent Skeletal Effects of Erythropoietin. *Vitam. Horm.* 105, 161–179. doi: 10.1016/bs.vh.2017.02.003

Hojman, P., Brolin, C., Gissel, H., Brandt, C., Zerahn, B., Pedersen, B. K., et al. (2009). Erythropoietin over-expression protects against diet-induced obesity in mice through increased fat oxidation in muscles. *PLoS One* 4:e5894. doi: 10.1371/journal.pone.0005894

Holstein, J. H., Menger, M. D., Scheuer, C., Meier, C., Culemann, U., Wirbel, R. J., et al. (2007). Erythropoietin (EPO): EPO-receptor signaling improves early endochondral ossification and mechanical strength in fracture healing. *Life Sci.* 80, 893–900. doi: 10.1016/j.lfs.2006.11.023

Jais, A., and Bruning, J. C. (2017). Hypothalamic inflammation in obesity and metabolic disease. *J. Clin. Invest.* 127, 24–32. doi: 10.1172/jci88878

Kang, H., Yang, K., Xiao, L., Guo, L., Guo, C., and Yan, Y. (2017). Osteoblast Hypoxia-Inducible Factor-1alpha Pathway Activation Restrains Osteoclastogenesis via the Interleukin-33-MicroRNA-34a-Notch1 Pathway. *Front. Immunol.* 8:1312. doi: 10.3389/fimmu.2017.01312

Katz, O., Stuible, M., Golishevski, N., Lifshitz, L., Tremblay, M. L., Gassmann, M., et al. (2010). Erythropoietin treatment leads to reduced blood glucose levels and body mass: insights from murine models. *J. Endocrinol.* 205, 87–95. doi: 10.1677/joe-09-0425

Kertesz, N., Wu, J., Chen, T. H., Sucov, H. M., and Wu, H. (2004). The role of erythropoietin in regulating angiogenesis. *Dev .Biol.* 276, 101–110. doi: 10.1016/j.ydbio.2004.08.025

Kim, J. H., and Kim, N. (2014). Regulation of NFATc1 in Osteoclast Differentiation. *J. Bone Metab.* 21, 233–241. doi: 10.11005/jbm.2014.21.4.233

Kim, J., Jung, Y., Sun, H., Joseph, J., Mishra, A., Shiozawa, Y., et al. (2012). Erythropoietin mediated bone formation is regulated by mTOR signaling. *J. Cell Biochem.* 113, 220–228. doi: 10.1002/jcb.23347

Kodo, K., Sugimoto, S., Nakajima, H., Mori, J., Itoh, I., Fukuhara, S., et al. (2017). Erythropoietin (EPO) ameliorates obesity and glucose homeostasis by promoting thermogenesis and endocrine function of classical brown adipose tissue (BAT) in diet-induced obese mice. *PLoS One* 12:e0173661. doi: 10.1371/journal.pone.0173661

Kristjansdottir, H. L., Lewerin, C., Lerner, U. H., Herlitz, H., Johansson, P., and Johansson, H. (2020). High Plasma Erythropoietin Predicts Incident Fractures in Elderly Men with Normal Renal Function: The MrOS Sweden Cohort. *J. Bone Miner. Res.* 35, 298–305. doi: 10.1002/jbmr.3900

Kubatzky, K. F., Uhle, F., and Eigenbrod, T. (2018). From macrophage to osteoclast - How metabolism determines function and activity. *Cytokine* 112, 102–115. doi: 10.1016/j.cyto.2018.06.013

Lauterbach, M. A., and Wunderlich, F. T. (2017). Macrophage function in obesity-induced inflammation and insulin resistance. *Pflugers Arch.* 469, 385–396. doi: 10.1007/s00424-017-1955-5

Li, C., Shi, C., Kim, J., Chen, Y., Ni, S., Jiang, L., et al. (2015). Erythropoietin promotes bone formation through EphrinB2/EphB4 signaling. *J. Dent. Res.* 94, 455–463. doi: 10.1177/0022034514566431

Li, D., Hu, Q., Tan, G., Xie, X., Yang, Z., and Kang, P. (2018). Erythropoietin Enhances Bone Repair Effects via the Hypoxia-Inducible Factor Signal Pathway in Glucocorticoid-Induced Osteonecrosis of the Femoral Head. *Am. J. Med. Sci.* 355, 597–606. doi: 10.1016/j.amjms.2018.03.010

Li, Y., Lu, Z., Keogh, C. L., Yu, S. P., and Wei, L. (2007). Erythropoietin-induced neurovascular protection, angiogenesis, and cerebral blood flow restoration after focal ischemia in mice. *J. Cereb Blood Flow Metab.* 27, 1043–1054. doi: 10.1038/sj.jcbfm.9600417

Luk, C. T., Shi, S. Y., Choi, D., Cai, E. P., Schroer, S. A., and Woo, M. (2013). In vivo knockdown of adipocyte erythropoietin receptor does not alter glucose or energy homeostasis. *Endocrinology* 154, 3652–3659. doi: 10.1210/en.2013-1113

Lumeng, C. N., Bodzin, J. L., and Saltiel, A. R. (2007). Obesity induces a phenotypic switch in adipose tissue macrophage polarization. *J. Clin. Invest.* 117, 175–184. doi: 10.1172/jci29881

Maiese, K. (2008). Triple play: promoting neurovascular longevity with nicotinamide, WNT, and erythropoietin in diabetes mellitus. *Biomed. Pharmacother.* 62, 218–232. doi: 10.1016/j.biopha.2008.01.009

Marti, H. H., Gassmann, M., Wenger, R. H., Kvietikova, I., Morganti-Kossmann, M. C., Kossmann, T., et al. (1997). Detection of erythropoietin in human liquor: intrinsic erythropoietin production in the brain. *Kidney Int.* 51, 416–418. doi: 10.1038/ki.1997.55

Meng, R., Zhu, D., Bi, Y., Yang, D., and Wang, Y. (2013). Erythropoietin inhibits gluconeogenesis and inflammation in the liver and improves glucose intolerance in high-fat diet-fed mice. *PLoS One* 8:e53557. doi: 10.1371/journal.pone.0053557

Mihmanli, A., Dolanmaz, D., Avunduk, M. C., and Erdemli, E. (2009). Effects of recombinant human erythropoietin on mandibular distraction osteogenesis. *J. Oral. Maxillofac. Surg.* 67, 2337–2343. doi: 10.1016/j.joms.2008.06.082

Min, S. Y., Learnard, H., Kant, S., Gealikman, O., Rojas-Rodriguez, R., DeSouza, T., et al. (2019). Exercise Rescues Gene Pathways Involved in Vascular Expansion and Promotes Functional Angiogenesis in Subcutaneous White Adipose Tissue. *Int. J. Mol. Sci.* 20:2046. doi: 10.3390/ijms20082046

Muruganandan, S., Govindarajan, R., and Sinal, C. J. (2018). Bone Marrow Adipose Tissue and Skeletal Health. *Curr. Osteoporos Rep.* 16, 434–442. doi: 10.1007/s11914-018-0451-y

Nachbauer, W., Boesch, S., Reindl, M., Eigentler, A., Hufler, K., Poewe, W., et al. (2012). Skeletal muscle involvement in friedreich ataxia and potential effects of recombinant human erythropoietin administration on muscle regeneration and neovascularization. *J. Neuropathol. Exp. Neurol.* 71, 708–715. doi: 10.1097/nen.0b013e31825fed76

Oikonomidou, P. R., Casu, C., Yang, Z., Crielaard, B., Shim, J. H., Rivella, S., et al. (2016). Polycythemia is associated with bone loss and reduced osteoblast activity in mice. *Osteoporos. Int.* 27, 1559–1568. doi: 10.1007/s00198-015-3412-7

Omlor, G. W., Kleinschmidt, K., Gantz, S., Speicher, A., Guehring, T., and Richter, W. (2016). Increased bone formation in a rabbit long-bone defect model after single local and single systemic application of erythropoietin. *Acta Orthop.* 87, 425–431. doi: 10.1080/17453674.2016.1198200

Ott, S. M. (2018). Cortical or Trabecular Bone: What's the Difference? *Am. J. Nephrol.* 47, 373–375. doi: 10.1159/000489672

Rankin, E. B., Wu, C., Khatri, R., Wilson, T. L., Andersen, R., Araldi, E., et al. (2012). The HIF signaling pathway in osteoblasts directly modulates erythropoiesis through the production of EPO. *Cell* 149, 63–74. doi: 10.1016/j.cell.2012.01.051

Rauner, M., Franke, K., Murray, M., Singh, R. P., Hiram-Bab, S., Platzbecker, U., et al. (2016). Increased EPO Levels Are Associated With Bone Loss in Mice Lacking PHD2 in EPO-Producing Cells. *J. Bone Miner. Res.* 31, 1877–1887. doi: 10.1002/jbmr.2857

Reinhardt, M., Dey, S., Tom Noguchi, C., Zhang, Y., Krakoff, J., and Thearle, M. S. (2016). Non-hematopoietic effects of endogenous erythropoietin on lean mass and body weight regulation. *Obesity* 24, 1530–1536. doi: 10.1002/oby.21537

Ribatti, D., Presta, M., Vacca, A., Ria, R., Giuliani, R., Dell'Era, P., et al. (1999). Human erythropoietin induces a pro-angiogenic phenotype in cultured endothelial cells and stimulates neovascularization in vivo. *Blood* 93, 2627–2636. doi: 10.1182/blood.v93.8.2627.408k21_2627_2636

Rivella, S., May, C., Chadburn, A., Riviere, I., and Sadelain, M. (2003). A novel murine model of Cooley anemia and its rescue by lentiviral-mediated human beta-globin gene transfer. *Blood* 101, 2932–2939. doi: 10.1182/blood-2002-10-3305

Rolfing, J. H., Baatrup, A., Stiehler, M., Jensen, J., Lysdahl, H., and Bunger, C. (2014a). The osteogenic effect of erythropoietin on human mesenchymal stromal cells is dose-dependent and involves non-hematopoietic receptors and multiple intracellular signaling pathways. *Stem Cell Rev. Rep.* 10, 69–78. doi: 10.1007/s12015-013-9476-x

Rolfing, J. H., Jensen, J., Jensen, J. N., Greve, A. S., Lysdahl, H., Chen, M., et al. (2014b). A single topical dose of erythropoietin applied on a collagen carrier enhances calvarial bone healing in pigs. *Acta Orthop.* 85, 201–209. doi: 10.3109/17453674.2014.889981

Shao, J., Zhang, Y., Yang, T., Qi, J., Zhang, L., and Deng, L. (2015). HIF-1alpha disturbs osteoblasts and osteoclasts coupling in bone remodeling by up-regulating OPG expression. *Vitro. Cell Dev. Biol. Anim.* 51, 808–814. doi: 10.1007/s11626-015-9895-x

Shingo, T., Sorokan, S. T., Shimazaki, T., and Weiss, S. (2001). Erythropoietin regulates the in vitro and in vivo production of neuronal progenitors by mammalian forebrain neural stem cells. *J. Neurosci.* 21, 9733–9743. doi: 10.1523/jneurosci.21-24-09733.2001

Shiozawa, Y., Jung, Y., Ziegler, A. M., Pedersen, E. A., Wang, J., Wang, Z., et al. (2010). Erythropoietin couples hematopoiesis with bone formation. *PLoS One* 5:e10853. doi: 10.1371/journal.pone.0010853

Sinder, B. P., Pettit, A. R., and McCauley, L. K. (2015). Macrophages: Their Emerging Roles in Bone. *J. Bone Miner. Res.* 30, 2140–2149. doi: 10.1002/jbmr.2735

Singbrant, S., Russell, M. R., Jovic, T., Liddicoat, B., Izon, D. J., Purton, L. E., et al. (2011). Erythropoietin couples erythropoiesis, B-lymphopoiesis, and bone homeostasis within the bone marrow microenvironment. *Blood* 117, 5631–5642. doi: 10.1182/blood-2010-11-320564

Soliz, J., Khemiri, H., Caravagna, C., and Seaborn, T. (2012). Erythropoietin and the sex-dimorphic chemoreflex pathway. *Adv. Exp. Med. Biol.* 758, 55–62. doi: 10.1007/978-94-007-4584-1_8

Sun, H., Jung, Y., Shiozawa, Y., Taichman, R. S., and Krebsbach, P. H. (2012). Erythropoietin modulates the structure of bone morphogenetic protein 2-engineered cranial bone. *Tissue Eng. Part A* 18, 2095–2105. doi: 10.1089/ten.tea.2011.0742

Suresh, S., Alvarez, J. C., Dey, S., and Noguchi, C. T. (2020a). Erythropoietin-Induced Changes in Bone and Bone Marrow in Mouse Models of Diet-Induced Obesity. *Int. J. Mol. Sci.* 21:1657. doi: 10.3390/ijms21051657

Suresh, S., de Castro, L. F., Dey, S., Robey, P. G., and Noguchi, C. T. (2019a). Erythropoietin modulates bone marrow stromal cell differentiation. *Bone Res.* 7:21.

Suresh, S., Lee, J., and Noguchi, C. T. (2020b). Erythropoietin signaling in osteoblasts is required for normal bone formation and for bone loss during erythropoietin-stimulated erythropoiesis. *FASEB J.* 00, 1–13. doi: 10.1016/s8756-3282(02)00716-0

Suresh, S., Rajvanshi, P. K., and Noguchi, C. T. (2019b). The Many Facets of Erythropoietin Physiologic and Metabolic Response. *Front. Physiol.* 10:1534. doi: 10.3389/fphys.2019.01534

Suzuki, N., Ohneda, O., Takahashi, S., Higuchi, M., Mukai, H. Y., Nakahata, T., et al. (2002). Erythroid-specific expression of the erythropoietin receptor rescued its null mutant mice from lethality. *Blood* 100, 2279–2288. doi: 10.1182/blood-2002-01-0124

Teng, R., Gavrilova, O., Suzuki, N., Chanturiya, T., Schimel, D., Hugendubler, L., et al. (2011). Disrupted erythropoietin signalling promotes obesity and alters hypothalamus proopiomelanocortin production. *Nat. Commun.* 2:520.

Villa, P., Bigini, P., Mennini, T., Agnello, D., Laragione, T., Cagnotto, A., et al. (2003). Erythropoietin selectively attenuates cytokine production and inflammation in cerebral ischemia by targeting neuronal apoptosis. *J. Exp. Med.* 198, 971–975. doi: 10.1084/jem.20021067

Vogiatzi, M. G., Tsay, J., Verdelis, K., Rivella, S., Grady, R. W., Doty, S., et al. (2010). Changes in bone microarchitecture and biomechanical properties in the th3 thalassemia mouse are associated with decreased bone turnover and occur during the period of bone accrual. *Calcif. Tissue Int.* 86, 484–494. doi: 10.1007/s00223-010-9365-0

Voss, J. D., Allison, D. B., Webber, B. J., Otto, J. L., and Clark, L. L. (2014). Lower obesity rate during residence at high altitude among a military population with frequent migration: a quasi experimental model for investigating spatial causation. *PLoS One* 9:e93493. doi: 10.1371/journal.pone.0093493

Wang, B., Fu, X., Liang, X., Deavila, J. M., Wang, Z., Zhao, L., et al. (2017). Retinoic acid induces white adipose tissue browning by increasing adipose vascularity and inducing beige adipogenesis of PDGFRalpha(+) adipose progenitors. *Cell Discov.* 3:17036.

Wang, L., Di, L., and Noguchi, C. T. (2014). Erythropoietin, a novel versatile player regulating energy metabolism beyond the erythroid system. *Int. J. Biol. Sci.* 10, 921–939. doi: 10.7150/ijbs.9518

Wang, L., Teng, R., Di, L., Rogers, H., Wu, H., Kopp, J. B., et al. (2013). PPARalpha and Sirt1 mediate erythropoietin action in increasing metabolic activity and browning of white adipocytes to protect against obesity and metabolic disorders. *Diabetes* 62, 4122–4131. doi: 10.2337/db13-0518

Wang, L., Zhang, Z., Wang, Y., Zhang, R., and Chopp, M. (2004). Treatment of stroke with erythropoietin enhances neurogenesis and angiogenesis and

improves neurological function in rats. *Stroke* 35, 1732–1737. doi: 10.1161/01.str.0000132196.49028.a4

Wong, P., Fuller, P. J., Gillespie, M. T., and Milat, F. (2016). Bone Disease in Thalassemia: A Molecular and Clinical Overview. *Endocr. Rev.* 37, 320–346. doi: 10.1210/er.2015-1105

Yasuda, Y., Masuda, S., Chikuma, M., Inoue, K., Nagao, M., and Sasaki, R. (1998). Estrogen-dependent production of erythropoietin in uterus and its implication in uterine angiogenesis. *J. Biol. Chem.* 273, 25381–25387. doi: 10.1074/jbc.273.39.25381

Ye, J. (2011). Adipose tissue vascularization: its role in chronic inflammation. *Curr. Diab. Rep.* 11, 203–210. doi: 10.1007/s11892-011-0183-1

Zhang, Y., Rogers, H. M., Zhang, X., and Noguchi, C. T. (2017). Sex difference in mouse metabolic response to erythropoietin. *FASEB J.* 31, 2661–2673. doi: 10.1096/fj.201601223rrr

Zhang, Y., Wang, L., Dey, S., Alnaeeli, M., Suresh, S., Rogers, H., et al. (2014). Erythropoietin action in stress response, tissue maintenance and metabolism. *Int. J. Mol. Sci.* 15, 10296–10333. doi: 10.3390/ijms150610296

**Conflict of Interest:** The authors declare that the research was conducted in the absence of any commercial or financial relationships that could be construed as a potential conflict of interest.

frontiers in Molecular Biosciences

ORIGINAL RESEARCH
published: 26 November 2020
doi: 10.3389/fmolb.2020.585056

# Osteoblast and Osteoclast Activity Affect Bone Remodeling Upon Regulation by Mechanical Loading-Induced Leukemia Inhibitory Factor Expression in Osteocytes

*Jingke Du[1†], Jiancheng Yang[2†], Zihao He[1,3†], Junqi Cui[4], Yiqi Yang[1], Mingming Xu[1], Xinhua Qu[5], Ning Zhao[6], Mengning Yan[1], Hanjun Li[1]* and Zhifeng Yu[1]**

[1] Shanghai Key Laboratory of Orthopedic Implants, Department of Orthopedic Surgery, Shanghai Ninth People's Hospital, Shanghai Jiao Tong University School of Medicine, Shanghai, China, [2] Department of Spinal Surgery, People's Hospital of Longhua Shenzhen, Shenzhen, China; School of Life Sciences, Northwestern Polytechnical University, Xi'an, China; Key Laboratory for Space Bioscience and Biotechnology, Northwestern Polytechnical University, Xi'an, China, [3] Arthritis Clinic and Research Center, Peking University People's Hospital, Peking University, Beijing, China, [4] Department of Pathology, Shanghai Ninth People's Hospital Affiliated to Shanghai Jiao Tong University School of Medicine, Shanghai, China, [5] Department of Bone and Joint Surgery, Renji Hospital, School of Medicine, Shanghai Jiao Tong University, Shanghai, China, [6] Department of Orthodontics, Shanghai Ninth People's Hospital, Shanghai Jiao Tong University School of Medicine, Shanghai, China

**Purpose:** Bone remodeling is affected by mechanical stimulation. Osteocytes are the primary mechanical load-sensing cells in the bone, and can regulate osteoblast and osteoclast activity, thus playing a key role in bone remodeling. Further, bone mass during exercise is also regulated by Leukemia inhibitory factor (LIF). This study aimed to investigate the role of LIF in the mechanical response of the bone, *in vivo* and *in vitro*, and to elucidate the mechanism by which osteocytes secrete LIF to regulate osteoblasts and osteoclasts.

**Methods:** A tail-suspension (TS) mouse model was used in this study to mimic muscular disuse. ELISA and immunohistochemistry were performed to detect bone and serum LIF levels. Micro-computed tomography (CT) of the mouse femurs was performed to measure three-dimensional bone structure parameters. Fluid shear stress (FSS) and microgravity simulation experiments were performed to study mechanical stress-induced LIF secretion and its resultant effects. Bone marrow macrophages (BMMs) and bone mesenchymal stem cells (BMSCs) were cultured to induce *in vitro* osteoclastogenesis and osteogenesis, respectively.

**Results:** Micro-CT results showed that TS mice exhibited deteriorated bone microstructure and lower serum LIF expression. LIF secretion by osteocytes was promoted by FSS and was repressed in a microgravity environment. Further experiments showed that LIF could elevate the tartrate-resistant acid phosphatase activity in BMM-derived osteoclasts through the STAT3 signaling pathway. LIF also

OPEN ACCESS

**Edited by:**
*Yankel Gabet,*
*Tel Aviv University, Israel*

**Reviewed by:**
*Przemko Tylzanowski,*
*KU Leuven, Belgium*
*Turabe M. H. U. Fazil,*
*Nanyang Technological University, Singapore*

***Correspondence:**
*Hanjun Li*
*hanjun_li@aliyun.com*
*Zhifeng Yu*
*zfyu@outlook.com*

[†] *These authors share first authorship*

**Specialty section:**
*This article was submitted to Cellular Biochemistry, a section of the journal Frontiers in Molecular Biosciences*

**Received:** *19 July 2020*
**Accepted:** *22 October 2020*
**Published:** *26 November 2020*

**Citation:**
*Du J, Yang J, He Z, Cui J, Yang Y, Xu M, Qu X, Zhao N, Yan M, Li H and Yu Z (2020) Osteoblast and Osteoclast Activity Affect Bone Remodeling Upon Regulation by Mechanical Loading-Induced Leukemia Inhibitory Factor Expression in Osteocytes. Front. Mol. Biosci. 7:585056. doi: 10.3389/fmolb.2020.585056*

enhanced alkaline phosphatase staining and osteogenesis-related gene expression during the osteogenic differentiation of BMSCs.

**Conclusion:** Mechanical loading affected LIF expression levels in osteocytes, thereby altering the balance between osteoclastogenesis and osteogenesis.

**Keywords: bone remodeling, osteocytes, leukemia inhibitory factor, osteoblasts, osteoclasts**

## INTRODUCTION

Mechanical loading plays an essential role in the maintenance of bone quality and quantity, and osteocytes are critical for sensing mechanical stimulation (Dallas et al., 2013; Bellido, 2014; Choy et al., 2020). *In vivo* studies have shown that osteocytes always exist in a complex mechanical environment, which includes shear stress, tensile strain, and pressure (Iolascon et al., 2013). When stimulated by mechanical strain (Wang et al., 2019), osteocytes can regulate osteoblast proliferation and differentiation by releasing signaling molecules, such as nitric oxide, prostaglandin E2, and adenosine triphosphate (Bakker et al., 2001; Genetos et al., 2005). Studies have shown that bed-ridden patients and astronauts develop osteoporosis due to reduced mechanical bone stimulation, but the mechanism of this phenomenon remains unclear (Norvell et al., 2004; Sibonga, 2013; Yang et al., 2018).

Leukemia inhibitory factor (LIF) belongs to the interleukin (IL)-6 family of cytokines; it has been detected in hypertrophic chondrocytes and vascular sprouts (Grimaud et al., 2002), hematopoietic and (Hilton et al., 1991), osteoblasts (Allan et al., 1990), skeletal (Broholm et al., 2011), and osteocytes (Marusić et al., 1993). Previous studies have shown that muscle loading impact bone development, and LIF influences this process (Broholm et al., 2008). Furthermore, IL-6 expression in osteocytes dramatically increases rats are subjected to mechanical loading-induced stress fractures (Wu et al., 2014), and IL-6 messenger RNA (mRNA) levels are elevated under fluid shear stress (FSS) (Bakker et al., 2014). Hence, we hypothesized that mechanical loading-induced LIF in osteocytes might regulate bone remodeling.

Leukemia inhibitory factor has diverse biological functions; for instance, it can promote proliferation of multiple types of hematopoietic cells, trigger platelet formation, facilitate neuronal survival and formation, and accelerate lipid transport in adipocytes (Metcalf, 2003; Brandt et al., 2015). However, LIF may exhibit contradictory effects in some cells (Nicola and Babon, 2015). Previous reports have shown that LIF has controversial effects on bone mass; some reports suggested that LIF causes a decrease in bone mass, whereas some claimed that LIF causes an increase in bone production (Cornish et al., 1993; Falconi and Aubin, 2007; Nicolaidou et al., 2012; Matsushita et al., 2014). Further, it was also reported that LIF promotes osteoclast differentiation (Richards et al., 2000); however, some studies demonstrated that Fra-2 regulates osteoclast size through LIF/LIF-receptor (LIFR) signaling and hypoxia. In addition, LIF- (Bozec et al., 2008) or LIFR- (Ware et al., 1995) knockout mice exhibit increase in osteoclast numbers and size. In the tail-suspension (TS) model, the hind limbs are free from the weight-bearing load, thus mimicking muscular disuse osteoporosis *in vivo*; thereby providing a suitable approach for elucidating the relationship between mechanical loading and bone metabolism (Morey-Holton and Globus, 1998). Hence, in this study, we aimed to investigate whether osteocytes can regulate bone remodeling by secreting LIF under mechanical stress.

## MATERIALS AND METHODS

### TS Mouse Model

Two-month-old male C57BL/6J mice were purchased from Shanghai SLAC laboratory animal company (Shanghai, China), and the study was approved by the animal ethics committee of Shanghai ninth people's hospital, China. All applicable institutional and national guidelines for the care and use of animals were followed. Mice were provided with commercial food and water under specific aseptic (specific pathogen free [SPF]) conditions. Twenty mice were randomly divided into two groups – the TS and control (Ctrl) groups, with ten mice per group. Both groups were maintained in the same environmental conditions. For this study, we applied the TS protocol described by Morey-Holton, with modifications (Morey-Holton and Globus, 1998). Briefly, the tail of each mouse was suspended by applying adhesive tape on its lateral surfaces. Three surgical tapes were then applied circularly at the base, middle, and end of the region to secure the adhesion between the tapes and the tail. The adhesive tape loop at the tip of the tail was passed through a metallic hollow column, which was then connected to a 360° free rotating hook via a metallic wire. The hook was placed on an overhead bar in the middle part of the top of the cage. Thus, these mice were maintained at an approximately 35° head-down tilt, with their hind limbs unloaded. The forelimbs could be used for locomotion. The overall suspension period was 28 days.

### Immunohistochemical

Samples were decalcified in 10% ethylenediaminetetraacetic acid (EDTA) for 3 weeks and embedded in paraffin. For microstructure observation, 4-μm-thick sagittal sections of the medial compartment of the knee joint were cut, and immunohistochemical staining with anti-tartrate-resistant acid phosphatase (TRAP) antibody (ab185716, Abcam, United Kingdom) and anti-LIF antibody (AB-449-NA, R&D Systems, United States) was performed.

## Micro-Computed Tomography (CT) Scanning

At the end of the suspension period, the femurs of the mice were fixed with 4% paraformaldehyde and then maintained in 75% ethanol. Specimens were scanned by micro-CT (μCT 80; Scanco Medical, Zurich, Switzerland), as described previously (Zhou et al., 2019). The micro-CT parameters were as follows: voltage, 70 kV; electric current, 114 μA; and resolution, 10 μm per pixel. The three-dimensional structural parameters, including bone volume fraction (BV/TV), trabecular number (Tb.N), trabecular thickness (Tb.Th), trabecular separation (Tb.Sp), and trabecular bone surface (BS/BV), were analyzed in the same region.

## Enzyme-Linked Immunosorbent Assay (ELISA)

Leukemia inhibitory factor levels in the Ctrl and TS groups were detected using the ELISA kit (MLF00, R&D Systems, United States), according to the manufacturer's instructions. A microplate reader (Bioteck, Arcugnano [Vicenza], Italy) was used to determine the density OD) of each well. We selected 450 and 540 for wavelength correction.

## Osteocyte Culture and Mechanical Loading

To study osteocytes *in vitro*, we used the osteocyte-like MLO-Y4 cells, which were kindly provided by Dr. Lynda Bonewald (University of Missouri-Kansas City, Kansas City, MO, United States). MLO-Y4 cells were cultured on rat tail collagen type I-coated dishes (Solarbio, Beijing, China) with α-minimum essential medium (α-MEM; Gibco, Grand Island, NY, United States), which contained 5% fetal bovine serum (FBS; Gibco), 5% fetal calf serum (FCS, Gibco), and 1% penicillin/streptomycin (Sigma-Aldrich, St. Louis, MO, United States). The osteocytes were then used for investigating FSS and microgravity loading.

MLO-Y4 cells ($2 \times 10^5$ cells/slide) were seeded on glass slides (75 mm × 38 mm × 1 mm), which were coated with rat tail collagen type 1 (BD Biosciences, Bedford, MA, United States). They were then cultured (37°C, 5% $CO_2$) for 48 h to ensure 80–90% confluence at the time of the flow experiment. FSS was generated using a Streamer® Shear Stress Device (flexercell STR-4000, Flexcell, NC, United States). Some MLO-Y4 cells were exposed to FSS (4 dyne/cm$^2$, 5 Hz) for 2 h and then harvested immediately. MLO-Y4 cells in the control group were seeded on the same slides, but were not exposed to FSS.

Microgravity simulation experiments were performed with a random positioning machine (RPM) (made by the Center for Space Science and Applied Research, the Chinese Academy of Sciences, Beijing, China). The RPM was placed in an air incubator at 37°C in 5% $CO_2$, and rotation mode of the RPM was set to the random mode at a speed range of 0–10 rpm. MLO-Y4 cells ($2 \times 10^4$ cells/cm$^2$) were seeded in a gas-permeable cell culture disk (Opticell, Nunc) and grown in α-MEM, which contained 5% FBS and 5% FCS, at 37°C in humidified air with 5% $CO_2$ for 2 day. Cells were then collected and divided into two groups, the control and RPM groups. After fixing the Opticell disks into the inner frame of RPM and ensuring that there were no air bubbles in the medium, the RPM was rotated randomly at a range of 0–10 rpm for 24 h to simulate microgravity. Cells of the control group were cultured under normal conditions (1G).

## *In vitro* Osteoclastogenesis

Bone marrow macrophages (BMMs) were obtained from the long bones of 4-week-old C57BL/6J mice. Mice were sacrificed, and their femurs and tibias were separated under sterile conditions. Bone marrow was flushed from the mouse femurs and tibias, re−suspended in complete α-MEM, which contained macrophage-colony stimulating factor (M-CSF, 30 ng/mL), and cultured in a 10-cm dish at 37°C in 5% $CO_2$. The medium was changed every alternate day to remove the non-adherent cells. At 80% confluence, cells were washed thrice with phosphate-buffered saline (PBS), and then BMMs were collected using trypsin for subsequent experiments. Bone mesenchymal stem cells (BMSCs) were obtained in the same way, but were cultured without M-CSF. For BMM differentiation, BMMs ($10^5$ cells/well) were seeded in a 24-well plate and then treated with receptor activator of nuclear factor kappa-B ligand (RANKL, 50 ng/mL) and M-CSF (30 ng/mL) after 12 h, as described in a previous study (Song et al., 2019). We then added LIF (10 ng/mL) to some of the wells and changed the media every alternate day for 7 days until osteoclasts were formed. After fixing the cells with 4% paraformaldehyde for 30 min, anti-TRAP antibody immunohistochemical staining was performed to detect TRAP activity. The Image-Pro Plus software (Media Cybernetics Bethesda, MD, United States) was used to calculate the number of TRAP-positive cells in each well.

## *In vitro* Osteogenesis

After reaching 80–90% density in a 24-well plate, BMSCs were cultured with osteogenesis assay kit (MUBMX-90021, Cyagen, CA, United States) at 37°C in humidified air with 5% $CO_2$ for 21 days to induce osteoblasts. Alkaline (ALP) or Alizarin red staining was performed after 14 and 21 days of culture. ALP presence in the cell layers was assessed as follows: the cultured cells were washed thrice with PBS, fixed with 4% paraformaldehyde for 10 min at room temperature (25°C), and then stained using the BCIP/NBT Alkaline Phosphatase Color Development Kit (Beyotime Institute of Biotechnology, Shanghai, China), according to the manufacturer's instructions. For Alizarin red staining, the cultured cells were fixed with 4% paraformaldehyde for 30 min, and then Alizarin red dye (contained in the MUBMX-90021 kit) was added to the 24-well plate for 3–5 min at room temperature (25°C). The plate was then washed five times with PBS. Semi-quantitative analysis was performed by adding 10% cetylpyridinium chloride (500 μL) (H811089, Macklin, CA, United States) to each well, and absorbance of the supernatant at 562 nm was detected after incubation for 30 min at room temperature.

## Quantitative Reverse-Transcription Polymerase Chain Reaction (qRT-PCR)

Total RNA was extracted using TRIzol reagent (Thermo Scientific, United States) and converted to complementary DNA (cDNA) using the Quantscript RT Kit (Promega, Madison, WI, United States). Next, PCR reactions of the cDNA and SYBR Premix Ex Taq Mix (10 μL) (Selleck, TX, United States) were performed. Real-Time PCR System (Light Cycler 2.0; Roche Diagnostics GmbH, Mannheim, Germany) was employed to determine mRNA levels. The data were analyzed by the $2^{-\Delta\Delta Ct}$ method, where Ct is threshold cycle. The primer sequences are presented in **Table 1**.

## Western Blot (WB) Analysis

To separate differently sized proteins in the samples, sodium dodecylsulfate-polyacrylamide gel (10% concentration) electrophoresis was performed. The proteins were then transferred onto polyvinylidene difluoride (PVDF) membranes (Millipore, Billerica, MA, United States). The PVDF membranes were blocked using 5% non-fat milk for 30 min and then incubated with primary antibodies against STAT3 (1:1,000; Cell Signaling Technology, MA, United States), p-STAT3 (1:1,000; Cell Signaling Technology), ERK (1:1,000; Cell Signaling Technology), p-ERK (1:2,000; Cell Signaling Technology), and β-actin (1:1,000; Cell Signaling Technology) at 4°C overnight. The membranes were washed four times with tris-buffered saline with Tween 20, and then incubated with horseradish peroxidase-conjugated secondary antibodies (1:10,000; Laizee Biotech, Shanghai, China) at room temperature for 1 h. Chemiluminescence detection was performed using an enhanced chemiluminescence Kit (Beyotime Institute of Biotechnology) and an Omega Lum$^{TM}$ C Imaging System (Gel Company, San Francisco, CA, United States) (Han et al., 2018). The relative intensity of the bands is quantified by ImageJ.

## Cell Viability Assay

MLO-Y4 cells (10000/cm$^2$) were seeded in 96-well plates, and some of them were treated with LIF (10 ng/mL). The cells were then incubated for 24 h. CCK-8 (C6005, NCM Biotech, United States) was added to the wells to obtain a final concentration of 10%, and incubated at 37°C for 2 h. The microplate reader (Bioteck, Arcugnano [Vicenza], Italy) was used to detect absorbance at 450 nm (Liu et al., 2017).

## Microarray Analysis

Three independent biological replicates of the FSS and Ctrl groups were used to perform microarray analysis. Briefly, after FSS treatment, MLO-Y4 cells were dissolved in TRIzol and sent for microarray analysis to Oebiotech (Shanghai, China[1]). Construction of an Illumina library and sequencing on an Illumina His Eq. 2000 platform were conducted by Oebiotech.

## Statistical Analysis

Statistical analyses of data were performed using GraphPad Prism 5.0 (GraphPad Software Inc., CA, United States). Each experiment was repeated at least thrice. All quantitative values were presented as the mean ± standard deviation (SD), and the differences were evaluated by one−way analysis of variance (ANOVA) or Student's *t*-test, followed by Bonferroni correction for multiple comparisons. $P < 0.05$ was considered statistically significant.

[1]https://www.oebiotech.com/

# RESULTS

At the end of the suspension period, femurs of the TS mice showed low bone mass. Bone volume/total volume(BV/TV), trabecular number(Tb.N), trabecular thickness(Tb.Th), trabecular separation(Tb.Sp), and bone surface/bone volume(BS/BV) (**Figure 1A**) were decreased and osteoclast number(OC.N/BS) (**Figures 1C,E**) was increased in the TS group, compared to the values in the control group. Micro-CT 3D reconstruction pictures are shown in **Figure 1B**. Additionally, TS mice showed lower LIF expression levels in both bone tissues and serum, as detected by immunohistochemistry (**Figure 1D**) and ELISA (**Figure 1G**), respectively. Quantitative analysis of immunohistochemistry is shown in **Figure 1F**.

RNA sequencing was conducted for the FSS-treated and control MLO-Y4 cells. After performing Gene Ontology (GO) (**Figure 2A**) and Kyoto Encyclopedia of Genes and Genomes (KEGG) pathway (**Figure 2B**) enrichment analyses, we found that differential genes were enriched in the cytokine-related pathways. According to the RNA sequencing results, the expression levels of various cytokines, including LIF, CXCL1, and CXCL2, were altered (**Figure 2C**). Thus, we validated a series of cytokine expression levels by qRT-PCR (**Figure 2D**) and confirmed that LIF expression increased on FSS treatment. This finding was consistent with the RNA sequencing results. Simultaneously, pro-apoptotic genes, such as BAX and BAD, were downregulated after FSS treatment, indicating that FSS exposure possibly prevented MLO-Y4 cell apoptosis. Meanwhile, MLO-Y4 cells were cultivated in a microgravity environment after RPM treatment for 24 h, and the LIF gene expression levels were observed to decrease dramatically with the increase in gene expression levels of apoptosis-related genes (**Figure 2E**).

Bone marrow macrophages were treated with LIF at different concentrations, and then CCK-8 (**Figure 3A**) and EdU (**Figures 3B,C**) assays were performed. Results of both assays showed that LIF had no significant influence on BMM cell viability. Verify the effects of LIF on osteoclastogenesis, different concentrations of LIF were added to the BMMs during their differentiation process. As shown in **Figure 3D**, when LIF concentration was >2 ng/mL, especially at concentration 10 ng/mL, expression of osteoclast-related genes was enhanced. Thus, 10 ng/mL was chosen as the final experimental concentration. Then, BMMs were treated with M−CSF (30 ng/mL), RANKL (50 ng/mL), and LIF (10 ng/mL), with or without LIF-neutralizing (20 ng/mL), until

**TABLE 1 |** Primer sequences for the quantitative reverse-transcription polymerase chain reaction.

| Target genes | Forward (5′-3′) | Reverse (5′-3′) |
|---|---|---|
| β-Actin | AGCCATGTACGTAGCCATCC | CTCTCAGCTGTGGTGGTGAA |
| Gapdh | ACCCAGAAGACTGTGGATGG | CACATTGGGGGTAGGAACAC |
| Lif | ATTGTGCCCTTACTGCTGCTG | GCCAGTTGATTCTTGATCTGGT |
| Bad | AAGTCCGATCCCGGAATCC | GCTCACTCGGCTCAAACTCT |
| Bax | TGAAGACAGGGGCCTTTTTG | AATTCGCCGGAGACACTCG |
| Ocn | CTGACCTCACAGATCCCAAGC | TGGTCTGATAGCTCGTCACAAG |
| Alp | GCCTGGATCTCATCAGTATTTGG | GTTCAGTGCGGTTCCAGACAT |
| Runx2 | CCGGGAATGATGAGAACTA | ACCGTCCACTGTCACTTT |
| Osteorix | CTCTCTGCTTGAGGAAGAAG | GTCCATTGGTGCTTGAGAAG |
| Opg | ACCCAGAAACTGGTCATCAGC | CTGCAATACACACACTCATCACT |
| Traf6 | AAACCACGAAGAGGTCATGG | GCGGGTAGAGACTTCACAGC |
| Ctsk | GGACCCATCTCTGTGTCCAT | CCGAGCCAAGAGAGCATATC |
| Dcst | AAAACCCTTGGGCTGTTCTT | AATCATGGACGACTCCTTGG |
| c-Fos | CCAGTCAAGAGCATCAGCAA | AAGTAGTGCAGCCCGGAGTA |

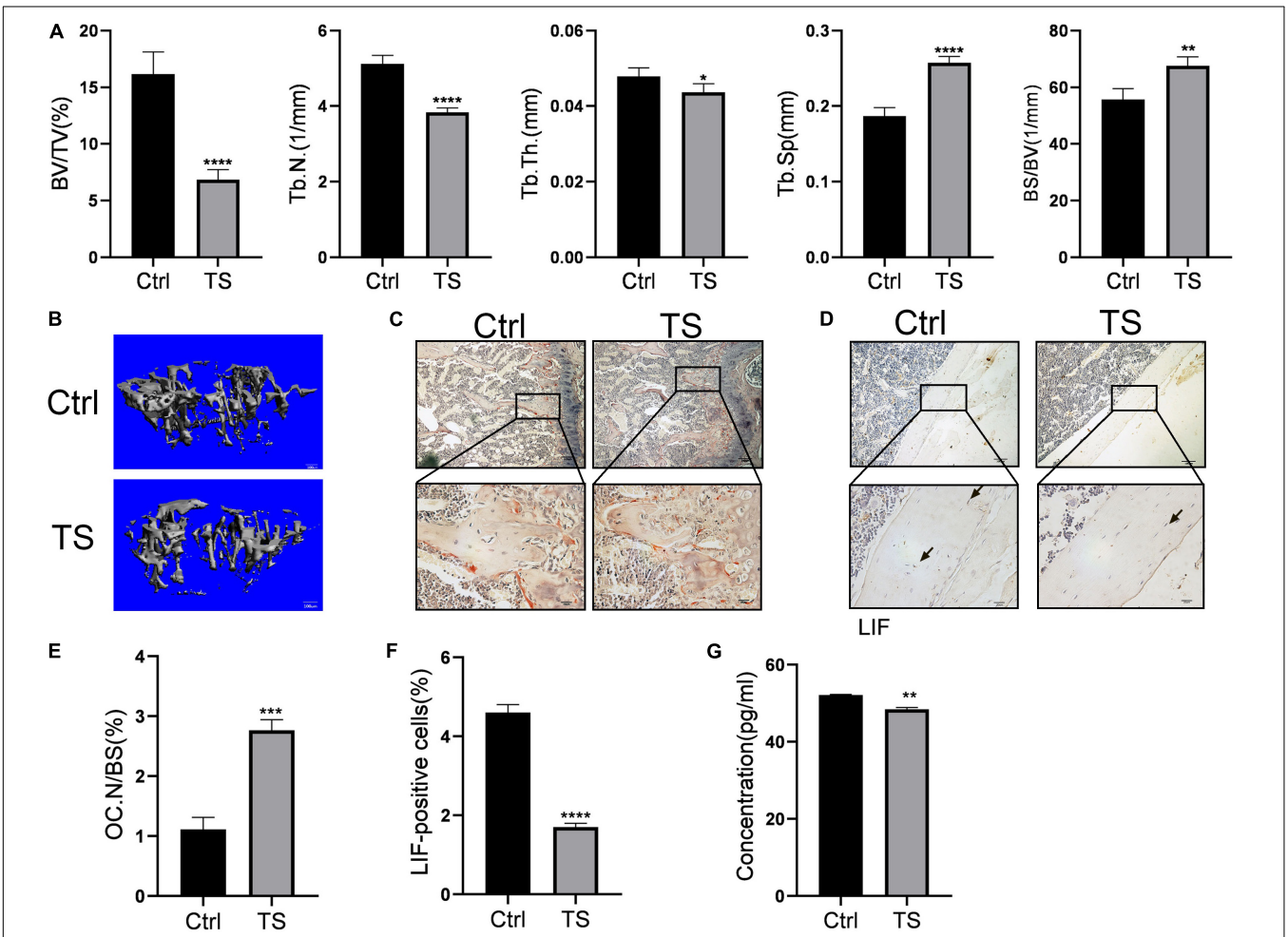


**FIGURE 1 |** Micro-CT analysis of Tail-suspension mice **(A)** Quantitative analysis of BV/TV, Tb.N, Tb.Th, BS/BV and Tb.Sp. **(B)** Micro-CT 3D reconstruction pictures. **(C)** Osteoclasts in the sub-growth-plate bone of tibia were stained using tartrate-resistant acid phosphatase. **(D)** The expression of LIF in tibias was detected by immunohistochemical staining. **(E)** Osteoclast numbers in **Figure 1C** were counted. **(F)** LIF positive cells in **Figure 1D** were counted. **(F)** Expression level of LIF in the serum was detected by ELISA. Black arrow: LIF positive osteocyte. All data are shown as means ± standard deviations ($n = 10$), $^{*}p < 0.05$, $^{**}p < 0.01$, $^{***}p < 0.005$ and $^{****}p < 0.001$.

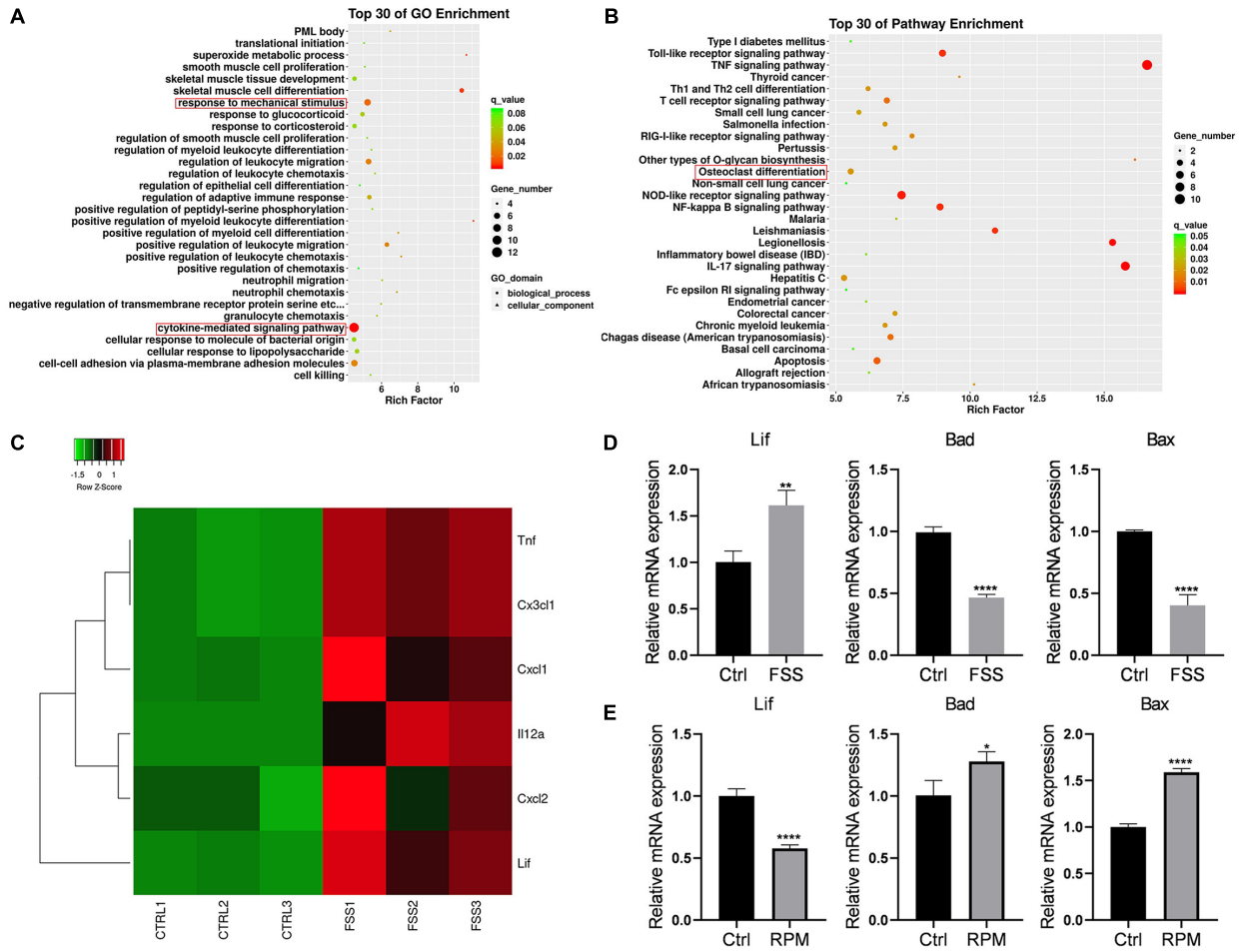


**FIGURE 2 |** LIF expression in the FSS or microgravity-treated MLO-Y4 cells **(A)** GO and **(B)** KEGG pathway enrichment analyses were performed. **(C)** Heatmap of the expression levels of various cytokines based on the RNA sequencing results is shown. **(D)** LIF expression was increased under FSS, as determined by RT-PCR. **(E)** LIF expression was reduced in the microgravity environment, as determined by RT-PCR. All data are shown as means ± standard deviations ($n = 3$), $^{*}p < 0.05$, $^{**}p < 0.01$, $^{***}p < 0.005$ and $^{****}p < 0.001$.

mature osteoclasts were formed. Numerous TRAP-positive multinucleated osteoclasts, formed in the three groups of treated BMMs, are shown in **Figure 3F**. The results (**Figure 3G**) showed more osteoclasts in the LIF-treated group than those in the control group, and this could be reversed by using LIF-neutralizing. Osteoclast-related gene expression levels (**Figure 3E**) also indicated that LIF promoted osteoclast formation, but LIF-neutralizing moderated this facilitation function of LIF. After starvation for 3 h, protein samples of the LIF-treated BMMs were extracted at different times. **Figure 3H** shows that after treatment for 5 min, LIF promoted STAT3 phosphorylation, but had no effects on ERK. These results showed that LIF promoted BMM differentiation via the STAT3 signaling pathway.

To detect the best concentration of LIF for osteogenesis using the osteogenesis assay kit, LIF was added at different concentrations to the BMSCs. Osteogenesis-related genes were tested on day 14. Consistent with osteoclastogenesis, osteogenesis was greatly promoted by LIF (10 ng/mL) (**Figure 4A**). As shown in **Figure 4B**, LIF promoted osteogenesis-related genes, including RUNX2, OCN, and ALP. After 14- and 21-day differentiation culture, BMSCs were stained with ALP (**Figure 4C**) or Alizarin red (**Figure 4D**). Images showed that the LIF-treated group presented more ALP- and Alizarin-positive nodules, and this finding was consistent with the results of semi-quantitative analysis of Alizarin red staining (**Figure 4E**). Western blot analysis showed that LIF activated the STAT3 signaling pathway in the BMSCs (**Figure 4F**), indicating that LIF exerted influence BMSCs through the STAT3 signaling pathway.

## DISCUSSION

In this study, the TS model was adopted to mimic muscular disuse *in vivo* and investigate the relationship between mechanical stimulation and bone quality.

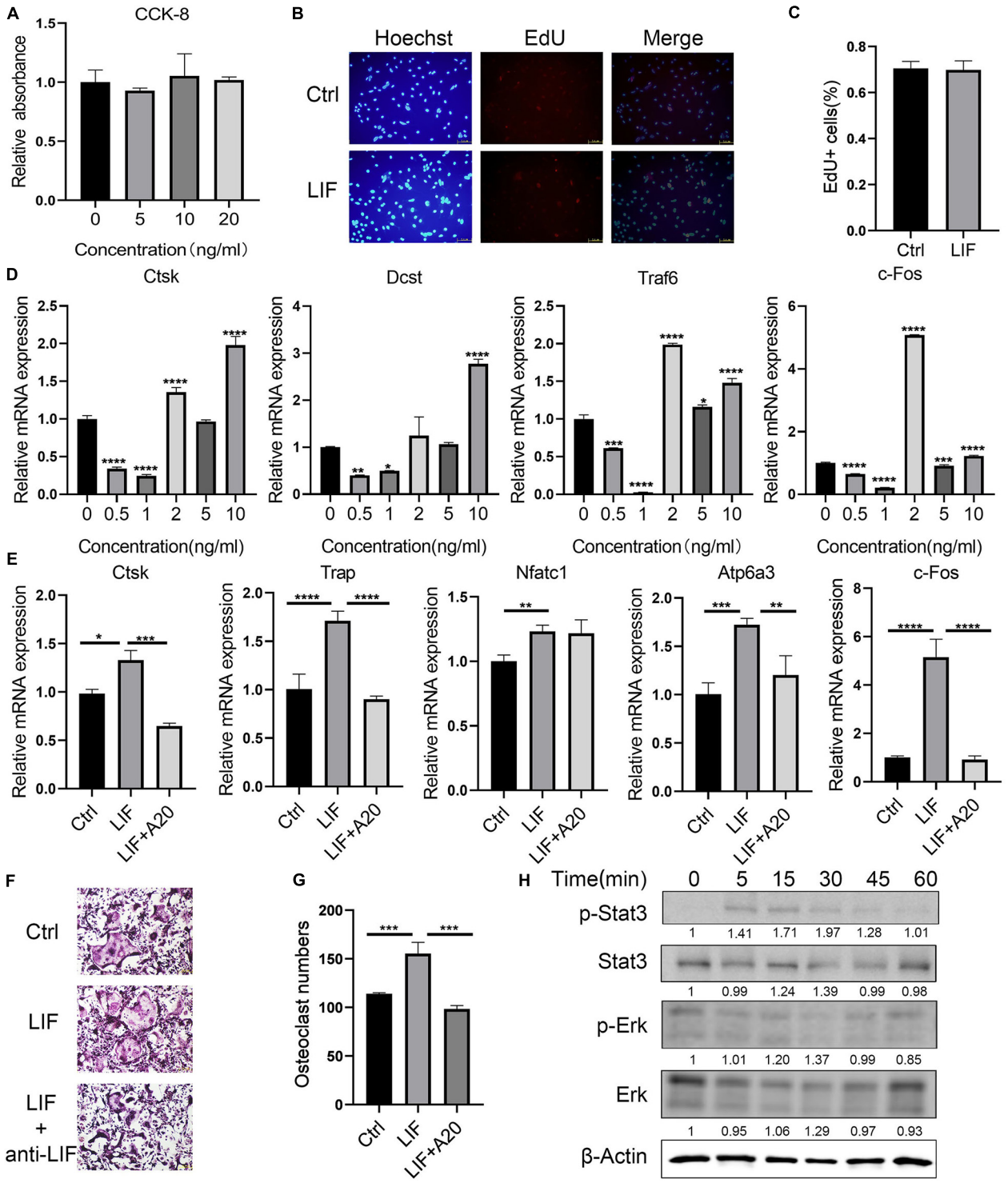


**FIGURE 3 |** LIF promotes BMM differentiation into osteoclasts **(A)** LIF, at different concentrations, did not affect BMM proliferation, as shown by the OD value calculated during CCK-8 analysis. **(B)** BMM cells were treated with LIF (10 ng/mL) for 24 h, and then EdU assay was performed. **(C)** EdU-positive cells were counted. **(D)** BMM cells were treated with LIF at different concentrations, and then osteoclast-related genes were detected. **(E)** RT-PCR results showed that LIF promoted osteoclast-related gene expression. **(F)** Representative images of TRAP staining of osteoclasts are shown. **(G)** The number of osteoclasts in each well (96-well plate) and all the cells with ≥3 nuclei were counted. **(H)** After treatment with LIF at different times, STAT3 and p-STAT3 protein levels in BMMs were determined by western blot analysis. All data are shown as the mean ± SD ($n = 3$); $^{*}p < 0.05$, $^{**}p < 0.01$, $^{***}p < 0.005$ and $^{****}p < 0.001$.

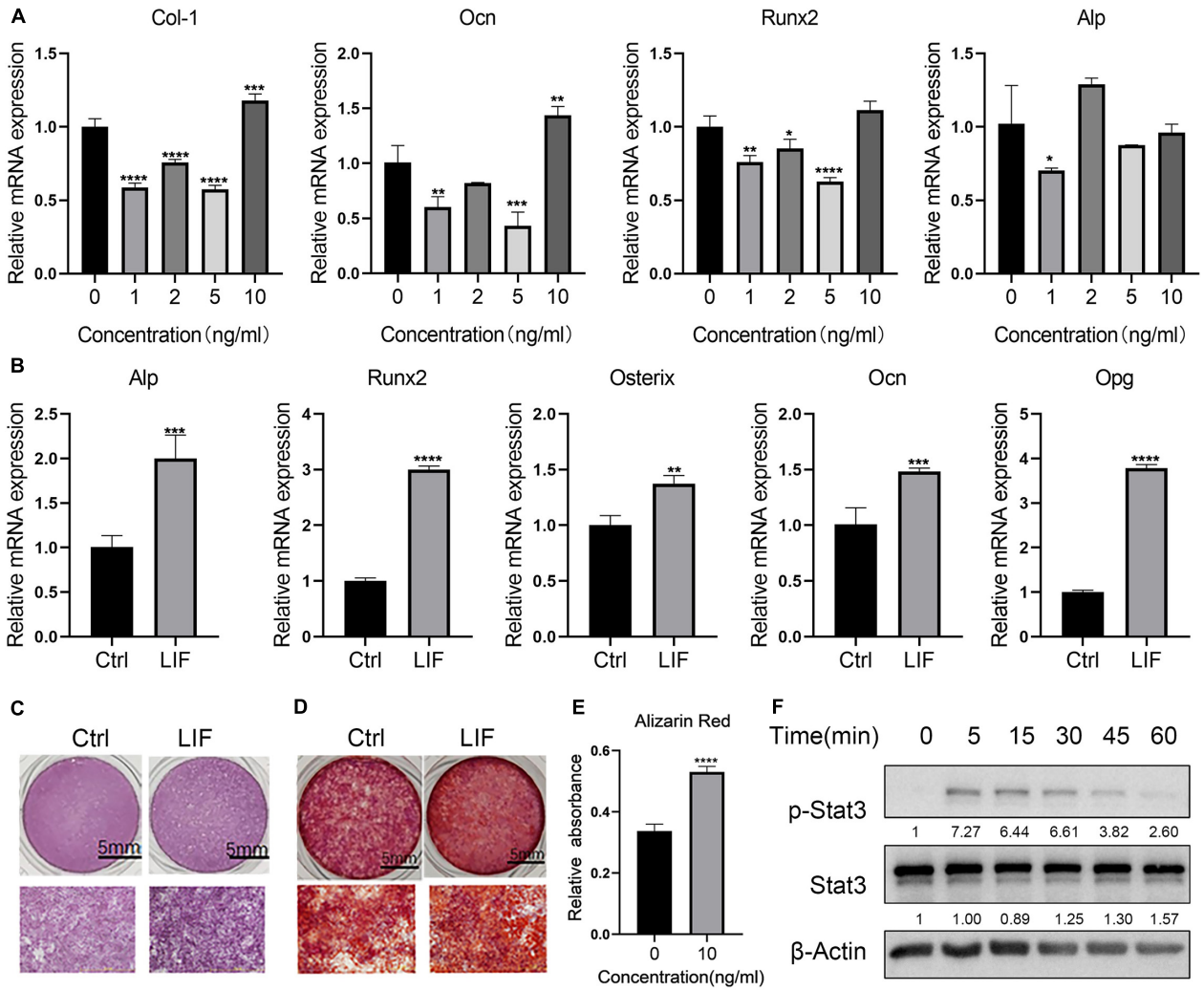


**FIGURE 4 |** LIF promotes the osteogenesis of BMSC **(A)** after treated with different concentration of LIF, osteogenesis-related genes were detected by RT-PCR. **(B)** After 14 days of culture, osteogenesis-related gene expression levels were tested using RT-PCR. **(C)** Representative ALP staining image of BMSC after being cultured 7 days in the osteogenic medium. **(D)** Alizarin red staining was performed after 21 days. **(E)** Semiquantitative analysis of Alizarin red staining. **(F)** Western blot results of BMSCs after being treated with LIF at different times. All data are shown as means ± standard deviations ($n = 3$), $^{*}p < 0.05$, $^{**}p < 0.01$, $^{***}p < 0.005$ and $^{****}p < 0.001$.

At the end of the tail suspension period, BV/TV, Tb.N, and Tb.Th of the TS mice were decreased significantly. Consistent with our findings, it was reported that hind limb unloading promotes osteocyte apoptosis and decreases bone mass (Swift et al., 2010; Cabahug-Zuckerman et al., 2016).

Both FSS exposure and a microgravity environment can affect LIF expression levels. Previous reports showed the effects of LIF on muscle load and exercise, further influencing bone mineral mass (Rauch and Schoenau, 2001; Brotto and Bonewald, 2015; Jia et al., 2018). Liang et al. (2011) found that continuous orthodontic forces promoted LIF/LIFR expression in the periodontal tissue. These findings showed that LIF plays a role in the mechanical response of the bone. Besides, evidence on the promotion of the anabolic response of bones by low-magnitude mechanical stimulation has also been reported (Ozcivici et al., 2010). Additionally, studies have shown that LIF can promote multinucleated giant cell number and nucleation (Gouin et al., 1999). In our study, LIF (10 ng/mL) was co-cultured with BMMs to investigate whether LIF affected osteoclast formation, indicating greater differentiation ability of LIF. However, when anti-LIF antibody was added to the osteoclastogenesis medium, LIF auxo-action was moderated, demonstrating that LIF could promote BMM differentiation. Several signaling pathways have been shown to be related to osteoclast differentiation and function. Many reports show that STAT3 drives NFATc1 transcription and osteoclast differentiation (Yang et al., 2019), indicating that LIF affects osteoclastogenesis by promoting STAT3 phosphorylation.

Metcalf and Gearing (1989) reported that LIF overexpression *in vivo* increases trabecular bone mass. In our study, during BMSC differentiation, ALP staining and RT-PCR results in the first 14 days demonstrated that LIF promoted osteogenesis, and this finding is consistent with previously reported data (Poulton et al., 2012). STAT3 phosphorylation level in BMSCs was determined after LIF (10 ng/mL) treatment, and it was found that LIF influenced BMSCs via the same signaling pathway (STAT3 signaling pathway).

Nevertheless, there are some limitations of our study. We observed that FSS promoted LIF expression, but the mechanism of this phenomenon remains unknown. In this study, a TS model corresponding to the microgravity experiment *in vitro* is designed, but osteocytes in TS mice are not in a microgravity environment. Besides, we tested LIF function only in BMSCs, whether LIF affected other cell lines, such as 3T3-E1, remains unknown. Last, we tested only the phosphorylation levels of STAT3, and not the downstream pathway, which could partly explain why exercise promoted bone mass increase. The promoting effects of LIF on the two cell lines used in this study showed that it possibly affected bone reconstruction and the decrease in its expression levels resulted in the reduction of bone renewal ability. This, in turn, resulted in poor replacement of the old bone by the new one.

In conclusion, our study demonstrated that mechanical stress could stimulate LIF expression in osteocytes. Besides, LIF simultaneously promoted osteoclastogenesis and osteogenesis. Mechanistically, LIF could increase the phosphorylation levels of STAT3, which is related to osteoclast and osteoblast formation.

## DATA AVAILABILITY STATEMENT

The datasets presented in this study can be found in online repositories. The names of the repository/repositories and accession number(s) can be found in the article/supplementary material.

## ETHICS STATEMENT

The animal study was reviewed and approved by Animal Ethics Committee of Shanghai Ninth People's Hospital, China.

## AUTHOR CONTRIBUTIONS

All authors listed have made a substantial, direct and intellectual contribution to the work, and approved it for publication.

## FUNDING

This work was supported by grants from the National Natural Science Foundation of China (Nos 11572197 and 11872251) to ZY, and National Natural Science Foundation of China (81802679) and China Postdoctoral Science Foundation (2018M632136 and 2019T120348) to HL.

## REFERENCES

Allan, E. H., Hilton, J. D., Brown, A. M., Evely, S. R., Yumita, S., Metcalf, D., et al. (1990). Osteoblasts display receptors for and responses to leukemia-inhibitory factor. *J. Cell. Physiol.* 145, 110–119. doi: 10.1002/jcp.1041450116

Bakker, A. D., Kulkarni, R. N., Klein-Nulend, J., and Lems, W. F. (2014). IL-6 alters osteocyte signaling toward osteoblasts but not osteoclasts. *J. Dent. Res.* 93, 394–399. doi: 10.1177/0022034514522485

Bakker, A. D., Soejima, K., Klein-Nulend, J., and Burger, E. H. (2001). The production of nitric oxide and prostaglandin E(2) by primary bone cells is shear stress dependent. *J. Biomech.* 34, 671–677. doi: 10.1016/s0021-9290(00)00231-1

Bellido, T. (2014). Osteocyte-driven bone remodeling. *Calcif. Tissue Int.* 94, 25–34. doi: 10.1007/s00223-013-9774-y

Bozec, A., Bakiri, L., Hoebertz, A., Eferl, R., Schilling, A. F., Komnenovic, K., et al. (2008). Osteoclast size is controlled by Fra-2 through LIF/LIF-receptor signalling and hypoxia. *Nature* 454, 221–225. doi: 10.1038/nature07019

Brandt, N., O'Neill, H. M., Kleinert, M., Schjerling, P., Vernet, E., Steinberg, G. R., et al. (2015). Leukemia inhibitory factor increases glucose uptake in mouse skeletal muscle. *Am. J. Physiol. Endocrinol. Metab.* 309, E142–E153.

Broholm, C., Laye, J. M., Brandt, C., Vadalasetty, R., Pilegaard, H., Pedersen, K. B., et al. (2011). LIF is a contraction-induced myokine stimulating human myocyte proliferation. *J. Appl. Physiol. (1985)* 111, 251–259. doi: 10.1152/japplphysiol.01399.2010

Broholm, C., Mortensen, O. H., Nielsen, S., Akerstrom, T., Zankari, A., Dahl, B., et al. (2008). Exercise induces expression of leukaemia inhibitory factor in human skeletal muscle. *J. Physiol.* 586, 2195–2201. doi: 10.1113/jphysiol.2007.149781

Brotto, M., and Bonewald, L. (2015). Bone and muscle: Interactions beyond mechanical. *Bone* 80, 109–114. doi: 10.1016/j.bone.2015.02.010

Cabahug-Zuckerman, P., Frikha-Benayed, D., Majeska, R. J., Tuthill, A., Yakar, S., Judex, S., et al. (2016). Osteocyte apoptosis caused by hindlimb unloading is required to trigger osteocyte rankl production and subsequent resorption of cortical and trabecular bone in mice femurs. *J. Bone Miner. Res.* 31, 1356–1365. doi: 10.1002/jbmr.2807

Choy, M. H. V., Wong, Y. M. R., Chow, H. K. S., Li, C. M., Chim, N. Y., Li, K. T., et al. (2020). How much do we know about the role of osteocytes in different phases of fracture healing? A systematic review. J. Orthop. Translat. 21, 111–121. doi: 10.1016/j.jot.2019.07.005

Cornish, J., Callon, K., King, A., Edgar, S., and Reid, I. R. (1993). The effect of leukemia inhibitory factor on bone *in vivo*. *Endocrinology* 132, 1359–1366. doi: 10.1210/endo.132.3.8440191

Dallas, S. L., Prideaux, M., and Bonewald, L. F. (2013). The osteocyte: an endocrine cell and more. *Endocr. Rev.* 34, 658–690. doi: 10.1210/er.2012-1026

Falconi, D., and Aubin, J. E. (2007). LIF inhibits osteoblast differentiation at least in part by regulation of HAS2 and its product hyaluronan. *J. Bone Miner. Res.* 22, 1289–1300. doi: 10.1359/jbmr.070417

Genetos, D. C., Geist, J. G., Liu, D., Donahue, J. H., and Duncan, L. R. (2005). Fluid shear-induced ATP secretion mediates prostaglandin release in MC3T3-E1 osteoblasts. *J. Bone Miner. Res.* 20, 41–49. doi: 10.1359/jbmr.041009

Gouin, F., Couillaud, S., Cottrel, M., Godard, A., Passuti, N., and Heymann, D. (1999). Presence of leukaemia inhibitory factor (LIF) and LIF-receptor chain (gp190) in osteoclast-like cells cultured from human giant cell tumour of bone. Ultrastructural distribution. Cytokine 11, 282–289. doi: 10.1006/cyto.1998.0429

Grimaud, E., Blanchard, F., Charrier, C., Gouin, F., Redini, F., and Heymann, D. (2002). Leukaemia inhibitory factor (lif) is expressed in hypertrophic chondrocytes and vascular sprouts during osteogenesis. *Cytokine* 20, 224–230. doi: 10.1006/cyto.2002.2002

Han, J., Gao, W., Su, D., and Liu, Y. (2018). Gypenoside inhibits RANKL-induced osteoclastogenesis by regulating NF-kappaB, AKT, and MAPK

signaling pathways. *J. Cell. Biochem.* 119, 7310–7318. doi: 10.1002/jcb.27028

Hilton, D. J., Nicola, N. A., and Metcalf, D. (1991). Distribution and comparison of receptors for leukemia inhibitory factor on murine hemopoietic and hepatic cells. *J. Cell. Physiol.* 146, 207–215. doi: 10.1002/jcp.1041460204

Iolascon, G., Resmini, G., and Tarantino, U. (2013). Mechanobiology of bone. *Aging Clin. Exp. Res.* 25(Suppl. 1), S3–S7.

Jia, D., Cai, M., Xi, Y., Du, S., and ZhenjunTian. (2018). Interval exercise training increases LIF expression and prevents myocardial infarction-induced skeletal muscle atrophy in rats. *Life Sci.* 193, 77–86. doi: 10.1016/j.lfs.2017.12.009

Liang, Y., Zhou, Y., Jiang, T., Zhang, Z., Wang, S., and Wang, Y. (2011). Expression of LIF and LIFR in periodontal tissue during orthodontic tooth movement. *Angle Orthod.* 81, 600–608. doi: 10.2319/102510-622.1

Liu, X., Chin, J.-F., Qu, X., Bi, H., Liu, Y., Yu, Z., et al. (2017). The beneficial effect of praeruptorin C on osteoporotic bone in ovariectomized mice via suppression of osteoclast formation and bone Resorption. *Front. Pharmacol.* 8:627. doi: 10.3389/fphar.2017.00627

Marusić, A., Kalinowski, F. J., Jastrzebski, S., and Lorenzo, A. J. (1993). Production of leukemia inhibitory factor mRNA and protein by malignant and immortalized bone cells. *J. Bone Miner. Res.* 8, 617–624. doi: 10.1002/jbmr.5650080513

Matsushita, K., Itoh, S., Ikeda, S., Yamamoto, Y., Yamauchi, Y., and Hayashi, M. (2014). LIF/STAT3/SOCS3 signaling pathway in murine bone marrow stromal cells suppresses osteoblast differentiation. *J. Cell. Biochem.* 115, 1262–1268. doi: 10.1002/jcb.24777

Metcalf, D. (2003). The unsolved enigmas of leukemia inhibitory factor. *Stem Cell.* 21, 5–14. doi: 10.1634/stemcells.21-1-5

Metcalf, D., and Gearing, D. P. (1989). Fatal syndrome in mice engrafted with cells producing high levels of the leukemia inhibitory factor. *Proc. Natl. Acad. Sci. U. S. A.* 86, 5948–5952. doi: 10.1073/pnas.86.15.5948

Morey-Holton, E. R., and Globus, R. K. (1998). Hindlimb unloading of growing rats: a model for predicting skeletal changes during space flight. *Bone* 22(5 Suppl.), 83S–88S.

Nicola, N. A., and Babon, J. J. (2015). Leukemia inhibitory factor (LIF). *Cytokine Growth Factor Rev.* 26, 533–544.

Nicolaidou, V., Wong, M. M., Redpath, A. N., Ersek, A., Baban, D. F., Williams, L. M., et al. (2012). Monocytes induce STAT3 activation in human mesenchymal stem cells to promote osteoblast formation. *PLoS One* 7:e39871. doi: 10.1371/journal.pone.0039871

Norvell, S. M., Alvarez, M., Bidwell, P. J., and Pavalko, M. F. (2004). Fluid shear stress induces beta-catenin signaling in osteoblasts. *Calcif. Tissue Int.* 75, 396–404. doi: 10.1007/s00223-004-0213-y

Ozcivici, E., Luu, Y. K., Adler, B., Qin, Y.-X., Rubin, J., Judex, S., et al. (2010). Mechanical signals as anabolic agents in bone. *Nat. Rev. Rheumatol.* 6, 50–59. doi: 10.1038/nrrheum.2009.239

Poulton, I. J., McGregor, N., Pompolo, S., Walker, E. C., and Sims, N. A. (2012). Contrasting roles of leukemia inhibitory factor in murine bone development and remodeling involve region-specific changes in vascularization. *J. Bone Miner. Res.* 27, 586–595. doi: 10.1002/jbmr.1485

Rauch, F., and Schoenau, E. (2001). The developing bone: slave or master of its cells and molecules? *Pediatr. Res.* 50, 309–314. doi: 10.1203/00006450-200109000-00003

Richards, C. D., Langdon, C., Deschamps, P., Pennica, D., and Shaughnessy, S. G. (2000). Stimulation of osteoclast differentiation in vitro by mouse oncostatin M, leukaemia inhibitory factor, cardiotrophin-1 and interleukin 6: synergy with dexamethasone. *Cytokine* 12, 613–621. doi: 10.1006/cyto.1999.0635

Sibonga, J. D. (2013). Spaceflight-induced bone loss: is there an osteoporosis risk? *Curr. Osteoporos. Rep.* 11, 92–98. doi: 10.1007/s11914-013-0136-5

Song, C., Yang, X., Lei, Y., Zhang, Z., Smith, W., Yan, J., et al. (2019). Evaluation of efficacy on RANKL induced osteoclast from RAW264.7 cells. *J. Cell. Physiol.* 234, 11969–11975. doi: 10.1002/jcp.27852

Swift, J. M., Nilsson, M. I., Hogan, H. A., Sumner, L. R., and Bloomfield, S. A. (2010). Simulated resistance training during hindlimb unloading abolishes disuse bone loss and maintains muscle strength. *J. Bone Miner. Res.* 25, 564–574. doi: 10.1359/jbmr.090811

Wang, T., Yang, L., Jiang, J., Liu, Y., Fan, Z., Zhong, C., et al. (2019). Pulsed electromagnetic fields: promising treatment for osteoporosis. *Osteoporos. Int.* 30, 267–276. doi: 10.1007/s00198-018-04822-6

Ware, C. B., Horowitz, M. C., Renshaw, B. R., Hunt, J. S., Liggitt, D., Koblar, S. A., et al. (1995). Targeted disruption of the low-affinity leukemia inhibitory factor receptor gene causes placental, skeletal, neural and metabolic defects and results in perinatal death. *Development* 121, 1283–1299.

Wu, A. C., Kidd, L. J., Cowling, N. R., Kelly, W. L., and Forwood, M. R. (2014). Osteocyte expression of caspase-3, COX-2, IL-6 and sclerostin are spatially and temporally associated following stress fracture initiation. *Bonekey Rep.* 3, 571.

Yang, J., Zhang, G., Dong, D., and Shang, P. (2018). Effects of iron overload and oxidative damage on the musculoskeletal system in the space environment: data from spaceflights and ground-based simulation models. *Int. J. Mol. Sci.* 19:2608. doi: 10.3390/ijms19092608

Yang, Y., Chung, M. R., Zhou, S., Gong, X., Xu, H., Hong, Y., et al. (2019). STAT3 controls osteoclast differentiation and bone homeostasis by regulating NFATc1 transcription. *J. Biol. Chem.* 294, 15395–15407. doi: 10.1074/jbc.ra119.010139

Zhou, F., Mei, J., Yuan, K., Han, X., Qiao, H., and Tang, T. (2019). Isorhamnetin attenuates osteoarthritis by inhibiting osteoclastogenesis and protecting chondrocytes through modulating reactive oxygen species homeostasis. *J. Cell. Mol. Med.* 23, 4395–4407. doi: 10.1111/jcmm.14333

**Conflict of Interest:** The authors declare that the research was conducted in the absence of any commercial or financial relationships that could be construed as a potential conflict of interest.

frontiers in Cell and Developmental Biology

REVIEW
published: 26 February 2021
doi: 10.3389/fcell.2021.644986

# Membrane Transport Proteins in Osteoclasts: The Ins and Outs

*Amy B. P. Ribet, Pei Ying Ng and Nathan J. Pavlos**

*Bone Biology and Disease Laboratory, School of Biomedical Sciences, The University of Western Australia, Nedlands, WA, Australia*

During bone resorption, the osteoclast must sustain an extraordinarily low pH environment, withstand immense ionic pressures, and coordinate nutrient and waste exchange across its membrane to sustain its unique structural and functional polarity. To achieve this, osteoclasts are equipped with an elaborate set of membrane transport proteins (pumps, transporters and channels) that serve as molecular 'gatekeepers' to regulate the bilateral exchange of ions, amino acids, metabolites and macromolecules across the ruffled border and basolateral domains. Whereas the importance of the vacuolar-ATPase proton pump and chloride voltage-gated channel 7 in osteoclasts has long been established, comparatively little is known about the contributions of other membrane transport proteins, including those categorized as secondary active transporters. In this Special Issue review, we provide a contemporary update on the 'ins and outs' of membrane transport proteins implicated in osteoclast differentiation, function and bone homeostasis and discuss their therapeutic potential for the treatment of metabolic bone diseases.

**Keywords: osteoclast, membrane transporter, V-ATPase, bone disease, ion channel, CLCN7, solute carrier, osteoporosis**

OPEN ACCESS

***Edited by:***
*Yankel Gabet,*
*Tel Aviv University, Israel*

***Reviewed by:***
*Wei Zou,*
*Washington University in St. Louis, United States*
*Mariafrancesca Scalise,*
*University of Calabria, Italy*

***Correspondence:**
*Nathan J. Pavlos*
*nathan.pavlos@uwa.edu.au*

***Specialty section:***
*This article was submitted to Cellular Biochemistry, a section of the journal Frontiers in Cell and Developmental Biology*

***Received:*** *22 December 2020*
***Accepted:*** *09 February 2021*
***Published:*** *26 February 2021*

***Citation:***
*Ribet ABP, Ng PY and Pavlos NJ (2021) Membrane Transport Proteins in Osteoclasts: The Ins and Outs. Front. Cell Dev. Biol. 9:644986. doi: 10.3389/fcell.2021.644986*

## INTRODUCTION

Osteoclasts (OCs) are large bone-digesting (resorbing) cells that play a central role in the regulation of skeletal bone mass and bone pathologies such as osteoporosis. These multinucleated giants arise from the fusion of mononuclear progenitor cells of the monocyte/macrophage lineage in response to macrophage-colony stimulating factor (M-CSF) and receptor activator of nuclear factor-κB ligand (RANKL) (for review see Teitelbaum and Ross (2003)). Upon contact with mineralized bone, OCs adopt a polarized anatomy that denotes their active bone-resorbing status (**Figure 1**). First, the bone-facing 'apical' membrane is hermetically sealed to the bone surface via podosomes; a dense network of actin filaments connected to transmembrane adhesion proteins (e.g., β3-integrin). The membrane entrapped within this 'sealing zone', in turn, assumes a highly convoluted morphology termed the ruffled border. The ruffled border serves as the OC bone-resorbing apparatus and is formed upon the rapid fusion of secretory lysosomes with the bone-apposed plasmalemma (reviewed in Ng et al. (2019)). Thus, the composition of the ruffled border shares close analogy with endolysosomal membranes (Weivoda and Oursler, 2014; Roy and Roux, 2018) and together with the underlying resorptive space (hemivacuole or resorptive pit) is viewed akin

**Abbreviations:** OC, osteoclast; $V_1$, V-ATPase ATP-hydrolytic domain; $V_0$, V-ATPase proton-translocation domain; BMD, bone mineral density; ARO, autosomal recessive osteopetrosis.

to a giant digestive 'extracellular lysosome'. Reflecting this, the resorptive hemivacuole is highly acidified (pH ∼4.5). Acidification is driven by the efflux of protons ($H^+$) and chloride ions ($Cl^-$) across the OC ruffled border membrane. This process is requisite to dissolve the inorganic phase of bone (hydroxyapatite) and the activation of acidic hydrolysases (chiefly cathepsin K) that digest the underlying organic collagen (Type 1a) matrix.

Being semipermeable, the ruffled border permits passive diffusion of small non-charged molecules (e.g., oxygen, carbon dioxide and water) across its membrane in-folds but restricts the influx of charged ions such as $H^+$ and $Cl^-$, leading to increased membrane potential and ionic pressure within the resorptive space. In addition, the dissolution of hydroxyapatite crystals ($Ca_{10}(PO_4)_6(OH)_2$) back into its elemental forms further exposes the ruffled border membrane to high ambient concentrations of calcium ions ($Ca^{2+}$) and inorganic phosphate (Pi). In order to sustain OC cell volume and polarity, these resorption by-products must be removed and transported across the OC ruffled border and basolateral membranes. Some of these materials (e.g., degraded collagen) are internalized by bulk endocytosis at the ruffled border and transported apico-basolaterally via transcytotic carriers before being expelled at the functional secretory domain (FSD) (Nesbitt and Horton, 1997; Salo et al., 1997). By comparison, other by-products, such as ions and metabolites, are translocated by sets of structurally and functionally diverse membrane transport proteins, enriched on the opposing ruffled border and basolateral membranes (**Figure 2**). In their simplest form, membrane transport proteins are considered 'gatekeepers' of molecular exchanges across biological membranes and are operationally categorized according to their mode, direction and molecule of transport: i.e., (i) channels, (ii) gated channels, (iii) primary active transporters and (iv) secondary active transporters (uniporters, symporters and antiporters, inclusive) (**Figure 2A**). These integral transmembrane proteins can be further subdivided into four main superfamilies: (i) the ATP-binding cassette (ABC) transporters, (ii) ATPases, (iii) ion channels, and (iv) solute carrier proteins (SLCs) (reviewed extensively in (Pizzagalli et al., 2020)).

Collectively, membrane transport proteins not only facilitate complex and rich exchanges at the interface between the OC ruffled border or the basolateral surface with the extracellular milieu but also between membranes of intracellular organelles (such as lysosomes, the endoplasmic reticulum and mitochondria) and the cytosol (**Figure 2B**). In this way, they ensure that every functional unit of the OC receives its necessary complement of ions, metabolites and nutrients required for cellular homeostasis. In a giant energetic cell so heavily subjected to large ionic fluxes and membrane turnover, it is therefore unsurprising that an increasing number of mutations in membrane transport proteins have been implicated in the pathogenesis of bone diseases, in particular bone sclerosing (high bone mass) diseases associated with OC dysfunction (**Table 1**). For example, most of the known forms of OC-rich autosomal recessive osteopetrosis (ARO) have been linked to mutations in subunits of the multimolecular vacuolar-ATPase (V-ATPase) proton pump and chloride voltage-gated channel 7 (CLCN7), both indispensable components of the OC acidification machinery as described herein.

In this Special Issue, we briefly review the 'ins and outs' of membrane transport proteins in OCs. We highlight the contributions of established OC membrane transporters and channels (e.g., V-ATPases and CLCN7) as well as shed light on lesser-known membrane transport proteins whose physiological contributions in OCs and bone health have only just begun to emerge. We describe the structure, localization and function of these membrane transport proteins in OCs and bone as well as discuss their therapeutic utility as molecular targets for the treatment of metabolic bone diseases such as osteoporosis.

## PROTON TRANSPORT IN OSTEOCLASTS: THE V-ATPASE COMPLEX

The transport of protons ($H^+$) across biological membranes is one of the most important physiological functions of cellular homeostasis, governing the regulation of intracellular pH, facilitating the generation of pH gradients in localized regions of cells, and maintaining the pH of the extracellular fluid. Aberrant regulation of pH in tissues and in cells leads to conditions such as acidosis and has been increasingly linked to the onset and progression of cancer (Parks et al., 2013; Aoi and Marunaka, 2014).

To maintain intracellular pH homeostasis, cells have evolved sophisticated proton extrusion mechanisms and complementary buffering systems (e.g., CA2 and SLC4A2 reviewed below). Of these, the vacuolar $H^+$-ATPase (V-ATPase) is among the most conspicuous features of eukaryotic endocytic and secretory organelle membranes and is arguably the keystone transporter for OC acidification and bone resorptive function. This large macromolecular complex is powered by the hydrolysis of ATP to extrude hydrogen ions ($H^+$) across biological membranes. In OCs, the V-ATPase complex is enriched on the OC ruffled border membrane and decorates the surface of secretory lysosomes (Baron et al., 1985). Here, it facilitates the transport of protons necessary for acidification of the underlying resorptive space and activation of acidic hydrolysases (e.g., cathepsin K). Structurally, the V-ATPase proton pump is composed of 14 subunits and is the sum of two domains: (i) the ATP-hydrolytic domain ($V_1$) and (ii) the proton-translocation domain ($V_0$) (**Figure 3**). The $V_1$ domain is composed of eight subunits (A to H) and is anchored indirectly to membranes through its interaction with the $V_0$ domain. The $V_0$ domain contains six subunits named a, d, e, c, c′, and c″, that assemble into a complex embedded into the membrane (**Figure 3**; Qin et al., 2012b; Duan et al., 2018). Following assembly, hydrolysis of ATP by the $V_1$ domain generates the energy required to initiate $V_0$ domain rotation. It is this active rotational movement that drives proton-translocation across the membrane (Forgac, 2007; Jefferies et al., 2008). For an extensive review see (Qin et al., 2012b).

The V-ATPase complex is obligatory for OC function and bone homeostasis. Accordingly, the gene expression levels of V-ATPase subunits are robustly amplified during RANKL-induced OC differentiation (Toyomura et al., 2000;

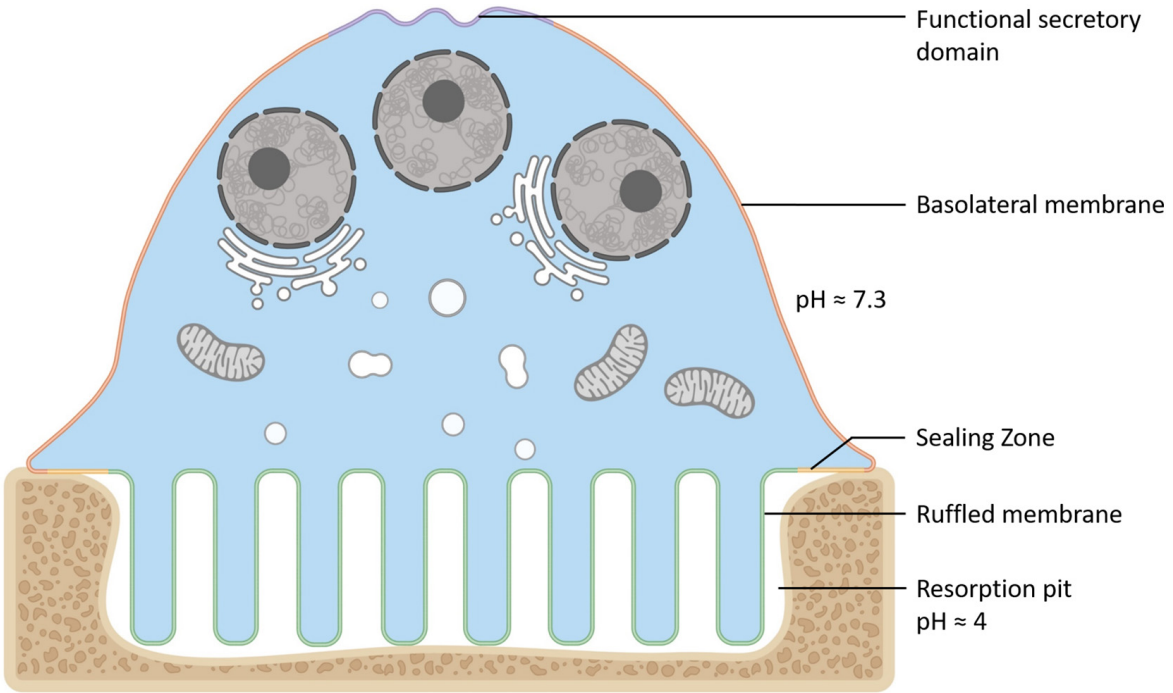


**FIGURE 1 |** Anatomy of the Osteoclast. Illustration of the unique configuration and membrane organization of an osteoclast during active bone resorption. The osteoclast's specialized plasma membrane domains are labeled and color-coded: Purple = the functional secretory domain, Orange = the basolateral membrane, Yellow = the sealing zone and Green = the ruffled border membrane. Created with BioRender.com.

Manolson et al., 2003). Transcriptionally, this is regulated by MITF (Microphthalmia-associated transcription factor) (Zhang et al., 2015), a transcription factor of the MiT-TFE family of basic helix-loop-helix leucine-zipper transcription factors that serve collectively as master regulators of lysosomal biogenesis, autophagy and osteoclastogenesis (Hershey and Fisher, 2004). Owing to its unique demands for acidification, the OC has also evolved cell-specific V-ATPase subunits. In particular, the OC-specific a3 subunit of the $V_0$ domain encoded by *TCIRG1* in humans or *ATP6i* in mice, respectively. The a3 subunit has been shown to facilitate trafficking of the V-ATPase pump to the ruffled border (Sun-Wada et al., 2000; Futai et al., 2019) in collaboration with the small regulatory GTPases Rab7 and Rab27A (Matsumoto et al., 2018; Futai et al., 2019). Not surprisingly, mutations in *TCIRG1* account for ∼50% of OC-rich ARO in humans (Frattini et al., 2000; Sobacchi et al., 2013), a skeletal phenotype that is recapitulated in mice upon genetic ablation of *ATP6i* (Li et al., 1999).

## NEUTRALIZING MEMBRANE POTENTIALS WITH CHLORIDE IONS DURING BONE RESORPTION

The electrogenic efflux of $H^+$ into the bone resorptive space generates a large membrane potential across the OC ruffled border (Kuno, 2018). To balance this charge, the OC must transport negatively charged counter-ions (anions) such as chloride ($Cl^-$) across the ruffled border membrane. Failure to neutralize this membrane potential inhibits the acidification of the underlying resorption pit (Kornak et al., 2001). To achieve this, the OC furnishes its ruffled border membrane with complementary chloride-proton antiporters and secondary active transporters, described herein, that cooperatively facilitate $Cl^-$ exchange across membranes.

## CLIC1

Chloride intracellular channel 1 (CLIC1) is a highly conserved chloride ion channel (Ulmasov et al., 2007) that exists intracellularly in a soluble state but undergoes reversible conformational changes that give rise to a dimeric integral membrane channel (Varela et al., 2019). The precise mechanisms governing CLIC1 membrane insertion remain unclear although oxidizing conditions, pH, $Ca^{2+}$ and $Zn^{2+}$ ion availability and membrane cholesterol have all been reported to influence its membrane integration (Valenzuela et al., 2013; Hossain et al., 2019). In OCs, the physiological role of CLIC1 has been contentious. Initial studies by Schaller et al. (2004) demonstrated that the chloride channel inhibitor NS3736 protected against ovariectomy-induced bone loss in rats owing to a dose-dependent inhibition of OC bone resorption. In keeping with this position, NS3736 was found to block OC acidification and bone resorption under *in vitro* settings. Based on these observations, the authors speculated that NS3736 inhibits the transport activity of either

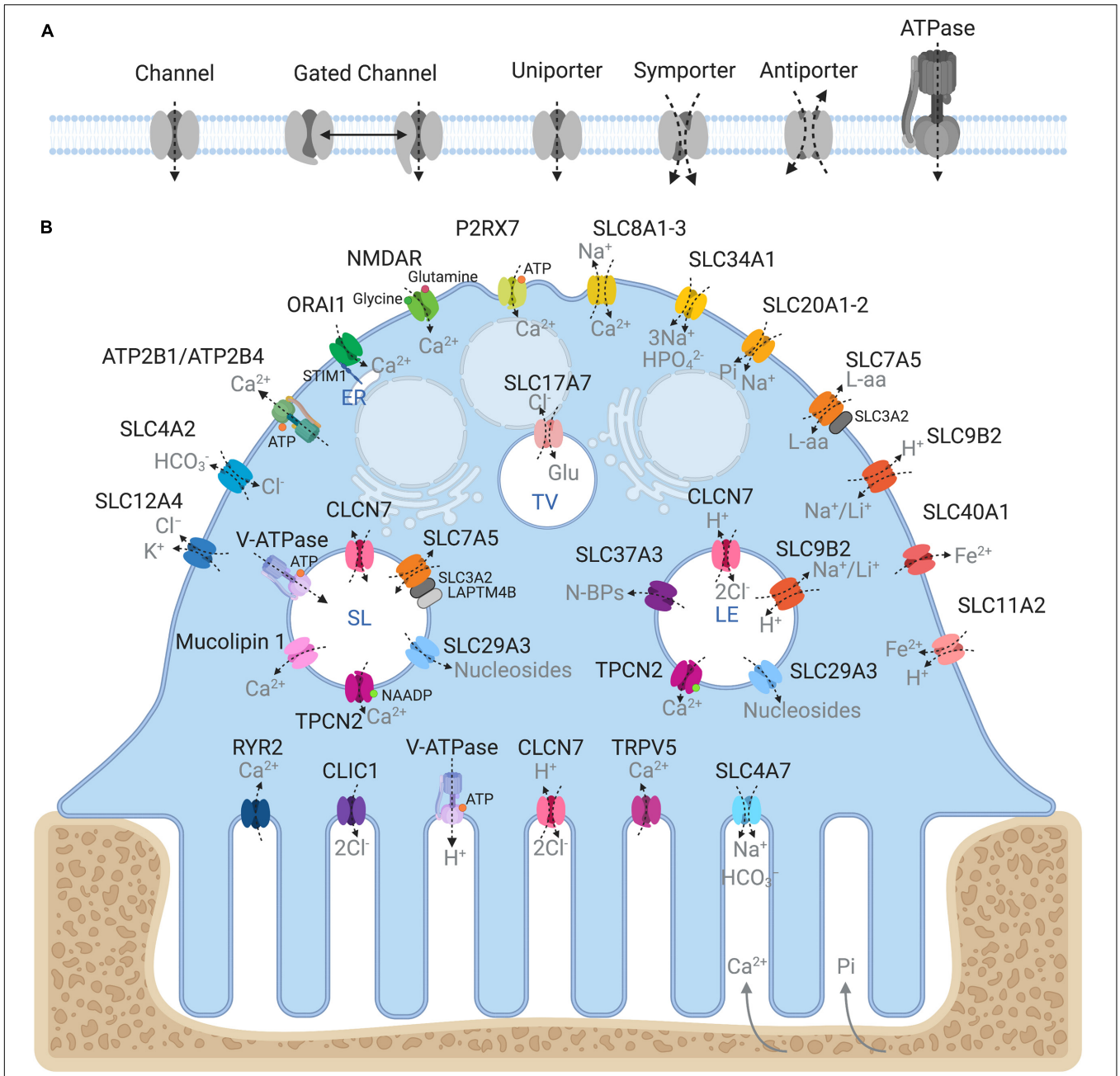


**FIGURE 2 |** Ins and outs of membrane transport proteins in osteoclasts. **(A)** Schema depicting the major types of transport proteins and their modes of substrate movement across biological membranes. **(B)** Model summarizing the reported membrane localization of all the major membrane transport proteins expressed in osteoclasts. Known substrates are indicated in gray. Intracellular compartments correspond to: ER, endoplasmic reticulum; SL, Secretory lysosome; LE, Late endosome; TV, Transcytotic vesicle. Created with BioRender.com.

CLIC1 or CLCN7. Closer inspection of the expression levels of CLIC1 and CLCN7 revealed that whereas CLCN7 is highly expressed in OCs, CLIC1 is expressed widely in peripheral tissues, implying that NS3736 acted primarily on CLCN7 rather than CLIC1. Consistently, mice deficient in *CLIC1* lack an overt bone phenotype but rather exhibit bleeding abnormalities owing to platelet dysfunction (Qiu et al., 2010). Collectively, these data point to a physiological role for CLIC1 outside of the skeleton.

## CLCN7

Unlike CLIC1, the chloride voltage-gated channel 7 (CLCN7) (also known as CLC-7, OPTA2, and PPP1R63) is indispensable for OC function and bone homeostasis (Kornak et al., 2001). Intracellularly, CLCN7 exists as a homodimer residing on the membranes of late endosomes, lysosomes and the ruffled border where it functions as a $2Cl^-/H^+$ antiporter with a fixed

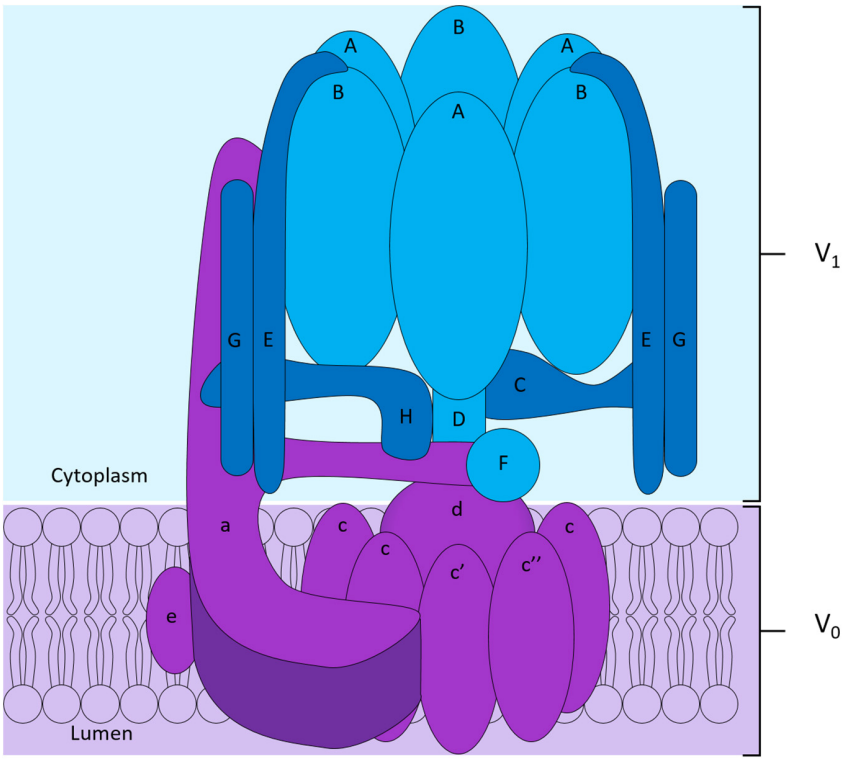


**FIGURE 3 |** Structure of the V-ATPase proton pump. The V-ATPase complex is composed of two domains: the peri-membranous $V_1$ domain composed of subunits A to H responsible for the hydrolysis of ATP shown in blue, and the intramembranous $V_0$ domain who allows the translocation of protons across the membrane shown in purple in the diagram. The V0 domain is composed of the subunits a, e, d and of a hexameric ring formed by subunits c, c′ and c″.

stoichiometry of $2Cl^-$ for each $H^+$ transported (Graves et al., 2008). Unique among mammalian CLCN transporters, CLCN7 requires an obligatory β-subunit: osteoclastogenesis associated transmembrane protein 1 (Ostm1) (also known as CLCN7 accessory beta subunit) (Lange et al., 2006). This association is critical for the stability of CLCN7 and Ostm1 expression and $Cl^-/H^+$ exchange (Stauber and Jentsch, 2010). Similar to the V-ATPase proton pump subunits, the expression of both CLCN7 and Ostm1 is regulated by the transcription factor MITF (Meadows et al., 2007). CLCN7 traffics to late endosomes and lysosomes via interaction of its [DE]XXXL[LI] dileucine lysosomal targeting motifs with cognate adaptor proteins (Stauber and Jentsch, 2010). The mechanisms by which Ostm1 and CLCN7 cooperate on lysosome membranes has long remained unclear. However, recent cryoelectron microscopy studies by two independent groups demonstrated that the highly glycosylated Ostm1 serves as a molecular shield by covering the luminal surface of CLCN7 thereby protecting it from proteolysis in acidic environments that occur inside lysosomes and the resorptive space (Schrecker et al., 2020; Zhang et al., 2020). The importance of this intimate molecular association is exemplified in the skeleton where mutations in either CLCN7 or Ostm1 correspond with severe osteopetrosis in humans and in mice (Kornak et al., 2001; Chalhoub et al., 2003). The G215R mutation in CLCN7, for example, leads to autosomal dominant osteopetrosis type 2 that does not abolish the transport function of the channel but rather causes a severe trafficking defect with the G215R-CLCN7 mutation rendering CLCN7 retention in the ER (Schulz et al., 2010). OCs derived from both CLCN7 and Ostm1 mutant mice form normally but fail to form a ruffled border and resorb bone (Kornak et al., 2001; Chalhoub et al., 2003).

In addition to CLCN7, CLCN3 and CLCN5 have also been reported to reside on late endosomes in OCs (Okamoto et al., 2008) and mineralizing osteoblasts (Larrouture et al., 2015). Genetic ablation and siRNA-mediated depletion of *Clcn3* was found to reduce the acidification and bone resorptive capabilities of mouse OCs cultured *in vitro* (Okamoto et al., 2008). *Clcn3* knockout mice lack a bone phenotype although, like their *Clcn7* knockout counterparts, they exhibit severe neurodegeneration (Yoshikawa et al., 2002; Kasper et al., 2005; Okamoto et al., 2008). This indicates that CLCN3 is dispensable for OC function and skeletal homeostasis.

## SLC12A4

Outside the CLCN family, solute carrier family 12 member 4 (SLC12A4), also known as the electroneutral potassium-chloride cotransporter 1 (KCC1), has been shown to facilitate $Cl^-$ extrusion in OCs. SLC12A4 localizes exclusively to the OC basolateral surface where it has been proposed to function in

the cotransport of $K^+$ and $Cl^-$ simultaneously in the outward direction. Unlike other members of the SLC12 family, SLC12A4 $K^+/Cl^-$ cotransport is not dependent on the presence of $Na^+$ (Hebert et al., 2004). Structurally, SLC12A4 is composed of 1085 amino acids forming a 12 transmembrane domain structure with a large extracellular loop containing potential N-linked glycosylation sites, and cytoplasmic N- and C-terminal domains (Gillen et al., 1996). To enable transporter function, SLC12A4 dimerises through links in both transmembrane and extracellular domains (Liu et al., 2019). Although ubiquitously expressed, the function of *Slc12a4* has been explored in mouse OCs in *in vitro* settings (Kajiya et al., 2006). Studies by Kajiya et al. (2006) demonstrated that Slc12a4 is the primary potassium-chloride transporter expressed in OCs. Moreover, treatment of OCs with the KCC transporter inhibitor R(+)-butylindazone (DIOA), or knockdown of *Slc12a4* expression using siRNA, decreased $Cl^-$ extrusion resulting in increased OC alkalinisation and, in turn, reduced capacity to resorb bone (Kajiya et al., 2006). It remains to be seen whether these *in vitro* defects in OC activity extend to physiological impacts on the skeleton in intact mice.

## INTERNAL BUFFERING AND $HCO_3^-$ TRANSPORT IN OSTEOCLASTS

To sustain acidification during ongoing cycles of bone resorption, the V-ATPase pump requires a continuous supply of protons. Protons are supplied to the V-ATPase pump by the cytoplasmic carbonic anhydrase 2 (CA2), an enzyme that catalyses the reversible hydration of carbon dioxide along the following equation: $CO_2 + H_2O \rightarrow H^+ + HCO_3^-$. Unsurprisingly, defects in CA2 activity lead to osteopetrosis and extra-skeletal disturbances including renal tubular acidosis and cerebral calcification, reminiscent of the clinical features observed in patients harboring mutations in *TCIRG1*. At the same time, CA2 stabilizes intracellular pH (pHi) and alkalinisation in OCs through the liberation of $HCO_3^-$ ions. $HCO_3^-$ ions are, in turn, exchanged for $Cl^-$ by select members of the solute carrier protein family 4 (SLC4), thereby ensuring an electroneutral supply of $Cl^-$ to the OC (Teti et al., 1989).

## SLC4A2

SLC4A2, previously known as EPB3L1 or AE2, is a member of the SLC4 family of $Cl^-/HCO_3^-$ exchangers. SLC4 family members are important for the modulation of pHi and have been implicated in the regulation of cell volume, migration, and transepithelial movement of ions in various tissues (Alper, 2006). The SLC4 family comprises 10 members divided into three major clades; (i) the $Na^+$-independent electroneutral $Cl^-/HCO_3^-$ exchangers (e.g., SLC4A1), (ii) the $Na^+$-dependent $HCO_3^-$ transporters (e.g., SLC4A4) and, (iii) borate transporters comprised of a singular member in mammals, SLC4A11 (Cordat and Casey, 2008; Liu et al., 2015). In mice, due to different promoter regions *Slc4a2* can be transcribed as five different N-terminal variants: Slc4a2a, Slc4a2$b_1$, Slc4a2$b_2$, Slc4a2$c_1$, and Slc4a2$c_2$. Slc4a2a and Slc4a2b are ubiquitously expressed while Slc4a2c expression is restricted to the stomach. In OCs, *Slc4a2* expression is upregulated during differentiation in an NFATc1-dependent manner (Wu et al., 2008) and has been localized to the basolateral plasma membrane. *Slc4a2* knockout mice are viable and have been used as a model to study the role of the transporter in different tissues including the stomach, intestines, colon, biliary epithelial cells, testes, and ameloblasts (Rossmann et al., 2000; Medina et al., 2003; Lyaruu et al., 2008; Gawenis et al., 2010; Concepcion et al., 2013).

In bone, four independent studies have investigated the impact of *Slc4a2* deletion on skeletal homeostasis in mice. The first by Wu et al. (2008) assessed the bone phenotypes of mice globally lacking all *Slc4a2* isoforms. In this study *Slc4a2*-deficient mice were shown to manifest osteopetrosis with growth retardation and clubbing of the long bones. The authors went on to show that this disruption in bone homeostasis was related to a cell-autonomous defect in OCs and concluded that the primary function of Slc4a2 in OCs is to facilitate bone resorption by suppressing OC apoptosis (Wu et al., 2008). The second, by Josephsen et al. employed a global deletion mouse model of *Slc4a2*. In this instance, the knockout mice presented with an osteopetrotic phenotype affecting the skull and long bones. This high bone mass phenotype was attributed to defects in OCs, which where morphologically enlarged and possessed rudimentary ruffled borders. Soon after, Jansen et al. (2009) confirmed the osteopetrotic phenotypes of long bones in *Slc4a2a-b* knockout mice. However, in contrast to global *Slc4a2*-deficient mice, calvarias of *Slc4a2a-b* knockout mice are indistinguishable from wild-type littermates implying partial compensation from untargeted Slc4 isoforms. More recent studies by Coury et al. (2013) used an OC-specific conditional deletion of *Slc4a2* in mice. In this study, specific loss of Slc4a2 in OCs corresponded with a high bone mass phenotype and dysfunctional OCs which exhibited impaired bone resorption capacity owing to a dysregulation of calpain-dependent podosomal disassembly (Coury et al., 2013). The importance of SLC4A2 is not limited to mice, but has also been shown to underpin the osteopetrotic phenotype observed in Red Angus cattle (Meyers et al., 2010). Taken together, these findings highlight the indispensable role for the SLC4A2 transporter in buffering HCO3$^-$ / $Cl^-$ exchange during OC bone resorption. A future challenge will be deciphering the exact contribution of each SLC4A2 variant in OCs as well as exploiting this transporter family for therapeutic targeting. A recent study demonstrating that the anion exchange inhibitor 4, 4′-diisothiocyano-2,2′-stilbenedisulfonic acid (DIDS) is capable of suppressing OC activity in a mouse model of wear-particle-induced osteolysis (Wu et al., 2018) lends 'proof of principal' toward this.

## SLC4A7

Solute carrier family 4 member 7 (SLC4A7), also known as NBC2, NBC3 and NBCn1, is responsible for the electroneutral cotransport of $Na^+$ and $HCO_3^-$ with a stoichiometry of one for one (Pushkin et al., 1999; Choi et al., 2000). SLC4A7 is

expressed in many human tissues including the kidneys and gastrointestinal tract where it localizes to basolateral and apical cell membranes and participates in net cellular acid extrusion. The transporter is predicted to homodimerise and is understood to have 14 transmembrane domains with a long intracellular N-terminal and short C-terminal presenting a PDZ domain. SLC4A7 possesses a dileucine motif in its cytoplasmic C-terminal tail indicating potential lysosomal residency supported by reports of co-localization with LAMP1. The C-terminal of the protein has also been shown to interact with RACK1. In addition, some putative binding candidates for this terminal have been identified and include LAMP1, LAMP2, AP2A1, AP2B1, Rab5A, 5B, 5C, 8A, 11, and SNX1, 2, 5, 6, 27 (Olesen et al., 2018). The PDZ domain of Slc4a7 has been shown to interact with NHERF-1, PSD-95, and CFTR. There is also evidence for interactions between the C-terminal PDZ domain and V-ATPase subunits in renal tissues (Pushkin et al., 2003) and CA2, consequently recruiting CA2 to the plasma membrane (Loiselle et al., 2004).

*Slc4a7* expression has been detected at both the mRNA and protein level in neonatal rat OCs and murine OC-like cells where it has been suggested to function as a key participant in M-CSF-induced cellular alkalinisation (Bouyer et al., 2007). Indeed, *Slc4a7* expression is upregulated during osteoclastogenesis and had been localized to the ruffled border membrane (Riihonen et al., 2010). Consistently, knockdown of Slc4a7 expression using a shRNA lentivirus-mediated delivery impairs OC bone resorption and cytosolic pH homeostasis but does not alter OC formation or survival. To date, *Slc4a7* knockout mice have been generated although their skeletal phenotype remains unknown (Lee et al., 2016).

## CALCIUM TRANSPORTERS IN OSTEOCLAST SIGNALING, DIFFERENTIATION AND FUNCTION

$Ca^{2+}$ is a universal second messenger required for cell signaling and plays multiple roles in OC formation, survival and activity (Robinson et al., 2010). It is liberated from bone during resorption by OCs, which, in turn, exposes the ruffled border membrane to high concentrations of the ion (up to 40mM $Ca^{2+}$) (Silver et al., 1988). Aforementioned, some of this $Ca^{2+}$ is removed by transcytotic mechanisms or through passive leakage from the resorptive compartment during OC migration. However, a portion of this solubilized $Ca^{2+}$ is exchanged transcellularly across OC membranes via a number of structurally diverse calcium transport proteins embedded on the surface of the OC ruffled border and basolateral domain that are described here (Berger et al., 2001).

## RYANODINE RECEPTOR 2

Being enriched in the OC plasma membrane, the Ryanodine receptor 2 (RYR2) was initially proposed to be the major $Ca^{2+}$channel controlling $Ca^{2+}$ influx in OCs, a position supported by several lines of biophysical, pharmacological and immunochemical evidence in the early 2000s (Zaidi et al., 1995, 1999; Baljit et al., 2002; Datta and Horrocks, 2003). The role of the RYR2 in OCs has been reviewed extensively in Robinson et al. (2010) and thus will not be discussed further herein. Instead, we will focus on the contribution of more recently identified transporters and channels that have been implicated in modulating the exchange of $Ca^{2+}$ across OC membranes.

## ATP2B1 AND ATP2B4

*ATP2B1* and *ATP2B4*, also known as *PMCA1* and *PMCA4* respectively, belong to the P-type $Ca^{2+}$ ATPase family that maintains intracellular homeostasis by exporting $Ca^{2+}$ from the cytoplasm to the extracellular space. These pumps are powered by the hydrolysis of ATP, with one $Ca^{2+}$ ion removed from the cell for each molecule of ATP hydrolysed. Calmodulin increases the affinity of the proteins' alternatively spliced $Ca^{2+}$-binding site and also increases the rate at which the pump extrudes $Ca^{2+}$ (Keeton et al., 1993; Tidow et al., 2012). *ATP2B1* and *ATP2B4* are highly expressed in OCs and transcriptionally regulated by NFATc1 (Kim et al., 2012). Both ATP2B1 and ATP2B4 pumps reside on the basolateral membrane of OCs where they have been proposed to function to extrude superfluous intracellular $Ca^{2+}$ and thus prevent $Ca^{2+}$-induced apoptosis. Studies by Kim et al. (2012) demonstrated that siRNA-mediated double knockdown of *ATP2B1* and *ATP2B4* led to a significantly reduced bone volume to trabecular volume ratio and a significant increase in OC surface to bone surface ratio using a mouse calvarial injection model. Genetic ablation of *Atp2b1* in mice is lethal during early embryonic development and thus far has precluded assessment of the skeleton (Okunade et al., 2004). Similarly, there has been no reported bone phenotype for *Atp2b4* knockout mice, however males are infertile owing to reduced sperm motility (Okunade et al., 2004; Schuh et al., 2004).

## TRPV4-6

In addition to $Ca^{2+}$ ATPases, OCs possess an array of $Ca^{2+}$ channels including several members belonging to the transient receptor potential (TRP) channel family. TRP channels are a class of 6-membrane-spanning helices ion channels primarily located on the plasma membrane of several mammalian cell types. They can be divided into Groups 1 and Group 2 channels; with each possessing their own subfamilies. TRP channels mediate several sensory functions including pain, temperature, taste, pressure, and vision but have also been linked to regulatory mechanisms. Trpv1-6 (Transient receptor potential cation channel subfamily V member 1 to 6) are members for the TRPV subfamily of Group 1 TRP channels. Several TRPV members including TRPV4, 5 and 6 are known to be expressed in OCs. *TRPV4* mRNA and protein expression has been reported to be upregulated during OC differentiation. *In vitro,* TRPV4 has been implicated in OC formation, with overexpression or knockdown of the channel correlating to increased and decreased OC numbers, respectively (Cao et al., 2019).

In comparison, TRPV5 is primarily expressed in the kidney, intestines and OCs where it plays a central role in the

systemic regulation of $Ca^{2+}$ homeostasis by facilitating: (i) $Ca^{2+}$ reabsorption in the kidneys, (ii) absorption of dietary $Ca^{2+}$ by intestinal cells, and (iii) the release of the ion by active OCs. The importance of TRPV5 in $Ca^{2+}$ homeostasis is exemplified in *Trpv5* knockout mice, which exhibit reduced renal $Ca^{2+}$ reabsorption leading to hypercalciuria-induced polyuria coupled with urine acidification (Hoenderop et al., 2003). The $Ca^{2+}$ lost through urine in *Trpv5* knockout mice is compensated by hyperabsorption of dietary $Ca^{2+}$, which, in turn, leads to reduced bone cortical and trabecular thickness. In these mice, serum peptide hormones (PTH), $Ca^{2+}$ and $K^{+}$ levels are normal despite increased 1,25-(OH)2D3, implying that the decreased cortical and trabecular bone thickness observed in *Trpv5* knockout mice is an indirect consequence of prolonged elevations in 1,25-(OH)2D3 (Hoenderop et al., 2003). However, studies by the same group later reported a cell-autonomous defect in *Trpv5*-deficient OCs. In OCs, Trpv5 localizes to the ruffled border suggestive of a role in modulating bone resorption. Closer inspection of the bones of *Trpv5* knockout mice revealed that loss of *Trpv5* was associated with increased OC numbers and an increase in the number of nuclei per OC. Moreover, *Trpv5* knockout OCs exhibited reduced bone resorptive capacity in line with a intrinsic cellular defect (van der Eerden et al., 2005). Further, alendronate has been shown to normalize the reduced bone thickness in *Trpv5* knockout mice (Nijenhuis et al., 2008). It is noteworthy that Econazole (Yan et al., 2011), TH-1177 (Landowski et al., 2011), and selected cannabinoids (Janssens et al., 2018) have been reported to modulate TRPV5 but have potencies in the mid-micromolar range and are not selective for TRPV5 over its close homolog TRPV6. Hughes et al. (2019) identified three novel TRPV5 inhibitors through structural-based virtual screening. One of which was selective for TRPV5 over TRPV6 as revealed through the identification of a previously uncharacterised TRPV5 binding site by cryoelectron microscopy (Hughes et al., 2019). The apparent importance of TRPV5 in OC function along with recent development of selective TRPV5 inhibitors makes this channel a potential candidate for the therapeutic modulation of bone homeostasis.

Finally, similar to *TRPV5*, *Trvp6* knockout mice manifest a low bone mass (osteopenia) phenotype owing to increased OC numbers, and hence a net increase in OC bone resorptive activity *in vivo* (Chen et al., 2014).

## MUCOLIPIN-1

Mucolipin-1 (also known as TRPML1) is the first member of the transient receptor potential cation channel, mucolipin subfamily and is widely recognized as a major calcium release channel residing on lysosomal membranes (Vergarajauregui and Puertollano, 2006; Thompson et al., 2007). Mucolipin-1 plays critical roles in a variety of membrane trafficking processes such as retrograde trafficking of lysosomes to the trans-Golgi network, autophagic maturation and lysosomal homeostasis (Haoxing and Dejian, 2015; Scotto Rosato et al., 2019). This non-selective cation channel is modulated by changes in $Ca^{2+}$ concentration, phosphoinositides and pH. Mutations in *MCOLN1* lead to Mucolipidosis type IV, an autosomal recessive neurodegenerative lysosomal storage disorder (Bargal et al., 2000). The importance of Mucolipin-1 extends to bone. Genetic deletion of Mucolipin-1 in mice correlates with impaired osteoclastogenesis, altered lysosomal homeostasis and attenuated OC bone resorption pointing to an indispensable and physiological role for this cation channel in bone remodeling (Erkhembaatar et al., 2017). For an extensive review see (Wang et al., 2014).

## ORAI1

ORAI calcium release-activated calcium modulator 1 (ORAI1), also known as CRACM1 and TMEM142A, is a plasma membrane localized $Ca^{2+}$ channel. It associates with stromal interaction molecule 1 (STIM1), an endoplasmic reticulum transmembrane protein, to modulate $Ca^{2+}$ cellular entry through a process termed calcium release-activated calcium (CRAC) (Lunz et al., 2019). Upon depletion of luminal endoplasmic reticulum $Ca^{2+}$ stores, the CRAC assembly formed by ORAI1 and STIM1 opens to refill depleted stores. To achieve channel opening, the cytoplasmic portion of STIM1 must come into contact with the intracellular portion of ORAI1 after which ORAI1, in turn, allows extracellular $Ca^{2+}$ influx into the cell to replenish stores. Studies by Zhou et al. (2011) reported a decline in both *ORAI1* and *STIM1* expression during osteoclastogenesis in human cells. Moreover, they found that siRNA-mediated knockdown of *ORAI1* decreased OC formation. The authors further demonstrated that pharmacological inhibition of the CRAC channel assembly prevented OC differentiation. Using a shRNA knockdown approach, Hwang and Putney (2012) similarly reported that depletion of *Orai1* impairs OC differentiation *in vitro* owing to a decreased in NFATc1 transcritpional activity and associated downstream genes. Importantly, *Orai1* knockout mice exhibit a clear skeletal phenotype (Robinson et al., 2012). *Orai1* knockout mice are anatomically smaller than their wild-type counterparts and show less post-natal growth. In addition, they exhibit tooth abnormalities and bone defects, including the existence of unresorbed cartilage remnants and decreased bone mineralization. Accordingly, OCs from *Orai1* knockout mice are morphologically smaller (mononuclear) and osteoblastic maturation was impaired. Thus, the skeletal abnormalities observed in *Orai1* knockout mice appear to arise from cell-autonomous defects in both OCs and osteoblasts highlighting a general role for this $Ca^{2+}$ channel in bone homeostasis.

## NMDAR

The N-methyl-D-aspartate receptor (NMDAR) is a glutamate receptor and ion channel found on the plasma membrane of OCs whose physiological function has long been debated. The channel is composed of three subunits: NMDAR1 associates with one or more NMDAR2 and/or NMDAR3 subunits. The multiple receptor subunit combinations along with the existence of 8 different NMDAR1 splice variants allows diversity in glutamate receptor function (Spencer et al., 2007). When activated by the

binding of glutamate and glycine, the NMDAR allows for the flow of $Ca^{2+}$ across the membrane. At present the role of NMDAR in OCs physiology remains contentious with several conflicting reports in the literature (Spencer et al., 2007). For instance, Chenu et al. (1998) reported that MK-801, an NMDAR inhibitor, had no effect on adhesion or survival of OCs but caused the disruption of actin ring formation. In contrast, studies by Peet et al. (1999) found no effect of MK-801 on OC actin ring formation but instead showed that MK-801 prevented OC differentiation and bone resorption in a co-culture model *in vitro*. Further, Merle et al. (2003) reported that MK-801 inhibited osteoclastogenesis and that activation of NMDAR induced the nuclear translocation of NFκB. Thus, further study using *in vivo* models will be required to resolve the physiological contribution of this $Ca^{2+}$ channel in OCs and bone homeostasis.

## P2RX7

ATP-activated $Ca^{2+}$ channel Purinergic receptor P2X 7 (P2RX7), also known under the alias P2X7, is a member of the Purinergic receptors P2X group that mediate $Ca^{2+}$ fluxes across membranes in response to extracellular ATP. Following activation, P2RX7 forms a homotrimeric pore that facilitates the movement of organic ions including N-methyl-D-glucamine, choline and fluorescent dyes such as ethidium and YO-PRO-12 across membranes (Alves et al., 2014; Sluyter, 2017). P2RX7 is the major PX2 family member expressed in OCs (Naemsch et al., 2001) and its role in skeletal and joint diseases has been extensively reviewed (Zeng et al., 2019). P2RX7 has been implicated in OC fusion in both mice (Ke et al., 2003) and humans (Pellegatti et al., 2011). In humans, the formation of OCs is inhibited by an anti-P2RX7 monoclonal antibody and by specific P2RX7 pharmacological antagonists A740003 and AZ11645363 (Pellegatti et al., 2011). There is also accumulated evidence implicating several P2RX7 SNPs in postmenopausal osteoporosis (Ohlendorff et al., 2007; Gartland et al., 2012; Jørgensen et al., 2012). In keeping with this position, genetic deletion of *P2RX7* in mice corresponds with a significant reduction in total and cortical bone content and periosteal circumference in femurs, and reduced periosteal bone formation and increased trabecular bone resorption in tibias (Ke et al., 2003). Consistently, Wang et al. (2018a) reported increased OC formation in *P2RX7* knockout mice compared to wild-type littermates following ovariectomy (OVX)-induced bone loss. Further, whereas both the cortical and trabecular bone volume fractions were significantly decreased in the tibias of *P2RX7* knockout mice compared to knockout sham controls at 6-weeks post-OVX, no statistically significant change was observed in the corresponding bone parameters in OVX and sham operated wild-type mice 6-weeks post-surgery (Wang et al., 2018a).

## TPCN2

Two pore segment channel 2 (TPCN2), also known as TPC2, is a member of the Two pore channel family of intracellular voltage-gated and ligand-gated cation-selective channels that enables $Ca^{2+}$ ion release in response to NAADP binding. Intracellularly, TPCN2 localizes to lysosome-related organelles via a lysosomal targeting motif (Brailoiu et al., 2010; Schieder et al., 2010; Ambrosio et al., 2015) where it has been shown to contribute to the regulation of their biogenesis (Ambrosio et al., 2015). In OCs, *Tpcn2* mRNA expression is upregulated in response to RANKL and has been proposed to play a role in maintaining intracellular $Mg^{2+}$ rather than $Ca^{2+}$ homeostasis. At steady-state $Mg^{2+}$ levels, siRNA-mediated knockdown of *Tpcn2* has been shown to impair OC differentiation and bone resorption *in vitro*. Conversely, under low $Mg^{2+}$ culture conditions, OC formation was accelerated suggesting that Tpcn2 functions to regulates OC differentiation and activity in response to circulating $Mg^{2+}$ levels (Notomi et al., 2012, 2017).

## SLC8A1-3

Solute carrier family 8 member A1, A2 and A3 (SLC8A1, SLC8A2, SLC8A3), previously known as NCX1, NCX2 and NCX3, respectively, are $Na^{+}/Ca^{2+}$ antiporters from the SLC8 family. All three SLC8A transporters are expressed in OCs and are reported to localize to the basolateral membrane. Of these transporters, SLC8A1 has received the most attention in OCs (Li et al., 2007; Albano et al., 2017). The use of chemical inhibitors or siRNA to inhibit SLC8A1 and SLC8A3 leads to reduced bone resorption *in vitro* (Moonga et al., 2001; Li et al., 2007). Using an OC-specific *Slc8a1* knockout mouse model Albano et al. (2017) reported that *Slc8a1* knockout OCs form normally but resorb significantly more bone than their wild-type counterparts *in vitro*. However, no obvious skeletal changes were detected in *Slc8a1* knockout mice at 3 months of age with only very minor differences appreciable at 6 months of age. The findings *in vivo* suggest that Slc8a1 plays an accessory but not essential role in OC $Ca^{2+}$ homeostasis.

# PHOSPHATE HANDLING IN THE OSTEOCLAST

Inorganic phosphate (Pi) is an essential molecule for cellular homeostasis and is the major anionic component of hydroxyapatite. Therefore, in addition to $Ca^{2+}$, OCs are exposed to high ambient concentrations of Pi during bone resorption. Although the exact Pi concentration liberated into the resorption pit remains to be established, it is predicted to reach upward of 20 mM (Kuno, 2018). High ambient Pi has been shown to influence OC differentiation and resorptive activity underlying the importance of appropriate Pi handling by the cell (Kanatani et al., 2003). It has also been hypothesized that part of the Pi released from bone may be utilized by the OC to maintain cellular ATP during the energy requiring cyclical processes of migration, attachment, and resorption (Gupta et al., 1997). Typically, Pi influx has been reported to require extensive V-ATPase activity and thus a large amount of energy. Evidence of the existence of $Na^{+}$-dependent Pi transport systems in OCs was first demonstrated by Gupta et al. (1996) and later confirmed

by the Miyamoto and Gupta laboratories who demonstrated the presence of Pi influx and efflux systems in OC-like cells derived from RAW264.7 macrophages and primary mouse OCs (Khadeer et al., 2003; Mikiko et al., 2005). The expression of several $Na^+$-dependent Pi transporters have been assessed in OCs including SLC17A1 (previously NPT1), SLC34A1 (previously Npt2a or SLC17A2), SLC34A2 (previously Npt2b), SLC34A3 (previously Npt2c), SLC20A1 (previously Pit-1), SLC20A2 (previously Pit-2) and SLC37A3. Of these, SLC34A1, SLC20A1/2 and SLC37A3 have been functionally characterized in OCs.

## SLC34A1

Solute carrier family 34 member 1 (SLC34A1), previously known as NPT2a or SLC17A2 is an 80-90 kDa sodium cation/divalent phosphate cotransporter with a stoichiometry of three $Na^+$ to one $HPO_4^{2-}$ (Forster et al., 1999). It resides on cell membranes where it preferentially cotransports $Na^+$ and $HPO_4^{2-}$, although it has also been reported to transport $Li^+$ as a driving cation (Olga et al., 2012; Schlingmann et al., 2016). SLC34A1 sequentially binds two $Na^+$ cations, a $HPO_4^{2-}$ and a third $Na^+$ before undergoing conformational changes allowing the release of the ions on the opposite side of the membrane (Forster, 2019).

Several independent studies have implicated a role for *SLC34A1* in OC differentiation, bone resorption and skeletal homeostasis albeit with conflicting reports (Gupta et al., 2001; Khadeer et al., 2003; Albano et al., 2015). On one hand, studies by Albano et al. (2015) reported that SLC34A1 is dispensable for OC differentiation and bone resorption. On the other, studies by Gupta et al. (2001) reported that *Slc34a1* knockout mice exhibit an age-dependent bone phenotype associated with a reduction in OC numbers that accompanied increases in bone formation. The precise reasons for these discrepancies is unclear but may reflect differences in the targeting approach and mouse strains used. Alternatively, they might point to extra-skeletal disturbances in Pi homeostasis influencing the magnitude of bone phenotypes observed. For instance, outside of bone, *SLC34A1* is highly expressed in the kidneys. Inactivating mutations in *SLC34A1* have been associated with idiopathic infantile hypercalcemia 2 (IIH2), a disease usually attributed to mutations in CYP24A1 (Schlingmann et al., 2011; De Paolis et al., 2019). Thus, a major role of SLC34A1 is to facilitate reabsorption of glomerular-filtered phosphate in the proximal tubule, with disruption of this transporter leading to hypophosphatemia. Mutations in *SLC34A1* result in surplus active vitamin D in the body. This vitamin D excess, in turn, increases calcium absorption into the bloodstream, resulting in hypercalcemia (Schlingmann et al., 2016). Consistently, global *Slc34a1* knockout mice manifest hypophosphatemia and hyperphosphaturia associated with hypercalcemia and hypercalciuria all of which are known to influence bone mass.

## SLC20A1 AND SLC20A2

SLC20A1 (also known as PiT-1 and Glvr-1) and SLC20A2 (also known as PiT-2, Glvr-2 and Ram-1) are sodium-phosphate ($Na^+$/Pi) electrogenic cotransporters that are widely expressed. These transporters share 60% of their amino acid sequence although their precise stoichiometry remains to be established (Kavanaugh and Kabat, 1996; Bai et al., 2000). In OCs, both SLC20A isoforms are constitutively expressed throughout osteoclastogenesis (Khadeer et al., 2003; Albano et al., 2015). Of these, SLC20A1 has been localized to the basolateral membrane of bone-resorbing OCs (Khadeer et al., 2003). Global genetic ablation of *Slc20a1* in mice leads to embryonic lethality. However, a *Slc20a1* variant mouse in which both alleles code for a gene with 85% reduced expression (knockdown) are viable but manifest multiple abnormalities that do not extend to bone (Beck et al., 2010; Bourgine et al., 2013). Interestingly, *Slc20a1* knockdown mice exhibit an upregulation of *Slc20a2* implying functional redundancy. *Slc20a2* knockdown mice, however, show no overt bone phenotype but rather manifest features consistent with familial idiopathic infantile ganglia calcification as observed in humans harboring mutations in *SLC20A2* (Wang et al., 2012; Jensen et al., 2013). Future generation of a double *Slc20a1-Slc20a2* OC-specific knockout model might prove valuable toward resolving the ambiguity around the physiological importance of these two $Na^+$/Pi transporters in OC function.

## SLC37A3

Solute carrier family 37 member 3 (SLC37A3) is a little studied member of the SLC37 family of glucose-6-phosphate (G6P)/Pi antiporters (Chou et al., 2013; Cappello et al., 2018). SLC37A3 is highly expressed in neutrophils and the pancreas implying an important role for this transporter in these systems. SLC37A3 has been shown to localize to the endoplasmic reticulum but unlike other SLC37 family members does not transport G6P (Pan et al., 2011). Instead, SLC37A3 has been recently implicated in the translocation of nitrogen-containing bisphosphonates (N-BPs) from lysosomes to the cytosol (Drake et al., 2008). Using a CRISPRi-mediated genome-wide screen, Yu et al. (2018) identified SLC37A3 among the top genes to confer resistance to N-BPs. They further demonstrated that SLC37A3 interacts with ATRAID, a type I transmembrane protein on lysosomes, that stabilizes SLC37A3 expression thereby allowing the transport of N-BPs into the cytosol. In keeping with this position, deletion of *SLC37A3* and/or *ATRAID* conferred resistance to alendronate in OC-like cells derived from RAW 264.7 cells. While SLC37A3 appears to facilitate efflux of N-BPs from the lysosome, its endogenous substrate remains to be defined.

# OTHER SOLUTE CARRIER TRANSPORTERS IN OSTEOCLASTS

Among the multitude of membrane transporters known to exist in OCs (**Figure 2**), a growing number of members of the solute carrier (SLC) transporter superfamily have recently been identified in OCs and implicated in bone health and disease. SLC proteins constitute a large group of transmembrane transporters spanning 65 gene families and having more than 400 putatively

functional protein-coding genes (He et al., 2009; Schlessinger et al., 2013). These transporters are organized into families based on predicted protein sequence homology and predicted substrate specificity (Chou et al., 2013). Some of these transporters are ubiquitously expressed while others are a specialized feature of terminally differentiated cell types like neurons and OCs. All members of this superfamily have a preferred substrate and subcellular localization allowing for a vast number of varied exchanges across biological membranes intracellularly and with the extracellular environment (Pizzagalli et al., 2020). A number of diverse SLC transporters have been recently linked to OC function involved in the exchange of a range of fundamental biological substrates including amino acids (SLC7A5/LAT1, SLC9B, SLC17A7/VGLUT1), nucleosides (SLC29A3) and iron (SLC40A1 and SLC11A2) that are described briefly herein.

## AMINO ACID AND NUCLEOSIDE TRANSPORTERS

Amino acids and nucleosides are utilized as the building blocks for proteins, DNA and RNA, respectively, as well as serving critical roles in a variety of cellular signaling functions including synaptic neurotransmitter in neurons (e.g., the glutamate transporter SLC17A7/VGLUT1). Dysregulation of amino acid and nucleoside transporters have been increasingly implicated in various human metabolic diseases as well as cancer pathogenesis (Kandasamy et al., 2018; Pastor-Anglada and érez-Torras, 2018). Thus, it is not surprising that the importance of these membrane transporters has been extended to OC formation and function.

### SLC7A5

The solute carrier family 7 member 5 (SLC7A5), also known as L-type amino acid transporter (LAT1), mediates the cellular uptake of phenylalanine, tyrosine, L-DOPA, leucine, histidine, methionine and tryptophan. SLC7A5 forms a heterodimer through the formation of a disulfide bond with the solute carrier family 3 member 2 (SLC3A2). The heterodimer functions as a $Na^+$-independent large neutral L-amino acid exchanger where SLC7A5 is the transport component (Napolitano et al., 2015). Whereas the heterodimer localizes to the plasma membrane, it translocates to lysosomes upon heterotrimerisation with LAPTM4B. At the lysosomal membrane, the heterotrimer allows for entry of amino acids into the lysosomal lumen leading to the V-ATPase mediated activation of mTORC1 (Milkereit et al., 2015).

Slc7a5 has been linked to the pathogenesis of various cancers (e.g., highly proliferative breast cancer subtypes and small cell lung cancer) where it is thought to modulate cell proliferation (El Ansari et al., 2018). More recently, the role of Slc7a5 has been extended to bone homeostasis. Studies by Ozaki et al. (2019) demonstrated that *Slc7a5* is expressed in both OCs and osteoblasts, with expression of the transporter found to decline in preosteoclasts of ovariectomized mice. Conditional deletion of *Slc7a5* in OCs yields a low bone mass phenotype associated with an elevation in the bone resorption marker CTx, whereas bone formation markers remained unchanged. Moreover, loss of Slc7a5 accelerates osteoclastogenesis and bone resorption in an mTORC1-dependent manner that, in turn, contributes to the nuclear accumulation of the pro-osteoclastogenic transcription factor NFATc1.

### SLC9B2

Solute carrier family 9 member 2 (SLC9B2), also known as FLJ23984 or NHA2 and NHEDC2, is a 547 amino acid antiporter that regulates the exchange of extracellular $H^+$ for cytosolic $Na^+$ or $Li^+$. SLC9B2 is highly expressed in OCs and is transcriptionally regulated by TFEB (Sardiello et al., 2009). This transporter possesses an N-terminal lysosomal targeting motif and accordingly is localized to late endosomes as well as the OC basolateral membrane (Pham et al., 2007; Battaglino et al., 2008; Hilton et al., 2008; Lee et al., 2008). Despite its abundance in OCs, *Slc9b2* knockout mice lack a prominent skeletal phenotype (Hofstetter et al., 2010). Further, OCs from *Slc9b2* deficient mice differentiate normally and are capable of bone resorption *in vitro*, suggesting that SLC9B2 is dispensable in OCs or may be compensated by a hitherto unidentified transporter that fulfills its function (Pizzagalli et al., 2020).

### SLC17A7

SLC17A7, also known as BNPI or VGLUT1, is an electrogenic $Cl^-$ dependent glutamate transporter of the SLC17 family. SLC17A7 is best recognized for its function in mediating the uptake of glutamate into synaptic vesicles in neurons, with a preference for L-glutamate over D-glutamate (Voglmaier et al., 2006). The importance of glutamate in bone homeostasis has long been recognized (Serre et al., 1999; Hinoi et al., 2001; Skerry and Taylor, 2001; Mason, 2004). In OCs, glutamate is secreted through the process of transcytosis. Studies by Morimoto et al. (2006) were the first to demonstrate the existence of the glutamate transporter in OCs where it was localized to transcytotic vesicles. Using OCs from *Slc17a7* knockout mice they further demonstrated that whereas the number and morphology of *Slc17a7* knockout OCs are comparable to those derived from wild-type littermates, loss of the transporter corresponded with altered glutamate signaling and significantly increased OC bone resorption. Accordingly, *Slc17a7* knockout mice exhibit reduced bone mass at 4 months of age (Morimoto et al., 2006).

### SLC29A3

Solute carrier family 29 member 3 (SLC29A3), also known as ENT3 or FLJ11160, is one of the four members of the SLC29 family. It is highly expressed in macrophages and OCs and encodes an equilibrative nucleoside transporter. SLC29A3 possesses an N-terminal dileucine motif necessary for its targeting to endosomal and lysosomal membranes (Baldwin et al., 2005). Various IDELS of *SLC29A3* have been linked to diseases

**TABLE 1 |** Summary of known osteoclast membrane transport proteins, their localizations, substrates, associated disease phenotypes and impacts on osteoclasts.

| Name | Subcellular localization | Primary substrate | Human-Mouse protein sequence identity (%) | Known disease associations | Knockout or knockdown impacts OC function | |
|---|---|---|---|---|---|---|
| | | | | | *in vitro* | *in vivo* |
| V-type ATPase | Lysosome, Ruffled border | ATP, $H^+$ | | Osteopetrosis (Frattini et al., 2000; Sobacchi et al., 2013) | Yes | Yes |
| CLIC1 | Apical membrane | $Cl^-$ | 98 | | No | No |
| CLCN7 | Late endosome, Lysosome, Ruffled border | $2Cl^-$, $H^+$ | 96 | Osteopetrosis, Hypopigmentation, organomegaly, and delayed myelination and development (Nicoli et al., 2019) | Yes | Yes |
| SLC12A4 | Cell membrane | $K^+$, $Cl^-$ | 96 | | Yes | |
| SLC4A2 | Basolateral membrane | $Cl^-$, $HCO_3^-$ | 94 | | | Yes |
| SLC4A7 | Cell membrane | $Na^+$, $HCO_3^-$ | 74 | | Yes | |
| Ryanodine receptor 2 | Cell membrane | $Ca2^+$ | 97 | Arrhythmogenic right ventricular dysplasia 2 (214) Catecholaminergic polymorphic ventricular tachycardia (215) | | |
| ATP2B1 | Basolateral membrane | $Ca^{2+}$ | 99 | | Yes | |
| ATP2B4 | Basolateral membrane | $Ca^{2+}$ | 81 | Variants may confer resistance to sever malaria (Timmann et al., 2012) | Yes | |
| TRPV4 | | $Ca^{2+}$ | 95 | Multiple neuromuscular disorders (Auer-Grumbach et al., 2010; Deng et al., 2010; Landouré et al., 2010) | Yes | |
| TRPV5 | Ruffled border | $Ca^{2+}$ | 81 | Variant association with recurrent kidney stones (Palsson et al., 2019) | | Yes |
| TRPV6 | | $Ca^{2+}$ | 88 | Transient neonatal hyperparathyroidism (Suzuki et al., 2018) | | Yes |
| Mucolipin 1 | Late endosome, Lysosome | $Ca^{2+}$, $Fe^{2+}$, $Na^+$, $K^+$, $H^+$ | 91 | Mucolipidosis IV (Boudewyn and Walkley, 2019) | | Yes |
| ORAI1 | Cell membrane | $Ca2^+$ | 90 | Immunodeficiency 9 (Feske et al., 2006). Tubular Aggregate Myopathy 2 (Nesin et al., 2014) | Yes | Yes |
| NMDA receptor | Cell membrane | $Ca2^+$ | 99 (NMDAR1) | Neurodevelopmental disorder with or without hyperkinetic movements and seizures (Hamdan et al., 2011; Lemke et al., 2016) | | |
| P2RX7 | Cell membrane | $Ca2^+$ | 80 | | | Yes |
| TPCN2 | Acidic organelles | $Na^+$, $Ca^{2+}$, $H^+$ | 73 | No link to disease but it has been linked to human pigmentation characteristics (Sulem et al., 2008) | Yes | |
| SLC8A1-3 | Cell membrane | $Na^+$, $Ca^{2+}$ | 94, 94,96 | | Yes | |
| SLC34A1 | Cell membrane | $Na^+$, $HPO_4^{2-}$ | 90 | Hypophosphatemic Nephrolithiasis/Osteoporosis 1 (Prié et al., 2002) Fanconi Renotubular Syndrome 2 (Magen et al., 2010) Infantile Hypercalcemia 2 (Schlingmann et al., 2016) | | Yes |
| SLC20A1-A2 | Basolateral membrane | $Na^+$, Pi | 93, 92 | Idiopathic basal ganglia calcification (Wang et al., 2012; Jensen et al., 2013) | | No |
| SLC37A3 | Vesicles | | 89 | | Yes | |
| SLC7A5 | Cell membrane, Lysosome | L-type amino acids | 92 | | Yes | Yes |
| SLC9B2 | Basolateral membrane | $H^+$, $Na^+$ | 81 | | No | No |
| SLC17A7 | Synaptic vesicles | Glutamate | 98 | | | Yes |
| SLC29A3 | Endosome, Lysosome | Nucleosides | 74 | H syndrome (Farooq et al., 2012) Dysosteosclerosis (Campeau et al., 2012) | Yes | |
| SLC40A1 | Cell membrane | Iron | 90 | Hemochromatosis (Montosi et al., 2001; Njajou et al., 2001) | | Yes (LysM-Cre) |

*Human-Mouse protein sequence identity were obtained using BLAST.*

including Faisalabad histiocytosis (FHC), H syndrome, sinus histiocytosis with massive lymphadenopathy (also known as familial Rosai-Dorfman disease), pigmented hypertrichosis and insulin-dependent diabetes have all been proposed to form part of a continuous 'SLC29A3 spectrum disorder' (Morgan et al., 2010).

Campeau et al. (2012) identified SLC29A3 as the causative gene underpinning two cases of dysosteosclerosis, a rare bone sclerosing dysplasia. OCs derived from peripheral blood mononuclear cells isolated from these patients exhibited reduced differentiation and resorption capacity *in vitro* (Campeau et al., 2012). Howaldt et al. (2019) also reported sclerosing bone dysplasias in two patients with SLC29A3 mutations.

## IRON TRANSPORTERS

In addition to $Ca^{2+}$ and Pi, iron (ferritin) is an important element for OC differentiation and bone homeostasis. This is exemplified in patients with iron overload conditions such as hemochromatosis, thalassemia and sickle cell disease, which frequently suffer osteoporosis and associated fragility fractures (Guggenbuhl et al., 2005; Fung et al., 2008). Hemochromatosis, in particular, has been reported to arise from mutations in *SLC40A1* (Zhang et al., 2017; Ka et al., 2018; Yin et al., 2019). SLC40A1, also known as Ferroportin 1 and SLC11A3, is a 571-amino acid transporter localized to cell membranes where it functions to facilitate iron export (Hentze et al., 2004).

### SLC40A1

Global *Slc40a1* knockout, myeloid lineage-specific (*LysM*-Cre) and mature OC-specific (*Ctsk*-Cre) conditional *Slc40a1* knockout mice have been generated and characterized by several independent groups (Wang et al., 2018b; Pereira et al., 2020). Global deletion of *Slc40a1* in mice leads to embryonic lethality (Donovan et al., 2005). On the other hand, myeloid lineage-specific and mature OC conditional *Slc40a1* knockout mice are viable but exhibit mild or little bone phenotypes, respectively, which also depend on the sex, age and Cre-driver employed. For instance, *LysM*-Cre *Slc40a1* conditional knockout mice exhibit decreased trabecular bone mass of both long bones and vertebrae in female, but not in male littermates at 2-months of age. By comparison, specific deletion of *Slc40a1* in the late stages of OC differentiation by *Ctsk*-Cre has no obvious effects on either trabecular or cortical bone mass of both the long bones and vertebrae, suggesting that the importance of *Slc40a1* in OC bone remodeling occurs indirectly through myeliod projenitors. In keeping with this position, *Slc40a1*-deficient OC precurors (from female mice) have increased intracellular iron accumulation and exhibit accelerated OC formation *in vitro* but this was not observed in *Ctsk*-Cre conditional *Slc40a1* knockout mice.

In contrast, independent studies by Pereira et al. (2020) recently reported a high bone mass phenotype in 16 week-old female and male *LysM*-Cre *Slc40a1* conditional knockout mice associated with reduced OC formation *in vivo*. While the precise reasons for these discrepancies warrant further study, it may reflect differences in the age at which mice were phenotyped and the strain of Slc40a1 floxed mice investigated (C57BL/6N-Slc40a1tm1c(EUCOMM)Hmgu/H in the Pereira study compared to 129S-Slc40a1tm2Nca/J by Wang et al., 2018b) (Pereira et al., 2020). Regardless, together these findings highlight a role for Slc40a1 in the regulation of bone structure and strength via direct actions in the macrophage-OC lineage. In keeping with the importance of Slc40a1 in iron handling during OC differentiation, hepcidin, an upstream modulator of Slc40a1 has also been reported to modulate osteoclastogenesis *in vitro* (Xie et al., 2016).

### SLC11A2

Finally, like SLC40A1, the SLC11A2 transporter (also known as DMT1) has been shown to regulate iron uptake (Knutson, 2017). Currently, very little is known about the role of SLC11A2 in OCs. Nonetheless, at steady-state conditions, the expression of *SLC11A2* has been shown to be upregulated during OC maturation. Conversly, the expression of *SLC11A2* is downregulated in mature OCs following addition of exogenous iron to cell culture media *in vitro* (Xie et al., 2016).

## THERAPEUTIC POTENTIAL OF MEMBRANE TRANSPORT PROTEINS FOR METABOLIC BONE DISEASES

Over the past few decades, the advent of genomic sequencing coupled with genome-wide association studies has rapidly expanded our knowledge of the number of membrane transport proteins underpinning the pathophysiology of various human diseases ranging from cancer to metabolic diseases such as obesity, type 2 diabetes and osteoporosis (reviewed extensively in Lin et al. (2015a), Zhang Y. et al. (2018), Schumann et al. (2020)). Not surprisingly, unraveling the substrates transported and molecular mechanisms regulating transporter activity has been the focus of intense scientific and pharmaceutical inquiry in recent years, in pursuit of lucrative therapeutic targets against these critical yet largely untapped protein superfamilies (ésar-Razquin et al., 2015). In fact, outside of G-protein coupled receptors (GPCRs), the most intensively studied drug targets, membrane transport proteins constitute the largest but most understudied group of potential new drug targets (Schumann et al., 2020). For example, more than 30 transporters of the SLC superfamily have recently been presented as current, prospective, or potential drug targets (Lin et al., 2015b; Schumann et al., 2020; Wang et al., 2020) and spawned strategic partnerships between pharmaceutical industry and academia, the largest conglomerate called RESOLUTE (Research Empowerment on Solute Carriers) (Pizzagalli et al., 2020). In addition, multiple drug classes targeting membrane transporters have already reached the market, with several additional drugs in phase II clinical trials, many aimed at targeting metabolic diseases (Lin et al., 2015b; Zhang Y. et al., 2018; Schumann et al., 2020).

Osteoporosis, defined as low bone mass associated with skeletal fragility and increased bone fracture risk (Lane, 2006), is by far the most prominent of all OC-mediated metabolic bone diseases. Frontline treatments for osteoporosis use remedies aimed at reducing further bone loss termed 'anti-resorptive' agents such as bisphosphonates and antibodies directed against the key OC differentiation cytokine RANKL (i.e., Denosumab) (Langdahl, 2020). Alternate treatments that help stimulate new bone formation (anabolic agents) are also available but the approved arsenal is small. These include parathyroid/parathyroid-related peptide hormones (PTH/rP) and the recently approved anti-sclerostin therapy "EVENITY" (Romosozumab-aqqg). While each drug is capable of building new bone, they remain (i) expensive; (ii) require subcutaneous injection (PTH/rP-daily; EVENITY-monthly); (iii) have limited efficacy (PTH/rP ∼18-months; EVENITY 12-doses, switching to standard anti-resorptives thereafter); (iv) carry increased treatment risks (PTH/rP-osteosarcoma; EVENITY-cardiovascular) and thus; (v) are restricted to patients with the most severe osteoporosis. Similarly, despite several anti-resorptive drugs on the market, issues remain concerning patient compliance and rare but unwanted side effects such as osteonecrosis of the jaw or atypical sub-trochanteric femoral fractures with prolonged use (Langdahl, 2020). Moreover, current anti-resorptive agents suppress OC differentiation and survival. This results in arrested bone turnover, as OC help regulate bone remodeling by communicating with osteoblasts and encouraging their recruitment, a process termed 'coupling' (Sims and Martin, 2020). Therefore, there remains an unmet need for alternative and better next-generation therapies for which membrane transporter proteins may serve as a promising and tractable drug target.

As detailed above, OCs possess a multitude of membrane transporters, many that are indispensable for OC formation and function. However, despite their obvious importance, to date very few have been targeted therapeutically for OC-mediated diseases. This is partly due to the technical limitations when designing inhibitors against integral membrane proteins. First, membrane transporters are very difficult to express and purify biochemically and thus the majority lack available high-resolution crystal structures required to inform the design of small molecule inhibitors and channel blockers. Second,

**TABLE 2 |** V-ATPase inhibitors, targeting selectively and their impact on osteoclasts *in vitro* and *in vivo*.

| V-ATPase inhibitor | Target | Selectivity | *In vitro* | *In vivo* |
|---|---|---|---|---|
| Bafilomycin | $V_0$c $V_0$a | Low | Widely used in experimental cell biology. Prevents OC resorption, and inhibits endocytosis and apoptosis (Xu et al., 2003) | Prevents OC resorption. Toxic upon systemic administration due to low OC specificity |
| Concanamycin | $V_0$c | Low | Inhibits OC resorption and contributes to apoptosis (Okahashi et al., 1997) | Toxic due to low OC specificity |
| SB242784 | $V_0$c | High | Inhibits human OC resorption (Nadler et al., 1998) | Limits bone loss in thyroparathyroidectomy and ovariectomy rats (Visentin et al., 2000) |
| Iejimalides | $V_0$ | Low | Iejimalides A and B inhibit OC formation and cellular acidification. They also have anti-tumor activity (Kazami et al., 2006; McHenry et al., 2010) | |
| FR167356 | Unknown | V-ATPase-High OC-Low | Seven-fold greater inhibitory effect of cell membrane V-ATPase than lysosomal V-ATPase. Inhibits resorption when accompanied by PTH, IL-1, and IL-6 (Niikura et al., 2004, 2005b) | Dose-dependently reduces retinoic acid-induced hypercalcemia in thyroparathyroidectomy and ovariectomy rats (Niikura et al., 2005b) |
| FR202126 | Unknown | High | Inhibits resorption in the presence of IL-1, IL-6 and PTH (Niikura et al., 2005a) | Inhibits resorption (Niikura et al., 2005a) |
| FR177995 | Unknown | Low | Inhibits resorption and does not affect OC numbers (Niikura et al., 2007) | Administration dose-dependently improves the BMD of the distal femur in adjuvant-induced arthritic rats (Niikura et al., 2007) |
| Diphyllin | Unknown | Low | Inhibits lysosomal acidification (Sorensen et al., 2007) | |
| KM91104 | $V_0$a3-$V_1$B2 interaction | Medium | Inhibits OC formation and resorption (Kartner et al., 2010) | |
| Enoxacin<br>Bis-enoxacin | $V_1$B2-actin interaction | Low | Enoxacin dose-dependently inhibits OC formation (Toro et al., 2012). Bis-enoxacin also inhibits osteoclastogenesis and resorption | Bis-enoxacin inhibits resorption (Toro et al., 2013; Zhang Y. et al., 2018) |
| Salicylihalamide A<br>Saliphenylhalamide | $V_0$ (Xie et al., 2004) | Low | Saliphenylhalamid inhibits OC differentiation | Saliphenylhalamide inhibits OC resorption in a titanium particle-induced osteolysis mouse model (Qin et al., 2012a) |
| Artemisia capillaris extract | Unknown | Low | Inhibits differentiation and resorption by mature OCs | |
| Luteolin | $V_0$a3-$V_0$d2 interaction | Low | Controversial (Lee et al., 2009; Crasto et al., 2013) | Has a protective effect against ovariectomy-induced bone loss (Kim et al., 2011) |

there remain many membrane transport proteins for which the substrate transported is unknown, i.e., 'orphans' making drug targeting difficult. Third, the development and delivery of specific inhibitors that can readily penetrate OC membranes and target to specific intracellular transporters also remains a considerable challenge. This is perhaps best exemplified by drugs targeting the V-ATPase complex. Despite having attracted intense interest by bone researchers and spawned the development of a vast number of pharmacological V-ATPase inhibitors (summarized in **Table 2**), so far all have lacked targeting specificity to OCs and bone, precluding there clinical use for the treatment of OC-mediated diseases like osteoporosis. Similarly, given the high expression levels of CLCN7 in OCs and its indispensable role in bone homeostasis, CLCN7 has also received considerable attention as a potential therapeutic target for the treatment of osteoporosis. However, thus far pharmacological compounds targeting CLCN7 have been limited to preclinical studies owing to safety concerns regarding their extra-skeletal effects on retinal cells and the central nervous system given that CLCN7 knockout mice also manifest severe retinal and neuronal degeneration (Li et al., 1999). Nonetheless, CLCN7 inhibitors have been trialed successfully *in vitro* and in ovariectomized rat models and found to attenuate bone resorption while maintaining bone formation rates (Chalhoub et al., 2003; Valenzuela et al., 2013).

We anticipate therefore that new and enabling technologies, together with increased recognition of membrane transport protein importance, will bring about significant advances in the ability to develop new and selective next-generation therapies targeting specific OC membrane transport proteins that may serve as an alternative to conventional anti-osteoporosis therapies.

## SUMMARY AND PERSPECTIVES

In this review, we have summarized the 'ins and outs' of the main families of membrane transport proteins that regulate OC homeostasis. Briefly, the well-established V-ATPase proton pump is responsible for acidification and the formation of a membrane potential at the ruffled border that is neutralized by $Cl^-$ transport while CA2 and SLC4 family members offer an internal buffering system for $H^+$ and $Cl^-$ levels. Mass release of $Ca^{2+}$ by the bone is handled by a disproportionately large number of $Ca^{2+}$ channels compared to only a few known Pi handling proteins. To date, intensive research has focused on understanding the transport of $H^+$, $Cl^-$ and $Ca^{2+}$ across OC membranes, whereas our understanding of other small molecule transporters, including secondary active transporters (e.g., SLCs), remains comparatively underrepresented.

In spite of considerable progress over the past few decades toward the identification and expansion of the OC membrane transport protein inventory, very few transporters have been characterized functionally in OCs. This is, in part, due to several inherent challenges encountered when working with proteins embedded deeply in cellular membranes, which are not readily accessible to standard biochemical methods, together with a giant cell that is notoriously impervious to conventional cell biology manipulations such as transfection. Further, attempts to identify and characterize new membrane transport proteins in OCs have thus far been largely unsystematic, informed instead by research in more advanced polarized systems such as neurons and epithelial cells. It is likely, however, that OCs possess their own unique complement of membrane transport proteins necessary to fulfill their specialized requirement for rapid molecular exchanges during bone resorption. In this regard, an unbiased approach to identify OC-specific membrane transport proteins would therefore be a valuable future line of inquiry. Recent developments in 'omics' technologies coupled with genome-wide association studies may prove useful toward this goal.

## AUTHOR CONTRIBUTIONS

AR contributed to the writing, tables, and accompanying figures. NP contributed to the conceptualization and writing and editing of the manuscript. PN contributed to the editing of the manuscript. All authors contributed to the article and approved the submitted version.

## FUNDING

This work was supported, in part, by funding from the National Health and Medical Research Council of Australia (NHMRC) (APP1143921) to NP. Arthritis Australia to NP and PN and a Faculty of Health and Medical Sciences Research Grant Scheme (SE Ohman Medical Research Fund) to NP and PN. AR is supported by Australian Government Research Training Program Scholarship.

## ACKNOWLEDGMENTS

We apologize to colleagues whose work could not be cited owing to space limitations. We thank members of Bone Biology and Disease Laboratory for their enthusiastic input and insightful discussions. In particular, we also thank Laila Abudulai for her valuable feedback.

## REFERENCES

Albano, G., Dolder, S., Siegrist, M., Mercier-Zuber, A., Auberson, M., Stoudmann, C., et al. (2017). Increased bone resorption by osteoclast-specific deletion of the sodium/calcium exchanger isoform 1 (NCX1). *Pflugers Arch.* 469, 225–233. doi: 10.1007/s00424-016-1923-5

Albano, G., Moor, M., Dolder, S., Siegrist, M., Wagner, C. A., Biber, J., et al. (2015). Sodium-dependent phosphate transporters in osteoclast differentiation and function. *PLoS One* 10:e0125104. doi: 10.1371/journal.pone.0125104

Alper, S. L. (2006). Molecular physiology of SLC4 anion exchangers. *Exp. Physiol.* 91, 153–161. doi: 10.1113/expphysiol.2005.031765

Alves, L. A., de Melo Reis, R. A., de Souza, C. A., de Freitas, M. S., Teixeira, P. C., Ferreira, D. N. M., et al. (2014). The P2X7 receptor: shifting from a low- to a

high-conductance channel - an enigmatic phenomenon? *Biochim. Biophys. Acta* 1838, 2578–2587. doi: 10.1016/j.bbamem.2014.05.015

Ambrosio, A. L., Boyle, J. A., and Di Pietro, S. M. (2015). TPC2 mediates new mechanisms of platelet dense granule membrane dynamics through regulation of Ca2+ release. *Mol. Biol. Cell* 26, 3263–3274. doi: 10.1091/mbc.e15-01-0058

Aoi, W., and Marunaka, Y. (2014). Importance of pH homeostasis in metabolic health and diseases: crucial role of membrane proton transport. *BioMed Res. Int.* 2014:598986.

Auer-Grumbach, M., Olschewski, A., Papić, L., Kremer, H., McEntagart, M. E., Uhrig, S., et al. (2010). Alterations in the ankyrin domain of TRPV4 cause congenital distal SMA, scapuloperoneal SMA and HMSN2C. *Nat. Genet.* 42, 160–164. doi: 10.1038/ng.508

Bai, L., Collins, J. F., and Ghishan, F. K. (2000). Cloning and characterization of a type III Na-dependent phosphate cotransporter from mouse intestine. *Am. J. Physiol. Cell Physiol.* 279, C1135–C1143.

Baldwin, S. A., Yao, S. Y., Hyde, R. J., Ng, A. M., Foppolo, S., Barnes, K., et al. (2005). Functional characterization of novel human and mouse equilibrative nucleoside transporters (hENT3 and mENT3) located in intracellular membranes. *J. Biol. Chem.* 280, 15880–15887. doi: 10.1074/jbc.m414337200

Baljit, S. M., Sun, L., Jameel, I., Robert, D., Vijai, S. S., Peter, J. R. B., et al. (2002). Ca2+ influx through the osteoclastic plasma membrane ryanodine receptor. *Am. J. Physiol. Renal Physiol.* 282, F921–F932.

Bargal, R., Avidan, N., Ben-Asher, E., Olender, Z., Zeigler, M., Frumkin, A., et al. (2000). Identification of the gene causing mucolipidosis type IV. *Nat. Genet.* 26, 118–123. doi: 10.1038/79095

Baron, R., Neff, L., Louvard, D., and Courtoy, P. J. (1985). Cell-mediated extracellular acidification and bone resorption: evidence for a low pH in resorbing lacunae and localization of a 100-kD lysosomal membrane protein at the osteoclast ruffled border. *J. Cell Biol.* 101, 2210–2222. doi: 10.1083/jcb.101.6.2210

Battaglino, R. A., Pham, L., Morse, L. R., Vokes, M., Sharma, A., Odgren, P. R., et al. (2008). NHA-oc/NHA2: a mitochondrial cation-proton antiporter selectively expressed in osteoclasts. *Bone* 42, 180–192. doi: 10.1016/j.bone.2007.09.046

Beck, L., Leroy, C., Beck-Cormier, S., Forand, A., Salaün, C., Paris, N., et al. (2010). The phosphate transporter PiT1 (Slc20a1) revealed as a new essential gene for mouse liver development. *PLoS One* 5:e9148. doi: 10.1371/journal.pone.0009148

Berger, C. E., Rathod, H., Gillespie, J. I., Horrocks, B. R., and Datta, H. K. (2001). Scanning electrochemical microscopy at the surface of bone-resorbing osteoclasts: evidence for steady-state disposal and intracellular functional compartmentalization of calcium. *J. Bone Miner. Res.* 16, 2092–2102. doi: 10.1359/jbmr.2001.16.11.2092

Boudewyn, L. C., and Walkley, S. U. (2019). Current concepts in the neuropathogenesis of mucolipidosis type IV. *J. Neurochem.* 148, 669–689. doi: 10.1111/jnc.14462

Bourgine, A., Pilet, P., Diouani, S., Source, S., Lesoeur, J., Beck-Cormier, S., et al. (2013). Mice with hypomorphic expression of the sodium-phosphate cotransporter PiT1/Slc20a1 have an unexpected normal bone mineralization. *PLoS One* 8:e65979. doi: 10.1371/journal.pone.0065979

Bouyer, P., Sakai, H., Itokawa, T., Kawano, T., Fulton, C. M., Boron, W. F., et al. (2007). Colony-stimulating factor-1 increases osteoclast intracellular pH and promotes survival via the electroneutral Na/HCO3 cotransporter NBCn1. *Endocrinology* 148, 831–840. doi: 10.1210/en.2006-0547

Brailoiu, E., Rahman, T., Churamani, D., Prole, D. L., Brailoiu, G. C., Hooper, R., et al. (2010). An NAADP-gated two-pore channel targeted to the plasma membrane uncouples triggering from amplifying Ca2+ signals. *J. Biol. Chem.* 285, 38511–38516. doi: 10.1074/jbc.m110.162073

Campeau, P. M., Lu, J. T., Sule, G., Jiang, M. M., Bae, Y., Madan, S., et al. (2012). Whole-exome sequencing identifies mutations in the nucleoside transporter gene SLC29A3 in dysosteosclerosis, a form of osteopetrosis. *Hum. Mol. Genet.* 21, 4904–4909. doi: 10.1093/hmg/dds326

Cao, B., Dai, X., and Wang, W. (2019). Knockdown of TRPV4 suppresses osteoclast differentiation and osteoporosis by inhibiting autophagy through Ca(2+) - calcineurin-NFATc1 pathway. *J. Cell Physiol.* 234, 6831–6841. doi: 10.1002/jcp.27432

Cappello, A. R., Curcio, R., Lappano, R., Maggiolini, M., and Dolce, V. (2018). The physiopathological role of the exchangers belonging to the SLC37 family. *Front. Chem.* 6:122. doi: 10.3389/fchem.2018.00122

Chalhoub, N., Benachenhou, N., Rajapurohitam, V., Pata, M., Ferron, M., Frattini, A., et al. (2003). Grey-lethal mutation induces severe malignant autosomal recessive osteopetrosis in mouse and human. *Nat. Med.* 9, 399–406. doi: 10.1038/nm842

Chen, F., Ni, B., Yang, Y. O., Ye, T., and Chen, A. (2014). Knockout of TRPV6 causes osteopenia in mice by increasing osteoclastic differentiation and activity. *Cell Physiol. Biochem.* 33, 796–809. doi: 10.1159/000358653

Chenu, C., Serre, C. M., Raynal, C., Burt-Pichat, B., and Delmas, P. D. (1998). Glutamate receptors are expressed by bone cells and are involved in bone resorption. *Bone* 22, 295–299. doi: 10.1016/s8756-3282(97)00295-0

Choi, I., Aalkjaer, C., Boulpaep, E. L., and Boron, W. F. (2000). An electroneutral sodium/bicarbonate cotransporter NBCn1 and associated sodium channel. *Nature* 405, 571–575. doi: 10.1038/35014615

Chou, J. Y., Sik Jun, H., and Mansfield, B. C. (2013). The SLC37 family of phosphate-linked sugar phosphate antiporters. *Mol. Aspects Med.* 34, 601–611. doi: 10.1016/j.mam.2012.05.010

Concepcion, A. R., Lopez, M., Ardura-Fabregat, A., and Medina, J. F. (2013). Role of AE2 for pHi regulation in biliary epithelial cells. *Front. Physiol.* 4:413. doi: 10.3389/fphys.2013.00413

Cordat, E., and Casey, J. R. (2008). Bicarbonate transport in cell physiology and disease. *Biochem. J.* 417, 423–439. doi: 10.1042/bj20081634

Coury, F., Zenger, S., Stewart, A. K., Stephens, S., Neff, L., Tsang, K., et al. (2013). SLC4A2-mediated Cl-/HCO3- exchange activity is essential for calpain-dependent regulation of the actin cytoskeleton in osteoclasts. *Proc. Natl. Acad. Sci. U.S.A.* 110, 2163–2168. doi: 10.1073/pnas.1206392110

Crasto, G. J., Kartner, N., Yao, Y., Li, K., Bullock, L., Datti, A., et al. (2013). Luteolin inhibition of V-ATPase a3-d2 interaction decreases osteoclast resorptive activity. *J. Cell Biochem.* 114, 929–941. doi: 10.1002/jcb.24434

Datta, H. K., and Horrocks, B. R. (2003). Mechanisms of calcium disposal from osteoclastic resorption hemivacuole. *J. Endocrinol.* 176, 1–5. doi: 10.1677/joe.0.1760001

De Paolis, E., Scaglione, G. L., De Bonis, M., Minucci, A., and Capoluongo, E. (2019). CYP24A1 and SLC34A1 genetic defects associated with idiopathic infantile hypercalcemia: from genotype to phenotype. *Clin. Chem. Lab. Med.* 57, 1650–1667. doi: 10.1515/cclm-2018-1208

Deng, H.-X., Klein, C. J., Yan, J., Shi, Y., Wu, Y., Fecto, F., et al. (2010). Scapuloperoneal spinal muscular atrophy and CMT2C are allelic disorders caused by alterations in TRPV4. *Nat. Genet.* 42, 165–169. doi: 10.1038/ng.509

Donovan, A., Lima, C. A., Pinkus, J. L., Pinkus, G. S., Zon, L. I., Robine, S., et al. (2005). The iron exporter ferroportin/Slc40a1 is essential for iron homeostasis. *Cell Metab.* 1, 191–200. doi: 10.1016/j.cmet.2005.01.003

Drake, M. T., Clarke, B. L., and Khosla, S. (2008). Bisphosphonates: mechanism of action and role in clinical practice. *Mayo Clin. Proc.* 83, 1032–1045. doi: 10.4065/83.9.1032

Duan, X., Yang, S., Zhang, L., and Yang, T. (2018). V-ATPases and osteoclasts: ambiguous future of V-ATPases inhibitors in osteoporosis. *Theranostics* 8, 5379–5399. doi: 10.7150/thno.28391

El Ansari, R., Craze, M. L., Miligy, I., Diez-Rodriguez, M., Nolan, C. C., Ellis, I. O., et al. (2018). The amino acid transporter SLC7A5 confers a poor prognosis in the highly proliferative breast cancer subtypes and is a key therapeutic target in luminal B tumours. *Breast Cancer Res.* 20:21.

Erkhembaatar, M., Gu, D. R., Lee, S. H., Yang, Y. M., Park, S., Muallem, S., et al. (2017). Lysosomal Ca(2+) signaling is essential for osteoclastogenesis and bone remodeling. *J. Bone Miner. Res.* 32, 385–396. doi: 10.1002/jbmr.2986

ésar-Razquin, A. C., Snijder, B., Frappier-Brinton, T., Isserlin, R., Gyimesi, G., Bai, X., et al. (2015). A call for systematic research on solute carriers. *Cell* 162, 478–487. doi: 10.1016/j.cell.2015.07.022

Farooq, M., Moustafa, R. M., Fujimoto, A., Fujikawa, H., Abbas, O., Kibbi, A. G., et al. (2012). Identification of two novel mutations in SLC29A3 encoding an equilibrative nucleoside transporter (hENT3) in two distinct Syrian families with H syndrome: expression studies of SLC29A3 (hENT3) in human skin. *Dermatology* 224, 277–284. doi: 10.1159/000338886

Feske, S., Gwack, Y., Prakriya, M., Srikanth, S., Puppel, S.-H., Tanasa, B., et al. (2006). A mutation in Orai1 causes immune deficiency by abrogating CRAC channel function. *Nature* 441, 179–185.

Forgac, M. (2007). Vacuolar ATPases: rotary proton pumps in physiology and pathophysiology. *Nat. Rev. Mol. Cell Biol.* 8, 917–929. doi: 10.1038/nrm2272

Forster, I. C. (2019). The molecular mechanism of SLC34 proteins: insights from two decades of transport assays and structure-function studies. *Pflugers Arch.* 471, 15–42. doi: 10.1007/s00424-018-2207-z

Forster, I. C., Loo, D. D., and Eskandari, S. (1999). Stoichiometry and Na+ binding cooperativity of rat and flounder renal type II Na+-Pi cotransporters. *Am. J. Physiol.* 276, F644–F649.

Frattini, A., Orchard, P. J., Sobacchi, C., Giliani, S., Abinun, M., Mattsson, J. P., et al. (2000). Defects in TCIRG1 subunit of the vacuolar proton pump are responsible for a subset of human autosomal recessive osteopetrosis. *Nat. Genet.* 25, 343–346. doi: 10.1038/77131

Fung, E. B., Harmatz, P. R., Milet, M., Coates, T. D., Thompson, A. A., Ranalli, M., et al. (2008). Fracture prevalence and relationship to endocrinopathy in iron overloaded patients with sickle cell disease and thalassemia. *Bone* 43, 162–168. doi: 10.1016/j.bone.2008.03.003

Futai, M., Sun-Wada, G. H., Wada, Y., Matsumoto, N., and Nakanishi-Matsui, M. (2019). Vacuolar-type ATPase: a proton pump to lysosomal trafficking. *Proc. Jpn. Acad. Ser. B Phys. Biol. Sci.* 95, 261–277. doi: 10.2183/pjab.95.018

Gartland, A., Skarratt, K. K., Hocking, L. J., Parsons, C., Stokes, L., Jørgensen, N. R., et al. (2012). Polymorphisms in the P2X7 receptor gene are associated with low lumbar spine bone mineral density and accelerated bone loss in post-menopausal women. *Eur. J. Hum. Genet.* 20, 559–564. doi: 10.1038/ejhg.2011.245

Gawenis, L. R., Bradford, E. M., Alper, S. L., Prasad, V., and Shull, G. E. (2010). AE2 Cl-/HCO3- exchanger is required for normal cAMP-stimulated anion secretion in murine proximal colon. *Am. J. Physiol. Gastrointest. Liver Physiol.* 298, G493–G503.

Gillen, C. M., Brill, S., Payne, J. A., and Forbush, B. III (1996). Molecular cloning and functional expression of the K-Cl cotransporter from rabbit, rat, and human. A new member of the cation-chloride cotransporter family. *J. Biol. Chem.* 271, 16237–16244. doi: 10.1074/jbc.271.27.16237

Graves, A. R., Curran, P. K., Smith, C. L., and Mindell, J. A. (2008). The Cl-/H+ antiporter ClC-7 is the primary chloride permeation pathway in lysosomes. *Nature* 453, 788–792. doi: 10.1038/nature06907

Guggenbuhl, P., Deugnier, Y., Boisdet, J. F., Rolland, Y., Perdriger, A., Pawlotsky, Y., et al. (2005). Bone mineral density in men with genetic hemochromatosis and HFE gene mutation. *Osteoporos Int.* 16, 1809–1814. doi: 10.1007/s00198-005-1934-0

Gupta, A., Guo, X. L., Alvarez, U. M., and Hruska, K. A. (1997). Regulation of sodium-dependent phosphate transport in osteoclasts. *J. Clin. Invest.* 100, 538–549. doi: 10.1172/jci119563

Gupta, A., Miyauchi, A., Fujimori, A., and Hruska, K. A. (1996). Phosphate transport in osteoclasts: a functional and immunochemical characterization. *Kidney Int.* 49, 968–974. doi: 10.1038/ki.1996.137

Gupta, A., Tenenhouse, H. S., Hoag, H. M., Wang, D., Khadeer, M. A., Namba, N., et al. (2001). Identification of the type II Na(+)-Pi cotransporter (Npt2) in the osteoclast and the skeletal phenotype of Npt2-/- mice. *Bone* 29, 467–476. doi: 10.1016/s8756-3282(01)00601-9

Hamdan, F. F., Gauthier, J., Araki, Y., Lin, D.-T., Yoshizawa, Y., Higashi, K., et al. (2011). Excess of de novo deleterious mutations in genes associated with glutamatergic systems in nonsyndromic intellectual disability. *Am. J. Hum. Genet.* 88, 306–316. doi: 10.1016/j.ajhg.2011.02.001

Haoxing, X., and Dejian, R. (2015). Lysosomal physiology. *Annu. Rev. Physiol.* 77, 57–80. doi: 10.1146/annurev-physiol-021014-071649

He, L., Vasiliou, K., and Nebert, D. W. (2009). Analysis and update of the human solute carrier (SLC) gene superfamily. *Hum. Genomics* 3, 195–206. doi: 10.1186/1479-7364-3-2-195

Hebert, S. C., Mount, D. B., and Gamba, G. (2004). Molecular physiology of cation-coupled Cl- cotransport: the SLC12 family. *Pflugers Arch.* 447, 580–593. doi: 10.1007/s00424-003-1066-3

Hentze, M. W., Muckenthaler, M. U., and Andrews, N. C. (2004). Balancing acts: molecular control of mammalian iron metabolism. *Cell* 117, 285–297.

Hershey, C. L., and Fisher, D. E. (2004). Mitf and Tfe3: members of a b-HLH-ZIP transcription factor family essential for osteoclast development and function. *Bone* 34, 689–696. doi: 10.1016/j.bone.2003.08.014

Hilton, M. J., Tu, X., Wu, X., Bai, S., Zhao, H., Kobayashi, T., et al. (2008). Notch signaling maintains bone marrow mesenchymal progenitors by suppressing osteoblast differentiation. *Nat. Med.* 14, 306–314. doi: 10.1038/nm1716

Hinoi, E., Fujimori, S., Nakamura, Y., and Yoneda, Y. (2001). Group III metabotropic glutamate receptors in rat cultured calvarial osteoblasts. *Biochem. Biophys. Res. Commun.* 281, 341–346. doi: 10.1006/bbrc.2001.4355

Hoenderop, J. G., van Leeuwen, J. P., van der Eerden, B. C., Kersten, F. F., van der Kemp, A. W., Merillat, A. M., et al. (2003). Renal Ca2+ wasting, hyperabsorption, and reduced bone thickness in mice lacking TRPV5. *J. Clin. Invest.* 112, 1906–1914. doi: 10.1172/jci200319826

Hofstetter, W., Siegrist, M., Simonin, A., Bonny, O., and Fuster, D. G. (2010). Sodium/hydrogen exchanger NHA2 in osteoclasts: subcellular localization and role *in vitro* and *in vivo*. *Bone* 47, 331–340. doi: 10.1016/j.bone.2010.04.605

Hossain, K. R., Turkewitz, D. R., Holt, S. A., Herson, L., Brown, L. J., Cornell, B. A., et al. (2019). A conserved GXXXG motif in the transmembrane domain of CLIC proteins is essential for their cholesterol-dependant membrane interaction. *Biochim. Biophys. Acta Gen. Subj.* 8:8.

Howaldt, A., Nampoothiri, S., Quell, L.-M., Ozden, A., Fischer-Zirnsak, B., Collet, C., et al. (2019). Sclerosing bone dysplasias with hallmarks of dysosteosclerosis in four patients carrying mutations in SLC29A3 and TCIRG1. *Bone* 120, 495–503. doi: 10.1016/j.bone.2018.12.002

Hughes, T. E., Del Rosario, J. S., Kapoor, A., Yazici, A. T., Yudin, Y., Fluck, E. C. III, et al. (2019). Structure-based characterization of novel TRPV5 inhibitors. *Elife* 8:e49572.

Hwang, S. Y., and Putney, J. W. (2012). Orai1-mediated calcium entry plays a critical role in osteoclast differentiation and function by regulating activation of the transcription factor NFATc1. *FASEB J.* 26, 1484–1492. doi: 10.1096/fj.11-194399

Jansen, I. D. C., Mardones, P., Lecanda, F., de Vries, T. J., Recalde, S., Hoeben, K. A., et al. (2009). Ae2a,b-Deficient mice exhibit osteopetrosis of long bones but not of calvaria. *FASEB J.* 23, 3470–3481. doi: 10.1096/fj.08-122598

Janssens, A., Silvestri, C., Martella, A., Vanoevelen, J. M., Di Marzo, V., and Voets, T. (2018). Delta(9)-tetrahydrocannabivarin impairs epithelial calcium transport through inhibition of TRPV5 and TRPV6. *Pharmacol. Res.* 136, 83–89. doi: 10.1016/j.phrs.2018.08.021

Jefferies, K. C., Cipriano, D. J., and Forgac, M. (2008). Function, structure and regulation of the vacuolar (H+)-ATPases. *Arch. Biochem. Biophys.* 476, 33–42. doi: 10.1016/j.abb.2008.03.025

Jensen, N., Schrøder, H. D., Hejbøl, E. K., Füchtbauer, E.-M., de Oliveira, J. R. M., and Pedersen, L. (2013). Loss of function of Slc20a2 associated with familial idiopathic basal ganglia calcification in humans causes brain calcifications in mice. *J. Mol. Neurosci.* 51, 994–999. doi: 10.1007/s12031-013-0085-6

Jørgensen, N. R., Husted, L. B., Skarratt, K. K., Stokes, L., Tofteng, C. L., Kvist, T., et al. (2012). Single-nucleotide polymorphisms in the P2X7 receptor gene are associated with post-menopausal bone loss and vertebral fractures. *Eur. J. Hum. Genet.* 20, 675–681. doi: 10.1038/ejhg.2011.253

Ka, C., Guellec, J., Pepermans, X., Kannengiesser, C., Ged, C., Wuyts, W., et al. (2018). The SLC40A1 R178Q mutation is a recurrent cause of hemochromatosis and is associated with a novel pathogenic mechanism. *Haematologica* 103, 1796–1805. doi: 10.3324/haematol.2018.189845

Kajiya, H., Okamoto, F., Li, J.-P., Nakao, A., and Okabe, K. (2006). Expression of mouse osteoclast K-Cl Co-transporter-1 and its role during bone resorption. *J. Bone Mineral Res.* 21, 984–992. doi: 10.1359/jbmr.060407

Kanatani, M., Sugimoto, T., Kano, J., Kanzawa, M., and Chihara, K. (2003). Effect of high phosphate concentration on osteoclast differentiation as well as bone-resorbing activity. *J. Cell. Physiol.* 196, 180–189. doi: 10.1002/jcp.10270

Kandasamy, P., Gyimesi, G., Kanai, Y., and Hediger, M. A. (2018). Amino acid transporters revisited: new views in health and disease. *Trends Biochem. Sci.* 43, 752–789. doi: 10.1016/j.tibs.2018.05.003

Kartner, N., Yao, Y., Li, K., Crasto, G. J., Datti, A., and Manolson, M. F. (2010). Inhibition of osteoclast bone resorption by disrupting vacuolar H+-ATPase a3-B2 subunit interaction. *J. Biol. Chem.* 285, 37476–37490. doi: 10.1074/jbc.m110.123281

Kasper, D., Planells-Cases, R., Fuhrmann, J. C., Scheel, O., Zeitz, O., Ruether, K., et al. (2005). Loss of the chloride channel ClC-7 leads to lysosomal storage disease and neurodegeneration. *EMBO J.* 24, 1079–1091. doi: 10.1038/sj.emboj.7600576

Kavanaugh, M. P., and Kabat, D. (1996). Identification and characterization of a widely expressed phosphate transporter/retrovirus receptor family. *Kidney Int.* 49, 959–963. doi: 10.1038/ki.1996.135

Kazami, S., Muroi, M., Kawatani, M., Kubota, T., Usui, T., Kobayashi, J., et al. (2006). Iejimalides show anti-osteoclast activity via V-ATPase inhibition. *Biosci. Biotechnol. Biochem.* 70, 1364–1370. doi: 10.1271/bbb.50644

Ke, H. Z., Qi, H., Weidema, A. F., Zhang, Q., Panupinthu, N., Crawford, D. T., et al. (2003). Deletion of the P2X7 nucleotide receptor reveals its regulatory roles in bone formation and resorption. *Mol. Endocrinol.* 17, 1356–1367. doi: 10.1210/me.2003-0021

Keeton, T. P., Burk, S. E., and Shull, G. E. (1993). Alternative splicing of exons encoding the calmodulin-binding domains and C termini of plasma membrane Ca (2+)-ATPase isoforms 1, 2, 3, and 4. *J. Biol. Chem.* 268, 2740–2748. doi: 10.1016/s0021-9258(18)53836-9

Khadeer, M. A., Tang, Z., Tenenhouse, H. S., Eiden, M. V., Murer, H., Hernando, N., et al. (2003). Na+-dependent phosphate transporters in the murine osteoclast: cellular distribution and protein interactions. *Am. J. Physiol. Cell Physiol.* 284, C1633–C1644.

Kim, H. J., Prasad, V., Hyung, S. W., Lee, Z. H., Lee, S. W., Bhargava, A., et al. (2012). Plasma membrane calcium ATPase regulates bone mass by fine-tuning osteoclast differentiation and survival. *J. Cell Biol.* 199, 1145–1158. doi: 10.1083/jcb.201204067

Kim, T. H., Jung, J. W., Ha, B. G., Hong, J. M., Park, E. K., Kim, H. J., et al. (2011). The effects of luteolin on osteoclast differentiation, function in vitro and ovariectomy-induced bone loss. *J. Nutr. Biochem.* 22, 8–15. doi: 10.1016/j.jnutbio.2009.11.002

Knutson, M. D. (2017). Iron transport proteins: gateways of cellular and systemic iron homeostasis. *J. Biol. Chem.* 292, 12735–12743. doi: 10.1074/jbc.r117.786632

Kornak, U., Kasper, D., Bösl, M. R., Kaiser, E., Schweizer, M., Schulz, A., et al. (2001). Loss of the ClC-7 chloride channel leads to osteopetrosis in mice and man. *Cell* 104, 205–215. doi: 10.1016/s0092-8674(01)00206-9

Kuno, M. (2018). Cooperative electrogenic proton transport pathways in the plasma membrane of the proton-secreting osteoclast. *Pflügers Archiv. Eur. J. Physiol.* 470, 851–866. doi: 10.1007/s00424-018-2137-9

Landouré, G., Zdebik, A. A., Martinez, T. L., Burnett, B. G., Stanescu, H. C., Inada, H., et al. (2010). Mutations in TRPV4 cause charcot-marie-tooth disease type 2C. *Nat. Genet.* 42, 170–174.

Landowski, C. P., Bolanz, K. A., Suzuki, Y., and Hediger, M. A. (2011). Chemical inhibitors of the calcium entry channel TRPV6. *Pharm. Res.* 28, 322–330. doi: 10.1007/s11095-010-0249-9

Lane, N. E. (2006). Epidemiology, etiology, and diagnosis of osteoporosis. *Am. J. Obstet. Gynecol.* 194, S3–S11.

Langdahl, B. L. (2020). Overview of treatment approaches to osteoporosis. *Br. J. Pharmacol.* doi: 10.1111/bph.15024 [Epub ahead of print].

Lange, P. F., Wartosch, L., Jentsch, T. J., and Fuhrmann, J. C. (2006). ClC-7 requires Ostm1 as a β-subunit to support bone resorption and lysosomal function. *Nature* 440, 220–223. doi: 10.1038/nature04535

Larrouture, Q. C., Nelson, D. J., Robinson, L. J., Liu, L., Tourkova, I., Schlesinger, P. H., et al. (2015). Chloride–hydrogen antiporters ClC-3 and ClC-5 drive osteoblast mineralization and regulate fine-structure bone patterning *in vitro*. *Physiol. Rep.* 3:e12607. doi: 10.14814/phy2.12607

Lee, J. W., Ahn, J. Y., Hasegawa, S., Cha, B. Y., Yonezawa, T., Nagai, K., et al. (2009). Inhibitory effect of luteolin on osteoclast differentiation and function. *Cytotechnology* 61, 125–134. doi: 10.1007/s10616-010-9253-5

Lee, S., Axelsen, T. V., Andersen, A. P., Vahl, P., Pedersen, S. F., and Boedtkjer, E. (2016). Disrupting $Na^+$, $HCO3^-$-cotransporter NBCn1 (Slc4a7) delays murine breast cancer development. *Oncogene* 35, 2112–2122. doi: 10.1038/onc.2015.273

Lee, S. H., Kim, T., Park, E. S., Yang, S., Jeong, D., Choi, Y., et al. (2008). NHE10, an osteoclast-specific member of the Na+/H+ exchanger family, regulates osteoclast differentiation and survival [corrected]. *Biochem. Biophys. Res. Commun.* 369, 320–326. doi: 10.1016/j.bbrc.2008.01.168

Lemke, J. R., Geider, K., Helbig, K. L., Heyne, H. O., Schütz, H., Hentschel, J., et al. (2016). Delineating the GRIN1 phenotypic spectrum. a distinct genetic NMDA receptor encephalopathy. *Neurology* 86, 2171–2178. doi: 10.1212/wnl.0000000000002740

Li, J. P., Kajiya, H., Okamoto, F., Nakao, A., Iwamoto, T., and Okabe, K. (2007). Three Na+/Ca2+ exchanger (NCX) variants are expressed in mouse osteoclasts and mediate calcium transport during bone resorption. *Endocrinology* 148, 2116–2125. doi: 10.1210/en.2006-1321

Li, Y. P., Chen, W., Liang, Y., Li, E., and Stashenko, P. (1999). Atp6i-deficient mice exhibit severe osteopetrosis due to loss of osteoclast-mediated extracellular acidification. *Nat. Genet.* 23, 447–451. doi: 10.1038/70563

Lin, L., Yee, S. W., Kim, R. B., and Giacomini, K. M. (2015a). SLC transporters as therapeutic targets: emerging opportunities. *Nat. Rev. Drug Discov.* 14, 543–560. doi: 10.1038/nrd4626

Lin, L., Yee, S. W., Kim, R. B., and Giacomini, K. M. (2015b). SLC transporters as therapeutic targets: emerging opportunities. *Nat. Rev. Drug Discov.* 14, 543–560.

Liu, S., Chang, S., Han, B., Xu, L., Zhang, M., Zhao, C., et al. (2019). Cryo-EM structures of the human cation-chloride cotransporter KCC1. *Science* 366, 505–508. doi: 10.1126/science.aay3129

Liu, Y., Yang, J., and Chen, L. M. (2015). Structure and function of SLC4 family [Formula: see text] transporters. *Front. Physiol.* 6:355. doi: 10.3389/fphys.2015.00355

Loiselle, F. B., Morgan, P. E., Alvarez, B. V., and Casey, J. R. (2004). Regulation of the human NBC3 Na+/HCO3- cotransporter by carbonic anhydrase II and PKA. *Am. J. Physiol. Cell Physiol.* 286, C1423–C1433.

Lunz, V., Romanin, C., and Frischauf, I. (2019). STIM1 activation of Orai1. *Cell Calcium* 77, 29–38. doi: 10.1016/j.ceca.2018.11.009

Lyaruu, D. M., Bronckers, A. L., Mulder, L., Mardones, P., Medina, J. F., Kellokumpu, S., et al. (2008). The anion exchanger Ae2 is required for enamel maturation in mouse teeth. *Matrix Biol.* 27, 119–127. doi: 10.1016/j.matbio.2007.09.006

Magen, D., Berger, L., Coady, M. J., Ilivitzki, A., Militianu, D., Tieder, M., et al. (2010). A loss-of-function mutation in NaPi-IIa and renal fanconi's syndrome. *N. Engl. J. Med.* 362, 1102–1109. doi: 10.1056/nejmoa0905647

Manolson, M. F., Yu, H., Chen, W., Yao, Y., Li, K., Lees, R. L., et al. (2003). The a3 isoform of the 100-kDa V-ATPase subunit is highly but differentially expressed in large (= 10 nuclei) and small (= 5 nuclei) osteoclasts. *J. Biol. Chem.* 278, 49271–49278. doi: 10.1074/jbc.m309914200

Mason, D. J. (2004). Glutamate signalling and its potential application to tissue engineering of bone. *Eur. Cell. Mater.* 7, 12–25;discussion25–6.

Matsumoto, N., Sekiya, M., Tohyama, K., Ishiyama-Matsuura, E., Sun-Wada, G. H., Wada, Y., et al. (2018). Essential role of the a3 Isoform of V-ATPase in secretory lysosome trafficking via rab7 recruitment. *Sci. Rep.* 8:6701.

McHenry, P., Wang, W. L., Devitt, E., Kluesner, N., Davisson, V. J., McKee, E., et al. (2010). Iejimalides A and B inhibit lysosomal vacuolar H+-ATPase (V-ATPase) activity and induce S-phase arrest and apoptosis in MCF-7 cells. *J. Cell Biochem.* 109, 634–642.

Meadows, N. A., Sharma, S. M., Faulkner, G. J., Ostrowski, M. C., Hume, D. A., and Cassady, A. I. (2007). The expression of Clcn7 and Ostm1 in osteoclasts is coregulated by microphthalmia transcription factor. *J. Biol. Chem.* 282, 1891–1904. doi: 10.1074/jbc.m608572200

Medina, J. F., Recalde, S., Prieto, J., Lecanda, J., Saez, E., Funk, C. D., et al. (2003). Anion exchanger 2 is essential for spermiogenesis in mice. *Proc. Natl. Acad. Sci. U.S.A.* 100, 15847–15852. doi: 10.1073/pnas.2536127100

Merle, B., Itzstein, C., Delmas, P. D., and Chenu, C. (2003). NMDA glutamate receptors are expressed by osteoclast precursors and involved in the regulation of osteoclastogenesis. *J. Cell. Biochem.* 90, 424–436. doi: 10.1002/jcb.10625

Meyers, S. N., McDaneld, T. G., Swist, S. L., Marron, B. M., Steffen, D. J., O'Toole, D., et al. (2010). A deletion mutation in bovine SLC4A2 is associated with osteopetrosis in Red Angus cattle. *BMC Genomics* 11:337. doi: 10.1186/1471-2164-11-337

Mikiko, I., Naoko, M., Michiyo, I., Sakiko, H., Yuko, S., Rie, N., et al. (2005). Characterization of inorganic phosphate transport in osteoclast-like cells. *Am. J. Physiol. Cell Physiol.* 288, C921–C931.

Milkereit, R., Persaud, A., Vanoaica, L., Guetg, A., Verrey, F., and Rotin, D. (2015). LAPTM4b recruits the LAT1-4F2hc Leu transporter to lysosomes and promotes mTORC1 activation. *Nat. Commun.* 6:7250.

Montosi, G., Donovan, A., Totaro, A., Garuti, C., Pignatti, E., Cassanelli, S., et al. (2001). Autosomal-dominant hemochrom-atosis is associated with a mutation in the ferroportin (SLC11A3) gene. *J. Clin. Invest.* 108, 619–623. doi: 10.1172/jci200113468

Moonga, B. S., Davidson, R., Sun, L., Adebanjo, O. A., Moser, J., Abedin, M., et al. (2001). Identification and characterization of a sodium/calcium exchanger, NCX-1, in osteoclasts and its role in bone resorption. *Biochem. Biophys. Res. Commun.* 283, 770–775. doi: 10.1006/bbrc.2001.4870

Morgan, N. V., Morris, M. R., Cangul, H., Gleeson, D., Straatman-Iwanowska, A., Davies, N., et al. (2010). Mutations in SLC29A3, encoding an equilibrative nucleoside transporter ENT3, cause a familial histiocytosis syndrome (Faisalabad histiocytosis) and familial Rosai-Dorfman disease. *PLoS Genet.* 6:e1000833. doi: 10.1371/journal.pgen.1000833

Morimoto, R., Uehara, S., Yatsushiro, S., Juge, N., Hua, Z., Senoh, S., et al. (2006). Secretion of L-glutamate from osteoclasts through transcytosis. *Embo J.* 25, 4175–4186. doi: 10.1038/sj.emboj.7601317

Nadler, G., Morvan, M., Delimoge, I., Belfiore, P., Zocchetti, A., James, I., et al. (1998). (2Z,4E)-5-(5,6-dichloro-2-indolyl)-2-methoxy-N-(1,2,2,6,6-pentamethylpiperidin-4-yl)-2,4-pentadienamide, a novel, potent and selective inhibitor of the osteoclast V-ATPase. *Bioorg. Med. Chem. Lett.* 8, 3621–3626. doi: 10.1016/s0960-894x(98)00660-x

Naemsch, L. N., Dixon, S. J., and Sims, S. M. (2001). Activity-dependent development of P2X7 current and Ca2+ entry in rabbit osteoclasts. *J. Biol. Chem.* 276, 39107–39114. doi: 10.1074/jbc.m105881200

Napolitano, L., Scalise, M., Galluccio, M., Pochini, L., Albanese, L. M., and Indiveri, C. (2015). LAT1 is the transport competent unit of the LAT1/CD98 heterodimeric amino acid transporter. *Int. J. Biochem. Cell Biol.* 67, 25–33. doi: 10.1016/j.biocel.2015.08.004

Nesbitt, S. A., and Horton, M. A. (1997). Trafficking of matrix collagens through bone-resorbing osteoclasts. *Science* 276, 266–269. doi: 10.1126/science.276.5310.266

Nesin, V., Wiley, G., Kousi, M., Ong, E. C., Lehmann, T., Nicholl, D. J., et al. (2014). Activating mutations in STIM1 and ORAI1 cause overlapping syndromes of tubular myopathy and congenital miosis. *Proc. Nat. Acad. Sci. U.S.A.* 111, 4197–4202. doi: 10.1073/pnas.1312520111

Ng, P. Y., Ribet, A. B. P., and Pavlos, N. J. (2019). Membrane trafficking in osteoclasts and implications for osteoporosis. *Biochem. Soc. Trans.* 47, 639–650. doi: 10.1042/bst20180445

Nicoli, E. R., Weston, M. R., Hackbarth, M., Becerril, A., Larson, A., Zein, W. M., et al. (2019). Lysosomal storage and albinism due to effects of a de novo CLCN7 variant on lysosomal acidification. *Am. J. Hum. Genet.* 104, 1127–1138.

Niikura, K., Nakajima, S., Takano, M., and Yamazaki, H. (2007). FR177995, a novel vacuolar ATPase inhibitor, exerts not only an inhibitory effect on bone destruction but also anti-immunoinflammatory effects in adjuvant-induced arthritic rats. *Bone* 40, 888–894. doi: 10.1016/j.bone.2006.10.015

Niikura, K., Takano, M., and Sawada, M. (2004). A novel inhibitor of vacuolar ATPase, FR167356, which can discriminate between osteoclast vacuolar ATPase and lysosomal vacuolar ATPase. *Br. J. Pharmacol.* 142, 558–566. doi: 10.1038/sj.bjp.0705812

Niikura, K., Takeshita, N., and Chida, N. (2005a). A novel inhibitor of vacuolar ATPase, FR202126, prevents alveolar bone destruction in experimental periodontitis in rats. *J. Toxicol. Sci.* 30, 297–304. doi: 10.2131/jts.30.297

Niikura, K., Takeshita, N., and Takano, M. (2005b). A vacuolar ATPase inhibitor, FR167356, prevents bone resorption in ovariectomized rats with high potency and specificity: potential for clinical application. *J. Bone Miner. Res.* 20, 1579–1588. doi: 10.1359/jbmr.050517

Nijenhuis, T., van der Eerden, B. C., Hoenderop, J. G., Weinans, H., van Leeuwen, J. P., and Bindels, R. J. (2008). Bone resorption inhibitor alendronate normalizes the reduced bone thickness of TRPV5(-/-) mice. *J. Bone Miner. Res.* 23, 1815–1824. doi: 10.1359/jbmr.080613

Njajou, O. T., Vaessen, N., Joosse, M., Berghuis, B., van Dongen, J. W. F., Breuning, M. H., et al. (2001). A mutation in SLC11A3 is associated with autosomal dominant hemochromatosis. *Nat. Genet.* 28, 213–214. doi: 10.1038/90038

Notomi, T., Ezura, Y., and Noda, M. (2012). Identification of two-pore channel 2 as a novel regulator of osteoclastogenesis. *J. Biol. Chem.* 287, 35057–35064. doi: 10.1074/jbc.m111.328930

Notomi, T., Kuno, M., Hiyama, A., Nozaki, T., Ohura, K., Ezura, Y., et al. (2017). Role of lysosomal channel protein TPC2 in osteoclast differentiation and bone remodeling under normal and low-magnesium conditions. *J. Biol. Chem.* 292, 20998–21010. doi: 10.1074/jbc.m117.780072

Ohlendorff, S. D., Tofteng, C. L., Jensen, J. E., Petersen, S., Civitelli, R., Fenger, M., et al. (2007). Single nucleotide polymorphisms in the P2X7 gene are associated to fracture risk and to effect of estrogen treatment. *Pharm. Genomics* 17, 555–567. doi: 10.1097/fpc.0b013e3280951625

Okahashi, N., Nakamura, I., Jimi, E., Koide, M., Suda, T., and Nishihara, T. (1997). Specific inhibitors of vacuolar H(+)-ATPase trigger apoptotic cell death of osteoclasts. *J. Bone Miner. Res.* 12, 1116–1123. doi: 10.1359/jbmr.1997.12.7.1116

Okamoto, F., Kajiya, H., Toh, K., Uchida, S., Yoshikawa, M., Sasaki, S., et al. (2008). Intracellular ClC-3 chloride channels promote bone resorption in vitro through organelle acidification in mouse osteoclasts. *Am. J. Physiol. Cell Physiol.* 294, C693–C701.

Okunade, G. W., Miller, M. L., Pyne, G. J., Sutliff, R. L., O'Connor, K. T., Neumann, J. C., et al. (2004). Targeted ablation of plasma membrane Ca2+-ATPase (PMCA) 1 and 4 indicates a major housekeeping function for PMCA1 and a critical role in hyperactivated sperm motility and male fertility for PMCA4. *J. Biol. Chem.* 279, 33742–33750. doi: 10.1074/jbc.m404628200

Olesen, C. W., Vogensen, J., Axholm, I., Severin, M., Schnipper, J., Pedersen, I. S., et al. (2018). Trafficking, localization and degradation of the Na(+),HCO3(-) co-transporter NBCn1 in kidney and breast epithelial cells. *Sci. Rep.* 8:7435.

Olga, A., Anne-Kristine, M., Chiara, G., Heini, M., and Ian, C. F. (2012). Lithium interactions with Na+-coupled inorganic phosphate cotransporters: insights into the mechanism of sequential cation binding. *Am. J. Physiol. Cell Physiol.* 302, C539–C554.

Ozaki, K., Yamada, T., Horie, T., Ishizaki, A., Hiraiwa, M., Iezaki, T., et al. (2019). The L-type amino acid transporter LAT1 inhibits osteoclastogenesis and maintains bone homeostasis through the mTORC1 pathway. *Sci. Signal.* 12:eaaw3921. doi: 10.1126/scisignal.aaw3921

Palsson, R., Indridason, O. S., Edvardsson, V. O., and Oddsson, A. (2019). Genetics of common complex kidney stone disease: insights from genome-wide association studies. *Urolithiasis* 47, 11–21. doi: 10.1007/s00240-018-1094-2

Pan, C.-J., Chen, S.-Y., Jun, H. S., Lin, S. R., Mansfield, B. C., and Chou, J. Y. (2011). SLC37A1 and SLC37A2 are phosphate-linked, glucose-6-phosphate antiporters. *PLoS One* 6:e23157. doi: 10.1371/journal.pone.0023157

Parks, S. K., Chiche, J., and Pouysségur, J. (2013). Disrupting proton dynamics and energy metabolism for cancer therapy. *Nat. Rev. Cancer* 13, 611–623. doi: 10.1038/nrc3579

Pastor-Anglada, M., and érez-Torras, S. P. (2018). Who is who in adenosine transport. *Front. Pharmacol.* 9:627. doi: 10.3389/fphar.2018.00627

Peet, N. M., Grabowski, P. S., Laketić-Ljubojević, I. R. A., and Skerry, T. M. (1999). The glutamate receptor antagonist MK801 modulates bone resorption in vitro by a mechanism predominantly involving osteoclast differentiation. *FASEB J.* 13, 2179–2185. doi: 10.1096/fasebj.13.15.2179

Pellegatti, P., Falzoni, S., Donvito, G., Lemaire, I., and Di Virgilio, F. (2011). P2X7 receptor drives osteoclast fusion by increasing the extracellular adenosine concentration. *FASEB J.* 25, 1264–1274. doi: 10.1096/fj.10-169854

Pereira, M., Ko, J. H., Logan, J., Protheroe, H., Kim, K. B., Tan, A. L. M., et al. (2020). A trans-eQTL network regulates osteoclast multinucleation and bone mass. *Elife* 19:55549.

Pham, L., Purcell, P., Morse, L., Stashenko, P., and Battaglino, R. A. (2007). Expression analysis of nha-oc/NHA2: a novel gene selectively expressed in osteoclasts. *Gene Expr. Patterns* 7, 846–851. doi: 10.1016/j.modgep.2007.07.002

Pizzagalli, M. D., Bensimon, A., and Superti-Furga, G. (2020). A guide to plasma membrane solute carrier proteins. *FEBS J.*

Prié, D., Huart, V., Bakouh, N., Planelles, G., Dellis, O., Gérard, B., et al. (2002). Nephrolithiasis and osteoporosis associated with hypophosphatemia caused by mutations in the type 2a sodium–phosphate cotransporter. *N. Engl. J. Med.* 347, 983–991. doi: 10.1056/nejmoa020028

Pushkin, A., Abuladze, N., Lee, I., Newman, D., Hwang, J., and Kurtz, I. (1999). Cloning, tissue distribution, genomic organization, and functional characterization of NBC3, a new member of the sodium bicarbonate cotransporter family. *J. Biol. Chem.* 274, 16569–16575. doi: 10.1074/jbc.274.23.16569

Pushkin, A., Abuladze, N., Newman, D., Muronets, V., Sassani, P., Tatishchev, S., et al. (2003). The COOH termini of NBC3 and the 56-kDa H+-ATPase subunit are PDZ motifs involved in their interaction. *Am. J. Physiol. Cell Physiol.* 284, C667–C673.

Qin, A., Cheng, T. S., Lin, Z., Cao, L., Chim, S. M., Pavlos, N. J., et al. (2012a). Prevention of wear particle-induced osteolysis by a novel V-ATPase inhibitor saliphenylhalamide through inhibition of osteoclast bone resorption. *PLoS One* 7:e34132. doi: 10.1371/journal.pone.0034132

Qin, A., Cheng, T. S., Pavlos, N. J., Lin, Z., Dai, K. R., and Zheng, M. H. (2012b). V-ATPases in osteoclasts: structure, function and potential inhibitors of bone

resorption. *Int. J. Biochem. Cell Biol.* 44, 1422–1435. doi: 10.1016/j.biocel.2012.05.014

Qiu, M. R., Jiang, L., Matthaei, K. I., Schoenwaelder, S. M., Kuffner, T., Mangin, P., et al. (2010). Generation and characterization of mice with null mutation of the chloride intracellular channel 1 gene. *Genesis* 48, 127–136.

Riihonen, R., Nielsen, S., Vaananen, H. K., Laitala-Leinonen, T., and Kwon, T. H. (2010). Degradation of hydroxyapatite *in vivo* and *in vitro* requires osteoclastic sodium-bicarbonate co-transporter NBCn1. *Matrix Biol.* 29, 287–294. doi: 10.1016/j.matbio.2010.01.003

Robinson, L. J., Blair, H. C., Barnett, J. B., Zaidi, M., and Huang, C. L. (2010). Regulation of bone turnover by calcium-regulated calcium channels. *Ann. N. Y. Acad. Sci.* 1192, 351–357. doi: 10.1111/j.1749-6632.2009.05219.x

Robinson, L. J., Mancarella, S., Songsawad, D., Tourkova, I. L., Barnett, J. B., Gill, D. L., et al. (2012). Gene disruption of the calcium channel Orai1 results in inhibition of osteoclast and osteoblast differentiation and impairs skeletal development. *Lab. Invest.* 92, 1071–1083. doi: 10.1038/labinvest.2012.72

Rossmann, H., Alper, S. L., Nader, M., Wang, Z., Gregor, M., and Seidler, U. (2000). Three 5′-variant mRNAs of anion exchanger AE2 in stomach and intestine of mouse, rabbit, and rat. *Ann. N. Y. Acad. Sci.* 915, 81–91. doi: 10.1111/j.1749-6632.2000.tb05226.x

Roy, M., and Roux, S. (2018). Rab GTPases in osteoclastic endomembrane systems. *BioMed Res. Int.* 2018:4541538.

Salo, J., Lehenkari, P., Mulari, M., Metsikkö, K., and Väänänen, H. K. (1997). Removal of osteoclast bone resorption products by transcytosis. *Science* 276, 270–273. doi: 10.1126/science.276.5310.270

Sardiello, M., Palmieri, M., di Ronza, A., Medina, D. L., Valenza, M., Gennarino, V. A., et al. (2009). A gene network regulating lysosomal biogenesis and function. *Science* 325, 473–477. doi: 10.1126/science.1174447

Schaller, S., Henriksen, K., Sveigaard, C., Heegaard, A. M., Helix, N., Stahlhut, M., et al. (2004). The chloride channel inhibitor NS3736 [corrected] prevents bone resorption in ovariectomized rats without changing bone formation. *J. Bone Miner. Res.* 19, 1144–1153. doi: 10.1359/jbmr.040302

Schieder, M., Rötzer, K., Brüggemann, A., Biel, M., and Wahl-Schott, C. A. (2010). Characterization of two-pore channel 2 (TPCN2)-mediated Ca2+ currents in isolated lysosomes. *J. Biol. Chem.* 285, 21219–21222. doi: 10.1074/jbc.c110.143123

Schlessinger, A., Yee, S. W., Sali, A., and Giacomini, K. M. (2013). SLC classification: an update. *Clin. Pharmacol. Ther.* 94, 19–23. doi: 10.1038/clpt.2013.73

Schlingmann, K. P., Kaufmann, M., Weber, S., Irwin, A., Goos, C., John, U., et al. (2011). Mutations in CYP24A1 and idiopathic infantile hypercalcemia. *N. Engl. J. Med.* 365, 410–421.

Schlingmann, K. P., Ruminska, J., Kaufmann, M., Dursun, I., Patti, M., Kranz, B., et al. (2016). Autosomal-recessive mutations in SLC34A1 encoding sodium-phosphate cotransporter 2A cause idiopathic infantile hypercalcemia. *J. Am. Soc. Nephrol.* 27, 604–614. doi: 10.1681/asn.2014101025

Schrecker, M., Korobenko, J., and Hite, R. K. (2020). Cryo-EM structure of the lysosomal chloride-proton exchanger CLC-7 in complex with OSTM1. *Elife* 9:e59555.

Schuh, K., Cartwright, E. J., Jankevics, E., Bundschu, K., Liebermann, J., Williams, J. C., et al. (2004). Plasma membrane Ca2+ ATPase 4 is required for sperm motility and male fertility. *J. Biol. Chem.* 279, 28220–28226. doi: 10.1074/jbc.m312599200

Schulz, P., Werner, J., Stauber, T., Henriksen, K., and Fendler, K. (2010). The G215R mutation in the Cl-/H+-antiporter ClC-7 found in ADO II osteopetrosis does not abolish function but causes a severe trafficking defect. *PLoS One* 5:e12585. doi: 10.1371/journal.pone.0012585

Schumann, T., König, J., Henke, C., Willmes, D. M., Bornstein, S. R., Jordan, J., et al. (2020). Solute carrier transporters as potential targets for the treatment of metabolic disease. *Pharmacol. Rev.* 72, 343–379. doi: 10.1124/pr.118.015735

Scotto Rosato, A., Montefusco, S., Soldati, C., Di Paola, S., Capuozzo, A., Monfregola, J., et al. (2019). TRPML1 links lysosomal calcium to autophagosome biogenesis through the activation of the CaMKKβ/VPS34 pathway. *Nat. Commun.* 10:5630.

Serre, C. M., Farlay, D., Delmas, P. D., and Chenu, C. (1999). Evidence for a dense and intimate innervation of the bone tissue, including glutamate-containing fibers. *Bone* 25, 623–629. doi: 10.1016/s8756-3282(99)00215-x

Silver, I. A., Murrills, R. J., and Etherington, D. J. (1988). Microelectrode studies on the acid microenvironment beneath adherent macrophages and osteoclasts. *Exp. Cell Res.* 175, 266–276. doi: 10.1016/0014-4827(88)90191-7

Sims, N. A., and Martin, T. J. (2020). Osteoclasts provide coupling signals to osteoblast lineage cells through multiple mechanisms. *Annu. Rev. Physiol.* 82, 507–529. doi: 10.1146/annurev-physiol-021119-034425

Skerry, T. M., and Taylor, A. F. (2001). Glutamate signalling in bone. *Curr. Pharm. Des.* 7, 737–750. doi: 10.2174/1381612013397771

Sluyter, R. (2017). The P2X7 receptor. *Adv. Exp. Med. Biol.* 1051, 17–53.

Sobacchi, C., Schulz, A., Coxon, F. P., Villa, A., and Helfrich, M. H. (2013). Osteopetrosis: genetics, treatment and new insights into osteoclast function. *Nat. Rev. Endocrinol.* 9, 522–536. doi: 10.1038/nrendo.2013.137

Sorensen, M. G., Henriksen, K., Neutzsky-Wulff, A. V., Dziegiel, M. H., and Karsdal, M. A. (2007). Diphyllin, a novel and naturally potent V-ATPase inhibitor, abrogates acidification of the osteoclastic resorption lacunae and bone resorption. *J. Bone Miner. Res.* 22, 1640–1648. doi: 10.1359/jbmr.070613

Spencer, G. J., McGrath, C. J., and Genever, P. G. (2007). Current perspectives on NMDA-type glutamate signalling in bone. *Int. J. Biochem. Cell Biol.* 39, 1089–1104. doi: 10.1016/j.biocel.2006.11.002

Stauber, T., and Jentsch, T. J. (2010). Sorting motifs of the endosomal/lysosomal CLC chloride transporters. *J. Biol. Chem.* 285, 34537–34548. doi: 10.1074/jbc.m110.162545

Sulem, P., Gudbjartsson, D. F., Stacey, S. N., Helgason, A., Rafnar, T., Jakobsdottir, M., et al. (2008). Two newly identified genetic determinants of pigmentation in Europeans. *Nat. Genet.* 40, 835–837. doi: 10.1038/ng.160

Sun-Wada, G., Murata, Y., Yamamoto, A., Kanazawa, H., Wada, Y., and Futai, M. (2000). Acidic endomembrane organelles are required for mouse postimplantation development. *Dev. Biol.* 228, 315–325. doi: 10.1006/dbio.2000.9963

Suzuki, Y., Chitayat, D., Sawada, H., Deardorff, M. A., McLaughlin, H. M., Begtrup, A., et al. (2018). TRPV6 variants interfere with maternal-fetal calcium transport through the placenta and cause transient neonatal hyperparathyroidism. *Am. J. Hum. Genet.* 102, 1104–1114. doi: 10.1016/j.ajhg.2018.04.006

Teitelbaum, S. L., and Ross, F. P. (2003). Genetic regulation of osteoclast development and function. *Nat. Rev. Genet.* 4, 638–649. doi: 10.1038/nrg1122

Teti, A., Blair, H. C., Teitelbaum, S. L., Kahn, A. J., Koziol, C., Konsek, J., et al. (1989). Cytoplasmic pH regulation and chloride/bicarbonate exchange in avian osteoclasts. *J. Clin. Invest.* 83, 227–233. doi: 10.1172/jci113863

Thompson, E. G., Schaheen, L., Dang, H., and Fares, H. (2007). Lysosomal trafficking functions of mucolipin-1 in murine macrophages. *BMC Cell Biol.* 8:54. doi: 10.1186/1471-2121-8-54

Tidow, H., Poulsen, L. R., Andreeva, A., Knudsen, M., Hein, K. L., Wiuf, C., et al. (2012). A bimodular mechanism of calcium control in eukaryotes. *Nature* 491, 468–472. doi: 10.1038/nature11539

Timmann, C., Thye, T., Vens, M., Evans, J., May, J., Ehmen, C., et al. (2012). Genome-wide association study indicates two novel resistance loci for severe malaria. *Nature* 489, 443–446. doi: 10.1038/nature11334

Toro, E., Zuo, J., Guiterrez, A., La Rosa, R., Gawron, A., Bradaschia-Correa, V., et al. (2013). Bis-enoxacin inhibits bone resorption and orthodontic tooth movement. *J. Dental Res.* 92, 925–931. doi: 10.1177/0022034513501876

Toro, E. J., Zuo, J., Ostrov, D. A., Catalfamo, D., Bradaschia-Correa, V., Arana-Chavez, V., et al. (2012). Enoxacin directly inhibits osteoclastogenesis without inducing apoptosis. *J. Biol. Chem.* 287, 17894–17904. doi: 10.1074/jbc.m111.280511

Toyomura, T., Oka, T., Yamaguchi, C., Wada, Y., and Futai, M. (2000). Three subunit a isoforms of mouse vacuolar H+-ATPase preferential expression of the a3 isoform during osteoclast differentiation. *J. Biol. Chem.* 275, 8760–8765. doi: 10.1074/jbc.275.12.8760

Ulmasov, B., Bruno, J., Woost, P. G., and Edwards, J. C. (2007). Tissue and subcellular distribution of CLIC1. *BMC Cell Biol.* 8:8. doi: 10.1186/1471-2121-8-8

Valenzuela, S. M., Alkhamici, H., Brown, L. J., Almond, O. C., Goodchild, S. C., Carne, S., et al. (2013). Regulation of the membrane insertion and conductance activity of the metamorphic chloride intracellular channel protein CLIC1 by cholesterol. *PLoS One* 8:e56948. doi: 10.1371/journal.pone.0056948

van der Eerden, B. C., Hoenderop, J. G., de Vries, T. J., Schoenmaker, T., Buurman, C. J., Uitterlinden, A. G., et al. (2005). The epithelial Ca2+ channel TRPV5 is

essential for proper osteoclastic bone resorption. *Proc. Natl. Acad. Sci. U.S.A.* 102, 17507–17512. doi: 10.1073/pnas.0505789102

Varela, L., Hendry, A. C., Medina-Carmona, E., Cantoni, D., and Ortega-Roldan, J. L. (2019). Membrane insertion of soluble CLIC1 into active chloride channels is triggered by specific divalent cations. *bioRxiv [Preprint]* doi: 10.1101/638080

Vergarajauregui, S., and Puertollano, R. (2006). Two di-leucine motifs regulate trafficking of mucolipin-1 to lysosomes. *Traffic* 7, 337–353. doi: 10.1111/j.1600-0854.2006.00387.x

Visentin, L., Dodds, R. A., Valente, M., Misiano, P., Bradbeer, J. N., Oneta, S., et al. (2000). A selective inhibitor of the osteoclastic V-H(+)-ATPase prevents bone loss in both thyroparathyroidectomized and ovariectomized rats. *J. Clin. Invest.* 106, 309–318. doi: 10.1172/jci6145

Voglmaier, S. M., Kam, K., Yang, H., Fortin, D. L., Hua, Z., Nicoll, R. A., et al. (2006). Distinct endocytic pathways control the rate and extent of synaptic vesicle protein recycling. *Neuron* 51, 71–84. doi: 10.1016/j.neuron.2006.05.027

Wang, C., Li, Y., Shi, L., Ren, J., Patti, M., Wang, T., et al. (2012). Mutations in SLC20A2 link familial idiopathic basal ganglia calcification with phosphate homeostasis. *Nat. Genet.* 44, 254–256.

Wang, L., Fang, B., Fujiwara, T., Krager, K., Gorantla, A., Li, C., et al. (2018b). Deletion of ferroportin in murine myeloid cells increases iron accumulation and stimulates osteoclastogenesis *in vitro* and *in vivo*. *J. Biol. Chem.* 293, 9248–9264. doi: 10.1074/jbc.ra117.000834

Wang, N., Agrawal, A., Jørgensen, N. R., and Gartland, A. (2018a). P2X7 receptor regulates osteoclast function and bone loss in a mouse model of osteoporosis. *Sci. Rep.* 8:3507.

Wang, W., Zhang, X., Gao, Q., and Xu, H. (2014). TRPML1: an ion channel in the lysosome. *Handb. Exp. Pharmacol.* 222, 631–645. doi: 10.1007/978-3-642-54215-2_24

Wang, W. W., Gallo, L., Jadhav, A., Hawkins, R., and Parker, C. G. (2020). The druggability of solute carriers. *J. Med. Chem.* 63, 3834–3867. doi: 10.1021/acs.jmedchem.9b01237

Weivoda, M. M., and Oursler, M. J. (2014). The roles of small GTPases in osteoclast biology. *Orthop. Muscular Syst. Curr. Res.* 3:1000161.

Wu, C., Liu, X., Sun, R., Qin, Y., Liu, Z., Yang, S., et al. (2018). Targeting anion exchange of osteoclast, a new strategy for preventing wear particles induced-osteolysis. *Front. Pharmacol.* 9:1291. doi: 10.3389/fphar.2018.01291

Wu, J., Glimcher, L. H., and Aliprantis, A. O. (2008). HCO3-/Cl- anion exchanger SLC4A2 is required for proper osteoclast differentiation and function. *Proc. Natl. Acad. Sci. U.S.A.* 105, 16934–16939. doi: 10.1073/pnas.0808763105

Xie, W., Lorenz, S., Dolder, S., and Hofstetter, W. (2016). Extracellular Iron is a modulator of the differentiation of osteoclast lineage cells. *Calcif. Tissue Int.* 98, 275–283. doi: 10.1007/s00223-015-0087-1

Xie, X. S., Padron, D., Liao, X., Wang, J., Roth, M. G., and De Brabander, J. K. (2004). Salicylihalamide A inhibits the V0 sector of the V-ATPase through a mechanism distinct from bafilomycin A1. *J. Biol. Chem.* 279, 19755–19763. doi: 10.1074/jbc.m313796200

Xu, J., Feng, H. T., Wang, C., Yip, K. H., Pavlos, N., Papadimitriou, J. M., et al. (2003). Effects of Bafilomycin A1: an inhibitor of vacuolar H (+)-ATPases on endocytosis and apoptosis in RAW cells and RAW cell-derived osteoclasts. *J. Cell Biochem.* 88, 1256–1264. doi: 10.1002/jcb.10477

Yan, P., Li, T., Bo, M., Die, L., and Xing, L. (2011). Inhibition of bone resorption by econazole in rat osteoclast-like cells through suppressing TRPV5. *Arch. Pharm. Res.* 34, 1007–1013. doi: 10.1007/s12272-011-0618-x

Yin, X., Zhang, Y., Gao, H., Jin, Q. L., and Wen, X. Y. (2019). A case report of hereditary hemochromatosis caused by mutation of SLC40A1 gene. *Medicine (Baltimore)* 98:e17526. doi: 10.1097/md.0000000000017526

Yoshikawa, M., Uchida, S., Ezaki, J., Rai, T., Hayama, A., Kobayashi, K., et al. (2002). CLC-3 deficiency leads to phenotypes similar to human neuronal ceroid lipofuscinosis. *Genes Cells* 7, 597–605. doi: 10.1046/j.1365-2443.2002.00539.x

Yu, Z., Surface, L. E., Park, C. Y., Horlbeck, M. A., Wyant, G. A., Abu-Remaileh, M., et al. (2018). Identification of a transporter complex responsible for the cytosolic entry of nitrogen-containing bisphosphonates. *Elife* 7:e36620.

Zaidi, M., Moonga, B. S., and Adebanjo, O. A. (1999). Novel mechanisms of calcium handling by the osteoclast: a review–hypothesis. *Proc. Assoc. Am. Phys.* 111, 319–327. doi: 10.1046/j.1525-1381.1999.99233.x

Zaidi, M., Shankar, V. S., Tunwell, R., Adebanjo, O. A., Mackrill, J., Pazianas, M., et al. (1995). A ryanodine receptor-like molecule expressed in the osteoclast plasma membrane functions in extracellular Ca2+ sensing. *J. Clin. Invest.* 96, 1582–1590. doi: 10.1172/jci118197

Zeng, D., Yao, P., and Zhao, H. (2019). P2X7, a critical regulator and potential target for bone and joint diseases. *J. Cell. Physiol.* 234, 2095–2103. doi: 10.1002/jcp.27544

Zhang, S., Liu, Y., Zhang, B., Zhou, J., Li, T., Liu, Z., et al. (2020). Molecular insights into the human CLC-7/Ostm1 transporter. *Sci. Adv.* 6:eabb4747. doi: 10.1126/sciadv.abb4747

Zhang, T., Zhou, Q., Ogmundsdottir, M. H., Moller, K., Siddaway, R., Larue, L., et al. (2015). Mitf is a master regulator of the v-ATPase, forming a control module for cellular homeostasis with v-ATPase and TORC1. *J. Cell Sci.* 128, 2938–2950. doi: 10.1242/jcs.173807

Zhang, W., Lv, T., Huang, J., and Ou, X. (2017). Type 4B hereditary hemochromatosis associated with a novel mutation in the SLC40A1 gene: a case report and a review of the literature. *Medicine (Baltimore)* 96:e8064. doi: 10.1097/md.0000000000008064

Zhang, X., Xu, X., Liu, X., Mao, C., Qin, A., and Lu, E. (2018). Bisenoxacin blocks alveolar bone resorption in rats with ovariectomyinduced osteoporosis. *Mol. Med. Rep.* 17, 3232–3238.

Zhang, Y., Zhang, Y., Sun, K., Meng, Z., and Chen, L. (2018). The SLC transporter in nutrient and metabolic sensing, regulation, and drug development. *J. Mol. Cell Biol.* 11, 1–13. doi: 10.1093/jmcb/mjy052

Zhou, Y., Lewis, T. L., Robinson, L. J., Brundage, K. M., Schafer, R., Martin, K. H., et al. (2011). The role of calcium release activated calcium channels in osteoclast differentiation. *J. Cell. Physiol.* 226, 1082–1089. doi: 10.1002/jcp.22423

**Conflict of Interest:** The authors declare that the research was conducted in the absence of any commercial or financial relationships that could be construed as a potential conflict of interest.

frontiers in Cell and Developmental Biology

REVIEW
published: 18 March 2021
doi: 10.3389/fcell.2021.658893

# Hypoxia-Inducible Factors Regulate Osteoclasts in Health and Disease

*Xianyi Meng[1], Ben Wielockx[2], Martina Rauner[3†] and Aline Bozec[1*†]*

*[1] Department of Internal Medicine 3 – Rheumatology and Immunology, Friedrich-Alexander-University Erlangen-Nurnberg (FAU) and Universitatsklinikum Erlangen, Erlangen, Germany, [2] Institute of Clinical Chemistry and Laboratory Medicine, Technische Universität Dresden, Dresden, Germany, [3] Department of Medicine 3 – Division of Molecular Bone Biology, Medical Faculty of the Technische Universität Dresden, Dresden, Germany*

Hypoxia-inducible factors (HIFs) have become key transcriptional regulators of metabolism, angiogenesis, erythropoiesis, proliferation, inflammation and metastases. HIFs are tightly regulated by the tissue microenvironment. Under the influence of the hypoxic milieu, HIF proteins allow the tissue to adapt its response. This is especially critical for bone, as it constitutes a highly hypoxic environment. As such, bone structure and turnover are strongly influenced by the modulation of oxygen availability and HIFs. Both, bone forming osteoblasts and bone resorbing osteoclasts are targeted by HIFs and modulators of oxygen tension. Experimental and clinical data have delineated the importance of HIF responses in different osteoclast-mediated pathologies. This review will focus on the influence of HIF expression on the regulation of osteoclasts in homeostasis as well as during inflammatory and malignant bone diseases.

**Keywords: hypoxia, HIF, osteoclast, osteoblast, bone homeostasis, inflammation, malignant bone disease**

OPEN ACCESS

***Edited by:***
*Ari Elson,*
*Weizmann Institute of Science, Israel*

***Reviewed by:***
*Cormac Taylor,*
*University College Dublin, Ireland*
*Joachim Fandrey,*
*University of Duisburg-Essen, Germany*

****Correspondence:***
*Aline Bozec*
*aline.bozec@uk-erlangen.de*

*† These authors have contributed equally to this work*

***Specialty section:***
*This article was submitted to Cellular Biochemistry, a section of the journal Frontiers in Cell and Developmental Biology*

***Received:*** *26 January 2021*
***Accepted:*** *18 February 2021*
***Published:*** *18 March 2021*

***Citation:***
*Meng X, Wielockx B, Rauner M and Bozec A (2021) Hypoxia-Inducible Factors Regulate Osteoclasts in Health and Disease. Front. Cell Dev. Biol. 9:658893. doi: 10.3389/fcell.2021.658893*

## INTRODUCTION

Bone is a highly dynamic tissue that undergoes constant remodeling to adapt to changing functional and metabolic demands, but also to repair microdamages that naturally occur throughout life. For example, bone sensitively reacts to loading (e.g., weight-lifting activities) or unloading conditions (e.g., space flight) by increasing or decreasing bone mass, respectively. In addition, bone also adapts to meet changing metabolic demands (Zhang et al., 2015; Shahi et al., 2017; Loeffler et al., 2018), such as during lactation, when bone resorption increases to provide sufficient calcium for milk production (Kovacs, 2005). Thus, bone remodeling is a finely tuned and dynamic system that is required to maintain bone mass as well as mineral homeostasis during adulthood (Al-Bari and Al Mamun, 2020).

Bone remodeling is a temporally and spatially controlled process (Frost, 1963). In adults, about 10% of the bone surface is undergoing remodeling at a given time. The cells that contribute to bone remodeling are grouped into the basic multicellular unit (BMU) (Hauge et al., 2001; Andersen et al., 2009). Therein, osteoclasts, which are of hematopoietic origin, resorb bone (Teitelbaum, 2000). This is followed by a reversal phase, in which osteoclasts vacate the bone remodeling area and allow for osteoblasts, the bone-forming cells, to locate and refill the resorbed area with new bone matrix (Matsuo and Irie, 2008; Sims and Gooi, 2008). This process is estimated to take about 3 months in humans (Eriksen et al., 1984a,b). It is a coupled process, where osteoclasts regulate the differentiation and activity of osteoblasts and vice versa. Besides osteoclasts and osteoblasts, which are the two most important specialized cell types for bone remodeling, several other cell

types have been shown to contribute to bone remodeling, such as the osteocytes, which appear to coordinate bone remodeling by sending signals to the osteoclasts and osteoblasts to regulate their activity (Sims and Martin, 2015).

In healthy adults, the amount of newly formed bone equals the amount of resorbed bone, thus, ensuring the maintenance of bone mass. However, several disease conditions including estrogen deficiency, chronic inflammation, and malignant disease lead to uncoupling of bone resorption and bone formation in which bone resorption exceeds bone formation, leading to bone loss and fragility (Roodman, 2004; Pacifici, 2008; Redlich and Smolen, 2012; Klein-Nulend et al., 2015). As such, osteoclasts play a prominent role in diseases characterized by bone loss and therefore are the main therapeutic target of anti-resorptive strategies to treat osteoporosis.

Importantly, both, inflammation and malignancy are characterized by hypoxia and also physiological bone remodeling is under the strict control of hypoxia-related signaling pathways. The latter may be explained by the rather hypoxic microenvironment of bone niche, with *in vivo* measurements in mice demonstrating local oxygen tension as low as 1.3 kPa (10 mmHg; tissues less than this are generally defined as hypoxic) (McNamee et al., 2013; Spencer et al., 2014).

Hypoxia-inducible factors (HIF) are heterodimeric transcription factors, consisting of an oxygen-labile alpha subunit (HIFα) and a constitutively-stable beta subunit (HIF1β), that exert pivotal roles in inducing cellular responses to hypoxia (Wang et al., 1995; Tian et al., 1997). HIF1α and HIF2α are structurally similar (Loboda et al., 2010). Their stability is post-transcriptionally regulated by oxygen availability through the iron-dependent enzymes prolylhydroxylases (PHDs) (Mole, 2010). In well-oxygenated environment, HIFα is subject to oxygen-dependent hydroxylation at proline residues 564 and/or 402 by PHDs, which leads to binding of the von Hippel Lindau protein (VHL) and an associated ubiquitin protein ligase complex. This leads to ubiquitination and proteasomal degradation of HIFα (Lee et al., 2004). Conversely, the hydroxylation reaction is inhibited under hypoxic condition, HIFα subunits are stabilized and translocate to the nucleus, where they heterodimerize with HIF1β and bind to HRE located within regulatory elements of HIF target genes (Dengler et al., 2014). These are involved in multiple processes such as angiogenesis (*Vegf*, *Pdgf*, and *Fgf2*), erythropoiesis (*Epo*, *Tfr1*, and *Cp*), metabolism (*Glut1*, *Pdk1*, *Hk2*, *Ldha*, and *Mct4*), proliferation (*Tnfa*, *Ccnd1*, and *Igf2*), inflammation (*Il1b*, *Il6*, and *Il17*) and metastasis (*Met1*, *Lox1*) (Flamme et al., 1997; Jaakkola et al., 2001; Mahon et al., 2001; Wenger et al., 2005; Semenza, 2014). Recent studies showed that many other proteins are involved in the regulation of basal HIF1α levels in an oxygen-independent manner. Luo et al. (2010) delineated that the heat shock protein 70 (HSP70) binds *via* its carboxy-terminus to HIF1α, leading to recruitment of HSP70-interaction protein (CHIP), a chaperone-dependent E3 ubiquitin ligase, which mediates HIF1α ubiquitination and proteasomal degradation. Additionally, it has been shown that PTEN-PI3K-AKT signaling axis controls E3 ubiquitin-protein ligase Murine double minute 2 (MDM2), which mediates HIF1α ubiquitination under hypoxic conditions in a proteasome-dependent manner (Joshi et al., 2014; **Figure 1**).

Besides the post-transcriptional regulation of HIF1α protein stability, HIFα is also regulated at the transcriptional level. Increased transcription of *Hif1a* was found in cells after the stimulation of growth factors (FGF, EGF, and Heregulin), cytokines (TNF-α, IL-1, and IL-6) and pathogen associated molecular patterns (PAMP) (LPS and HBx) *via* the JAK/STAT and NF-κB signaling pathways (Frede et al., 2006; **Figure 1**). Recognition of pathogens by immune cells activates the mitogen activated protein kinase (MAPK) pathway *via* pattern recognition receptors signaling, such as toll like receptors (TLRs) (Frede et al., 2006), which leads to the induction of NF-κB and transactivation of *Hif1a* under normoxia (Rius et al., 2008). In addition, T cell receptor ligation induces substantial accumulation of HIF1α mRNA and protein, especially in the pro-inflammatory T helper 17 (Th17) cell lineage by a mechanism dependent of STAT3 signaling activation (Dang et al., 2011). Besides, MYD88-dependent NF-κB activity is crucial for LPS-induced HIF1α accumulation in dendritic cells (Jantsch et al., 2011). Taken together, growth factors, cytokines and factors stimulating PAMP are critical regulators of HIF1α or HIF2α level in normoxic and hypoxic conditions.

Given the pertinent role of osteoclasts in bone homeostasis and bone disease, and their regulation *via* hypoxia signaling, this review will summarize the current knowledge on the role of hypoxia signaling on osteoclasts and its potential as therapeutic target to inhibit osteoclast function in inflammatory and malignant bone diseases.

## OSTEOCLASTS AND THEIR REGULATION BY HYPOXIC SIGNALING PATHWAYS

Osteoclasts originate from the erythromyeloid progenitors during embryogenesis and throughout life fuse with hematopoietic stem cells to produce long-lived, multinucleated cells that are capable to resorb bone (Jacome-Galarza et al., 2019). Mononuclear cells also appear to dissociate again from multinucleated osteoclasts, suggesting that osteoclasts are undergoing constant remodeling themselves. Receptor activator of NF-κB ligand (RANKL) is the key cytokine driving osteoclastogenesis. Upon binding to its receptor RANK, RANKL induces differentiation, fusion, and life span of osteoclasts *via* the activation of pathways downstream of TRAF6 including MAPK, NF-κB, and PI3K/Akt (Nakagawa et al., 1998; Kong et al., 1999; Yahara et al., 2020). These pathways culminate in the activation of NFATc1, AP-1, and NF-κB transcription factors, which induce the expression of typical osteoclastic genes such as cathepsin K or tartrate-resistant acid phosphatase (TRAP). RANKL is mainly produced by cells from the osteogenic lineage (i.e., osteoblasts and osteocytes) together with its natural antagonist osteoprotegerin (OPG). OPG is able to bind RANKL and prevent it from binding to RANK and thus initiating osteoclastogenesis. Therefore, the RANKL/OPG ratio is crucial for predicting the osteoclastic milieu of the environment. Once osteoclasts are

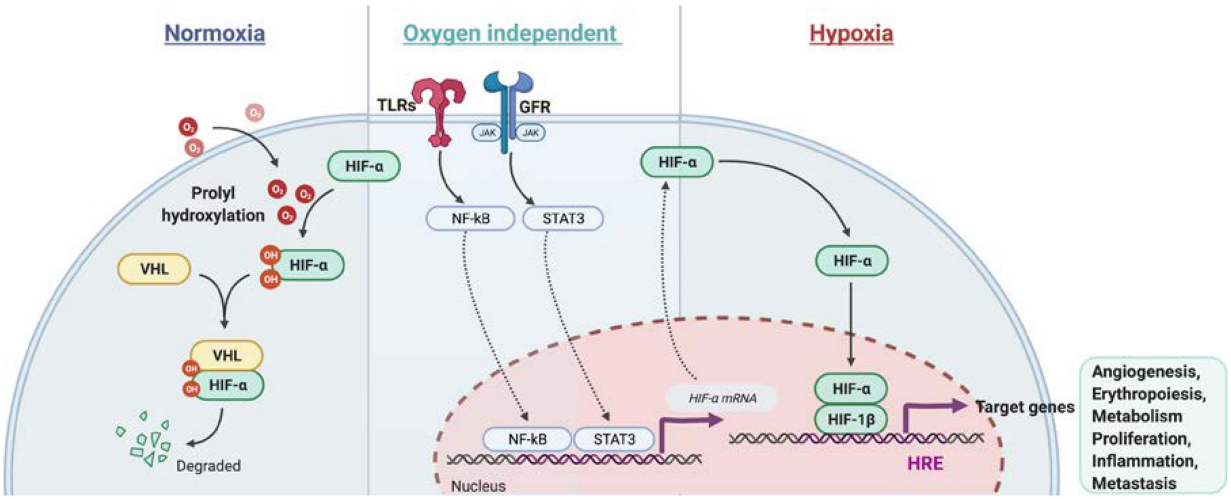


**FIGURE 1 |** Regulation of HIFα stabilization in normoxia and hypoxia conditions as well in an oxygen independent pathway. In normoxia, HIFα is hydroxylated by prolyl hydroxylase domain (PHD) protein. The proline-hydroxylated HIFα is then recognized by von Hippel-Lindau E3 ubiquitin ligase (VHL) and subjected to be degraded *via* proteasome. In hypoxia, HIFα becomes stable and dimeries with HIF-1β. After translocation to the nucleus, the HIF heterodimer binds the hypoxia response element (HRE) of target genes to regulate transcription. Besides, NF-κb and STAT3 signaling activation induce *Hifa* mRNA transcription under normoxia or hypoxia.

formed they attach tightly to the bone matrix *via* integrins, most prominently $\alpha_v\beta_3$, and seal off the environment from the area that will be resorbed. Within this sealing zone, osteoclasts acidify the environment and secrete matrix-degrading enzymes such as cathepsin K into the resorption lacunae to resorb the mineralized and organic components of bone. Until recently, osteoclasts have been proposed to undergo apoptosis after bone resorption. However, newer concepts suggest that osteoclasts may recycle (parts) of themselves to fuse with new osteoclast syncytia and engage in new remodeling cycles (McDonald et al., 2019).

Hypoxia is a critical stimulator of osteoclastogenesis in mouse and human cell culture systems. Early studies have shown that low oxygen tension (2% $O_2$) increases osteoclast differentiation and bone resorption *in vitro* (Arnett et al., 2003; Muzylak et al., 2006; Bozec et al., 2008), while hyperoxia suppresses osteoclastogenesis (Al Hadi et al., 2013; Yu et al., 2020). In an effort to analyze whether HIF1α was responsible for the pro-osteoclast effects, HIF1α protein was expressed in osteoclasts *in vitro* (Leger et al., 2010). However, in this study, osteoclast generation was inhibited by expression of a constitutively active form of HIF1α, suggesting that other hypoxia-responsive factors may contribute to osteoclastogenesis (Leger et al., 2010). Another study that investigated the potential of hypoxia mimetic PHD inhibitor dimethyloxallyl glycine (DMOG) to rescue ovariectomy-induced bone loss similarly found no effect of DMOG on osteoclast activity (Peng et al., 2014). Finally, Hulley et al. (2017) have shown that activation of HIF1α *via* deficiency of PHD2 does not affect osteoclast differentiation, but impairs bone resorption *in vitro*, suggesting that HIF1α may affect the bone resorbing activity of osteoclasts. However, it should be noted that *in vivo*, PHD2 +/− mice showed normal serum levels of CTX, a bone resorption marker, despite low bone mass (Rauner et al., 2016), suggesting that rather defective osteoblast function contributed to the low bone mass. HIFs are the canonical substrates for PHD-mediated protein hydroxylation. Increasing *in vitro* evidence indicates that PHD may also have alternative targets such as IKK-β, p105, p53, and FOXO3a (Cockman et al., 2019; Lee, 2019). However, the role of these non-HIF substrates in osteoclastogenesis under hypoxia is still elusive. Besides, neither osteoclast-specific knockout nor treatment with a HIF1α inhibitor altered bone mass or osteoclast numbers under physiological conditions, but in states of estrogen or testosterone deficiency, when osteoclasts are activated, HIF1α deficiency prevented bone loss by suppressing osteoclast activation (Miyauchi et al., 2013; Tando et al., 2016). Overall, direct effects of HIF1α on osteoclastogenesis during physiology appear negligible. However, metabolically, osteoclasts require oxidative phosphorylation during differentiation, while for bone resorption, osteoclasts rely on energy production *via* glycolysis (Czupalla et al., 2005; Jin et al., 2014; Lemma et al., 2016). As HIFs activate glycolysis, this may in part explain the stronger effect of HIF1α activation on osteoclastic bone resorption rather than differentiation. In fact, HIF1α has been identified as a critical metabolic switch to turn on anaerobic respiration to rapidly increase ATP production in osteoclasts (Morten et al., 2013).

Importantly, there is strong evidence that HIF1α controls osteoclastogenesis *via* the regulation of the RANKL/OPG ratio and also IL-33 levels in osteoblasts (Wu et al., 2015; Kang et al., 2017; Zhu et al., 2019) and osteocytes even under physiological conditions (Stegen et al., 2018).

In contrast to HIF1α, HIF2α appears to have direct effects on osteoclasts. Overexpression of HIF2α in progenitors increased osteoclast numbers and marker gene expression *in vitro* (Lee et al., 2019) by upregulating TRAF6 expression. Moreover,

osteoclast-specific knockout of HIF2α increased bone mass by decreasing osteoclast numbers (Lee et al., 2019). However, also in case of HIF2α, osteoblast-mediated regulation of osteoclastogenesis *via* RANKL/OPG seems to play an important role as osteoblast-specific knockout of HIF2α also decreased osteoclast numbers *in vivo*.

Taken together, HIFs appear to play a more prominent role in osteoblast-to-osteoclast communication rather than directly affecting osteoclastogenesis. Moreover, activation of hypoxia signaling pathways may be more relevant in disease states than during physiological bone remodeling. In the following sections, we will discuss the role of hypoxia-related proteins in inflammatory and malignant diseases.

## ROLE OF HYPOXIA IN THE REGULATION OF OSTEOCLASTS IN RHEUMATOID ARTHRITIS AS A PROTOTYPICAL INFLAMMATORY DISEASE

Rheumatoid arthritis (RA) is a systemic autoimmune disorder that manifests as chronic inflammation and joint tissue destruction (Komatsu and Takayanagi, 2012). Macrophages, T lymphocytes and B lymphocytes are crucial cells in the development and progression of RA (Ma and Pope, 2005; Cope et al., 2007; Marston et al., 2010). Oxygen tension in the synovial fluid of RA patients (range from 18 to 33 mmHg, equivalent to 2 to 4%) was found lower than in healthy controls (range from 69 to 89 mmHg, equivalent to 9 to 12%) (Giatromanolaki et al., 2003; Muz et al., 2009). In addition, tissue oximeters were used to confirm that hypoxia is a feature of RA synovial tissue and correlates with the intensity of the inflammatory process during RA development (Quinonez-Flores et al., 2016). HIFs (HIF1α and HIF2α) could therefore interfere with joint inflammation, angiogenesis and cartilage destruction in RA (Westra et al., 2010; Quinonez-Flores et al., 2016). Different aspects of RA are influenced by the expression of HIFs in stromal cells and immune cells. Hypoxia induces vascular cell adhesion molecule-1 (VCAM1) and stromal cell-derived factor-1 (SDF-1) expression in synovial fibroblasts and promotes lymphocyte homing to joints of RA patients (Hitchon et al., 2002; Hu et al., 2016). Studies have also shown that NF-κB-HIF1α pathway activation drives the migration and invasion of synovial fibroblasts by increasing the expression of MMP2 and MMP9 (Lee et al., 2012). Interestingly, HIF2α was expressed mainly in fibroblast-like synoviocytes (FLS) of RA synovium and regulated the production of RANKL and several catabolic factors such as matrix-degrading enzymes (MMP3, MMP9, MMP12, MMP13, and ADAMTS4), chemokines (CCL2, CCL5, CCL7, CXCL1, CXCL2, CXCL4, CXCL5, and CXCL10) and inflammatory mediators (COX2 and iNOS) (Huh et al., 2015). Moreover, HIF2α expression in FLS controls IL-6 induction and enhances Th17 cell differentiation during RA pathogenesis (Ryu et al., 2014). Also the induction of IL-1, TNF-α, and IL-33 was reported to be increased in FLS *via* HIFs, which subsequently was reflected by T cell functions with expansion of Th1 and Th17 cells (Sarkar et al., 2010; Samarpita et al., 2018), but also B cell autoantibody production. By a feedback loop by TNF-α, IL-33 manages the control of HIF. Besides HIF2α, also HIF1α increases IL-6 production in RA. Further evidence shows that HIF1α is highly expressed in Th17 cells and that loss of HIF1α in Th17 cells impairs their differentiation and IL-17 production, suggesting that HIF1α expression in Th17 cells might control synovial inflammation in arthritis (Dang et al., 2011). Finally, HIF1α participation in collagen-induced arthritis has been demonstrated by studying conditional HIF1α deletion in B cells, which results in less IL-10-producing B cells and exacerbated Th17 cells mediated inflammation (Meng et al., 2018; **Figure 2**).

Altogether, HIF1α and HIF2α indirectly regulate osteoclast-induced bone erosion through the control of the pro-inflammatory milieu. However, it remains unclear whether there is a direct involvement of these factors in osteoclasts under inflammatory conditions. Several therapeutic agents use the hypoxic milieu to get activated and to deliver the therapeutic agents to hypoxic cells on a site specific. However, the off-target effects might be an important challenge since hypoxic conditions also appear physiologically (Phillips, 2016). Several agents targeting the HIF pathway, such as specific HIF inhibitors, showed promising results in cancers or in hypoxia-related diseases (Fallah and Rini, 2019). Regarding RA, it has been suggested that local administration of these compounds could avoid their early systemic degradation. Another promising route may be achieved *via* delivery carriers for example *via* the delivery of gene therapy targeting HIFs. However, before these therapies approach clinics, several challenges still need to be addressed. In RA, downstream targets of HIFs have been therapeutically targeted, such as antibodies against VEGF, or small molecules against its receptor. In preclinical studies, these approaches showed a significant reduction of inflammation, particularly in the early phase of inflammatory RA development (Lu et al., 2000; De Bandt et al., 2003; Maruotti et al., 2014). Based on the above-mentioned studies, it is evident that HIFs are promising targets for RA.

## ROLE OF HYPOXIA IN THE REGULATION OF OSTEOCLASTS IN OSTEOLYTIC BONE DISEASE

Bone metastases are incurable, cause pathological fractures, hypercalcemia and reduce the quality of life (Macedo et al., 2017). Initially, the hypoxic bone microenvironment provides an excellent soil for tumor cells to thrive. Once homed, these cells start producing a variety of cytokines and growth factors that activate cells, including osteoclasts (Maurizi and Rucci, 2018). In turn, this will lead to bone absorption and destruction of the microenvironment, which eventually stimulates the proliferation of tumor cells. As such a vicious cycle between tumor cells and osteoclasts is established (Huang et al., 2020). Although osteolytic lesions have been observed in several cancer types, it has been especially detected in breast cancers; a tumor with great avidity for bone metastasizing in up to 80% of stage IV breast cancer patients (Brook et al., 2018). These tumor cells typically produce

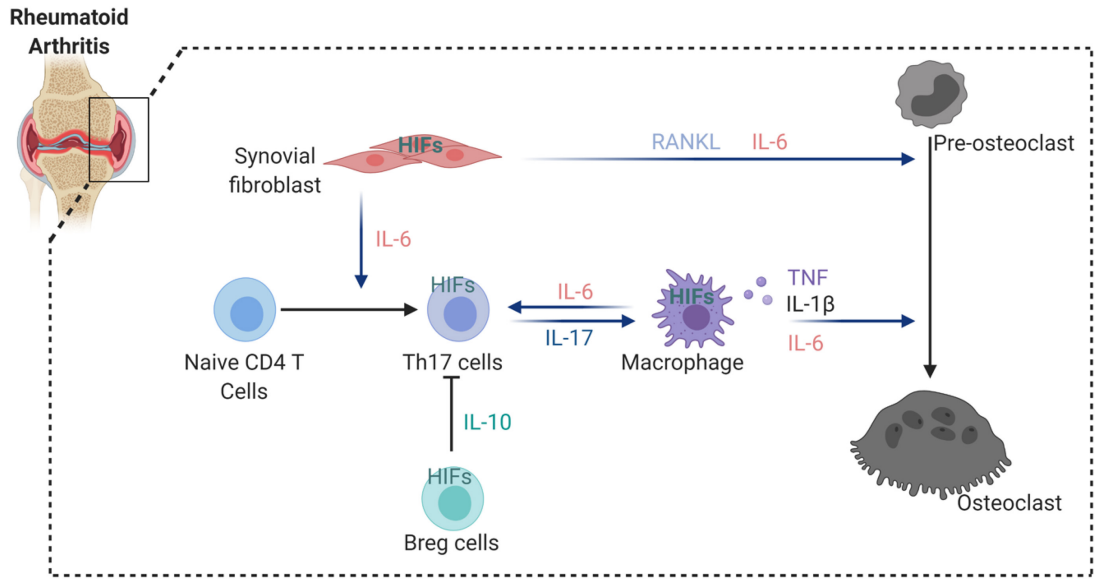


**FIGURE 2 |** HIFs involvement in the regulation of osteoclastogenesis in arthritic joint. HIFs expression induce the secretion of a number of cytokines from synovial fibroblast and macrophages that enhance osteoclastogenesis. In addition, hypoxia stimulates IL-6 production by synovial fibroblast and macrophages, thereby increasing Th17 differentiation from naïve CD4 T cells. However, HIFs activation in Breg cells inhibit Th17 differentiation *via* suppressive factor IL-10.

parathyroid hormone related protein (PTHrP), which stimulates calcium release from bone (Poole and Reeve, 2005), just like PTH. Interestingly, the expression of PTHrP is driven by HIF2α, but not HIF1α, and is not only confined to metastatic tumor cells, but has also been detected in chondrocytes where it is also induced by HIF1α (Browe et al., 2019). PTHrP stimulates osteoblasts to generate RANKL, simultaneously preventing OPG production (Huang et al., 2004). RANKL and RANK have also been shown to be produced by tumor cells in a HIF1α-dependent manner (Tang et al., 2011), suggesting that osteolysis is potentially also feasible through an interaction between the tumor cells and osteoclasts. As mentioned before, in this setting, osteoclastogenesis is driven forward due to an enhanced RANKL/OPG ratio. The consequence is enhanced bone resorption and release of other growth factors including TGFα and PDGF, both stimulating tumor growth and eventually also osteolysis (Janssens et al., 2005). Nevertheless, there are also other reports suggesting RANKL is not HIF-dependent. In that respect, deletion of PHD2 and PHD3 in osteoblast (progenitors) (Osx:cre line) resulted in increased bone volume as a consequence of OPG induction, whereas RANKL levels were not changed (Wu et al., 2015). This finding was also confirmed using a VHL knock-out strategy in primary osteoblasts (Shao et al., 2015) and by us, showing that PHD2 deletion in osteoblasts (Osx:cre line) causes high bone density (Rauner et al., 2016; Stegen et al., 2016). Although more research will be necessary to unravel the background of these opposing results, hypoxia and hypoxia pathway proteins have an impact on stromal cells of the bone/bone marrow environment that directly regulate bone homeostasis and therefore probably also osteolytic lesions.

Interestingly, the impact of hypoxia signaling in bone can also influence the growth and dissemination of external tumors finally ending up in the bone. Devignes and colleagues elegantly showed that HIF-induced CXCL12 production in osteoblast progenitors directly promotes systemic tumor growth and dissemination. In fact, mice conditionally deficient for HIF1α in osteoprogenitors displayed reduced $CXCL12^{+}$ cells whereas VHL deficiency resulted in the opposite outcome (Devignes et al., 2018). The chemokine CXCL12/stromal cell-derived factor 1 alpha (SDF1) has not only been shown in a variety of different tumor types (Shi et al., 2020), but also plays a central role in the bone marrow niche where it controls hematopoietic stem cell quiescence in conjunction with its receptor CXCR4. In the context of breast cancer cell dissemination, this signaling appears to work *via* CXCR4 on the tumor cells, underscoring local hypoxic signaling in the BM niche exerting control on distant tumors, impacting growth and metastasis (Xu et al., 2015). This suggests that targeting CXCL12/CXCR4 would be beneficial, but different experimental approaches reveal case-by-case differences (Zielinska and Katanaev, 2020). Indeed, although systemic CXCR4 inhibition might be beneficial in breast cancer growth, deficiency of CXCR4 in osteoclasts was shown to enhance osteoclastogenesis, which in turn may again promote bone metastasis and stimulate the vicious cycle (Zielinska and Katanaev, 2020).

Conversely, hypoxia in a variety of different tumors outside the bone/bone marrow area can also affect the bone and its environment by enhancing future colonization of tumor cells and even promoting pre-osteolysis. First indications for this paradigm were reported almost two decades ago, as researchers found a clear correlation between HIF1α expression in primary breast cancers and the presence of (micro)metastasis in the bone marrow of these patients

(Woelfle et al., 2003). HIF1α-induced lysyl oxidase (LOX), a copper-dependent amine oxidases, is such a molecule that can cause tumor cell dissemination and tumor driven osteolytic lesions (Bondareva et al., 2009). At the same time, it promotes RANKL-dependent differentiation of osteoclasts, while inhibiting osteoblast differentiation (Reynaud et al., 2017). This suggests that LOX secreted by tumor cells induces osteoclastogenesis thereby creating a pre-metastatic niche that would favor tumor homing and growth. Interestingly, LOX induction itself also enhances HIF1α expression, underscoring the synergism between LOX/HIF in regulating the adaptation of tumor cells to hypoxia (Pez et al., 2011) and beyond.

## CONCLUSION

The role of hypoxia and HIFs is evident in bone physiology and in numerous pathophysiological diseases where osteoclasts are activated and induce bone loss. However, the exact role of HIF1α or HIF2α in osteoclast remains quite vague and largely appear to be mediated indirectly *via* other cells like stromal cells. However, they should be taken into consideration when thinking of the indirect pathway of osteoclast activation, notably by their function in the immune cells, in particular in Th17/Treg cells or in macrophages. Therefore, HIF inhibitors would likely target osteoclast activation and secondary bone loss in numerous diseases. As example, a recent study discovered an increased bone mass in mice treated with HIF1α inhibitor 2ME2 (Miyauchi et al., 2013). However, it still remains inconclusive whether HIF inhibitors would act the same way in human bone diseases as in murine models. Future studies on HIF signaling and its clinical relevance may improve our understanding of the role of HIF in osteoclastogenesis and eventually lead to effective treatments for human diseases involving bone homeostasis.

## AUTHOR CONTRIBUTIONS

MR and AB contributed equally to the work. XM, BW, MR, and AB conceived and wrote the review. All authors contributed to the article and approved the submitted version.

## FUNDING

This work was supported by grants from the German Research Foundation (μBone SPP 2084) to BW, MR, and AB as well as a grant from the German-Israeli-Foundation (No. I-1433-203.13_2017) to BW and MR.

## REFERENCES

Al Hadi, H., Smerdon, G. R., and Fox, S. W. (2013). Hyperbaric oxygen therapy suppresses osteoclast formation and bone resorption. *J. Orthop. Res.* 31, 1839–1844. doi: 10.1002/jor.22443

Al-Bari, A. A., and Al Mamun, A. (2020). Current advances in regulation of bone homeostasis. *FASEB Bioadv.* 2, 668–679. doi: 10.1096/fba.2020-00058

Andersen, T. L., Sondergaard, T. E., Skorzynska, K. E., Dagnaes-Hansen, F., Plesner, T. L., Hauge, E. M., et al. (2009). A physical mechanism for coupling bone resorption and formation in adult human bone. *Am. J. Pathol.* 174, 239–247. doi: 10.2353/ajpath.2009.080627

Arnett, T. R., Gibbons, D. C., Utting, J. C., Orriss, I. R., Hoebertz, A., Rosendaal, M., et al. (2003). Hypoxia is a major stimulator of osteoclast formation and bone resorption. *J. Cell Physiol.* 196, 2–8. doi: 10.1002/jcp.10321

Bondareva, A., Downey, C. M., Ayres, F., Liu, W., Boyd, S. K., Hallgrimsson, B., et al. (2009). The lysyl oxidase inhibitor, beta-aminopropionitrile, diminishes the metastatic colonization potential of circulating breast cancer cells. *PLoS One* 4:e5620. doi: 10.1371/journal.pone.0005620

Bozec, A., Bakiri, L., Hoebertz, A., Eferl, R., Schilling, A. F., Komnenovic, V., et al. (2008). Osteoclast size is controlled by Fra-2 through LIF/LIF-receptor signalling and hypoxia. *Nature* 454, 221–225. doi: 10.1038/nature07019

Brook, N., Brook, E., Dharmarajan, A., Dass, C. R., and Chan, A. (2018). Breast cancer bone metastases: pathogenesis and therapeutic targets. *Int. J. Biochem. Cell Biol.* 96, 63–78. doi: 10.1016/j.biocel.2018.01.003

Browe, D. C., Coleman, C. M., Barry, F. P., and Elliman, S. J. (2019). Hypoxia activates the PTHrP -MEF2C pathway to attenuate hypertrophy in mesenchymal stem cell derived cartilage. *Sci. Rep.* 9:13274. doi: 10.1038/s41598-019-49499-x

Cockman, M. E., Lippl, K., Tian, Y. M., Pegg, H. B., Figg, W. D. J., Abboud, M. I., et al. (2019). Lack of activity of recombinant HIF prolyl hydroxylases (PHDs) on reported non-HIF substrates. *Elife* 8:e46490. doi: 10.7554/eLife.46490

Cope, A. P., Schulze-Koops, H., and Aringer, M. (2007). The central role of T cells in rheumatoid arthritis. *Clin. Exp. Rheumatol.* 25(5 Suppl. 46), S4–S11.

Czupalla, C., Mansukoski, H., Pursche, T., Krause, E., and Hoflack, B. (2005). Comparative study of protein and mRNA expression during osteoclastogenesis. *Proteomics* 5, 3868–3875. doi: 10.1002/pmic.200402059

Dang, E. V., Barbi, J., Yang, H. Y., Jinasena, D., Yu, H., Zheng, Y., et al. (2011). Control of T(H)17/T(reg) balance by hypoxia-inducible factor 1. *Cell* 146, 772–784. doi: 10.1016/j.cell.2011.07.033

De Bandt, M., Ben Mahdi, M. H., Ollivier, V., Grossin, M., Dupuis, M., Gaudry, M., et al. (2003). Blockade of vascular endothelial growth factor receptor I (VEGF-RI), but not VEGF-RII, suppresses joint destruction in the K/BxN model of rheumatoid arthritis. *J. Immunol.* 171, 4853–4859. doi: 10.4049/jimmunol.171.9.4853

Dengler, V. L., Galbraith, M., and Espinosa, J. M. (2014). Transcriptional regulation by hypoxia inducible factors. *Crit. Rev. Biochem. Mol. Biol.* 49, 1–15. doi: 10.3109/10409238.2013.838205

Devignes, C. S., Aslan, Y., Brenot, A., Devillers, A., Schepers, K., Fabre, S., et al. (2018). HIF signaling in osteoblast-lineage cells promotes systemic breast cancer growth and metastasis in mice. *Proc. Natl. Acad. Sci. U.S.A.* 115, E992–E1001. doi: 10.1073/pnas.1718009115

Eriksen, E. F., Gundersen, H. J., Melsen, F., and Mosekilde, L. (1984a). Reconstruction of the formative site in iliac trabecular bone in 20 normal individuals employing a kinetic model for matrix and mineral apposition. *Metab. Bone Dis. Relat. Res.* 5, 243–252. doi: 10.1016/0221-8747(84)90066-3

Eriksen, E. F., Melsen, F., and Mosekilde, L. (1984b). Reconstruction of the resorptive site in iliac trabecular bone: a kinetic model for bone resorption in 20 normal individuals. *Metab. Bone Dis. Relat. Res.* 5, 235–242. doi: 10.1016/0221-8747(84)90065-1

Fallah, J., and Rini, B. I. (2019). HIF inhibitors: status of current clinical development. *Curr. Oncol. Rep.* 21:6. doi: 10.1007/s11912-019-0752-z

Flamme, I., Frohlich, T., von Reutern, M., Kappel, A., Damert, A., and Risau, W. (1997). HRF, a putative basic helix-loop-helix-PAS-domain transcription factor is closely related to hypoxia-inducible factor-1 alpha and developmentally expressed in blood vessels. *Mech. Dev.* 63, 51–60. doi: 10.1016/s0925-4773(97)00674-6

Frede, S., Stockmann, C., Freitag, P., and Fandrey, J. (2006). Bacterial lipopolysaccharide induces HIF-1 activation in human monocytes via p44/42 MAPK and NF-kappaB. *Biochem. J.* 396, 517–527. doi: 10.1042/BJ20051839

Frost, H. M. (1963). *Bone Remodelling Dynamics*. New York, NY: Thomas.

Giatromanolaki, A., Sivridis, E., Maltezos, E., Athanassou, N., Papazoglou, D., Gatter, K. C., et al. (2003). Upregulated hypoxia inducible factor-1alpha and -2alpha pathway in rheumatoid arthritis and osteoarthritis. *Arthritis Res. Ther.* 5, R193–R201. doi: 10.1186/ar756

Hauge, E. M., Qvesel, D., Eriksen, E. F., Mosekilde, L., and Melsen, F. (2001). Cancellous bone remodeling occurs in specialized compartments lined by cells expressing osteoblastic markers. *J. Bone Miner. Res.* 16, 1575–1582. doi: 10.1359/jbmr.2001.16.9.1575

Hitchon, C., Wong, K., Ma, G., Reed, J., Lyttle, D., and El-Gabalawy, H. (2002). Hypoxia-induced production of stromal cell-derived factor 1 (CXCL12) and vascular endothelial growth factor by synovial fibroblasts. *Arthritis Rheum.* 46, 2587–2597. doi: 10.1002/art.10520

Hu, F., Liu, H., Xu, L., Li, Y., Liu, X., Shi, L., et al. (2016). Hypoxia-inducible factor-1alpha perpetuates synovial fibroblast interactions with T cells and B cells in rheumatoid arthritis. *Eur. J. Immunol.* 46, 742–751. doi: 10.1002/eji.201545784

Huang, J. C., Sakata, T., Pfleger, L. L., Bencsik, M., Halloran, B. P., Bikle, D. D., et al. (2004). PTH differentially regulates expression of RANKL and OPG. *J. Bone Miner. Res.* 19, 235–244. doi: 10.1359/JBMR.0301226

Huang, Y., Xiao, Z., Guan, Z., Zeng, Z., Shen, Y., Xu, X., et al. (2020). Bone-seeking nanoplatform co-delivering cisplatin and zoledronate for synergistic therapy of breast cancer bone metastasis and bone resorption. *Acta Pharm. Sin. B* 10, 2384–2403. doi: 10.1016/j.apsb.2020.06.006

Huh, Y. H., Lee, G., Lee, K. B., Koh, J. T., Chun, J. S., and Ryu, J. H. (2015). HIF-2alpha-induced chemokines stimulate motility of fibroblast-like synoviocytes and chondrocytes into the cartilage-pannus interface in experimental rheumatoid arthritis mouse models. *Arthritis Res. Ther.* 17:302. doi: 10.1186/s13075-015-0816-x

Hulley, P. A., Bishop, T., Vernet, A., Schneider, J. E., Edwards, J. R., Athanasou, N. A., et al. (2017). Hypoxia-inducible factor 1-alpha does not regulate osteoclastogenesis but enhances bone resorption activity via prolyl-4-hydroxylase 2. *J. Pathol.* 242, 322–333. doi: 10.1002/path.4906

Jaakkola, P., Mole, D. R., Tian, Y. M., Wilson, M. I., Gielbert, J., Gaskell, S. J., et al. (2001). Targeting of HIF-alpha to the von Hippel-Lindau ubiquitylation complex by O2-regulated prolyl hydroxylation. *Science* 292, 468–472. doi: 10.1126/science.1059796

Jacome-Galarza, C. E., Percin, G. I., Muller, J. T., Mass, E., Lazarov, T., Eitler, J., et al. (2019). Developmental origin, functional maintenance and genetic rescue of osteoclasts. *Nature* 568, 541–545. doi: 10.1038/s41586-019-1105-7

Janssens, K., ten Dijke, P., Janssens, S., and Van Hul, W. (2005). Transforming growth factor-beta1 to the bone. *Endocr. Rev.* 26, 743–774. doi: 10.1210/er.2004-0001

Jantsch, J., Wiese, M., Schodel, J., Castiglione, K., Glasner, J., Kolbe, S., et al. (2011). Toll-like receptor activation and hypoxia use distinct signaling pathways to stabilize hypoxia-inducible factor 1alpha (HIF1A) and result in differential HIF1A-dependent gene expression. *J. Leukoc. Biol.* 90, 551–562. doi: 10.1189/jlb.1210683

Jin, Z., Wei, W., Yang, M., Du, Y., and Wan, Y. (2014). Mitochondrial complex I activity suppresses inflammation and enhances bone resorption by shifting macrophage-osteoclast polarization. *Cell Metab.* 20, 483–498. doi: 10.1016/j.cmet.2014.07.011

Joshi, S., Singh, A. R., and Durden, D. L. (2014). MDM2 regulates hypoxic hypoxia-inducible factor 1alpha stability in an E3 ligase, proteasome, and PTEN-phosphatidylinositol 3-kinase-AKT-dependent manner. *J. Biol. Chem.* 289, 22785–22797. doi: 10.1074/jbc.M114.587493

Kang, H., Yang, K., Xiao, L., Guo, L., Guo, C., Yan, Y., et al. (2017). Osteoblast hypoxia-inducible factor-1alpha pathway activation restrains osteoclastogenesis via the interleukin-33-MicroRNA-34a-Notch1 pathway. *Front. Immunol.* 8:1312. doi: 10.3389/fimmu.2017.01312

Klein-Nulend, J., van Oers, R. F., Bakker, A. D., and Bacabac, R. G. (2015). Bone cell mechanosensitivity, estrogen deficiency, and osteoporosis. *J. Biomech.* 48, 855–865. doi: 10.1016/j.jbiomech.2014.12.007

Komatsu, N., and Takayanagi, H. (2012). Inflammation and bone destruction in arthritis: synergistic activity of immune and mesenchymal cells in joints. *Front. Immunol.* 3:77. doi: 10.3389/fimmu.2012.00077

Kong, Y. Y., Yoshida, H., Sarosi, I., Tan, H. L., Timms, E., Capparelli, C., et al. (1999). OPGL is a key regulator of osteoclastogenesis, lymphocyte development and lymph-node organogenesis. *Nature* 397, 315–323. doi: 10.1038/16852

Kovacs, C. S. (2005). Calcium and bone metabolism during pregnancy and lactation. *J. Mammary Gland Biol. Neoplasia* 10, 105–118. doi: 10.1007/s10911-005-5394-0

Lee, F. S. (2019). Substrates of PHD. *Cell Metab.* 30, 626–627. doi: 10.1016/j.cmet.2019.08.008

Lee, J. W., Bae, S. H., Jeong, J. W., Kim, S. H., and Kim, K. W. (2004). Hypoxia-inducible factor (HIF-1)alpha: its protein stability and biological functions. *Exp. Mol. Med.* 36, 1–12. doi: 10.1038/emm.2004.1

Lee, S. Y., Park, K. H., Yu, H. G., Kook, E., Song, W. H., Lee, G., et al. (2019). Controlling hypoxia-inducible factor-2alpha is critical for maintaining bone homeostasis in mice. *Bone Res.* 7:14. doi: 10.1038/s41413-019-0054-y

Lee, Y. A., Choi, H. M., Lee, S. H., Hong, S. J., Yang, H. I., Yoo, M. C., et al. (2012). Hypoxia differentially affects IL-1beta-stimulated MMP-1 and MMP-13 expression of fibroblast-like synoviocytes in an HIF-1alpha-dependent manner. *Rheumatology (Oxford)* 51, 443–450. doi: 10.1093/rheumatology/ker327

Leger, A. J., Altobelli, A., Mosquea, L. M., Belanger, A. J., Song, A., Cheng, S. H., et al. (2010). Inhibition of osteoclastogenesis by prolyl hydroxylase inhibitor dimethyloxallyl glycine. *J. Bone Miner. Metab.* 28, 510–519. doi: 10.1007/s00774-010-0171-6

Lemma, S., Sboarina, M., Porporato, P. E., Zini, N., Sonveaux, P., Di Pompo, G., et al. (2016). Energy metabolism in osteoclast formation and activity. *Int. J. Biochem. Cell Biol.* 79, 168–180. doi: 10.1016/j.biocel.2016.08.034

Loboda, A., Jozkowicz, A., and Dulak, J. (2010). HIF-1 and HIF-2 transcription factors–similar but not identical. *Mol. Cells* 29, 435–442. doi: 10.1007/s10059-010-0067-2

Loeffler, J., Duda, G. N., Sass, F. A., and Dienelt, A. (2018). The metabolic microenvironment steers bone tissue regeneration. *Trends Endocrinol. Metab.* 29, 99–110. doi: 10.1016/j.tem.2017.11.008

Lu, J., Kasama, T., Kobayashi, K., Yoda, Y., Shiozawa, F., Hanyuda, M., et al. (2000). Vascular endothelial growth factor expression and regulation of murine collagen-induced arthritis. *J. Immunol.* 164, 5922–5927. doi: 10.4049/jimmunol.164.11.5922

Luo, W., Zhong, J., Chang, R., Hu, H., Pandey, A., and Semenza, G. L. (2010). Hsp70 and CHIP selectively mediate ubiquitination and degradation of hypoxia-inducible factor (HIF)-1alpha but not HIF-2alpha. *J. Biol. Chem.* 285, 3651–3663. doi: 10.1074/jbc.M109.068577

Ma, Y., and Pope, R. M. (2005). The role of macrophages in rheumatoid arthritis. *Curr. Pharm. Des.* 11, 569–580. doi: 10.2174/1381612053381927

Macedo, F., Ladeira, K., Pinho, F., Saraiva, N., Bonito, N., Pinto, L., et al. (2017). Bone metastases: an overview. *Oncol. Rev.* 11:321. doi: 10.4081/oncol.2017.321

Mahon, P. C., Hirota, K., and Semenza, G. L. (2001). FIH-1: a novel protein that interacts with HIF-1alpha and VHL to mediate repression of HIF-1 transcriptional activity. *Genes Dev.* 15, 2675–2686. doi: 10.1101/gad.924501

Marston, B., Palanichamy, A., and Anolik, J. H. (2010). B cells in the pathogenesis and treatment of rheumatoid arthritis. *Curr. Opin. Rheumatol.* 22, 307–315. doi: 10.1097/BOR.0b013e3283369cb8

Maruotti, N., Cantatore, F. P., and Ribatti, D. (2014). Putative effects of potentially anti-angiogenic drugs in rheumatic diseases. *Eur. J. Clin. Pharmacol.* 70, 135–140. doi: 10.1007/s00228-013-1605-6

Matsuo, K., and Irie, N. (2008). Osteoclast-osteoblast communication. *Arch. Biochem. Biophys.* 473, 201–209. doi: 10.1016/j.abb.2008.03.027

Maurizi, A., and Rucci, N. (2018). The osteoclast in bone metastasis: player and target. *Cancers (Basel)* 10:218. doi: 10.3390/cancers10070218

McDonald, M., Khoo, W. H., Mohanty, S., Terry, R., Chai, R., Quinn, J., et al. (2019). Intravital imaging of osteoclasts in vivo reveals novel osteoclast fate which may underlie the therapeutic response to Denosumab withdrawal. *J. Bone Miner. Res.* 34, 44–45.

McNamee, E. N., Korns Johnson, D., Homann, D., and Clambey, E. T. (2013). Hypoxia and hypoxia-inducible factors as regulators of T cell development, differentiation, and function. *Immunol. Res.* 55, 58–70. doi: 10.1007/s12026-012-8349-8

Meng, X., Grotsch, B., Luo, Y., Knaup, K. X., Wiesener, M. S., Chen, X. X., et al. (2018). Hypoxia-inducible factor-1alpha is a critical transcription factor for IL-10-producing B cells in autoimmune disease. *Nat. Commun.* 9:251. doi: 10.1038/s41467-017-02683-x

Miyauchi, Y., Sato, Y., Kobayashi, T., Yoshida, S., Mori, T., Kanagawa, H., et al. (2013). HIF1alpha is required for osteoclast activation by estrogen deficiency in postmenopausal osteoporosis. *Proc. Natl. Acad. Sci. U.S.A.* 110, 16568–16573. doi: 10.1073/pnas.1308755110

Mole, D. R. (2010). Iron homeostasis and its interaction with prolyl hydroxylases. *Antioxid. Redox Signal.* 12, 445–458. doi: 10.1089/ars.2009.2790

Morten, K. J., Badder, L., and Knowles, H. J. (2013). Differential regulation of HIF-mediated pathways increases mitochondrial metabolism and ATP production in hypoxic osteoclasts. *J. Pathol.* 229, 755–764. doi: 10.1002/path.4159

Muz, B., Khan, M. N., Kiriakidis, S., and Paleolog, E. M. (2009). Hypoxia. The role of hypoxia and HIF-dependent signalling events in rheumatoid arthritis. *Arthritis Res. Ther.* 11:201. doi: 10.1186/ar2568

Muzylak, M., Price, J. S., and Horton, M. A. (2006). Hypoxia induces giant osteoclast formation and extensive bone resorption in the cat. *Calcif. Tissue Int.* 79, 301–309. doi: 10.1007/s00223-006-0082-7

Nakagawa, N., Kinosaki, M., Yamaguchi, K., Shima, N., Yasuda, H., Yano, K., et al. (1998). RANK is the essential signaling receptor for osteoclast differentiation factor in osteoclastogenesis. *Biochem. Biophys. Res. Commun.* 253, 395–400. doi: 10.1006/bbrc.1998.9788

Pacifici, R. (2008). Estrogen deficiency, T cells and bone loss. *Cell Immunol.* 252, 68–80. doi: 10.1016/j.cellimm.2007.06.008

Peng, J., Lai, Z. G., Fang, Z. L., Xing, S., Hui, K., Hao, C., et al. (2014). Dimethyloxalylglycine prevents bone loss in ovariectomized C57BL/6J mice through enhanced angiogenesis and osteogenesis. *PLoS One* 9:e112744. doi: 10.1371/journal.pone.0112744

Pez, F., Dayan, F., Durivault, J., Kaniewski, B., Aimond, G., Le Provost, G. S., et al. (2011). The HIF-1-inducible lysyl oxidase activates HIF-1 via the Akt pathway in a positive regulation loop and synergizes with HIF-1 in promoting tumor cell growth. *Cancer Res.* 71, 1647–1657. doi: 10.1158/0008-5472.CAN-10-1516

Phillips, R. M. (2016). Targeting the hypoxic fraction of tumours using hypoxia-activated prodrugs. *Cancer Chemother. Pharmacol.* 77, 441–457. doi: 10.1007/s00280-015-2920-7

Poole, K. E., and Reeve, J. (2005). Parathyroid hormone – a bone anabolic and catabolic agent. *Curr. Opin. Pharmacol.* 5, 612–617. doi: 10.1016/j.coph.2005.07.004

Quinonez-Flores, C. M., Gonzalez-Chavez, S. A., and Pacheco-Tena, C. (2016). Hypoxia and its implications in rheumatoid arthritis. *J. Biomed. Sci.* 23:62. doi: 10.1186/s12929-016-0281-0

Rauner, M., Franke, K., Murray, M., Singh, R. P., Hiram-Bab, S., Platzbecker, U., et al. (2016). Increased EPO levels are associated with bone loss in mice lacking PHD2 in EPO-producing cells. *J. Bone Miner. Res.* 31, 1877–1887. doi: 10.1002/jbmr.2857

Redlich, K., and Smolen, J. S. (2012). Inflammatory bone loss: pathogenesis and therapeutic intervention. *Nat. Rev. Drug Discov.* 11, 234–250. doi: 10.1038/nrd3669

Reynaud, C., Ferreras, L., Di Mauro, P., Kan, C., Croset, M., Bonnelye, E., et al. (2017). Lysyl oxidase is a strong determinant of tumor cell colonization in bone. *Cancer Res.* 77, 268–278. doi: 10.1158/0008-5472.CAN-15-2621

Rius, J., Guma, M., Schachtrup, C., Akassoglou, K., Zinkernagel, A. S., Nizet, V., et al. (2008). NF-kappaB links innate immunity to the hypoxic response through transcriptional regulation of HIF-1alpha. *Nature* 453, 807–811. doi: 10.1038/nature06905

Roodman, G. D. (2004). Pathogenesis of myeloma bone disease. *Blood Cells Mol. Dis.* 32, 290–292. doi: 10.1016/j.bcmd.2004.01.001

Ryu, J. H., Chae, C. S., Kwak, J. S., Oh, H., Shin, Y., Huh, Y. H., et al. (2014). Hypoxia-inducible factor-2alpha is an essential catabolic regulator of inflammatory rheumatoid arthritis. *PLoS Biol.* 12:e1001881. doi: 10.1371/journal.pbio.1001881

Samarpita, S., Doss, H. M., Ganesan, R., and Rasool, M. (2018). Interleukin 17 under hypoxia mimetic condition augments osteoclast mediated bone erosion and expression of HIF-1alpha and MMP-9. *Cell Immunol.* 332, 39–50. doi: 10.1016/j.cellimm.2018.07.005

Sarkar, S., Cooney, L. A., and Fox, D. A. (2010). The role of T helper type 17 cells in inflammatory arthritis. *Clin. Exp. Immunol.* 159, 225–237. doi: 10.1111/j.1365-2249.2009.04016.x

Semenza, G. L. (2014). Oxygen sensing, hypoxia-inducible factors, and disease pathophysiology. *Annu. Rev. Pathol.* 9, 47–71. doi: 10.1146/annurev-pathol-012513-104720

Shahi, M., Peymani, A., and Sahmani, M. (2017). Regulation of bone metabolism. *Rep. Biochem. Mol. Biol.* 5, 73–82.

Shao, J., Zhang, Y., Yang, T., Qi, J., Zhang, L., and Deng, L. (2015). HIF-1alpha disturbs osteoblasts and osteoclasts coupling in bone remodeling by up-regulating OPG expression. *In Vitro Cell. Dev. Biol. Anim.* 51, 808–814. doi: 10.1007/s11626-015-9895-x

Shi, Y., Riese, D. J. II, and Shen, J. (2020). The role of the CXCL12/CXCR4/CXCR7 chemokine axis in cancer. *Front. Pharmacol.* 11:574667. doi: 10.3389/fphar.2020.574667

Sims, N. A., and Gooi, J. H. (2008). Bone remodeling: multiple cellular interactions required for coupling of bone formation and resorption. *Semin. Cell Dev. Biol.* 19, 444–451. doi: 10.1016/j.semcdb.2008.07.016

Sims, N. A., and Martin, T. J. (2015). Coupling signals between the osteoclast and osteoblast: how are messages transmitted between these temporary visitors to the bone surface? *Front. Endocrinol. (Lausanne)* 6:41. doi: 10.3389/fendo.2015.00041

Spencer, J. A., Ferraro, F., Roussakis, E., Klein, A., Wu, J., Runnels, J. M., et al. (2014). Direct measurement of local oxygen concentration in the bone marrow of live animals. *Nature* 508, 269–273. doi: 10.1038/nature13034

Stegen, S., Stockmans, I., Moermans, K., Thienpont, B., Maxwell, P. H., Carmeliet, P., et al. (2018). Osteocytic oxygen sensing controls bone mass through epigenetic regulation of sclerostin. *Nat Commun.* 9:2557. doi: 10.1038/s41467-018-04679-7

Stegen, S., van Gastel, N., Eelen, G., Ghesquiere, B., D'Anna, F., Thienpont, B., et al. (2016). HIF-1alpha promotes glutamine-mediated redox homeostasis and glycogen-dependent bioenergetics to support postimplantation bone cell survival. *Cell Metab.* 23, 265–279. doi: 10.1016/j.cmet.2016.01.002

Tando, T., Sato, Y., Miyamoto, K., Morita, M., Kobayashi, T., Funayama, A., et al. (2016). Hif1alpha is required for osteoclast activation and bone loss in male osteoporosis. *Biochem. Biophys. Res. Commun.* 470, 391–396. doi: 10.1016/j.bbrc.2016.01.033

Tang, Z. N., Zhang, F., Tang, P., Qi, X. W., and Jiang, J. (2011). Hypoxia induces RANK and RANKL expression by activating HIF-1alpha in breast cancer cells. *Biochem. Biophys. Res. Commun.* 408, 411–416. doi: 10.1016/j.bbrc.2011.04.035

Teitelbaum, S. L. (2000). Bone resorption by osteoclasts. *Science* 289, 1504–1508. doi: 10.1126/science.289.5484.1504

Tian, H., McKnight, S. L., and Russell, D. W. (1997). Endothelial PAS domain protein 1 (EPAS1), a transcription factor selectively expressed in endothelial cells. *Genes Dev.* 11, 72–82. doi: 10.1101/gad.11.1.72

Wang, G. L., Jiang, B. H., Rue, E. A., and Semenza, G. L. (1995). Hypoxia-inducible factor 1 is a basic-helix-loop-helix-PAS heterodimer regulated by cellular O2 tension. *Proc. Natl. Acad. Sci. U.S.A.* 92, 5510–5514. doi: 10.1073/pnas.92.12.5510

Wenger, R. H., Stiehl, D. P., and Camenisch, G. (2005). Integration of oxygen signaling at the consensus HRE. *Sci. STKE* 2005:re12. doi: 10.1126/stke.3062005re12

Westra, J., Molema, G., and Kallenberg, C. G. (2010). Hypoxia-inducible factor-1 as regulator of angiogenesis in rheumatoid arthritis – therapeutic implications. *Curr. Med. Chem.* 17, 254–263. doi: 10.2174/092986710790149783

Woelfle, U., Cloos, J., Sauter, G., Riethdorf, L., Janicke, F., van Diest, P., et al. (2003). Molecular signature associated with bone marrow micrometastasis in human breast cancer. *Cancer Res.* 63, 5679–5684.

Wu, C., Rankin, E. B., Castellini, L., Alcudia, J. F., LaGory, E. L., Andersen, R., et al. (2015). Oxygen-sensing PHDs regulate bone homeostasis through the modulation of osteoprotegerin. *Genes Dev.* 29, 817–831. doi: 10.1101/gad.255000.114

Xu, C., Zhao, H., Chen, H., and Yao, Q. (2015). CXCR4 in breast cancer: oncogenic role and therapeutic targeting. *Drug Des. Devel. Ther.* 9, 4953–4964. doi: 10.2147/DDDT.S84932

Yahara, Y., Barrientos, T., Tang, Y. J., Puviindran, V., Nadesan, P., Zhang, H., et al. (2020). Erythromyeloid progenitors give rise to a population of osteoclasts that contribute to bone homeostasis and repair. *Nat. Cell Biol.* 22, 49–59. doi: 10.1038/s41556-019-0437-8

Yu, X., Jiang, H., Cheng, G., Shang, W., and Zhang, S. (2020). High levels of HIF-1a in hypoxic dental pulps associated with teeth with severe periodontitis. *J. Mol. Histol.* 51, 265–275. doi: 10.1007/s10735-020-09878-5

Zhang, Q., Riddle, R. C., and Clemens, T. L. (2015). Bone and the regulation of global energy balance. *J. Intern. Med.* 277, 681–689. doi: 10.1111/joim.12348

Zhu, J., Tang, Y., Wu, Q., Ji, Y. C., Feng, Z. F., and Kang, F. W. (2019). HIF-1alpha facilitates osteocyte-mediated osteoclastogenesis by activating JAK2/STAT3 pathway in vitro. *J. Cell. Physiol.* 234, 21182–21192. doi: 10.1002/jcp.28721

Zielinska, K. A., and Katanaev, V. L. (2020). The signaling duo CXCL12 and CXCR4: chemokine fuel for breast cancer tumorigenesis. *Cancers (Basel)* 12:3071. doi: 10.3390/cancers12103071

**Conflict of Interest:** The authors declare that the research was conducted in the absence of any commercial or financial relationships that could be construed as a potential conflict of interest.

frontiers in Cell and Developmental Biology

ORIGINAL RESEARCH
published: 26 March 2021
doi: 10.3389/fcell.2021.646803

# Sestrin2 Regulates Osteoclastogenesis via the p62-TRAF6 Interaction

*Sue Young Oh[1†], Namju Kang[1,2†], Jung Yun Kang[1,2,3], Ki Woo Kim[1], Jong-Hoon Choi[4], Yu-Mi Yang[1*†] and Dong Min Shin[1,2*]*

[1] Department of Oral Biology, Yonsei University College of Dentistry, Seoul, South Korea, [2] BK21 FOUR Project, Yonsei University College of Dentistry, Seoul, South Korea, [3] Department of Dental Hygiene, Yonsei University Wonju College of Medicine, Wonju, South Korea, [4] Department of Orofacial Pain & Oral Medicine, Yonsei University College of Dentistry, Seoul, South Korea

The receptor activator of nuclear factor-kappa B ligand (RANKL) mediates osteoclast differentiation and functions by inducing $Ca^{2+}$ oscillations, activating mitogen-activated protein kinases (MAPKs), and activating nuclear factor of activated T-cells type c1 (NFATc1) via the RANK and tumor necrosis factor (TNF) receptor-associated factor 6 (TRAF6) interaction. Reactive oxygen species (ROS) also plays an important role during osteoclastogenesis and Sestrin2, an antioxidant, maintains cellular homeostasis upon stress injury via regulation of ROS, autophagy, and inflammation. However, the role of Sestrin2 in osteoclastogenesis remains unknown. In this study, we investigated the role of Sestrin2 in the RANKL-RANK-TRAF6 signaling pathway during osteoclast differentiation. Deletion of *Sestrin2* (*Sesn2*) increased bone mass and reduced the number of multinucleated osteoclasts on bone surfaces. RANKL-induced osteoclast differentiation and function decreased in *Sesn2* knockout (KO) bone marrow-derived monocytes/macrophages (BMMs) due to inhibition of NFATc1 expression, but osteoblastogenesis was not affected. mRNA expression of RANKL-induced specific osteoclastogenic genes and MAPK protein expression were lower in *Sesn2* KO BMMs than wild-type (WT) BMMs after RANKL treatment. However, the *Sesn2* deletion did not affect ROS generation or intracellular $Ca^{2+}$ oscillations during osteoclastogenesis. In contrast, the interaction between TRAF6 and p62 was reduced during osteoclasts differentiation in *Sesn2* KO BMMs. The reduction in the TRAF6/p62 interaction and TRAP activity in osteoclastogenesis in *Sesn2* KO BMMs was recovered to the WT level upon expression of Flag-*Sesn2* in *Sesn2* KO BMMs. These results suggest that Sestrin2 has a novel role in bone homeostasis and osteoclasts differentiation through regulation of NFATc1 and the TRAF6/p62 interaction.

**Keywords: reactive oxygen species, autophagy inducer, osteoclast differentiation, antioxidant proteins, bone homeostasis**

OPEN ACCESS

***Edited by:***
*Drorit Neumann,*
*Tel Aviv University, Israel*

***Reviewed by:***
*Eleni Douni,*
*Agricultural University of Athens, Greece*
*Yuqi Wang,*
*Saint Louis University, United States*

****Correspondence:***
*Dong Min Shin*
*dmshin@yuhs.ac*
*Yu-Mi Yang*
*ymyang@yuhs.ac*

*† These authors have contributed equally to this work*

***Specialty section:***
*This article was submitted to Cellular Biochemistry, a section of the journal Frontiers in Cell and Developmental Biology*

***Received:*** *28 December 2020*
***Accepted:*** *09 March 2021*
***Published:*** *26 March 2021*

***Citation:***
*Oh SY, Kang N, Kang JY, Kim KW, Choi JH, Yang YM and Shin DM (2021) Sestrin2 Regulates Osteoclastogenesis via the p62-TRAF6 Interaction. Front. Cell Dev. Biol. 9:646803. doi: 10.3389/fcell.2021.646803*

## INTRODUCTION

Bone is a living organ that renews throughout life via bone remodeling. Bone remodeling results from a balanced collaboration between bone formation by osteoblasts and bone resorption by osteoclasts. When the homeostatic equilibrium of this process is broken, bone diseases, such as periodontitis, osteoporosis, osteopetrosis, autoimmune arthritis, and bone tumors, develop

(Takayanagi, 2007; Crockett et al., 2011; Okamoto et al., 2017; Tsukasaki and Takayanagi, 2019). Mature osteoclasts are differentiated multinucleated cells (MNCs) derived from hematopoietic cells of the mononuclear lineage; the two essential factors required for osteoclast formation are macrophage colony-stimulating factor (M-CSF) and receptor activator of nuclear factor-κB ligand (RANKL), which is secreted by osteoblasts (Boyle et al., 2003; Takayanagi, 2007). The interaction between RANKL and RANK receptor activates tumor necrosis factor (TNF) receptor-associated factor 6 (TRAF6). TRAF6 activates downstream signals, including nuclear factor-κB (NF-κB), and mitogen-activated protein kinases (MAPKs), such as extracellular regulated kinase (ERK), c-jun N-terminal kinase (JNK), and p38 (Takayanagi et al., 2002b). In addition, the RANKL-RANK interaction leads to an increase in the intracellular reactive oxygen species (ROS) level and to oscillations in the intracellular $Ca^{2+}$ concentration ($[Ca^{2+}]_i$). Ultimately, RANKL-mediated ROS generation and $[Ca^{2+}]_i$ oscillations induce nuclear translocation of nuclear factor of activated T-cells cytoplasmic 1 (NFATc1), formation of MNCs, and bone resorption (Takayanagi et al., 2002a; Lee et al., 2005; Kim et al., 2010).

$Ca^{2+}$ is an essential second messenger in universal signaling cascade and plays a critical role in cellular life and death decisions, such as cell proliferation, gene expression, contraction, secretion, metabolism, cell survival, and apoptosis (Hempel and Trebak, 2017). The $Ca^{2+}$ signaling pathways associate with other cellular signaling systems, including the ROS pathway. Although ROS can damage cellular components, including protein, lipids, and DNA, at moderate levels, ROS function as crucial signaling molecules in some physiological processes via their oxidizing activity (Gorlach et al., 2015; Hempel and Trebak, 2017). ROS and $Ca^{2+}$ signaling can be regarded as bidirectional actions because ROS can regulate cellular $Ca^{2+}$ signaling and $Ca^{2+}$ signaling is key for ROS production during bone remodeling (Agidigbi and Kim, 2019). Thus, dysfunction in one of these systems might affect the other system leading to harmful effects and various disorders (Lee et al., 2005; Kim et al., 2010, 2012, 2013; Srinivasan et al., 2010; Domazetovic et al., 2017).

Sestrins, a highly conserved protein family, are induced by various environmental stresses, including DNA damage, oxidative stress, and nutritional stress. Sestrins protect and maintain cell and tissues homeostasis upon stress injury by negatively regulating ROS accumulation and the mammalian target of rapamycin (mTOR) protein kinase signaling. There are three Sestrin isoforms in vertebrates: Sestrin1 (Sesn1, PA26), Sestrin2 (Sesn2, Hi95), and Sestrin3 (Sesn3). Sesn1 associates with autophagy-related genes and negatively regulates the mTOR complex 1 (mTORC1) and ROS production in immune cells. Sesn2, an antioxidant, activates AMP-activated protein kinase (AMPK) and inhibits mTORC1 signaling. Sesn3 also suppresses mTORC1 activity and maintains Akt activity by activating the AMPK-TSC1/2 signaling axis (Wang et al., 2019; Kim et al., 2020).

Human Sestrin2 (hSestrin2) consists of three subdomains: Sesn-A, Sesn-B, and Sesn-C. Sesn-A functions as an active alkyl hydroperoxide reductase and is essential for the antioxidant effect. Sesn-B contains a leucine-binding site and interacts with leucine. Sesn-C interacts with the Rag GTPase-activating protein complex to regulate AMPK and mTORC1 signaling (Kim H. et al., 2015; Saxton et al., 2016). Sesn2 also protects cells from oxidative stresses by activating autophagic regulators through the kelch-like ECH-associated protein 1 (Keap1)-nuclear factor erythroid-2-related factor 2 (Nrf2) pathway and through interaction with p62, an adaptor protein for autophagy (Bae et al., 2013; Rhee and Bae, 2015). p62 activates mTORC1-dependent nutrient sensing, NF-κB-mediated inflammatory responses, and the Nrf2-activated antioxidant defense in hepatocarcinoma cells (Taniguchi et al., 2016). Interestingly, several studies have shown that p62 is an atypical protein kinase C (aPKC) interacting protein that mediates the TRAF6-p62-aPKC signaling axis in RANKL-induced osteoclastogenesis (Duran et al., 2004; McManus and Roux, 2012; Li et al., 2014). Expression of NF-κB and MAPKs associate with activation of RANKL-RANK-TRAF6 downstream signaling, which regulates expression of NFATc1 and the functions of MNCs during osteoclastogenesis (Takayanagi et al., 2000; Boyle et al., 2003). Although it has been shown that Sesn2 protects cells from harmful stresses by inhibiting mTORC1 and ROS and by regulating autophagy via the Sesn2 and Keap1-p62 interaction, the regulatory role of Sesn2 during the maintenance of bone homeostasis remains unknown.

In this study, we used *Sesn2* knockout (KO) mice to investigate the role of Sesn2 in the RANK-TRAF6 downstream signaling pathway and during RANKL-induced osteoclasts differentiation and bone metabolism.

# MATERIALS AND METHODS

## Reagents

Sesn2 plasmid (pcDNA3.1 Flag-Sesn2; plasmid #61868) was obtained from Addgene (Cambridge, MA, United States). Lentiviral pLVX-EF1α-IRES-Puro (EIP) vector (#631988) was obtained from Takara Bio United States, Inc. (Mountain View, CA, United States). Anti- Sesn2 antibodies were obtained from ProteinTech (Rosemont, IL, United States). Anti-NFATc1 and anti-TRAF6 antibodies were obtained from Santa Cruz Biotechnology (Santa Cruz, CA, United States). Anti-phosphor (p)-p38, anti-p-ERK, anti-p-JNK, and anti-IκBα antibodies were obtained from Cell Signaling (Beverly, MA, United States). Anti-p62 antibodies were obtained from Abnova (Taipei City, Taiwan). Anti-tubulin antibodies were obtained from Developmental Studies Hybridoma Bank (Iowa city, IA, United States). Fura-2/AM was purchased from Invitrogen (Carlsbad, CA, United States). Pluronic F-127 was obtained from Molecular Probes (Eugene, OR, United States). RANKL was purchased from R&D Systems (Minneapolis, MN, United States). All other chemicals were purchased from Sigma-Aldrich (St. Louis, MO, United States).

## Animals and Cell Culture

*Sesn2* KO mice in the C57BL/6 background were generated as described (Woo et al., 2009) and all animal care and experimental procedures complied with institutional guidelines

and were approved by the Institutional Animal Care and Use Committee (IACUC) in Yonsei University (IACUC approval no. 2020-0031). The femur and tibia were isolated from 4 to 6-week-old male mice as described previously (Son et al., 2019). All cells derived from bone marrow of femur and tibia were collected and cultured in α-minimum essential medium (α-MEM) (Gibco, Grand Island, NY, United States) medium containing 10% fetal bovine serum (FBS) (Gibco) and 30 ng/mL M-CSF. The following day, non-adherent cells in media were collected and seeded on adequate plates containing 30 ng/mL M-CSF (PeproTech, Rocky Hill, NJ, United States). After 3 days, non-adherent cells were washed out with fresh media, and adherent cells were used as bone marrow-derived monocytes/macrophages (BMMs). Primary osteoblast cell cultures were prepared as described previously (Son et al., 2018). In brief, the calvariae of 1∼3-day-old mice were digested with an enzyme solution containing 0.1% collagenase and 0.1% dispase. The isolated osteoblastic cells were cultured for 4 days in α-MEM supplemented with 10% FBS and 1% antibiotic-antimycotic solution in a humidified incubator containing 5% $CO_2$. Cells were plated at a density of $3 \times 10^4$ cells/well in 24-well plates. Osteoblastic differentiation of cells was induced by 50 μg/ml ascorbic acid and 10 mM β-glycerophosphate when cells reached confluence.

## Micro-CT Scanning and Bone Histomorphometry

The distal femoral bone structure was analyzed by Advanced Institutes of Convergence Technology (Genoss Co., Ltd., Suwon, South Korea) after removing soft tissues. Two-dimensional images were analyzed using CTAn software (v.1.16, Bruker, Billerica, MA, United States). The dissected femurs of 13∼15-week-old male mice were fixed in 4% paraformaldehyde overnight at 4°C, decalcified in 15% ethylenediaminetetraacetic acid and embedded in paraffin. Paraffin-embedded sections were cut and stained with tartrate-resistant acid phosphatase (TRAP)/alkaline phosphatase (ALP) stain kit (Wako, Osaka, Japan) according to the manufacturer's protocols. Staining was visualized with an Olympus IX71/F22PH microscope (Tokyo, Japan) and measurements performed with Bio-Quant software (Bioquant Image Analysis Co., Nashville, TN, United States).

## Alkaline Phosphatase (ALP) Activity Assay and Alizarin Red S (ARS) Staining

After osteogenic induction, cells were rinsed two times with phosphate buffered saline, fixed in 4% paraformaldehyde for 10 min, and then rinsed with deionized water three times. ALP and alizarin red S (ARS) were added into cells for the staining during 30 min. Images of each sample were acquired using a CCD camera. To quantify matrix mineralization, cells were washed once with PBS solution and incubated in 100 mM cetylpyridinium chloride for ARS and alkaline phosphatase yellow for ALP. The concentration of ARS was measured using a microplate spectrophotometer at a 562 nm wavelength and ALP activity was measured at the wavelength of 405 nm.

## Tartrate-Resistant Acid Phosphatase (TRAP) Stain Assay

Bone marrow-derived monocytes/macrophages of WT and *Sesn2* KO mice were seeded in 48-well plates at a concentration of $3 \times 10^4$ cells/well and cultured in α-MEM containing 10% FBS with 30 ng/ml M-CSF and 60 ng/ml RANKL. The culture medium was replaced every 2 days. After 6 days, a TRAP stain assay was performed to confirm the cell differentiation rate. $TRAP^+$ cells were stained using a Leukocyte Acid Phosphate Assay Kit (Sigma-Aldrich) by following the manufacturer's procedure and number of $TRAP^+$ cells (containing ≥3 nuclei) were counted.

## Resorption Assay

Bone marrow-derived monocytes/macrophages were seeded on Osteo Assay surface (Corning, Corning, NY, United States) and differentiated into osteoclasts. After 6 days, cells were washed with sodium hypochlorite solution for 1 h at room temperature. Bone slices were imaged, and resorption pits were photographed and analyzed by using Bio-Quant software.

## Real-Time RT-PCR Analysis

Total RNA was isolated by using Trizol reagent (Thermo Fisher Scientific, Waltham, MA, United States) according to the manufacturer's instruction. Total RNA was reverse transcribed to cDNA with the use of MultiScribe™ Reverse Transcriptase (Applied Biosystems, Foster City, CA, United States). Quantitative PCR was performed to measure the relative mRNA levels using the StepOnePlus Real-Time PCR System (Applied Biosystems) with a 20 μl reaction mix containing cDNA, 0.2 μM primers, and 10 μl of SensiFAST™ SYBR® Hi-ROX Kit (BIOLINE, London, United Kingdom). The relative amount of mRNA normalized to 18S was calculated using the delta-delta method. The following primers were used: cathepsin K (CTSK) forward: 5′-GAAGAAGACTCACCAGAAG CAG-3′, reverse: 5′-YCCAGGTTATGGGCAGAGATT-3′; tartrate-resistant acid phosphatase 5 (ACP5, TRAP) forward: 5′-GCAACATCCCCT GGTATGTG-3′, reverse: 5′-GCAAACGGTAGTAAGGGCTG-3′; dendrocyte expressed seven transmembrane protein (DC-STAMP) forward: 5′-GGGGACTTATGTGTTTCCACG-3′, reverse: 5′-ACAAAGCAACAGACTCCCAAAT-3′; d2 isoform of the vacuolar ATPase v0 domain (Atp6v0d2) forward: 5′-CTGGTTCGAGGATGCAAAGC-3′, reverse: 5′-GTTGCCATA GTCCGTGGTCTG-3′; osteoclast-associated receptor (OSCAR) forward: 5′-CCTAGCCTCATACCCCCAG-3′, reverse: 5′-CGTTGATCCCAGGAGTCACAA-3′; αv integrin forward: 5′-CCGTGGACTTCTTCGAGCC-3′, reverse: 5′-CT GTTGAATCAAACTCAATGGGC-3′; β3 integrin forward: 5′-CCACACGAGGCGTGAACTC-3′, reverse: 5′-CTTCAGGTT ACATCGGGGTGA-3′; macrophage colony-stimulating factor 1 receptor (mCsf1r, M-CSFR) forward: 5′-GGACCTACC GTTGTACCGAG-3′, reverse: 5′-CAAGAGTGGGCCGGATC TTT-3′; Sestrin2 (Sesn2) forward: 5′-GCAGATCTATGATCG TAGCGGA-3′, reverse: 5′-GCTCTAGATCAGGTCATGTAGC-3′; NFATc1 forward: 5′-CAAGTCTCACCACAGGGCTCAC TA-3′, reverse: 5′-GCGTGAGAGGTTCATTCTCCAAGT-3′;

18S forward: 5′-ACCGCAGCTAGGAATGGA-3′, reverse: 5′-GCCTCAGTTCCGAAAACCA-3′.

## Measurement of $[Ca^{2+}]_i$

The cells were seeded on cover glass in a 35-mm dishes ($5 \times 10^4$ cells/coverslip) and stimulated with RANKL for the indicated times. The cells were loaded with 5 μM Fura-2/AM and 0.05% Pluronic F-127 for 30 min in physiological salt solution (140 mM NaCl, 5 mM KCl, 1 mM $MgCl_2$, 1 mM $CaCl_2$, 10 mM HEPES, 10 mM glucose, 310 mOsm, pH 7.4) at room temperature. Fura-2/AM fluorescence was measured using excitation wavelengths of 340 and 380 nm, and emitted fluorescence 510 nm (Ratio = $F_{340}/F_{380}$) was collected and monitored at 2 s intervals using a CCD camera (Universal Imaging Co., Downingtown, PA, United States). All data were analyzed using MetaFluor software (Molecular Devices, San Jose, CA, United States).

## Measurement of Intracellular ROS

The cells were seeded in 12-well plate with cover glass at a density of $1.5 \times 10^5$ cells/well. ROS was detected using the fluorescent probe 5-(and-6)-carboxy-2′,7′ dichlorofluorescein diacetate (DCFDA). The cells were exposed to 60 ng/ml RANKL and 10 μM DCFDA for 30 min and examined with a laser-scanning confocal microscope (model LSM 510; Carl Zeiss) with a GFP filter set. The mean relative fluorescence intensity for each field was measured with a Zeiss vision system and averaged.

## Western Blot and Immunoprecipitation

Whole cell lysates were extracted in RIPA buffer (Tech & Innovation, Seoul, South Korea), and centrifuged at 12,000 × *g* for 10 min at 4°C. Supernatant was collected, and protein was measured using Pierce BCA Protein Assay Kit (Thermo Fisher Scientific, Waltham, MA, United States). Extracts were subjected to 8–10% SDS-PAGE and transferred to polyvinylidene difluoride membranes (Immobilon-P, Millipore Corp., Bedford, MA, United States). The membranes were blocked with 5% skimmed milk and probed with primary antibodies in 5% BSA in TBS-T overnight at 4°C. The primary antibodies were used as follows: NFATc1 (1:750), Sesn2 (1:1000), p-JNK (1:1000), p-ERK (1:1000), p-p38 (1:1000), IκBα (1:1000), TRAF6 (1:1000), p62 (1:4000), actin (1:1000), and tubulin (1:5000). Membranes were washed and exposed to horseradish peroxidase-conjugated secondary antibodies for 1 h. The antigen-antibody complexes were detected with an ECL™ Prime Western Blotting Detection Reagent (Amersham Biosciences, Piscataway, NJ, United States). Quantification was performed by densitometry using ImageJ. For immunoprecipitation, 700–1000 μg of protein was incubated with 1 μg anti–rabbit TRAF6 antibody at 4°C overnight with rotation. Protein G-Sepharose was added and incubated with rotation for 2 h at 4°C. Beads were collected by centrifugation at 5000 rpm for 30 s, boiled in 2× SDS sample buffer at 95–100 centigrade for 10 min, loaded on an SDS-PAGE, and analyzed by immunoblotting for TRAF6 and p62.

## DNA Transfection

Approximately $1 \sim 5 \times 10^5$ BMMs were seeded on a 35-mm dish and incubated in antibiotic-free medium. After 24 h, DNA was mixed with 250 μl of Lipofectamine 2000 (Invitrogen) and 250 μl of Opti-MEM, incubated for 20 min at room temperature before adding the cell. The transfected cells were assayed at 24 h after post-transfection.

## Vector Construction and Transfection Using Lentiviral System

A 1.4 kb full-length human Flag-Sesn2 cDNA was subcloned into the pLVX-EIP vector (Takara) according to the manufacturer's instructions. The recombinant reaction was generated pLVX-EIP-Flag-Sesn2, which is engineered to express Flag-Sesn2, and pLVX-EIP was a control. Lentivirus packaging was performed according to the manufacturer's instruction by co-transfection of these vectors and packaging mixtures (Addgene) into 293T cells using Lipofectamine 2000 and incubated for 24 h. The viral supernatant was harvested after 48–72 h, and titers were determined. Cultured BMMs were infected with the pLVX-EIP-Flag-Sesn2 or control virus pLVX-EIP and incubated for 24 h before treatment with 50 ng/ml RANKL for the indicated times to induce osteoclastogenesis.

## Statistical Analysis

Data were presented as mean ± standard error of the mean (S.E.M.) from at least 3 independent experiments. Statistical significance was determined by using a Student's *t*-test or ANOVA test. Statistical significance was set at $p < 0.05$ level.

# RESULTS

## Deficiency of *Sesn2* Increases Bone Mass

Intracellular ROS levels directly affected RANKL-induced osteoclast differentiation and bone density, and Sens2 functions as an antioxidant that suppresses ROS by activating AMPK and inhibiting mTORC1. Therefore, we examined whether the deletion of *Sesn2* alters bone phenotypes *in vivo* by dissecting the femurs from wild-type (WT) and *Sesn2* KO male mice, measuring bone mass by micro-radiographical analysis, and measuring osteoclastogenesis by histomorphological analysis using TRAP staining. The bone mass [bone volume/total volume (BV/TV)] and trabecular number (Tb.N) of *Sesn2* KO femurs were higher than WT femurs (∼35.6 and ∼31.8%, respectively), whereas trabecular separation (Tb.Sp) was ∼21.9% lower in femurs of *Sesn2* KO mice than WT femurs (**Figure 1A**). TRAP-stained bone sections were used to identify osteoclasts within femoral metaphysis and to quantify surface measurements. Osteoclast surface as a percentage of total bone surface (Oc.S/BS) and the number of osteoclasts over total bone surface (N.Oc/BS) in *Sesn2* KO sections were lower than WT sections (∼30.2 and ∼33.5%, respectively; **Figure 1B**). These results indicated that the increase in bone density in *Sens2* KO mice may result from

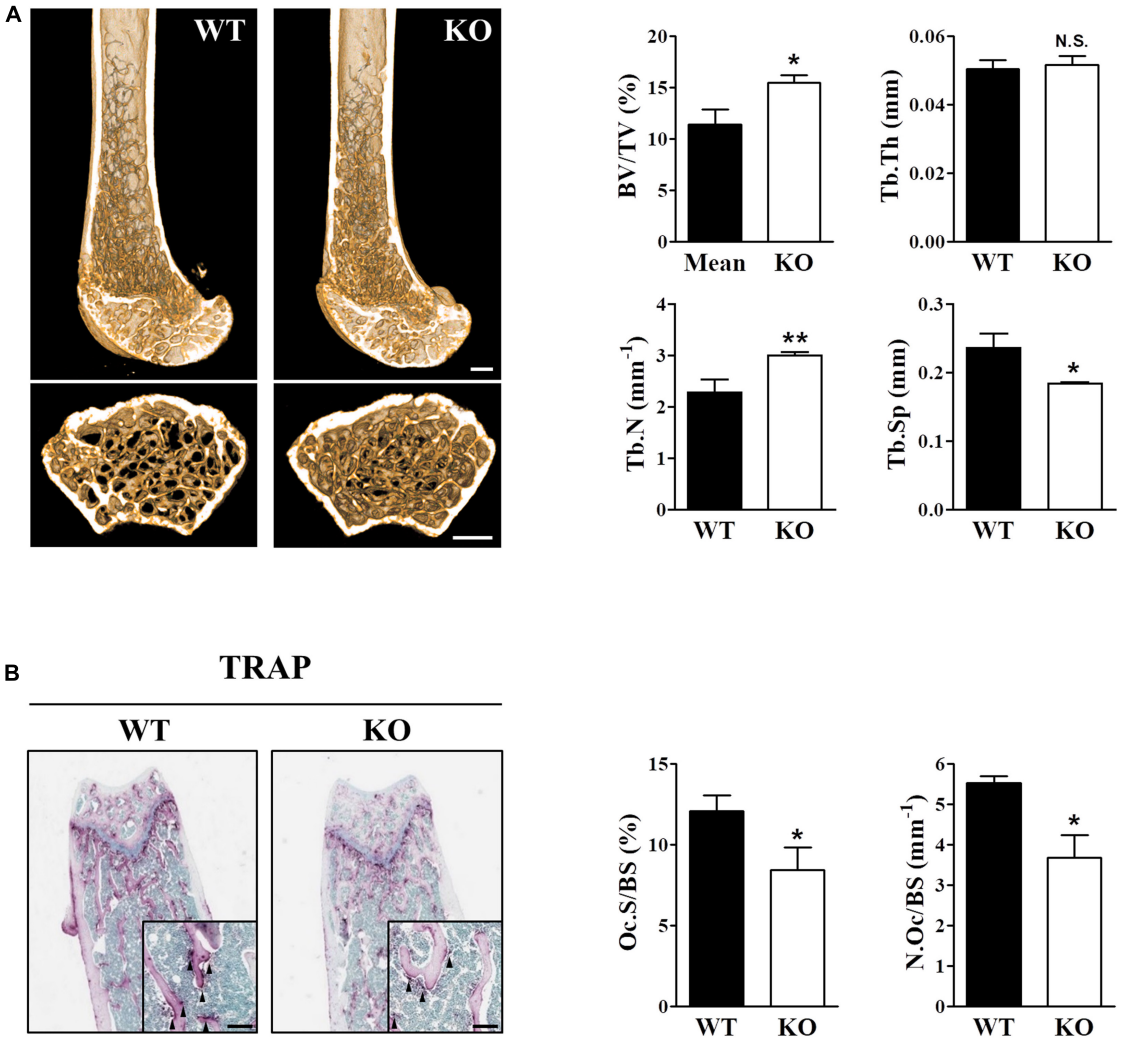


**FIGURE 1 |** The skeletal phenotype is altered in *Sesn2* KO mice. For the *in vivo* experiments, distal femoral bones were isolated from WT and *Sesn2* KO male mice and analyzed histologically and by micro-computed tomography (μCT). **(A)** Micro-radiographic analyses of femur obtained from 13 to 15-week old WT ($n = 6$) and *Sesn2* KO mice ($n = 9$). The bone mass increased in *Sesn2* KO mice. Bone volume over total volume (BV/TV), trabecular thickness (Tb.Th), trabecular number (Tb.N), and trabecular separation (Tb.Sp) were expressed as mean ± S.E.M. $^{*}p < 0.05$ and $^{**}p < 0.01$ compared with WT mice. N.S. = not significant (Scale bar = 500 μm). **(B)** Trabecular surfaces of sectioned femurs from WT ($n = 5$) and *Sesn2* KO mice ($n = 7$) were TRAP-stained. TRAP$^{+}$ osteoclasts along the trabecular surfaces on bone sections are indicated by arrows. There were fewer osteoclasts on the bone surface of *Sesn2* KO mice than WT mice. The percentages of TRAP-labeled osteoclast surface over bone surface (Oc.S/BS) were calculated, and the results are presented as fold-change relative to WT mice (Scale bar = 100 μm). Oc.S/BS and number of osteoclast over bone surface (N.Oc/BS) were measured using Bio-Quant software and expressed as mean ± S.E.M. $^{*}p < 0.05$ compared with WT.

decreases in the ratio and number for TRAP$^{+}$ osteoclasts on the bone surface.

## Sens2 Modulates Osteoclast Differentiation and Function *in vitro*

We examined the effects of Sens2 on osteoblast differentiation in calvarial cells after treatments of ascorbic acid and β-glycerophosphate and on osteoclast differentiation of BMMs after RANKL treatment. ARS and ALP activity data showed that *Sesn2* expression did not affect osteoblastogenesis (**Figure 2A**). We then investigated the roles of Sens2 on osteoclastogenesis in M-SCF-treated and RANKL-treated WT and *Sesn2* KO BMMs. The number of TRAP$^{+}$ osteoclasts, especially TRAP$^{+}$ MNCs with more than 10 nuclei, was ∼46.3% lower in *Sesn2* KO BMMs than in WT BMMs (**Figure 2B**). To evaluate whether defects in osteoclastogenesis result in osteoclasts with impaired function in *Sesn2* KO mice, we performed a pit formation assay in WT and *Sesn2* KO BMMs. The formation of pits and resorbed areas were ∼51.5% lower in *Sesn2* KO BMMs than in WT BMMs (**Figure 2C**). To confirm the inhibitory effect of the *Sesn2* KO on osteoclastogenesis, we examined NFATc1 expression. Upon RANKL treatment, NFATc1 protein expression was induced and sustained in WT

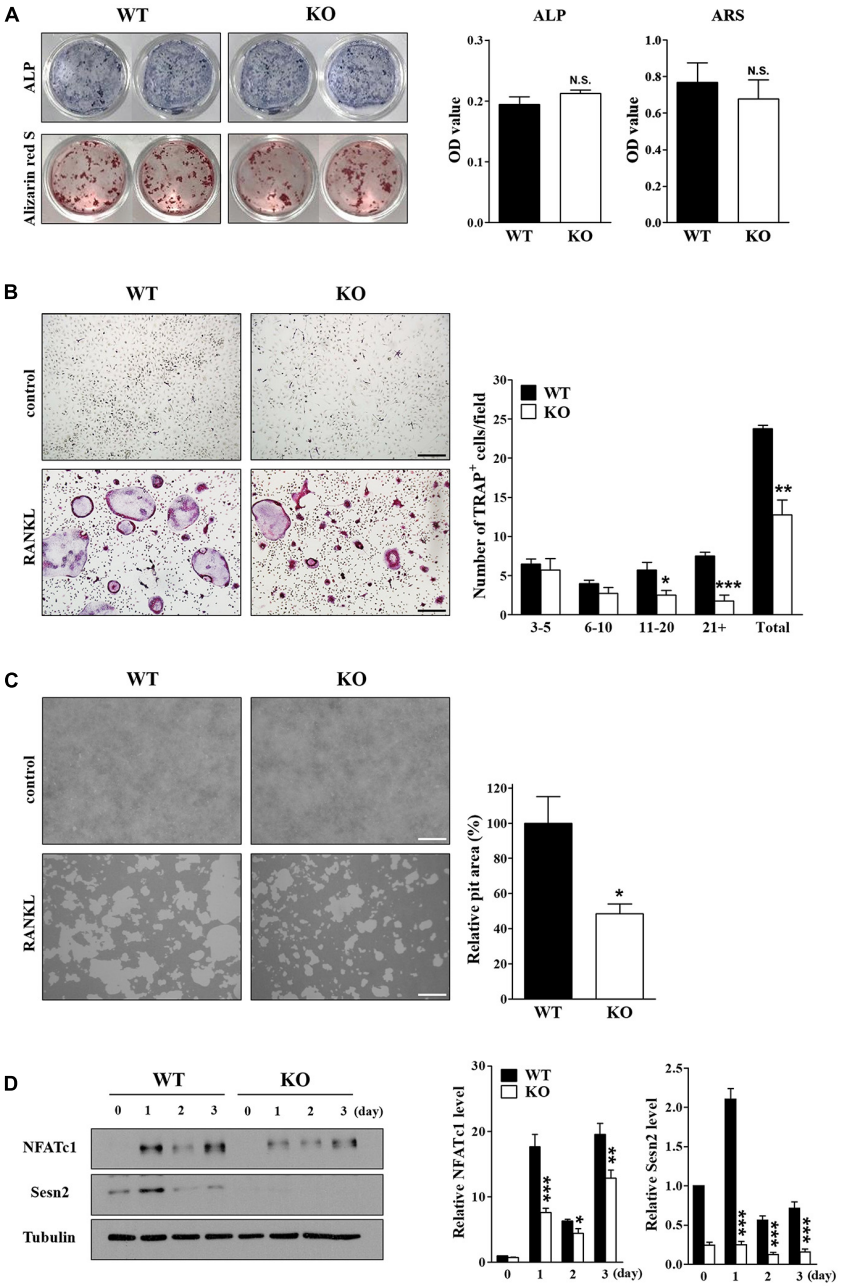


**FIGURE 2 |** Deletion of *Sesn2* inhibits osteoclast differentiation. **(A)** Primary calvarial osteoblasts derived from WT and *Sesn2* KO mice were stained for ALP and ARS after 14 day of cell culture ($n = 4$). The *Sesn2* deletion had no effects on osteoblast differentiation in *Sesn2* KO mice. N.S. = not significant. **(B)** Primary BMMs derived from WT and *Sesn2* KO mice were TRAP-stained after 6 days of cell culture ($n = 4$). After staining, $TRAP^+$ MNCs with more than three nuclei were scored as osteoclasts. Osteoclast differentiation was reduced in *Sesn2* KO mice (Scale bar = 50 μm). Data were expressed as mean ± S.E.M. $^*p < 0.05$, $^{**}p < 0.01$, and $^{***}p < 0.001$ compared with RANKL-treated WT mice. **(C)** BMMs were plated on a pit assay plate and cultured for 6 days ($n = 4$). The attached cells were removed and photographed under a light microscope. Pit areas were quantified using Bio-Quant software (Scale bar = 50 μm). RANKL-induced bone resorption was inhibited in *Sesn2* KO BMMs. The data were normalized to the resorptive area in RANKL-treated BMMs from WT mice. Results were expressed as mean ± S.E.M. $^*p < 0.05$ compared with RANKL-treated WT mice. **(D)** Expression of NFATc1 (90∼110 kDa), Sestrin2 (54 kDa), and tubulin (50 kDa) in WT and *Sesn2* KO BMMs after RANKL stimulation were quantified by immunoblotting and ImageJ analysis ($n = 6$). Expression of NFATc1 was lower in *Sesn2* KO BMM cells than in WT BMM cells. Data were normalized to the expression in cells from WT mice and expressed as mean ± S.E.M. $^*p < 0.05$, $^{**}p < 0.01$, and $^{***}p < 0.001$ compared with WT.

BMMs, whereas NFATc1 protein expression was reduced in *Sesn2* KO BMMs (∼88.0% in day 1 of RANKL treatments). The Sens2 protein level increased in WT BMMs on day 1 after RANKL treatment, but reduced thereafter (**Figure 2D**). These results demonstrated that Sens2 regulates osteoclasts, but not osteoblasts, differentiation and function.

## Deletion of *Sesn2* Correlates Negatively With Genes That Regulate Osteoclast Differentiation

Osteoclast differentiation, maturation, and function are regulated by specific osteoclastogenic genes, including NFATc1, CTSK, TRAP, DC-STAMP, Atp6v0d2, OSCAR, αvβ3 integrin, and mCsf1r (Boyle et al., 2003; Asagiri and Takayanagi, 2007; Okamoto et al., 2017; Tsukasaki and Takayanagi, 2019). We used real-time PCR to investigate the effects of *Sesn2* on expression of these genes during osteoclast differentiation of BMMs after 2 days of RANKL treatments. Except for mCsf1r, mRNA expression of most of the genes was lower in *Sesn2* KO BMMs indicating that Sens2 regulates maturation and function during osteoclast differentiation (**Figure 3A**). Expressions of NF-κB and MAPKs including ERK, JNK, and p38, correlate closely with activation of RANKL-TRAF6 downstream signals during osteoclastogenesis (Boyle et al., 2003). To confirm the effect of *Sesn2* on expressions of MAPKs, we examined protein expression of MAPKs and IκBα upon RANKL stimulation in WT and *Sesn2* KO BMMs. Activations of NF-κB by reduced degradation of IκBα proteins and MAPKs after RANKL treatment was lower in *Sesn2* KO BMMs than in WT BMMs. p-ERK expression increased in WT BMMs during the first 10 min of RANKL treatment, but expression diminished thereafter (**Figure 3B**). These results suggested that Sens2 acts on osteoclast differentiation and function by regulating osteoclastogenic genes in RANKL-TRAF6 downstream pathway.

## Sens2 Regulates Osteoclastogenesis Through Interaction Between TRAF6 and p62

Sens2 suppresses the generation and action of ROS, thus we examined the effects of Sens2 on ROS generation and induction of $[Ca^{2+}]_i$ oscillations upon RANKL stimulations in WT and *Sesn2* KO BMMs. We observed that the lack of *Sesn2* did not affect the amount of ROS produced and the number of $[Ca^{2+}]_i$ oscillation spikes upon RANKL treatment (**Figures 4A,B**). Because Sesn2 activates autophagic degradation and interaction with p62 (Bae et al., 2013), we examined the interaction of TRAF6 with p62 in WT and *Sesn2* KO BMMs to determine if Sesn2 affects the TRAF6-p62 interaction and induction of osteoclastogenesis. Co-immunoprecipitation of p62 and TRAF6 upon RANKL stimulation showed that fewer TRAF6-p62 complexes were present in *Sesn2* KO BMMs than in WT BMMs, thus dissociation of TRAF6-p62 complexes were facilitated in *Sesn2* KO BMMs (**Figure 4C**). We also performed co-immunoprecipitation and TRAP assays after transient expression of *Sesn2* in WT and *Sesn2* KO BMM to determine whether TRAF6-p62 interactions increase upon recovery of Sesn2 expression and whether abnormal osteoclastogenesis is rescued by overexpression of *Sesn2*. Upon Sesn2 expression and RANKL stimulation, binding of TRAF6 to p62 in *Sesn2* KO BMMs increased to levels observed in WT BMMs (**Figure 4D**). In addition, upon *Sens2* overexpression, the abnormal osteoclast differentiation observed in *Sesn2* KO BMMs was returned to normal and levels of $TRAP^+$ MNCs increased to levels found in WT BMMs (**Figure 4E**). These results indicated that Sesn2 regulates RANKL-induced osteoclast differentiation and function by mediating the interaction between TRAF6 and p62.

# DISCUSSION

In this study, we demonstrated a novel role of Sesn2 to regulate interactions between TRAF6 and p62 during osteoclastogenesis. We also provided evidence that Sesn2 modulates the activities of NF-κB, MAPKs, as well as NFATc1 downstream signaling during osteoclasts differentiation. *Sesn2* KO mice had an high bone mass phenotype caused by a reduction in osteoclast differentiation through inhibition of expression of the osteoclastogenic genes NF-κB, MAPKs, and NFATc1, but not dependent on the rate of osteoblast differentiation or changes in intracellular ROS and $Ca^{2+}$ levels (**Figure 5**). These findings suggest that Sesn2 regulates RANKL-induced NFATc1 activation during late stage osteoclast differentiation through the TRAF6/p62 interaction-mediated NF-κB and MAPKs pathways.

It has been shown that increases in $[Ca^{2+}]_i$ and induction of $Ca^{2+}$ oscillations play important roles in RANKL-induced osteoclastogenesis (Takayanagi et al., 2002a). Increases in ROS through the RANKL-RANK-TRAF6 signaling axis activate MAPKs and differentiation to multinucleated osteoclasts, and these ROS-induced effects are inhibit by antioxidants, such as nicotinamide adenine dinucleotide phosphate (NADPH) oxidases 1 (NOX1) and Rac1, an activator of the various NOX family members (Lee et al., 2005). We demonstrated previously that Rac1-mediated ROS levels increased in a deletion mutant of peroxiredoxin II, a thiol-based peroxide reductase, and induced $Ca^{2+}$ oscillations, as well as osteoclast differentiation and function during osteoclastogenesis (Kim et al., 2010). Previous reports on ROS production and RANKL-induced osteoclastogenesis have shown that ROS levels regulate expression and activity of differentiation factors during osteoclastogenesis, thereby determining the number of mature osteoclasts and bone density, but that ROS levels do not affect osteoblastogenesis (Kim et al., 2010, Kim J.H. et al., 2015; Goettsch et al., 2013; Hyeon et al., 2013; Kang and Kim, 2016; Lee et al., 2019; Ng et al., 2019; Han et al., 2020). Lee et al. (2019) has recently reported that reduction in osteoclast differentiation and increased bone density through regulation of ROS signaling result from reduced RANKL secretion by osteoblasts. However, we found that Sesn2 regulated osteoclastogenesis through the NF-κB and MAPK pathways and that Sesn2 did not affect osteoblast differentiation, ROS generation, or induction of $Ca^{2+}$ oscillations. Activations of the antioxidant enzymes NAD-dependent deacetylase sirtuin 3 (Sirt3) and superoxide dismutase 2 (SOD2) inhibited osteoclastogenic genes and NFATc1 expression, formation of mature osteoclasts, and osteoclast functional activity by reducing mitochondrial ROS production (Kim et al., 2017). On the other hand, knock-down of Sesn2 increased lipopolysaccharide-induced ROS production and apoptosis by inhibiting SOD2 and catalase activity in heart

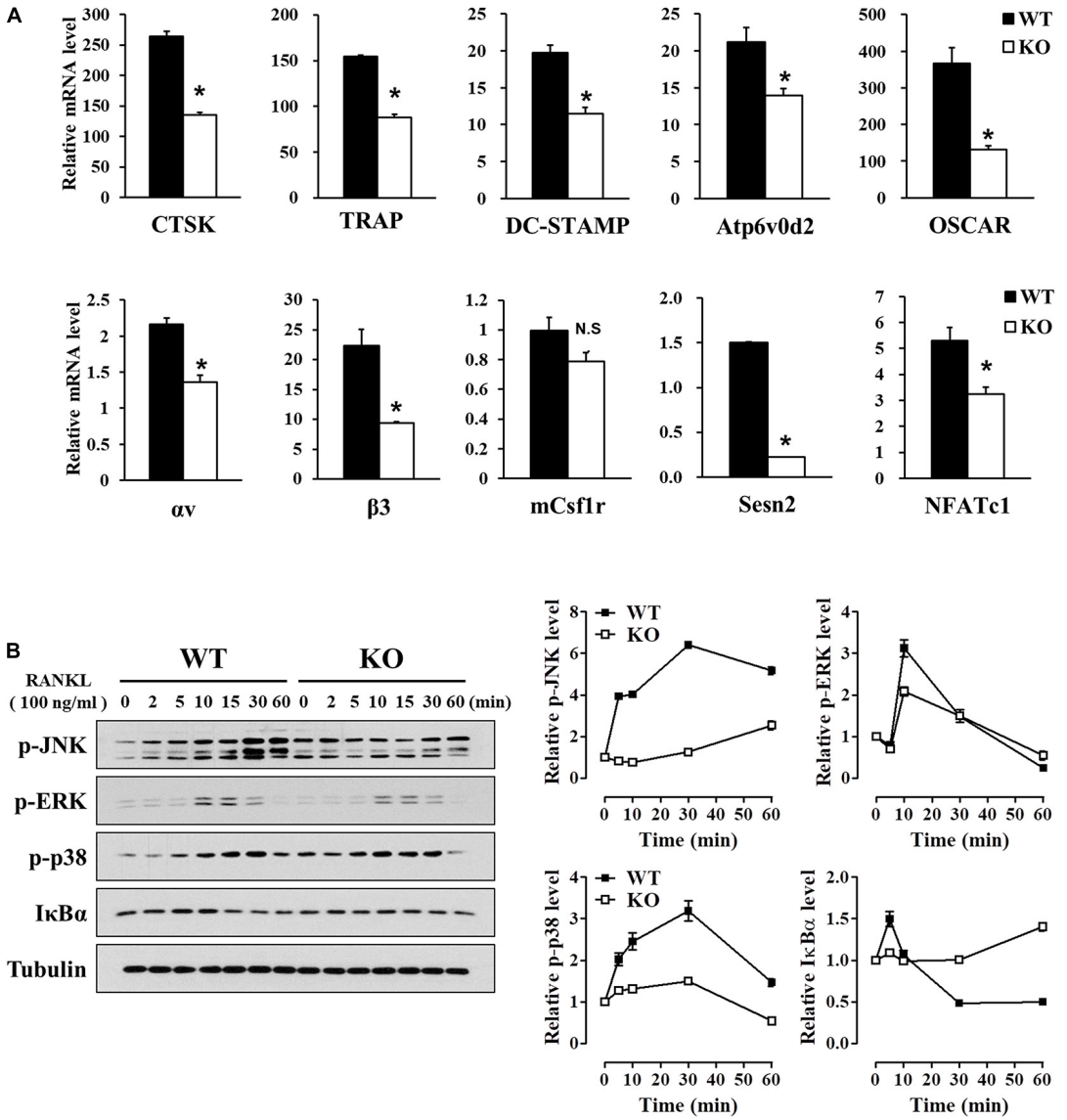


**FIGURE 3 |** Reduced expression of osteoclast differentiation marker genes in *Sesn2* KO mice. **(A)** Expression of mRNAs for the master regulators of osteoclastogenesis were measured on 2 days after RANKL treatment. Osteoclastogenesis-related gene expression diminished in *Sesn2* KO BMMs during osteoclast differentiation ($n = 4$). Data were expressed as mean ± S.E.M. *$p < 0.05$ compared with WT. N.S. = not significant. **(B)** BMM cells were treated with 100 ng/ml RANKL for the period indicated. Protein expression of p-JNK (90∼110 kDa), p-ERK (44, 42 kDa), p-p38 (41 kDa), and IκBα (35 kDa) was quantified by immunoblotting and ImageJ analysis ($n = 3$). The RANKL-induced activation of the TRAF6 downstream pathways was reduced in *Sesn2* KO osteoclasts. Data were normalized to expression in WT cells and expressed as mean ± S.E.M.

(Hwang et al., 2018). Therefore, Sesn2 may exert its antioxidant effects via multiple regulatory pathways.

A previous report showed that the TRAF6/p62 interaction and activation of the NF-kB and/or MAPK pathways play important roles in RANKL-induced osteoclast differentiation (Duran et al., 2004). CYLD, a de-ubiquitinating enzyme, physically interacts with p62, the CYLD/TRAF6 complex negatively regulates TRAF6 ubiquitination and regulates the sustained inhibitory actions of NF-kB and NFATc1 during RANKL-induced osteoclastogenesis (Jin et al., 2008). Bae et al. (2013) demonstrated that Sesn2 interacts with Keap1, p62, and ubiquitin ligase and that the antioxidant activity of Sesn2 is mediated by activation of Nrf2 and p62-dependent autophagic degradation of Keap1 when ROS is increased as a result of an increase in mTORC1 activity and ER stress due to environmental stresses. According to these reports, it has a possibility to regulate the osteoclastogenesis via interactions between p62/Sesn2 and TRAF6/p62. Although we did not confirmed the Sesn2 interaction with TRAF6 or p62 under RANKL-induced osteoclast differentiation, our results combined with previous reports suggest that Sesn2 promotes a strong interaction between TRAF6 and p62 and promotes RANKL-induced osteoclastogenesis via activations of NF-κB and MAPK

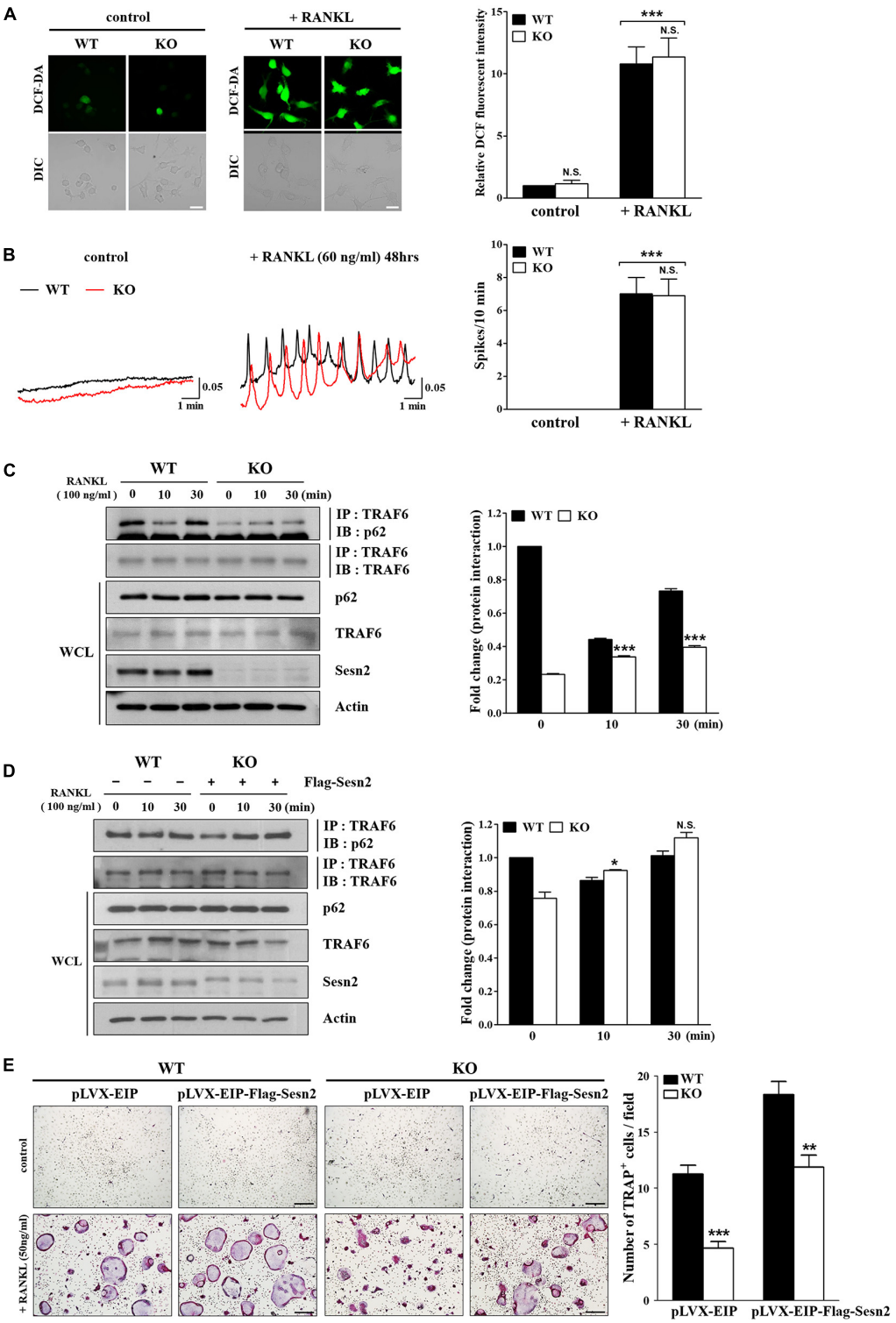


**FIGURE 4 |** The p62 and TRAF6 interaction is inhibited in *Sesn2* KO mice. **(A)** RANKL-induced ROS generation was measured in WT and *Sesn2* KO BMMs ($n = 7$). Deletion of *Sesn2* had no effect on ROS generation in *Sesn2* KO BMMs. The data were normalized to the amount of ROS generated in WT cells and expressed as mean ± S.E.M. $^{***}p < 0.001$ compared with control. N.S. = not significant (Scale bar = 10 μm). **(B)** The number of RANKL-induced $[Ca^{2+}]_i$ oscillations were measured in WT and *Sesn2* KO BMMs ($n = 5$). Deletion of *Sesn2* had no effects on $[Ca^{2+}]_i$ oscillations. The data were expressed as means ± S.E.M. $^{***}p < 0.001$ compared with control. N.S. = not significant. **(C)** BMMs from WT and *Sesn2* KO mice were treated with RANKL for the period indicated, immunoprecipitated with anti-TRAF6 antibody, and the precipitates were immunoblotted for p62 (55 kDa) and TRAF6 (60 kDa; $n = 3$). The *Sesn2* deletion inhibited the interaction between

*(Continued)*

**FIGURE 4 |** Continued
p62 and TRAF6. Data were expressed as mean ± SEM. ***$p < 0.001$ compared with WT. **(D)** BMMs from *Sesn2* KO mice were transfected with Flag-*Sesn2* ($n = 3$). At 24 h post-transfection, cells were harvested and lysed, and cell lysates were subjected to immunoprecipitation with anti-TRAF6 antibody. The inhibition of interaction between p62 and TRAF6 in the *Sesn2* deletion was recovered by transfection of *Sesn2* KO BMMs with Flag-*Sesn2*. Data were expressed as mean ± SEM. *$p < 0.05$ compared with transfected WT. N.S. = not significant. **(E)** BMMs from WT and *Sesn2* KO mice were transfected with pLVX-EIP and pLVX-EIP-Flag-*Sesn2* ($n = 3$). At 24 h post-infection, cells were treated 50 ng/ml RANKL for 6 days, and then TRAP-stained. $TRAP^+$ MNCs with more than ten nuclei were scored as osteoclasts. The reduction in $TRAP^+$ osteoclasts in the *Sesn2* deletion was recovered to WT levels by transfection of pLVX-EIP-Flag-*Sesn2* into *Sesn2* KO BMMs when compared to transfection of pLVX-EIP into WT BMMs. Data were expressed as mean ± SEM (Scale bar = 50 μm). **$p < 0.01$ and ***$p < 0.001$ compared with RANKL-treated WT BMMs.

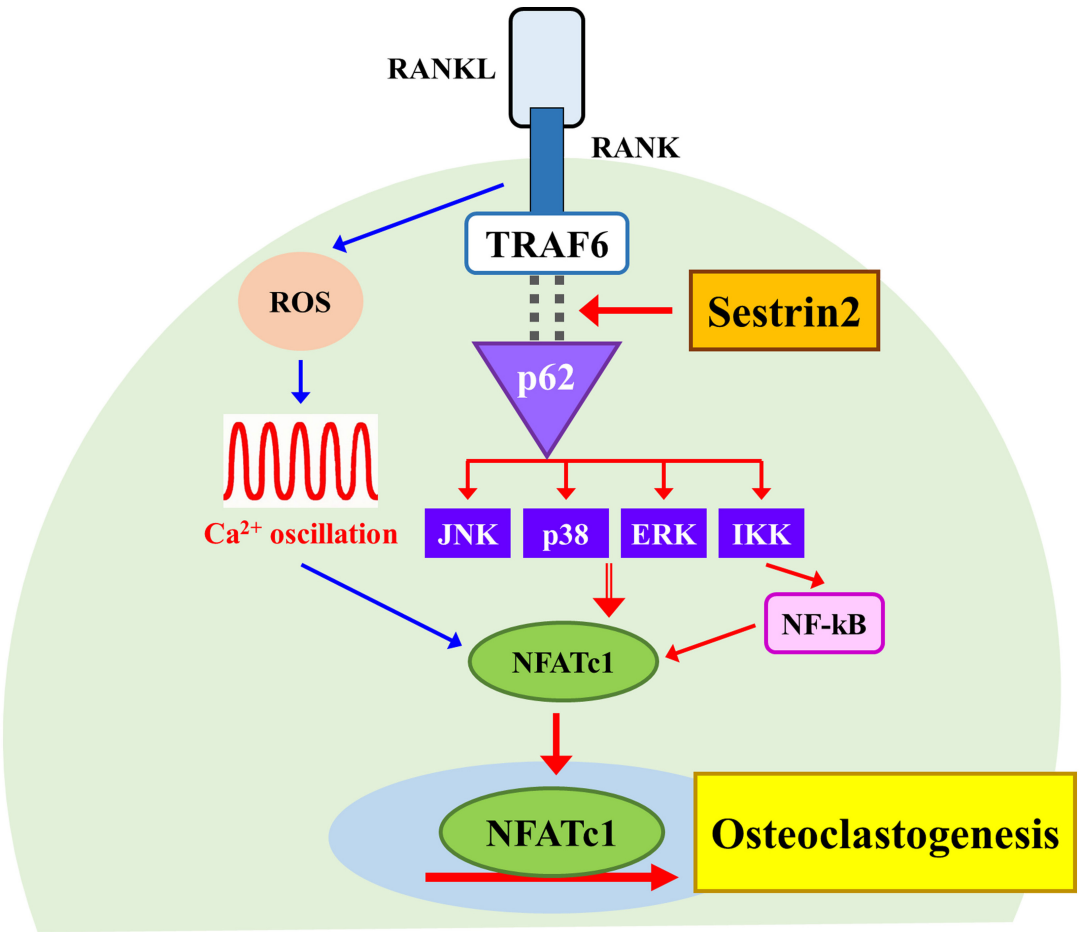


**FIGURE 5 |** A schematic diagram for the regulatory mechanism of osteoclast differentiation by Sestrin2. The model shows the activation of NFATc1 requires Sestrin2-mediated activation for the TRAF6/p62 interaction (red arrows). The sequence of events activated by RANKL also induces the ROS generation and $Ca^{2+}$ oscillations that are required for the activation of NFATc1 regardless of Sesstrin2 (blue arrows).

downstream signaling pathways. In addition, to protect cells against endotoxicity, such as inflammation and aging, Sesn2 is activated by an increase in oxidative stress-induced Nrf2 and AP-1 via activation of toll-like receptors, by inhibition of ubiquitin-mediated Sestrin degradation, and by an increase in Sestrin-MAPK complexes in immune cells (Wang et al., 2019; Kim et al., 2020). Further, it has been shown that p62 is highly expressed in osteoclasts in periapicitis and periodontitis models and that NOX4 is highly expressed in bones obtained from patients with osteoporosis and Paget disease, a focal disorder of enhanced bone remodeling (Goettsch et al., 2013; Li et al., 2014). Recently, it has been reported that Sestrin expression is suppressed in knee joint cartilage obtained from osteoarthritis and aging donors (Shen et al., 2017). Other reports are also showed that Sesn2 expression reduction in skeletal muscles of old mice is increased expression and induced autophagy by physical exercise, and Sesn1 and Sesn2 expression are increased by acute aerobic exercise in skeletal muscle of young mice (Lenhare et al., 2017; Crisol et al., 2018). Therefore, we suggest that Sesn2 protects against stimulation of the immune response and aging.

In summary, our results provide strong evidence for the role of Sesn2 in regulation of RANKL-induced osteoclasts differentiation

and bone metabolism via the NF-κB and MAPK pathways and the TRAF6/p62 interactions. Specifically, our findings suggest that Sesn2 regulates bone remodeling by balancing autophagy and antioxidant signaling. We believe that our findings may be clinically relevance for pathological conditions of the immune and skeletal systems. We demonstrated the essential roles of Sesn2 in the TRAF6/p62 downstream signaling pathway during RANKL-induced osteoclast differentiation. These findings suggest a novel and potent therapeutic target for various bone and skeletal disorders caused by the abnormal formation of osteoclasts.

## DATA AVAILABILITY STATEMENT

The raw data supporting the conclusions of this article will be made available by the authors, without undue reservation.

## ETHICS STATEMENT

The animal study was reviewed and approved by the Institutional Animal Care and Use Committee (IACUC) in Yonsei University (IACUC approval no. 2020-0031).

## AUTHOR CONTRIBUTIONS

SYO and NK contributed to the data acquisition, analysis, and interpretation and drafted the manuscript. YMY contributed to the data acquisition, analysis, and interpretation, and drafted and critically revised the manuscript. JYK contributed to the conception and drafted the manuscript. KWK and JHC contributed to conception and revised the manuscript. DMS contributed to conception, design, and data interpretation and critically revised the manuscript. All authors gave final approval and agreed to be accountable for all aspects of the work.

## FUNDING

This study was supported by the Yonsei University College of Dentistry Fund (6-2020-0012).

## SUPPLEMENTARY MATERIAL

The Supplementary Material for this article can be found online at: https://www.frontiersin.org/articles/10.3389/fcell.2021.646803/full#supplementary-material

## REFERENCES

Agidigbi, T. S., and Kim, C. (2019). Reactive oxygen species in osteoclast differentiation and possible pharmaceutical targets of ROS-mediated osteoclast diseases. *Int. J. Mol. Sci.* 20:3576. doi: 10.3390/ijms20143576

Asagiri, M., and Takayanagi, H. (2007). The molecular understanding of osteoclast differentiation. *Bone* 40, 251–264. doi: 10.1016/j.bone.2006.09.023

Bae, S. H., Sung, S. H., Oh, S. Y., Lim, J. M., Lee, S. K., Park, Y. N., et al. (2013). Sestrins activate Nrf2 by promoting p62-dependent autophagic degradation of Keap1 and prevent oxidative liver damage. *Cell Metab.* 17, 73–84. doi: 10.1016/j.cmet.2012.12.002

Boyle, W. J., Simonet, W. S., and Lacey, D. L. (2003). Osteoclast differentiation and activation. *Nature* 423, 337–342. doi: 10.1038/nature01658

Crisol, B. M., Lenhare, L., Gaspar, R. S., Gaspar, R. C., Munoz, V. R., da Silva, A. S. R., et al. (2018). The role of physical exercise on Sestrin1 and 2 accumulations in the skeletal muscle of mice. *Life Sci.* 194, 98–103. doi: 10.1016/j.lfs.2017.12.023

Crockett, J. C., Rogers, M. J., Coxon, F. P., Hocking, L. J., and Helfrich, M. H. (2011). Bone remodelling at a glance. *J. Cell Sci.* 124(Pt 7), 991–998. doi: 10.1242/jcs.063032

Domazetovic, V., Marcucci, G., Iantomasi, T., Brandi, M. L., and Vincenzini, M. T. (2017). Oxidative stress in bone remodeling: role of antioxidants. *Clin. Cases Miner. Bone Metab.* 14, 209–216. doi: 10.11138/ccmbm/2017.14.1.209

Duran, A., Serrano, M., Leitges, M., Flores, J. M., Picard, S., Brown, J. P., et al. (2004). The atypical PKC-interacting protein p62 is an important mediator of RANK-activated osteoclastogenesis. *Dev. Cell* 6, 303–309.

Goettsch, C., Babelova, A., Trummer, O., Erben, R. G., Rauner, M., Rammelt, S., et al. (2013). NADPH oxidase 4 limits bone mass by promoting osteoclastogenesis. *J. Clin. Invest.* 123, 4731–4738. doi: 10.1172/JCI67603

Gorlach, A., Bertram, K., Hudecova, S., and Krizanova, O. (2015). Calcium and ROS: a mutual interplay. *Redox Biol.* 6, 260–271. doi: 10.1016/j.redox.2015.08.010

Han, B., Geng, H., Liu, L., Wu, Z., and Wang, Y. (2020). GSH attenuates RANKL-induced osteoclast formation in vitro and LPS-induced bone loss in vivo. *Biomed. Pharmacother.* 128:110305. doi: 10.1016/j.biopha.2020.110305

Hempel, N., and Trebak, M. (2017). Crosstalk between calcium and reactive oxygen species signaling in cancer. *Cell Calcium* 63, 70–96. doi: 10.1016/j.ceca.2017.01.007

Hwang, H. J., Kim, J. W., Chung, H. S., Seo, J. A., Kim, S. G., Kim, N. H., et al. (2018). Knockdown of Sestrin2 increases lipopolysaccharide-induced oxidative stress, apoptosis, and fibrotic reactions in H9c2 cells and heart tissues of mice via an AMPK-dependent mechanism. *Mediators Inflamm.* 2018:6209140. doi: 10.1155/2018/6209140

Hyeon, S., Lee, H., Yang, Y., and Jeong, W. (2013). Nrf2 deficiency induces oxidative stress and promotes RANKL-induced osteoclast differentiation. *Free Radic. Biol. Med.* 65, 789–799. doi: 10.1016/j.freeradbiomed.2013.08.005

Jin, W., Chang, M., Paul, E. M., Babu, G., Lee, A. J., Reiley, W., et al. (2008). Deubiquitinating enzyme CYLD negatively regulates RANK signaling and osteoclastogenesis in mice. *J. Clin. Invest.* 118, 1858–1866. doi: 10.1172/JCI34257

Kang, I. S., and Kim, C. (2016). NADPH oxidase gp91(phox) contributes to RANKL-induced osteoclast differentiation by upregulating NFATc1. *Sci. Rep.* 6:38014. doi: 10.1038/srep38014

Kim, H., An, S., Ro, S. H., Teixeira, F., Park, G. J., Kim, C., et al. (2015). Janus-faced Sestrin2 controls ROS and mTOR signalling through two separate functional domains. *Nat. Commun.* 6:10025. doi: 10.1038/ncomms10025

Kim, H., Kim, T., Jeong, B. C., Cho, I. T., Han, D., Takegahara, N., et al. (2013). Tmem64 modulates calcium signaling during RANKL-mediated osteoclast differentiation. *Cell Metab.* 17, 249–260. doi: 10.1016/j.cmet.2013.01.002

Kim, H., Lee, Y. D., Kim, H. J., Lee, Z. H., and Kim, H. H. (2017). SOD2 and Sirt3 control osteoclastogenesis by regulating mitochondrial ROS. *J. Bone Miner. Res.* 32, 397–406. doi: 10.1002/jbmr.2974

Kim, H. J., Prasad, V., Hyung, S. W., Lee, Z. H., Lee, S. W., Bhargava, A., et al. (2012). Plasma membrane calcium ATPase regulates bone mass by fine-tuning osteoclast differentiation and survival. *J. Cell Biol.* 199, 1145–1158. doi: 10.1083/jcb.201204067

Kim, J. H., Kim, K., Kim, I., Seong, S., and Kim, N. (2015). NRROS negatively regulates osteoclast differentiation by inhibiting RANKL-mediated NF-N:B and reactive oxygen species pathways. *Mol. Cells* 38, 904–910. doi: 10.14348/molcells.2015.0177

Kim, M., Kowalsky, A. H., and Lee, J. H. (2020). Sestrins in physiological stress responses. *Annu. Rev. Physiol.* 83, 381–403. doi: 10.1146/annurev-physiol-031620-092317

Kim, M. S., Yang, Y. M., Son, A., Tian, Y. S., Lee, S. I., Kang, S. W., et al. (2010). RANKL-mediated reactive oxygen species pathway that induces long lasting Ca2+ oscillations essential for osteoclastogenesis. *J. Biol. Chem.* 285, 6913–6921. doi: 10.1074/jbc.M109.051557

Lee, N. K., Choi, Y. G., Baik, J. Y., Han, S. Y., Jeong, D. W., Bae, Y. S., et al. (2005). A crucial role for reactive oxygen species in RANKL-induced osteoclast differentiation. *Blood* 106, 852–859. doi: 10.1182/blood-2004-09-3662

Lee, S. H., Lee, S. H., Lee, J. H., Park, J. W., and Kim, J. E. (2019). IDH2 deficiency increases bone mass with reduced osteoclastogenesis by limiting RANKL expression in osteoblasts. *Bone* 129:115056. doi: 10.1016/j.bone.2019.115056

Lenhare, L., Crisol, B. M., Silva, V. R. R., Katashima, C. K., Cordeiro, A. V., Pereira, K. D., et al. (2017). Physical exercise increases Sestrin 2 protein levels and induces autophagy in the skeletal muscle of old mice. *Exp. Gerontol.* 97, 17–21. doi: 10.1016/j.exger.2017.07.009

Li, R. F., Chen, G., Ren, J. G., Zhang, W., Wu, Z. X., Liu, B., et al. (2014). The adaptor protein p62 is involved in RANKL-induced autophagy and osteoclastogenesis. *J. Histochem. Cytochem.* 62, 879–888. doi: 10.1369/0022155414551367

McManus, S., and Roux, S. (2012). The adaptor protein p62/SQSTM1 in osteoclast signaling pathways. *J. Mol. Signal.* 7:1. doi: 10.1186/1750-2187-7-1

Ng, A. Y. H., Li, Z., Jones, M. M., Yang, S., Li, C., Fu, C., et al. (2019). Regulator of G protein signaling 12 enhances osteoclastogenesis by suppressing Nrf2-dependent antioxidant proteins to promote the generation of reactive oxygen species. *Elife* 8:e42951. doi: 10.7554/eLife.42951

Okamoto, K., Nakashima, T., Shinohara, M., Negishi-Koga, T., Komatsu, N., Terashima, A., et al. (2017). Osteoimmunology: the conceptual framework unifying the immune and skeletal systems. *Physiol. Rev.* 97, 1295–1349. doi: 10.1152/physrev.00036.2016

Rhee, S. G., and Bae, S. H. (2015). The antioxidant function of sestrins is mediated by promotion of autophagic degradation of Keap1 and Nrf2 activation and by inhibition of mTORC1. *Free Radic. Biol. Med.* 88(Pt B), 205–211. doi: 10.1016/j.freeradbiomed.2015.06.007

Saxton, R. A., Knockenhauer, K. E., Wolfson, R. L., Chantranupong, L., Pacold, M. E., Wang, T., et al. (2016). Structural basis for leucine sensing by the Sestrin2-mTORC1 pathway. *Science* 351, 53–58. doi: 10.1126/science.aad2087

Shen, T., Alvarez-Garcia, O., Li, Y., Olmer, M., and Lotz, M. K. (2017). Suppression of Sestrins in aging and osteoarthritic cartilage: dysfunction of an important stress defense mechanism. *Osteoarthritis Cartilage* 25, 287–296. doi: 10.1016/j.joca.2016.09.017

Son, A., Kang, N., Kang, J. Y., Kim, K. W., Yang, Y. M., and Shin, D. M. (2018). TRPM3/TRPV4 regulates Ca2+-mediated RANKL/NFATc1 expression in osteoblasts. *J. Mol. Endocrinol.* 61, 207–218. doi: 10.1530/JME-18-0051

Son, A., Kang, N., Oh, S. Y., Kim, K. W., Muallem, S., Yang, Y. M., et al. (2019). Homer2 and Homer3 modulate RANKL-induced NFATc1 signaling in osteoclastogenesis and bone metabolism. *J. Endocrinol.* 242, 241–249. doi: 10.1530/joe-19-0123

Srinivasan, S., Koenigstein, A., Joseph, J., Sun, L., Kalyanaraman, B., Zaidi, M., et al. (2010). Role of mitochondrial reactive oxygen species in osteoclast differentiation. *Ann. N. Y. Acad. Sci.* 1192, 245–252. doi: 10.1111/j.1749-6632.2009.05377.x

Takayanagi, H. (2007). The role of NFAT in osteoclast formation. *Ann. N. Y. Acad. Sci.* 1116, 227–237. doi: 10.1196/annals.1402.071

Takayanagi, H., Kim, S., Koga, T., Nishina, H., Isshiki, M., Yoshida, H., et al. (2002a). Induction and activation of the transcription factor NFATc1 (NFAT2) integrate RANKL signaling in terminal differentiation of osteoclasts. *Dev. Cell* 3, 889–901. doi: 10.1016/s1534-5807(02)00369-6

Takayanagi, H., Kim, S., Matsuo, K., Suzuki, H., Suzuki, T., Sato, K., et al. (2002b). RANKL maintains bone homeostasis through c-Fos-dependent induction of interferon-beta. *Nature* 416, 744–749. doi: 10.1038/416744a

Takayanagi, H., Ogasawara, K., Hida, S., Chiba, T., Murata, S., Sato, K., et al. (2000). T-cell-mediated regulation of osteoclastogenesis by signalling cross-talk between RANKL and IFN-gamma. *Nature* 408, 600–605. doi: 10.1038/35046102

Taniguchi, K., Yamachika, S., He, F., and Karin, M. (2016). p62/SQSTM1-Dr. Jekyll and Mr. Hyde that prevents oxidative stress but promotes liver cancer. *FEBS Lett.* 590, 2375–2397. doi: 10.1002/1873-3468.12301

Tsukasaki, M., and Takayanagi, H. (2019). Osteoimmunology: evolving concepts in bone-immune interactions in health and disease. *Nat. Rev. Immunol.* 19, 626–642. doi: 10.1038/s41577-019-0178-8

Wang, L. X., Zhu, X. M., and Yao, Y. M. (2019). Sestrin2: its potential role and regulatory mechanism in host immune response in diseases. *Front. Immunol.* 10:2797. doi: 10.3389/fimmu.2019.02797

Woo, H. A., Bae, S. H., Park, S., and Rhee, S. G. (2009). Sestrin 2 is not a reductase for cysteine sulfinic acid of peroxiredoxins. *Antioxid. Redox Signal.* 11, 739–745. doi: 10.1089/ars.2008.2360

**Conflict of Interest:** The authors declare that the research was conducted in the absence of any commercial or financial relationships that could be constructed as a potential conflict of interest.

frontiers in Cell and Developmental Biology

HYPOTHESIS AND THEORY
published: 30 March 2021
doi: 10.3389/fcell.2021.644503

# The Mechanism Switching the Osteoclast From Short to Long Duration Bone Resorption

*Jean-Marie Delaisse[1,2,3]*, Kent Søe[1,2,3], Thomas Levin Andersen[1,2,3,4], Aleksandra Maria Rojek[3] and Niels Marcussen[3]*

*[1] Clinical Cell Biology, Department of Pathology, Odense University Hospital, Odense, Denmark, [2] Clinical Cell Biology, Pathology Research Unit, Department of Clinical Research, University of Southern Denmark, Odense, Denmark, [3] Department of Molecular Medicine, University of Southern Denmark, Odense, Denmark, [4] Department of Forensic Medicine, Aarhus University, Aarhus, Denmark*

The current models of osteoclastic bone resorption focus on immobile osteoclasts sitting on the bone surface and drilling a pit into the bone matrix. It recently appeared that many osteoclasts also enlarge their pit by moving across the bone surface while resorbing. Drilling a pit thus represents only the start of a resorption event of much larger amplitude. This prolonged resorption activity significantly contributes to pathological bone destruction, but the mechanism whereby the osteoclast engages in this process does not have an answer within the standard bone resorption models. Herein, we review observations that lead to envision how prolonged resorption is possible through simultaneous resorption and migration. According to the standard pit model, the "sealing zone" which surrounds the ruffled border (i.e., the actual resorption apparatus), "anchors" the ruffled border against the bone surface to be resorbed. Herein, we highlight that continuation of resorption demands that the sealing zone "glides" inside the cavity. Thereby, the sealing zone emerges as the structure responsible for orienting and displacing the ruffled border, e.g., directing resorption against the cavity wall. Importantly, sealing zone displacement stringently requires thorough collagen removal from the cavity wall - which renders strong cathepsin K collagenolysis indispensable for engagement of osteoclasts in cavity-enlargement. Furthermore, the sealing zone is associated with generation of new ruffled border at the leading edge, thereby allowing the ruffled border to move ahead. The sealing zone and ruffled border displacements are coordinated with the migration of the cell body, shown to be under control of lamellipodia at the leading edge and of the release of resorption products at the rear. We propose that bone resorption demands more attention to osteoclastic models integrating resorption and migration activities into just one cell phenotype.

**Keywords: osteoporosis, ruffled border, resorption trenches, cathepsin K, collagen, sealing zone, osteoclast**

OPEN ACCESS

***Edited by:***
*Ari Elson,*
*Weizmann Institute of Science, Israel*

***Reviewed by:***
*Anna Teti,*
*University of L'Aquila, Italy*
*Helen Knowles,*
*University of Oxford, United Kingdom*

****Correspondence:***
*Jean-Marie Delaisse*
*jean-marie.delaisse@rsyd.dk*

***Specialty section:***
*This article was submitted to Cellular Biochemistry, a section of the journal Frontiers in Cell and Developmental Biology*

***Received:*** *21 December 2020*
***Accepted:*** *22 February 2021*
***Published:*** *30 March 2021*

***Citation:***
*Delaisse J-M, Søe K, Andersen TL, Rojek AM and Marcussen N (2021) The Mechanism Switching the Osteoclast From Short to Long Duration Bone Resorption. Front. Cell Dev. Biol. 9:644503. doi: 10.3389/fcell.2021.644503*

## 1. AN OSTEOCLASTIC RESORPTION EVENT OFTEN GOES BEYOND THE FORMATION OF A PIT

Bone resorption is necessary to allow bone modeling and remodeling, and may become deleterious in pathological situations. The cell performing bone resorption is the multinucleated osteoclast. The main components of the resorption machinery have been identified (Väänänen et al., 2000; Coxon and Taylor, 2008; Feng and Teitelbaum, 2013; Ng et al., 2019) and are usually pictured as

in **Figure 1A** (shown here for the main subcellular components – not for the molecular details). (i) The ruffled border is a zone of the plasma membrane facing the bone surface and is specialized in secretion of resorption agents and uptake of resorption products - much like the boring head of a tunneling machine integrating destruction and evacuation of debris. (ii) The sealing zone (SZ) surrounds the ruffled border and delineates the area of bone surface to be resorbed. Together with the ruffled border it delimits the actual "subosteoclastic resorption compartment." The SZ is commonly believed to prevent the diffusion of resorption agents to the surrounding bone surface and to anchor the bone resorption compartment to the bone surface. (iii) An intricate network of vesicles trafficking through the cell deliver resorption agents to the resorption compartment and transport resorption products from the ruffled border to the basolateral domain. (iv) A complex cytoskeletal organization is involved in this intracellular trafficking and connected to the SZ. Of note, in this setup the SZ is positioned on the native bone surface as a planar ring surrounding the ruffled border (**Figure 1A**). In this way, the ruffled border invades the bone matrix perpendicularly to the bone surface and generates a pit (**Figure 1A**). According to this model, the resorption event remains stationary on the bone surface for its whole duration (typically 2-24 h in bone resorption assays) (Søe and Delaissé, 2017). This model became the standard reference of most studies. We refer to it as the pit resorption mode (Søe and Delaissé, 2010, 2017; Søe et al., 2013; Merrild et al., 2015).

It follows from this standard view that extension of the resorption activity to the bone surface and enlargement of the initial pit were proposed to occur by repeated pit formations, separated by migration/stretching episodes (Lakkakorpi and Vaananen, 1991; Saltel et al., 2004; Novack and Faccio, 2011; Vives et al., 2011; Rumpler et al., 2013; Georgess et al., 2014; **Figure 2A**). Thus the elongated excavations on bone surfaces, called herein trenches (**Figure 3**), were ascribed to a series of confluent pits (**Figure 2A**). Clusters or trails of pits generated by osteoclasts cultured on bone slices were considered to support the existence of alternations between pit formation and migration episodes (**Figure 3**). Recent time lapse observations of these osteoclasts directly confirmed this hypothesis (Søe and Delaissé, 2017). However, time lapse revealed as well that many osteoclasts do not stop resorbing after the generation of a pit, but instead enlarge it laterally thereby making a trench (Søe and Delaissé, 2017). These time lapse observations also stressed that when the osteoclasts do so, they do not disassemble the extracellular resorption compartment as commonly believed (Lakkakorpi and Vaananen, 1991; Saltel et al., 2004; Georgess et al., 2014), but instead displace it continuously parallel to the bone surface (Søe and Delaissé, 2017). Thus one should be aware that pit formation is for many osteoclasts only the start of a resorption event of much larger amplitude [typically days in bone resorption assays (Søe and Delaissé, 2017)] (**Figure 2B**). We call this process the trench resorption mode (Søe and Delaissé, 2010, 2017; Søe et al., 2013; Merrild et al., 2015; Borggaard et al., 2020).

This newly discovered trench resorption mode deserves much attention. First, trenches represent typically more than 50% of the resorption events achieved on bone slices by osteoclasts generated from blood donors (Søe and Delaissé, 2017). Thus more than 50% of the osteoclasts are enlarging their original pit in this bone resorption assay. Second, the trench resorption mode shows higher resorption performances in terms of duration, speed, and depth, compared with the pit resorption mode, and is thus more aggressive (Merrild et al., 2015; Søe and Delaissé, 2017; **Table 1**). Of note, less than 15% of the osteoclasts that started to make a trench stop resorbing within a 72 h culture period (Søe and Delaissé, 2017; Borggaard et al., 2020). Third, the trench mode appears to have clinical relevance (**Table 1**). Glucocorticoids were found to increase the prevalence of trenches generated in the *in vitro* resorption assays (Søe and Delaissé, 2010), and significantly more trenches were produced by osteoclasts generated from aged blood donors (Møller et al., 2020c). More trenches were also produced by osteoclasts generated from males compared to females (Merrild et al., 2015). In contrast, pharmacological agents like bisphosphonates decrease the prevalence of trenches (Møller et al., 2020a) and cathepsin K inhibitors completely abrogate them (Søe et al., 2013; Merrild et al., 2015; Panwar et al., 2016, 2017; Borggaard et al., 2020). Furthermore, pit and trenches appear to differently affect bone strength (Vanderoost et al., 2013). Scanning electron microscopy pictures of bone surfaces of osteoporotic patients, which are regularly used to highlight extended erosion, actually show a high prevalence of trenches (**Figure 3B**). Thus trenches are also generated *in vivo* and their prevalence in osteoporosis seems to have been mostly overlooked. Overall, it thus seems that the trench mode, i.e., cavity enlargement, is an important contributor to pathological bone resorption.

It is obviously important to know the mechanism driving resorption beyond the formation of a pit. Knowledge of this mechanism is expected to answer a number of intriguing questions of relevance for the clinic. What determines the duration of a resorption event and the size of the excavation? What controls the orientation of the resorption axis in other directions than perpendicular to the bone surface as in the pit mode? How is simultaneous resorption and displacement of the SZ possible, since they are classically considered mutually exclusive (Lakkakorpi and Vaananen, 1991; Takahashi et al., 2007; Novack and Faccio, 2011; Georgess et al., 2014)? Why is resorption in the trench mode more powerful? We review herein both published and unpublished observations that may help understanding the mechanistic peculiarities of the trench mode vs. the pit mode and thereby help comprehending the resorption power beyond what is classically investigated. They let us proposing a previously underestimated regulatory role of the collagenolysis rate vs. demineralization rate, as it determines whether the SZ can move into the excavation - thereby re-orienting the ruffled border and the resorption axis for cavity enlargement. This leads to envision a bone resorption model that takes into account the full resorption program. Overall, the present analysis invites to improve our view of the bone resorbing osteoclast by taking into account combined resorption and migration.

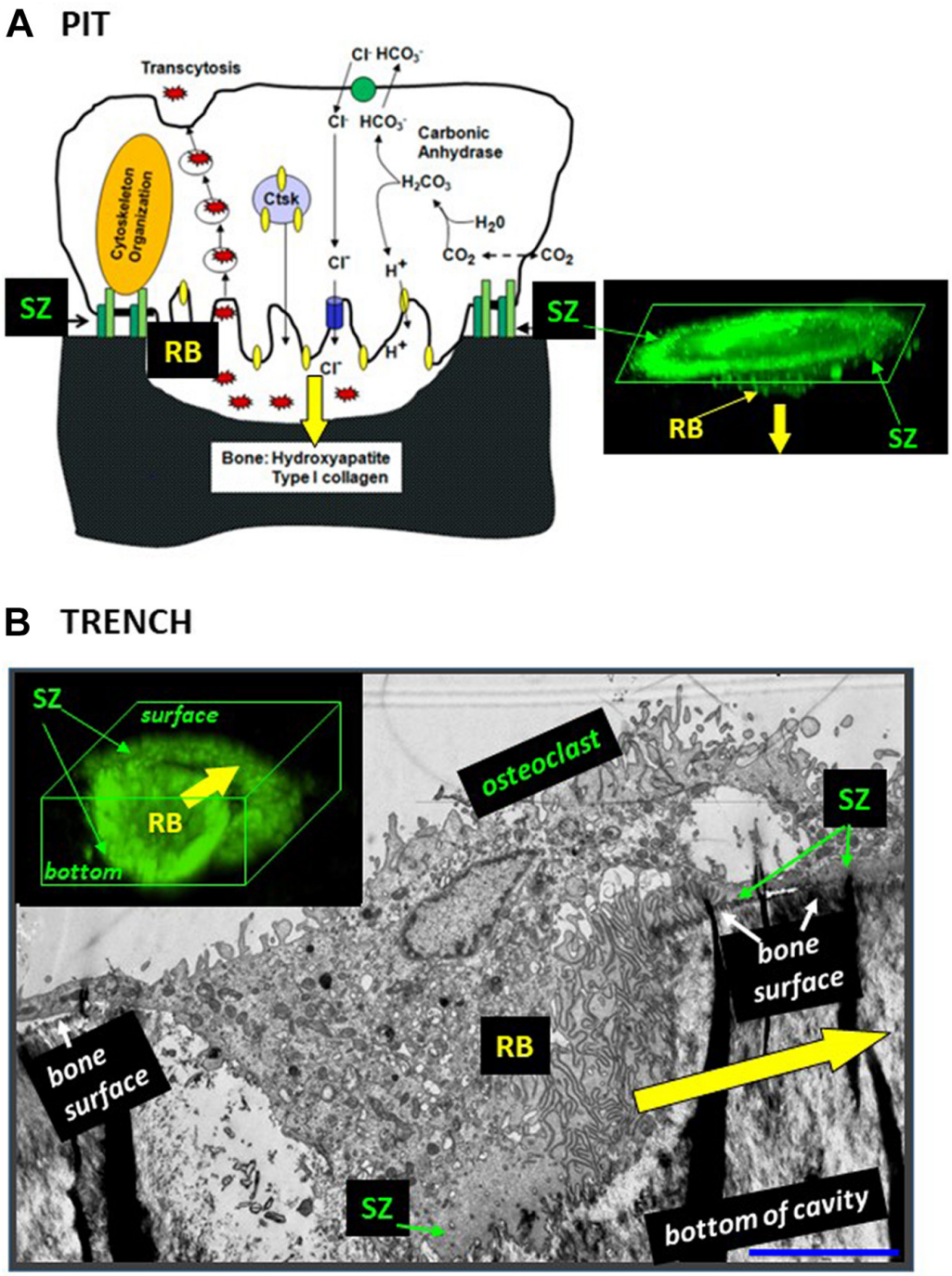


**FIGURE 1 |** The configuration of the ruffled border and the SZ is different in osteoclasts making pits **(A)** and trenches **(B)**. **(A)** Pit mode. Classical model of the bone resorption mechanism [reproduced from Feng and Teitelbaum (2013) with permission] and confocal microscopy image showing the corresponding 3D configuration of the SZ and the ruffled border (RB) [reproduced from Søe and Delaissé (2017) with permission; SZ and ruffled border were visualized by staining actin with phalloidin]. Note the planar SZ on the bone surface. It surrounds the ruffled border and consequently the ruffled border is directed against the bone surface, so that resorption occurs perpendicularly to the bone surface (yellow arrow). **(B)** Trench mode. Osteoclasts were generated from blood donors and cultured on bone slices. An osteoclast was sectioned parallel to its resorption/migration axis (identified beforehand through light microscopy), processed for electron microscopy (Kristensen et al., 2013), and a picture was taken (unpublished). The corresponding 3D configuration of the SZ and the ruffled border (RB) is shown on a confocal picture [reproduced from Søe and Delaissé (2017) with permission; stainings as in panel **(A)**]. Note that the front side of the SZ is on the bone surface and the rear side of the SZ in the cavity. Consequently, the ruffled border is rotated compared with the pit mode and resorbs parallel to the bone surface (yellow arrow). Scale bar in panel **(B)**: 5 μm.

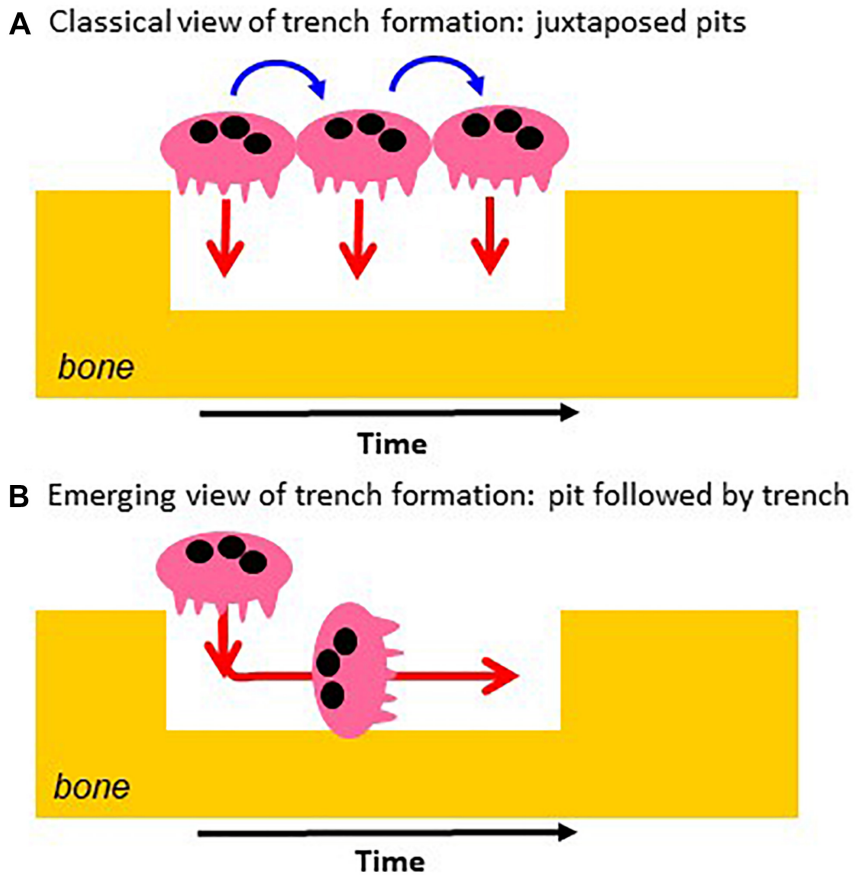


**FIGURE 2 |** Classical vs. novel view of the mechanism of trench formation. **(A)** The classical view of trench formation is based on the traditional pit model and ascribed to successive pit formations (red arrows). They are separated by cell migration/stretching episodes (blue arrows). **(B)** The novel view is directly based on the course of events revealed by time lapse: the osteoclast starts making a pit and then enlarges it laterally. The change of orientation of the resorption axis results from the re-orientation of the ruffled border (see **Figure 1**).

## 2. A KEY EVENT FOR ENLARGEMENT OF RESORPTION CAVITIES: THE SZ "STEPPING" IN THE CAVITY AND REORIENTING THE RUFFLED BORDER

Osteoclasts initiating bone resorption show SZs positioned on the native bone surface as a planar ring surrounding the ruffled border (**Figure 1A**). As mentioned above, in this way, the ruffled border invades the bone matrix perpendicularly to the bone surface and generates a pit. This invasion is unlikely to be able to proceed beyond a certain depth by simple extension of the ruffled border. Interestingly in this regard, osteoclasts forming a trench have only the leading edge of the SZ positioned on the native bone surface, whereas the rear part of the SZ is lining the freshly resorbed walls of the cavity (making the SZ appearing as a crescent when viewed from above: see e.g., Mulari et al., 2003; Rumpler et al., 2013; Merrild et al., 2015; **Figure 1B**). Important to note, this means that the transition from the pit to the trench mode goes along with the displacement of the rear part of the SZ into the excavation. This displacement re-orients the penetration angle of the ruffled border into the bone matrix: it becomes directed against one of the walls of the excavation so that the cavity enlarges in this direction – which is parallel to the bone surface (**Figures 1**, **2B**). Further enlargement in a given direction, thus generating a trench, goes along with the continuous displacement of the rear part of the SZ along the walls of the trench, and of the leading edge of the SZ on the bone surface (**Figure 1B**).

## 3. THOROUGH COLLAGEN DEGRADATION IS MANDATORY FOR DISPLACEMENT OF THE SZ IN THE RESORPTION CAVITY

### 3.1. Collagen Prevents SZ Formation Required for Initiation of Bone Resorption

Common experience is that osteoclasts seeded on bone slices (obtained by sawing and therefore exposing mineralized bone

**TABLE 1 |** Overview of differences between the pit and trench resorption mode.

| | Pit mode* *Standard model* | → *Trench mode *Mostly disregarded* | References |
|---|---|---|---|
| Basic characteristics | • Resorbs without moving | • Resorbs while moving | Søe and Delaissé, 2017 |
| | • Drills perpendicularly to the bone surface | • Erodes parallel to the bone surface *(enlarging laterally the initial pit)* | Søe and Delaissé, 2017 |
| | • Short duration (hours) | • Long duration (days) | Søe and Delaissé, 2017 |
| | • Slower (50 $\mu m^2$/h) | • Faster (100 $\mu m^2$/h) | Søe and Delaissé, 2017 |
| | • Shallower (8 $\mu m$) | • Deeper (12 $\mu m$) | Merrild et al., 2015 |
| Mechanistic features | • Collagenolysis rate slower than demineralization rate | • Balanced rate of collagenolysis and demineralization | Søe et al., 2013 and section 3.2 |
| | • Lower active cathepsin K level | • Higher active cathepsin K level | Borggaard et al., 2020 and section 3.3 |
| | • Sealing zone (SZ) on bone surface (*planar – believed to anchor the ruffled border*) | • Sealing zone (SZ) partially in cavity (*(folded – believed to orient and transport the ruffled border)* | Søe and Delaissé, 2017 and section 2 |
| | • No detection of phagocytic features | • Phagocytic features | Borggaard et al., 2020 and section 6 |
| | • No significant relation with number of nuclei per osteoclast | • Increases with number of nuclei per osteoclast | Møller et al., 2020c |
| Clinical significance | | • Increased contribution: | |
| | | with glucocorticoids | Søe and Delaissé, 2010 |
| | | with age | Møller et al., 2020c |
| | | in males | Merrild et al., 2015 |
| | | • Abolished by cathepsin K inhibitors | Søe et al., 2013; Merrild et al., 2015; Panwar et al., 2016, 2017; Borggaard et al., 2020 |
| | | • Decreased by bisphosphonates | Møller et al., 2020a |
| | • Appears to favor coupling with bone formation | | Delaisse et al., 2020 |

*See section 1 for the definition of pit and trench modes. *Note that in a typical in vitro experiment, (performed with osteoclasts generated from CD14-positive monocytes from blood donors) 90% of the trench formation events start as a pit which is thereafter enlarged laterally, whereas half of the resorption events do not go beyond the formation of a pit (Søe and Delaissé, 2017).*

matrix) readily generate a SZ and start resorbing. However, it is also well established that when osteoclasts are exposed to collagen surfaces, they do not show a SZ and do not start resorbing (Saltel et al., 2004; Takahashi et al., 2007). So, osteoclasts are unable to resorb non-mineralized bone in rickets (Nordahl et al., 2000), and osteoclasts cannot resorb native bone surfaces unless the superficial layer of collagenous matrix has been removed (Chambers et al., 1985). Actually, osteoclasts on collagen present a set of distinct phenotypic characteristics (Sato et al., 1998; Saltel et al., 2004; Takahashi et al., 2007). These have been described as a mesenchymal migratory phenotype (Søe and Delaissé, 2010, 2017; Søe et al., 2013), because the response of the osteoclast to collagen vs. bone is reminiscent of epithelial-mesenchymal transitions (Kalluri et al., 2009). One of the characteristics of osteoclasts on collagen is that podosomes are either isolated, or in clusters, or in belts (Saltel et al., 2004; Takahashi et al., 2007). These podosomes are mechanosensing the rigidity of the surface they are in contact with (van den Dries et al., 2019). If the collagen becomes mineralized, the podosomes sense greater rigidity and recognize that the cell is dealing with bone, thereby "authorizing" the activation of the degradation machinery (Saltel et al., 2004). Thus podosomes appear to contribute in making sure that osteoclasts degrade only bone (and only when presenting a "collagen-free" surface) and no other tissue. After having recognized bone, the podosomes can organize themselves into a superstructure called the SZ, allowing for the polarized secretory phenotype of bone resorbing osteoclasts (Saltel et al., 2004; Luxenburg et al., 2007; Georgess et al., 2014). SZ formation is thus a prerequisite for bone resorption. The therefore required collagen removal from native bone surfaces has been ascribed to matrix metalloproteinases (MMPs) of bone lining cells and perhaps osteocytes (Chambers and Fuller, 1985; Nakamura et al., 2004; Abdelgawad et al., 2016; Delaisse et al., 2020).

## 3.2. A High Rate of Collagenolysis vs. Demineralization Is Necessary for Displacement of the SZ in the Resorption Cavity and Continuation of Resorption

The bone matrix consists of collagen embedded in mineral. Bone resorption thus requires demineralization, which is achieved by proton secretion (Baron et al., 1985), and collagen degradation, which is achieved by cathepsin K, a powerful proteinase degrading collagen once it is demineralized (Saftig et al., 1998; Garnero et al., 1999). Hence, one should be aware that presence of collagen can be "generated" in the excavation when the rate of demineralization exceeds the rate of collagen degradation. This

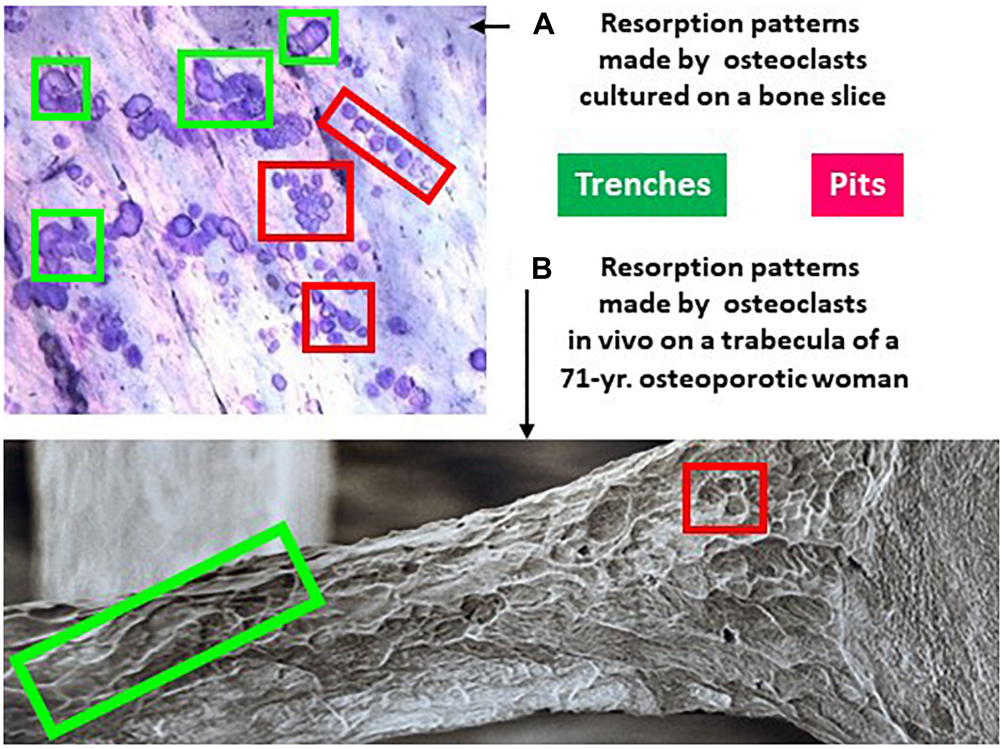


**FIGURE 3 |** Resorption patterns of osteoclasts in culture **(A)** and *in vivo* **(B)** show both pits and trenches. **(A)** Picture of the surface of a bone slice exposed to the resorptive activity of osteoclasts generated from blood donors (unpublished illustration). The slices were stained with toluidine blue as explained in Søe and Delaissé, 2010. **(B)** Trabecula of the third lumbar vertebra of a 71-year old osteoporotic woman, processed for scanning electron microscopy (reproduced from the British Bone Research Society with kind permission of Tim Arnett, University College London). Both **(A,B)** show two types of resorption cavities: trenches representing continuous resorption events parallel to the bone surface (green frames), and pits representing resorption events perpendicular to the bone surface. Pits are often seen in groups - which reflects repeated resorption events separated by migration episodes.

collagen is then very likely to prevent SZ displacement in the excavation and to stop resorption just as mentioned in section 3.1 in relation with the initiation of a resorption event. So, collagen and mineral should not merely be considered as substrates to be resorbed, but also as important regulators of the resorptive activity: mineral activates resorption whereas collagen acts as a brake (**Figure 4**). Furthermore, solubilization of mineral is by nature a fast process, whereas collagen fragmentation and the evacuation of the collagen fragments is by nature more complex and slower (**Figure 4**). It is thus a challenge for the osteoclast to coordinate the speed of demineralization and collagenolysis, which by nature occur at very different rates (**Figure 4**). Collagen will automatically operate as a brake in case of excessive demineralization activity and will thereby protect bone against too high resorption. This brake is not activated when collagen degradation is as fast as demineralization, thereby allowing the SZ to move in the cavity.

Evidence for this view is provided by the analysis of collagen remnants in the excavations – whether through immunoreactivity (Leung et al., 2011; Abdelgawad et al., 2014; **Figures 5A,B**), spectroscopy (Panwar et al., 2016), SEM (Søe and Delaissé, 2010; Panwar et al., 2016), or measurements of thickness of collagen fringes (Søe et al., 2013). Pits show almost always plenty of collagen remnants (**Figure 5A**) - meaning that collagenolysis has been slower than demineralization, thereby leading to accumulation of collagen which then does not allow the SZ to move in the pit and prevents transition to the trench mode. In contrast, trenches do not show presence of collagen (**Figure 5B**), which means that collagenolysis has been as fast as demineralization, and thus the rear part of the SZ could move along the walls of the cavity, which can therefore be continuously enlarged. Very thorough collagen removal along the side walls of trenches is in line with the highly polarized secretion of cathepsin K at the periphery of the ruffled border (Mulari et al., 2003; Lemaire et al., 2014) (see section 5). Besides, prolonged resorption is also seen if osteoclasts are seeded on pure mineral (Saltel et al., 2004; Geblinger et al., 2009; Wijenayaka et al., 2009), or on bone rendered anorganic (Søe et al., 2013) - which is consistent with the absence of the "collagen brake".

The hypothesis that the collagenolysis/demineralization balance determines the ability to switch into the trench mode is further supported by pharmacological evidence (Søe et al., 2013). The presence of a low dose of carbonic anhydrase inhibitor slowing down demineralization vs. collagenolysis in osteoclast cultures on bone slices, leads to absence of collagen accumulation and a 2-fold increase in the proportion of trenches at the expense of pits (Søe et al., 2013). Thus, slowing down the demineralization vs. collagenolysis rate renders collagenolysis fast enough to prevent collagen accumulation, and so more trenches and less pits are generated. Conversely, the presence

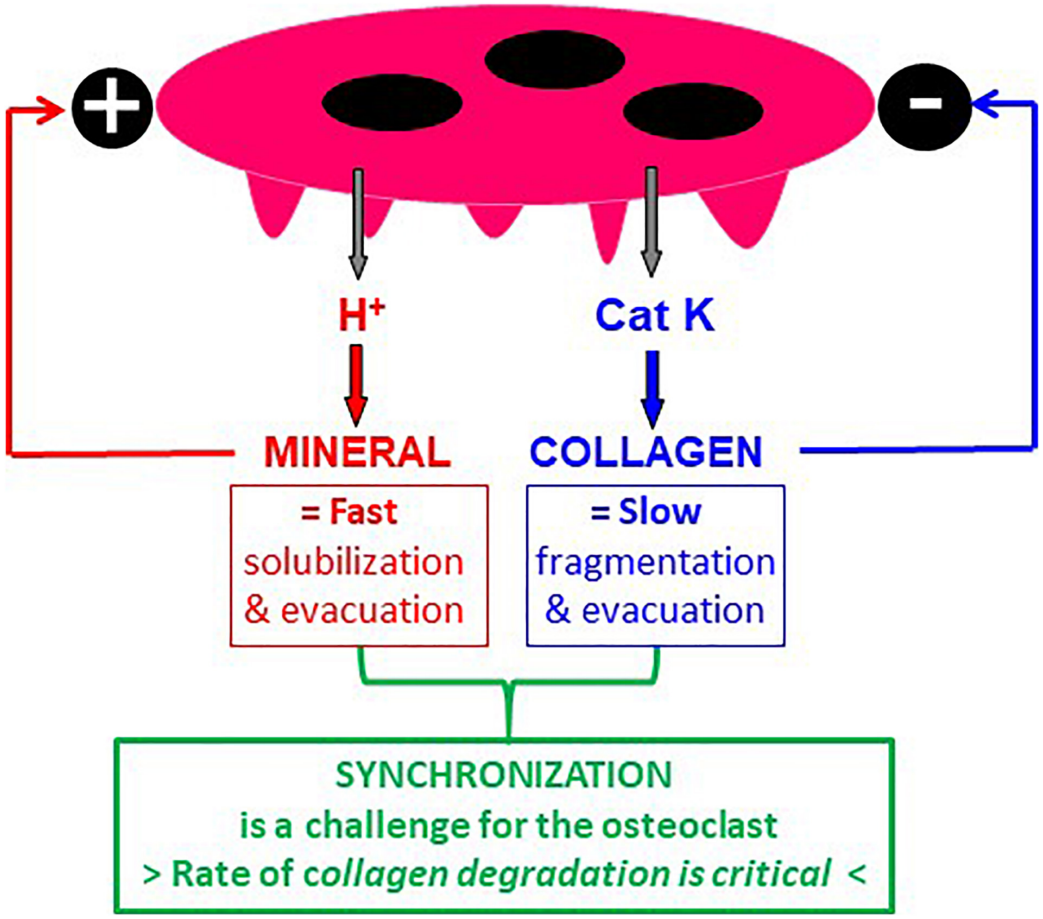


**FIGURE 4 |** Mineral and collagen are not only substrates to be resorbed, but also regulators of osteoclastic bone resorption. It is well established that mineral is solubilized by protons and collagen by cathepsin K. However, it is often neglected (i) that mineral is an activator of resorption and collagen an inhibitor of resorption (see section 3), and (ii) that solubilization of mineral is by nature a faster process compared with collagen degradation and clearance. Hence, the challenge for the osteoclast is to degrade collagen at the same rate as demineralization – otherwise collagen accumulates and stops resorption.

of a cathepsin K inhibitor slowing down collagenolysis, allows fast collagen accumulation, prevents formation of trenches, and concomitantly induces an increase in pit number (Søe et al., 2013; Panwar et al., 2016, 2017; Borggaard et al., 2020). Thus slowing down the collagenolysis vs. demineralization rate prompts a fast accumulation of collagen and thereby an early arrest of resorption, and so the transition to trench formation does not occur. These observations link collagen degradation rates vs. demineralization rates, transition from pit to trench resorption mode, SZ displacement, and prolongation of the resorption event. The association of these events stresses the contribution of collagen degradation for positioning the SZ and the ruffled border it surrounds (**Figure 5C**). Thereby the SZ appears as a navigation wheel operated by collagen degradation, and orienting the direction of resorption. (i) The displacement of the SZ along the freshly resorbed walls of the excavation is conditioned by fast degradation of demineralized collagen by cathepsin K (**Figure 5C**). Therefore, cathepsin K activity levels are expected to be especially critical for regulating the duration of resorption events/enlargement of resorption cavities (section 3.3). (ii) If dealing with native bone surfaces, one should also take into account the displacement of the leading edge of the SZ on the bone surface (Chambers and Fuller, 1985; Everts et al., 2002; Delaisse et al., 2020). Collagen degradation on the bone surface immediately in front of the moving osteoclast, is conditioned by removal of collagen by MMPs of the bone lining cells known to support the osteoclastic resorptive activity (Chambers and Fuller, 1985; Nakamura et al., 2004; Abdelgawad et al., 2016; Delaisse et al., 2020; **Figure 5C**).

## 3.3. Clinical Significance of High Levels of Active Cathepsin K for Enlargement of Resorption Cavities

The need for sufficient cathepsin K to allow transition from pit to trench mode is clearly demonstrated by the concomitant abolishment of trench formation and increase in pit formation in response to cathepsin K inhibitors (Søe et al., 2013; Panwar et al., 2016, 2017; Borggaard et al., 2020), as mentioned in section 3.2. It is interesting to note the relevance of this finding to the variations

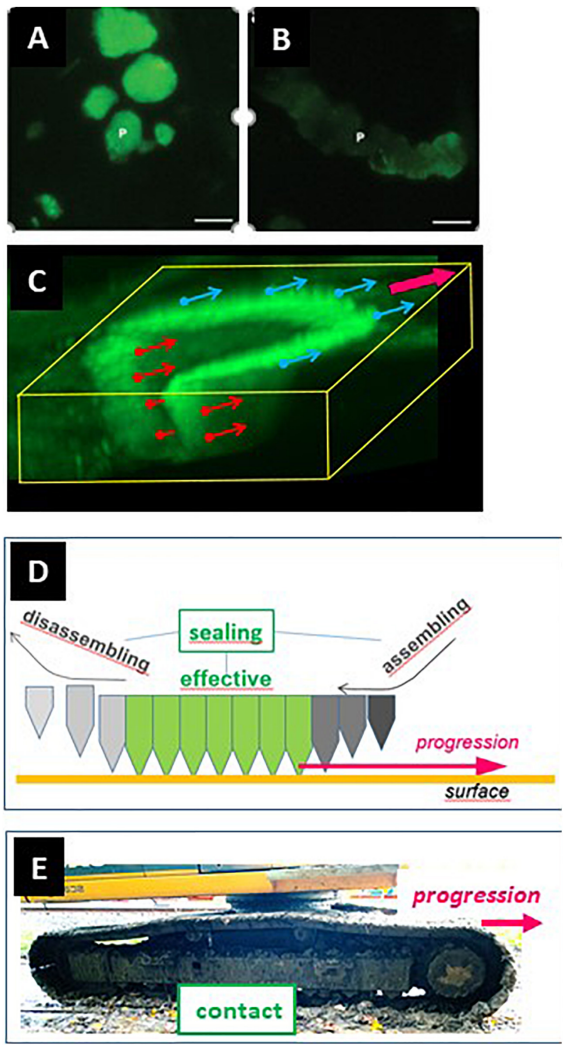


**FIGURE 5 |** Absence of collagen on the cavity walls is a prerequisite for SZ displacement in a resorption cavity and for trench formation. **(A,B)** Bone slices were exposed to resorptive activity of human osteoclasts, stained for collagen immunoreactivity, and visualized through fluorescence microscopy [**panels (A,B)**, reproduced from Leung et al. (2011) with permission]. Pits **(A)** show strong signals (green). In contrast, trenches **(B)** show weak collagen signal (green). **(C)** Confocal picture showing the 3D configuration of the SZ of a trench forming osteoclast (unpublished). The SZ was visualized through staining of actin with phalloidin (Søe and Delaissé, 2017). The osteoclast is moving in the direction of the magenta arrow shown at the upper right corner. The small arrows originating from the SZ indicate the surface that must be devoid of collagen to allow the displacement of the SZ. The blue ones concern the displacement on the bone surface (and may depend on collagen degradation by MMPs of bone lining cells). The red ones concern the displacement along the cavity walls (and depend on collagen degradation by cathepsin K). **(D)** Displacement of the SZ is dependent on assembly of new podosomes at the leading edge and disassembly at the rear of the podosome band. Note that this means that the assembly site is at the outer rim of the SZ domain laying on the bone surface and of the inner rim of the SZ domain lining the cavity walls. Interestingly, these respective assembly sites correspond with the surfaces devoid of collagen shown in **panel (C)**. **(E)** Caterpillar track allowing simultaneous movement and contact. This picture is shown as a comparison with the posodosome band shown in **panel (E)**, to make understood that seal and movement do not exclude each other.

in osteoclast aggressiveness in the human population. Healthy blood donors show a great inter-individual variation in cathepsin K expression levels in their osteoclasts (Merrild et al., 2015), and the levels of active cathepsin K (directly titrated in the osteoclasts from these respective donors) explain 70% of the variations in prevalence of trench formation by the osteoclasts generated from these different donors (Borggaard et al., 2020). Furthermore, the age of the donor proves to be an important determinant of levels of both active cathepsin K and prevalence of trench formation (not of pit formation) (Møller et al., 2020c), thus suggesting that enlargement of resorption cavities is an important contributor of the age effect on bone quality. Menopause status is associated with increased levels of active cathepsin K (Møller et al., 2020c) whereas estrogen represses cathepsin K levels (Mano et al., 1996) and leads to more collagen remnants in the excavations in osteoclast cultures (Parikka et al., 2001). Osteoclasts generated from males were reported both to express higher cathepsin K levels and to generate more trenches (Merrild et al., 2015). Glucocorticoids were reported to increase both cathepsin K levels (Swanson et al., 2006) and trench formation (Søe and Delaissé, 2010). Interestingly, the number of nuclei per osteoclast (supporting protein-synthesis power) is another characteristic that shows variability amongst donors (Møller et al., 2020b) and that positively correlates with cathepsin K levels (Møller et al., 2020a) and prevalence of trenches (Møller et al., 2020c). Overall, one may conclude that the differences in active cathepsin K levels amongst individuals will affect the duration of the resorption events and the size of the resorption cavities. Whether this mechanism also contributes to differences in bone resorption depending on inflammatory conditions (Redlich and Smolen, 2012; Madel et al., 2020) or, the skeletal site (Everts et al., 1999) remains to be investigated. Still, regarding the latter, it is of interest to mention that osteoclasts generated from human bone marrow show a higher propensity to make trenches, compared with those generated from blood (Merrild et al., 2015), and that mouse long bone osteoclasts show higher levels of cathepsin K than calvaria osteoclasts (Everts et al., 1999).

## 4. SIMULTANEOUS RESORPTION AND OSTEOCLAST DISPLACEMENT IN THE TRENCH RESORPTION MODE

According to the classical pit model, the osteoclastic resorptive activity is stationary and cannot occur simultaneously with osteoclast displacement (Lakkakorpi and Vaananen, 1991; Saltel et al., 2004; Georgess et al., 2014). The direct demonstration of the trench resorption mode through time lapse obliges to reconsider this classical view (Søe and Delaissé, 2017). Sections 2 and 3 focused on the displacement of the SZ and the resorption compartment it delineates. They highlighted that a high rate of collagenolysis vs. demineralization is permissive for this displacement. The present section reports additional observations throwing light on SZ displacement. Furthermore, it takes into consideration the displacement of the cell body, which

brings the resorption compartment to critical areas of the bone surface to be resorbed.

## 4.1. SZ Displacement

As mentioned above, the SZ is known to consist of a superstructure of densely interconnected podosomes (Saltel et al., 2004; Luxenburg et al., 2007; van den Dries et al., 2019). Interestingly with respect to SZ displacement, podosomes have a half-life of about 2-12 min (Linder, 2007; Luxenburg et al., 2012). The SZ is thus undergoing constant remodeling. This is very well reflected by the somewhat unsteady appearance of the SZ of pit forming osteoclasts observed in time-lapse (Søe and Delaissé, 2017), and in accordance with the concept of a "dynamic" SZ (Stenbeck and Horton, 2000; Saltel et al., 2004; Geblinger et al., 2010). Therefore, one may envision that in trench mode, the SZ remodeling is organized in such a way that new podosomes are appended at the leading edge of the podosome band and removed at the rear edge of the podosome band (**Figure 5D**). It is remarkable that these podosome appositional areas of the SZ exactly correspond to the areas where full clearance of collagen is critical for SZ displacement: i.e., to the outer rim of the SZ domain positioned on top of the bone surface, and the inner rim of the SZ domain positioned inside the excavation (**Figure 5C**) (see section 3). Of note, movement of "podosome groups" in migrating cells (Linder and Kopp, 2005) as well as of podosome belts in osteoclasts (Tehrani et al., 2006) is also achieved by assembly at the front and disassembly at the rear. Together these observations lead to propose that the coordinated formation and removal of podosomes allows a unidirectional displacement of the SZ, while an effective seal is maintained in the center of the podosome band. This working principle is reminiscent of a caterpillar track simultaneously allowing movement and strong contact (**Figure 5E**). The mechanism coordinating site specific podosome recruitment and migratory cues of the cell body remains to be investigated.

## 4.2. Cell Body Displacement

While SZ displacement responds to "rigidity-sensing" (van den Dries et al., 2019), and therefore to collagen degradation (section 3), the cell body responds to signals ordering where erosion should occur (Niwa et al., 2013; Brylka and Schinke, 2019), and guides the resorption compartment over the bone surfaces to be eroded. Time lapse and confocal microscopy show that osteoclasts forming a trench have similar migratory features as purely migrating osteoclasts (Wheal et al., 2014): (i) lamellipodia ahead of the front part of the SZ, and (ii) a rear edge showing intermittent and abrupt displacements compared with the steady speed of the SZ and the ruffled border, as can be very well appreciated on kymographs (Søe and Delaissé, 2017). This intermittent displacement of the rear results in alternations of stretching and retraction of the cell body (Wheal et al., 2014; Søe and Delaissé, 2017). In purely migrating osteoclasts, stretching was ascribed to attachment of the rear and proposed to relate to accumulation of $\alpha_v\beta_3$ integrins as seen in neutrophils, whereas retraction was shown to result from disassembly of cell adhesion complexes at the rear (Wheal et al., 2014). In this respect, it is of interest that trench-forming osteoclasts show abundant $\alpha_v\beta_3$ integrins at the rear (Mulari et al., 2003), allowing them to attach in the same way.

A recent observation shows particularly well that detachment of the rear is indeed a critical event involved in the displacement of trench-forming osteoclasts: this detachment is prevented by a low dose of chloroquine, a compound that interferes with lysosomal function and trafficking (Borggaard et al., 2020). This low dose does not affect pit formation, nor the transition from pit to trench, nor displacement of the front, nor resorption speed (Borggaard et al., 2020). The immobilization of the rear makes the osteoclast stretching extensively, but at some point, the front of the osteoclast detaches and bounces backward while the rear remains attached (Borggaard et al., 2020). This reflects a progressive imbalance in the strength of cell adhesion between the front and the rear. Furthermore, this imbalance coincides with prevention of exocytosis of resorption products, which then accumulate at the rear (Borggaard et al., 2020) (see section 5). This dual effect of chloroquine thus points to a mechanism that connects exocytosis with coordination of attachment/detachment of the rear and the front of trench forming osteoclasts (Borggaard et al., 2020) (see section 5). In line with this, resorption products were proposed to disrupt cell adhesion complexes upon termination of bone resorption (Wilson et al., 2009). Again, this mechanism remains to be investigated.

# 5. EVACUATION OF THE RESORPTION PRODUCTS

Maintenance of contact of the SZ with fully mineralized collagen, and hence long duration resorption events, does not only demand efficient collagen degradation, but also fast evacuation of the collagen fragments from the resorption compartment (Nesbitt and Horton, 1997; Salo et al., 1997). As mentioned in section 3.2, proper resorption requires thorough fragmentation of demineralized collagen in the resorption compartment, and at the electron microscopy level, it appears to melt between the folds of the ruffled border (Miller, 1977; Stenbeck and Horton, 2000). Accordingly, the evacuation of these fragments is proposed to involve fluid phase and clathrin-mediated endocytosis (Mulari et al., 2003; Stenbeck and Horton, 2004). The internalized vesicles are then crossing the cytoplasm and are exocytosed at the basolateral domain opposite to the ruffled border which is called the functional secretory domain (FSD) (Salo et al., 1996, 1997; Coxon and Taylor, 2008; Hirvonen et al., 2013; Ng et al., 2019). The half-life of the endocytosed material is only 22 min (Stenbeck and Horton, 2004). Striking pictures of release of resorption products at the FSD were reported (Nesbitt and Horton, 1997; Salo et al., 1997; Rogers et al., 2011; Ng et al., 2019), but the mechanism of this exocytosis is poorly known. The coordination of endocytosis at the RB, transcytosis, and exocytosis at the FSD is suspected to be important to cycle integrins and plasma membrane, and considered necessary to meet the demands of the ruffled border for large amounts of plasma membrane (Palokangas et al., 1997; Stenbeck, 2002; Mulari et al., 2008). Overexpression of dynamin - which pinches off the vesicles budding inside the cytoplasm (von Kleist and

Haucke, 2012) - makes osteoclasts generating long trenches instead of round pits in bone slices (Bruzzaniti et al., 2005). This effect points to endocytosis as a critical component of the mechanism allowing trench formation/sustained resorption. We mention here two characteristics of this evacuation that appear different in the trench mode compared to the pit mode. First, the spatial organization of this evacuation system is distinct, as based on the positioning of specific markers, such as clathrin, dynamin and $\alpha_v\beta_3$ for evacuation, compared to Rab7 and v-$H^+$-ATPase for secretion (Mulari et al., 2003). The ruffled border of pit forming osteoclasts appears organized in two concentric zones: internalization of resorption products occurs in the middle part, whereas the resorption agents are secreted at its periphery (Mulari et al., 2003). In trench forming osteoclasts, these two zone appear as imbricated crescents. Internalization occurs at the inner crescent whereas the resorption agents are secreted at the level of the outer one (Mulari et al., 2003) (thereby favoring collagen removal along the cavity walls as mentioned in section 3.2). Furthermore, the FSD is at the opposite side of the ruffled border, which is thus distal to the bone surface in the pit mode, but at proximity to the bone surface in the trench mode (Stenbeck and Horton, 2004), thereby allowing exocytosis at the FSD to interfere with cell attachment (Borggaard et al., 2020). With respect to the latter, a second point of interest was highlighted by time-lapse: trench forming osteoclasts show evidence for traffic of big vacuoles carrying resorption products from the front to the rear, where they disappear (Søe and Delaissé, 2017; Borggaard et al., 2020). As mentioned in section 4, chloroquine induces accumulation of these vacuoles at the rear, indicating impaired exocytosis (likely because digestion of their content is prevented by the presence of chloroquine) (Borggaard et al., 2020). This evacuation route is poorly characterized, but is intriguing because it is not detected in the pit mode, and is blocked simultaneously to the prevention of detachment of the rear/attachment of the leading edge (Borggaard et al., 2020) (see section 4). These observations highlight a link between a seemingly trench-specific membrane cycling route, and displacement of osteoclasts (see section 6). This link deserves attention in future studies.

## 6. EVIDENCE FOR PRE-CAVITATION ACTIVITIES PREPARING RESORPTION

An interesting implication of the trench resorption mode is that the leading edge of the cell body is laying on the bone surface to be eroded. This can be clearly appreciated when sectioning trench-making osteoclasts parallel to their resorption/migration axis, and observing them through confocal and electron microscopy. These images show lamellipodia at the very front, followed by an actin rich cytoplasm [called clear zone (CZ) in electron microscopy terminology and appearing to coincide with the SZ defined in confocal microscopy], and only thereafter the actual cavitation together with the ruffled border (**Figures 1B**, **6A,B**, **7E**, **8**; Møller et al., 2018). Interestingly, nascent folds of ruffled border are visible over this pre-cavitation surface. This means that the "import" of membrane into the ruffled border [as a compensation for ruffled border uptake at the resorption cavity (Palokangas et al., 1997; Stenbeck, 2002; Mulari et al., 2008)], is directed to the leading edge of trench forming osteoclasts. This targeted import supports the displacement of the ruffled border and is part of the mechanism displacing the resorption compartment. Morphologically, this ruffled border formation appears as an increasing number of tiny folds of the plasma membrane with deeper and deeper interdigitations (**Figures 6A,B**). This gradient is immediately adjacent to an area of the CZ crossed by tiny canals (**Figures 6C-E**), some of which open extracellularly (**Figure 6E**). The continuum between these features suggests that the recruitment of these tiny canals and their fusion with the plasma membrane could represent the first step of the ruffled border formation mechanism. Such a link between CZ and ruffled border generation would explain the intriguing inverse variation in CZ size and ruffled border size, in response to variations in small GTPases or PLEKHM1 (Reinholt et al., 1999; Zhao et al., 2001; Alakangas et al., 2002; Van Wesenbeeck et al., 2007). Explorations of these pre-cavitation areas may refine the knowledge on ruffled border formation, which is often merely claimed to be due to massive fusion of lysosomes with the plasma membrane (Ng et al., 2019).

Furthermore, the electron microscopy pictures of these osteoclast sections reveal superficial disruptions of the matrix beneath the CZ (**Figures 6A**, **7A-D**). The attention on an irregular nanotopography beneath the CZ has already been drawn in earlier publications (Holtrop and King, 1977; Zambonin-Zallone et al., 1988; Pierce, 1989; Sasaki et al., 1989), but their significance could not be understood, as the pit model did not allow thinking of them as bone surfaces to be resorbed. It is tempting to reconsider these alterations as part of the trench resorption process where they would represent the initial step of matrix disruption. One may speculate that the above mentioned canals crossing the CZ deliver resorption agents onto these pre-cavitation surfaces (**Figure 6**), and the fact that some of these canals are connected to vacuoles is compatible with this speculation (**Figure 6E**). Superficial disruptions may also result from podosomes (**Figures 7B,C**), which are associated with proteinases (Linder, 2007; Saltel et al., 2008), and exert dislocating mechanical forces by penetrating into the matrix (van den Dries et al., 2019). A link between podosomes, SZ/CZ, and nanotopography has been mentioned (Holtrop and King, 1977; Zambonin-Zallone et al., 1988; Shemesh et al., 2016). It is not unlikely that these superficial disruptions would lead to release of matrix clumps (including mineral), which would then be taken up by phagocytosis due to their size. This is very much in contrast with the mode of uptake of the thoroughly solubilized matrix "melting" between the deep folds of the fully developed ruffled border (see section 5). This hypothesis of phagocytosis in the pre-cavitation area is supported by electron dense vacuoles in the pre-cavitation area of trench forming osteoclasts sectioned along their migration/resorption axis (**Figure 7D**). Intracytoplasmic vacuoles of the same appearance were reported in the earlier literature at the level of the CZ (Pierce, 1989) and of poorly developed ruffled border (Bonucci, 1974). Evidence for uptake of collagen at that level is provided by collagen immunoreactivity in the osteoclast cytoplasm covering the pre-cavitation surface (**Figure 7E**). All these observations taken together suggest that

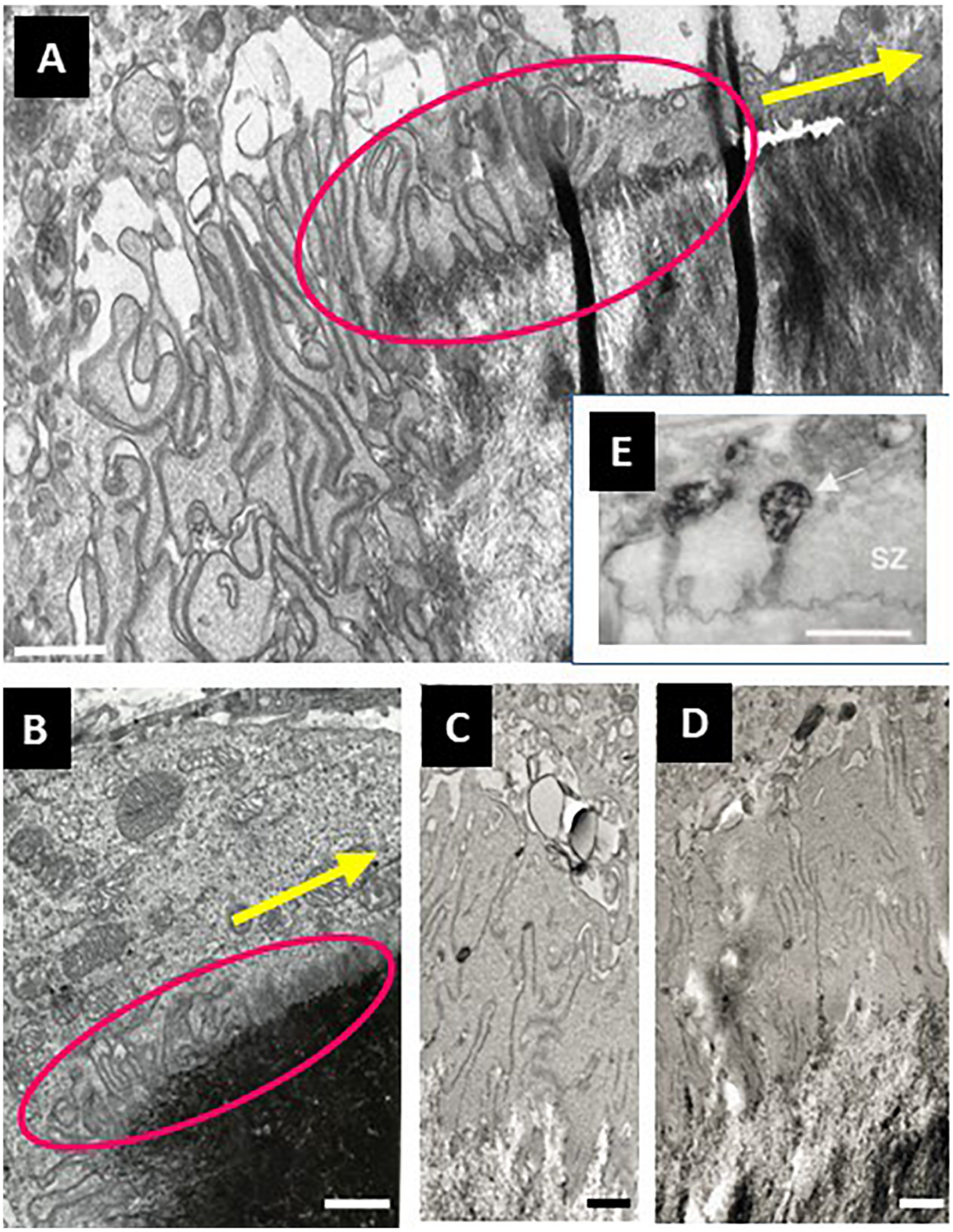


**FIGURE 6 |** Electron microscopy pictures in the area of pre-cavitation surfaces of trench forming osteoclasts: peculiarities of the CZ, nascent ruffled border, and underlying bone surface. **(A–D)** Electron microscopy pictures of osteoclasts sectioned parallel to their resorption/migration axis were obtained in the same way as in **Figure 1B** (unpublished, A is a higher magnification of the pre-cavitation area shown in **Figure 1B**). **(A,B)** Pre-cavitation areas are framed in magenta and the resorption/migration axis is shown by the yellow arrow. Note the gradient of plasma membrane folds over the pre-cavitation surface toward the edge of the cavity, and as well the corresponding gradient of alterations of the surface of the bone matrix. Interestingly, these folds appear in a "clear cytoplasm" typical of the CZ/SZ. **(C–E)** Narrow canals are visible across the CZ suggesting communication between the cytoplasm and the pre-cavitation surface. It is speculated that these canals may represent a preparative step of ruffled border formation. Interestingly, the canals of the CZ of a trench forming osteoclast in E are connected to vacuoles at the cytoplasmic side and show clear openings toward the bone surface [reproduced from Mulari et al. (2003) with permission). Scale bars 1 μm.

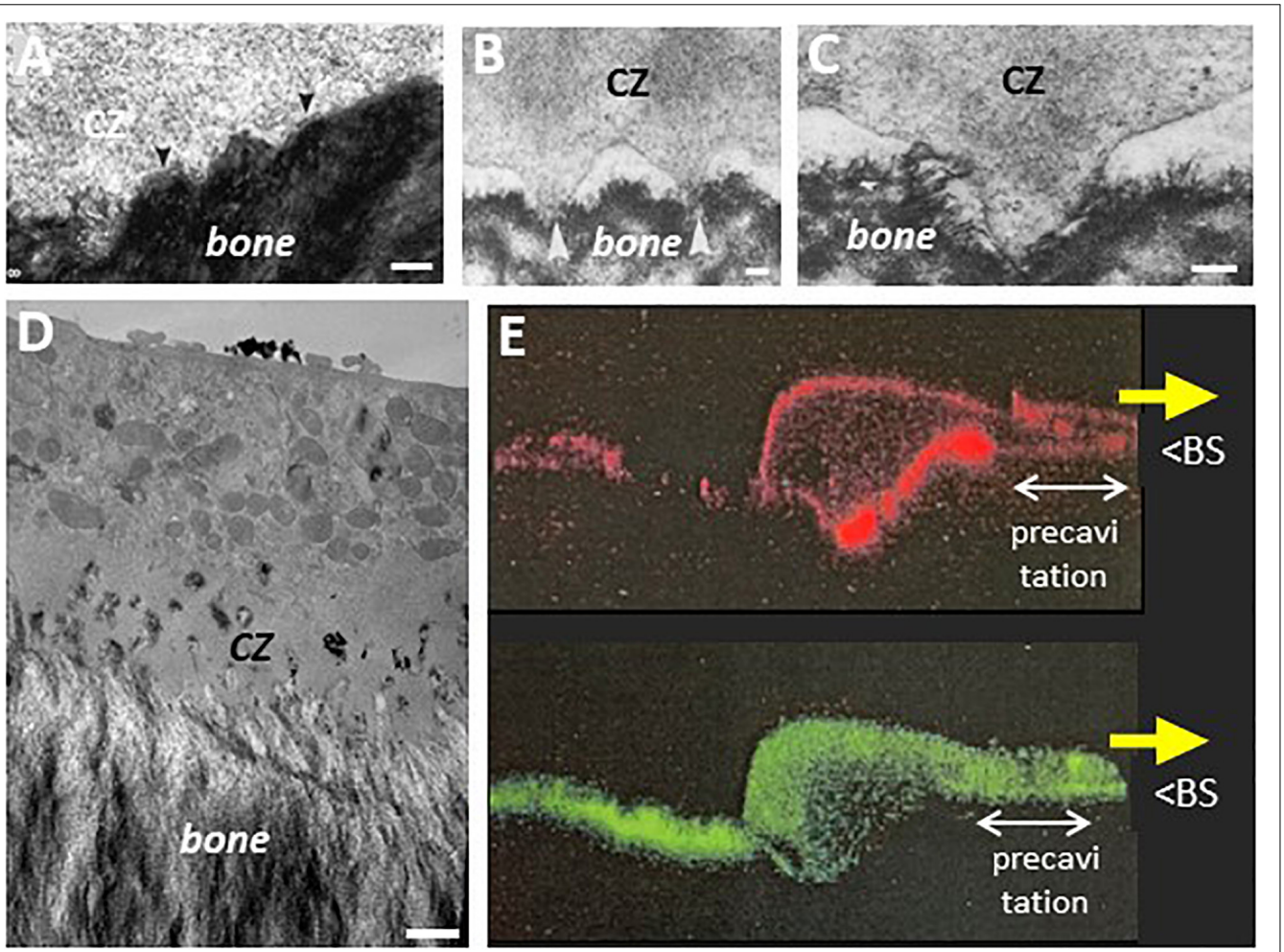


**FIGURE 7 |** Electron microscopy pictures in the area of pre-cavitation surfaces: podosomes, superficial disruptions of the bone matrix, and evidence for uptake of resorption products. **(A)** Uneven interface between CZ and underlying bone surface that received attention in Pierce (1989) [rat maxillary osteoclast, reproduced from Pierce (1989)]. **(B,C)** Podosomes in the CZ of hen osteoclast. Note they protrude in the matrix of medullary bone [reproduced from Zambonin-Zallone et al. (1988) with permission]. **(D)** EM picture of the pre-cavitation area of an osteoclast sectioned along the resorption/migration axis (obtained as in **Figures 1B**, **6**, unpublished). Note the disrupted bone surface, the nascent ruffled border in the CZ, and the electron dense vacuoles in the CZ, similar to the phagocytic features reported earlier in this area (Bonucci, 1974; Pierce, 1989). **(E)** Confocal picture of a trench forming osteoclast sectioned along its resorption/migration axis and perpendicularly to the bone surface (unpublished). The osteoclast is moving in the direction of the yellow arrow. Human osteoclasts were obtained and analyzed on dentine as in Nesbitt and Horton (1997) (red: actin; green: collagen fragments stained with a collagen antibody as in Nesbitt and Horton (1997); unpublished picture of S. Nesbitt (The Royal Institution, London) with kind permission). BS: bone surface. Note the ruffled border and the SZ are at the typical position seen in trench forming osteoclasts. Note the intracellular collagen signal in the pre-cavitation area and all along the basolateral domain up to the rear of the osteoclast (- which fits the route of resorption products shown by time lapse). Scale bars in **(A)** 100 nm; **(B)** 1 μm; **(C)** 250 nm; **(D)** 1 μm.

the superficial disruptions on the pre-cavitation surfaces are directly due to osteoclasts and do not merely represent pre-existing irregularities of the bone surface. Regarding the electron microscopy phagocytic features, one should also mention that they may well relate to the vacuoles identified in time lapse of trench making osteoclasts (section 5). (i) They transport resorption products from the leading edge to the rear where they disappear. (ii) Their site of origin at the front edge of the cavity would explain their detection specifically in the trench mode. (iii) Phagocytosis would explain the large size of these vacuoles. (iv) This phagocytic process requires membrane consumption at the front, which may put at risk attachment/protrusion ability of the front, unless membrane is returned to the plasma membrane by exocytosis at the rear. Blockage of exocytosis at the rear by chloroquine (section 5) would prevent this return and therefore lead to detachment of the front (section 4).

Thus, the trench resorption mode allows for a series of pre-cavitation activities that may contribute importantly to osteoclast aggressiveness, but that are not taken into account in the standard models of osteoclastic bone resorption.

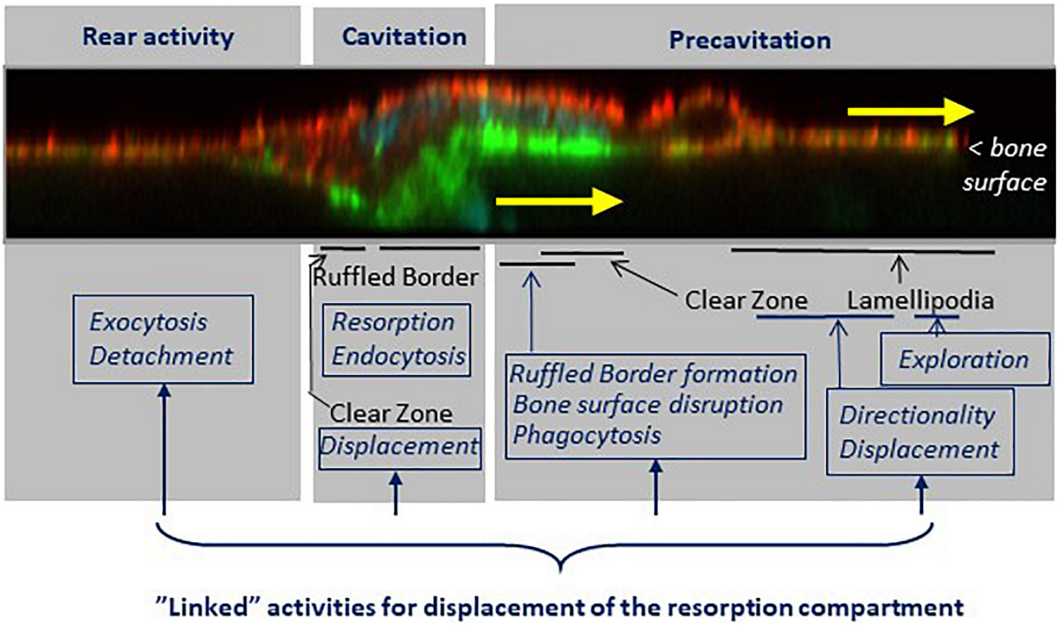


**FIGURE 8 |** The shift from the pit to the trench resorption mode goes along with a specific arrangement of cellular domains responsible of the respective tasks supporting trench formation. Key features (black fonts) and related tasks (blue fonts) are mapped on a confocal picture of a trench forming osteoclast sectioned along its resorption/migration axis and perpendicularly to the bone surface (actin stained with phalloidin, green; $\alpha_v\beta_3$ stained with $\alpha_v\beta_3$ antibody, red, unpublished). The osteoclast is moving in the direction of the yellow arrows. (i) The pre-cavitation domain harbors lamellipodia and the front part of the SZ. This domain plays a major role in exploration, displacement and in determining the direction of resorption. It supports ruffled border formation, damages superficially the bone surfaces, and shows phagocytic events. (ii) The cavitation domain shows the same well known characteristics as in the pit mode: a fully developed ruffled border, thorough resorption and endocytosis. A critical difference, however, is that the cavitation harbors part of the SZ, which moves along the cavity walls. (iii) The rear appears to be an exit site for resorption products, and their release is involved in the mechanism allowing the rear to detach from the bone surface, thereby allowing the cell body to migrate. Of note, the continuous displacement of the resorption compartment requires the coordination of all these tasks. See sections 4 to 6.

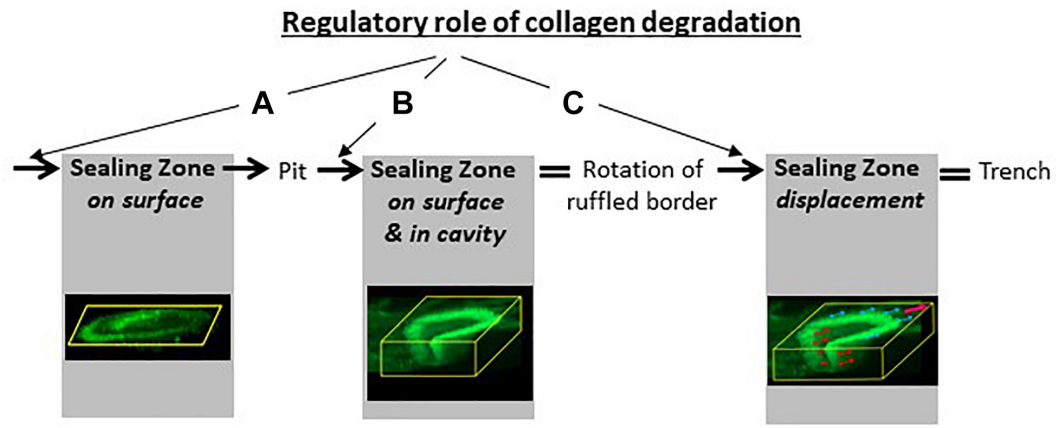


**FIGURE 9 |** Collagen degradation as a "regulator" of SZ and bone resorption. Next to its obvious direct role in the formation of a cavity, collagen degradation has a key role for SZ formation **(A)**, orientation **(B)** and displacement **(C)** (see section 3). **(A)** The formation of a planar SZ on the bone surface depends on thorough collagen degradation by MMPs of bone lining cells and orients the ruffled border against the bone surface for drilling a pit (see **Figure 1A**). **(B)** The movement of part of the SZ into the pit depends on thorough collagen removal from the pit by cathepsin K and orients the ruffled border against the cavity wall to resorb parallel to the bone surface (see **Figure 2B**). **(C)** The continuous displacement of the SZ parallel to the bone surface depends on thorough collagen removal from the cavity walls by cathepsin K and from the bone surface by MMPs of bone lining cells, and leads to the formation of a trench (sections 3.2 and 4). The confocal pictures are from **Figures 1** and **5**.

## 7. KEY MESSAGES AND PERSPECTIVES

- The observations reviewed herein lead to envision the mechanism that allows the osteoclast extensively enlarging its resorption cavity by making a trench. As explained in section 1, this enlargement is at the basis of bone erosion and pathological bone destruction, and therefore its mechanism is important to know.
- This mechanism corresponds to a unique osteoclastic phenotype characterized by integrated resorption and migration activities. **Figure 8** shows a spatial model of this phenotype, taking into account the characteristic configuration of a trench-forming osteoclast: its front on the bone surface and its main body in the resorption cavity. (i) The front domain laying over the bone surface is responsible for guiding resorption on the bone surface (see section 4), for continuously generating new ruffled border (which appears to arise from inside the CZ itself) (see section 6), and for disrupting superficially the bone surface and taking up matrix clumps through phagocytosis (see section 6). (ii) The "cavity domain" corresponds to the classical resorption compartment. Importantly, however, this is also where the SZ surrounding the ruffled border has to displace itself along the cavity wall (see sections 3 and 4). (iii) The "rear domain" is responsible for a process linking the release of resorption products and the disassembly of attachment complexes between the cell and he bone surface (see section 5). The standard model of the resorption mechanism shown in **Figure 1A** thus gives only a partial view of the machinery involved in the "large size" resorption events.
- The special role of the SZ has to be underscored. Rather than anchoring the bone resorption compartment, it emerges as the structure transporting the resorption compartment/ruffled border (just like the structure bearing the boring head in a tunneling machine) (see sections 2 and 4), and it is closely associated with ruffled border formation at the leading edge (see section 6). Accordingly, the SZ governs the "resorption route" during the long duration resorption events (**Figure 9**): as explained in section 2, it directs the resorptive activity first against the bone surface and thereafter against the cavity wall. This resorption route is in line with the fact that 90% of trench resorption events start as a pit (Søe and Delaissé, 2017).
- The principle linking collagen removal, SZ formation and "initiation" of resorption is well known (see section 3.1). Here we highlight that this principle also rules all the subsequent steps involved in the "enlargement" of a resorption cavity, since collagen removal must be as fast as demineralization to allow SZ displacement in the cavity, thereby allowing trench formation (see section 3.2) (**Figure 9**). Accordingly, it is of big interest to investigate which are the upstream effectors that affect the coordination between collagen degradation and demineralization, as already discussed by Søe et al. (2013).
- The collagen degradation required for SZ displacement in the excavation is performed by cathepsin K. This stresses that in addition to the obvious role of cathepsin K to resorb the bulk of collagen of the bone matrix, thereby creating a cavity, cathepsin K has also a regulatory role to remove the "negative collagen signaling" toward osteoclasts. This regulatory role is permissive to initiate and continue cavity enlargement. Therefore, high levels of the collagen degrading cathepsin K is at the heart of the resorption efficacy of trench forming osteoclasts (**Figure 9**).
- This observation draws the attention on cathepsin K as a favorite target for anti-resorptives in the clinic (especially in cases of aging, glucocorticoid treatment, and menopause: see section 3.3). The upcoming cathepsin K exosite inhibitors appear interesting candidates, since they inhibit specifically collagen degradation without inhibiting the other cathepsin K activities, and therefore avoid the side effects of odanacatib (Panwar et al., 2016, 2017). Also from a diagnostic point of view, the variation in cathepsin K activity levels amongst individuals may be interesting to consider, when evaluating the risk of bone fragilization (see section 3.3).
- Understanding extended bone erosion requires thinking of osteoclasts beyond the standard bone resorption models, and therefore paying attention in the coordination between demineralization, collagen degradation, podosome dynamics in the SZ, continuous ruffled border formation and secretion of resorption agents at the leading edge, release of resorption products at the rear, and cell body displacement.

## DATA AVAILABILITY STATEMENT

The original contributions presented in the study are included in the article, further inquiries can be directed to the corresponding author.

## AUTHOR CONTRIBUTIONS

J-MD and KS generated the concept. TA, NM, and AR provided the unpublished transmission electron microscopy pictures. J-MD wrote the manuscript. All authors approved the final text.

## FUNDING

The Research Council of Lillebaelt Hospital (Vejle, Denmark) was the main source of support to the studies of the authors reported herein. Support was also obtained from the Region of Southern Denmark (08/8932 and 15/24819).

## REFERENCES


Abdelgawad, M. E., Delaisse, J.-M., Hinge, M., Jensen, P. R., Alnaimi, R. W., Rolighed, L., et al. (2016). Early reversal cells in adult human bone remodeling: osteoblastic nature, catabolic functions and interactions with osteoclasts. *Histochem. Cell Biol.* 145, 603–615. doi: 10.1007/s00418-016-1414-y

Abdelgawad, M. E., Søe, K., Andersen, T. L., Merrild, D. M. H., Christiansen, P., Kjærsgaard-Andersen, P., et al. (2014). Does collagen trigger the recruitment of osteoblasts into vacated bone resorption lacunae during bone remodeling? *Bone* 67, 181–188. doi: 10.1016/j.bone.2014.07.012

Alakangas, A., Selander, K., Mulari, M., Halleen, J., Lehenkari, P., Mönkkönen, J., et al. (2002). Alendronate disturbs vesicular trafficking in osteoclasts. *Calcif. Tissue Int.* 70, 40–47. doi: 10.1007/s002230010047

Baron, R., Neff, L., Louvard, D., and Courtoy, P. J. (1985). Cell-mediated extracellular acidification and bone resorption: evidence for a low pH in resorbing lacunae and localization of a 100-kD lysosomal membrane protein at the osteoclast ruffled border. *J. Cell Biol.* 101, 2210–2222. doi: 10.1083/jcb.101.6.2210

Bonucci, E. (1974). The organic-inorganic relationships in bone matrix undergoing osteoclastic resorption. *Calcif. Tissue Res.* 16, 13–36. doi: 10.1007/BF02008210

Borggaard, X. G., Pirapaharan, D. C., Delaissé, J. M., and Søe, K. (2020). Osteoclasts' ability to generate trenches rather than pits depends on high levels of active cathepsin k and efficient clearance of resorption products. *Int. J. Mol. Sci.* 21:5924. doi: 10.3390/ijms21165924

Bruzzaniti, A., Neff, L., Sanjay, A., Horne, W. C., De Camilli, P., and Baron, R. (2005). Dynamin forms a Src kinase-sensitive complex with Cbl and regulates podosomes and osteoclast activity. *Mol. Biol. Cell* 16, 3301–3313. doi: 10.1091/mbc.e04-12-1117

Brylka, L. J., and Schinke, T. (2019). Chemokines in physiological and pathological bone remodeling. *Front. Immunol.* 10:2182. doi: 10.3389/fimmu.2019.02182

Chambers, T. J., and Fuller, K. (1985). Bone cells predispose bone surfaces to resorption by exposure of mineral to osteoclastic contact. *J. Cell Sci.* 76, 155–165.

Chambers, T. J., Darby, J. A., and Fuller, K. (1985). Mammalian collagenase predisposes bone surfaces to osteoclastic resorption. *Cell Tissue Res.* 241, 671–675. doi: 10.1007/BF00214590

Coxon, F. P., and Taylor, A. (2008). Vesicular trafficking in osteoclasts. *Semin. Cell Dev. Biol.* 19, 424–433. doi: 10.1016/j.semcdb.2008.08.004

Delaisse, J.-M., Andersen, T. L., Kristensen, H. B., Jensen, P. R., Andreasen, C. M., and Søe, K. (2020). Re-thinking the bone remodeling cycle mechanism and the origin of bone loss. *Bone* 141:115628. doi: 10.1016/j.bone.2020.115628

Everts, V., Delaissé, J. M., Korper, W., Jansen, D. C., Tigchelaar-Gutter, W., Saftig, P., et al. (2002). The bone lining cell: its role in cleaning Howship's lacunae and initiating bone formation. *J. Bone Miner. Res.* 17, 77–90. doi: 10.1359/jbmr.2002.17.1.77

Everts, V., Korper, W., Jansen, D. C., Steinfort, J., Lammerse, I., Heera, S., et al. (1999). Functional heterogeneity of osteoclasts: matrix metalloproteinases participate in osteoclastic resorption of calvarial bone but not in resorption of long bone. *FASEB J.* 13, 1219–1230. doi: 10.1096/fasebj.13.10.1219

Feng, X., and Teitelbaum, S. L. (2013). Osteoclasts: new insights. *Bone Res.* 1, 11–26. doi: 10.4248/BR201301003

Garnero, P., Borel, O., Byrjalsen, I., Ferreras, M., Drake, F. H., McQueney, M. S., et al. (1999). The collagenolytic activity of cathepsin K is unique among mammalian proteinases. *J. Biol. Chem.* 273, 32347–32352. doi: 10.1074/jbc.273.48.32347

Geblinger, D., Addadi, L., and Geiger, B. (2010). Nano-topography sensing by osteoclasts. *J. Cell Sci.* 123, 1503–1510. doi: 10.1242/jcs.060954

Geblinger, D., Geiger, B., and Addadi, L. (2009). Surface-induced regulation of podosome organization and dynamics in cultured osteoclasts. *ChemBioChem* 10, 158–165. doi: 10.1002/cbic.200800549

Georgess, D., Machuca-Gayet, I., Blangy, A., and Jurdic, P. (2014). Podosome organization drives osteoclast-mediated bone resorption. *Cell Adhes. Migr.* 8, 192–204. doi: 10.4161/cam.27840

Hirvonen, M. J., Fagerlund, K., Lakkakorpi, P., Väänänen, H. K., and Mulari, M. T. K. (2013). Novel perspectives on the transcytotic route in osteoclasts. *Bonekey Rep.* 2:306. doi: 10.1038/bonekey.2013.40

Holtrop, M. E., and King, G. J. (1977). The ultrastructure of the osteoclast and its functional implications. *Clin. Orthop. Relat. Res.* 123, 177–196. doi: 10.1097/00003086-197703000-00062

Kalluri, R., Weinberg, R. A., Kalluri, R., and Weinberg, R. A. (2009). The basics of epithelial-mesenchymal transition. *J. Clin. Invest.* 119, 1420–1428. doi: 10.1172/JCI39104

Kristensen, H. B., Andersen, T. L., Marcussen, N., Rolighed, L., and Delaisse, J.-M. (2013). Increased presence of capillaries next to remodeling sites in adult human cancellous bone. *J. Bone Miner. Res.* 28, 574–585. doi: 10.1002/jbmr.1760

Lakkakorpi, P. T., and Vaananen, H. K. (1991). Kinetics of the osteoclast cytoskeleton during the resorption cycle in vitro. *J. Bone Miner. Res.* 6, 817–826. doi: 10.1002/jbmr.5650060806

Lemaire, P. A., Huang, L., Zhuo, Y., Lu, J., Bahnck, C., Stachel, S. J., et al. (2014). Chondroitin sulfate promotes activation of cathepsin K. *J. Biol. Chem.* 289, 21562–21572. doi: 10.1074/jbc.M114.559898

Leung, P., Pickarski, M., Zhuo, Y., Masarachia, P. J., and Duong, L. T. (2011). The effects of the cathepsin K inhibitor odanacatib on osteoclastic bone resorption and vesicular trafficking. *Bone* 49, 623–635. doi: 10.1016/j.bone.2011.06.014

Linder, S. (2007). The matrix corroded: podosomes and invadopodia in extracellular matrix degradation. *Trends Cell Biol.* 17, 107–117. doi: 10.1016/j.tcb.2007.01.002

Linder, S., and Kopp, P. (2005). Podosomes at a glance. *J. Cell Sci.* 118, 2079–2082. doi: 10.1242/jcs.02390

Luxenburg, C., Geblinger, D., Klein, E., Anderson, K., Hanein, D., Geiger, B., et al. (2007). The architecture of the adhesive apparatus of cultured osteoclasts: from podosome formation to sealing zone assembly. *PLoS One* 2:e179. doi: 10.1371/journal.pone.0000179

Luxenburg, C., Winograd-Katz, S., Addadi, L., and Geiger, B. (2012). Involvement of actin polymerization in podosome dynamics. *J. Cell Sci.* 125, 1666–1672. doi: 10.1242/jcs.075903

Madel, M. B., Ibáñez, L., Ciucci, T., Halper, J., Rouleau, M., Boutin, A., et al. (2020). Dissecting the phenotypic and functional heterogeneity of mouse inflammatory osteoclasts by the expression of cx3cr1. *Elife* 9:e54493. doi: 10.7554/eLife.54493.sa2

Mano, H., Yuasa, T., Kameda, T., Miyazawa, K., Nakamaru, Y., Shiokawa, M., et al. (1996). Mammalian mature osteoclasts as estrogen target cells. *Biochem. Biophys. Res. Commun.* 223, 637–642. doi: 10.1006/bbrc.1996.0947

Merrild, D. M. H., Pirapaharan, D. C., Andreasen, C. M., Kjærsgaard-Andersen, P., Møller, A. M. J., Ding, M., et al. (2015). Pit- and trench-forming osteoclasts: a distinction that matters. *Bone Res.* 3:15032. doi: 10.1038/boneres.2015.32

Miller, S. C. (1977). Osteoclast cell-surface changes during the egg-laying cycle in Japanese quail. *J. Cell Bol.* 75, 104–118. doi: 10.1083/jcb.75.1.104

Møller, A. M. J., Delaisse, J. M., Olesen, J. B., Bechmann, T., Madsen, J. S., and Søe, K. (2020a). Zoledronic acid is not equally potent on osteoclasts generated from different individuals. *JBMR Plus* 4:e10412. doi: 10.1002/jbm4.10412

Møller, A. M. J., Delaissé, J. M., Olesen, J. B., Canto, L. M., Rogatto, S. R., Madsen, J. S., et al. (2020b). Fusion potential of human osteoclasts in vitro reflects age, menopause, and in vivo bone resorption levels of their donors—a possible involvement of DC-STAMP. *Int. J. Mol. Sci.* 21:6368. doi: 10.3390/ijms21176368

Møller, A. M. J., Delaisse, J. M., Olesen, J. B., Madsen, J. S., Canto, L. M., Bechmann, T., et al. (2020c). Aging and menopause reprogram osteoclast precursors for aggressive bone resorption. *Bone Res.* 8:27. doi: 10.1038/s41413-020-0102-7

Møller, A. M. J., Füchtbauer, E. M., Brüel, A., Andersen, T. L., Borggaard, X. G., Pavlos, N. J., et al. (2018). Septins are critical regulators of osteoclastic bone resorption. *Sci. Rep.* 8:13016. doi: 10.1038/s41598-018-31159-1

Mulari, M. T. K., Nars, M., Laitala-Leinonen, T., Kaisto, T., Metsikkö, K., Sun, Y., et al. (2008). Recombinant VSV G proteins reveal a novel raft-dependent endocytic pathway in resorbing osteoclasts. *Exp. Cell Res.* 314, 1641–1651. doi: 10.1016/j.yexcr.2008.02.011

Mulari, M. T. K., Zhao, H., Lakkakorpi, P. T., and Väänänen, H. K. (2003). Osteoclast ruffled border has distinct subdomains for secretion and

degraded matrix uptake. *Traffic* 4, 113–125. doi: 10.1034/j.1600-0854.2003.40206.x

Nakamura, H., Sato, G., Hirata, A., and Yamamoto, T. (2004). Immunolocalization of matrix metalloproteinase-13 on bone surface under osteoclasts in rat tibia. *Bone* 34, 48–56. doi: 10.1016/j.bone.2003.09.001

Nesbitt, S. A., and Horton, M. A. (1997). Trafficking of matrix collagens through bone-resorbing osteoclasts. *Science* 276, 266–269. doi: 10.1126/science.276.5310.266

Ng, P. Y., Patricia Ribet, A. B., and Pavlos, N. J. (2019). Membrane trafficking in osteoclasts and implications for osteoporosis. *Biochem. Soc. Trans.* 47, 639–650. doi: 10.1042/BST20180445

Niwa, T., Mizukoshi, K., Azuma, Y., Kashimata, M., and Shibutani, T. (2013). Fundamental study of osteoclast chemotaxis toward chemoattractants expressed in periodontitis. *J. Periodontal. Res.* 48, 773–780. doi: 10.1111/jre.12068

Nordahl, J., Hollberg, K., Mengarelli-Widholm, S., Andersson, G., and Reinholt, F. P. (2000). Morphological and functional features of clasts in low phosphate, vitamin D-deficiency rickets. *Calcif. Tissue Int.* 67, 400–407. doi: 10.1007/s002230001151

Novack, D. V., and Faccio, R. (2011). Osteoclast motility: putting the brakes on bone resorption. *Ageing Res. Rev.* 10, 54–61. doi: 10.1016/j.arr.2009.09.005

Palokangas, H., Mulari, M., and Väänänen, H. K. (1997). Endocytic pathway from the basal plasma membrane to the ruffled border membrane in bone-resorbing osteoclasts. *J. Cell Sci.* 110, 1767–1780.

Panwar, P., Søe, K., Guido, R. V., Bueno, R. V. C., Delaisse, J.-M., and Brömme, D. (2016). A novel approach to inhibit bone resorption: exosite inhibitors against cathepsin K. *Br. J. Pharmacol.* 173, 396–410. doi: 10.1111/bph.13383

Panwar, P., Xue, L., Søe, K., Srivastava, K., Law, S., Delaisse, J. M., et al. (2017). An ectosteric inhibitor of cathepsin K inhibits bone resorption in ovariectomized mice. *J. Bone Miner. Res.* 32, 2415–2430. doi: 10.1002/jbmr.3227

Parikka, V., Lehenkari, P., Sassi, M. L., Halleen, J., Risteli, J., Härkönen, P., et al. (2001). Estrogen reduces the depth of resorption pits by disturbing the organic bone matrix degradation activity of mature osteoclasts. *Endocrinology* 142, 5371–5378. doi: 10.1210/endo.142.12.8533

Pierce, A. M. (1989). Attachment to and phagocytosis of mineral by alveolar bone osteoclasts. *J. Submicrosc. Cytol. Pathol.* 21, 63–71.

Redlich, K., and Smolen, J. S. (2012). Inflammatory bone loss: pathogenesis and therapeutic intervention. *Nat. Rev. Drug Discov.* 11, 234–250. doi: 10.1038/nrd3669

Reinholt, F. P., Hultenby, K., Heinegård, D., Marks, S. C., Norgård, M., and Anderson, G. (1999). Extensive clear zone and defective ruffled border formation in osteoclasts of osteopetrotic (ia/ia) rats: implications for secretory function. *Exp. Cell Res.* 251, 477–491. doi: 10.1006/excr.1999.4585

Rogers, M. J., Crockett, J. C., Coxon, F. P., and Mönkkönen, J. (2011). Biochemical and molecular mechanisms of action of bisphosphonates. *Bone* 49, 34–41. doi: 10.1016/j.bone.2010.11.008

Rumpler, M., Würger, T., Roschger, P., Zwettler, E., Sturmlechner, I., Altmann, P., et al. (2013). Osteoclasts on bone and dentin in vitro: mechanism of trail formation and comparison of resorption behavior. *Calcif. Tissue Int.* 93, 526–539. doi: 10.1007/s00223-013-9786-7

Saftig, P., Hunziker, E., Wehmeyer, O., Jones, S., Boyde, A., Rommerskirch, W., et al. (1998). Impaired osteoclastic bone resorption leads to osteopetrosis in cathepsin-K-deficient mice. *Proc. Natl. Acad. Sci. U S A.* 95, 13453–13458. doi: 10.1073/pnas.95.23.13453

Salo, J., Lehenkari, P., Mulari, M., Metsikkö, K., and Väänänen, H. K. (1997). Removal of osteoclast bone resorption products by transcytosis. *Science* 276, 270–273. doi: 10.1126/science.276.5310.270

Salo, J., Metsikkö, K., Palokangas, H., Lehenkari, P., and Kalervo Väänänen, H. (1996). Bone-resorbing osteoclasts reveal a dynamic division of basal plasma membrane into two different domains. *J. Cell Sci.* 109, 301–307.

Saltel, F., Chabadel, A., Bonnelye, E., and Jurdic, P. (2008). Actin cytoskeletal organisation in osteoclasts: a model to decipher transmigration and matrix degradation. *Eur. J. Cell Biol.* 87, 459–468. doi: 10.1016/j.ejcb.2008.01.001

Saltel, F., Destaing, O., Bard, F., Eichert, D., and Jurdic, P. (2004). Apatite-mediated actin dynamics in resorbing osteoclasts. *Mol. Biol. Cell* 15, 5231–5241. doi: 10.1091/mbc.e04-06-0522

Sasaki, T., Takahashi, N., Higashi, S., and Suda, T. (1989). Multinucleated cells formed on calcified dentine from mouse bone marrow cells treated with 1α,25-dihydroxyvitamin D3 have ruffled borders and resorb dentine. *Anat. Rec.* 224, 379–391. doi: 10.1002/ar.1092240307

Sato, T., Foged, N. T., and Delaissé, J.-M. (1998). The migration of purified osteoclasts through collagen is inhibited by matrix metalloproteinase inhibitors. *J. Bone Miner. Res.* 13, 59–66. doi: 10.1359/jbmr.1998.13.1.59

Shemesh, M., Addadi, S., Milstein, Y., Geiger, B., and Addadi, L. (2016). Study of osteoclast adhesion to cortical bone surfaces: a correlative microscopy approach for concomitant imaging of cellular dynamics and surface modifications. *ACS Appl. Mater. Interfaces* 8, 14932–14943. doi: 10.1021/acsami.5b08126

Søe, K., and Delaissé, J.-M. (2010). Glucocorticoids maintain human osteoclasts in the active mode of their resorption cycle. *J. Bone Miner. Res.* 25, 2184–2192. doi: 10.1002/jbmr.113

Søe, K., and Delaissé, J.-M. (2017). Time-lapse reveals that osteoclasts can move across the bone surface while resorbing. *J. Cell Sci.* 130, 2026–2035. doi: 10.1242/jcs.202036

Søe, K., Merrild, D. M. H., and Delaissé, J.-M. (2013). Steering the osteoclast through the demineralization-collagenolysis balance. *Bone* 56, 191–198. doi: 10.1016/j.bone.2013.06.007

Stenbeck, G. (2002). Formation and function of the ruffled border in osteoclasts. *Semin. Cell Dev. Biol.* 13, 285–292. doi: 10.1016/S1084952102000587

Stenbeck, G., and Horton, M. A. (2000). A new specialized cell-matrix interaction in actively resorbing osteoclasts. *J. Cell Sci.* 113, 1577–1587.

Stenbeck, G., and Horton, M. A. (2004). Endocytic trafficking in actively resorbing osteoclasts. *J. Cell Sci.* 117, 827–836. doi: 10.1242/jcs.00935

Swanson, C., Lorentzon, M., Conaway, H. H., and Lerner, U. H. (2006). Glucocorticoid regulation of osteoclast differentiation and expression of receptor activator of nuclear factor-κB (NF-κB) ligand, osteoprotegerin, and receptor activator of NF-κB in mouse calvarial bones. *Endocrinology* 147, 3613–3622. doi: 10.1210/en.2005-0717

Takahashi, N., Ejiri, S., Yanagisawa, S., and Ozawa, H. (2007). Regulation of osteoclast polarization. *Odontology* 95, 1–9. doi: 10.1007/s10266-007-0071-y

Tehrani, S., Faccio, R., Chandrasekar, I., Ross, F. P., and Cooper, J. A. (2006). Cortactin has an essential and specific role in osteoclast actin assembly. *Mol. Biol. Cell* 17, 2882–2895. doi: 10.1091/mbc.e06-03-0187

Väänänen, H. K., Zhao, H., Mulari, M., and Halleen, J. M. (2000). The cell biology of osteoclast function. *J. Cell Sci.* 113, 377–381.

van den Dries, K., Linder, S., Maridonneau-Parini, I., and Poincloux, R. (2019). Probing the mechanical landscape – new insights into podosome architecture and mechanics. *J. Cell Sci.* 132:jcs236828. doi: 10.1242/jcs.236828

Van Wesenbeeck, L., Odgren, P. R., Coxon, F. P., Frattini, A., Moens, P., Perdu, B., et al. (2007). Involvement of PLEKHM1 in osteoclastic vesicular transport and osteopetrosis in incisors absent rats and humans. *J. Clin. Invest.* 117, 919–930. doi: 10.1172/JCI30328

Vanderoost, J., Søe, K., Merrild, D. M. H., Delaissé, J.-M., and Van Lenthe, G. H. (2013). Glucocorticoid-induced changes in the geometry of osteoclast resorption cavities affect trabecular bone stiffness. *Calcif. Tissue Int.* 92, 240–250. doi: 10.1007/s00223-012-9674-6

Vives, V., Laurin, M., Cres, G., Larrousse, P., Morichaud, Z., Noel, D., et al. (2011). The Rac1 exchange factor Dock5 is essential for bone resorption by osteoclasts. *J. Bone Miner. Res.* 26, 1099–1110. doi: 10.1002/jbmr.282

von Kleist, L., and Haucke, V. (2012). At the crossroads of chemistry and cell biology: inhibiting membrane traffic by small molecules. *Traffic* 13, 495–504. doi: 10.1111/j.1600-0854.2011.01292.x

Wheal, B. D., Beach, R. J., Tanabe, N., Dixon, S. J., and Sims, S. M. (2014). Subcellular elevation of cytosolic free calcium is required for osteoclast migration. *J. Bone Miner. Res.* 29, 725–734. doi: 10.1002/jbmr.2068

Wijenayaka, A. K. A. R., Colby, C. B., Atkins, G. J., and Majewski, P. (2009). Biomimetic hydroxyapatite coating on glass coverslips for the assay of osteoclast activity in vitro. *J. Mater. Sci. Mater. Med.* 20, 1467–1473. doi: 10.1007/s10856-009-3718-0

Wilson, S. R., Peters, C., Saftig, P., and Brömme, D. (2009). Cathepsin K activity-dependent regulation of osteoclast actin ring formation and bone resorption. *J. Biol. Chem.* 284, 2584–2592. doi: 10.1074/jbc.M805280200

Zambonin-Zallone, A., Teti, A., Carano, A., and Marchisio, P. C. (1988). The distribution of podosomes in osteoclasts cultured on bone laminae: effect of retinol. *J. Bone Miner. Res.* 3, 517–523. doi: 10.1002/jbmr.5650030507

Zhao, H., Laitala-Leinonen, T., Parikka, V., and Väänänen, H. K. (2001). Downregulation of small GTPase Rab7 impairs osteoclast polarization and bone resorption. *J. Biol. Chem.* 276, 39295–39302. doi: 10.1074/jbc.M010999200

**Conflict of Interest:** The authors declare that the research was conducted in the absence of any commercial or financial relationships that could be construed as a potential conflict of interest.

frontiers in Cell and Developmental Biology

ORIGINAL RESEARCH
published: 01 April 2021
doi: 10.3389/fcell.2021.627153

# Lack of Adiponectin Drives Hyperosteoclastogenesis in Lipoatrophic Mice

*Maria-Bernadette Madel[1†], He Fu[2†], Dominique D. Pierroz[3], Mariano Schiffrin[2], Carine Winkler[2], Anne Wilson[4], Cécile Pochon[5], Barbara Toffoli[2], Mahdia Taïeb[1], Jean-Yves Jouzeau[5], Federica Gilardi[2‡], Serge Ferrari[6], Nicolas Bonnet[7], Claudine Blin-Wakkach[1], Béatrice Desvergne[2]* and David Moulin[5]**

[1] Université Côte d'Azur, CNRS, UMR 7370, Laboratoire de PhysioMédecine Moléculaire, Nice, France, [2] Center for Integrative Genomics, Genopode, Lausanne Faculty of Biology and Medicine, Lausanne, Switzerland, [3] International Osteoporosis Foundation, Nyon, Switzerland, [4] Department of Oncology, University of Lausanne, Epalinges, Switzerland, [5] Université de Lorraine, CNRS, IMoPA, Nancy, France, [6] Division of Bone Diseases, Department of Internal Medicine Specialties, Geneva University Hospital, Faculty of Medicine, Geneva, Switzerland, [7] Nestlé Research, Lausanne, Switzerland

OPEN ACCESS

**Edited by:**
Natalie A. Sims,
University of Melbourne, Australia

**Reviewed by:**
Natalie Wee,
University of Melbourne, Australia
Jiake Xu,
University of Western Australia, Australia

***Correspondence:**
Béatrice Desvergne
beatrice.desvergne@unil.ch
David Moulin
david.moulin@univ-lorraine.fr

[†] These authors have contributed equally to this work and share first authorship

[‡] **Present address:**
Federica Gilardi,
Faculty Unit of Toxicology, CURML, Faculty of Biology and Medicine, University of Lausanne, Lausanne, Switzerland

**Specialty section:**
This article was submitted to Cellular Biochemistry, a section of the journal Frontiers in Cell and Developmental Biology

**Received:** 08 November 2020
**Accepted:** 22 February 2021
**Published:** 01 April 2021

**Citation:**
Madel M-B, Fu H, Pierroz DD, Schiffrin M, Winkler C, Wilson A, Pochon C, Toffoli B, Taïeb M, Jouzeau J-Y, Gilardi F, Ferrari S, Bonnet N, Blin-Wakkach C, Desvergne B and Moulin D (2021) Lack of Adiponectin Drives Hyperosteoclastogenesis in Lipoatrophic Mice. Front. Cell Dev. Biol. 9:627153. doi: 10.3389/fcell.2021.627153

Long bones from mammals host blood cell formation and contain multiple cell types, including adipocytes. Physiological functions of bone marrow adipocytes are poorly documented. Herein, we used adipocyte-deficient PPARγ-whole body null mice to investigate the consequence of total adipocyte deficiency on bone homeostasis in mice. We first highlighted the dual bone phenotype of PPARγ null mice: one the one hand, the increased bone formation and subsequent trabecularization extending in the long bone diaphysis, due to the well-known impact of PPARγ deficiency on osteoblasts formation and activity; on the other hand, an increased osteoclastogenesis in the cortical bone. We then further explored the cause of this unexpected increased osteoclastogenesis using two independent models of lipoatrophy, which recapitulated this phenotype. This demonstrates that hyperosteoclastogenesis is not intrinsically linked to PPARγ deficiency, but is a consequence of the total lipodystrophy. We further showed that adiponectin, a cytokine produced by adipocytes and mesenchymal stromal cells is a potent inhibitor of osteoclastogenesis *in vitro* and *in vivo*. Moreover, pharmacological activation of adiponectin receptors by the synthetic agonist AdipoRon inhibited mature osteoclast activity both in mouse and human cells by blocking podosome formation through AMPK activation. Finally, we demonstrated that AdipoRon treatment blocks bone erosion *in vivo* in a murine model of inflammatory bone loss, providing potential new approaches to treat osteoporosis.

**Keywords: adiponectin, osteoclast, bone marrow adiposity, cortical bone porosity, AMPK**

## INTRODUCTION

Bone homeostasis is a result of constant remodeling activities, with a balance of bone resorption and bone formation. The most prevalent disorder of bone homeostasis is osteoporosis, affecting men and women, with a particular high prevalence in post-menopausal women. The low efficacy of actual anti-osteoporotic therapeutic options highlights the need of better understanding the pathophysiological processes at work.

The role of adipocyte in bone homeostasis is one of the factors raising great interest, but it faces quite some complexity. An illustration of this complexity is the fact that obesity is traditionally considered to be protective against osteoporosis, consequently to an increased proliferation and differentiation of osteoblasts and osteocytes stimulated by mechanical load (Felson et al., 1993). However, obesity in post-menopausal women and in men correlates with increased marrow adiposity, alteration of the bone microarchitecture, and increased risk of fracture (Sheu and Cauley, 2011). Thus, the respective roles of aging, increased BMI, and visceral *vs.* bone marrow fat on bone homeostasis remain difficult to disentangle (Horowitz et al., 2017; Cornish et al., 2018).

Peroxisome proliferator-activated receptors (PPARs) are ligand-activated transcription factors that belong to the nuclear hormone receptor superfamily. PPARγ is a key factor and master regulator in adipocytes development and functions (Tontonoz and Spiegelman, 2008). Indeed, loss-of-function studies both *in vitro* and *in vivo* have clearly demonstrated that PPARγ is essential for the formation of adipose tissue (Barak et al., 1999; Rosen et al., 1999; Wang et al., 2013) and mature adipocyte homeostasis (Imai et al., 2004). Recently, we demonstrated that mice carrying a full body deletion of PPARγ ($Pparg^{\Delta/\Delta}$) are totally devoid of adipocytes (Sardella et al., 2018). The activity of PPARγ is also central in bone homeostasis by modulating both bone formation by osteoblasts and bone resorption due to osteoclast activity. First, adipocytes and osteoblasts share same mesenchymal progenitors, and the cell fate decision between adipocyte and osteoblast lineages depends on various signals (Idris et al., 2009; Calo et al., 2010; Kawai and Rosen, 2010; Wan, 2010). Activation of PPARγ inhibits osteoblast formation, and thus bone formation, by favoring adipocyte differentiation (Rzonca et al., 2004; Ali et al., 2005). Along this line, *in vivo* evidence indicates that mice heterozygous for a null allele of the gene encoding PPARγ (*Pparγ*) exhibit increased osteoblastogenesis, which results in increased bone mass with a doubling of the rate of new bone formation, when compared to control mice. Moreover, PPARγ also directly inhibits osteoblast activity, independently of adipogenesis, as demonstrated by the consequence of osteoblast-specific *Pparγ* deletion in osteoblast differentiation and trabecular bone formation (Sun et al., 2013). Second, in bone resorption, PPARγ promotes osteoclastogenesis, as illustrated by increased osteoclast numbers in aged mice treated with thiazolidinediones, which are high-affinity synthetic *PPARγ* agonists (Lazarenko et al., 2007). Conversely, mice in which *Pparγ* is specifically deleted in endothelial and hematopoietic cells (i.e., affecting osteoclast progenitors but not osteoblasts), exhibit decreased osteoclastogenesis compared to wild-type mice, provoking osteopetrosis with impaired bone resorption and reduced medullary cavities (Wan et al., 2007). However, a recent controversy on the role of PPARγ in osteoclast was raised by Zou et al. who found that only the pharmacological, and not the physiological activation of PPARγ affects osteoclastogenesis (Zou et al., 2016). Finally, hyperactivation of PPARγ via agonist treatment causes accumulation of adipocytes in the bone marrow in thiazolidinedione-treated rodents, whereas increased bone loss and bone fractures have been correlated with thiazolidinedione therapy in humans (Lazarenko et al., 2007; Grey, 2008; Kahn et al., 2008).

Herein, we used mice carrying a PPARγ full body deletion to explore the consequences of the lack of adipocyte on bone homeostasis, and demonstrate that as expected, there is a strong increased bone density of the trabecular bone. However, this phenotype was associated with an exacerbated osteoclastogenesis. Using two other complementary models of genetically-induced lipoatrophic mice, *i.e.* mice carrying an adipose-tissue specific deletion of PPARγ and AZIP mice, we then further explore the cross-talk between adipocytes and osteoclasts, whose alteration leads to hyperosteoclastogenesis and osteoporosis.

## RESULTS

In order to evaluate the impact of adipose tissue on bone homeostasis, we studied lipoatrophic mice, that we recently generated. These mice, hereby called $Pparg^{\Delta/\Delta}$ carry a whole body deletion of PPARγ and were obtained through epiblastic (Sox2 promoter) *cre* deletion of the *Pparγ* allele (Sardella et al., 2018). Bone analyses of female one-year-old mice first showed that these mice displayed dramatic alterations of both trabecular and cortical bones (**Figure 1**). The three-dimensional images generated by trabecular bone microcomputed tomography (3D micro-CT) reconstruction of the femurs of one-year old female mice highlighted a remarkably high trabecularization of the bone architecture in $Pparg^{\Delta/\Delta}$ mice, which extended along the shaft and almost reached the mid-diaphysis (**Supplementary Video S1**, **Figures 1A**, and **Table 1A**). In contrast, the cortical bone was found to be extremely porous at the epiphysis and the diaphysis. Owing to hypertrabecularization and high cortical porosity, the frontier between these two types of bone along the diaphysis remained difficult to establish. The phenotype was also observed in $Pparg^{\Delta/\Delta}$ male mice. However, the difficulties to obtain an appropriate number of old $Pparg^{\Delta/\Delta}$ males (due to premature death, still being investigated), and the fact that old female mice had a marked phenotype lead us to pursue all further explorations in females.

We first further evaluated in female whether the bone alterations appear during development or appear progressively with age, by performing micro CT measurements at 5–6 months. A quantification of the diverse parameters is shown in **Table 1B**. More particularly, we found that the increased trabecular number and connectivity density in both vertebral bodies and distal femoral metaphysic bones appeared at 5–6 months of age, whereas the alteration of cortical parameters were only seen in 1 year-old mice.

Molecular analyses confirmed an increased trabecular bone formation, as exemplified by increased levels of alkaline phosphatase mRNA (*Alp1*) in the bone, evaluated by RT-qPCR and increased levels of alkaline phosphatase (ALP) and osteocalcin (OCN) in the serum measured by ELISA (**Figures 1B,C**). To evaluate whether osteocytes, which come from osteoblasts and are mature permanent bone cells, *versus* osteoblast populations were altered in these mice,

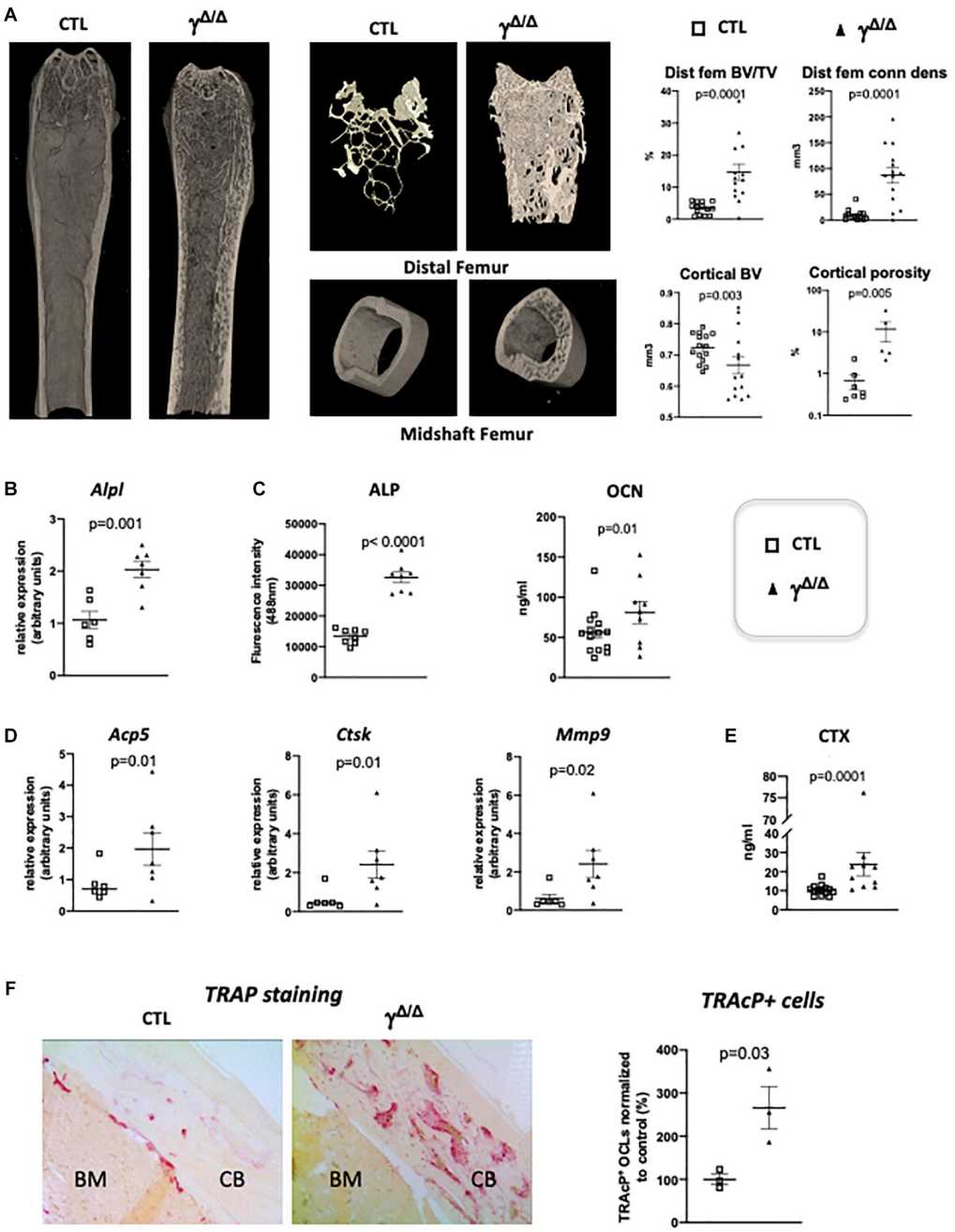


**FIGURE 1 |** Epiblastic PPARγ-deletion induces trabecular and cortical bone alteration. **(A)** Micro-CT analysis of femur from *Pparg*$^{\Delta/\Delta}$ ($\gamma^{\Delta/\Delta}$) one-year old female mice or control female littermates (CTL). Dot plots on the right show for the different genotypes (empty square for CTL and black triangle for $\gamma^{\Delta/\Delta}$) the percentage bone volume/trabecular volume (BV/TV) in % and connectivity density (ConnDens) of distal femoral trabecular bone (upper panels), and the cortical bone volume (BV) in mm$^3$ and the percentage of cortical porosity of femur (lower panels). All mice were 1-year-old. **(B)** RT-qPCR analysis of Alkaline phosphatase (*Alpl*) gene expression in femur from CTL and $\gamma^{\Delta/\Delta}$. **(C)** ELISA measurements of serum Alkaline phosphatase (ALP) and osteocalcin (OCN). **(D)** RT-qPCR analysis of Acid Phosphatase 5-Tartrate Resistant (*Acp5*), Cathepsin K (*Ctsk*), and Matrix Metallopeptidase 9 (*Mmp9*) expression in femur from CTL and $\gamma^{\Delta/\Delta}$. **(E)** ELISA measurements of serum Carboxy-terminal Collagen I telopeptide (CTX). **(F)** Representative images of TRAcP staining of decalcified sections of femurs, at mid-shaft levels, from control (CTL) or *Pparg*$^{\Delta/\Delta}$ ($\gamma^{\Delta/\Delta}$) mice. CB, cortical bone; BM, bone marrow. Data are presented as mean ± S.E.M. Each dot represents an individual animal. Statistical significance was determined by two-tailed unpaired *t*-test.

we measured the mRNA levels of sclerostin (*Sost*) and keratocan (*Kera*), which are expressed by osteocytes and osteoblasts, respectively (Jilka et al., 2014). Both markers were unchanged (**Supplementary Figure S1**). Three-D micro-CT of the fourth lumbar vertebrae clearly demonstrated increased trabecular bone volume fraction and trabecular connectivity

**TABLE 1 | (A)** Micro-CT data were obtained from various bones in $Pparg^{fl/+}$ and $Pparg^{\Delta/\Delta}$ of 1 year-old female mice. **(B)** Similar evaluation of bones from 5/6 month-old female mice.

**A. Micro CT analyses of 1 year-old female mice**

| 1 year | $Pparg^{fl/+}$ | $Pparg^{\Delta/\Delta}$ |
|---|---|---|
| No. of animals assessed | 15 | 14 |
| Cortical TV ($mm^3$) | 1.498 ± 0.023 | 1.327 ± 0.031* |
| Cortical BV ($mm^3$) | 0.723 ± 0.012 | 0.667 ± 0.028* |
| Cortical thickness (μm) | 241.8 ± 4.5 | 208.0 ± 10.4* |
| Dist femoral BV/TV (%) | 3.41 ± 0.49 | 14.38 ± 2.26* |
| Dist femoral conn density ($mm^3$) | 9.18 ± 2.57 | 81.89 ± 13.62* |
| Dist femoral Tb N (/mm) | 2.39 ± 0.09 | 3.61 ± 0.22* |
| Dist femoral Tb Th (μm) | 54.37 ± 2.48 | 57.28 ± 3.52* |
| Dist femoral Tb Sp (μm) | 431.34 ± 18.4 | 291.10 ± 9.70* |
| Vertebral BV/TV (%) | 17.33 ± 1.38 | 29.57 ± 3.30* |
| Vertebral conn density ($mm^3$) | 127.02 ± 14.89 | 519.44 ± 73.33* |
| Vertebral Tb N (/mm) | 3.42 ± 0.17 | 6.29 ± 0.53* |
| Vertebral Tb Th (μm) | 51.43 ± 1.88 | 47.04 ± 2.30 |
| Vertebral Tb Sp (μm) | 311.13 ± 16.23 | 177.30 ± 15.73* |

**B. Complete bone analysis by micro CT of 5/6 month-old female mice**

| 5–6 months | $Pparg^{fl/+}$ | $Pparg^{\Delta/\Delta}$ |
|---|---|---|
| No. of animals assessed | 8 | 10 |
| Cortical TV ($mm^3$) | 1.18 ± 0.05 | 1.18 ± 0.04 |
| Cortical BV ($mm^3$) | 0.0541 ± 0.023 | 0.0548 ± 0.014 |
| Cortical thickness (μm) | 203.75 ± 4.80 | 202.80 ± 5.33 |
| Dist femoral BV/TV (%) | 7.78 ± 1.17 | 8.55 ± 1.07 |
| Dist femoral conn density ($mm^3$) | 38.90 ± 8.70 | 84.30 ± 14.85* |
| Dist femoral Tb N (/mm) | 3.13 ± 0.13 | 3.75 ± 0.22* |
| Dist femoral Tb Th (μm) | 53.01 ± 1.62 | 45.93 ± 2.24* |
| Dist femoral Tb Sp (μm) | 327.46 ± 15.03 | 283.59 ± 21.33 |
| Vertebral BV/TV (%) | 15.49 ± 1.31 | 21.44 ± 1.79* |
| Vertebral conn density ($mm^3$) | 112.73 ± 12.56 | 275.53 ± 33.10* |
| Vertebral Tb N (/mm) | 3.71 ± 0.13 | 4.76 ± 0.17* |
| Vertebral Tb Th (μm) | 49.03 ± 1.17 | 46.39 ± 1.14 |
| Vertebral Tb Sp (μm) | 278.37 ± 10.66 | 215.1 ± 8.32* |

*Values are given as mean ± standard deviation. TV, total volume; BV, bone volume; Tb N, trabecular number; Tb Th, trabecular thickness; Tb Sp, trabecular separation. *$p < 0.05$ vs. $Pparg^{fl/+}$.*

density, indicating increased osteoblastogenesis in $Pparg^{\Delta/\Delta}$ (**Supplementary Figure S1**), in agreement with previous report (Akune et al., 2004). These results are consistent with the pivotal role of PPARγ on the fate of bone marrow mesenchymal stromal cells, with previous reports showing increased osteoblastogenesis when PPARγ signaling is pharmacologically or genetically blocked (Takada et al., 2009). As mentioned above, the role of PPARγ in osteoblastogenesis has been well documented and was therefore not further investigated in the present report.

Remarkably, the expression of bone resorbing markers such as the Tartrate-Resistant Acid Phosphatase Type 5 (*Acp5*), cathepsin K (*Ctsk*) was increased in the long bones of $Pparg^{\Delta/\Delta}$ mice compared to control mice. Mmp9, which is a key proteinase involved in the recruitment and activity of osteoclasts and endothelial cells for the development of long bones, particularly in the diaphysis core (Jemtland et al., 1998; Engsig et al., 2000), was also increased (**Figure 1D**) suggesting an increase in osteoclastogenesis. This is further supported by an augmentation of serum levels of carboxy-terminal collagen I telopeptide (CTX) (**Figure 1E**). Indeed, TRAcP staining on femoral sections (**Figure 1F**) confirmed the increased presence of bone-resorbing osteoclasts explaining the observed cortical porosity.

PPARγ is known to play a role in activating osteoclastogenesis. Wan et al. (2007) used a Tie2Cre-directed *Pparγ* deletion, which specifically target endothelial cells among which the myeloid-lineage cells —from which the osteoclast is derived. These authors show that this cell-specific *Pparγ* deletion severely impaired osteoclastogenesis, whereas PPARγ synthetic agonists exacerbated it (Wan et al., 2007). This role of Pparγ in osteoclast has been recently questioned by the study of Zou et al. (2016), showing that the *in vivo* effect of PPARγ on osteoclast formation is only seen upon pharmacological activation of PPARγ but neither on physiological nor on pathological osteoclast formation. This raised the question whether the elevated osteoclast activity observed in cortical bone is attributable to lipoatrophy, or to unforeseen intrinsic effects of PPARγ deficiency in the osteoclast lineage. To disentangle these two possibilities, we used another PPARγ-independent lipodystrophic mouse model. $AZIP^{tg/+}$ mouse is a hemizygote transgenic mouse strain in which a dominant negative protein of key B-ZIP transcription factors (A-ZIP) blocks adipocyte development. $AZIP^{tg/+}$ mice are born with no white adipose tissue and markedly decreased brown adipose tissue (Moitra et al., 1998). In support of the lipoatrophy hypothesis, micro-CT analyses of the femur of 1 year old female $AZIP^{tg/+}$ mice revealed an increased cortical porosity (**Figure 2A**). As observed in $Pparg^{\Delta/\Delta}$ mice, TRAcP staining of longitudinal bone sections revealed increased osteoclast numbers (**Figure 2B**), further confirmed by the increased expression levels of the osteoclastogensis markers (**Figure 2C**). Finally, we generated a third mouse model by invalidating *Pparγ* in adipose tissue ($Adipoq^{cre}$ Pparγ fl/fl, $\gamma^{FatKO}$ (Wang et al., 2013), called herein $Pparg^{adipoKO}$). These mice are lipoatrophic, but in contrast to $Pparg^{\Delta/\Delta}$, they have an unaltered hematopoietic lineage. Here again, micro-CT analysis and osteoclastogenesis markers in one-year old females revealed increased osteoclast numbers and activity with an enhanced cortical porosity, as observed in $Pparg^{\Delta/\Delta}$ mice (**Figures 2D,E**). These two independent mouse models confirmed that adipocyte deficiency is pivotal to the cortical bone phenotype and the increased osteoclast number observed here.

One consequence of lipodystrophy observed in all three models is a severe type 2 diabetes with signs of diabetic nephropathy (Moitra et al., 1998; Toffoli et al., 2017; Wang et al., 2013). Given that chronic kidney diseases are often accompanied by hyperparathyroidism and result in complex, combined catabolic and anabolic activities in the bones (Levin et al., 2007), we evaluated parathyroid hormone (PTH) levels. As shown in **Supplementary Figure S2**, no statistically significant differences were observed between $Pparg^{\Delta/\Delta}$ mice and their control littermates in either the circulating levels of PTH or the mRNA levels of the PTH receptor Pth1r in the bones or kidneys.

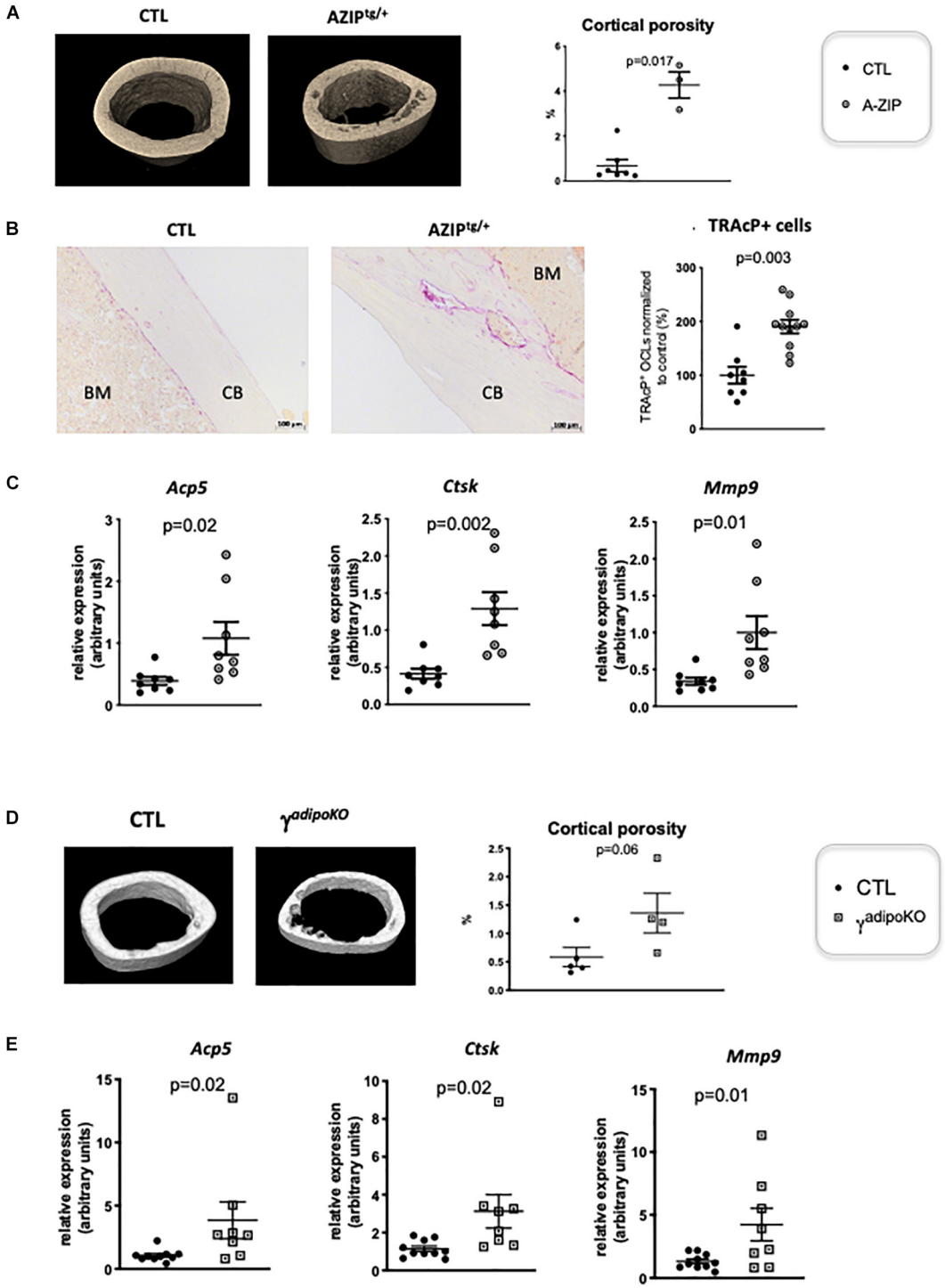


**FIGURE 2 |** Lipoatrophy is responsible for unregulated osteoclastogenesis. **(A)** Representative 3D sections of midshaft femur from 1 year-old female A-ZIP$^{tg/+}$ and CTL littermates (left panels) and femoral cortical porosity measured by micro-CT analysis of femur from A-ZIP$^{tg/+}$ and control (CTL) littermates (right panel). **(B)** Representative images of TRAcP staining of longitudinal sections of decalcified femurs, at mid-shaft levels, from control (CTL) or A-ZIP$^{tg/+}$ mice (left panels; CB, cortical bone; BM, bone marrow). The right panel is a quantification of TRAcP positive osteoclasts. **(C)** RT-qPCR analysis of Acid Phosphatase 5-Tartrate Resistant (*Acp5*) Cathepsin K (*Ctsk*) and Matrix Metallopeptidase 9 (*Mmp9)* expression in femur from A-ZIP$^{tg/+}$ mice and their control littermates. **(D)** Representative 3D sections of midshaft femur from 1 year-old females PPARγ$^{adipoKO}$ and CTL littermates (left panels) and femoral cortical porosity measured by micro-CT analysis of femur from PPARγ$^{adipoKO}$ and control (CTL) littermates (right panel). **(E)** RT-qPCR analysis of Acid Phosphatase 5-Tartrate Resistant (*Acp5*) Cathepsin K (*Ctsk*) and Matrix Metallopeptidase 9 (*Mmp9)* expression in femur from PPARγ$^{adipoKO}$ mice and their control littermates. Each dot represents an individual animal. Statistical significance was determined by two-tailed unpaired *t*-test.

Notably, serum PTH levels were also unchanged in AZIP$^{tg/+}$ mice (**Supplementary Figure S2**), suggesting that the PTH pathway is unlikely to support the increased bone remodeling observed in lipodystrophic mice.

To investigate how adipocytes regulate osteoclastogenesis, and to evaluate whether factors produced by adipocytes within the bone marrow can influence osteoclastogenesis, we performed an osteoclastogenesis assay using bone marrow cells from wild-type mice cultured in the presence of either control medium (CTL in **Figure 3**) or adipocyte-conditioned medium (ACM) (see **Figure 3A** for a graphic summary of the experiment). Adipocyte-conditioned medium was isolated from culture of adipocyte-differentiated 3T3-L1 cells whereas control medium was obtained from cultures of undifferentiated pre-adipocytes 3T3-L1 cells. The presence in bone marrow cells culture of adipocyte-conditioned medium, compared to pre-adipocyte-conditioned medium, provoked a substantial decrease in the number of mature osteoclasts (**Figure 3B**). Consistently, adipocyte-conditioned medium significantly inhibited bone resorption as assessed by the decrease number of resorption pits in the calvaria resorption assay (**Figure 3C**). These data demonstrate that adipocyte-secreted mediators are responsible for the inhibition of RANKL-induced osteoclast differentiation *in vitro*.

Next, we searched for component(s) of ACM responsible for this anti-osteoclastogenic activity. Interestingly, the ACM inhibitory activity was maintained after filtering out all components larger than 35 kDa from the conditioned medium. The molecular weights of the major adipokines, adiponectin and leptin, are below 35 kDa and their circulating levels are not or barely detectable in *Pparg*$^{\Delta/\Delta}$ mice, as we previously demonstrated (Gilardi et al., 2019). As expected, the gene expression levels of *Leptin* and *Adiponectin* in long bones *of Pparg*$^{\Delta/\Delta}$ mice as well as AZIP$^{tg/+}$ mice were extremely low (**Supplementary Figure S3**). Unlike *Leptin*, *Adiponectin* is preferentially expressed by adipocyte and by bone-marrow MSC, and is a well-characterized target gene of Pparγ (Iwaki et al., 2003). Western-blot analyses confirmed that adiponectin was present in large amounts in ACM but not in CTL medium (**Figure 3D**). We therefore tested whether blocking adiponectin would affect ACM-mediated inhibition of osteoclastogenesis *in vitro*. As shown in **Figure 3B**, the addition of a blocking adiponectin antibody reversed the reduction in osteoclast number in a dose-dependent manner. These results support that the soluble factors secreted by adipocytes, in particular adiponectin, are inhibitors of osteoclastogenesis. Consistently, the total lack of adipocytes, including in the bone marrow, results in a complete absence of this adipokine, leading to the loss of its repressive activity in osteoclast differentiation.

AdipoRon is a non-peptidic agonist of adiponectin receptors (Okada-Iwabu et al., 2013). We thus perform the reverse experiment of the antibody blocking assay, adding AdipoRon to culture of bone marrow cells. Consistently, AdipoRon recapitulated the blocking effect of ACM on osteoclast differentiation irrespective of the origin of the osteoclast progenitors (bone marrow, spleen, or monocytic-enriched fraction) with IC50 in the micromolar range (**Figures 4A,B** and **Supplementary Figure S4**). Furthermore, AdipoRon blocked osteoclast differentiation in *Pparγ* deficient cells, confirming that intrinsic PPARγ alterations do not play a role in the observed phenotype (**Figure 4C**).

Previous studies demonstrated *in vivo* that mice treated with adiponectin expressing adenovirus have reduced osteoclast numbers and bone-resorption markers (Oshima et al., 2005). Using the macrophage cell line RAW264, prone to differentiate in osteoclasts, these authors further showed that adiponectin blocked *in vitro* osteoclastogenesis by inhibiting NFATc1. Blockade of NFATc1 was suggested to occur through activation of the AMPK signaling pathway, a key integrator of metabolic signals and target of adiponectin signaling (Yamaguchi et al., 2008). We thus tested whether this mechanism would apply *in vivo* and to primary cells. Flow cytometry analysis combining nuclei staining (Madel et al., 2018) and anti-AdipoR1 antibody, confirmed that the adiponectin receptor AdipoR1 is expressed also by mature osteoclasts generated from murine bone marrow cells (**Figure 4D**). Furthermore, RT-PCR performed on osteoclasts from different origins (bone marrow, bone marrow-derived dendritic cells, bone marrow monocytic cells) showed that osteoclasts express both adiponectin receptors AdipoR1 and AdipoR2 (**Figure 4E**). In agreement, western-blot analysis of AMPK phosphorylation confirmed that the Adiponectin signaling pathway is active in both precursors and mature osteoclasts sorted on the basis of their nuclei number ($\geq$3) (Madel et al., 2018; **Figures 4F–H**).

AdipoRon was thus used to investigate the consequences of adiponectin receptor activation on murine and human osteoclasts. AICAR was used as a synthetic activator of AMPK. As seen in **Figures 5A,B** each of these molecules inhibited the formation of podosomes that are essential for bone resorption. Moreover, dorsomorphin, a reversible AMP-kinase inhibitor, could reverse the AdipoRon inhibitory effect (**Figure 5B**). This is in line with the recently published effect of recombinant adiponectin on RAW264.7 cells, confirming the impact of adiponectin on both osteoclasts differentiation and podosome formation (Chen et al., 2018) and endorsing the use of AdipoRon as a surrogate activator for adiponectin receptors. Finally, adiponectin signaling regulates numerous cellular metabolic pathways including mitochondrial functions (Iwabu et al., 2010). AdipoRon treatment provoked disruption of the perinuclear mitochondrial network when added to culture of mature osteoclasts (**Figure 5C**). Altogether, these results indicate that, beside its inhibiting action in osteoclast differentiation, adiponectin signaling exerts a pivotal role in mature osteoclast energy homeostasis regulation.

The inhibitory effect of AdipoRon was further tested *in vivo* on the well-described model of osteoclast bone resorption induced by lipopolysaccharide (LPS) injection into the mouse calvaria. Both micro-CT and TRAcP staining (**Figure 5D**) showed that AdipoRon administration resulted in a strong decrease in osteoclast numbers and bone resorption pits on calvaria.

We thus aimed to validate our findings on human cells and therefore investigated the impact of AdipoRon on hPBMC-derived osteoclasts. Consistent with the results

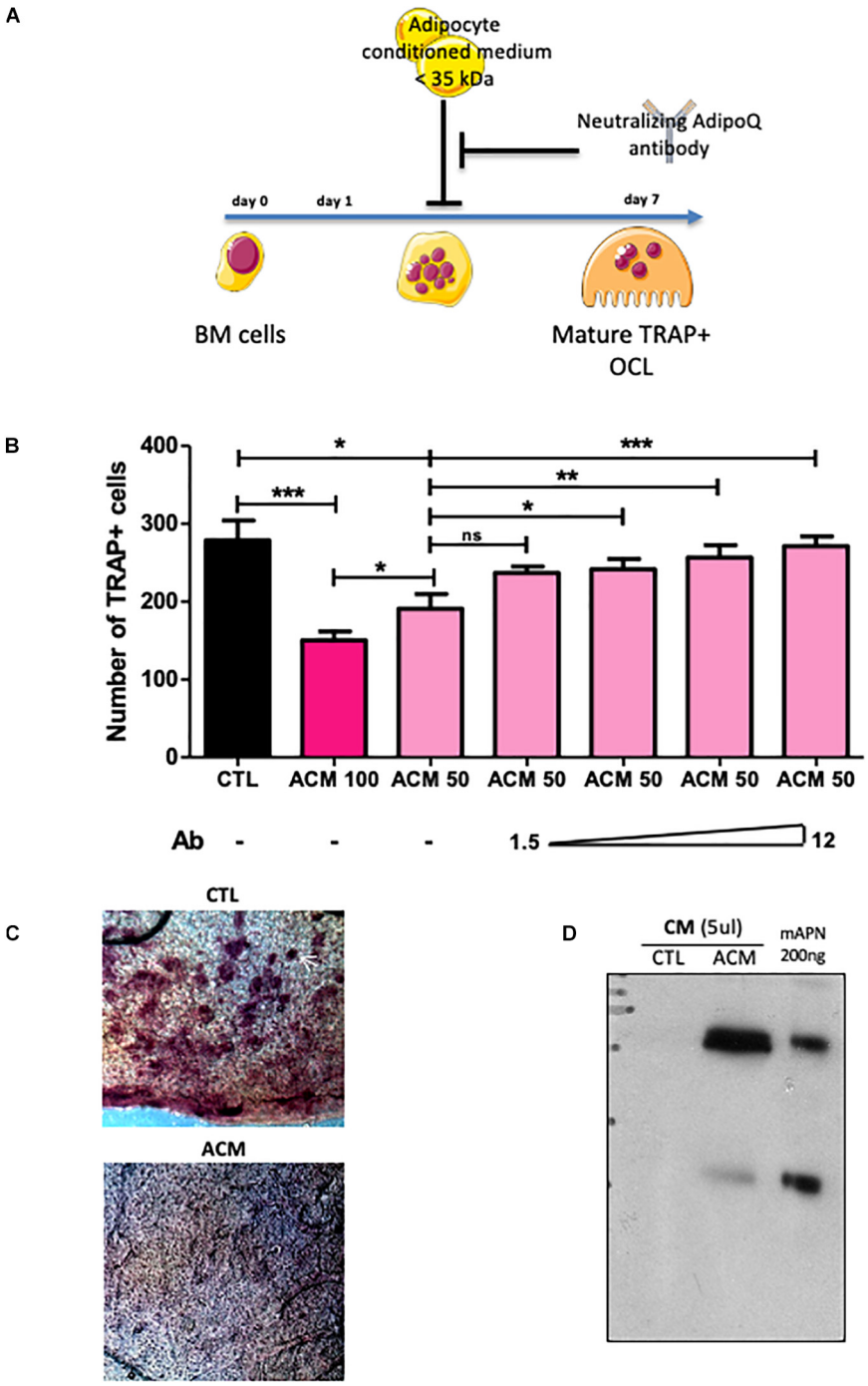


**FIGURE 3 |** Adipocyte conditioned medium inhibits osteoclastogenesis. **(A)** Experimental design of the *in vitro* assay used to test anti-osteoclastogenic activity from mature adipocyte secreted factors. **(B)** One day after plating, wild type BM cells were cultured for 6 more days in the presence of M-CSF and RANKL (osteoclast differentiation media) in addition to conditioned medium prepared from differentiated (ACM, adipocyte-conditioned medium) or undifferentiated (CTL: control-conditioned medium) 3T3-L1 preadipocytes. Different doses of a specific blocking antibody against adiponectin (1.5–12.0 μg/ml) were added to the conditioned medium (ACM50) during osteoclast differentiation (ACM 100 means pure ACM; ACM50 means 1:1 diluted ACM with osteoclast differentiation medium). Data are presented as mean ± SEM of biological triplicates. Statistical significance was determined by two-tailed unpaired *t*-test. $*p < 0.05$, $**p < 0.01$, $***p < 0.001$. **(C)** Calvaria resorption pit assay. Representative sections of skulls from 14 day-old wild-type pups cultured for 2 weeks in complete αMEM in the presence of conditioned medium from either undifferentiated 3T3-L1 preadipocytes (CTL, $n = 3$) or mature 3T3-L1 adipocytes (ACM, $n = 3$), after TRAP staining. Top panel: the white arrow indicates one example of resorption pit seen in many places on the skull with CTL medium, while absent with the ACM culture medium. **(D)** Western-blot analysis of conditioned medium from undifferentiated (CTL) and differentiated 3T3-L1 adipocyte (A-CM) against adiponectin. Recombinant mouse adiponectin (200 ng rmAdiponectin) was added to demonstrate specificity of the signal.

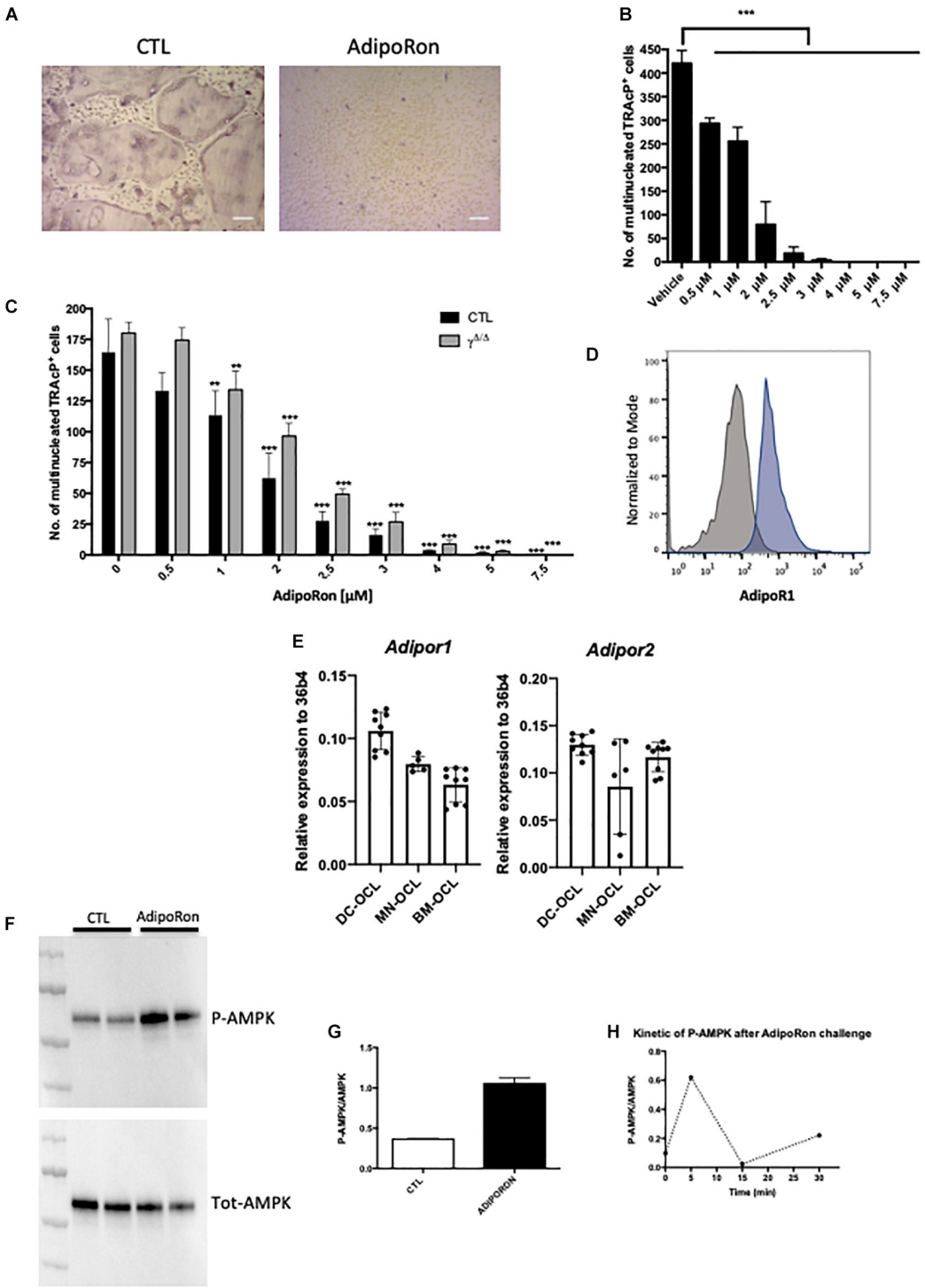


**FIGURE 4 |** Adiponectin signalling activation blocks osteoclast differentiation. **(A)** Representative images of TRAcP stained BM-derived osteoclasts differentiated in the presence or absence of AdipoRon (5 μM). Scale bars = 100 μm. **(B)** Dose response effect of AdipoRon on osteoclast differentiation using RAW264.7 cells ($n$ = 3). **(C)** Effect of AdipoRon on osteoclast differentiation assay using bone marrow cells from *Pparg*$^{\Delta/\Delta}$ ($\gamma^{\Delta/\Delta}$, grey bars) mice and control littermates (CTL, black bars). **(D)** Expression of Type 1 Adiponectin Receptor (AdipoR1) at the surface of BM- derived osteoclasts demonstrated by flow cytometry. Grey curve represents unstained negative control; blue curve represents BM-derived osteoclasts. **(E)** RT-qPCR analysis of Adiponectin Receptor 1 and 2 (*Adipor1* and *Adipor2*) on osteoclasts differentiated from bone marrow (BM) cells (BM-OCL), from BM-derived dendritic cells (DC-OCL) and BM monocytic cells (MN-OCLs). **(F)** Western-blot analysis of sorted mature bone marrow-derived osteoclasts treated with AdipoRon (5 μM). AdipoRon treatment activates AMPK phosphorylation (p-AMPK) in murine BM-derived osteoclasts. **(G)** Ratio of P-AMPK over total AMPK measured by densitometry. **(H)** Kinetic of AMPK phosphorylation (P-AMPK) after AdipoRon challenge in RAW264.7-derived osteoclasts. Data are presented as mean ± S.E.M. Statistical significance was determined by two-tailed unpaired $t$-test. $^{**}p < 0.01$, $^{***}p < 0.001$.

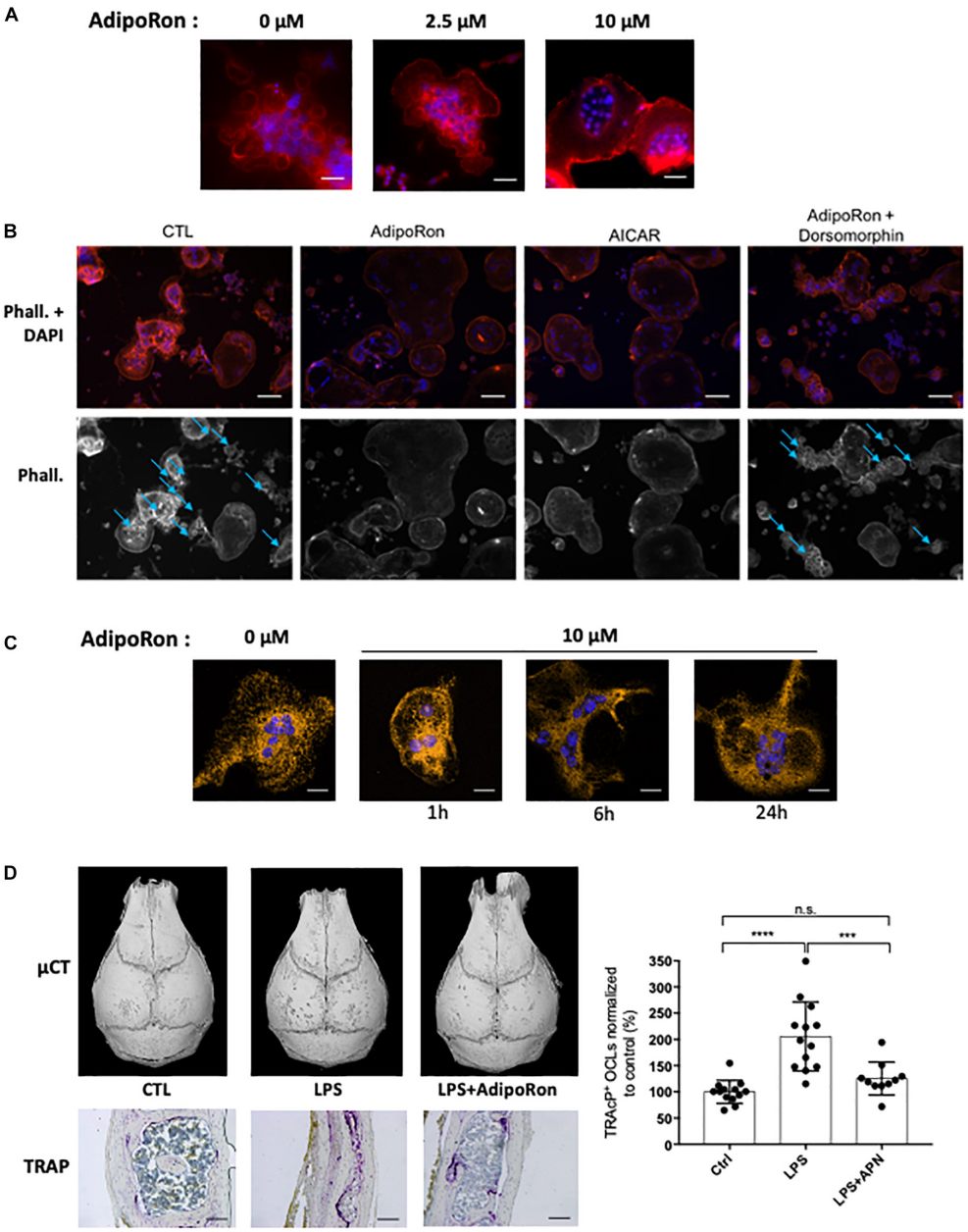


**FIGURE 5 |** Adiponectin regulates OCL activity and podosome formation. **(A)** Confocal microscopy of phalloidin-marked podosomes in RAW264.7-OCL in the presence of increasing concentrations of AdipoRon (representative images of $n = 3$ per concentration) Scale bars = 100 µm. **(B)** Confocal microscopy of phalloidin-marked podosomes in the presence of AMPK modulating drugs (AdipoRon, 10 µM; AICAR, 50 nM; Dorsomorphin, 1.2 µM) (representative image of $n = 3$ per conditions white asterisks marking the podosomes). Scale bars = 50 µm. Blue arrows indicate podosome rings. **(C)** Confocal microscopy of MitoTracker Orange in mature RAW264.7-OCL after AdipoRon (10 µM) challenge at different time points. Scale bars = 20 µm. **(D)** Mice received daily *s.c.* injections on the calvaria. Mice were injected with either 100 µg lipopolysaccharide from *Salmonella abortus equi* (LPS), or 100 µg LPS + 500 ng AdipoRon (LPS + AdipoRon) or vehicle (PBS) injection (control, CTL). Mouse skulls were collected on the 3rd day ($n = 3$ animals per group); Top panels: Micro-CT of the mouse skulls; Bottom panels: TRAcP staining of mouse skull after LPS +/− AdipoRon challenge, (representative sections from 3 animals per group), scale bars = 100 µm. Right panel: quantification of the TRAcP staining. Two-group comparisons were performed using the Student's t-test. ***$p < 0.001$, ****$p < 0.0001$.

obtained with mouse cells, low dose of AdipoRon significantly inhibited RANKL-induced human osteoclast differentiation (**Supplementary Figures S5A,B**). AdipoRon also activated AMPK phosphorylation in human PBMC-derived osteoclasts within minutes (**Supplementary Figure S5C**). At later time-point, i.e., within hours after the challenge with AdipoRon, the number of actin-containing podosome was drastically reduced in human osteoclasts (**Supplementary Figure S5D**).

These original findings offer new therapeutic perspectives in inflammatory bone loss management by targeting adiponectin/AdipoR.

## DISCUSSION

In the present report, using lipodystrophic mouse models, we evaluated how the total lack of adipose tissue may affect bone homeostasis. Taken together our results demonstrate that mature osteoclasts are sensitive to extrinsic adipose-derived metabolic signals such as adipokine and that bone marrow adiposity must be considered as a physiological regulator of bone homeostasis. Consistently with the literature, we identified adiponectin as one main inhibitory signal for osteoclastogenesis. Herein, we further showed that AdipoRon, a pharmacological agonist of adiponectin receptors, inhibits osteoclast differentiation of precursors from different origins (bone marrow, dendritic and monocytic cells). We also demonstrated that adiponectin signaling inhibits human osteoclast differentiation as well as activity of human mature osteoclast and explored how AMPK signaling act on mature osteoclast activity via podosome formation blockade. These original findings reveal a conserved adiponectin-mediated metabolic control of osteoclast activity and are clinically promising, in particular with regard to the treatment and prevention of excessive pathological bone-resorption conditions, such as in osteoporotic patients.

The first model used in the present study, the *Pparγ* null mice, is bringing up some decisive arguments with respect to the controversy on the role of PPARγ in osteoclastogenesis. Whereas initial studies reported that PPARγ is a key factor for osteoclastogenesis (Wan et al., 2007), they could not confirm such activity and proposed that only pharmacological activation of PPARγ had impact on osteoclastogenesis (Zou et al., 2016). Herein, we definitely demonstrate that osteoclastogenesis can occur in the absence of PPARγ signal, and that other adipose tissue-derived signals, such as adipokines, affect osteoclast differentiation and activity. In contrast, the increase trabecular bone formation seen in vertebrae, in femoral epiphyses and distal diaphysis of $Pparg^{\Delta/\Delta}$ mouse is consistent with the known role of PPARγ in inhibiting osteogenesis.

Using three complementary genetic models (2 distinct conditional null mice of *Pparγ* and the $AZIP^{tg/+}$ mice, a PPARγ-independent lipoatrophy model), we showed that the dramatic cortical bone alteration due to an excessive osteoclastogenesis in mice is linked to the lack of adipocyte and adipocyte-derived signals. The systemic and local activities of adipokines such as leptin and adiponectin have been recently reviewed (Cornish et al., 2018). Although leptin can act as a positive regulator of osteogenesis in *in vitro* systems, other studies in mice show that systemic leptin acting via the central nervous system is a potent inhibitor of bone formation (Ducy et al., 2000). Systemic adiponectin was reported to promote bone formation through its depressive action on the sympathetic tone in mice in age-dependent manner (Kajimura et al., 2013). However, *in vitro* differentiation assay showed that adiponectin inhibits osteoclast formation (Oshima et al., 2005; Yamaguchi et al., 2008). The observations *in vivo* are more controversial. Adiponectin-null mice exhibit an increased trabecular volume and fewer osteoclasts according to Wang et al. (2014), whereas Shinoda et al. (2006) found normal bone development in these mice. In contrast, Naot et al. (2016) described a decreased cortical thickness in adiponectin-null female mice and Yang et al. (2019) a decreased bone mass. Interestingly, the female bias of the phenotype observed herein was also found in adiponectin-null mice. Thus, adiponectin may have different effects on bone remodeling, depending on the activated autocrine, paracrine or systemic pathways (Tu et al., 2011). Our results from the osteoclastogenesis assay using bone marrow-derived cells and adiponectin-specific blocking antibodies support the important paracrine role of adiponectin in the inhibition of osteoclastogenesis in the normal BM environment. Direct paracrine activity is also consistent with the presence of the adiponectin receptors, AdipoR1 and AdipoR2, on the surface of differentiating osteoclasts (Pacheco-Pantoja et al., 2013). Nonetheless, we cannot exclude that other adipokines may also contribute to the paracrine effects of adipocytes on osteoclasts.

Identifying the source of adiponectin in the vicinity of osteoclast precursors and/or mature osteoclasts in bone marrow and bone compartment is challenging. Indeed, levels of adiponectin production by BM adipocytes remain controversial. Cawthorn et al. (2014) reported that BM adipocytes serve as a major source of circulating adiponectin exerting systemic effects during caloric restriction whereas others groups reported that bone marrow adipocytes express lower levels of adiponectin than adipocytes in adipose tissue (Liu et al., 2011; Poloni et al., 2013; Li et al., 2019). Others sources of bone marrow adiponectin have been recently described. Bone marrow $PDGFR\beta^{+}VCAM\text{-}1^{+}$ stromal cells have been identified as major producers of adiponectin in the bone marrow (Mukohira et al., 2019). Single cell transcriptomic profiling of the mouse bone marrow stromal compartment indicated that $LepR^{+}$ bone marrow mesenchymal stromal cells, which form a functional continuum with osteolineage cells, are expressing adiponectin (Baryawno et al., 2019). Beside their proliferative action on HSC and antiproliferative effects on myelomonocytic and early B lymphoid cells, these adiponectin-producing cells appears to be essential to the hematopoietic niche. In this context, our finding that adiponectin regulates osteoclast activity and differentiation in bone further strengthens the argument that a metabolic pathway driven by adiponectin controls many osteoimmunology processes, including remodeling of bone marrow hematopoietic stem cell niche, with potential implications for multiple human disease states including cancer.

The distinct behavior and response of trabecular bone versus cortical bone is particularly highlighted in $Pparg^{\Delta/\Delta}$ mice. Such contrasting phenotype has been previously observed. For example, increased or decreased mechanical strain (Ausk et al., 2013) or fluoride treatment increase the density of trabecular bone but decrease the density of cortical bone (Connett, Fluoride Action network, April 2012)[1]. This bivalent phenotype

[1]http://fluoridealert.org/studies/bone03/

is reminiscent of that observed when osteoblast and osteocyte apoptosis is prevented via targeted deletion of the proapoptotic proteins Bak/Bax (Jilka et al., 2014). In this context, a severe increase in cortical porosity was accompanied by increased osteoclast formation. The prolonged lifespan of osteoblasts was proposed by the authors to trigger diametrically opposed biological effects on bone homeostasis with an exaggeration of the adverse effects of aging due to long-lived osteocytes (Jilka et al., 2014). In particular, osteocytes may increase intracortical remodeling via their secretion of RANKL and the subsequent activation of osteoclasts (Fuller et al., 1998; Jilka et al., 2014; Rinotas et al., 2014). In $Pparg^{\Delta/\Delta}$ mice, the levels of *Sost* and *Keratocan* gene expression as markers of osteocytes and osteoblasts, respectively, are unchanged with respect to those found in their control littermates, thus refuting the possibility of an increased number of both cell types. In parallel, the increased expression of *Ctsk* and *Mmp9* likely contributes to the loss of cortical bone owing to high osteoclast activity, whereas the well-established role of PPARγ deficiency in bone formation via osteoblast activation is particularly highlighted by the increased trabecular bone density. Finally, it has been recently shown that osteoclasts have some site-dependent specificities and heterogeneity (Madel et al., 2019), that could contribute to the distinct behavior of the cortical bone *vs.* trabecular bone.

The difference in the intensity of the cortical porosity observed between the three lipodystrophic models we used may stem from different causes. On the one hand, the fact that the phenotype is more marked in the $Pparg^{\Delta/\Delta}$ mice indicates that the expression of PPARγ in other cell types including osteoblasts and osteoclasts may dampen the phenotype in the AZIP and in the $Pparg^{adipoKO}$ models, irrespectively of adiponectin signals. However, a clear contribution of adipocytes remains highlighted by the results in AZIP mice which expressed functional PPARγ in all cell types. On the other hand, adiponectin gene expression, barely detectable in $Pparg^{\Delta/\Delta}$ mice, is still present in the AZIP model and could contribute to the difference of phenotype penetrance between these two mouse models.

One important finding of the present report is the mechanism by which AdipoR signaling affects osteoclast activity. Indeed, here we demonstrated that AMPK was activated following AdipoRon challenge, which resulted in alteration of osteoclast metabolism, as exemplified by the alteration of the perinuclear mitochondrial network. We cannot exclude that direct or indirect signaling events may occur following adipoRon challenge that could interfere with osteoclast activity genetic program, such as Akt or NFATc1 signaling pathway as previously demonstrated with recombinant adiponectin (Yamaguchi et al., 2008; Tu et al., 2011). However, AMPK is central in this process, since its activation induced mitochondrial network alteration and podosome formation blockade, whereas AMPK blockade reverted these effects. Similarly, we also demonstrated that adiponectin signaling inhibits human osteoclast differentiation as well as activity of human mature osteoclast.

Altogether, these original findings reveal a conserved adiponectin-mediated metabolic control of osteoclast activity and are clinically promising, in particular with regard to the treatment and prevention of excessive pathological bone-resorption conditions, such as in osteoporotic patients. The present study implies that preserving functional adiponectin sensitivity in patients suffering from metabolic diseases (e.g., diabetes, obesity, metabolic syndrome) might be also beneficial for preventing bone fragility.

# MATERIALS AND METHODS

## Key Resources Table

| Reagent or resource | Source | Identifier |
|---|---|---|
| **Antibodies** | | |
| Neutralizing adiponectin receptor 1 polyclonal antibody | Enzo life science | ALX-210-645-C200 |
| Adiponectin rabbit monoclonal antibody | Cell signaling technology | #2789 |
| AMPK(Rabbit mAb (D63G4) | Cell signaling technology | #5832 |
| Phospho-AMPKα (Thr172) (40H9) Rabbit mAb | Cell signaling technology | #2535 |
| **Chemicals, peptides, and recombinant proteins** | | |
| Fetal Bovine Serum | GIBCO | 10082139 |
| Alpha MEM with NTP, dNTP | GIBCO | 22571 |
| AdipoRon | SIGMA | SML0998 |
| mRANKL | R&D systems | 462-TEC |
| hRANKL | R&D systems | 6449-TEC |
| **Critical commercial assays** | | |
| Acid Phosphatase, Leukocyte (TRAP) assay | SIGMA | 387A |
| murine serum CTX ELISA | LSBio | F21349 |
| murine serum OCN ELISA | LSBio | F12227 |
| murine serum PTH ELISA | LSBio | F23085 |
| **Experimental models: cell lines** | | |
| 3T3-L1 pre adipose murine cell line | ATCC | CL-173 |
| RAW 264.7 murine macrophage | ATCC | TIB-71 |
| **Experimental models: organisms/strains** | | |
| Sox2-Cre mouse | The Jackson Laboratory | 004783 |
| Adipoq-Cre mouse | The Jackson Laboratory | 010803 |
| Pparγ L2/L2 mouse | B Desvergne | |
| AZIP/F1 tg mouse | C Vinson | |
| **Oligonucleotides (primers): see Supplementary Table 1** | | |
| **Software and algorithms** | | |
| CTan CTVol | Skyscan | |
| ImageJ | Fiji | |

## Mouse Models

Genotype denomination follows the rules recommended by the Mouse Genome Database (MGD) Nomenclature Committee. Animal procedures were authorized by the Canton of Vaud veterinary service. Sox2CRE transgenic mice [$SOX2CRE^{tg/+}$; Tg(Sox2-cre)1Amc/J] and AdipoQCRE ($Adipoq\text{-}Cre^{tg/+}$) from The Jackson Laboratory, were maintained in the University of Lausanne Animal Facility. The series of matings allowing the

generation of the SOX2CRE$^{tg/+}$*Pparg*$^{em\,\Delta/\Delta}$ mouse (hereafter called *Pparg*$^{\Delta/\Delta}$), which expressed the SOX2CRE transgene and have no *Pparγ* functional alleles, as well as their control littermates (CTL) that have no SOX2CRE transgene and two functional *Pparγ* alleles (*Pparg*$^{fl/+}$) have been described in Gilardi et al. (2019). The resulting genetic background of these mice are a mix of C57Bl6 and SV129L. Pparg$^{adipoKO}$ and their control littermates were generated as described in Wang et al. (2013), in a mixed genetic background C57Bl6 and SV129L. AZIP/F1 mice on FVB background [Tg(AZIP/F)1Vsn in MGD, herein called AZIP$^{tg/+}$] and wild type FVB controls were a kind gift from Dr. Charles Vinson and were generated as previously described (Moitra et al., 1998).

## Primary Cell Culture

Mouse bone marrow cells were isolated by crushing entire long bones into DMEM/3% FCS (GIBCO). Bone fragments were removed by filtration through a 70 μm filter mesh. Splenocyte suspensions were obtained by mashing the spleen through sieves into DMEM/3% FCS, washing by centrifugation then filtering through 70 μm filter caps. Primary osteoblasts from neonatal calvaria of *Pparg*$^{fl/+}$ and *Pparg*$^{\Delta/\Delta}$ were harvested by sequential collagenase type II (3 mg/mL) digestions of individual calvarium from 2 to 3-day-old mice. After genotyping, calvaria cells of the same genotype were pooled and plated accordingly. The cells were incubated at 37°C with 5% CO2 and media was changed every 2 days until they reached 80% confluency. To assess proliferation, primary osteoblasts were plated in 24-well plates at a concentration of 10,000 cells/well in EMEM media (GIBCO) containing 10% FBS, 100 U/ml penicillin and 100 ug/ml streptomycin (GIBCO).

## Osteoclastogenesis Assays and TRAcP Staining of Murine and Human Primary Cells

Erythrocytes were eliminated from murine splenocyte and BM preparation or human PBMC using ACK lysis buffer. When indicated, osteoclasts were also derived from CD11b$^{+}$ monocytic cells (MN-OCLs) and bone marrow-derived CD11c$^{+}$ dendritic cells (DC-OCLs) as described previously (Ibáñez et al., 2016). Cells were cultured in complete αMEM with 40 ng/ml M-CSF (ProSpec-Tany TechnoGene, Rehovat, Israel) and l0 ng/ml RANKL (R&D Systems, MN). Tartrate-resistant acid phosphatase (TRAcP) staining was performed after 4–6 days, using the Acid Phosphatase, Leukocyte (TRAP) Kit according to the manufacturer's instructions (Sigma). Mature osteoclasts were identified as multi-nucleate TRAcP$^{+}$ cells using light microscopy. 3T3-L1 cells (ATCC) were grown to sub-confluence in DMEM/10% FBS. Cells were then cultured in adipogenic conditions [DMEM/10%FBS, 0.5 mM 3-isobutyl-1-methylxanthine, 1 μM dexamethasone (Sigma), and 10 μg/ml bovine insulin (Sigma)] for 2 weeks, after which the medium was changed back to DMEM/10% FBS. Adipocyte Conditioned Medium (A-CM) was collected after 24 hours exposure to differentiated cells. Similarly, conditioned control medium (CTL) was obtained from undifferentiated 3T3-L1 cells. A-CM and CTL were concentrated 5X using Centriprep$^{TM}$ (Millipore). Conditioned medium from either differentiated or undifferentiated 3T3-L1 cells was added during osteoclastogenesis from multipotent progenitor cells. For neutralization experiments, 50% CM was incubated with different amounts of anti-adiponectin antibody (Enzo Life Sciences) for 30 min at room temperature then added during osteoclastogenesis. TRAcP staining to evaluate osteoclast numbers was performed as mentioned above.

## Osteoclast Differentiation and TRAcP Staining of RAW 264.7 Cells

For osteoclastogenesis, a total of $1 \times 10^4$ RAW 264.7 (ATCC) cells were seeded per well on 24-well plates in 500 μl αMEM containing 5% FCS (Hyclone, GE Healthcare), 1% penicillin-streptomycin (Gibco) as well as 50 μM β-mercaptoethanol (Gibco) and 30 ng/ml murine RANKL (R&D Systems). To study the impact of adiporon on osteoclast differentiation, 10 μM AdipoRon (Sigma-Aldrich) were added to the culture medium. Tartrate-resistant acid phosphatase (TRAcP) activity was examined using the leucocyte acid phosphatase kit (Sigma-Aldrich) according to manufacturer's specifications. TRAcP$^{+}$ cells with ≥3 nuclei were considered as osteoclasts. In addition, $5 \times 10^3$ RAW 264.7 cells were seeded per well in a Nunc Lab-Tek II 8-well Chamber Slide system (ThermoFisher Scientific) in a total of 300 μl osteoclast differentiation medium containing 30 ng/ml RANKL. Fully differentiated osteoclasts were treated with 10 μM AdipoRon for the indicated time points. FACS analysis as well as sorting of mature OCLs for subsequent Western-blot analyses was performed as described previously (Madel et al., 2018).

## Measurement of Bone Morphology and Microarchitecture

Unless otherwise indicated, 1-year old females of each genotype were used for bone analyses.

High-resolution micro-computed tomography (UCT40, ScancoMedical AG, Bassdorf, Switzerland) was used to scan the femur and the 5th lumber vertebral body. Data were calibrated against a phantom, which has a known hydroxyapatite value. For the vertebral trabecular region, we evaluated ∼300 transverse CT slices between the cranial and caudal end plates, excluding 100 μm near each endplate. Femoral cortical geometry was assessed in a 1 mm−long region centered at the femoral midshaft. CT images were reconstructed in 1,024 × 1,024 pixel matrices using a standard convolution-backprojection procedure, and the resulting gray−scale images were segmented using a constrained 3D Gaussian filter ($\sigma = 0.8$, support = 1.0) to remove noise, and a fixed threshold (22 and 30% of maximal gray scale value for trabecular bone and cortical bone, respectively) was used to extract the structure of mineralized tissue.

Cortical and trabecular bones were evaluated using isotropic 12μm voxels. For trabecular bones, we assessed bone volume fraction (BV/TV,%), trabecular thickness (Tb.Th, μm), trabecular number (Tb.N, $mm^{-1}$), and trabecular separation (Tb.Sp, μm). For cortical midshaft femur, we measured the average total

volume (TV, $mm^3$), bone volume (BV, $mm^3$), and average cortical thickness (μm). SkyScan software (CTAn and CTVol) was employed to calculate cortical bone porosity of femur using a dedicate method after acquisition using a Skyscan 1272 (SkyScan 1272, Bruker, Brussels, Belgium) at a resolution of 10 μm/pix, and a threshold set up at 100–255, finally visualized in 3D.

## Serum Protein Assays

Blood was obtained by cardiac puncture immediately after euthanasia. After clotting and centrifugation, serum was collected and stored at −80°C until use. Serum CTX (carboxy-terminal collagen crosslinks), osteocalcin (OCN), alkaline phosphatase (ALP), and parathyroid hormone (PTH) were measured by ELISA assays according to the manufacturer's protocol (LifeSpan Biosciences, Inc., Seattle, WA).

## Calvaria Injection

Nine 6-week old C57/BL6 male mice were purchased from Envigo and housed in the local animal facility under a 12 h light/12 h dark cycle. The animals were randomly divided into three experimental groups, each group comprising three mice. Mice received daily *s.c.* injections on the calvaria before analysis on the third day. Group 1 was injected with 100 μg lipopolysaccharide from *Salmonella abortus equi* (LPS, Sigma-Aldrich), group 2 with 100 μg LPS + 500 ng AdipoRon (Sigma-Aldrich) and experimental group 3 underwent vehicle (PBS) injection. Calvariae were collected and fixed overnight in 4% formaldehyde at 4°C and then stored in 70% EtOH. Subsequent micro-CT analysis were used to evaluate the resorbed area. Calvariae were decalcified in 10% EDTA, embedded in paraffin and 5-micron sections were cut and stained for tartrate-resistant acid phosphatase (TRAcP, Sigma-Aldrich).

## Quantitative RT-PCR

Total RNA was isolated from total long bones, including the crude BM, or primary cell cultures, using TRIzol LS (Invitrogen) and purified with the RNeasy kit (Qiagen). RNA quality was verified by microfluidic (Agilent 2100 Bioanalyzer) and concentration determined with a NanoDrop spectrophotometer (Wilmington). Total RNA (500 ng/μg) was reverse transcribed using Script™ cDNA synthesis kit (Bio-Rad) according to the manufacturer's instructions. Real time qPCR was performed with SYBR® Green PCR mastermix using an ABI PRISM® 7900 PCR machine (Applied Biosystems). Results were normalized to glyceraldehyde-3-phosphate dehydrogenase (*Gapdh*) or beta-actin beta (*Actb*). The primer sets are indicated in the **Supplementary Table S1**.

## Western Blot Analysis

Mature OCLs were sorted based on their nuclei number (≥3) following the protocol described in Madel et al. (2018). This protocol ensures that further analyses (FACS and western-blot analysis) are made with a pure mature cell population, avoiding contaminant effects due to the important number of non-osteoclastic cells always present in classical culture, as reported (Madel et al., 2018). The sorted mature OCLs were washed twice with ice-cold PBS and scraped in 1X Laemmli buffer. Cells were disrupted by sonication and centrifuged at 3,000 rpm for 10 min. Protein samples were analyzed by SDS/PAGE (gradient 4–15% acrylamide, Criterion, BioRad) and electroblotted onto 0.2% PVDF membrane using Transblot Turbo (BioRad). After 1 h in blocking buffer (Tris-buffered saline (TBS)–Tween 20 with 5% fat free dry milk), membranes were blotted overnight at 4°C with Rabbit mAb against AMPKα (D63G4) (dilution 1:1,000, Cell Signaling Technology) or Phospho-AMPKα (Thr172) (40H9) (dilution 1:1,000, Cell Signaling Technology), diluted in TBS–Tween with 5% BSA. After three washing steps with TBS–Tween 20, blot was incubated for 1 h at room temperature with anti-rabbit IgG conjugated with horseradish peroxidase diluted 1:2,000 in blocking buffer. After four additional washing steps with TBS–Tween 20, protein bands were detected by chemiluminescence using Chemi Doc XRS + (BioRad).

## Imaging

Podosomes were visualized by phalloidin staining (Sigma-Aldrich) following manufacturer's instructions. After removing unbound phalloidin conjugates, cells were labeled with 1 μg/ml DAPI (Sigma-Aldrich). Microscopic imaging was performed using a fluorescence microscope (Zeiss Axio Observer D1). For mitochondrial analysis, live cells were labeled with 200 nM MitoTracker Orange (ThermoFisher) according to manufacturer's recommendations. After staining, cells were fixed in 4% formaldehyde, labeled with 1 μg/ml DAPI and subjected to z-stack confocal microscopy analyses (Zeiss LSM 710 on an inverted Axio Observer.Z1 stand). Images were processed using Fiji/Image J software (Schindelin et al., 2012).

## Statistical Analysis

The data were analyzed using one- or two-factor ANOVA for multiple comparisons as appropriate. Two-group comparisons were performed using the Student's *t*-test. ns: non-significant, $^{*}p < 0.05$, $^{**}p < 0.01$, $^{***}p < 0.001$, $^{****}p < 0.0001$.

# DATA AVAILABILITY STATEMENT

The original contributions presented in the study are included in the article/**Supplementary Material**, further inquiries can be directed to the corresponding author/s.

# ETHICS STATEMENT

The animal study was reviewed and approved by the Canton of Vaud Veterinary Service.

# AUTHOR CONTRIBUTIONS

HF designed the experimental plan, performed the experiments, analyzed the data, and contribute to the original draft preparation. M-BM, DP, MS, CW, AW, CP, MT, and BT performed experiments, analyzed the data, and prepared the visualization. J-YJ, FG, SF, NB, and CB-W contributed to the

conceptualization, analyzed the data, and reviewed/edited the manuscript. BD and DM conceived the study, designed the experimental plan, supervised the study, analyzed the data, wrote the manuscript, and acquired financial support for the project, were the guarantors of this work and, as such, had full access to all the data in the study and take responsibility for the integrity of the data and the accuracy of the data analyses. All authors read and edited the manuscript.

## FUNDING

This work was supported by the Etat de Vaud (BD and AW) the FNRS 31003A-135583/1 (BD), the Région Grand Est (J-YJ), the Fondation Arthritis (DM), the French PIA project Lorraine Université d'Excellence, reference ANR-15-IDEX-04-LUE (J-YJ and DM) and the Fondation pour la Recherche Médicale (FRM, ECO20160736019) (M-BM).

## ACKNOWLEDGMENTS

We would like to acknowledge the Montpellier preclinical platform of ECELLFRANCE for the μCT analysis (IRMB, Montpellier, France) and the microCT platform SC3M from the RMeS Lab, INSERM UMRS 1229 (Nantes, France).

## SUPPLEMENTARY MATERIAL

The Supplementary Material for this article can be found online at: https://www.frontiersin.org/articles/10.3389/fcell.2021.627153/full#supplementary-material

**Supplementary Video 1 |** Video of 3D micro-CT reconstruction of genetically induced lipoatrophic mice showing alterations of both trabecular and cortical femoral bone.

**Supplementary Figure 1 |** Osteoblastic activity is increased in mice with epiblastic deletion of PPAR**g**. **(A)** Representative 3-D micro-CT of the fourth lumbar vertebrae of CTL and *Pparg*$^{\Delta/\Delta}$ ($\gamma^{\Delta/\Delta}$) mice. $n$ = 5 WT and 5 $\gamma^{\Delta/\Delta}$. **(B)** Trabecular bone volume fraction measured by micro-CT analysis of vertebra from $\gamma^{\Delta/\Delta}$ ($n$ = 5) and control (CTL; $n$ = 5) littermates. **(C)** Trabecular connectivity density measured by micro-CT analysis of vertebra from $\gamma^{\Delta/\Delta}$ ($n$ = 5) and control (CTL; $n$ = 5) littermates. **(D)** *Keratocan* and *Sost* mRNA levels in long bones of CTL ($n$ = 6) and $\gamma^{\Delta/\Delta}$ ($n$ = 6) mice.

**Supplementary Figure 2 |** Parathyroid hormone (PTH) signaling. The serum levels of PTH were assessed by Elisa Assay in 1-year-old male and female mice (*Pparg*$^{\Delta/\Delta}$, AZIP$^{tg/+}$, and their control littermates). Six males and six females were included per genotype. As there were no statistically significant differences between males and females, the analysis was performed using the total number of mice (mean ± *SD*). Lower panels: mRNA expression levels of Pth1r in the bones and in the kidneys of CTL vs. *Pparg*$^{\Delta/\Delta}$ mice.

**Supplementary Figure 3 |** Adiponectin expression levels in long bone and in adipocyte-conditioned medium. RT-qPCR analysis of *Leptin* and *AdipoQ* mRNA levels in long bone from A-ZIP$^{tg/+}$ ($n$ = 8) and their CTL littermates ($n$ = 8) and from $\gamma^{\Delta/\Delta}$ ($n$ = 7) and their CTL littermates ($n$ = 6). Data are presented as mean ± S.E.M. Statistical significance was determined by two-tailed unpaired *t*-test.

**Supplementary Figure 4 |** AdipoRon inhibits osteoclast (OCL) differentiation of various origins. Left panels: representative images of TRAcP stained **(A)** BM-derived, **(B)** spleen derived, and **(C)** macrophages enriched fraction osteoclasts differentiated in the presence or absence of AdipoRon (5 μM). *Right panels*: the mean IC50 of AdipoRon inhibition of OCL differentiation was determined from the curve with the error of the fit (S.E.M.) Data are mean ± S.E.M. ($n$ = 3 biological replicates).

**Supplementary Figure 5 |** AdipoRon inhibits human osteoclast (OCL) differentiation and activity through AMPK activation. **(A)** Dose response effect of AdipoRon on osteoclast differentiation from hPBMC ($n$ = 5). **(B)** Representative images of TRAcP staining of hPBMC derived osteoclast differentiation in the presence or absence of AdipoRon (5(μM). **(C)** Western-blot analysis of hPBMC-derived osteoclasts treated with AdipoRon (5(μM). AdipoRon treatment activates AMPK phosphorylation (p-AMPK) in hPBMC after 5 min. **(D)** Fluorescence microscopy of phalloidin-marked podosomes in hPBMC derived OCL in the presence of AdipoRon (5 μM, 12 h) (representative images of $n$ = 5).

**Supplementary Table 1 |** Primers used for q-RT-PCR.

## REFERENCES

Akune, T., Ohba, S., Kamekura, S., Yamaguchi, M., Chung, U.-I., Kubota, N., et al. (2004). PPARgamma insufficiency enhances osteogenesis through osteoblast formation from bone marrow progenitors. *J. Clin. Invest.* 113, 846–855. doi: 10.1172/jci200419900

Ali, A. A., Weinstein, R. S., Stewart, S. A., Parfitt, A. M., Manolagas, S. C., and Jilka, R. L. (2005). Rosiglitazone causes bone loss in mice by suppressing osteoblast differentiation and bone formation. *Endocrinology* 146, 1226–1235. doi: 10.1210/en.2004-0735

Ausk, B. J., Huber, P., Srinivasan, S., Bain, S. D., Kwon, R. Y., McNamara, E. A., et al. (2013). Metaphyseal and diaphyseal bone loss in the tibia following transient muscle paralysis are spatiotemporally distinct resorption events. *Bone* 57, 413–422. doi: 10.1016/j.bone.2013.09.009

Barak, Y., Nelson, M. C., Ong, E. S., Jones, Y. Z., Ruiz-Lozano, P., Chien, K. R., et al. (1999). PPAR gamma is required for placental, cardiac, and adipose tissue development. *Mol. Cell* 4, 585–595. doi: 10.1016/s1097-2765(00)80209-9

Baryawno, N., Przybylski, D., Kowalczyk, M. S., Kfoury, Y., Severe, N., Gustafsson, K., et al. (2019). A cellular taxonomy of the bone marrow stroma in homeostasis and leukemia. *Cell* 177, 1915–1932.e16.

Calo, E., Quintero-Estades, J. A., Danielian, P. S., Nedelcu, S., Berman, S. D., and Lees, J. A. (2010). Rb regulates fate choice and lineage commitment in vivo. *Nature* 466, 1110–1114. doi: 10.1038/nature09264

Cawthorn, W. P., Scheller, E. L., Learman, B. S., Parlee, S. D., Simon, B. R., Mori, H., et al. (2014). Bone marrow adipose tissue is an endocrine organ that contributes to increased circulating adiponectin during caloric restriction. *Cell Metab.* 20, 368–375. doi: 10.1016/j.cmet.2014.06.003

Chen, G., Huang, L., Wu, X., Liu, X., Xu, Q., Li, F., et al. (2018). Adiponectin inhibits osteoclastogenesis by suppressing NF-(B and p38 signaling pathways. *Biochem. Biophys. Res. Commun.* 503, 2075–2082. doi: 10.1016/j.bbrc.2018.07.162

Cornish, J., Wang, T., and Lin, J.-M. (2018). Role of marrow adipocytes in regulation of energy metabolism and bone homeostasis. *Curr. Osteoporos. Rep.* 16, 116–122. doi: 10.1007/s11914-018-0425-0

Ducy, P., Amling, M., Takeda, S., Priemel, M., Schilling, A. F., Beil, F. T., et al. (2000). Leptin inhibits bone formation through a hypothalamic relay: a central control of bone mass. *Cell* 100, 197–207. doi: 10.1016/s0092-8674(00)81558-5

Engsig, M. T., Chen, Q. J., Vu, T. H., Pedersen, A. C., Therkidsen, B., Lund, L. R., et al. (2000). Matrix metalloproteinase 9 and vascular endothelial growth factor are essential for osteoclast recruitment into developing long bones. *J. Cell Biol.* 151, 879–889. doi: 10.1083/jcb.151.4.879

Felson, D. T., Zhang, Y., Hannan, M. T., and Anderson, J. J. (1993). Effects of weight and body mass index on bone mineral density in men and women: the framingham study. *J. Bone Miner. Res.* 8, 567–573. doi: 10.1002/jbmr.5650080507

Fuller, K., Wong, B., Fox, S., Choi, Y., and Chambers, T. J. (1998). TRANCE is necessary and sufficient for osteoblast-mediated activation of bone resorption in osteoclasts. *J. Exp. Med.* 188, 997–1001. doi: 10.1084/jem.188.5.997

Gilardi, F., Winkler, C., Quignodon, L., Diserens, J.-G., Toffoli, B., Schiffrin, M., et al. (2019). Systemic PPAR(deletion in mice provokes lipoatrophy, organomegaly, severe type 2 diabetes and metabolic inflexibility. *Metab. Clin. Exp.* 95, 8–20. doi: 10.1016/j.metabol.2019.03.003

Grey, A. (2008). Skeletal consequences of thiazolidinedione therapy. *Osteoporos. Int.* 19, 129–137. doi: 10.1007/s00198-007-0477-y

Horowitz, M. C., Berry, R., Holtrup, B., Sebo, Z., Nelson, T., Fretz, J. A., et al. (2017). Bone marrow adipocytes. *Adipocyte* 6, 193–204.

Ibáñez, L., Abou-Ezzi, G., Ciucci, T., Amiot, V., Belaïd, N., Obino, D., et al. (2016). Inflammatory osteoclasts prime TNF(-producing CD4(T cells and express CX3 CR1. *J. Bone Miner. Res.* 31, 1899–1908. doi: 10.1002/jbmr.2868

Idris, A. I., Sophocleous, A., Landao-Bassonga, E., Canals, M., Milligan, G., Baker, D., et al. (2009). Cannabinoid receptor type 1 protects against age-related osteoporosis by regulating osteoblast and adipocyte differentiation in marrow stromal cells. *Cell Metab.* 10, 139–147. doi: 10.1016/j.cmet.2009.07.006

Imai, T., Takakuwa, R., Marchand, S., Dentz, E., Bornert, J.-M., Messaddeq, N., et al. (2004). Peroxisome proliferator-activated receptor gamma is required in mature white and brown adipocytes for their survival in the mouse. *Proc. Natl. Acad. Sci. U.S.A.* 101, 4543–4547. doi: 10.1073/pnas.0400356101

Iwabu, M., Yamauchi, T., Okada-Iwabu, M., Sato, K., Nakagawa, T., Funata, M., et al. (2010). Adiponectin and AdipoR1 regulate PGC-1alpha and mitochondria by Ca(2() and AMPK/SIRT1. *Nature* 464, 1313–1319. doi: 10.1038/nature08991

Iwaki, M., Matsuda, M., Maeda, N., Funahashi, T., Matsuzawa, Y., Makishima, M., et al. (2003). Induction of adiponectin, a fat-derived antidiabetic and antiatherogenic factor, by nuclear receptors. *Diabetes* 52, 1655–1663. doi: 10.2337/diabetes.52.7.1655

Jemtland, R., Lee, K., and Segre, G. V. (1998). Heterogeneity among cells that express osteoclast-associated genes in developing bone. *Endocrinology* 139, 340–349. doi: 10.1210/endo.139.1.5664

Jilka, R. L., O'Brien, C. A., Roberson, P. K., Bonewald, L. F., Weinstein, R. S., and Manolagas, S. C. (2014). Dysapoptosis of osteoblasts and osteocytes increases cancellous bone formation but exaggerates cortical porosity with age. *J. Bone Miner. Res.* 29, 103–117. doi: 10.1002/jbmr.2007

Kahn, S. E., Zinman, B., Lachin, J. M., Haffner, S. M., Herman, W. H., Holman, R. R., et al. (2008). Rosiglitazone-associated fractures in type 2 diabetes: an analysis from a diabetes outcome progression trial (ADOPT). *Diabetes Care* 31, 845–851. doi: 10.2337/dc07-2270

Kajimura, D., Lee, H. W., Riley, K. J., Arteaga-Solis, E., Ferron, M., Zhou, B., et al. (2013). Adiponectin regulates bone mass via opposite central and peripheral mechanisms through FoxO1. *Cell Metab.* 17, 901–915. doi: 10.1016/j.cmet.2013.04.009

Kawai, M., and Rosen, C. J. (2010). PPAR(: a circadian transcription factor in adipogenesis and osteogenesis. *Nat. Rev. Endocrinol.* 6, 629–636. doi: 10.1038/nrendo.2010.155

Lazarenko, O. P., Rzonca, S. O., Hogue, W. R., Swain, F. L., Suva, L. J., and Lecka-Czernik, B. (2007). Rosiglitazone induces decreases in bone mass and strength that are reminiscent of aged bone. *Endocrinology* 148, 2669–2680. doi: 10.1210/en.2006-1587

Levin, A., Bakris, G. L., Molitch, M., Smulders, M., Tian, J., Williams, L. A., et al. (2007). Prevalence of abnormal serum vitamin D, PTH, calcium, and phosphorus in patients with chronic kidney disease: results of the study to evaluate early kidney disease. *Kidney Int.* 71, 31–38. doi: 10.1038/sj.ki.5002009

Li, Y., Meng, Y., and Yu, X. (2019). The unique metabolic characteristics of bone marrow adipose tissue. *Front. Endocrinol.* 10:69. doi: 10.1016/j.bone.2018.01.009

Liu, L.-F., Shen, W.-J., Ueno, M., Patel, S., and Kraemer, F. B. (2011). Characterization of age-related gene expression profiling in bone marrow and epididymal adipocytes. *BMC Genomics* 12:212.

Madel, M.-B., Ibáñez, L., Rouleau, M., Wakkach, A., and Blin-Wakkach, C. (2018). A novel reliable and efficient procedure for purification of mature osteoclasts allowing functional assays in mouse cells. *Front. Immunol.* 9:2567.

Madel, M.-B., Ibáñez, L., Wakkach, A., de Vries, T. J., Teti, A., Apparailly, F., et al. (2019). Immune function and diversity of osteoclasts in normal and pathological conditions. *Front. Immunol.* 10:1408.

Moitra, J., Mason, M. M., Olive, M., Krylov, D., Gavrilova, O., Marcus-Samuels, B., et al. (1998). Life without white fat: a transgenic mouse. *Genes Dev.* 12, 3168–3181. doi: 10.1101/gad.12.20.3168

Mukohira, H., Hara, T., Abe, S., Tani-ichi, S., Sehara-Fujisawa, A., Nagasawa, T., et al. (2019). Mesenchymal stromal cells in bone marrow express adiponectin and are efficiently targeted by an adiponectin promoter-driven cre transgene. *Int. Immunol.* 45, 1219–1213.

Naot, D., Watson, M., Callon, K. E., Tuari, D., Musson, D. S., Choi, A. J., et al. (2016). Reduced bone density and cortical bone indices in female adiponectin-knockout mice. *Endocrinology* 157, 3550–3561. doi: 10.1210/en.2016-1059

Okada-Iwabu, M., Yamauchi, T., Iwabu, M., Honma, T., Hamagami, K.-I., Matsuda, K., et al. (2013). A small-molecule AdipoR agonist for type 2 diabetes and short life in obesity. *Nature* 503, 493–499. doi: 10.1038/nature12656

Oshima, K., Nampei, A., Matsuda, M., Iwaki, M., Fukuhara, A., Hashimoto, J., et al. (2005). Adiponectin increases bone mass by suppressing osteoclast and activating osteoblast. *Biochem. Biophys. Res. Commun.* 331, 520–526. doi: 10.1016/j.bbrc.2005.03.210

Pacheco-Pantoja, E. L., Waring, V. J., Wilson, P. J. M., Fraser, W. D., and Gallagher, J. A. (2013). Adiponectin receptors are present in RANK-L-induced multinucleated osteoclast-like cells. *J. Recept. Signal Transduct. Res.* 33, 291–297. doi: 10.3109/10799893.2013.828070

Poloni, A., Maurizi, G., Serrani, F., Mancini, S., Zingaretti, M. C., Frontini, A., et al. (2013). Molecular and functional characterization of human bone marrow adipocytes. *Exp. Hematol.* 41, 558–566.e2.

Rinotas, V., Niti, A., Dacquin, R., Bonnet, N., Stolina, M., Han, C.-Y., et al. (2014). Novel genetic models of osteoporosis by overexpression of human RANKL in transgenic mice. *J. Bone Miner. Res.* 29, 1158–1169. doi: 10.1002/jbmr.2112

Rosen, E. D., Sarraf, P., Troy, A. E., Bradwin, G., Moore, K., Milstone, D. S., et al. (1999). PPAR gamma is required for the differentiation of adipose tissue in vivo and in vitro. *Mol. Cell* 4, 611–617.

Rzonca, S. O., Suva, L. J., Gaddy, D., Montague, D., and Lecka-Czernik, B. (2004). Bone is a target for the antidiabetic compound rosiglitazone. *Endocrinology* 145, 401–406. doi: 10.1210/en.2003-0746

Sardella, C., Winkler, C., Quignodon, L., Hardman, J. A., Toffoli, B., Giordano Attianese, G. M. P., et al. (2018). Delayed hair follicle morphogenesis and hair follicle dystrophy in a lipoatrophy mouse model of pparg total deletion. *J. Invest. Dermatol.* 138, 500–510. doi: 10.1016/j.jid.2017.09.024

Schindelin, J., Arganda-Carreras, I., Frise, E., Kaynig, V., Longair, M., Pietzsch, T., et al. (2012). Fiji: an open-source platform for biological-image analysis. *Nat. Methods* 9, 676–682. doi: 10.1038/nmeth.2019

Sheu, Y., and Cauley, J. A. (2011). The role of bone marrow and visceral fat on bone metabolism. *Curr. Osteoporos. Rep.* 9, 67–75. doi: 10.1007/s11914-011-0051-6

Shinoda, Y., Yamaguchi, M., Ogata, N., Akune, T., Kubota, N., Yamauchi, T., et al. (2006). Regulation of bone formation by adiponectin through autocrine/paracrine and endocrine pathways. *J. Cell. Biochem.* 99, 196–208. doi: 10.1002/jcb.20890

Sun, H., Kim, J. K., Mortensen, R., Mutyaba, L. P., Hankenson, K. D., and Krebsbach, P. H. (2013). Osteoblast-Targeted suppression of PPAR(increases osteogenesis through activation of mTOR signaling. *Stem Cell* 31, 2183–2192. doi: 10.1002/stem.1455

Takada, I., Kouzmenko, A. P., and Kato, S. (2009). Wnt and PPAR(signaling in osteoblastogenesis and adipogenesis. *Nat. Rev. Rheumatol.* 5, 442–447. doi: 10.1038/nrrheum.2009.137

Toffoli, B., Gilardi, F., Winkler, C., Soderberg, M., Kowalczuk, L., Arsenijevic, Y., et al. (2017). Nephropathy in Pparg-null mice highlights PPAR(systemic activities in metabolism and in the immune system. *PLoS One* 12:e0171474. doi: 10.1371/journal.pone.0171474

Tontonoz, P., and Spiegelman, B. M. (2008). Fat and beyond: the diverse biology of PPARgamma. *Annu. Rev. Biochem.* 77, 289–312. doi: 10.1146/annurev.biochem.77.061307.091829

Tu, Q., Zhang, J., Dong, L. Q., Saunders, E., Luo, E., Tang, J., et al. (2011). Adiponectin inhibits osteoclastogenesis and bone resorption via APPL1-mediated suppression of Akt1. *J. Biol. Chem.* 286, 12542–12553. doi: 10.1074/jbc.m110.152405

Wan, Y. (2010). PPAR in bone homeostasis. *Trends Endocrinol. Metab.* 21, 722–728.

Wan, Y., Chong, L.-W., and Evans, R. M. (2007). PPAR-gamma regulates osteoclastogenesis in mice. *Nat. Med.* 13, 1496–1503. doi: 10.1038/nm1672

Wang, F., Mullican, S. E., DiSpirito, J. R., and Peed, L. C. (2013). Lipoatrophy and severe metabolic disturbance in mice with fat-specific deletion of PPAR. *Proc. Natl. Acad. Sci. U.S.A.* 110, 18656–18661. doi: 10.1073/pnas.1314863110

Wang, Q.-P., Li, X.-P., Wang, M., Zhao, L.-L., Li, H., Xie, H., et al. (2014). Adiponectin exerts its negative effect on bone metabolism via OPG/RANKL pathway: an in vivo study. *Endocrine* 47, 845–853. doi: 10.1007/s12020-014-0216-z

Yamaguchi, N., Kukita, T., Li, Y.-J., Kamio, N., Fukumoto, S., Nonaka, K., et al. (2008). Adiponectin inhibits induction of TNF-alpha/RANKL-stimulated NFATc1 via the AMPK signaling. *FEBS Lett.* 582, 451–456. doi: 10.1016/j.febslet.2007.12.037

Yang, J., Park, O.-J., Kim, J., Han, S., Yang, Y., Yun, C.-H., et al. (2019). Adiponectin deficiency triggers bone loss by up-regulation of osteoclastogenesis and down-regulation of osteoblastogenesis. *Front. Endocrinol.* 10:815.

Zou, W., Rohatgi, N., Chen, T. H.-P., Schilling, J., Abu-amer, Y., and Teitelbaum, S. L. (2016). PPAR- regulates pharmacological but not physiological or pathological osteoclast formation. *Nat. Med.* 22, 1203–1205. doi: 10.1038/nm.4208

**Conflict of Interest:** The authors declare that the research was conducted in the absence of any commercial or financial relationships that could be construed as a potential conflict of interest.

frontiers in Cell and Developmental Biology

REVIEW
published: 12 April 2021
doi: 10.3389/fcell.2021.641162

# Role of OSCAR Signaling in Osteoclastogenesis and Bone Disease

*Iva R. Nedeva[1], Mattia Vitale[1], Ari Elson[2], Judith A. Hoyland[1]* and Jordi Bella[1]**

[1] Division of Cell Matrix Biology and Regenerative Medicine, Faculty of Biology, Medicine and Health, School of Biological Sciences, University of Manchester, Manchester, United Kingdom, [2] Department of Molecular Genetics, The Weizmann Institute of Science, Rehovot, Israel

Formation of mature bone-resorbing cells through osteoclastogenesis is required for the continuous remodeling and repair of bone tissue. In aging and disease this process may become aberrant, resulting in excessive bone degradation and fragility fractures. Interaction of receptor-activator of nuclear factor-κB (RANK) with its ligand RANKL activates the main signaling pathway for osteoclastogenesis. However, compelling evidence indicates that this pathway may not be sufficient for the production of mature osteoclast cells and that co-stimulatory signals may be required for both the expression of osteoclast-specific genes and the activation of osteoclasts. Osteoclast-associated receptor (OSCAR), a regulator of osteoclast differentiation, provides one such co-stimulatory pathway. This review summarizes our present knowledge of osteoclastogenesis signaling and the role of OSCAR in the normal production of bone-resorbing cells and in bone disease. Understanding the signaling mechanism through this receptor and how it contributes to the production of mature osteoclasts may offer a more specific and targeted approach for pharmacological intervention against pathological bone resorption.

**Keywords: osteoclastogenesis, osteoclast-associated receptor, OSCAR, bone remodeling, bone disease, collagen, cell signaling**

OPEN ACCESS

***Edited by:***
*Catalina Dirney Alba Soto, University of Buenos Aires, Argentina*

***Reviewed by:***
*Jiake Xu, University of Western Australia, Australia*
*An Qin, Shanghai Ninth People's Hospital, China*
*Kai Chen, University of Western Australia, Australia*

***Correspondence:**
*Jordi Bella*
*jordi.bella@manchester.ac.uk*
*Judith A. Hoyland*
*judith.a.hoyland@manchester.ac.uk*

***Specialty section:***
*This article was submitted to Cellular Biochemistry, a section of the journal Frontiers in Cell and Developmental Biology*

***Received:*** *13 December 2020*
***Accepted:*** *15 March 2021*
***Published:*** *12 April 2021*

***Citation:***
*Nedeva IR, Vitale M, Elson A, Hoyland JA and Bella J (2021) Role of OSCAR Signaling in Osteoclastogenesis and Bone Disease. Front. Cell Dev. Biol. 9:641162. doi: 10.3389/fcell.2021.641162*

## SIGNALING PATHWAYS IN OSTEOCLASTOGENESIS

Bone tissue undergoes continuous remodeling throughout life at a rate of approximately 10% per year (Kenkre and Bassett, 2018). Such remodeling allows adequate repair of microdamage, as well as adaptation of mass, size and shape to load requirements, thereby ensuring optimal bone strength. Bone remodeling is under the strict control of an array of regulatory molecules, and is largely accomplished by the balanced activity of osteoclasts (OCLs), which resorb bone, and osteoblasts (OBLs), which lay new bone (Rucci, 2008). Several pathological states, autoimmune conditions, certain malignancies and prolonged immobilization may tip the balance in favor of increased bone resorption (Brounais et al., 2008; Iseme et al., 2017; Napoli et al., 2017; Bilezikian et al., 2019). The normal process of aging also alters the activity of OCLs and OBLs in favor of increased bone degradation (Seeman, 2019).

Loss of bone mass is more often associated with dysregulated OCL production and function rather than impaired OBL activity (Feng and Teitelbaum, 2013). Thus, implementing successful strategies for inhibition of excessive bone resorption requires thorough understanding of the mechanisms governing the proliferation, differentiation and activation of OCLs (Yavropoulou and Yovos, 2008; Park-Min, 2018). While considerable research efforts have been dedicated to the main

osteoclastogenesis signaling pathway mediated through receptor activator of nuclear factor-κB (RANK), there are significant gaps in our understanding of the role of the co-stimulatory molecules in this process. Here we review briefly the key steps in OCL differentiation and summarize the current evidence relating to the role of the osteoclast-associated receptor (OSCAR).

## The Osteoclast Cell

OCLs develop from haematopoietic stem cells through a series of morphological and functional transformations that lead to the establishment of multinucleated polarized cells (Kodama and Kaito, 2020). These are able to migrate toward bone, adhere to it, and resorb the tissue beneath in a controlled manner (Bruzzaniti and Baron, 2006; Teitelbaum, 2007). OCLs express proteins that participate both in bone demineralisation and in the degradation of the demineralised organic matrix. Mutations affecting the expression or function of these proteins impair bone resorption and lead to osteopetrosis (Bruzzaniti and Baron, 2006; Teitelbaum, 2007; Sobacchi et al., 2013; Palagano et al., 2018). **Table 1** summarizes data on genetic knockout mice discussed in the text below.

OCL attachment to bone is largely mediated by $\alpha_v\beta_3$ integrin, which binds to matrix proteins containing arginine-glycine-aspartate (RGD) sequences such as bone sialoprotein and osteopontin. Failure of $\alpha_v\beta_3$ expression results in defective cell attachment and spreading, and in deficient bone resorption (Ross and Teitelbaum, 2005; Brunner et al., 2013). Once attached, OCLs undergo cytoskeletal rearrangement that leads to the establishment of distinct apical and basolateral membrane surfaces. The basolateral surface is located distal to the bone and is enriched in $Na^+/K^+$-ATPase, transport proteins, and receptors involved in the regulation of OCL survival, differentiation and activity (discussed below). The apical surface faces the bone and forms a ruffled border through multiple, deep infoldings of the cell membrane. This ruffled appearance is due to the continuous exocytosis of secretory vesicles containing enzymes such as matrix metalloproteinase 9 (MMP-9), tartrate-resistant acid phosphatase (TRAP) or cathepsin K, which degrade the organic components of the bone. The apical surface is also rich in $H^+$-ATPase, which actively secretes protons into the underlying extracellular compartment inducing acidification and demineralization of the bone area beneath the cell (Bruzzaniti and Baron, 2006). The membrane surrounding the ruffled border (sealing zone) seals off the resorption pit and creates an isolated microenvironment between cell and bone surface (Granot-Attas and Elson, 2008). OCLs adhere tightly to the bone surface through adhesion structures called podosomes, which contain an actin-rich central core and several actin-associated proteins. The region around this core contains $\alpha_v\beta_3$ integrin, adaptor proteins (e.g., vinculin, paxillin, talin), Rho GTPases, and kinases such as c-Src and Pyk2 (Granot-Attas and Elson, 2008).

## The M-CSF Pathway Controls the Survival and Proliferation of OCL Precursors

Proliferation and differentiation of OCLs require two key signaling molecules which are normally expressed by stromal cells and OBLs: macrophage colony stimulating factor (M-CSF) and RANK ligand (RANKL) (Feng and Teitelbaum, 2013). Bone morphogenetic proteins (BMPs) are also emerging as key players in osteoclast homeostasis and appear to interact with the RANKL pathway in OCL differentiation and activation. The role of BMPs in OCL signaling is reviewed on a separate contribution to this Research Topic (Lademann et al., 2020) and will not be further discussed here.

M-CSF is needed during all stages of OCL development for optimal cell production and function, but the role of this cytokine is critical for the proliferation of OCL precursor cells (OCLPs). M-CSF exerts its effects through binding to its receptor M-CSFR, which is expressed on the OCLP membrane. Downstream, this leads to activation of extracellular signal regulated kinases 1 and 2 (ERK1/2) and phosphoinositide 3 kinase (PI3K), which are key regulators of the survival and proliferation of OCLPs (Feng and Teitelbaum, 2013). Accordingly, defective signaling through this pathway, such as due to inactivating mutations in the Csf1 gene or deficiency in M-CSF, results in impaired production of OCLs and leads to an osteopetrotic phenotype in mice (op/op mice, **Table 1**) (Yoshida et al., 1990; Dai et al., 2002). A similar phenotype is seen in mice lacking the PU.1 transcription factor (**Table 1**), which positively regulates the expression of M-CSFR (Tondravi et al., 1997; Houston et al., 2007).

M-CSF-dependent activation of ERK1/2 leads to stimulation of microphthalmia-associated transcription factor (MITF) which, in turn, upregulates the expression of the B-cell lymphoma-2 (Bcl-2) anti-apoptotic protein (Weilbaecher et al., 2001; McGill et al., 2002). Mice expressing a mutant MITF (mi/mi mice) or lacking Bcl-2 also exhibit an osteopetrotic phenotype (**Table 1**) (Hodgkinson et al., 1993; McGill et al., 2002), again demonstrating the importance of the M-CSF signaling pathway in osteoclastogenesis.

## RANK/RANKL Signaling Is Required for OCL Differentiation

RANKL, a member of the tumor necrosis factor family, is expressed by OBLs in three forms – as a transmembrane protein, as a truncated ectodomain produced by cleavage of the membrane-bound ligand, and as a secreted protein (Findlay and Atkins, 2011). Activated T cells also produce the latter form, and this could be implicated in the bone loss seen in inflammatory and autoimmune disorders such as rheumatoid arthritis (Takahashi et al., 2008; Crotti et al., 2015).

RANKL stimulates OCL differentiation through binding to RANK, a member of the tumor necrosis factor receptor (TNFR) family that is expressed on the plasma membrane of precursor cells (Feng and Teitelbaum, 2013). Deletion of the genes coding for either RANK or RANKL (Tnfrsf11a and Tnfsf11, respectively), blocks OCL production and leads to severe osteopetrosis in mice (**Table 1**) and in humans (Dougall et al., 1999; Kong et al., 1999; Kim et al., 2000; Li et al., 2000; Sobacchi et al., 2013; Palagano et al., 2018), indicating that RANK-RANKL signaling is critical for osteoclastogenesis.

Binding of RANKL to RANK leads to recruitment of the adaptor protein TNFR-associated factor 6 (TRAF6) (Lomaga et al., 1999; Gohda et al., 2005). The cytoplasmic tail of RANK

**TABLE 1 |** Summary of skeleton-related phenotypes in knockout mice for genes involved in osteoclast differentiation in the order in which they are discussed in the text.

| Gene | Protein | Skeleton-related phenotypes and diseases | MGI IDs | References |
|---|---|---|---|---|
| Csf1 | M-CSF | Osteopetrosis, op/op mouse<br>Abnormal bone structure, morphology and remodeling<br>Abnormal bone and dentin mineralisation<br>Decreased bone resorption<br>Abnormal osteoblast morphology and differentiation<br>Abnormal osteoclast morphology and differentiation<br>Decreased osteoclast cell number | 1856333<br>5305707 | Yoshida et al., 1990; Naito et al., 1991, 1997; Begg et al., 1993; Harris et al., 2012; Nakamichi et al., 2013 |
| Csf1r | M-CSFR | Osteopetrosis<br>Abnormal bone structure, morphology, physiology and mineralisation<br>Failure of bone resorption<br>Abnormal osteoblast morphology<br>Abnormal osteoclast morphology and differentiation | 2181194 | Dai et al., 2002, 2004; Nakamichi et al., 2013 |
| Spi1 | PU.1 | Osteopetrosis<br>Failure of tooth eruption | 3717917 | Tondravi et al., 1997; Houston et al., 2007 |
| Mitf | MITF | Osteopetrosis, mi/mi mouse<br>Osteosclerosis<br>Abnormal bone morphology<br>Failure of tooth eruption<br>Abnormal osteoclast morphology and physiology | 1856087<br>1856085 | Hodgkinson et al., 1993; Nii et al., 1995; McGill et al., 2002; Steingrimsson et al., 2002 |
| Tnfrsf11a | RANK | Osteopetrosis<br>Abnormal bone and tooth morphology<br>Abnormal osteoclast differentiation<br>Decreased osteoclast cell number | 1860238<br>2183226<br>3664109 | Dougall et al., 1999; Li et al., 2000; Kapur et al., 2004 |
| Tnfsf11 | RANKL | Osteopetrosis<br>Abnormal bone and tooth morphology<br>Abnormal bone mineralisation<br>Decreased bone resorption<br>Abnormal osteoclast physiology<br>Decreased osteoclast cell number<br>Abnormal chondrocyte morphology and differentiation | 1859962<br>2386263<br>5297062<br>5307891<br>5614816 | Kong et al., 1999; Kim et al., 2000; Nakashima et al., 2011; Douni et al., 2012; Palmer et al., 2016 |
| Traf6 | TRAF6 | Osteopetrosis<br>Abnormal bone and tooth morphology<br>Decreased bone resorption<br>Abnormal osteoclast morphology and physiology | 1859953<br>2675469 | Lomaga et al., 1999; Naito et al., 1999 |
| Nfkb1<br>Nfkb2 | NF-κB | Osteopetrosis<br>Abnormal bone structure and morphology<br>Abnormal osteoclast differentiation<br>Decreased osteoclast cell number | 3852643 | Franzoso et al., 1997; Iotsova et al., 1997; Yamashita et al., 2007 |
| Fos | c-Fos | Osteopetrosis<br>Abnormal bone and tooth morphology<br>Decreased osteoclast cell number | 2181817 | Wang et al., 1992 |
| Nfatc1 | NFATc1 | Osteopetrosis<br>Abnormal bone and tooth morphology<br>Abnormal osteoclast differentiation<br>Decreased osteoclast cell number | 3831720 | Asagiri et al., 2005; Aliprantis et al., 2008 |
| Fcer1g | FcRγ | No skeletal effects<br>Normal bone volume and osteoclast function, size or number | 1857165 | Mócsai et al., 2004 |
| Fcer1g<br>Tyrobp | FcRγ<br>DAP12 | Osteopetrosis<br>Abnormal bone morphology<br>Increased bone mass<br>Decreased bone resorption<br>Abnormal osteoclast differentiation | 3818498 | Mócsai et al., 2004 |
| Tyrobp | DAP12 | Osteopetrosis<br>Nasu-Hakola disease<br>Abnormal bone morphology, remodeling and mineralisation<br>Decreased bone resorption<br>Abnormal osteoclast physiology and differentiation | 2386271<br>2386277 | Tomasello et al., 2000; Mócsai et al., 2004; Nataf et al., 2005 |

*(Continued)*

**TABLE 1** | Continued

| Gene | Protein | Skeleton-related phenotypes and diseases | MGI IDs | References |
|---|---|---|---|---|
| Btk<br>Tec | Btk<br>Tec | Osteopetrosis<br>Decreased bone resorption<br>Decreased osteoclast cell numbers | 3028887 | Ellmeier et al., 2000; Shinohara et al., 2008 |
| Itgb3 | Integrin β3 subunit | Osteosclerosis<br>Increased bone thickness<br>Abnormal osteoclast morphology and physiology<br>Increased osteoclast cell number | 2175913 | McHugh et al., 2000 |
| Oscar | Oscar | Abnormal osteoclast differentiation<br>Reduced osteoarthritis manifestation<br>Decreased chondrocyte apoptosis | 5301430 | Barrow et al., 2011; Park et al., 2020 |
| Oscar<br>Tyrobp | Oscar<br>DAP12 | Abnormal bone morphology<br>Abnormal osteoclast morphology, physiology and differentiation<br>Decreased osteoclast cell numbers | 5301435 | Barrow et al., 2011 |

*Data compiled from the Mouse Genome Informatics database (MGI) (http://www.informatics.jax.org/).*

lacks enzymatic activity, and thus interaction with TRAF6 is required for the activation of downstream pathways (Takayanagi, 2007; Kim and Kim, 2016). Other members of the TRAF family (e.g., TRAF2, 3 and 5) also bind RANK although their contribution to osteoclastogenesis appears to be limited (Takayanagi, 2007; Park et al., 2017).

RANK-recruited TRAF6 initiates signaling which ultimately leads to activation of nuclear factor kappa B (NF-κB), the kinase Akt (Wong et al., 1999; Wada et al., 2005), and several mitogen-activated protein kinases (MAPK) such as ERK1/2 (He et al., 2011), c-Jun N-terminal kinase (JNK) (David et al., 2002; Wada et al., 2005), and p38 (Li et al., 2002) (**Figure 1A**). One key consequence of MAPK stimulation is the induction of c-Fos and activator protein 1 (AP1), although the precise molecular mechanisms leading to this induction are not completely understood (Takayanagi, 2007; Park et al., 2017). AP1 functions as a homo/heterodimeric transcription factor, and is composed of members of the Fos, Jun and ATF (activating transcription factor) families (Hess et al., 2004). AP1/c-Fos and NF-κB directly regulate the expression of nuclear factor of activated T cells 1 (NFATc1) (**Figure 1A**), the key transcription factor of OCL-specific genes (Park et al., 2017). Thus, RANKL-stimulated induction of NF-κB and c-Fos is critical for the production of mature OCLs. Indeed, application of NF-κB inhibitors (Takatsuna et al., 2005) or deficiency in the NF-κB components p50/p52 (Yamashita et al., 2007) leads to impaired NFATc1 induction, while knockout of NF-κB in mice leads to osteopetrosis (**Table 1**) due to lack of mature OCLs (Franzoso et al., 1997; Iotsova et al., 1997). Similarly, deficiency of c-Fos abrogates NFATc1 induction and osteoclastogenesis *in vitro* (Takayanagi et al., 2002) and results in marked osteopetrosis *in vivo* (Wang et al., 1992) (**Table 1**), while overexpression of c-Fos can rescue NFATc1 expression in p50/p52 deficient cells (Yamashita et al., 2007).

NFATc1 upregulates the expression of TRAP, cathepsin K, calcitonin receptor, the β3 integrin subunit, DC-STAMP (dendritic cell-specific transmembrane protein) and $H^+$-ATPase (Matsumoto et al., 2004; Matsuo et al., 2004; Crotti et al., 2006; Kim et al., 2008). This is accomplished through the formation of a transcriptional complex which includes NFATc1, AP1 (Fos/Jun), MITF and PU.1 (Asagiri et al., 2005) (**Figure 1B**), although the components of this complex may vary depending on the target gene (Takayanagi, 2007). *In vitro* studies by Takayanagi et al. (2002) showed that deletion of NFATc1 leads to failure of OCL development while ectopic expression of the protein stimulates osteoclastogenesis in the absence of RANKL. The requirement of NFATc1 for the production of OCLs was also confirmed *in vivo* (Asagiri et al., 2005; Aliprantis et al., 2008) (**Table 1**). However, it must be noted that global disruption of this transcription factor is lethal since its activity is similarly required for the development of cardiac valves (de la Pompa et al., 1998).

Although NF-κB and c-Fos/AP1 have critical roles for the initial expression of NFATc1, its sustained induction necessitates the activity of the calcium-calmodulin dependent protein phosphatase calcineurin and the calcium-calmodulin dependent protein kinase IV (CAMK IV) (Takayanagi, 2007). Calcineurin dephosphorylates NFATc1, which leads to exposure of its nuclear translocation signal and localization to the nucleus where NFATc1 autoamplifies its own transcription. CAMK IV activation leads to phosphorylation of cAMP response element-binding protein (CREB), and subsequently, to the robust induction of c-Fos (Takayanagi, 2007) (**Figure 1B**). The importance of these pathways is demonstrated by the evidence that pharmacological inhibition of calcineurin (Ishida et al., 2002; Takayanagi et al., 2002) and CAMK IV (Sato et al., 2006) results in impaired osteoclastogenesis.

Activation of calcineurin and CAMK IV depends on the rise of intracellular free calcium concentration $[Ca^{2+}]_i$ (**Figure 1B**). Although stimulation with RANKL leads to increased $[Ca^{2+}]_i$ (Takayanagi et al., 2002), it appears that RANK is not the receptor that directly induces changes. Indeed, there is compelling evidence indicating that the rise of $[Ca^{2+}]_i$ requires activation and signaling through adaptors containing immunoreceptor tyrosine-based activation motifs (ITAMs), in particular DNAX-associated protein of 12 kDa (DAP12) and FcεRI γ chain (FcRγ)

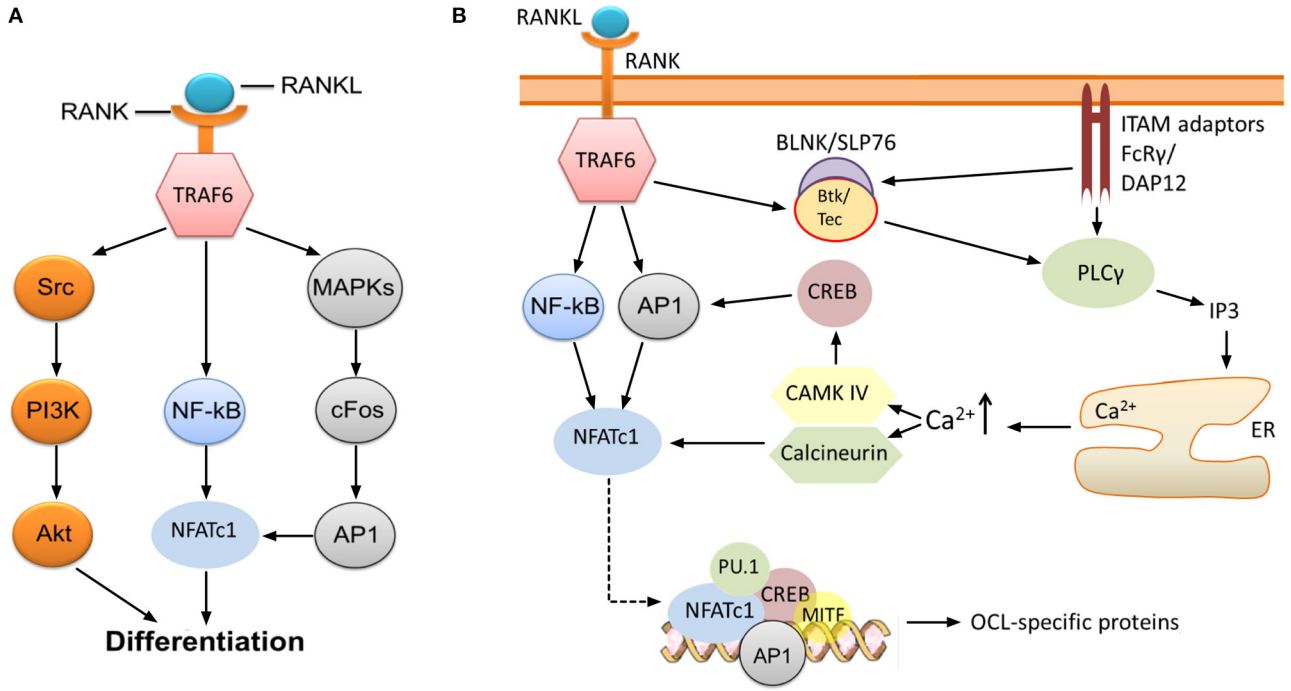


**FIGURE 1 |** RANK-NFATc1 signaling in OCL differentiation. **(A)** Binding of RANKL to RANK leads to induction of NF-κB and AP1, which, in turn, results in increased expression of NFATc1, a key transcription factor regulating the expression of OCL-specific genes. Src-mediated activation of the PI3K/Akt pathway downstream of TRAF6 is also required for OCL production, and inhibition of these pathways impairs osteoclastogenesis. **(B)** Sustained induction of NFATc1 leads to expression of OCL-specific proteins. The initial induction of NFATc1 mediated by NF-κB and AP1 is sustained through the activities of CAMK IV and the phosphatase calcineurin. This permits robust expression of NFATc1, which, together with several other transcription factors, upregulates the expression of OCL-specific genes (see text). Signaling through FcRγ and DAP12 ITAM adaptors is required for the sustained induction of NFATc1, specifically through activation of PLCγ and subsequent release of calcium from intracellular stores. Activation of PLCγ may also need phosphorylation by Btk/Tec–BLNK/SLP76 complex which is stimulated downstream of RANK/RANKL and ITAM adaptor signaling.

(Zou and Teitelbaum, 2015; Humphrey and Nakamura, 2016) (**Figure 1B**).

## Co-stimulatory Signals Are Necessary for Osteoclastogenesis

The requirement for co-stimulatory signaling through DAP12 and FcRγ for OCL differentiation was demonstrated by Koga et al. (2004), who found that NFATc1 expression was nearly undetectable in DAP12$^{-/-}$ FcRγ$^{-/-}$ cells following stimulation with RANKL, even though c-Fos and TRAF6 were expressed. Furthermore, RANKL-induced calcium oscillations, which normally lead to activation of NFATc1, were not apparent in these cells. Similarly, phosphorylation of phospholipase Cγ (PLCγ) was found to be impaired while phosphorylation of MAPK p38 and JNK was not affected. These results demonstrate that, in the absence of the ITAM adaptors FcRγ and DAP12, pathways downstream of RANK are activated normally but the PLCγ-calcium-NFATc1 activation pathway is impaired (**Figure 1B**). Consequently, DAP12$^{-/-}$ FcRγ$^{-/-}$ OCL precursor cells fail to differentiate into mature OCLs despite the presence of RANKL and M-CSF. Ectopic expression of NFATc1 rescued OCL maturation in the DAP12$^{-/-}$ FcRγ$^{-/-}$ cells, while stimulation of FcRγ in DAP12$^{-/-}$ cells restored the calcium oscillations and NFATc1 induction (Koga et al., 2004). Similarly, reintroduction of functional DAP12 in DAP12$^{-/-}$ FcRγ$^{-/-}$ cells rescued OCL differentiation in response to RANKL and M-CSF stimulation, whereas an ITAM-deficient DAP12 mutant failed to do so. Reintroduction of functional FcRγ was also able to rescue the osteoclastogenesis in cells doubly deficient in DAP12 and FcRγ, although this occurred only when OCL precursor cells were co-cultured with OBLs. Again, an ITAM-deficient FcRγ mutant did not rescue OCL differentiation (Koga et al., 2004). These results indicate that DAP12 and FcRγ may have overlapping roles in stimulating NFATc1 induction, although it appears that FcRγ requires a stimulus that is provided externally by OBL cells.

Similarly, Mócsai et al. (2004) observed that combined deficiency of DAP12 and FcRγ impairs osteoclastogenesis (**Table 1**). The precursor cells failed to form multinucleated OCLs, although they stained positive for TRAP, calcitonin receptor, cathepsin K, RANK, and integrin $\beta_3$ (Mócsai et al., 2004). This suggests that ITAM adaptor signaling is critical for the intermediate/late stages of osteoclastogenesis, such as OCL fusion and activation. Single deficiency of DAP12 was partly compensated by FcRγ. However, this only occurred in co-culture conditions with OBLs, which is in agreement with the findings of Koga et al. (2004).

Shinohara et al. (2008) further suggested that the Tec family of kinases, specifically Btk and Tec, are required to phosphorylate and activate PLCγ in the PLCγ-calcium-NFATc1 pathway (**Figure 1B**). Double deficiency of Btk and Tec was associated with severe impairment of osteoclastogenesis in mice resulting in an osteopetrotic phenotype (**Table 1**). Furthermore, phosphorylation of PLCγ and the oscillations of calcium were suppressed in $Btk^{-/-}$ $Tec^{-/-}$ cells, suggesting that the kinases regulate this pathway. The authors proposed that Btk and Tec are phosphorylated in response to RANKL stimulation, following which the kinases form a signaling complex with adaptor molecules such as B-cell linker protein (BLNK) and SH2-containing leucocyte protein of 76 kDa (SLP-76). These adaptors require activation by ITAM adaptor signaling, and formation of signaling complexes was not observed in $DAP12^{-/-}$ $FcR\gamma^{-/-}$ cells. Thus, Shinohara et al. (2008) suggested that the Btk/Tec–BLNK/SLP76 complex might bridge the ITAM and RANKL pathways (**Figure 1B**). Nevertheless, other adaptor molecules may also be involved since double deficiency of BLNK and SLP-76 does not appear to markedly alter bone phenotype *in vivo* (although *in vitro* this is associated with significant inhibition of osteoclastogenesis) (Shinohara et al., 2008).

*In vivo* studies indicate that mice deficient in DAP12 exhibit only a mild form of osteopetrosis and have normal numbers of OCLs (Koga et al., 2004; Mócsai et al., 2004) (**Table 1**). Similarly, mice deficient in FcRγ appear to have normal trabecular bone volume and OCL numbers. However, mice deficient in both DAP12 and FcRγ were found to be severely osteopetrotic, and showed increased numbers and thickness of bone trabeculae (Koga et al., 2004; Mócsai et al., 2004) (**Table 1**). The mice had few OCLs, indicating that the observed bone changes stem from defective osteoclastogenesis. Thus, in agreement with the *in vitro* studies, these findings indicate that the ITAM adaptors are essential for OCL production *in vivo*, and that signaling through FcRγ can largely compensate for deficiency in DAP12. Indeed, Nasu-Hakola (NH) disease in humans results from deficiency of DAP12 signaling (Paloneva et al., 2000, 2002). This condition is associated with the formation of bony cysts. However, patients with NH disease show normal OCL differentiation and do not suffer from osteopetrosis, likely as a result of compensation through FcRγ. Surprisingly, these patients may even present with loss of trabecular bone (Paloneva et al., 2000), suggesting that, at least in humans, DAP12 and FcRγ may not have completely overlapping roles.

## ITAM Adaptor Signaling Is Required for OCL Activity

As indicated earlier, OCLs must adhere to the bone matrix and undergo cytoskeletal rearrangement to acquire bone-resorbing activity. These processes occur during the late stages of osteoclastogenesis and require the expression of the integrin subunit $\beta_3$ which is not present in immature OCL precursor cells (Ross and Teitelbaum, 2005). OCLs use $\alpha_v\beta_3$ integrin not only to attach to the bone matrix but also to initiate signaling which leads to reorganization of the cell cytoskeleton. Research evidence suggests that FcRγ and DAP12 co-operate with $\alpha_v\beta_3$ integrin in a manner that requires the activities of the c-Src and Syk kinases (Zou et al., 2007) (**Figure 2**). Indeed, OCLs deficient in the integrin $\beta_3$ subunit, c-Src, or Syk fail to undergo cytoskeletal rearrangement and to form actin rings, which leads to impaired bone resorption and osteopetrosis *in vivo* (Jakus et al., 2007; Zou and Teitelbaum, 2015) (**Table 1**). In addition, OCLs doubly deficient in FcRγ and DAP12 have a phenotype similar to $\beta_3^{-/-}$ cells (McHugh et al., 2000; Faccio et al., 2003; Mócsai et al., 2004). Culture on $\alpha_v\beta_3$ ligands, such as vitronectin, leads to phosphorylation and activation of Syk in OCL precursors (Faccio et al., 2003; Zou et al., 2007) while in mature adherent OCLs Syk is constitutively phosphorylated (Mócsai et al., 2004). Syk phosphorylation, however, is absent in $DAP12^{-/-}$ $FcR\gamma^{-/-}$ cells, and is attenuated in $DAP12^{-/-}$ cells (Mócsai et al., 2004). Co-culture of OCLs with OBLs partially normalizes OCL differentiation and resorption activity in $DAP12^{-/-}$ cells, indicating again that FcRγ can compensate for the deficiency of DAP12 in co-culture conditions (Mócsai et al., 2004).

## The ITAM Adaptor FcRγ Associates With OSCAR to Provide Co-stimulatory Signals for Osteoclastogenesis

The tyrosine-based activation motif that gives name to the ITAM adaptor molecules FcRγ and DAP12 is a conserved, short cytoplasmic sequence with a repeated signature set of four amino acids YxxI/L, typically separated by 6–8 amino acids, $YxxI/Lx_{(6-8)}YxxI/L$ (Underhill and Goodridge, 2007; Ivashkiv, 2009). Phosphorylation of the two tyrosine residues by members of the Src family of kinases allows the recruitment of signal mediators such as the Syk kinase, which ultimately alter the activity of downstream effectors and cellular activity (Merck et al., 2004; Jakus et al., 2007). The ITAM adaptors, however, do not possess an extracellular ligand-binding domain and therefore require association with specific cell-surface receptors. FcRγ has been found to associate with several immunoreceptors including OSCAR, paired immunoglobulin receptor A (PIR-A) and Fc receptors, while DAP12 has been shown to pair with triggering receptor expressed on myeloid cells 2 (TREM2), signal-regulatory protein β1 (SIRPβ1), sialic acid-binding immunoglobulin-like lectin 15 (Siglec-15), and myeloid DAP12-associated lectin (MDL-1) (Humphrey and Nakamura, 2016). The role of these receptor molecules in osteoclastogenesis is not well-understood although evidence indicates that they are involved in the provision of co-stimulatory signals (Humphrey and Nakamura, 2016). Application of activating anti-TREM2 and anti-SIRPβ1 antibodies was shown to stimulate the differentiation of OCL precursor cells, and this was only observed in the presence of DAP12 (Koga et al., 2004). Similarly, application of stimulating anti-OSCAR and anti-PIR antibodies activated osteoclastogenesis *in vitro*, and this effect was not observed in $FcR\gamma^{-/-}$ OCLs (Koga et al., 2004). This evidence suggests that the ITAM adaptors may pair with more than one receptor to stimulate OCL maturation. However, it appears that receptors which pair with FcRγ do not pair with DAP12, and *vice versa*. Similar results were obtained by Merck et al. (2004), who used

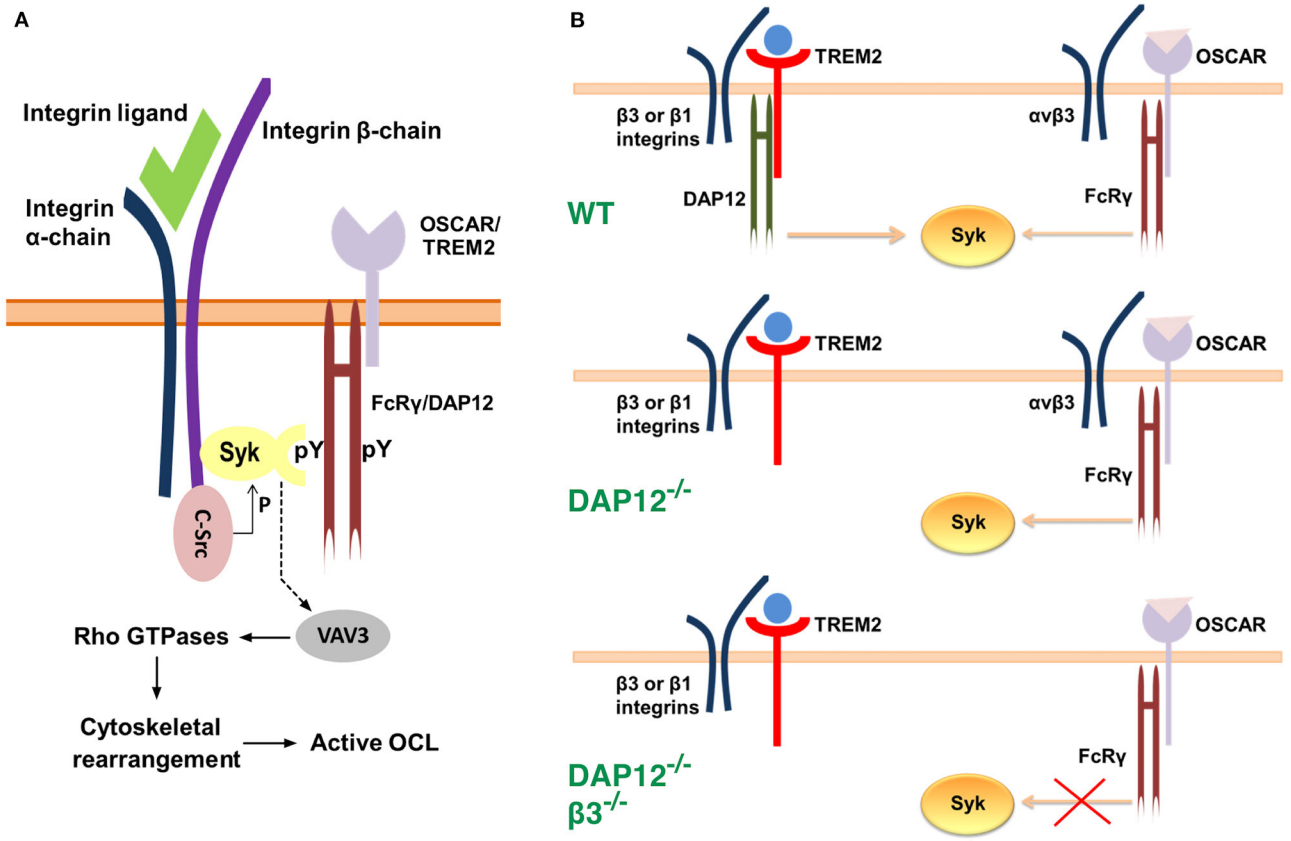


**FIGURE 2 |** Models for the interaction between $\alpha_v\beta_3$ integrins, c-Src, Syk and the ITAM adaptors. **(A)** Syk, c-Src and $\alpha_v\beta_3$ integrins associate into a multimeric complex (Zou et al., 2007). c-Src is associated constitutively with the three terminal amino acids of the $\beta_3$ integrin subunit. Binding of a ligand to $\alpha_v\beta_3$ integrin leads to phosphorylation and activation of c-Src, and to the recruitment of Syk. The latter is bound to the phosphotyrosine residues of an ITAM adaptor, FcRγ or DAP12, via its C-terminal SH2 (Src homology region 2) domain. The N-terminal SH2 domain of Syk associates with the cytoplasmic domain of the $\beta_3$ integrin subunit at a site which is distinct from that of c-Src. Activated c-Src phosphorylates Syk, which, in turn, leads to phosphorylation and activation of the guanine exchange factor Vav3. The latter alters the activity of Rho GTPases which ultimately results in reorganization of the cytoskeleton. **(B)** A model for OSCAR-FcRγ role in cytoskeletal rearrangement during osteoclastogenesis (Zou and Teitelbaum, 2015). In wild-type OCLs Syk activation is achieved mainly through TREM2-DAP12 signaling in association with $\beta_3$ or $\beta_1$ integrins. Syk activation leads to cytoskeletal rearrangement. Deficiency of DAP12 is compensated by OSCAR-FcRγ, which only associates with $\alpha_v\beta_3$ integrin. Thus, deficiency of both DAP12 and $\alpha_v\beta_3$ integrin leads to impaired signaling even in the presence of OSCAR-FcRγ and consequently to cytoskeletal disorganization.

immunoprecipitation to demonstrate that OSCAR specifically associates with FcRγ but not with DAP12. Blockade of OSCAR signaling was found to inhibit the formation of multinucleated OCLs as well as their bone resorption activity, as evidenced by the reduction in the number of resorption pits when cells were cultured on dentine slices in the presence of a soluble form of OSCAR (Kim et al., 2002). These findings indicate that OSCAR regulates OCL differentiation in a manner which agrees with the role of its adaptor FcRγ as discussed above.

Barrow et al. (2011) examined the effect of OSCAR deficiency *in vivo* by generating DAP12$^{-/-}$ Oscar$^{-/-}$ mice (**Table 1**). These mice displayed a phenotype similar to that of DAP12$^{-/-}$ FcRγ$^{-/-}$ mice (**Table 1**). Specifically, they showed decreased OCL differentiation as indicated by the number of TRAP positive cells, as well as decreased cell size and reduced activity as evidenced by the eroded bone areas. Bone formation and OBL numbers in these mice were not different from those observed in mice deficient in DAP12 only. Consistently, the number and volume of trabeculae in DAP12$^{-/-}$ Oscar$^{-/-}$ mice were increased compared to those in DAP12$^{-/-}$ mice (Barrow et al., 2011). In a different study, Zou and Teitelbaum (2015) demonstrated that activation of OSCAR with a stimulating antibody rescues the dysfunctional osteoclastogenesis in DAP12$^{-/-}$ cells. Additionally, when cultured on bone, where natural collagen ligands for OSCAR are present (discussed later), DAP12$^{-/-}$ OCLs were able to spread, form actin rings, and resorb bone (Zou and Teitelbaum, 2015). In agreement with the studies addressed above (section Co-stimulatory Signals are Necessary for Osteoclastogenesis), OSCAR-FcRγ rescue effects required the expression of integrin $\beta_3$ subunit. Indeed, the authors found that mice deficient in both DAP12 and the integrin $\beta_3$ subunit showed severe osteopetrosis with a 4-fold increase in trabecular mass. In contrast, DAP12 was found to enable cytoskeletal rearrangement via association

with either integrin $\beta_1$ or $\beta_3$ subunits (Zou and Teitelbaum, 2015) (**Figure 2B**). Collectively, these studies suggest that the co-stimulatory signals for osteoclastogenesis, which are mediated through FcRγ, occur in association with OSCAR, and require the expression of $\beta_3$ integrin subunit. As mentioned, however, the ITAM adaptor shows promiscuity and can pair with PIR-A and Fc receptors. Thus, further studies are required to establish whether these FcRγ/immunoreceptor complexes contribute to osteoclastogenesis, and whether particular conditions (e.g., injury/trauma, acute or chronic inflammation) favor signaling through a particular complex.

# A CLOSER LOOK AT OSCAR

## OSCAR Discovery and Structure

OSCAR (Osteoclast Associated Ig-like Receptor) was first identified by Kim et al. (2002), who coined this name since they observed that the receptor was expressed in murine preosteoclasts and mature OCLs, but not in macrophages or dendritic cells. The novel protein was found to be an immunoglobulin type receptor and a member of the leucocyte receptor complex (LRC) (Kim et al., 2002). The human version had also been annotated as polymeric immunoglobulin receptor 3 precursor (PIGR3), but the name OSCAR has been adopted in all literature ever since. Subsequent studies revealed that OSCAR expression in bone is conserved among species, suggesting that the protein has important functions in bone homeostasis (Nemeth et al., 2011). Unlike murine OSCAR, however, the human ortholog of the receptor is expressed not only in OCLs but also in other cells of the myeloid lineage, including monocytes, macrophages and dendritic cells (Merck et al., 2004).

In humans, the OSCAR gene maps to chromosome 19q13.42 in the LRC, where it lies in close proximity to other immunoreceptor genes such as those coding for leukocyte immunoglobulin (Ig)-like receptors (LILRs) and killer cell Ig-like receptors (KIRs) (Kim et al., 2002; So et al., 2003; Merck et al., 2004; Barrow and Trowsdale, 2008). These proteins share 70% amino acid sequence homology with OSCAR, they all show an Ig-like structure, and signal through FcRγ or DAP12 adaptors (Nemeth et al., 2011). Considering this similarity, it has been suggested that OSCAR might be able to interact with major histocompatibility complex (MHC) class I molecules similarly to KIR and LILR members (Ishikawa et al., 2004).

Several isoforms have been described for human OSCAR from alternative splicing of the human gene (**Table 2**, **Supplementary Figure 1**). The OSCAR-M1 isoform is a type I transmembrane protein of 263 amino acids (245 after signal peptide removal), with two Ig-like domains D1 and D2 in its N-terminal extracellular region, a predicted transmembrane (TM) region, and a short C-terminal cytoplasmic tail (Kim et al., 2002) (**Figure 3**). The transcript for OSCAR-M1 contains five exons. The sequence for D1 maps to exon 3, the sequence for D2 maps to exon 4, and the sequence for the TM region is in exon 5 (**Supplementary Figure 1**). A longer OSCAR-S1 isoform (282 amino acids) results from the alternative splicing of exons 4 and 5 and lacks the predicted TM region (**Supplementary Figure 1**). Additional isoforms for human OSCAR (**Table 2**) arise from either adding or skipping one exon in the N-terminal region (**Supplementary Figure 2**). The OSCAR-S isoforms could correspond to a secreted, soluble form of OSCAR (sOSCAR, discussed later). All OSCAR-M and OSCAR-S human isoforms have identical sequences in their D1-D2 extracellular regions. Similar sets of OSCAR-M and OSCAR-S isoforms have been predicted in the genomes of chimpanzee (**Table 2**) and several other primates, although the state of annotation of their OSCAR genes is still preliminary.

Two isoforms have been described for murine OSCAR (**Table 2**) that result from alternative splicing at the end of the first exon. Both are type I transmembrane proteins with the same domain composition as human OSCAR-M1 (Kim et al., 2002). No murine OSCAR-S type isoform has been described to date. The OSCAR gene appears to be conserved in mammals, marsupials and monotremes, and for most species only the transmembrane form is predicted. No reliable orthologs for OSCAR have been predicted to date in birds, amphibians, reptiles or fishes.

The three-dimensional structure of the extracellular region of human OSCAR has been determined by X-ray crystallography (Haywood et al., 2016; Zhou et al., 2016), both free and in complex with a collagen triple-helical peptide (discussed later) (**Figure 3B**). As predicted, OSCAR extracellular region consists of two Ig-like domains, D1 (membrane-distal) and D2 (membrane-proximal), connected by a short interdomain linker. The sequence of this linker diverges from the consensus linker sequence of other members of the LRC family and introduces a sharp β-turn that results an unusually obtuse interdomain angle of 241°. This obtuse angle differs significantly from the acute interdomain angles near 90° seen in other LRC receptors (Haywood et al., 2016; Zhou et al., 2016).

The cytoplasmic domain of OSCAR is short, and so far it has not been demonstrated to have a signaling function, although a putative guanylate cyclase activity has been suggested based on amino acid sequence homology analysis (Nemeth et al., 2011). In the transmembrane domain, similar to other receptors from the LRC family, OSCAR has an arginine residue at position 231 (R231) via which the receptor associates with FcRγ (**Figure 3A**) (Kim et al., 2002; Merck et al., 2004). This residue is conserved across OSCAR orthologs (**Supplementary Figure 3**). Indeed, the presence of this residue is critical for OSCAR signaling since a mutant protein in which R231 is substituted with a neutral residue fails to recruit FcRγ to the cell membrane (Merck et al., 2004).

## Regulation of OSCAR Expression

OSCAR expression appears to form a positive feedback loop with NFATc1 expression. As discussed earlier (section RANK/RANKL Signaling is Required for OCL Differentiation), RANKL stimulation in OCLs results in initial activation of NFATc1 and recruitment of other transcription factors such as PU.1 and MITF. These molecules bind to the OSCAR promoter and upregulate OSCAR expression (Kim et al., 2005b,c). Increased signaling through OSCAR-FcRγ, in turn, leads to rise in $[Ca^{2+}]_i$, which results in a sustained activation of NFATc1 through a $Ca^{2+}$-dependent calcineurin pathway

**TABLE 2 |** Representative entries for OSCAR genes and currently described or predicted isoforms in genome databases.

| Species | OSCAR gene links | Isoform | Naa | NCBI | Uniprot |
|---|---|---|---|---|---|
| Human | ENSG00000170909 | M1 | 263 | NP_573399 | Q8IYS5-2 |
| | NCBI 126014 | M2 | 267 | NP_570127 | Q8IYS5-3 |
| | | M3 | 252 | NP_573398 | Q8IYS5-6 |
| | | S1 | 282 | NP_001269278 | Q8IYS5-1 |
| | | S2 | 271 | NP_001269279 | Q8IYS5-4 |
| | | S3 | 286 | NP_996554 | Q8IYS5-7 |
| Chimpanzee | ENSPTRG00000048476 | M1 | 263 | PNI92300 | A0A2I3T010 |
| | NCBI 107966470 | M2 | 267 | PNI92298 | A0A2J8Q7Q1 |
| | | M3 | 252 | PNI92296 | A0A6D2X5E3 |
| | | S1 | 305 | PNI92297 | A0A2I3RTB0 |
| | | S2 | 294 | PNI92302 | A0A2I3TWJ1 |
| | | S3 | 309 | PNI92299 | A0A2J8Q7T4 |
| Mouse | ENSMUSG00000054594 | M1 M2 | 265 | NP_001277306 | Q8VBT3-1 |
| | NCBI 232790 | M3 | 271 | NP_783440 | Q8VBT3-2 |
| Rat | ENSRNOG00000055716 | M1 | 273 | NP_001171902 | D3ZCA1 |
| | NCBI 292537 | X1 | 267 | XP_006228082 | |
| Horse | ENSECAG00000039917 | X2 | 260 | XP_023506119 | A0A3Q2I9K5 |
| | NCBI 100051988 | X1 | 292 | XP_023506118 | |
| Pig | ENSSSCG00000003259 | X1 | 262 | XP_020950544 | A0A481CKH3 |
| | NCBI 100518788 | | | | |
| Dog | ENSCAFG00000024209 | X1 | 274 | XP_022283292 | E2RCM5 |
| | NCBI 484313 | X2 | 261 | | |

*Isoform names differ in different databases. The number of amino acids (Naa) corresponds to the unprocessed sequence of each isoform.*

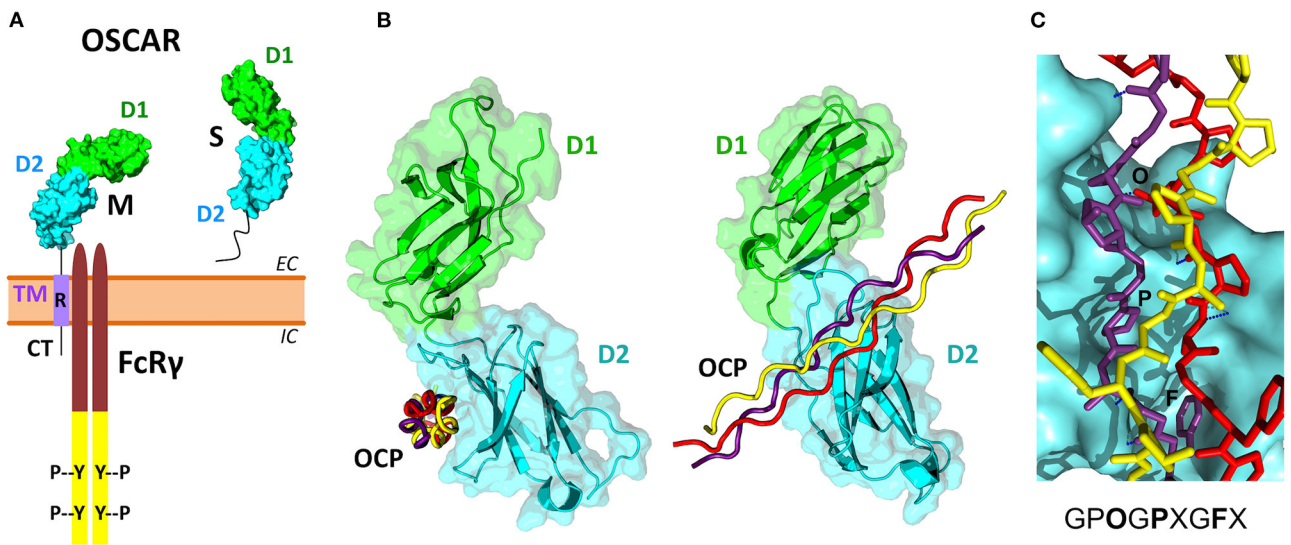


**FIGURE 3 |** OSCAR domain structure and its association with FcRγ and collagen ligands. **(A)** Several membrane-associated (M) and soluble (S) isoforms have been reported for human OSCAR (**Table 2**). The M isoforms contain two extracellular Ig-like domains D1 (green) and D2 (cyan), a single transmembrane region TM (purple), and a short cytoplasmic tail CT. An arginine residue (R) within the TM region links OSCAR with the FcRγ adaptor. The S isoforms result from alternative splicing of the human OSCAR gene that removes the TM region. **(B)** Two views of the crystal structure of the OSCAR ectodomain D1-D2 in complex with an OSCAR-binding collagen-like peptide (OCP) (Haywood et al., 2016; Zhou et al., 2016). D1 and D2 are shown as ribbon and surface diagrams, and the three OCP chains are shown as red, yellow and purple ropes. **(C)** Details of the OCP bound to the primary binding site on D2. The consensus OSCAR-binding sequence is shown. Two of the three peptide chains bind tightly to the D2 surface, with several hydrogen bonds (blue dotted lines) and side chains of several residues (O, P, F) fitting D2 surface pockets.

(**Figure 1B**) (Takayanagi et al., 2002), thus completing the positive feedback loop. Accordingly, application of the $Ca^{2+}$ chelator BAPTA inhibits activation of NFATc1 in RANKL-stimulated OCLPs and suppresses osteoclastogenesis (Takayanagi et al., 2002), while application of the specific calcineurin inhibitor FK506 suppresses the increase in NFATc1 expression levels and its nuclear localization (Takayanagi et al., 2002) and markedly suppresses OSCAR expression (Kim et al., 2005c).

Several negative regulators including protein inhibitor of activated Stat3 (PIAS3), inhibitors of DNA binding (ID) proteins and the transcription factor MafB have been shown to inhibit OSCAR and NFATc1 expression and thereby to suppress RANKL-induced osteoclastogenesis (Lee et al., 2006; Kim et al., 2007a,b). PIAS3 recruits histone deacetylase 1 co-repressor to the promoters of NFATc1 and OSCAR, thus leading to arrest of their transcription. Accordingly, silencing of PIAS3 using RNAi relieves the transcriptional block and enhances osteoclastogenesis (Kim et al., 2007b). Similarly, Lee et al. (2006) observed that ID proteins interact with MITF and attenuate its ability to bind to the promoter of OSCAR. Overexpression of the ID proteins was shown to suppress the induction of OSCAR and NFATc1, and to inhibit the formation of differentiated OCLs (Lee et al., 2006).

The expression of OSCAR may be modulated by factors downstream of NFATc1. The MHC class II transactivator (CIITA), which is upregulated by NFATc1, appears to provide a negative feedback attenuating OSCAR and NFATc1 expression through competition for transcriptional binding sites (Kim et al., 2010). Modulation of MAPK signaling was also demonstrated to alter OSCAR expression. Specifically, inhibition of RANKL-induced activation of ERK, p38 and JNK by the peroxisome proliferator-activated receptor-γ (PPARγ) agonist KR62776 (Park et al., 2009) and by silibinin (Kim et al., 2009) appears to attenuate OSCAR induction and to inhibit osteoclastogenesis.

## OSCAR Ligands

When Kim et al. (2002) identified OSCAR they observed that signaling through the receptor may be bypassed when M-CSF and RANKL were supplemented externally in supraphysiological concentrations. However, signaling through OSCAR was mandatory for osteoclastogenesis when the only source of these cytokines was OBLs in a co-culture system. Application of OSCAR-Fc fusion protein, an engineered, soluble form of OSCAR fused to the Fc portion of human IgG1a, inhibited the formation of mature OCLs in co-culture conditions with OBLs (Kim et al., 2002). The authors thus proposed that OBL cells were likely expressing a putative OSCAR ligand. These findings are in agreement with studies that demonstrate that the rescue effects of FcRγ in osteoclastogenesis of $DAP12^{-/-}$ cells are observable only when the OCL precursors are co-cultured with OBLs (Koga et al., 2004; Mócsai et al., 2004) (see section Co-stimulatory Signals are Necessary for Osteoclastogenesis). Other than type I collagen (see below), which is secreted in large amounts by OBLs, the identity of the putative OBL-expressed OSCAR ligand has not yet been confirmed. A recent review on OBL-OCL interactions summarizes the different factors involved in this cell-to-cell communication (Chen et al., 2018), some of which could indirectly affect OSCAR signaling or expression.

Nearly a decade following the discovery of OSCAR, Barrow et al. (2011) showed that collagens can serve as ligands for this receptor. They used OSCAR-Fc fusion protein and observed that it binds strongly to fibrillar collagens I, II and III. Furthermore, OSCAR-Fc did not bind to other extracellular matrix proteins such as vitronectin and fibronectin, or to collagen peptide ligands for $\alpha_2\beta_1$ integrin and glycoprotein VI, indicating that OSCAR recognizes collagens containing specific sequence motifs. In agreement with the findings of Kim et al. (2002), the OSCAR-Fc fusion protein was able to bind to OBLs and stromal cells. Treatment with collagenase inhibited this interaction indicating that the putative ligands expressed on these cells are likely to contain collagenous domains (Barrow et al., 2011). Indeed, in a subsequent study Barrow et al. (2015) demonstrated that OSCAR could bind surfactant protein D (SP-D), a molecule that contains a collagen triple helical domain.

Solid-phase binding experiments with collagen toolkits, libraries of overlapping triple helical collagen-like peptides (CLPs) that encompass the entire collagen II and III sequences, elucidated the main requirements for collagen recognition by OSCAR. Barrow et al. (2011) identified the minimal OSCAR-binding collagen sequence as GPOGPXGFX (**Figure 3C**), where O is the abbreviation for the imino acid 4-hydroxyproline, the usual post-translational modification of proline seen in collagens and collagen-like proteins (Bella, 2016). This consensus sequence is also conserved in both chains of type I collagen. A unique motif GAOGASGDR that is quite different from the consensus sequence was found in collagen II, and several lower affinity sites were also identified (Barrow et al., 2011; Zhou et al., 2016). Furthermore, the triple-helical structure of collagen was found to be critical for OSCAR binding and signaling. Indeed, no interaction was observed when cells were cultured on an immobilized CLP containing the minimal binding collagen sequence but too short to form a triple helical structure (Barrow et al., 2011).

Human monocytes cultured on CLPs containing the minimal OSCAR-binding sequence (OCPs), were found to exhibit greater frequency of $[Ca^{2+}]_i$ oscillations and increased TRAP staining compared to cells cultured on control peptides (Barrow et al., 2011). In addition, murine bone marrow macrophages (BMMs) cultured on OCPs showed enhanced osteoclastogenesis as evidenced by increased gene expression of NFATc1, TRAP, cathepsin K, and the calcitonin receptor, and this response was inhibited by an anti-OSCAR antibody. Importantly, enhanced osteoclastogenesis was not observed in cells deficient in OSCAR or FcRγ, which indicates that these effects are mediated by the receptor and its adaptor molecule (Barrow et al., 2011). It is still unclear, however, whether binding of OSCAR to endogenous collagens can stimulate osteoclastogenesis in a similar manner.

Ligand-bound OSCAR was also shown to rescue osteoclastogenesis in DAP12 deficient cells (Barrow et al., 2011). When cultured on OCPs, murine $DAP12^{-/-}$ BMMs were able to form multinucleated cells which stained positive for TRAP and exhibited well-defined podosomes. This response was absent in $DAP12^{-/-}$ $Oscar^{-/-}$ BMMs but was restored

by retroviral transduction of OSCAR, thus indicating that the rescue effect was OSCAR-specific. The authors made similar observations when monocytes from patients with Nasu-Hakola disease (i.e., DAP12$^{-/-}$ or TREM$^{-/-}$) were used, thereby indicating potential clinical significance of stimulating OSCAR signaling. Altogether, the findings of Barrow et al. (2011) suggest that collagen molecules that are normally found within the extracellular bone matrix may serve as ligands for co-stimulatory signaling through OSCAR during osteoclastogenesis.

Two crystal structures of OSCAR ectodomains in complex with an OCP, published independently by Zhou et al. (2016) and Haywood et al. (2016), provided a detailed molecular view of the binding mechanism between OSCAR and its collagen ligands (**Figure 3B**). The structure by Zhou et al. (2016) (PDB 5EIQ) revealed two OCP binding sites on D1 and D2, respectively, while the structure by Haywood et al. (2016) (PDB 5CJB) showed a single site on D2. Site-directed mutagenesis and direct binding assays confirmed D2 as the primary binding domain. Both groups concluded that binding of collagen to D2 (membrane proximal) is facilitated by the unique angle between the two domains. Zhou et al. (2016) suggested that the interaction between OSCAR and collagen might involve two phases: an initial low-affinity binding mediated by D1, followed by a subsequent stable adhesion to D2. Notably, this contrasts with the interaction of collagen with other related receptors (such as glycoprotein VI and leukocyte-associated immunoglobulin-like receptor 1), where the D1 domain serves as a primary binding site (Lecut et al., 2004; Brondijk et al., 2010). Furthermore, Zhou et al. (2016) speculated that this two-phase interaction might be of particular importance for cells within the circulation. The authors argue that the flexibility of the D1-D2 interdomain region would permit D1 to probe the environment and mediate a weak interaction if a suitable ligand is present, which would then be followed by a firm adhesion via D2 (Zhou et al., 2016).

Haywood et al. (2016) also investigated the effects of OCP binding on osteoclastogenesis, and found that peptides containing ≥40 amino acids were able to inhibit the differentiation of cells cultured on immobilized collagen. The authors thus proposed that synthetic OCPs could potentially be used as a pharmacological treatment of pathological bone resorption (Haywood et al., 2016). Indeed, further research in this area has the potential to bring novel therapeutic strategies considering the putative role of OSCAR in bone disease as addressed in the paragraphs below.

# PHYSIOLOGICAL SIGNIFICANCE OF OSCAR IN BONE HEALTH AND DISEASE

**Figure 4** summarizes the different signaling mechanisms addressed above and illustrates the current understanding of OSCAR contribution to signaling during osteoclastogenesis. Genetic variants for the human OSCAR gene are known and can be browsed in genome databases such as ENSEMBL (see **Table 2** for the link to the human gene entry). Nevertheless, information about the possible clinical outcomes of these variants is still very limited (one exception is discussed in section OSCAR in Pathological Bone Degradation below).

## OSCAR in Bone Development, Maintenance and Repair

The interaction between OSCAR and collagen may play a significant role in the normal development, maintenance and repair of bone. During bone development OCL precursors are deposited at sites rich in collagen, and this may facilitate the production of mature OCLs through OSCAR signaling (Barrow et al., 2011). During bone maintenance and repair the recruitment of precursor cells from the circulation to bone surfaces requires transendothelial migration through blood capillaries that express RANKL and collagen III (Kindle et al., 2006; Andersen et al., 2009). It is possible that RANK-RANKL signaling and collagen-OSCAR interaction at this stage begin the process of precursor cell differentiation. Once the cells arrive at the bone surface they may encounter osteoblastic lining cells or be exposed to collagens I and III from the bone matrix (Andersen et al., 2009; Barrow et al., 2011). Further interaction between OSCAR and these ligands in the presence of RANKL may facilitate the production of multinucleated OCLs, which adhere to the bone via integrins, polarize, undergo cytoskeletal rearrangement, and begin resorption.

## OSCAR in Pathological Bone Degradation

Defective OSCAR signaling may be linked to pathological bone degradation and increased bone fragility. Kim et al. (2005a) identified 10 polymorphisms of human OSCAR, one of which was caused by a single nucleotide substitution in the promoter region (2322A>G). Using regression analysis the researchers found that this allele was strongly linked to lower bone mineral density and increased fracture risk in postmenopausal women (Kim et al., 2005a). The authors noted that the mutation might affect a putative binding site for CREB, although further research is necessary to confirm this potential mechanism.

Deregulation of ITAM signaling has been shown to contribute to the pathogenesis of inflammatory bone disease including rheumatoid arthritis, periprosthetic osteolysis, and periodontal disease (Crotti et al., 2015). Increased OSCAR and FcRγ levels were found in human periprosthetic tissue near sites of bone loss (Alias et al., 2012). Furthermore, polyethylene particles were observed to stimulate resorption by OCLs *in vitro* as well as to significantly increase the levels of OSCAR and FcRγ (Alias et al., 2012). Similarly, OSCAR has been identified at sites of osteolysis in tissues with periodontitis and in mild gingivitis, where it co-localized with TRAP-positive cells (Crotti et al., 2015). Further studies, however, are required to investigate the association of OSCAR and other ITAM-related molecules with periprosthetic bone loss and periodontitis.

## OSCAR in Rheumatoid Arthritis: Increased Expression in Mononuclear OCL Precursors

Rheumatoid arthritis (RA) is an autoimmune condition characterized by inflammation of the synovial membranes,

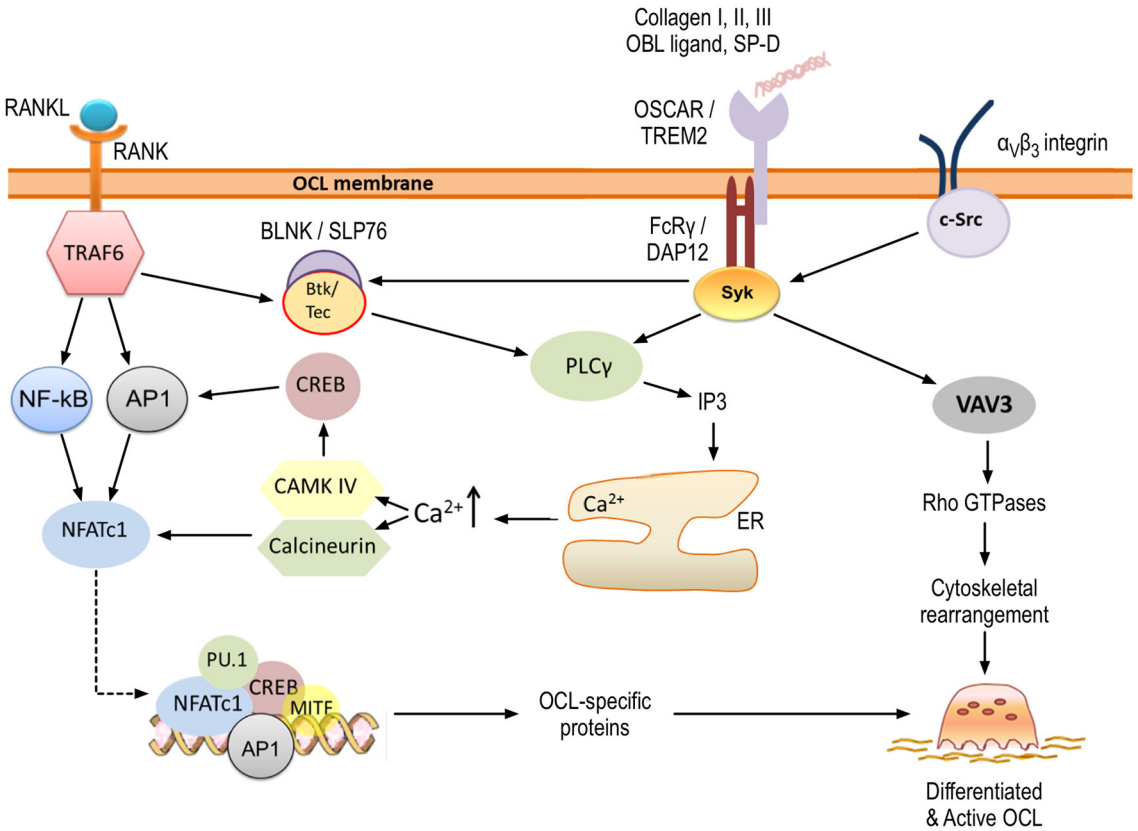


**FIGURE 4 |** OSCAR signaling in osteoclastogenesis. OSCAR associates with FcRγ and provides co-stimulatory signals for osteoclast maturation and activation. RANK-RANKL interaction leads to initial induction of NFATc1, which is amplified through OSCAR/FcRγ-mediated activation of CAMK IV and calcineurin. Ultimately, this leads to expression of osteoclast-specific proteins. In addition, OSCAR-FcRγ, in association with $\alpha_v\beta_3$ integrin, provides signals for cytoskeletal reorganization and thus osteoclast activation. Key tyrosine residues within FcRγ are phosphorylated by members of the Src family, leading to the recruitment of Syk kinase. The latter stimulates the activity of downstream effectors such as phospholipase PLCγ and guanine exchange factor VAV3, which subsequently activate further targets as shown. Details are provided within the body of the text.

infiltration of inflammatory cells, and increased production and activation of OCLs, which ultimately leads to bone erosion and joint destruction (Panagopoulos and Lambrou, 2018). Joints of RA patients only show mature OCLs close to the bone surface (Gravallese et al., 1998), but numerous mononuclear OCL precursors at different differentiation stages toward the OCL lineage are found in the vicinity of the joint, coming through the bloodstream and synovial microvasculature.

Not surprisingly, OSCAR has been detected in all these cells. Herman et al. (2008) showed that OSCAR is strongly expressed in the synovial tissue of RA patients. Staining of RA specimens revealed that OSCAR is expressed by multinucleated OCLs at the bone surface and approximately by 30% of mononuclear cells around synovial microvessels. Furthermore, circulating peripheral monocytes from RA patients showed 2-fold higher expression of OSCAR than monocytes from healthy individuals, suggesting that the receptor expression is increased before the cells enter the synovial tissue (Herman et al., 2008). *In vitro* culture demonstrated that these monocytes exhibited significantly higher differentiation into OCLs than cells with lower OSCAR levels from healthy individuals. Addition of OSCAR-Fc fusion protein to the culture inhibited the enhanced osteoclastogenesis and the effect was dose-dependent, reflecting competition for OSCAR ligand. These data suggest that the OSCAR pathway is activated in monocytes of RA patients, potentially exacerbating OCL differentiation and bone resorption (Herman et al., 2008). Similarly, Crotti et al. (2012) found that OSCAR and FcRγ were expressed in macrophage-like cells from the synovial tissue of active RA, and their levels were higher than those in tissue of inactive RA or healthy individuals. TREM2 and DAP12 were also found to be upregulated in inflammatory bone disease (Crotti et al., 2012; Chen et al., 2014). These results suggest that the enhanced destruction of bone seen in RA may partly be due to OSCAR-mediated differentiation of monocytes into OCLs, and further research is required to understand the relative contribution of TREM2-DAP12 and OSCAR-FcRγ complexes to bone disease.

## OSCAR Beyond OCLs: Excessive Activation of the Immune System

Excessive and inappropriate activation of the immune system presents another mechanism via which OSCAR may contribute

to the pathology of RA. Several studies have shown that human OSCAR is expressed not only in monocytes but also in other cells of the myeloid lineage, including macrophages, neutrophils and dendritic cells (Merck et al., 2004, 2005, 2006). Similarly to the signaling events in OCLs, activation of OSCAR in these cells was associated with an increase in $[Ca^{2+}]_i$ mediated through the ITAM-containing adaptor FcRγ. Dendritic cells (DCs) were found to express OSCAR continuously during all stages of differentiation, and the receptor was also maintained on the surface of mature cells (Merck et al., 2004). Ligation of OSCAR with an anti-OSCAR monoclonal antibody was shown to result in endocytosis of the receptor in a manner similar to the anti-mannose receptor internalization. The OSCAR-antibody complex was transported to vesicles associated with MHC class II-mediated antigen presentation. These findings indicate that in DCs OSCAR may be involved in antigen uptake and presentation (Merck et al., 2004). Furthermore, activation of OSCAR was shown to promote DC survival in a manner dependent on ERK and PI3K-induced expression of the anti-apoptotic proteins Bcl-2 and Bcl-xL (Merck et al., 2005). Stimulation of OSCAR was associated with increased maturation of DCs as well as with increased secretion of cytokines and chemokines such as the interleukins IL-8 and IL-12p40, monocyte chemoattractant protein-1 (MCP-1) and macrophage-derived chemokine (MDC). In addition, OSCAR signaling enhanced the stimulatory effects of Toll-like receptor ligands on DC maturation, cytokine release, and ability to induce T-cell proliferation and activation (Merck et al., 2005).

Following the identification of collagens as OSCAR ligands Schultz et al. (2015) demonstrated that collagen types I and II bind to OSCAR expressed on the surface of human DCs. Similar to the findings of Merck et al. (2004, 2005), the collagen-OSCAR interaction promoted the survival of DCs and enhanced the secretion of chemokines and proinflammatory cytokines, including tumor necrosis factor α (TNF-α), IL-6, IL-8, IL-10, IL-13, IL-23, and RANTES (Regulated on Activation, Normal T Cell Expressed and Secreted chemokine). Cells cultured on collagens I and II showed enhanced expression of maturation markers such as CD86 and CD83, and this effect was inhibited in a dose-dependent manner by the addition of OSCAR-blocking antibody (Schultz et al., 2015). These findings indicate that collagen-OSCAR interaction promotes DC maturation and activity, including secretion of pro-inflammatory cytokines, antigen uptake and induction of T lymphocytes.

Similar to the findings presented above, OSCAR signaling in monocytes was found to upregulate the expression of adhesion molecules and to increase the secretion of cytokines and chemokines including IL-8, MCP-1, MDC and ENA-78 (epithelial neutrophil-activating peptide-78) (Merck et al., 2006). The monocytes showed an increased lifespan when cultured in the absence of pro-survival factors. In contrast, OSCAR signaling did not affect the survival of neutrophils. However, the cells showed enhanced degranulation, synthesis of reactive oxygen species and cytokine release. Activation of OSCAR in neutrophils was also associated with changes in the expression of cell surface molecules involved in their recruitment (Merck et al., 2006). Collectively, these studies demonstrate that OSCAR signaling affects the function of both the innate and adaptive immune system, and thus it may play a role in inflammatory-mediated bone loss not only through supporting osteoclastogenesis but also through the enhanced recruitment and activation of immune cells.

Furthermore, a positive feedback loop may exist between OSCAR expression and immune cell activation in RA. As mentioned above, levels of OSCAR are higher in the synovial tissue of active RA compared to inactive RA (Crotti et al., 2012), suggesting that expression of OSCAR may be regulated by inflammatory cytokines. Indeed, Herman et al. (2008) investigated the effects of TNFα on OSCAR expression in monocytes *in vitro* and found that OSCAR mRNA was increased 4-fold in response to the treatment. OSCAR expression was also found to correlate with disease severity as indicated by the levels of C-reactive protein and erythrocyte sedimentation rate (which are markers of systemic inflammation), as well as by clinical assessment of RA activity (Herman et al., 2008).

Crotti et al. (2012) observed high OSCAR expression in the microvasculature of synovial tissue from RA patients and none in healthy control samples. OSCAR was detected on the luminal side of the microvasculature, suggesting association with endothelial cells. The authors hypothesized that the receptor is either expressed by endothelial cells or produced and secreted by other cells, following which it becomes bound to the endothelium at sites of inflammation (Crotti et al., 2012). Indeed, an earlier study by Goettsch et al. (2011) identified OSCAR in primary endothelial cells where its expression was found to be regulated by oxidized low density lipoprotein (oxLDL) via lectin-like oxidized LDL receptor 1 (LOX-1). The oxLDL-LOX1 interaction stimulated OSCAR induction in a manner that was dependent on activation of PI3K, calcium signaling and NFATc1. Similar to the anti-apoptotic effects of OSCAR in DCs and monocytes, stimulation of the receptor enhanced the survival of endothelial cells cultured in serum-free conditions (Goettsch et al., 2011). In a further study, the researchers found that OSCAR was upregulated in monocytes and macrophages from ApoE knockout mice fed on high-fat diet (Sinningen et al., 2013). TNFα and oxLDL produced an increase in OSCAR mRNA levels in RAW264.7 cells, while blockade of LOX-1 and NF-κB pathway abolished these effects (Sinningen et al., 2013). These studies, thereby, indicate that OSCAR expression is upregulated in endothelial cells and macrophages in response to pro-inflammatory stimuli.

Interestingly, changes in the level of OSCAR expression during bone disease may not be completely mirrored by those of FcRγ. Crotti et al. (2012) detected OSCAR but not FcRγ in the microvasculature of RA patients. In another study by Andersson et al. (2007), mouse calvarial bones cultured with synovial fluid from patients with osteoarthritis showed enhanced OSCAR and NFATc1 mRNA expression, while FcRγ levels remained unchanged relative to control. Considering this evidence, it may be speculated that in disease states OSCAR signaling may become uncoupled from FcRγ. As indicated earlier (section OSCAR Discovery and Structure) the cytoplasmic tail of OSCAR contains an amino acid sequence which suggests a potential guanylate cyclase activity (Nemeth et al., 2011). Furthermore,

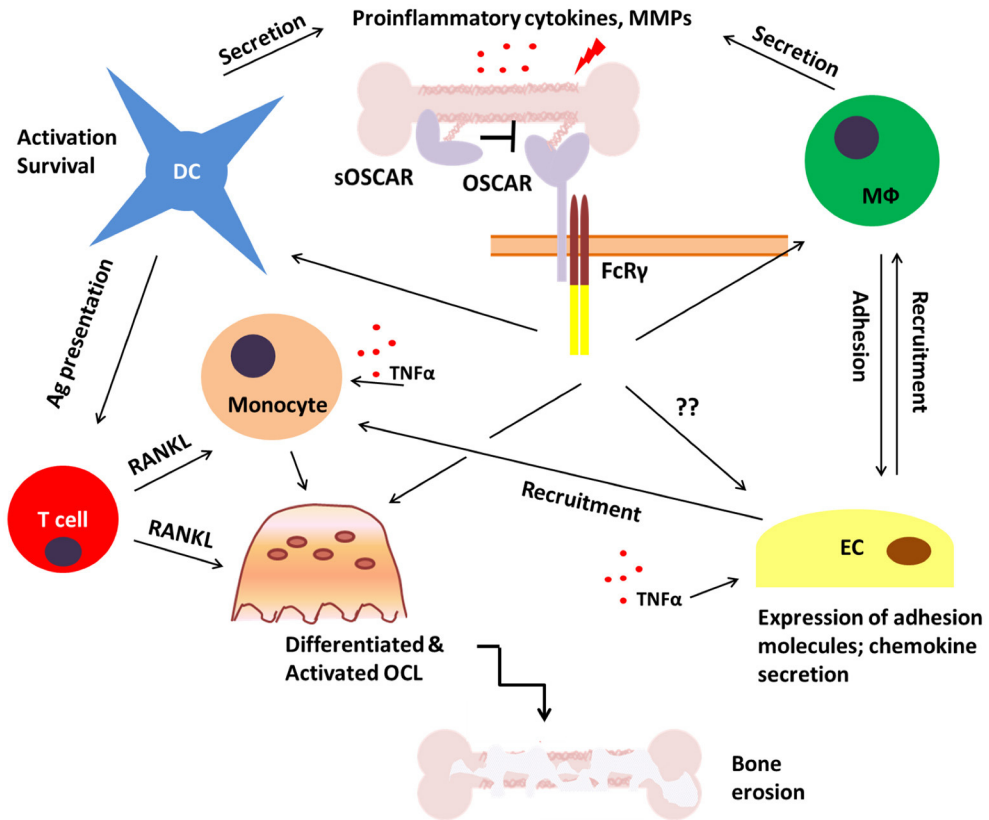


**FIGURE 5 |** Potential role of OSCAR in bone disease. During inflammatory bone disease inappropriate and prolonged activation of immune cells may lead to enhanced release of pro-inflammatory mediators such as cytokines, chemokines and matrix metalloproteinases (MMPs). This would stimulate the expression of adhesion molecules on endothelial cells (EC) and facilitate the recruitment of OSCAR-expressing immune cells including monocytes, dendritic cells (DC), and macrophages (Mϕ). This may lead to both amplification of the inflammatory process and enhanced osteoclastogenesis which would eventually result in bone erosion and fragility. A soluble form of OSCAR (sOSCAR) may prevent excessive signaling via OSCAR-FcRγ through competition for OSCAR ligands, although the current evidence for this is conflicting. OSCAR-FcRγ complex is also expressed on ECs, but little is known about its role in these cells in relation to bone disease.

OSCAR has been observed on the OCL surface in the absence of FcRγ, albeit the presence of the adaptor molecule was found to upregulate the receptor expression (Ishikawa et al., 2004). Thus, signaling through OSCAR independently of FcRγ may be possible, although evidence for this is lacking at present.

## OSCAR Expression in Chondrocytes: A Link to Osteoarthritis

Osteoarthritis (OA) has often been described as a degenerative joint disorder where the articular cartilage breaks down as a result of wear and tear, causing the bones to rub against each other, producing pain. However, OA is better defined as a whole joint disease that also affects subchondral bone, synovial membrane, ligaments and menisci (Loeser et al., 2012; Peng et al., 2021). Development of OA involves abnormal behavior of chondrocytes and altered metabolic homeostasis of the cartilage extracellular matrix. These result in chronic inflammation and defective remodeling of articular cartilage and neighboring bone driven by matrix degrading enzymes and inflammatory cytokines (Kapoor et al., 2011; Loeser et al., 2012; Hu and Ecker, 2021; Peng et al., 2021).

A recent study has reported for the first time a clear link between OA and OSCAR (Park et al., 2020). The authors demonstrated OSCAR expression in chondrocytes of wild-type mice, indicating that cells outside the non-myeloid lineage can also produce OSCAR. Furthermore, levels of expression were markedly elevated during OA pathogenesis in mouse and human articular cartilages. Genetic deletion of OSCAR in Oscar$^{-/-}$ mice (**Table 1**) reduced all hallmarks of OA pathology in an experimental model of induced OA. The study also demonstrated that OSCAR induces chondrocyte apoptosis during OA pathogenesis through its interaction with collagen, and that addition of a soluble OSCAR-Fc fusion protein attenuates OA pathogenesis in mouse models. Gene expression analysis identified a link between OSCAR and tumor necrosis factor-related apoptosis-inducing ligand (TRAIL), coded by the Tnfsf10 gene in mice and responsible for chondrocyte apoptosis in OA pathogenesis. TRAIL expression was downregulated in OA chondrocytes in Oscar$^{-/-}$ mice and in OA mice treated with OSCAR-Fc fusion protein. Thus, there seems to be an association between the interaction of OSCAR with collagen and the levels of TRAIL expression in the development and

progression of OA. Park et al. (2020) conclude that disruption of the OSCAR–collagen interaction is therefore a new avenue for the development of small molecule inhibitors or biologics as therapeutic agents against OA.

### A Secreted, Soluble Form of OSCAR in Serum

The discrepancy between the expression levels of OSCAR and FcRγ seen in diseased bone tissue may in part be associated with the detection of a secreted form of OSCAR. Indeed, a soluble form of OSCAR (sOSCAR) was initially identified in human blood serum (Herman et al., 2008), following which it was detected in the synovial fluid from RA patients (Crotti et al., 2012). Serum levels of sOSCAR were found to be decreased in RA patients compared to healthy individuals, and in a manner which correlated inversely with disease severity (Herman et al., 2008; Zhao et al., 2011). Furthermore, anti-TNFα therapy was demonstrated to significantly increase the levels of sOSCAR in serum (Herman et al., 2008). Given this evidence it may be hypothesized that in health OSCAR is either secreted or cleaved from the membrane surface after a certain signaling threshold is reached. The sOSCAR may bind pro-osteoclastogenic ligands and serve as a decoy receptor, thus limiting excessive production of OCLs and bone resorption. In inflammatory disorders, such as RA, pro-inflammatory mediators may lead to inhibition of OSCAR secretion/cleavage, which subsequently may result in decreased serum levels of sOSCAR and sustained pro-osteoclastogenic signaling.

It must be noted, however, that conflicting evidence has also been presented, indicating that sOSCAR levels may actually be positively regulated by pro-inflammatory cytokines. Crotti et al. (2012) cultured bone marrow endothelial cells in the presence of TNFα and IL-1β, and observed increased levels of OSCAR mRNA as well as the membrane-bound and secreted forms of the protein. In addition, Ndongo-Thiam et al. (2014) reported higher levels of sOSCAR in plasma from RA patients compared to healthy individuals. The authors concluded that levels of serum sOSCAR directly correlate with disease severity and may be predictive of bone destruction. A soluble form of OSCAR has also been detected in the synovial fluid of OA and RA patients with no significant difference between these groups (Crotti et al., 2012). It is not clear, however, whether and how levels of sOSCAR in serum and in synovial fluid correlate.

Considering the findings presented here, further research is imperative to resolve the discrepancy in the existing evidence and to clarify whether the soluble form of OSCAR is positively or negatively regulated by pro-inflammatory cytokines. In addition, further studies are required to identify the exact role and mechanism of sOSCAR production. It is unclear at present whether OSCAR is cleaved from the membrane and if so what signals regulate this process. Alternatively, sOSCAR may be produced as OSCAR-S via alternative splicing, and become exocytosed immediately following translation rather than being shed from the membrane. Answering these unknowns would help to understand better the role of OSCAR in physiological and pathological osteoclastogenesis, and may lead to the discovery of new therapeutics targeting excessive bone resorption.

## CONCLUDING REMARKS

OSCAR provides co-stimulatory signals which are required for osteoclast differentiation and activation (**Figure 4**). Furthermore, the expression of OSCAR and its adaptor molecule, FcRγ, is upregulated in inflammatory bone disease and osteoporosis (**Figure 5**). Given the available evidence it is plausible to consider that modulation of the signaling through OSCAR has the potential to suppress excessive osteoclastogenesis and bone resorption. Nevertheless, although this receptor has been identified nearly 20 years ago, many unanswered questions remain. For instance, what is the relative contribution of OSCAR-FcRγ complex to osteoclastogenesis considering that the FcRγ adaptor may couple with other immunoreceptors, or that other co-stimulatory molecules such as TREM2-DAP12 are also expressed by osteoclasts? Could OSCAR have an intrinsic signaling activity (i.e., independent of FcRγ) under certain conditions? What is the identity of the ligand expressed on osteoblast/stromal cells which activates OSCAR signaling? Could certain synthetic collagen-like peptides be used to inhibit the signaling through OSCAR-FcRγ complex? What signals are involved in termination of OSCAR-FcRγ activity? Is the soluble form of OSCAR produced by secretion or cleavage, and what are the signals that regulate its release? Do serum levels of sOSCAR increase or decrease during inflammatory bone disease, and could sOSCAR serve as a diagnostic marker?

Taking into consideration that OSCAR is expressed not only on osteoclasts but also on immune and other cell types such as endothelium, it is important to better understand the signaling through this receptor, and whether it contributes to chronic inflammatory disease. Since inflammation is at the core of many disorders affecting not only bone but also other body systems, modulation of OSCAR signaling may present new opportunities for alleviating disease activity and progression.

## AUTHOR CONTRIBUTIONS

IRN, MV, AE, JAH, and JB contributed to the literature research, discussion, and interpretation. IRN and JB drafted the manuscript. All the authors critically read, revised, and approved the final version of the manuscript.

## FUNDING

This work was supported by a Weizmann Institute-University of Manchester PhD studentship to IRN and a MRC CASE PhD studentship to MV (reference MR/R105767/1).

## SUPPLEMENTARY MATERIAL

The Supplementary Material for this article can be found online at: https://www.frontiersin.org/articles/10.3389/fcell.2021.641162/full#supplementary-material

## REFERENCES


Alias, E., Dharmapatni, A. S. S. K., Holding, A. C., Atkins, G. J., Findlay, D. M., Howie, D. W., et al. (2012). Polyethylene particles stimulate expression of ITAM-related molecules in peri-implant tissues and when stimulating osteoclastogenesis *in vitro*. *Acta Biomater.* 8, 3104–3112. doi: 10.1016/j.actbio.2012.04.037

Aliprantis, A. O., Ueki, Y., Sulyanto, R., Park, A., Sigrist, K. S., Sharma, S. M., et al. (2008). NFATc1 in mice represses osteoprotegerin during osteoclastogenesis and dissociates systemic osteopenia from inflammation in cherubism. *J. Clin. Invest.* 118, 3775–3789. doi: 10.1172/JCI35711

Andersen, T. L., Sondergaard, T. E., Skorzynska, K. E., Dagnaes-Hansen, F., Plesner, T. L., Hauge, E. M., et al. (2009). A physical mechanism for coupling bone resorption and formation in adult human bone. *Am. J. Pathol.* 174, 239–247. doi: 10.2353/ajpath.2009.080627

Andersson, M. K., Lundberg, P., Ohlin, A., Perry, M. J., Lie, A., Stark, A., et al. (2007). Effects on osteoclast and osteoblast activities in cultured mouse calvarial bones by synovial fluids from patients with a loose joint prosthesis and from osteoarthritis patients. *Arthritis Res. Ther.* 9:R18. doi: 10.1186/ar2127

Asagiri, M., Sato, K., Usami, T., Ochi, S., Nishina, H., Yoshida, H., et al. (2005). Autoamplification of NFATc1 expression determines its essential role in bone homeostasis. *J. Exp. Med.* 202, 1261–1269. doi: 10.1084/jem.20051150

Barrow, A. D., Palarasah, Y., Bugatti, M., Holehouse, A. S., Byers, D. E., Holtzman, M. J., et al. (2015). OSCAR is a receptor for surfactant protein D that activates TNF-α release from human CCR2+ inflammatory monocytes. *J. Immunol.* 194, 3317–3326. doi: 10.4049/jimmunol.1402289

Barrow, A. D., Raynal, N., Andersen, T. L., Slatter, D. A., Bihan, D., Pugh, N., et al. (2011). OSCAR is a collagen receptor that costimulates osteoclastogenesis in DAP12-deficient humans and mice. *J. Clin. Invest.* 121, 3505–3516. doi: 10.1172/JCI45913

Barrow, A. D., and Trowsdale, J. (2008). The extended human leukocyte receptor complex: diverse ways of modulating immune responses. *Immunol. Rev.* 224, 98–123. doi: 10.1111/j.1600-065X.2008.00653.x

Begg, S. K., Radley, J. M., Pollard, J. W., Chisholm, O. T., Stanley, E. R., and Bertoncello, I. (1993). Delayed hematopoietic development in osteopetrotic (op/op) mice. *J. Exp. Med.* 177, 237–242. doi: 10.1084/jem.177.1.237

Bella, J. (2016). Collagen structure: new tricks from a very old dog. *Biochem. J.* 473, 1001–1025. doi: 10.1042/BJ20151169

Bilezikian, J. P., Martin, T. J., Clemens, T. L., and Rosen, C. J. (2019). *Principles of Bone Biology. 4th Edn.* London: Academic Press.

Brondijk, T. H. C., De Ruiter, T., Ballering, J., Wienk, H., Lebbink, R. J., Van Ingen, H., et al. (2010). Crystal structure and collagen-binding site of immune inhibitory receptor LAIR-1: unexpected implications for collagen binding by platelet receptor GPVI. *Blood* 115, 1364–1373. doi: 10.1182/blood-2009-10-246322

Brounais, B., Ruiz, C., Rousseau, J., Lamoureux, F., Blanchard, F., Heymann, D., et al. (2008). Novel anti-cancer strategy in bone tumors by targeting molecular and cellular modulators of bone resorption. *Recent Pat. Anticancer Drug Discov.* 3, 178–186. doi: 10.2174/157489208786242269

Brunner, M., Jurdic, P., Tuckerman, J. P., Block, M. R., and Bouvard, D. (2013). New insights into adhesion signaling in bone formation. *Int. Rev. Cell Mol. Biol.* 305, 1–68. doi: 10.1016/B978-0-12-407695-2.00001-9

Bruzzaniti, A., and Baron, R. (2006). Molecular regulation of osteoclast activity. *Rev. Endocr. Metab. Disord.* 7, 123–139. doi: 10.1007/s11154-006-9009-x

Chen, D.-Y., Yao, L., Chen, Y.-M., Lin, C.-C., Huang, K.-C., Chen, S.-T., et al. (2014). A potential role of myeloid DAP12-associating lectin (MDL)-1 in the regulation of inflammation in rheumatoid arthritis patients. *PLoS ONE* 9:e86105. doi: 10.1371/journal.pone.0086105

Chen, X., Wang, Z., Duan, N., Zhu, G., Schwarz, E. M., and Xie, C. (2018). Osteoblast-osteoclast interactions. *Connect. Tissue Res.* 59, 99–107. doi: 10.1080/03008207.2017.1290085

Crotti, T. N., Dharmapatni, A., a,. S. S. K., Alias, E., and Haynes, D. R. (2015). Osteoimmunology: major and costimulatory pathway expression associated with chronic inflammatory induced bone loss. *J. Immunol. Res.* 2015, 281287. doi: 10.1155/2015/281287

Crotti, T. N., Dharmapatni, A. A., Alias, E., Zannettino, A. C. W., Smith, M. D., and Haynes, D. R. (2012). The immunoreceptor tyrosine-based activation motif (ITAM) -related factors are increased in synovial tissue and vasculature of rheumatoid arthritic joints. *Arthritis Res. Ther.* 14:R245. doi: 10.1186/ar4088

Crotti, T. N., Flannery, M., Walsh, N. C., Fleming, J. D., Goldring, S. R., and McHugh, K. P. (2006). NFATc1 regulation of the human β3 integrin promoter in osteoclast differentiation. *Gene* 372, 92–102. doi: 10.1016/j.gene.2005.12.012

Dai, X.-M., Ryan, G. R., Hapel, A. J., Dominguez, M. G., Russell, R. G., Kapp, S., et al. (2002). Targeted disruption of the mouse colony-stimulating factor 1 receptor gene results in osteopetrosis, mononuclear phagocyte deficiency, increased primitive progenitor cell frequencies, and reproductive defects. *Blood* 99, 111–120. doi: 10.1182/blood.V99.1.111

Dai, X. M., Zong, X. H., Akhter, M. P., and Stanley, E. R. (2004). Osteoclast deficiency results in disorganized matrix, reduced mineralization, and abnormal osteoblast behavior in developing bone. *J. Bone Miner. Res.* 19, 1441–1451. doi: 10.1359/JBMR.040514

David, J.-P., Sabapathy, K., Hoffmann, O., Idarraga, M. H., and Wagner, E. F. (2002). JNK1 modulates osteoclastogenesis through both c-Jun phosphorylation-dependent and -independent mechanisms. *J. Cell Sci.* 115, 4317–4325. doi: 10.1242/jcs.00082

de la Pompa, J. L., Timmerman, L. A., Takimoto, H., Yoshida, H., Elia, A. J., Samper, E., et al. (1998). Role of the NF-ATc transcription factor in morphogenesis of cardiac valves and septum. *Nature* 392, 182–186. doi: 10.1038/32419

Dougall, W. C., Glaccum, M., Charrier, K., Rohrbach, K., Brasel, K., De Smedt, T., et al. (1999). RANK is essential for osteoclast and lymph node development. *Genes Dev.* 13, 2412–2424. doi: 10.1101/gad.13.18.2412

Douni, E., Rinotas, V., Makrinou, E., Zwerina, J., Penninger, J. M., Eliopoulos, E., et al. (2012). A RANKL G278R mutation causing osteopetrosis identifies a functional amino acid essential for trimer assembly in RANKL and TNF. *Hum. Mol. Genet.* 21, 784–798. doi: 10.1093/hmg/ddr510

Ellmeier, W., Jung, S., Sunshine, M. J., Hatam, F., Xu, Y., Baltimore, D., et al. (2000). Severe B cell deficiency in mice lacking the tec kinase family members Tec and Btk. *J. Exp. Med.* 192, 1611–1624. doi: 10.1084/jem.192.11.1611

Faccio, R., Zou, W., Colaianni, G., Teitelbaum, S. L., and Ross, F. P. (2003). High dose M-CSF partially rescues the Dap12-/- osteoclast phenotype. *J. Cell. Biochem.* 90, 871–883. doi: 10.1002/jcb.10694

Feng, X., and Teitelbaum, S. L. (2013). Osteoclasts: new insights. *Bone Res.* 1, 11–26. doi: 10.4248/BR201301003

Findlay, D. M., and Atkins, G. J. (2011). Relationship between serum RANKL and RANKL in bone. *Osteoporos. Int.* 22, 2597–2602. doi: 10.1007/s00198-011-1740-9

Franzoso, G., Carlson, L., Xing, L., Poljak, L., Shores, E. W., Brown, K. D., et al. (1997). Requirement for NF-kappaB in osteoclast and B-cell development. *Genes Dev.* 11, 3482–3496. doi: 10.1101/gad.11.24.3482

Goettsch, C., Rauner, M., Sinningen, K., Helas, S., Al-Fakhri, N., Nemeth, K., et al. (2011). The osteoclast-associated receptor (OSCAR) is a novel receptor regulated by oxidized low-density lipoprotein in human endothelial cells. *Endocrinology* 152, 4915–4926. doi: 10.1210/en.2011-1282

Gohda, J., Akiyama, T., Koga, T., Takayanagi, H., Tanaka, S., and Inoue, J.-I. (2005). RANK-mediated amplification of TRAF6 signaling leads to NFATc1 induction during osteoclastogenesis. *EMBO J.* 24, 790–799. doi: 10.1038/sj.emboj.7600564

Granot-Attas, S., and Elson, A. (2008). Protein tyrosine phosphatases in osteoclast differentiation, adhesion, and bone resorption. *Eur. J. Cell Biol.* 87, 479–490. doi: 10.1016/j.ejcb.2008.01.006

Gravallese, E. M., Harada, Y., Wang, J. T., Gorn, A. H., Thornhill, T. S., and Goldring, S. R. (1998). Identification of cell types responsible for bone resorption in rheumatoid arthritis and juvenile rheumatoid arthritis. *Am. J. Pathol.* 152, 943–951.

Harris, S. E., Macdougall, M., Horn, D., Woodruff, K., Zimmer, S. N., Rebel, V. I., et al. (2012). Meox2Cre-mediated disruption of CSF-1 leads to osteopetrosis and osteocyte defects. *Bone* 50, 42–53. doi: 10.1016/j.bone.2011.09.038

Haywood, J., Qi, J., Chen, C.-C., Lu, G., Liu, Y., Yan, J., et al. (2016). Structural basis of collagen recognition by human osteoclast-associated receptor and design of osteoclastogenesis inhibitors. *Proc. Natl. Acad. Sci. U.S.A.* 113, 1038–1043. doi: 10.1073/pnas.1522572113

He, Y., Staser, K., Rhodes, S. D., Liu, Y., Wu, X., Park, S.-J., et al. (2011). Erk1 positively regulates osteoclast differentiation and bone resorptive activity. *PLoS ONE* 6:e24780. doi: 10.1371/journal.pone.0024780

Herman, S., Müller, R. B., Krönke, G., Zwerina, J., Redlich, K., Hueber, A. J., et al. (2008). Induction of osteoclast-associated receptor, a key osteoclast costimulation molecule, in rheumatoid arthritis. *Arthritis Rheum.* 58, 3041–3050. doi: 10.1002/art.23943

Hess, J., Angel, P., and Schorpp-Kistner, M. (2004). AP-1 subunits: quarrel and harmony among siblings. *J. Cell. Sci.* 117, 5965–5973. doi: 10.1242/jcs.01589

Hodgkinson, C. A., Moore, K. J., Nakayama, A., Steingrímsson, E., Copeland, N. G., Jenkins, N. A., et al. (1993). Mutations at the mouse microphthalmia locus are associated with defects in a gene encoding a novel basic-helix-loop-helix-zipper protein. *Cell* 74, 395–404. doi: 10.1016/0092-8674(93)90429-T

Houston, I. B., Kamath, M. B., Schweitzer, B. L., Chlon, T. M., and Dekoter, R. P. (2007). Reduction in PU.1 activity results in a block to B-cell development, abnormal myeloid proliferation, and neonatal lethality. *Exp. Hematol.* 35, 1056–1068. doi: 10.1016/j.exphem.2007.04.005

Hu, Q., and Ecker, M. (2021). Overview of MMP-13 as a promising target for the treatment of osteoarthritis. *Int. J. Mol. Sci.* 22:1742. doi: 10.3390/ijms22041742

Humphrey, M. B., and Nakamura, M. C. (2016). A comprehensive review of immunoreceptor regulation of osteoclasts. *Clin. Rev. Allergy Immunol.* 51, 48–58. doi: 10.1007/s12016-015-8521-8

Iotsova, V., Caamaño, J., Loy, J., Yang, Y., Lewin, A., and Bravo, R. (1997). Osteopetrosis in mice lacking NF-κB1 and NF-κB2. *Nat. Med.* 3, 1285–1289. doi: 10.1038/nm1197-1285

Iseme, R. A., Mcevoy, M., Kelly, B., Agnew, L., Walker, F. R., and Attia, J. (2017). Is osteoporosis an autoimmune mediated disorder? *Bone Rep.* 7, 121–131. doi: 10.1016/j.bonr.2017.10.003

Ishida, N., Hayashi, K., Hoshijima, M., Ogawa, T., Koga, S., Miyatake, Y., et al. (2002). Large scale gene expression analysis of osteoclastogenesis *in vitro* and elucidation of NFAT2 as a key regulator. *J. Biol. Chem.* 277, 41147–41156. doi: 10.1074/jbc.M205063200

Ishikawa, S., Arase, N., Suenaga, T., Saita, Y., Noda, M., Kuriyama, T., et al. (2004). Involvement of FcRγ in signal transduction of osteoclast-associated receptor (OSCAR). *Int. Immunol.* 16, 1019–1025. doi: 10.1093/intimm/dxh103

Ivashkiv, L. B. (2009). Cross-regulation of signaling by ITAM-associated receptors. *Nat. Immunol.* 10, 340–347. doi: 10.1038/ni.1706

Jakus, Z., Fodor, S., Abram, C. L., Lowell, C. A., and Mócsai, A. (2007). Immunoreceptor-like signaling by β2 and β3 integrins. *Trends Cell Biol.* 17, 493–501. doi: 10.1016/j.tcb.2007.09.001

Kapoor, M., Martel-Pelletier, J., Lajeunesse, D., Pelletier, J. P., and Fahmi, H. (2011). Role of proinflammatory cytokines in the pathophysiology of osteoarthritis. *Nat. Rev. Rheumatol.* 7, 33–42. doi: 10.1038/nrrheum.2010.196

Kapur, R. P., Yao, Z., Iida, M. H., Clarke, C. M., Doggett, B., Xing, L., et al. (2004). Malignant autosomal recessive osteopetrosis caused by spontaneous mutation of murine *Rank*. *J. Bone Miner. Res.* 19, 1689–1697. doi: 10.1359/JBMR.040713

Kenkre, J. S., and Bassett, J. H. D. (2018). The bone remodelling cycle. *Ann. Clin. Biochem.* 55, 308–327. doi: 10.1177/0004563218759371

Kim, G. S., Koh, J.-M., Chang, J. S., Park, B. L., Kim, L. H., Park, E. K., et al. (2005a). Association of the OSCAR promoter polymorphism with BMD in postmenopausal women. *J. Bone Miner. Res.* 20, 1342–1348. doi: 10.1359/JBMR.050320

Kim, J. H., Kim, K., Jin, H. M., Song, I., Youn, B. U., Lee, J., et al. (2009). Silibinin inhibits osteoclast differentiation mediated by TNF family members. *Mol. Cells* 28, 201–207. doi: 10.1007/s10059-009-0123-y

Kim, J. H., Kim, K., Youn, B. U., Jin, H. M., and Kim, N. (2010). MHC class II transactivator negatively regulates RANKL-mediated osteoclast differentiation by downregulating NFATc1 and OSCAR. *Cell. Signal.* 22, 1341–1349. doi: 10.1016/j.cellsig.2010.05.001

Kim, J. H., and Kim, N. (2016). Signaling pathways in osteoclast differentiation. *Chonnam Med. J.* 52, 12–17. doi: 10.4068/cmj.2016.52.1.12

Kim, K., Kim, J. H., Lee, J., Jin, H.-M., Lee, S.-H., Fisher, D. E., et al. (2005b). Nuclear factor of activated T cells c1 induces osteoclast-associated receptor gene expression during tumor necrosis factor-related activation-induced cytokine-mediated osteoclastogenesis. *J. Biol. Chem.* 280, 35209–35216. doi: 10.1074/jbc.M505815200

Kim, K., Kim, J. H., Lee, J., Jin, H. M., Kook, H., Kim, K. K., et al. (2007a). MafB negatively regulates RANKL-mediated osteoclast differentiation. *Blood* 109, 3253–3259. doi: 10.1182/blood-2006-09-048249

Kim, K., Lee, J., Kim, J. H., Jin, H. M., Zhou, B., Lee, S. Y., et al. (2007b). Protein inhibitor of activated STAT 3 modulates osteoclastogenesis by down-regulation of NFATc1 and osteoclast-associated receptor. *J. Immunol.* 178, 5588–5594. doi: 10.4049/jimmunol.178.9.5588

Kim, K., Lee, S.-H., Ha Kim, J., Choi, Y., and Kim, N. (2008). NFATc1 induces osteoclast fusion via up-regulation of Atp6v0d2 and the dendritic cell-specific transmembrane protein (DC-STAMP). *Mol. Endocrinol.* 22, 176–185. doi: 10.1210/me.2007-0237

Kim, N., Odgren, P. R., Kim, D. K., Marks, S. C., and Choi, Y. (2000). Diverse roles of the tumor necrosis factor family member TRANCE in skeletal physiology revealed by TRANCE deficiency and partial rescue by a lymphocyte-expressed TRANCE transgene. *Proc. Natl. Acad. Sci. U.S.A.* 97, 10905–10910. doi: 10.1073/pnas.200294797

Kim, N., Takami, M., Rho, J., Josien, R., and Choi, Y. (2002). A novel member of the leukocyte receptor complex regulates osteoclast differentiation. *J. Exp. Med.* 195, 201–209. doi: 10.1084/jem.20011681

Kim, Y., Sato, K., Asagiri, M., Morita, I., Soma, K., and Takayanagi, H. (2005c). Contribution of nuclear factor of activated T cells c1 to the transcriptional control of immunoreceptor osteoclast-associated receptor but not triggering receptor expressed by myeloid cells-2 during osteoclastogenesis. *J. Biol. Chem.* 280, 32905–32913. doi: 10.1074/jbc.M505820200

Kindle, L., Rothe, L., Kriss, M., Osdoby, P., and Collin-Osdoby, P. (2006). Human microvascular endothelial cell activation by IL-1 and TNF-α stimulates the adhesion and transendothelial migration of circulating human $CD14^+$ monocytes that develop with RANKL into functional osteoclasts. *J. Bone Miner. Res.* 21, 193–206. doi: 10.1359/JBMR.051027

Kodama, J., and Kaito, T. (2020). Osteoclast multinucleation: review of current literature. *Int. J. Mol. Sci.* 21:5685. doi: 10.3390/ijms21165685

Koga, T., Inui, M., Inoue, K., Kim, S., Suematsu, A., Kobayashi, E., et al. (2004). Costimulatory signals mediated by the ITAM motif cooperate with RANKL for bone homeostasis. *Nature* 428, 758–763. doi: 10.1038/nature02444

Kong, Y. Y., Yoshida, H., Sarosi, I., Tan, H. L., Timms, E., Capparelli, C., et al. (1999). OPGL is a key regulator of osteoclastogenesis, lymphocyte development and lymph-node organogenesis. *Nature* 397, 315–323. doi: 10.1038/16852

Lademann, F., Hofbauer, L. C., and Rauner, M. (2020). The bone morphogenetic protein pathway: the osteoclastic perspective. *Front. Cell Dev. Biol.* 8:586031. doi: 10.3389/fcell.2020.586031

Lecut, C., Arocas, V., Ulrichts, H., Elbaz, A., Villeval, J.-L., Lacapère, J.-J., et al. (2004). Identification of residues within human glycoprotein VI involved in the binding to collagen: evidence for the existence of distinct binding sites. *J. Biol. Chem.* 279, 52293–52299. doi: 10.1074/jbc.M406342200

Lee, J., Kim, K., Kim, J. H., Jin, H. M., Choi, H. K., Lee, S.-H., et al. (2006). Id helix-loop-helix proteins negatively regulate TRANCE-mediated osteoclast differentiation. *Blood* 107, 2686–2693. doi: 10.1182/blood-2005-07-2798

Li, J., Sarosi, I., Yan, X. Q., Morony, S., Capparelli, C., Tan, H. L., et al. (2000). RANK is the intrinsic hematopoietic cell surface receptor that controls osteoclastogenesis and regulation of bone mass and calcium metabolism. *Proc. Natl. Acad. Sci. U. S. A.* 97, 1566–1571. doi: 10.1073/pnas.97.4.1566

Li, X., Udagawa, N., Itoh, K., Suda, K., Murase, Y., Nishihara, T., et al. (2002). p38 MAPK-mediated signals are required for inducing osteoclast differentiation but not for osteoclast function. *Endocrinology* 143, 3105–3113. doi: 10.1210/endo.143.8.8954

Loeser, R. F., Goldring, S. R., Scanzello, C. R., and Goldring, M. B. (2012). Osteoarthritis: a disease of the joint as an organ. *Arthritis Rheum.* 64, 1697–1707. doi: 10.1002/art.34453

Lomaga, M. A., Yeh, W.-C., Sarosi, I., Duncan, G. S., Furlonger, C., Ho, A., et al. (1999). TRAF6 deficiency results in osteopetrosis and defective interleukin-1, CD40, and LPS signaling. *Genes Dev.* 13, 1015–1024. doi: 10.1101/gad.13.8.1015

Matsumoto, M., Kogawa, M., Wada, S., Takayanagi, H., Tsujimoto, M., Katayama, S., et al. (2004). Essential role of p38 mitogen-activated protein kinase in cathepsin K gene expression during osteoclastogenesis through association of NFATc1 and PU.1. *J. Biol. Chem.* 279, 45969–45979. doi: 10.1074/jbc.M408795200

Matsuo, K., Galson, D. L., Zhao, C., Peng, L., Laplace, C., Wang, K. Z. Q., et al. (2004). Nuclear factor of activated T-cells (NFAT) rescues osteoclastogenesis in precursors lacking c-Fos. *J. Biol. Chem.* 279, 26475–26480. doi: 10.1074/jbc.M313973200

McGill, G. G., Horstmann, M., Widlund, H. R., Du, J., Motyckova, G., Nishimura, E. K., et al. (2002). Bcl2 regulation by the melanocyte master regulator Mitf

modulates lineage survival and melanoma cell viability. *Cell* 109, 707–718. doi: 10.1016/S0092-8674(02)00762-6

McHugh, K. P., Hodivala-Dilke, K., Zheng, M.-H., Namba, N., Lam, J., Novack, D., et al. (2000). Mice lacking β3 integrins are osteosclerotic because of dysfunctional osteoclasts. *J. Clin. Invest.* 105, 433–440. doi: 10.1172/JCI8905

Merck, E., De Saint-Vis, B., Scuiller, M., Gaillard, C., Caux, C., Trinchieri, G., et al. (2005). Fc receptor γ-chain activation via hOSCAR induces survival and maturation of dendritic cells and modulates Toll-like receptor responses. *Blood* 105, 3623–3632. doi: 10.1182/blood-2004-07-2809

Merck, E., Gaillard, C., Gorman, D. M., Montero-Julian, F., Durand, I., Zurawski, S. M., et al. (2004). OSCAR is an FcRγ-associated receptor that is expressed by myeloid cells and is involved in antigen presentation and activation of human dendritic cells. *Blood* 104, 1386–1395. doi: 10.1182/blood-2004-03-0850

Merck, E., Gaillard, C., Scuiller, M., Scapini, P., Cassatella, M. A., Trinchieri, G., et al. (2006). Ligation of the FcRγ chain-associated human osteoclast-associated receptor enhances the proinflammatory responses of human monocytes and neutrophils. *J. Immunol.* 176, 3149–3156. doi: 10.4049/jimmunol.176.5.3149

Mócsai, A., Humphrey, M. B., Van Ziffle, J., a,. G., Hu, Y., Burghardt, A., et al. (2004). The immunomodulatory adapter proteins DAP12 and Fc receptor γ-chain (FcRγ) regulate development of functional osteoclasts through the Syk tyrosine kinase. *Proc. Natl. Acad. Sci. U. S. A.* 101, 6158–6163. doi: 10.1073/pnas.0401602101

Naito, A., Azuma, S., Tanaka, S., Miyazaki, T., Takaki, S., Takatsu, K., et al. (1999). Severe osteopetrosis, defective interleukin-1 signalling and lymph node organogenesis in TRAF6-deficient mice. *Genes Cells* 4, 353–362. doi: 10.1046/j.1365-2443.1999.00265.x

Naito, M., Hayashi, S., Yoshida, H., Nishikawa, S., Shultz, L. D., and Takahashi, K. (1991). Abnormal differentiation of tissue macrophage populations in 'osteopetrosis' (op) mice defective in the production of macrophage colony-stimulating factor. *Am. J. Pathol.* 139, 657–667.

Naito, M., Umeda, S., Takahashi, K., and Shultz, L. D. (1997). Macrophage differentiation and granulomatous inflammation in osteopetrotic mice (op/op) defective in the production of CSF-1. *Mol. Reprod. Dev.* 46, 85–91. doi: 10.1002/(SICI)1098-2795(199701)46:1<85::AID-MRD13>3.0.CO;2-2

Nakamichi, Y., Udagawa, N., and Takahashi, N. (2013). IL-34 and CSF-1: similarities and differences. *J. Bone Miner. Metab.* 31, 486–495. doi: 10.1007/s00774-013-0476-3

Nakashima, T., Hayashi, M., Fukunaga, T., Kurata, K., Oh-Hora, M., Feng, J. Q., et al. (2011). Evidence for osteocyte regulation of bone homeostasis through RANKL expression. *Nat. Med.* 17, 1231–1234. doi: 10.1038/nm.2452

Napoli, N., Chandran, M., Pierroz, D. D., Abrahamsen, B., Schwartz, A. V., Ferrari, S. L., et al. (2017). Mechanisms of diabetes mellitus-induced bone fragility. *Nat. Rev. Endocrinol.* 13, 208–219. doi: 10.1038/nrendo.2016.153

Nataf, S., Anginot, A., Vuaillat, C., Malaval, L., Fodil, N., Chereul, E., et al. (2005). Brain and bone damage in KARAP/DAP12 loss-of-function mice correlate with alterations in microglia and osteoclast lineages. *Am. J. Pathol.* 166, 275–286. doi: 10.1016/S0002-9440(10)62251-1

Ndongo-Thiam, N., Sallmard, G. D., Kastrup, J., and Miossec, P. (2014). Levels of soluble osteoclast-associated receptor (sOSCAR) in rheumatoid arthritis: link to disease severity and cardiovascular risk. *Ann. Rheum. Dis.* 73, 1276–1277. doi: 10.1136/annrheumdis-2013-204886

Nemeth, K., Schoppet, M., Al-Fakhri, N., Helas, S., Jessberger, R., Hofbauer, L. C., et al. (2011). The role of osteoclast-associated receptor in osteoimmunology. *J. Immunol.* 186, 13–18. doi: 10.4049/jimmunol.1002483

Nii, A., Steingrimsson, E., Copeland, N. G., Jenkins, N. A., and Ward, J. M. (1995). Mild osteopetrosis in the microphthalmia-oak ridge mouse. A model for intermediate autosomal recessive osteopetrosis in humans. *Am. J. Pathol.* 147, 1871–1882.

Palagano, E., Menale, C., Sobacchi, C., and Villa, A. (2018). Genetics of osteopetrosis. *Curr. Osteoporos. Rep.* 16, 13–25. doi: 10.1007/s11914-018-0415-2

Palmer, K., Fairfield, H., Borgeia, S., Curtain, M., Hassan, M. G., Dionne, L., et al. (2016). Discovery and characterization of spontaneous mouse models of craniofacial dysmorphology. *Dev. Biol.* 415, 216–227. doi: 10.1016/j.ydbio.2015.07.023

Paloneva, J., Kestil,ä, M., Wu, J., Salminen, A., Böhling, T., Ruotsalainen, V., et al. (2000). Loss-of-function mutations in *TYROBP* (*DAP12*) result in a presenile dementia with bone cysts. *Nat. Genet.* 25, 357–361. doi: 10.1038/77153

Paloneva, J., Manninen, T., Christman, G., Hovanes, K., Mandelin, J., Adolfsson, R., et al. (2002). Mutations in two genes encoding different subunits of a receptor signaling complex result in an identical disease phenotype. *Am. J. Hum. Genet.* 71, 656–662. doi: 10.1086/342259

Panagopoulos, P. K., and Lambrou, G. I. (2018). Bone erosions in rheumatoid arthritis: recent developments in pathogenesis and therapeutic implications. *J. Musculoskelet. Neuronal Interact.* 18, 304–319.

Park, D. R., Kim, J., Kim, G. M., Lee, H., Kim, M., Hwang, D., et al. (2020). Osteoclast-associated receptor blockade prevents articular cartilage destruction via chondrocyte apoptosis regulation. *Nat. Commun.* 11:4343. doi: 10.1038/s41467-020-18208-y

Park, J.-Y., Bae, M.-A., Cheon, H. G., Kim, S. S., Hong, J.-M., Kim, T.-H., et al. (2009). A novel PPARγ agonist, KR62776, suppresses RANKL-induced osteoclast differentiation and activity by inhibiting MAP kinase pathways. *Biochem. Biophys. Res. Commun.* 378, 645–649. doi: 10.1016/j.bbrc.2008.11.115

Park, J. H., Lee, N. K., and Lee, S. Y. (2017). Current understanding of RANK signaling in osteoclast differentiation and maturation. *Mol. Cells* 40, 706–713. doi: 10.14348/molcells.2017.0225

Park-Min, K. H. (2018). Mechanisms involved in normal and pathological osteoclastogenesis. *Cell. Mol. Life Sci.* 75, 2519–2528. doi: 10.1007/s00018-018-2817-9

Peng, Z., Sun, H., Bunpetch, V., Koh, Y., Wen, Y., Wu, D., et al. (2021). The regulation of cartilage extracellular matrix homeostasis in joint cartilage degeneration and regeneration. *Biomaterials* 268:120555. doi: 10.1016/j.biomaterials.2020.120555

Ross, F. P., and Teitelbaum, S. L. (2005). αvβ3 and macrophage colony-stimulating factor: partners in osteoclast biology. *Immunol. Rev.* 208, 88–105. doi: 10.1111/j.0105-2896.2005.00331.x

Rucci, N. (2008). Molecular biology of bone remodelling. *Clin. Cases Miner. Bone Metab.* 5, 49–56.

Sato, K., Suematsu, A., Nakashima, T., Takemoto-Kimura, S., Aoki, K., Morishita, Y., et al. (2006). Regulation of osteoclast differentiation and function by the CaMK-CREB pathway. *Nat. Med.* 12, 1410–1416. doi: 10.1038/nm1515

Schultz, H. S., Nitze, L. M., Zeuthen, L. H., Keller, P., Gruhler, A., Pass, J., et al. (2015). Collagen induces maturation of human monocyte-derived dendritic cells by signaling through osteoclast-associated receptor. *J. Immunol.* 194, 3169–3179. doi: 10.4049/jimmunol.1402800

Seeman, E. (2019). "Modeling and remodeling: the cellular machinery responsible for bone's material and structural strength during growth, aging and drug therapy," in *Principles of Bone Biology. 4th Edn*, eds J. P. Bilezikian, T. J. Martin, T. L. Clemens, and C. J. Rosen (London: Academic Press), 245–274.

Shinohara, M., Koga, T., Okamoto, K., Sakaguchi, S., Arai, K., Yasuda, H., et al. (2008). Tyrosine kinases Btk and Tec regulate osteoclast differentiation by linking RANK and ITAM signals. *Cell* 132, 794–806. doi: 10.1016/j.cell.2007.12.037

Sinningen, K., Rauner, M., Goettsch, C., Al-Fakhri, N., Schoppet, M., and Hofbauer, L. C. (2013). Monocytic expression of osteoclast-associated receptor (OSCAR) is induced in atherosclerotic mice and regulated by oxidized low-density lipoprotein *in vitro*. *Biochem. Biophys. Res. Commun.* 437, 314–318. doi: 10.1016/j.bbrc.2013.06.074

So, H., Rho, J., Jeong, D., Park, R., Fisher, D. E., Ostrowski, M. C., et al. (2003). Microphthalmia transcription factor and PU.1 synergistically induce the leukocyte receptor osteoclast-associated receptor gene expression. *J. Biol. Chem.* 278, 24209–24216. doi: 10.1074/jbc.M302940200

Sobacchi, C., Schulz, A., Coxon, F. P., Villa, A., and Helfrich, M. H. (2013). Osteopetrosis: genetics, treatment and new insights into osteoclast function. *Nat. Rev. Endocrinol.* 9, 522–536. doi: 10.1038/nrendo.2013.137

Steingrimsson, E., Tessarollo, L., Pathak, B., Hou, L., Arnheiter, H., Copeland, N. G., et al. (2002). Mitf and Tfe3, two members of the Mitf-Tfe family of bHLH-Zip transcription factors, have important but functionally redundant roles in osteoclast development. *Proc. Natl. Acad. Sci. U. S. A.* 99, 4477–4482. doi: 10.1073/pnas.072071099

Takahashi, N., Udagawa, N., Kobayashi, Y., Takami, M., Martin, T. J., and Suda, T. (2008). "Osteoclast generation," in *Principles of Bone Biology, 3rd Edn,* eds J. P. Bilezikian, L. G. Raisz, and T. J. Martin (San Diego: Academic Press), 175–192.

Takatsuna, H., Asagiri, M., Kubota, T., Oka, K., Osada, T., Sugiyama, C., et al. (2005). Inhibition of RANKL-induced osteoclastogenesis by (–)-DHMEQ, a

novel NF-κB inhibitor, through downregulation of NFATc1. *J. Bone Miner. Res.* 20, 653–662. doi: 10.1359/JBMR.041213

Takayanagi, H. (2007). Osteoimmunology: shared mechanisms and crosstalk between the immune and bone systems. *Nat. Rev. Immunol.* 7, 292–304. doi: 10.1038/nri2062

Takayanagi, H., Kim, S., Koga, T., Nishina, H., Isshiki, M., Yoshida, H., et al. (2002). Induction and activation of the transcription factor NFATc1 (NFAT2) integrate RANKL signaling in terminal differentiation of osteoclasts. *Dev. Cell* 3, 889–901. doi: 10.1016/S1534-5807(02)00369-6

Teitelbaum, S. L. (2007). Osteoclasts: what do they do and how do they do it? *Am. J. Pathol.* 170, 427–435. doi: 10.2353/ajpath.2007.060834

Tomasello, E., Desmoulins, P. O., Chemin, K., Guia, S., Cremer, H., Ortaldo, J., et al. (2000). Combined natural killer cell and dendritic cell functional deficiency in KARAP/DAP12 loss-of-function mutant mice. *Immunity* 13, 355–364. doi: 10.1016/S1074-7613(00)00035-2

Tondravi, M. M., Mckercher, S. R., Anderson, K., Erdmann, J. M., Quiroz, M., Maki, R., et al. (1997). Osteopetrosis in mice lacking haematopoietic transcription factor PU.1. *Nature* 386, 81–84. doi: 10.1038/386081a0

Underhill, D. M., and Goodridge, H. S. (2007). The many faces of ITAMs. *Trends Immunol.* 28, 66–73. doi: 10.1016/j.it.2006.12.004

Wada, T., Nakashima, T., Oliveira-Dos-Santos, A. J., Gasser, J., Hara, H., Schett, G., et al. (2005). The molecular scaffold Gab2 is a crucial component of RANK signaling and osteoclastogenesis. *Nat. Med.* 11, 394–399. doi: 10.1038/nm1203

Wang, Z.-Q., Ovitt, C., Grigoriadis, A. E., Möhle-Steinlein, U., Rüther, U., and Wagner, E. F. (1992). Bone and haematopoietic defects in mice lacking c-*fos*. *Nature* 360, 741–745. doi: 10.1038/360741a0

Weilbaecher, K. N., Motyckova, G., Huber, W. E., Takemoto, C. M., Hemesath, T. J., Xu, Y., et al. (2001). Linkage of M-CSF signaling to Mitf, TFE3, and the osteoclast defect in *Mitf*$^{mi/mi}$ mice. *Mol. Cell* 8, 749–758. doi: 10.1016/S1097-2765(01)00360-4

Wong, B., Besser, D., Kim, N., Arron, J., Vologodskaia, M., Hanafusa, H., et al. (1999). TRANCE, a TNF family member, activates Akt/PKB through a signaling complex involving TRAF6 and c-Src. *Mol. Cell* 4, 1041–1049. doi: 10.1016/S1097-2765(00)80232-4

Yamashita, T., Yao, Z., Li, F., Zhang, Q., Badell, I. R., Schwarz, E. M., et al. (2007). NF-κB p50 and p52 regulate receptor activator of NF-κB ligand (RANKL) and tumor necrosis factor-induced osteoclast precursor differentiation by activating c-Fos and NFATc1. *J. Biol. Chem.* 282, 18245–18253. doi: 10.1074/jbc.M610701200

Yavropoulou, M. P., and Yovos, J. G. (2008). Osteoclastogenesis–current knowledge and future perspectives. *J. Musculoskelet. Neuronal Interact.* 8, 204–216.

Yoshida, H., Hayashi, S.-I., Kunisada, T., Ogawa, M., Nishikawa, S., Okamura, H., et al. (1990). The murine mutation osteopetrosis is in the coding region of the macrophage colony stimulating factor gene. *Nature* 345, 442–444. doi: 10.1038/345442a0

Zhao, S., Guo, Y.-Y., Ding, N., Yang, L.-L., and Zhang, N. (2011). Changes in serum levels of soluble osteoclast-associated receptor in human rheumatoid arthritis. *Chin. Med. J.* 124, 3058–3060. doi: 10.3760/cma.j.issn.0366-6999.2011.19.019

Zhou, L., Hinerman, J. M., Blaszczyk, M., Miller, J. L. C., Conrady, D. G., Barrow, A. D., et al. (2016). Structural basis for collagen recognition by the immune receptor OSCAR. *Blood* 127, 529–537. doi: 10.1182/blood-2015-08-667055

Zou, W., Kitaura, H., Reeve, J., Long, F., Tybulewicz, V. L. J., Shattil, S. J., et al. (2007). Syk, c-Src, the αvβ3 integrin, and ITAM immunoreceptors, in concert, regulate osteoclastic bone resorption. *J. Cell Biol.* 176, 877–888. doi: 10.1083/jcb.200611083

Zou, W., and Teitelbaum, S. L. (2015). Absence of Dap12 and the αvβ3 integrin causes severe osteopetrosis. *J. Cell Biol.* 208, 125–136. doi: 10.1083/jcb.201410123

**Conflict of Interest:** The authors declare that the research was conducted in the absence of any commercial or financial relationships that could be construed as a potential conflict of interest.

frontiers in Cell and Developmental Biology

HYPOTHESIS AND THEORY
published: 20 May 2021
doi: 10.3389/fcell.2021.671210

# Sorting Nexin 10 as a Key Regulator of Membrane Trafficking in Bone-Resorbing Osteoclasts: Lessons Learned From Osteopetrosis

*Ari Elson[1]*, Merle Stein[2], Grace Rabie[3], Maayan Barnea-Zohar[1], Sabina Winograd-Katz[4], Nina Reuven[1], Moran Shalev[1], Juraj Sekeres[4], Moien Kanaan[3]*, Jan Tuckermann[2]* and Benjamin Geiger[4]**

[1] Department of Molecular Genetics, The Weizmann Institute of Science, Rehovot, Israel, [2] Institute of Comparative Molecular Endocrinology, University of Ulm, Ulm, Germany, [3] Hereditary Research Laboratory and Department of Life Sciences, Bethlehem University, Bethlehem, Palestine, [4] Department of Immunology, The Weizmann Institute of Science, Rehovot, Israel

OPEN ACCESS

**Edited by:**
Allen Liu,
University of Michigan, United States

**Reviewed by:**
Ya-Wen Liu,
National Taiwan University, Taiwan
Costin N. Antonescu,
Ryerson University, Canada

***Correspondence:**
Ari Elson
ari.elson@weizmann.ac.il
Moien Kanaan
mkanaan@bethlehem.edu
Jan Tuckermann
jan.tuckermann@uni-ulm.de
Benjamin Geiger
benny.geiger@weizmann.ac.il

**Specialty section:**
This article was submitted to Cellular Biochemistry, a section of the journal Frontiers in Cell and Developmental Biology

**Received:** 23 February 2021
**Accepted:** 23 April 2021
**Published:** 20 May 2021

**Citation:**
Elson A, Stein M, Rabie G, Barnea-Zohar M, Winograd-Katz S, Reuven N, Shalev M, Sekeres J, Kanaan M, Tuckermann J and Geiger B (2021) Sorting Nexin 10 as a Key Regulator of Membrane Trafficking in Bone-Resorbing Osteoclasts: Lessons Learned From Osteopetrosis. Front. Cell Dev. Biol. 9:671210. doi: 10.3389/fcell.2021.671210

Bone homeostasis is a complex, multi-step process, which is based primarily on a tightly orchestrated interplay between bone formation and bone resorption that is executed by osteoblasts and osteoclasts (OCLs), respectively. The essential physiological balance between these cells is maintained and controlled at multiple levels, ranging from regulated gene expression to endocrine signals, yet the underlying cellular and molecular mechanisms are still poorly understood. One approach for deciphering the mechanisms that regulate bone homeostasis is the characterization of relevant pathological states in which this balance is disturbed. In this article we describe one such "error of nature," namely the development of acute recessive osteopetrosis (ARO) in humans that is caused by mutations in sorting nexin 10 (SNX10) that affect OCL functioning. We hypothesize here that, by virtue of its specific roles in vesicular trafficking, SNX10 serves as a key selective regulator of the composition of diverse membrane compartments in OCLs, thereby affecting critical processes in the sequence of events that link the plasma membrane with formation of the ruffled border and with extracellular acidification. As a result, SNX10 determines multiple features of these cells either directly or, as in regulation of cell-cell fusion, indirectly. This hypothesis is further supported by the similarities between the cellular defects observed in OCLs form various models of ARO, induced by mutations in SNX10 and in other genes, which suggest that mutations in the known ARO-associated genes act by disrupting the same plasma membrane-to-ruffled border axis, albeit to different degrees. In this article, we describe the population genetics and spread of the original arginine-to-glutamine mutation at position 51 (R51Q)

in SNX10 in the Palestinian community. We further review recent studies, conducted in animal and cellular model systems, that highlight the essential roles of SNX10 in critical membrane functions in OCLs, and discuss possible future research directions that are needed for challenging or substantiating our hypothesis.

**Keywords: osteoclast, osteopetrosis, ARO, sorting nexin, SNX10, bone resorption**

# INTRODUCTION

## The Molecular Pathways That Regulate the Development and Function of Osteoclasts

Bone formation and homeostasis are tightly regulated processes, which depend on the concerted action of three major cell types: mesenchyme-derived OBs, which build bone, hematopoietic OCLs that degrade it, and osteocytes, which are also of mesenchymal origin and act as 'bone mechanosensors' that orchestrate the interplay between the former two cell types (Feng and Teitelbaum, 2013; Robling and Bonewald, 2020). The activities of OCLs and OBs are highly coordinated in time and space, leading to the replacement of old and damaged bone with new and intact tissue. This process of bone remodeling, in which OB and OCL activities are coordinated, removes micro-cracks and other structural defects that develop with time and maintains the physiological mass and physical properties of the bone matrix. Bones can be shaped or re-shaped also through the independent actions of these two cell types (Seeman, 2009; Feng and McDonald, 2011; Langdahl et al., 2016). Overall, bone production and degradation are well-regulated and balanced, and disruption of this balance can alter bone mass and cause serious disease.

Osteoclasts are giant, multinucleated phagocytes that originate in monocyte precursor cells. The cytokines M-CSF and RANKL trigger a complex and multi-stage process, in which mono-nuclear monocytes are induced to differentiate and fuse to form multi-nucleated cells that then differentiate further into mature bone-resorbing OCLs (Teitelbaum, 2007) (**Figure 1A**). It has been shown recently that mature OCLs can undergo fission *in vivo,* generating smaller multi-nucleated "osteomorphs" that can re-enter the fusion process and participate once again in forming mature OCLs (McDonald et al., 2021). Bone resorption is initiated when OCLs adhere to mineralized tissue via podosomes, specialized punctate integrin-based actin-rich adhesions that assemble into a peripheral belt-shaped array (also called a SZ) that confines the bone area destined for degradation (**Figures 1B,C**). Secretory lysosomes then fuse with the area of the ventral cell membrane that is delimited by the SZ to form a 'RB,' which is enriched with proton pumps and chloride transporters that drive the acidification of the OCL-bone interface. Fusion of lysosomes with the RB also discharges cathepsin K and other proteolytic enzymes onto the underlying bone surface. The combination of low pH and proteases leads to localized dissolution of the mineral and organic components of the bone matrix, and generates a resorption cavity (Novack and Teitelbaum, 2008; Teitelbaum, 2011). OCLs then endocytose the bone matrix debris from the resorption cavity through a specialized region of the RB. The debris are transported through the cell body to a specialized Functional Secretory Domain (FSD) located on the dorsal plasma membrane, through which the debris are secreted (Nesbitt and Horton, 1997; Salo et al., 1997; Mulari et al., 2003) (**Figure 1B**). Mature, functional OCLs are therefore polarized cells, in which directional transport takes place to and from their distinct dorsal and ventral membranes.

The process whereby uncommitted monocytes develop into mature, active OCLs includes several distinct stages that are driven by M-CSF, which promotes the survival and proliferation of the monocyte OCL precursor cells, and RANKL, which provides the major pro-osteoclastogenic signals. The molecular events and transcriptional programs that are induced by both cytokines are essential and sufficient for inducing monocyte precursor cells to differentiate into mature, bone-resorbing OCLs (Feng and Teitelbaum, 2013; Tsukasaki et al., 2020). Specifically, M-CSF activates its receptor tyrosine kinase, c-Fms, which, in turn, activates ERK1/2, PI3K, and Src signaling. Binding of RANKL to its receptor, RANK, induces the receptor to bind TNF Receptor-Associated Factors (TRAFs), which then activate the ERK, NFkB, and PI3K pathways and ultimately induce expression of NFATc1, the major fate-determining osteoclastogenic transcription factor (Wada et al., 2006; Feng and Teitelbaum, 2013; Takayanagi, 2021). Sustained activation of NFATc1 also requires its dephosphorylation by calcineurin, whose $Ca^{++}$-dependent activity requires signaling by the OSCAR and TREM2 receptors and their downstream ITAM-motif containing effectors DAP12 and FεRI (Zou and Teitelbaum, 2015; Humphrey and Nakamura, 2016). Finally, formation of resorption-competent OCLs also requires major cytoskeletal and membrane trafficking processes that act together to construct the resorptive apparatus of the cells. Attachment of OCLs to mineralized matrix is mediated by heterodimeric integrins, chiefly consisting of the αvβ3 chains. Binding of this integrin to RGD motifs in extracellular matrix proteins activates the Src tyrosine kinase, which leads to activation of Syk, Vav3, and the Rho-family GTPases Rac1 and Rac2. These integrin-driven signaling events ultimately lead to reorganization of the actin-based cytoskeleton and assembly of podosomes into SZs, enable lysosome fusion and formation of the RB, and induce OCL polarization (Feng and Teitelbaum, 2013; Georgess et al., 2014; Linder and Wiesner, 2016).

**Abbreviations:** ARO, autosomal recessive osteopetrosis; HSCT, hematopoietic stem cell transplantation; M-CSF, macrophage colony-stimulating factor; OB, osteoblast; OCL, osteoclast; RANKL, receptor activator of NFkB ligand; RB, ruffled border; R51Q, arginine-to-glutamine mutation at position 51; SNX10, sorting nexin 10; SZ, sealing zone.

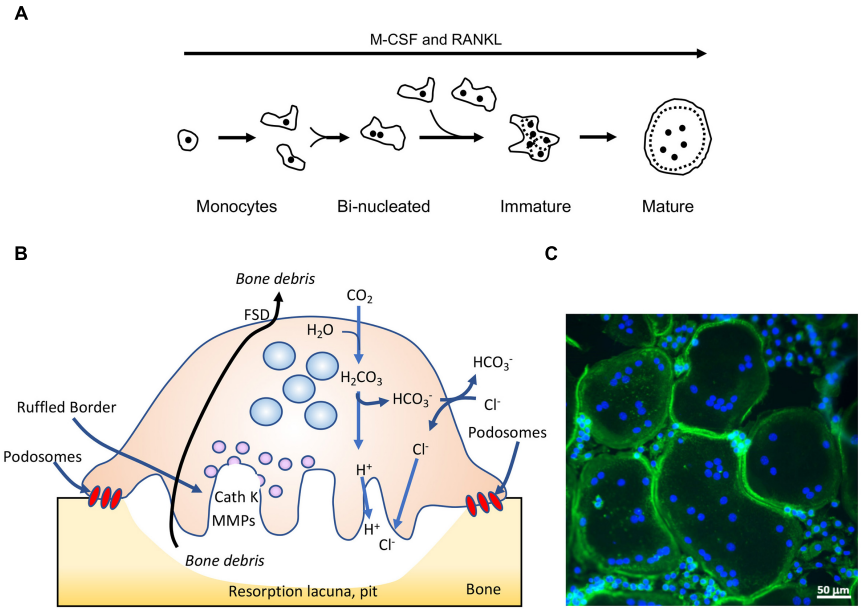


**FIGURE 1 |** Osteoclasts: form and function. **(A)** Outline of osteoclastogenesis in culture. M-CSF and RANKL induce mononucleated monocytes to differentiate and fuse to form bi-nucleated cells, which continue to fuse and form immature, multi-nucleated cells characterized by their random organization of podosomes (small black dots). The immature cells then mature and become rounder, and display a podosomal sealing zone-like belt at their periphery. **(B)** Schematic drawing of a mature, bone-resorbing osteoclast. OCLs adhere to bone using podosomes, actin-rich adhesion structures that, when grown on mineralized matrix, form a closed array (sealing zone) that isolates the area of bone that is to be degraded. The cells then secrete from their ventral ruffled border membrane protons, which dissolve the mineral components of the bone matrix, and proteases [such as cathepsin K (CathK) and matrix metalloproteases (MMPs)] that degrade its protein components. This combined activity results in formation of a resorption lacuna, or pit, in the bone surface. OCLs then endocytose the bone degradation products through their ruffled border membrane, transport them through the cell, and secrete them from the apical Functional Secretory Domain (FSD). **(C)** Mature mouse OCLs grown on glass coverslips, stained for actin (green, highlights the closed podosomal sealing zone-like array) and DNA (blue, nuclei). Note much smaller cells that have not fused and are located between the larger OCLs. Panels **(B,C)** were modified with permission from Shalev and Elson (2018).

Fine spatial and temporal tuning of membrane composition, compartmentalization, and dynamics play essential roles throughout the formation and development of OCLs, starting with the early stimulation of monocytes by M-CSF and RANKL and culminating in full OCL maturation and activation. This is evident in the extensive cell-cell fusion that occurs throughout osteoclastogenesis, until OCLs gain full resorption competence and stop fusing with other mature OCLs (Barnea-Zohar et al., 2021). It is also evident in the ability of OCLs to sense the properties of the underlying bone surface and to translate this information into cues that drive SZ formation at specific locations of the ventral cell membrane. The RB is then formed at these locations by another membranal event, namely the fusion of secretory lysosomes with the cell membrane. Membrane-related events also drive secretion of protons and proteases that degrade the underlying bone, endocytosis of bone matrix debris and their ultimate secretion via the dorsal FSD, leading to cell polarization (Feng and Teitelbaum, 2013; Georgess et al., 2014; Linder and Wiesner, 2016). That said, the nature of the molecular regulators of these processes is still unclear. We propose here that SNX10, which belongs to a large protein family that regulates vesicular trafficking in cells, plays a central role in spatially and temporally regulating the composition of diverse OCL membrane compartments. We further hypothesize that by doing so, SNX10 controls and affects membrane trafficking along the axis that links the plasma membrane with the RB, including processes, such as cell fusion and RB formation, in which it apparently plays an indirect role. We further propose that mutations in other known ARO-associated genes also disrupt the plasma membrane-to-RB axis, leading to related phenotypes. Here we examine this hypothesis in the context of a mutant of SNX10 that is associated with the genetic disease ARO.

## Learning About Osteoclasts From a Genetic Disease: The Case of Autosomal Recessive Osteopetrosis (ARO)

Decreased OCL-mediated bone resorption can occur as a result of genetic mutations that suppress the production of OCLs or inhibit their activity. Of particular importance in this context are genetic diseases whose mode of inheritance is autosomal recessive (AR), which allow linking individual genes and proteins with specific aspects of osteoclastogenesis or OCL function in a non-hypothesis driven, "real world" setting. Reduced bone resorption can disrupt the balance between bone formation and degradation and may lead to osteopetrosis, a heterogenous group of rare genetic diseases that are characterized by mild to life-threatening increases in bone mass. Osteopetrosis was initially described as "Marble Bone Disease" at the beginning of the 20th century by Albers-Schoenberg. This form of osteopetrosis

is inherited in an autosomal dominant manner, its symptoms are typically first detected in adults, and its progression is relatively benign (Balemans et al., 2005; Bollerslev et al., 2013). Another form of this disease is ARO, also known as malignant infantile osteopetrosis due to the tendency of its symptoms to become progressively worse. ARO is a rare disease with a global incidence of 1 in 250,000 live births, and is lethal unless treated by HSCT as noted further below (Sobacchi et al., 2013; Palagano et al., 2018). In ARO the trabecular pattern of the bone is lost and the differentiation between cortex and medulla is largely missing. Consequently, patients suffer from bone marrow failure as a result of bony encroachment into the hematopoietic niche, which leads to consequent pancytopenia and hepatosplenomegaly (Pangrazio et al., 2013). Skull changes may lead to hydrocephalus, choanal stenosis, and nerve compression, which can result in blindness, hearing loss, and cranial nerve palsies (Balemans et al., 2005). Additional symptoms include micrognathia, small thorax, pathological fractures, hypocalcemia, and severe dental defects as well as osteomyelitis of the jaw. Patients with more severe variants of this disease typically present also with severe failure to thrive during early infancy and do not survive past their first decade of life (Penna et al., 2019).

Most cases of ARO are caused by the presence of inactive OCLs ["OCL-rich ARO," (Sobacchi et al., 2013)] due to mutations in *TCIRG1, CLCN7,* or *OSTM1*, which encode components of the proton pump or $Cl^-/H^+$ antiporter of OCLs that are essential for acid secretion. Mutations in *PLEKHM1*, whose lysosome-associated protein product participates in vesicular trafficking, are another cause of this variant of ARO (Li et al., 1999; Frattini et al., 2000; Kornak et al., 2000, 2001; Chalhoub et al., 2003; Quarello et al., 2004; Van Wesenbeeck et al., 2007; Del Fattore et al., 2008; Sobacchi et al., 2013; Palagano et al., 2018). The less-frequent "OCL-poor" ARO variant is caused by absence of OCLs due to mutations in *TNFSF11*, which encodes RANKL, or in *TNFRSF11A*, which encodes RANK, the RANKL receptor, that are essential for OCL formation (Sobacchi et al., 2013; Palagano et al., 2018). HSCT from healthy donors can induce the formation of functional OCLs in the patients and significantly improve their clinical presentation (Hashemi Taheri et al., 2015; Orchard et al., 2015; Stepensky et al., 2019; Shapiro et al., 2020). However, because of the genetic heterogeneity of ARO, this treatment is often limited to cases where the underlying genetic mutation does not induce severe symptoms in other tissues, which cannot be corrected by HSCT.

# THE R51Q MUTATION IN SORTING NEXIN 10 – A CAUSE OF ARO IN PALESTINIAN COMMUNITIES AND ELSEWHERE

## ARO in Palestine

A major source of discovery of genes for AR diseases are consanguineous (inbred) populations (Antonarakis, 2019; Bamshad et al., 2019). Worldwide, ∼10% of marriages are estimated to be consanguineous (Bittles and Black, 2010), but this figure varies considerably between geographical regions. In a manner directly related to the topic discussed here, consanguinity rates are high among Arabs in the Middle East, in particular in Palestine, where 40–50% of marriages are consanguineous. Currently, 18–20% of all Palestinian marriages are between first cousins, a decrease from ∼25% in previous generations (Sharkia et al., 2008, 2016; Zlotogora and Shalev, 2014). Aker et al. (2012) described for the first time a link between ARO and a homozygous missense mutation in *SNX10* in three consanguineous families from the Palestinian village of Karma that is located near the city of Hebron (OMIM 614780). SNX10 belongs to the large family of sorting nexin proteins that, in eukaryotes, numbers over 30 structurally diverse members. All SNX proteins contain a phox-homology (PX) domain through which they bind phospholipids, mainly phosphatidylinositol-3-phosphate (PI3P) that is present in early endosomes. Indeed, a number of individual SNX proteins participate in the sorting of endocytosed proteins to degradation or to recycling, but many of the molecular details and cellular implications of these activities, including in OCLs, remain unknown (Worby and Dixon, 2002; Cullen, 2008; Teasdale and Collins, 2012; Gallon and Cullen, 2015). At 201 amino acids SNX10 is among the smaller SNX family members and, apart from an N-terminal extended PX domain, it lacks any known structural motifs (Cullen, 2008; Xu et al., 2014) (**Figure 2**).

The initial mutation described by Aker et al. (2012) was a missense mutation in exon 3 (c.152 G/A), leading to the replacement of a highly conserved arginine residue with a glutamine at position 51, which is located within the PX domain. OCLs from patients were fewer in number and smaller than OCLs from healthy controls, and their bone-resorbing activity was significantly inhibited (Aker et al., 2012). Following that study, eight additional families with multiple affected individuals suspected of suffering from ARO were recruited from the village of Karma and are presented here. All these families belonged to the same clan and bore the same family name. Upon interviewing, these families recognized that they most likely shared a common ancestor, but could not trace their relatedness despite frequent consanguineous marriages within each family. Following diagnosis, which was based mainly on clinical examination and on panoramic X-rays, similar findings were observed in affected individuals from all eight families, suggesting a common etiology. The most prominent features observed included early manifestation of disease, dysmorphic features, increased bone density, multiple fractures of legs and ribs, vision problems with either unilateral or bilateral vision loss, enlarged spleen and liver, pancytopenia and recurrent acute infections. The systemic findings suggested that these individuals suffer from the most severe manifestation of osteopetrosis, which is ARO.

Sequencing and segregation analyses confirmed that the *SNX10* p.R51Q variant was present in almost all affected individuals (B/III-15, C/IV-10, D/II-11, E/II-1, F/III-10, G/III-9, and I/II-2) (**Figure 3**) who were diagnosed with osteopetrosis, and their unaffected parents were heterozygous carriers for this mutation. Following whole exome sequencing, individual H/II-3 in family OST-H, who was wildtype for the *SNX10* p.R51Q variant, was found to be heterozygous for a frameshift mutation

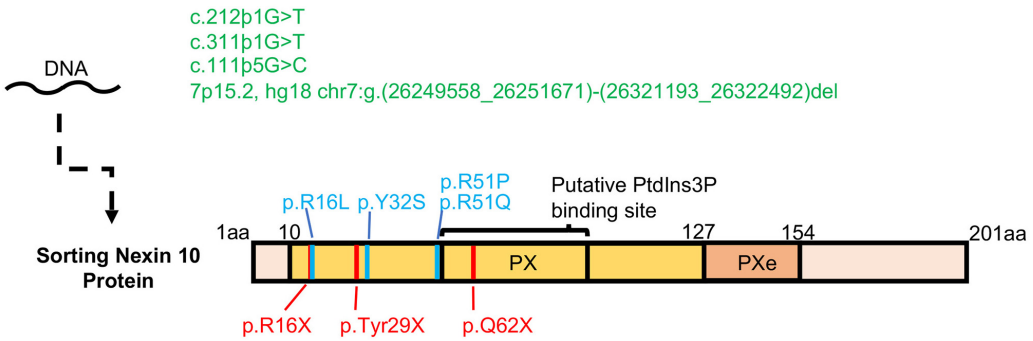


**FIGURE 2 |** Osteopetrotic mutations in SNX10. Three mutations that affect exon splicing and a large scale deletion in the *SNX10* locus are shown in green. Non-sense mutations leading to an early stop codon, which may produce a highly truncated and potentially unstable protein product are shown in red. Known missense mutations, which may affect the stability of the SNX10 protein or its ability to bind lipids and proteins, are shown in blue. A compound heterozygous nonsense mutation of p.Q62X with p.R16L has also been described. The PX and Pxe (extended PX domain, Xu et al., 2014 Proteins 82, 3483-3489, 2014) are marked in yellow and orange, respectively.

(p.C496fs*0, c.1485delC at Chr20:10,629,281) in the *JAG1* gene, which encodes the JAGGED 1 protein. Heterozygous mutations in this gene are known to cause Alagille syndrome (OMIM #118450), whose associated skeletal anomalies may be confused with osteopetrosis.

Four families from areas of the West Bank outside the village of Karma with affected individuals diagnosed with osteopetrosis were also enrolled in this study (**Figure 3**). Sanger sequencing of these affected individuals ruled out the *SNX10* p.R51Q mutation as cause for their disease, while whole exome sequencing revealed a different genetic basis for the disease in each case. These mutations all occur in genes that have been linked to ARO (Sobacchi et al., 2013; Palagano et al., 2018), and are described in **Figure 3**. The results obtained with these four families suggested that the *SNX10* p.R51Q mutation is localized to the village of Karma and could have appeared as a result of founder effect. Haplotype analyses, utilizing six short tandem repeat (STR) markers around the *SNX10* p.R51Q locus, were therefore conducted in order to trace the relatedness among the Karma families. From each family, one affected patient homozygous for the *SNX10* p.(R51Q) mutation, one heterozygous sibling, and both parents were examined. The OST-J family, which hails from a different geographical location and whose ARO is caused by a distinct genetic event (**Figure 3**), was also screened for the same microsatellite markers as a control. Haplotype analysis revealed that all Karma patients who were homozygous for p.R51Q mutation and who had not undergone HSCT were also homozygous for all the chosen markers, as indicated in **Figure 4**. The minimum shared haplotype block linked to the mutation was found in all the affected *SNX10* patients, while a different haplotype block was found in the OST-J family. This data provides additional evidence that the shared haplotype block is linked to p.R51Q mutation, and excludes the possibility of sharing it by pure chance in this endogamous population. The shared haplotype block also suggests the p.R51Q mutation in the Karma patients originates in a common founder and was spread in this community by common ancestry. Further studies, in which whole exome sequencing data of 1352 Palestinian individuals from the West Bank and Gaza was examined, revealed only two individuals as carriers of the p.R51Q mutation, corresponding to an estimated allele frequency of 0.00074. In contrast, examination of 3700 individuals from Karma and the surrounding villages identified 89 individuals, belonging to 35 extended families, as heterozygous carriers of this mutation, indicating an allele frequency of 0.024.

## SNX10-Based ARO in Other Geographical Locations

Following the original discovery of the R51Q mutation in SNX10, other mutations in *SNX10*, often in exons 3 and 4, have been linked to this disease in other geographical regions (Mégarbané et al., 2013; Pangrazio et al., 2013; Simanovsky et al., 2016; Stattin et al., 2017; Baer et al., 2019; Kocak et al., 2019; Stepensky et al., 2019) (see **Table 1** and **Figure 2**). Overall, it is estimated that 4.5% of the cases of ARO worldwide are caused by mutations in this gene (Sobacchi et al., 2013; Palagano et al., 2018). Patients with different *SNX10* mutations show symptoms of sclerosis that often also include cranial malformation, secondary neurological defects, vision impairment, and anemia, but usually lack overt immunological symptoms (Pangrazio et al., 2013; Simanovsky et al., 2016; Kocak et al., 2019). Recent evidence also suggests that synonymous mutations, which do not lead to an exchange of an amino acid or truncated protein and previously considered silent, can still cause symptoms of osteopetrosis (Palagano et al., 2017). Mutations leading to an intermediate osteopetrosis form, not as severe as ARO nor as benign as the dominant autosomal form of osteopetrosis, have also been detected in *SNX10* (Stattin et al., 2017; Baer et al., 2019). Although the symptoms of this intermediate disease present during infancy, it does not require urgent intervention. Patients suffering from this variant of *SNX10*-based osteopetrosis, as well as from other forms of intermediate disease, nonetheless accumulate debilitating skeletal complications as they age, and may eventually require blood transfusions and curative treatment (Stepensky et al., 2019).

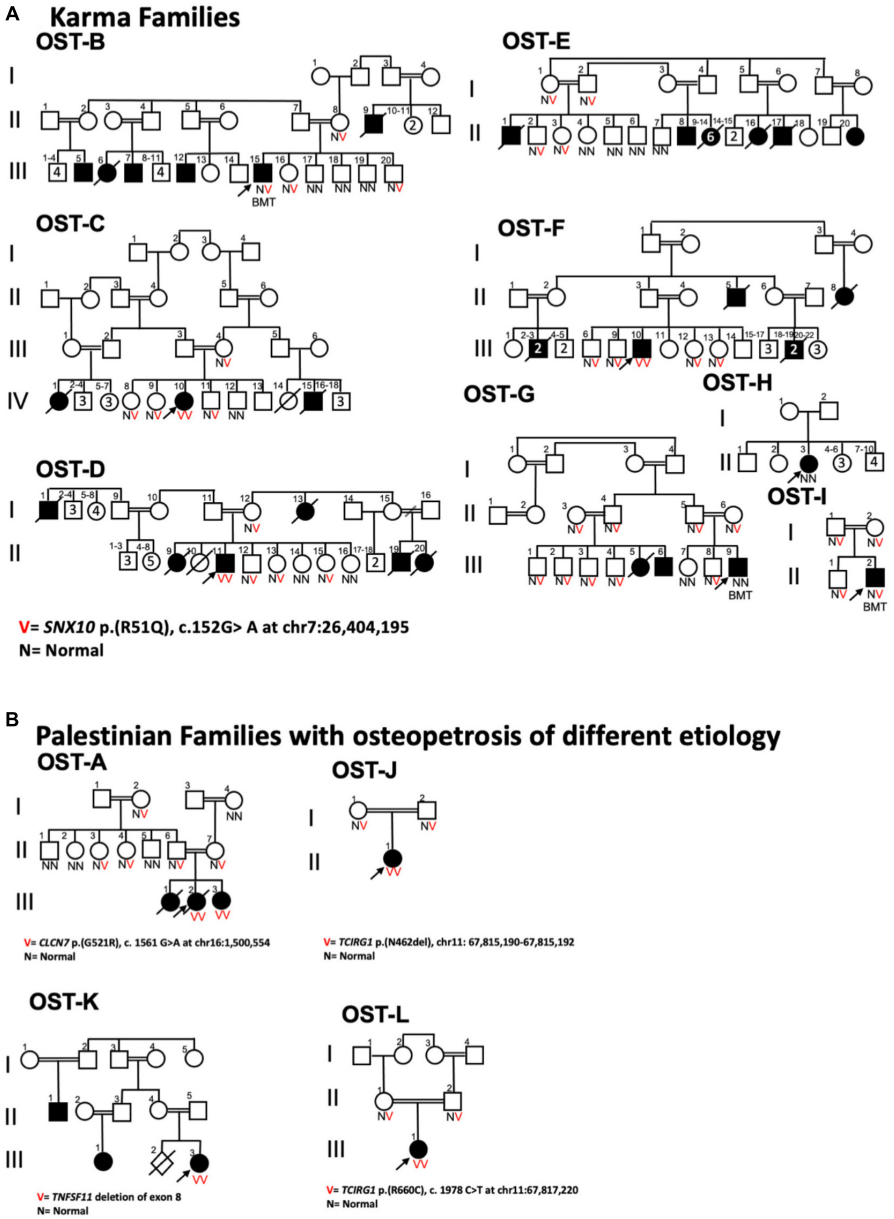


**FIGURE 3 |** Pedigrees of Palestinian families displaying ARO. **(A)** Karma village families displaying *SNX10* p.R51Q genotype of sampled individuals; arrows indicate probands. Highly consanguineous marital relationships produce offspring with two copies of the mutant *SNX10* allele that segregate with ARO phenotype. B/III-15, G/III-9, and I/II-2 ARO patients underwent hematopoietic stem cell transplantation, and thus their allele compositions reflect those of their unaffected donors. The only exception is the affected individual H/II-3 in OST-H Family, who was wildtype for SNX10_p.R51Q variant as discussed in the text. **(B)** Pedigrees of four Palestinian families from other regions of the West Bank with affected individuals diagnosed with osteopetrosis displaying different genetic mutations. The affected individual of a family from Ramallah (OST-J family) was homozygous for a frameshift mutation (p.N462del) in the *TCIRG1* gene, and the affected individual from the Bethlehem family (OST-L family) was homozygous for a non-synonymous mutation (p.R660C) in the same gene. The affected individual from the family from Yatta (OST-A family) was homozygous for a missense mutation in *ClCN7* gene: *CLCN7* p.G521R. A second family from Ramallah (OST-K family) carries a deletion mutation of exon 8 in *TNFSF11* gene.

A group of nine *SNX10* intermediate osteopetrosis patients was described in the Swedish county of Västerbotten, which were caused by a splice site mutation in the *SNX10* gene that led to a frameshift and premature termination of translation of the protein product (Stattin et al., 2017). Individuals with this variant of osteopetrosis have survived without HSCT up to the age of 47 years (Stattin et al., 2017).

Studies conducted during the last decade have taught us that *SNX10*-based osteopetrosis is heterogeneous in nature. Rare *de novo* mutations as well as related patient clusters sharing the

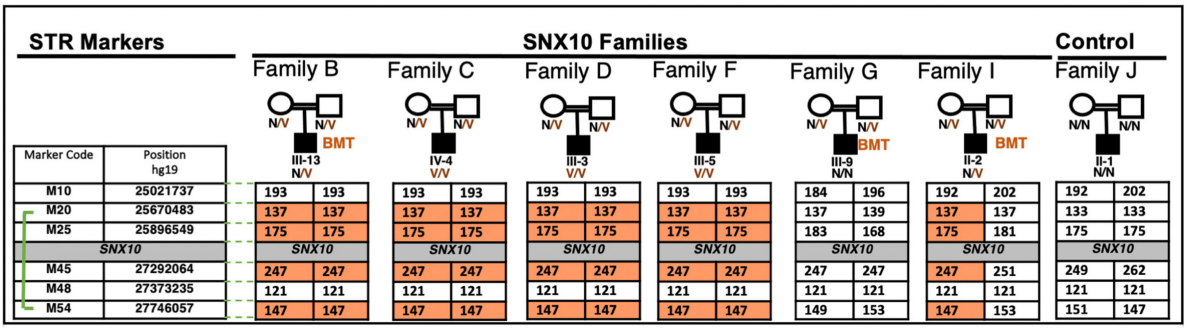


| Chr | position hg19 | Repeat | Marker | Distance from mutation |
|---|---|---|---|---|
| chr7 | 25021737 | 22xTG | M10 | -1309778 |
| chr7 | 25670483 | 20xTG | M20 | -661032 |
| chr7 | 25896549 | 20xAC | M25 | -434966 |
| *SNX10* Gene | | | | |
| chr7 | 27292064 | 24xGT | M45 | 960549 |
| chr7 | 27373235 | 22xGT | M48 | 1041720 |
| chr7 | 27746057 | 24xAC | M54 | 1414542 |

**FIGURE 4 |** Haplotype analysis of the *SNX10* locus in affected Palestinian families from the village of Karma. Six microsatellite repeat markers that flank the *SNX10* gene, three on either side, were selected and amplified by PCR using fluorescent labeled primers and examined by capillary electrophoresis (CE). Haplotype analyses were analyzed using GeneScan. Selected markers were tested on SNX10 positive families on the affected individual and the parents, one heterozygous sibling (not shown here). Haplotype analysis revealed that all Karma patients who are homozygous for p.R51Q mutation were also homozygous for all studied markers. BMT denotes patients who had undergone hematopoietic stem cell transplantation prior to analysis. Different haplotypes were found in unrelated OST-J Family (**Figure 3**), as expected. The minimum shared haplotype block (orange) linked to the mutation was found in all the affected *SNX10* patients. For each repeat the following parameters are provided: its position [according to the Human Genome Assembly GRCh37 (hg19), https://www.ncbi.nlm.nih.gov/assembly/GCF_000001405.13/], the length and composition of the nucleotide repeat, and its distance in bps from the R51Q mutation in the SNX10 gene.

same mutation were found, with the severity of the resulting disease linked to the underlying mutation. It is interesting to note that most missense mutations in SNX10 that led to ARO were localized at the beginning of the protein (**Table 1**); missense mutations that affect more downstream residues remain to be discovered. Absence of such mutations in the population could mean that such mutations do not cause disease or, conversely, that the severity of the disease precludes survival.

## INSIGHTS FROM MODEL SYSTEMS INTO THE MOLECULAR ROLE OF SNX10 IN OCLs

The known functions of SNX proteins suggest that SNX10 regulates osteoclastogenesis by controlling cellular membrane trafficking, and that the underlying mechanism can be characterized through cellular and molecular studies of SNX10-based ARO. While some of these studies can be performed in OCLs grown from human monocytes, patients of ARO caused by mutations in *SNX10* are rare, and most are treated with HSCT. A significant part of our knowledge was therefore obtained from model systems, such as genetically manipulated cells or mice. Notably, studies of this nature have been most revealing, yet interpretation of data obtained from these model systems should be done with obvious care.

### Studies of Cells From Human Patients

In the original study that linked SNX10 to ARO, Aker et al. (2012) showed that OCLs prepared *in vitro* from mononuclear leukocytes of ARO patients who were homozygous for R51Q SNX10 were inactive in *in vitro* assays. The cells also contained large vacuoles (Aker et al., 2012), which may be caused by defects in the sorting and fusion of cellular vesicles. Subsequent studies of the intermediate ARO cluster of cases from Västerbotten revealed that OCLs prepared from peripheral blood of patients contained defective RBs, and the cells did not resorb bone in *in vitro* assays. The cells were also three- to four-fold larger than OCLs from healthy individuals, a finding attributed to increased spreading (Stattin et al., 2017). Induced pluripotent stem cells were more recently produced from a patient carrying the Västerbotten mutation (Xu et al., 2017). This approach may help bypass the difficulties in obtaining hematopoietic cells from patients and will likely further advance our understanding of how this mutation affects SNX10 and its function in OCLs.

### Mouse Models of SNX10 Mutations in ARO

Several mouse models in which the *Snx10* gene has been targeted globally or specifically in OCLs have been described (**Table 2**). Ye et al. (2015) presented global knockdown (KD) mice, in which a selection cassette was inserted into intron 3 of *Snx10* and inhibited its expression, resulting in a drop of 86% in *Snx10* mRNA levels in bone samples. The phenotype of these mice

**TABLE 1 |** Osteopetrotic SNX10 mutations.

| Genotype | Mutation | Effect on SNX10 protein | Source |
|---|---|---|---|
| p.Arg51Gln | Missense | Reduces protein stability/binding | Aker et al. (2012) |
| p.Arg16Leu | Missense | Disrupts interactions with other proteins | Pangrazio et al. (2013) |
| p.Tyr32Ser | Missense | Destabilizes internal packing | Pangrazio et al. (2013) |
| p.Arg51Pro | Missense | Alters the main chain conformation or affects binding to other proteins | Pangrazio et al. (2013) |
| p.Arg16X | Non-sense | Truncated form of SNX10 | Pangrazio et al. (2013) |
| p.Tyr29X | Non-sense | Truncated form of SNX10 | Pangrazio et al. (2013) |
| p.Gln62X | Non-sense | Truncated form of SNX10 | Pangrazio et al. (2013) |
| p.Arg16Leu and p.Gln62X | Non-sense (compound heterozygous) | Truncated form of SNX10 | Pangrazio et al. (2013) |
| c.212 þ1G>T | Splice site nucleotide change | Impairs the splicing between donor splice sites of exons 4 and 5 | Pangrazio et al. (2013) |
| c.311 þ1G>T | Splice site nucleotide change | Impairs the splicing between donor splice sites of exons 4 and 5 | Pangrazio et al. (2013) |
| c.111 þ5G>C | Splice site nucleotide change | Reduces strength of the donor splice site of exon 3 | Pangrazio et al. (2013) |
| c.43delG | Non-sense | Truncated form of SNX10 | Amirfiroozy et al. (2017) |
| c.284 G>A | Missense? | | Shamriz et al. (2017) |
| 7p15.2, hg18 chr7:g.(26249558 _26251671)-(26321193_26322492)del | Deletion | Del including a large region upstream of SNX10 and a partial non-coding region of SNX10 | Baer et al. (2019) |

was severe and combined osteopetrosis and rickets. Homozygous mice exhibited massive increases in bone mass, absent teeth and severely retarded growth, and survived up to the age of 3–4 weeks (Ye et al., 2015). SNX10 KD OCLs were nearly inactive *in vitro* due to presence of rudimentary RBs and an inability to acidify the extracellular space, processes that rely on proper vesicular trafficking and membranal function. Paradoxically, the serum levels of collagen I C-telopeptides (CTX), which are interpreted as a clinical indicator of OCL mediated bone resorption *in vivo*, were significantly increased in these mice (Ye et al., 2015). Similar observations were made in other models of osteopetrosis despite demonstrably low OCL activity (e.g., Neutzsky-Wulff et al., 2008; Stein et al., 2020), indicating that circulating CTX levels might not accurately reflect *in vivo* OCL activity in these cases. Bone formation, as assessed by the clinical marker P1NP, was unaltered.

Clear indications of rickets were detected in homozygous SNX10 KD mice, in the form decreased bone mineral density and bone mineral content values, presence of non-mineralized osteoid on trabecular surfaces, and metaphyseal fraying and cupping in femurs and tibias (Ye et al., 2015). Indeed, the mice were hypocalcemic and exhibited increased serum levels of PTH and reduced levels of 25-hydroxy-vitamin D3. Further studies suggested that this is caused by a severe reduction in the expression of SNX10 in gastric epithelial cells, which resulted in elevated gastric pH and stomach necrosis that led to reduced uptake of dietary calcium. Dietary supplementation with calcium gluconate resolved the rachitic phenotypes of these mice.

The same study also described mice in which SNX10 was targeted specifically in OCLs (SNX10 OCL mice), by crossing mice carrying a floxed allele of *Snx*10 that deleted exons 4 and 5 with mice expressing Cathepsin-K-Cre (Ye et al., 2015). While SNX10 OCL mice were osteopetrotic and lacked teeth, their overall phenotype was less severe than SNX10 KD mice: the mice exhibited mild growth retardation by 3 weeks of age, but were reported to survive and did not display rachitic or gastric abnormalities (Ye et al., 2015). An additional strain of mice in which the *Snx10* gene was targeted and which are also osteopetrotic has been described (Zhou et al., 2016). OCLs from these mice appear to resorb bone less well than WT OCLs and to express reduced amounts of beta 3 integrin, TRAP, Cathepsin K, MMP9, and possibly NFATc1. Unfortunately, the genetic manipulation that gave rise to these mice has not been described, preventing a more precise understanding of this model.

Stein and colleagues Stein et al. (2020) created a whole-body knock-in R51Q SNX10 mouse, modeling the first mutation in this protein that was linked to ARO (Aker et al., 2012). Homozygous R51Q SNX10 mice were massively osteopetrotic, lacked teeth, exhibited significant developmental delay at the age of 4 weeks, and generally did not survive past the age of 6–8 weeks (Stein et al., 2020). OCLs from these mice lacked RBs and could not acidify the cell-bone interface, in agreement with their complete lack of activity in *in vitro* pit resorption assays. R51Q SNX10 OCLs also stained poorly for TRAP, appeared to be less adherent, and were noticeably more fragile and shorter-lived than their wild-type or heterozygous counterparts (Barnea-Zohar et al., 2021). Levels of CTX in circulation were elevated in these mice

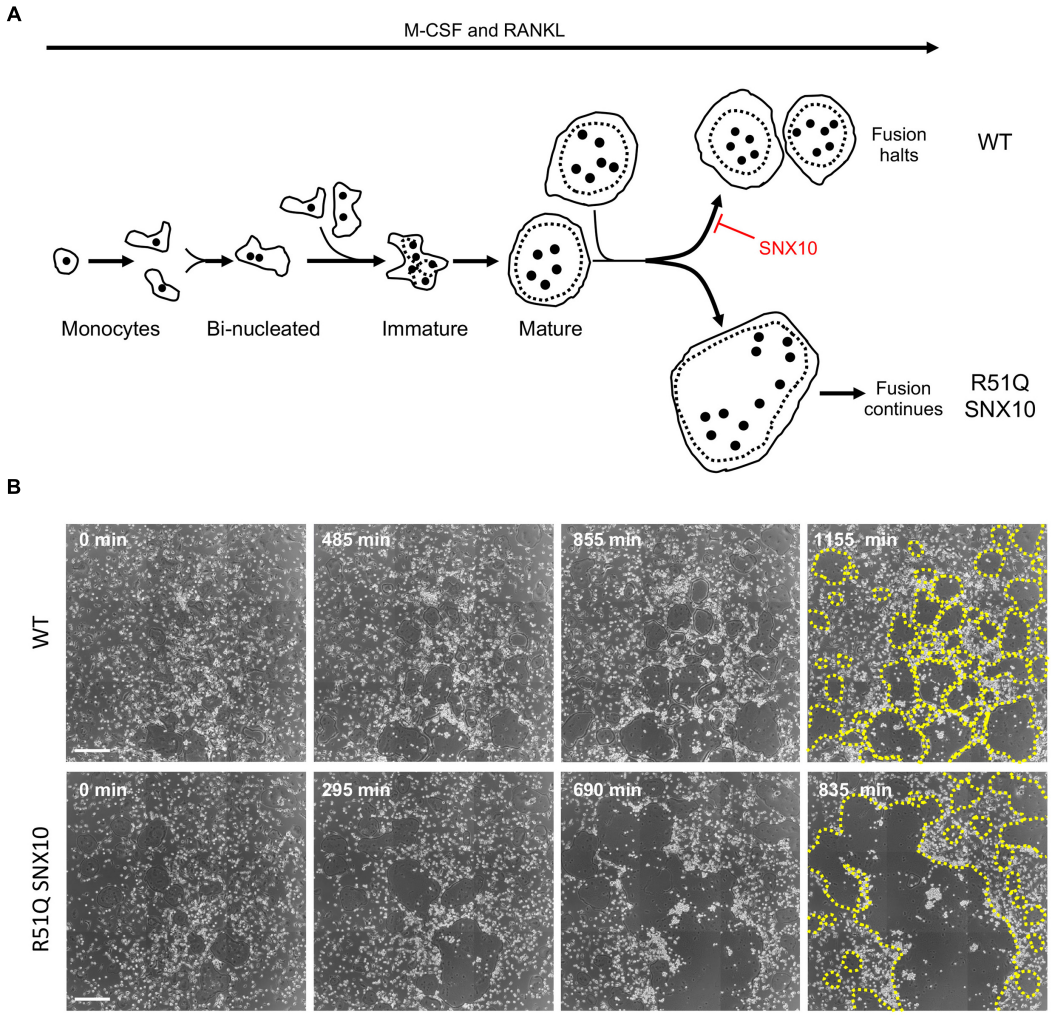


**FIGURE 5 |** Uncontrolled fusion of mature R51Q SNX10 OCLs. **(A)** Outline of osteoclastogenesis in culture, similar to **Figure 1A**. Top: WT mature OCLs do not fuse with each other. Bottom: Mature R51Q SNX10 OCLs readily fuse with each other and continue to fuse with other mature OCLs. **(B)** Phase light microscopy images of cultures of WT (top) and R51Q SNX10 (bottom) spleen-derived monocytes undergoing osteoclastic differentiation on glass coverslips in the presence of M-CSF and RANKL. Note development of mature, round WT OCLs that remain juxtaposed with each other, vs. continuous fusion that generates giant R51Q SNX10 OCLs (Barnea-Zohar et al., 2021). Times are noted from start of imaging; OCL boundaries are indicated by dashed yellow lines in the final image of each series. Each image is a composite of nine smaller images. Scale bars: 250 μm.

despite clear OCL inactivity (Stein et al., 2020), similar to the SNX10 KD mice (Ye et al., 2015). Osteoblast numbers were increased in R51Q SNX10 mice, but their bone formation rates, serum levels of P1NP, and *in vitro* differentiation of OBs were normal, indicating that their osteopetrotic phenotype was due to OCL dysfunction (Stein et al., 2020). This result is consistent with the very low expression of SNX10 in OBs relative to OCLs (Stein et al., 2020).

The bone-related phenotypes of the R51Q SNX10 knock-in mice and the SNX10 KD mice are overall similar and confirm a critical role for this protein in OCLs and in bone degradation. Nonetheless, R51Q SNX10 mice are not rachitic, an observation that agrees with the symptoms of human patients of SNX10-based ARO (Palagano et al., 2018). The rickets phenotype of SNX10-KD mice has been linked to dysfunction of gastric epithelial cells (Ye et al., 2015), which apparently does not occur in the R51Q SNX10 mice. This distinction may be caused by the differences between both model systems: the R51Q SNX10 mutation results in production of a mutant protein whose expression levels and functions in gastric epithelial cell are unknown, while the SNX10 KD model decreases expression of the WT protein to low levels (Ye et al., 2015; Stein et al., 2020).

## Cell-Based Studies

Studies of SNX proteins in cultured cell lines and in primary cells suggest that SNX10 functions in regulating vesicular trafficking in cells. In particular, the PX domain of SNX10, like those of most other SNX proteins (Teasdale and Collins, 2012), predominantly binds PI3P, which is found in early endosomes; SNX10 also binds phosphatidylinositol-3,5-diphosphate ($PI(3,5)P_2$) that is

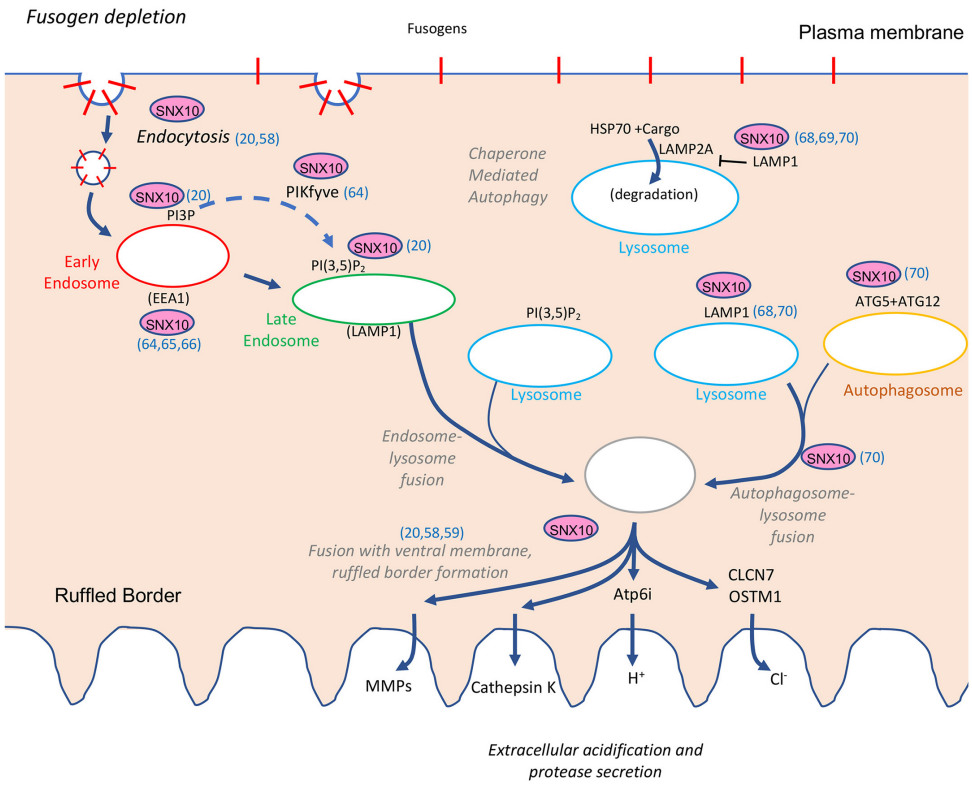


**FIGURE 6 |** Overview of the known functions of SNX10 along the plasma membrane-to-ruffled border axis. Functions or abilities indicated include support of endocytosis (references Ye et al., 2015 and Barnea-Zohar et al., 2021 noted in the figure), binding to PI3P and PI(3,5)$P_2$ (Barnea-Zohar et al., 2021), association with PIKfyve, EEA1, and early endosomal markers (Qin et al., 2006; Battaglino et al., 2019; Sultana et al., 2020), inhibition of chaperone mediated autophagy (You et al., 2018; Zhang et al., 2018, 2020), association with LAMP1 and ATG5 and promotion of lysosome-autophagosome fusion (Zhang et al., 2018, 2020), and ruffled border formation (Ye et al., 2015; Stein et al., 2020; Barnea-Zohar et al., 2021). See the section "Cell-Based Studies," for additional details. PI3P, phosphatidylinositol-3-phosphate; PI(3,5)$P_2$, phosphatidylinositol-3,5-diphosphate; Atp6i, the a3 subunit of the V0 domain of the OCL ATP-dependent proton pump; CLCN7, voltage-gated chloride/proton antiporter; OSTM1, beta subunit of the voltage-gated chloride/proton antiporter; CathK, cathepsin K; MMPs, matrix metalloproteases.

prominent in late endosomes (Haucke, 2005; Wallroth and Haucke, 2018; Barnea-Zohar et al., 2021). In agreement with these findings, studies in RAW264.7 cells indicated that SNX10 binds the lipid kinase PIKfyve, which phosphorylates PI3P into PI(3,5)2P, and both PIKfyve and SNX10 co-fractionate in these cells together with EEA1, a marker of early endosomes (Battaglino et al., 2019; Sultana et al., 2020). Qin et al. (2006) showed that SNX10 co-localizes with endosomal markers also in HeLa cells. Expression of exogenous SNX10, but not of several other SNX family members, in these cells led to accumulation of large vacuoles that required presence of both the PX domain of SNX10 and its C terminal sequence (Qin et al., 2006). These findings suggest that SNX10 performs a role in early endosomes, and consequently the effects of its disruption might be mediated by this cellular compartment.

SNX10 has also been shown to affect lysosomes and autophagosomes. SNX10 fulfills an essential role in chaperone-mediated autophagy (CMA), a process in which specific soluble cytosolic proteins are delivered to lysosomes for degradation in an autophagosome-independent manner. In CMA, target proteins associate initially with heat shock protein 70 (Hsc70), and the resulting complex binds LAMP2A at the lysosomal membrane and is translocated into the lysosomal lumen for degradation (Kaushik and Cuervo, 2018). SNX10 destabilizes LAMP2A, most likely by promoting maturation of cathepsin A that plays a major role in LAMP2A degradation (You et al., 2018; Zhang et al., 2018). Loss of SNX10 stabilizes LAMP2A and increases cellular CMA activity, which is associated with increased AMPK signaling in livers and in primary hepatocytes of SNX10 knockout mice (You et al., 2018; Zhang et al., 2018). Studies in the human carcinoma cell line HCT116 indicated that SNX10 interacts through specific residues located in its C-terminal sequence with the lysosomal protein LAMP1 (Zhang et al., 2018, 2020); this interaction was reported to be essential for inducing degradation of LAMP2A by a yet-unknown mechanism (Zhang et al., 2018).

In additional studies, expression of SNX10 was upregulated during autophagy in HCT116 and in various other cell lines (Zhang et al., 2020). SNX10 binds, through its C-terminus, the ATG5 protein in these cells, thereby associating also with the ATG12-ATG5 conjugate that is located on the surface of autophagosomes (Zhang et al., 2020) and which plays important

roles in the formation and maturation of autophagosomes and in their fusion with lysosomes (Chen et al., 2012). Further studies indicated that loss of SNX10 or mutation of specific C-terminal residues through which it binds ATG5 or LAMP1 inhibited autophagosome-lysosome fusion in HCT116 cells. According to the model that emerges from these findings, a population of SNX10 molecules associates with LAMP1 and with lysosomes, while other SNX10 molecules associate with the ATG12-ATG5 conjugate and with autophagosomes. Interactions between SNX10 molecules may bring these two organelles in close proximity and may promote their fusion (Zhang et al., 2020). Finally, SNX10 also enhances the bactericidal activity of macrophages by promoting acidification of their phagosomes, which occurs via phagosome maturation and fusion with lysosomes (Lou et al., 2017). Maturation of phagosomes and endosomes occurs by similar mechanisms, hence these studies further strengthen the conceptual link between SNX10 and early endosomes and the effect that this may have on lysosomes.

However, the effects of SNX10 are evident also in other cellular compartments, in which SNX10 is not known to function. One prominent example concerns OCL fusion, a process that initiates at the plasma membrane. When grown *in vitro* on mineralized or non-mineralized surfaces, R51Q SNX10 OCLs fuse repeatedly and continuously to form gigantic OCLs that can become 10- to 100-fold larger than controls (Barnea-Zohar et al., 2021). Examination of the fusion of mutant OCLs in culture by live-cell imaging revealed widespread fusion between mature OCLs, a fusion modality that was rarely observed among WT OCLs (**Figure 5**). In particular, mature juxtaposed R51Q SNX10 OCLs readily fused with each other and continued to fuse with additional mature OCLs, stopping only when no more fusion partners were available or when the cells died. In contrast, mature juxtaposed WT OCLs did not fuse with each other, and fusion ceased when such cells became surrounded by other similarly mature OCLs (**Figure 5**) (Barnea-Zohar et al., 2021). Molecularly, the R51Q mutation, which is located within the lipid-biding PX domain of SNX10, leads to the loss of PI3P binding and destabilizes the protein, severely reducing its levels in the cells (Barnea-Zohar et al., 2021). In agreement with this notion, expression of WT SNX10 rescued the deregulated fusion phenotype of primary R51Q SNX10 OCLs, while CRISPR-mediated knockout of the *Snx10* gene induced deregulated fusion in RAW264.7 cells (Barnea-Zohar et al., 2021). Taken together, these findings indicate that the hyper-fusion phenotype of R51Q SNX10 OCLs is induced by loss of function of SNX10. From a broader perspective, these findings indicate that fusion between mature OCLs is actively down-regulated by a cell-autonomous, genetically regulated mechanism, which requires SNX10 and is disrupted by the R51Q mutation. We note that in another study, knockdown of SNX10 by lentiviral-delivered shRNA prevented differentiation of RAW264.7 cells into mature OCLs (Zhu et al., 2012). The different results of this study vs. the CRISPR-mediated knockout of *Snx10* in RAW264.7 cells (Barnea-Zohar et al., 2021) may arise from distinct effects of acute (shRNA) vs. long-term, constitutive (CRISPR) elimination of *Snx10,* or from incomplete down-regulation of *Snx10* by shRNA.

How might R51Q SNX10 promote fusion between mature OCLs? Cell-cell fusion initiates when fusogens, specialized fusion-promoting molecules that are present at the cell surface, induce fusion of juxtaposed cells (Oren-Suissa and Podbilewicz, 2007; Chernomordik and Kozlov, 2008; Martens and McMahon, 2008; Helming and Gordon, 2009; Willkomm and Bloch, 2015; Brukman et al., 2019). Studies of OCLs from R51Q SNX10 and from SNX10KD mice revealed that internalization of dextran, which occurs by both fluid-phase and receptor-mediated endocytosis (Pustylnikov et al., 2014), is significantly reduced in these cells (Ye et al., 2015; Barnea-Zohar et al., 2021). Inhibition of endocytosis could result in aberrant retention of fusogens or of other fusion-promoting molecules at the cell surface, thereby enabling continuous fusion. In support of this proposal we note that endocytosis was shown to inhibit fusion of epidermal cells in *C. elegans* by selectively removing the fusogen EFF-1 from their surface (Smurova and Podbilewicz, 2016). However, endocytosis was also shown to promote fusion of monocytes in the early stages of osteoclastogenesis (Shin et al., 2014), suggesting that its role in cell-cell fusion might depend on the type and on the developmental stage of the fusing cells. This proposal can be tested directly by deep differential analysis of the plasma membrane proteome of R51Q SNX10 OCLs. Such analyses would help to identify putative fusion-promoting proteins that are downregulated in WT OCLs but are retained in the mutant cells.

A second example of a defect in R51Q SNX10 OCLs in a cellular compartment in which SNX10 does not function directly is the absence of the RB in mutant OCLs. The presence and function of SNX10 in autophagosomes, which fuse with lysosomes, and in lysosomes themselves suggest that loss of SNX10 or its R51Q mutant may adversely affect these compartments, thereby preventing subsequent fusion of lysosomes with the ventral cell membrane. Such an event would block formation of the RB and lead to OCL inactivity, as was indeed observed in R51Q SNX10 and in SNX10-KD mice (Ye et al., 2015; Stein et al., 2020; Barnea-Zohar et al., 2021). Collectively, the above results lead us to propose that the R51Q mutation in SNX10 leads to a loss-of-function of this protein that disrupts the formation or function of endosomes and lysosomes. The central role of these cellular compartments in vesicular trafficking results in disruption of events along the plasma membrane-to-RB axis, including some in which SNX10 is not known to play a direct role.

## DISCUSSION

In this article we have explored and discussed possible mechanisms whereby SNX10 might act as a key regulator of bone homeostasis via its involvement in OCL development and function. Starting with a specific monogenic disease (ARO in the Palestinian community) and an associated mutation (R51Q in SNX10) we discussed here both the population genetics background and the relevant mechanistic insights that may explain why individuals who are homozygous for this mutation develop osteopetrosis. While the direct role

**TABLE 2 |** Key cellular phenotypes in OCLs from "OCL-rich" ARO mouse models.

| Gene | *Snx10* | *Clcn7* | *Ostm1* | *Tcirg1* | *Plekhm1* |
|---|---|---|---|---|---|
| Protein | SNX10 Sorting nexin 10 | CLCN7 Chloride voltage-gated channel 7 (chloride/proton antiporter) | OSTM1 Osteoclastogenesis associated transmembrane protein 1 (beta subunit of CLCN7) | ATP6v0a3, Atp6i T cell immune regulator 1, ATPase H + transporting V0 subunit a3 (a3 subunit of the $H^+$-ATPase) | PLEKHM1 Plekstrin homology and RUN domain containing M1 |
| Mouse models | R51Q SNX10 knock-in, whole body (Stein et al., 2020; Barnea-Zohar et al., 2021). Conditional deletion of exons 4, 5 (Ye et al., 2015). | Whole-body knockout (Kornak et al., 2001; Kasper et al., 2005; Neutzsky-Wulff et al., 2008). Conditional deletion of exons 12, 13 (Wartosch et al., 2009)[2]. | Gray lethal (gl) mice (a naturally occurring mutant of *Ostm1*) (Rajapurohitam et al., 2001; Chalhoub et al., 2003; Lange et al., 2006; Héraud et al., 2014). Conditional in-frame deletion of exon 5 in *Ostm1* (Pata and Vacher, 2018). | Osteosclerotic (Oc) mice (a naturally occurring mutant of *Tcirg1*) (Ito et al., 2001; Schinke et al., 2009). Whole-body knockout of exons 2–5 (Li et al., 1999), conditional deletion of exons 14–20 (Sun-Wada et al., 2009). | Conditional deletion of exon 3 (Fujiwara et al., 2016). Gene-trap disruption of intron 1 (Brommage et al., 2014). |
| Bone phenotype | Osteopetrosis, growth retardation, no tooth eruption, death at 6–7 weeks (Ye et al., 2015; Stein et al., 2020). Rickets (whole-body Snx10 KD) (Ye et al., 2015). | Osteopetrosis, no rickets, growth retardation, no tooth eruption, death at 6–7 weeks (Kornak et al., 2001; Kasper et al., 2005; Neutzsky-Wulff et al., 2008). | Osteopetrosis, growth retardation, no tooth eruption, death at 3–4 weeks (Rajapurohitam et al., 2001; Chalhoub et al., 2003; Lange et al., 2006; Pata and Vacher, 2018). | Osteopetrosis, osteopetrorickets, growth retardation, no tooth eruption, death at 4–5 weeks (Li et al., 1999; Ito et al., 2001; Schinke et al., 2009; Sun-Wada et al., 2009). | Normal development, teeth present, increased trabecular bone mass (Fujiwara et al., 2016). No bone phenotype (Brommage et al., 2014). |
| TRAP-positive OCLs present | Yes (*in vivo*/*in vitro*)[1] (Ye et al., 2015; Stein et al., 2020; Barnea-Zohar et al., 2021). | Yes (*in vivo*/*in vitro*) (Kornak et al., 2001; Neutzsky-Wulff et al., 2008). | Yes. Increased OCL numbers (*in vivo*), TRAP staining *in vivo*/*in vitro* (Rajapurohitam et al., 2001; Pata and Vacher, 2018). | Yes. Increased OCL numbers (*in vivo*) (Li et al., 1999; Ito et al., 2001). | Yes (*in vitro*/*in vivo*). TRAP staining: *in vitro*, perinuclear accumulation (Fujiwara et al., 2016). |
| OCL activity | Inactive (*in vitro*) (Ye et al., 2015; Stein et al., 2020). | Inactive (*in vivo*/*in vitro*) (Kornak et al., 2001; Neutzsky-Wulff et al., 2008). | Virtually inactive (*in vitro*) (Rajapurohitam et al., 2001; Pata and Vacher, 2018). | Inactive (*in vivo*/*in vitro*) (Li et al., 1999). | Nearly absent (*in vitro*) (Fujiwara et al., 2016). |
| Lysosomes | | Present, normal pH (Kornak et al., 2001; Kasper et al., 2005). | Present, normal pH, dispersed organization (Pata and Vacher, 2018). | Present (Li et al., 1999). | Present, abnormal perinuclear positioning (Fujiwara et al., 2016). |
| Ruffled border | Absent (Stein et al., 2020) Rudimentary (Ye et al., 2015). | Nearly absent (Kornak et al., 2001). | Underdeveloped (Rajapurohitam et al., 2001). | Absent (Ito et al., 2001). | Absent (Fujiwara et al., 2016). |
| Extracellular acidification | Absent (Ye et al., 2015; Stein et al., 2020). | Absent (*in vitro*) (Kornak et al., 2001). | Absent (*in vitro*) (Pata and Vacher, 2018). | Absent (*in vitro*) (Li et al., 1999). | |
| Endocytosis | Impaired (Ye et al., 2015; Barnea-Zohar et al., 2021). | | | | Normal |
| OCL shape/size | *In vitro*: Gigantic OCLs, due to continuous cell-cell fusion. (Barnea-Zohar et al., 2021). | *In vivo*: abnormally elongated (Kornak et al., 2001), large OCLs (Neutzsky-Wulff et al., 2008). | *In vitro*: elongated. (Rajapurohitam et al., 2001), larger than WT, due to increased NFATc1 activity-? (Pata and Vacher, 2018). | | Abnormal, less round OCL shape, normal size, *in vitro* (Fujiwara et al., 2016). |
| Comments | | Accumulation of lysosomal storage materials in forebrain neurons and proximal tubule cells (Kasper et al., 2005; Wartosch et al., 2009). | Defective exocytosis of TRAP and Cathepsin K in OCLs (Pata and Vacher, 2018). Normal lysosomes, abnormal autophagosomes in neurons (Héraud et al., 2014). | | Inactive exocytosis (Fujiwara et al., 2016). Incisor absent (ia) rats, in which *Plekhm1* is disrupted, exhibit age-dependent osteopetrosis and lack teeth. Their OCLs are nearly inactive and lack ruffled borders (Reinholt et al., 1999; McDonald et al., 2011). |

[1] *In vitro: Determined in OCLs cultured on glass/plastic/bone/dentine from mice. in vivo: As observed in animals or directly in tissue samples collected from them.*
[2] *Whole-body E245A CLCN7 mice, in which CLCN7 was modified from a $Cl^-/H^+$ exchanger into an uncoupled Cl- conductor, display severe growth retardation and osteopetrosis and their OCLs display underdeveloped RBs, but these phenotypes are less severe than in whole body KO of CLCN7 (Weinert et al., 2010). Whole-body E312A CLCN7 mice, in which CLCN7 is transport-deficient, display phenotypes similar to whole-body CLCN7 knockouts (Weinert et al., 2014).*

of SNX10 in OCL function is still unknown, nearly all the manifestations of the R51Q mutation are related to aberrant membrane properties, including lipid interaction specificity, cell fusion, matrix adhesion, endocytosis, RB formation, and acidification of the resorption pit. Several of these phenotypes, e.g., deregulated cell fusion and RB formation, affect processes that SNX10 is not known to regulate directly, and most likely result from the broader disruption to the plasma membrane-RB axis (**Figure 6**).

The observation that severe membranal trafficking defects, such as those described here, are nonetheless compatible with embryo survival deserves some consideration. The phenotypes of the whole-body SNX10-KD and R51Q SNX10 mice are indeed severe, yet the mice are born and survive for several weeks. A possible explanation for this may be obtained from data from the Human Protein Atlas[1] that indicate that while SNX10 levels in OCLs are high, its expression in other cell types – and likely the consequences of its mutation – is not ubiquitous. Moreover, possible functional redundancies between SNX10 and other members of the SNX protein family may enable other cells and tissues, in which SNX10 is expressed, to escape the effects of its mutation.

It is noteworthy that most cases of ARO that are not SNX10-related, whose genetic basis is known, are caused by mutations in genes that also perform membrane regulatory functions in OCLs (Sobacchi et al., 2013; Palagano et al., 2018) (**Table 2**). Among these is the *TCIRG1* gene, which encodes the α3 subunit of the V0 domain of the ATP-dependent proton pump, the V-ATPase, mutations in which cause approximately half of ARO cases globally. Importantly, the lysosomal V-ATPase also participates in vesicle sorting and formation of RBs in addition to its role in acidifying lysosomes and the extracellular space (Coxon and Taylor, 2008; Sobacchi et al., 2013; Palagano et al., 2018). Also included are the *CLCN7* gene, whose product is the voltage-gated chloride/proton antiporter of late endosomes and lysosomes, as well as *OSTM1*, which encodes the beta subunit of this antiporter. Mutations in these two genes account for approximately 17.5% and 5%, respectively, of ARO cases. A small number of ARO cases are also caused by mutations in *PLEKHM1*, whose protein product functions in lysosomal trafficking and autophagosome-lysosome fusion, while 4.5% of ARO cases are linked to mutations in *SNX10*, whose relevance to membranal trafficking in OCLs has been discussed here (Sobacchi et al., 2013; Palagano et al., 2018). The finding that the major subtypes of ARO arise mostly by disruptions in genes that function in membranal trafficking in OCLs emphasizes the critical importance of this process in promoting properly regulated osteoclastogenesis and OCL resorption activity. Moreover, many of the mouse models developed to study mutations in these ARO-associated genes display several common phenotypes that include, in addition to massive osteopetrosis, absent or under-developed RBs, an inability to acidify the OCL-bone interface, reduced or absent bone-resorbing activity, and altered OCL shape or size (e.g., Kornak et al., 2001; Rajapurohitam et al., 2001; Kasper et al., 2005; Henriksen et al., 2006; Lange et al., 2006; Neutzsky-Wulff et al., 2008; Wartosch et al., 2009; Weinert et al., 2010; Héraud et al., 2014; Pata and Vacher, 2018) (**Table 2**). It is therefore tempting to propose that mutations in ARO-associated genes disrupt specific molecular functions that affect membrane and vesicular trafficking, leading to a wider but similar disruption of the membrane-to-RB axis and to a common set of phenotypes in OCLs. In this context it is of interest to examine OCLs from the various ARO models side by side and compare the precise details and characteristics of their cellular phenotypes. Uncovering these details is critical for obtaining a more complete understanding of OCL biology in particular, and of cellular membrane homeostasis and regulation of membrane trafficking and fusion in general. Furthermore, such information is important for devising novel therapeutic strategies for ARO and other diseases, such as osteoporosis and cancer-related bone loss, in which OCLs are known to play prominent roles. In light of the scarcity of ARO and the resulting small number of cases that can be studied in depth, it is reasonable to assume that studies in cell and animal models will continue to provide important mechanistic insights into these issues.

[1]www.proteinatlas.org

# MATERIALS AND METHODS

## Haplotype Analysis Using Microsatellite Markers

Six short tandem repeat (STR) markers around the SNX10_p.R51Q locus (**Figure 4**) were selected. Primer pairs were designed for amplification of the markers using the Hemi-NeSTR website with default parameters[2]. Each PCR product was mixed with 0.25 μl GeneScan™ 500 ROX™ Dye, and capillary electrophoresis was carried on an Applied Biosystems 3500 Genetic Analyzer (Thermo Fisher Scientific). Gene Mapper software (V5.2) was utilized to call and extract the genotypes from the electropherograms generated by the 3130XL Genetic Analyzer. Haplotypes were constructed manually.

## Whole-Exome Sequencing

Whole exome sequencing was performed at the Hereditary Research Laboratory, Bethlehem University, using Illumina's NextSeq™ 500 Sequencing System. DNA libraries were prepared using two preparation kits: the Illumina® TruSeq™ DNA Sample Prep Kit, or Nextera™ Flex for Enrichment Prep Kit. Following sequencing, reads were aligned to the reference human genome (hg19) using the Burrows-Wheeler (BWA) aligner. Prior to variant calling by the Genome Analysis Toolkit[3], mapped reads (BAM format) were re-processed by removing PCR duplicates, realigning around indels, and recalibrating base quality. The final list of variants was annotated by ANNOVAR[4] (Wang et al., 2010) using several databases of minor allele frequency including gnomAD[5] and PopFreqMax, as well as variant effect

[2]http://mpeters.net/primer.html

[3]https://gatk.broadinstitute.org

[4]http://annovar.openbioinformatics.org/

[5]https://gnomad.broadinstitute.org

predictors such as SIFT (Sorting Intolerant from Tolerant[6]), PolyPhen-2[7] and REVEL (Ioannidis et al., 2016). Candidate variants were validated by Sanger sequencing and then tested for co-segregation with the phenotype in additional family members.

### Culture of Primary OCLs

Culture of primary OCLs was performed as described in Barnea-Zohar et al. (2021). In brief, spleens from mice aged 4–8 weeks were dissociated into α-Minimal Eagle's Medium (α-MEM; Sigma-Aldrich, St. Louis, MO, United States). Following lysis of erythrocytes, $2 \times 10^6$ (WT) or $1 \times 10^6$ (R51Q SNX10) cells were seeded in 24-well plates. Cells were cultured in complete OCL medium [α-MEM containing 10% fetal calf serum, 2 mM glutamine, 50 units/ml penicillin, 50 μg/ml streptomycin, and M-CSF (20 ng/ml, Peprotech, Rehovot, Israel) for 2 days, after which RANKL (20 ng/ml, R&D Systems, Minneapolis, MN, United States)] was added. Cells were grown at 37°C in 5% $CO_2$ for a total of 5–7 days with daily changes of medium. Time-lapse images were acquired with an automated inverted microscope (DeltaVision Elite system IX71 with Resolve3D software modulus; Applied Precision, Inc., GE Healthcare, Issaquah, WA, United States) using a 10×/0.30 air objective (Olympus, Tokyo, Japan). The cells were maintained at 37°C with a 5% $CO_2$ humidified atmosphere throughout the imaging process.

### Ethics Board Approval

The human experiments described were approved by the Institutional Review Board of the Istishari Arab Hospital, Ramallah, Palestine. All family members gave their consent to participate in the study. All mouse experiments were approved by the Weizmann Institute IACUC and were conducted in accordance with Israeli law.

## DATA AVAILABILITY STATEMENT

The original contributions presented in the study are included in the article/supplementary material, further inquiries can be directed to the corresponding authors. The data presented in the study are deposited in the ClinVar repository, accession numbers: (1) NC_000018.10:g.60033942_60033993del (TNFRSF11A): SCV001571688/RCV001374875.1, (2) NM_001-199835.1(SNX10):c.152G>A (p.Arg51Gln): SCV001571689/RC-V000033149.3, (3) NM_001287.6(CLCN7):c.1561G>A (p.Gly5 21Arg): SCV001572330/RCV001375477.1, (4) NM_000-214.3 (JAG1):c.1485del (p.Cys496fs): SCV001572331/RCV0013-754 78.1, (5) NM_006019.4(TCIRG1):c.1384_1386del (p.Asn 462del): SCV001572332/RCV001375479.1, and (6) NM_00-6019.4(TCIRG1):c.1978C>T (p.Arg660Cys): SCV0015723-33/ RCV001375480.1.

[6] http://sift.bii.a-star.edu.sg

[7] http://genetics.bwh.harvard.edu/pph2/

## ETHICS STATEMENT

The studies involving human participants were reviewed and approved by Institutional Review Board of the Istishari Arab Hospital, Ramallah, Palestine. Written informed consent to participate in this study was provided by the participants' legal guardian/next of kin.

## AUTHOR CONTRIBUTIONS

AE, MK, JT, and BG wrote the manuscript, secured funding, and performed the analysis. MSt and GR wrote the manuscript, collected the data, and performed the analysis. MB-Z, SW-K, NR, MSh, and JS collected the data and performed the analysis. All authors contributed to the article and approved the submitted version.

## FUNDING

This study was supported by the Trilateral Deutsche Forschungsgemeinschaft (DFG) grant (Tu220/12) awarded to MK, JT, AE, and BG, by the DFG CRC Trauma grant (SFB1149) to JT, by grants from the Israel Science Foundation (grant #1734/20) and from the Kekst Family Institute for Medical Genetics and the David and Fela Shapell Center for Genetic Disorders Research, both of the Weizmann Institute, to AE. The funders were not involved in any aspect of this study or its publication.

## REFERENCES

Aker, M., Rouvinski, A., Hashavia, S., Ta-Shma, A., Shaag, A., Zenvirt, S., et al. (2012). An SNX10 mutation causes malignant osteopetrosis of infancy. *J. Med. Genet.* 49, 221–226. doi: 10.1136/jmedgenet-2011-100520

Amirfiroozy, A., Hamidieh, A. A., Golchehre, Z., Rezamand, A., Yahyaei, M., Beiranvandi, F., et al. (2017). A novel mutation in SNX10 gene causes malignant infantile osteopetrosis. *Avicenna J. Med. Biotechnol.* 9, 205–208.

Antonarakis, S. E. (2019). Carrier screening for recessive disorders. *Nat. Rev. Genet.* 20, 549–561. doi: 10.1038/s41576-019-0134-2

Baer, S., Schaefer, E., Michot, C., Fischbach, M., Morelle, G., Bendavid, M., et al. (2019). Intermediate autosomal recessive osteopetrosis with a large noncoding deletion in SNX10: a case report. *Pediatr. Blood Cancer* 66:e27751. doi: 10.1002/pbc.27751

Balemans, W., Van Wesenbeeck, L., and Van Hul, W. (2005). A clinical and molecular overview of the human osteopetroses. *Calcif. Tissue Int.* 77, 263–274. doi: 10.1007/s00223-005-0027-6

Bamshad, M. J., Nickerson, D. A., and Chong, J. X. (2019). Mendelian gene discovery: fast and furious with no end in sight. *Am. J. Hum. Genet.* 105, 448–455. doi: 10.1016/j.ajhg.2019.07.011

Barnea-Zohar, M., Winograd-Katz, S. E., Shalev, M., Arman, E., Reuven, N., Roth, L., et al. (2021). An SNX10-dependent mechanism down-regulates fusion between mature osteoclasts. *J. Cell Sci.* [Epub ahead of print]. doi: 10.1242/jcs.254979

Battaglino, R. A., Jha, P., Sultana, F., Liu, W., and Morse, L. R. (2019). FKBP12: a partner of Snx10 required for vesicular trafficking in osteoclasts. *J. Cell. Biochem.* 120, 13321–13329. doi: 10.1002/jcb.28606

Bittles, A. H., and Black, M. L. (2010). Evolution in health and medicine Sackler colloquium: consanguinity, human evolution, and complex diseases. *Proc. Natl. Acad. Sci. U.S.A.* 107(Suppl. 1), 1779–1786. doi: 10.1073/pnas.0906079106

Bollerslev, J., Henriksen, K., Nielsen, M. F., Brixen, K., and Van Hul, W. (2013). Autosomal dominant osteopetrosis revisited: lessons from recent studies. *Eur. J. Endocrinol.* 169, R39–R57.

Brommage, R., Liu, J., Hansen, G. M., Kirkpatrick, L. L., Potter, D. G., Sands, A. T., et al. (2014). High-throughput screening of mouse gene knockouts identifies established and novel skeletal phenotypes. *Bone Res.* 2:14034.

Brukman, N. G., Uygur, B., Podbilewicz, B., and Chernomordik, L. V. (2019). How cells fuse. *J. Cell Biol.* 218, 1436–1451. doi: 10.1083/jcb.201901017

Chalhoub, N., Benachenhou, N., Rajapurohitam, V., Pata, M., Ferron, M., Frattini, A., et al. (2003). Grey-lethal mutation induces severe malignant autosomal recessive osteopetrosis in mouse and human. *Nat. Med.* 9, 399–406. doi: 10.1038/nm842

Chen, D., Fan, W., Lu, Y., Ding, X., Chen, S., and Zhong, Q. (2012). A mammalian autophagosome maturation mechanism mediated by TECPR1 and the Atg12-Atg5 conjugate. *Mol. Cell.* 45, 629–641. doi: 10.1016/j.molcel.2011.12.036

Chernomordik, L. V., and Kozlov, M. M. (2008). Mechanics of membrane fusion. *Nat. Struct. Mol. Biol.* 15, 675–683.

Coxon, F. P., and Taylor, A. (2008). Vesicular trafficking in osteoclasts. *Semin. Cell Dev. Biol.* 19, 424–433. doi: 10.1016/j.semcdb.2008.08.004

Cullen, P. J. (2008). Endosomal sorting and signalling: an emerging role for sorting nexins. *Nat. Rev. Mol. Cell Biol.* 9, 574–582. doi: 10.1038/nrm2427

Del Fattore, A., Cappariello, A., and Teti, A. (2008). Genetics, pathogenesis and complications of osteopetrosis. *Bone* 42, 19–29. doi: 10.1016/j.bone.2007.08.029

Feng, X., and McDonald, J. M. (2011). Disorders of bone remodeling. *Annu. Rev. Pathol.* 6, 121–145.

Feng, X., and Teitelbaum, S. L. (2013). Osteoclasts: new insights. *Bone Res.* 1, 11–26. doi: 10.4248/br201301003

Frattini, A., Orchard, P. J., Sobacchi, C., Giliani, S., Abinun, M., Mattsson, J. P., et al. (2000). Defects in TCIRG1 subunit of the vacuolar proton pump are responsible for a subset of human autosomal recessive osteopetrosis. *Nat. Genet.* 25, 343–346. doi: 10.1038/77131

Fujiwara, T., Ye, S., Castro-Gomes, T., Winchell, C. G., Andrews, N. W., Voth, D. E., et al. (2016). PLEKHM1/DEF8/RAB7 complex regulates lysosome positioning and bone homeostasis. *JCI Insight* 1:e86330.

Gallon, M., and Cullen, P. J. (2015). Retromer and sorting nexins in endosomal sorting. *Biochem. Soc. Trans.* 43, 33–47. doi: 10.1042/bst20140290

Georgess, D., Machuca-Gayet, I., Blangy, A., and Jurdic, P. (2014). Podosome organization drives osteoclast-mediated bone resorption. *Cell Adh. Migr.* 8, 191–204.

Hashemi Taheri, A. P., Radmard, A. R., Kooraki, S., Behfar, M., Pak, N., Hamidieh, A. A., et al. (2015). Radiologic resolution of malignant infantile osteopetrosis skeletal changes following hematopoietic stem cell transplantation. *Pediatr. Blood Cancer* 62, 1645–1649. doi: 10.1002/pbc.25524

Haucke, V. (2005). Phosphoinositide regulation of clathrin-mediated endocytosis. *Biochem. Soc. Trans.* 33(Pt 6), 1285–1289. doi: 10.1042/bst0331285

Helming, L., and Gordon, S. (2009). Molecular mediators of macrophage fusion. *Trends Cell Biol.* 19, 514–522. doi: 10.1016/j.tcb.2009.07.005

Henriksen, K., Sørensen, M. G., Nielsen, R. H., Gram, J., Schaller, S., Dziegiel, M. H., et al. (2006). Degradation of the organic phase of bone by osteoclasts: a secondary role for lysosomal acidification. *J. Bone Miner. Res.* 21, 58–66. doi: 10.1359/jbmr.050905

Héraud, C., Griffiths, A., Pandruvada, S. N., Kilimann, M. W., Pata, M., and Vacher, J. (2014). Severe neurodegeneration with impaired autophagy mechanism triggered by ostm1 deficiency. *J. Biol. Chem.* 289, 13912–13925. doi: 10.1074/jbc.m113.537233

Humphrey, M. B., and Nakamura, M. C. A. (2016). Comprehensive review of immunoreceptor regulation of osteoclasts. *Clin. Rev. Allergy Immunol.* 51, 48–58. doi: 10.1007/s12016-015-8521-8

Ioannidis, N. M., Rothstein, J. H., Pejaver, V., Middha, S., McDonnell, S. K., Baheti, S., et al. (2016). REVEL: an ensemble method for predicting the pathogenicity of rare missense variants. *Am. J. Hum. Genet.* 99, 877–885.

Ito, M., Amizuka, N., Nakajima, T., and Ozawa, H. (2001). Bisphosphonate acts on osteoclasts independent of ruffled borders in osteosclerotic (oc/oc) mice. *Bone* 28, 609–616. doi: 10.1016/s8756-3282(01)00429-x

Kasper, D., Planells-Cases, R., Fuhrmann, J. C., Scheel, O., Zeitz, O., Ruether, K., et al. (2005). Loss of the chloride channel ClC-7 leads to lysosomal storage disease and neurodegeneration. *EMBO J.* 24, 1079–1091. doi: 10.1038/sj.emboj.7600576

Kaushik, S., and Cuervo, A. M. (2018). The coming of age of chaperone-mediated autophagy. *Nat. Rev. Mol. Cell Biol.* 19, 365–381. doi: 10.1038/s41580-018-0001-6

Kocak, G., Guzel, B. N., Mihci, E., Kupesiz, O. A., Yalcin, K., and Manguoglu, A. E. (2019). TCIRG1 and SNX10 gene mutations in the patients with autosomal recessive osteopetrosis. *Gene* 702, 83–88. doi: 10.1016/j.gene.2019.02.088

Kornak, U., Kasper, D., Bosl, M. R., Kaiser, E., Schweizer, M., Schulz, A., et al. (2001). Loss of the ClC-7 chloride channel leads to osteopetrosis in mice and man. *Cell* 104, 205–215. doi: 10.1016/s0092-8674(01)00206-9

Kornak, U., Schulz, A., Friedrich, W., Uhlhaas, S., Kremens, B., Voit, T., et al. (2000). Mutations in the a3 subunit of the vacuolar H(+)-ATPase cause infantile malignant osteopetrosis. *Hum. Mol. Genet.* 9, 2059–2063. doi: 10.1093/hmg/9.13.2059

Langdahl, B., Ferrari, S., and Dempster, D. W. (2016). Bone modeling and remodeling: potential as therapeutic targets for the treatment of osteoporosis. *Ther. Adv. Musculoskelet. Dis.* 8, 225–235. doi: 10.1177/1759720x16670154

Lange, P. F., Wartosch, L., Jentsch, T. J., and Fuhrmann, J. C. (2006). ClC-7 requires Ostm1 as a beta-subunit to support bone resorption and lysosomal function. *Nature* 440, 220–223. doi: 10.1038/nature04535

Li, Y. P., Chen, W., Liang, Y., Li, E., and Stashenko, P. (1999). Atp6i-deficient mice exhibit severe osteopetrosis due to loss of osteoclast-mediated extracellular acidification. *Nat. Genet.* 23, 447–451. doi: 10.1038/70563

Linder, S., and Wiesner, C. (2016). Feel the force: podosomes in mechanosensing. *Exp. Cell Res.* 343, 67–72. doi: 10.1016/j.yexcr.2015.11.026

Lou, J., Li, X., Huang, W., Liang, J., Zheng, M., Xu, T., et al. (2017). SNX10 promotes phagosome maturation in macrophages and protects mice against Listeria monocytogenes infection. *Oncotarget* 8, 53935–53947. doi: 10.18632/oncotarget.19644

Martens, S., and McMahon, H. T. (2008). Mechanisms of membrane fusion: disparate players and common principles. *Nat. Rev. Mol. Cell Biol.* 9, 543–556. doi: 10.1038/nrm2417

McDonald, M. M., Khoo, W. H., Ng, P. Y., Xiao, Y., Zamerli, J., Thatcher, P., et al. (2021). Osteoclasts recycle via osteomorphs during RANKL-stimulated bone resorption. *Cell* 184, 1330.e4–1347.e4.

McDonald, M. M., Morse, A., Peacock, L., Mikulec, K., Schindeler, A., and Little, D. G. (2011). Characterization of the bone phenotype and fracture repair in osteopetrotic incisors absent rats. *J. Orthop. Res.* 29, 726–733. doi: 10.1002/jor.21293

Mégarbané, A., Pangrazio, A., Villa, A., Chouery, E., Maarawi, J., Sabbagh, S., et al. (2013). Homozygous stop mutation in the SNX10 gene in a consanguineous Iraqi boy with osteopetrosis and corpus callosum hypoplasia. *Eur. J. Med. Genet.* 56, 32–35. doi: 10.1016/j.ejmg.2012.10.010

Mulari, M. T., Zhao, H., Lakkakorpi, P. T., and Väänänen, H. K. (2003). Osteoclast ruffled border has distinct subdomains for secretion and degraded matrix uptake. *Traffic* 4, 113–125. doi: 10.1034/j.1600-0854.2003.40206.x

Nesbitt, S. A., and Horton, M. A. (1997). Trafficking of matrix collagens through bone-resorbing osteoclasts. *Science* 276, 266–269. doi: 10.1126/science.276.5310.266

Neutzsky-Wulff, A. V., Karsdal, M. A., and Henriksen, K. (2008). Characterization of the bone phenotype in ClC-7-deficient mice. *Calcif. Tissue Int.* 83, 425–437. doi: 10.1007/s00223-008-9185-7

Novack, D. V., and Teitelbaum, S. L. (2008). The osteoclast: friend or foe? *Annu. Rev. Pathol.* 3, 457–484.

Orchard, P. J., Fasth, A. L., Le Rademacher, J., He, W., Boelens, J. J., Horwitz, E. M., et al. (2015). Hematopoietic stem cell transplantation for infantile osteopetrosis. *Blood* 126, 270–276.

Oren-Suissa, M., and Podbilewicz, B. (2007). Cell fusion during development. *Trends Cell Biol.* 17, 537–546. doi: 10.1016/j.tcb.2007.09.004

Palagano, E., Menale, C., Sobacchi, C., and Villa, A. (2018). Genetics of osteopetrosis. *Curr. Osteoporos. Rep.* 16, 13–25.

Palagano, E., Susani, L., Menale, C., Ramenghi, U., Berger, M., Uva, P., et al. (2017). Synonymous mutations add a layer of complexity in the diagnosis of human osteopetrosis. *J. Bone Miner. Res.* 32, 99–105. doi: 10.1002/jbmr.2929

Pangrazio, A., Fasth, A., Sbardellati, A., Orchard, P. J., Kasow, K. A., Raza, J., et al. (2013). SNX10 mutations define a subgroup of human autosomal recessive osteopetrosis with variable clinical severity. *J. Bone Miner. Res.* 28, 1041–1049.

Pata, M., and Vacher, J. (2018). Ostm1 bifunctional roles in osteoclast maturation: insights from a mouse model mimicking a human OSTM1 mutation. *J. Bone Miner. Res.* 33, 888–898. doi: 10.1002/jbmr.3378

Penna, S., Capo, V., Palagano, E., Sobacchi, C., and Villa, A. (2019). One disease, many genes: implications for the treatment of osteopetroses. *Front. Endocrinol.* 10:85. doi: 10.3389/fendo.2019.00085

Pustylnikov, S., Sagar, D., Jain, P., and Khan, Z. K. (2014). Targeting the C-type lectins-mediated host-pathogen interactions with dextran. *J. Pharm. Pharm. Sci.* 17, 371–392. doi: 10.18433/j3n590

Qin, B., He, M., Chen, X., and Pei, D. (2006). Sorting nexin 10 induces giant vacuoles in mammalian cells. *J. Biol. Chem.* 281, 36891–36896. doi: 10.1074/jbc.m608884200

Quarello, P., Forni, M., Barberis, L., Defilippi, C., Campagnoli, M. F., Silvestro, L., et al. (2004). Severe malignant osteopetrosis caused by a GL gene mutation. *J. Bone Miner. Res.* 19, 1194–1199. doi: 10.1359/jbmr.040407

Rajapurohitam, V., Chalhoub, N., Benachenhou, N., Neff, L., Baron, R., and Vacher, J. (2001). The mouse osteopetrotic grey-lethal mutation induces a defect in osteoclast maturation/function. *Bone* 28, 513–523. doi: 10.1016/s8756-3282(01)00416-1

Reinholt, F. P., Hultenby, K., Heinegård, D., Marks, S. C. Jr., Norgård, M., and Anderson, G. (1999). Extensive clear zone and defective ruffled border formation in osteoclasts of osteopetrotic (ia/ia) rats: implications for secretory function. *Exp. Cell Res.* 251, 477–491. doi: 10.1006/excr.1999.4585

Robling, A. G., and Bonewald, L. F. (2020). The osteocyte: new insights. *Annu. Rev. Physiol.* 82, 485–506. doi: 10.1146/annurev-physiol-021119-034332

Salo, J., Lehenkari, P., Mulari, M., Metsikkö, K., and Väänänen, H. K. (1997). Removal of osteoclast bone resorption products by transcytosis. *Science* 276, 270–273. doi: 10.1126/science.276.5310.270

Schinke, T., Schilling, A. F., Baranowsky, A., Seitz, S., Marshall, R. P., Linn, T., et al. (2009). Impaired gastric acidification negatively affects calcium homeostasis and bone mass. *Nat. Med.* 15, 674–681. doi: 10.1038/nm.1963

Seeman, E. (2009). Bone modeling and remodeling. *Crit. Rev. Eukaryot. Gene Expr.* 19, 219–233.

Shalev, M., and Elson, A. (2018). The roles of protein tyrosine phosphatases in bone-resorbing osteoclasts. *Biochim. Biophys. Acta* 1866, 114–123. doi: 10.1016/j.bbamcr.2018.07.005

Shamriz, O., Shaag, A., Yaacov, B., NaserEddin, A., Weintraub, M., Elpeleg, O., et al. (2017). The use of whole exome sequencing for the diagnosis of autosomal recessive malignant infantile osteopetrosis. *Clin. Genet.* 92, 80–85. doi: 10.1111/cge.12804

Shapiro, G., Fishleder, J., Stepensky, P., Simanovsky, N., Goldman, V., and Lamdan, R. (2020). Skeletal changes after hematopoietic stem cell transplantation in osteopetrosis. *J. Bone Miner. Res.* 35, 1645–1651.

Sharkia, R., Mahajnah, M., Athamny, E., Khatib, M., Sheikh-Muhammad, A., and Zalan, A. (2016). Changes in marriage patterns among the Arab community in Israel over a 60-year period. *J. Biosoc. Sci.* 48, 283–287. doi: 10.1017/s0021932015000103

Sharkia, R., Zaid, M., Athamna, A., Cohen, D., Azem, A., and Zalan, A. (2008). The changing pattern of consanguinity in a selected region of the Israeli Arab community. *Am. J. Hum. Biol.* 20, 72–77. doi: 10.1002/ajhb.20678

Shin, N. Y., Choi, H., Neff, L., Wu, Y., Saito, H., Ferguson, S. M., et al. (2014). Dynamin and endocytosis are required for the fusion of osteoclasts and myoblasts. *J. Cell. Biol.* 207, 73–89. doi: 10.1083/jcb.201401137

Simanovsky, N., Rozovsky, K., Hiller, N., Weintraub, M., and Stepensky, P. (2016). Extending the spectrum of radiological findings in patients with severe osteopetrosis and different genetic backgrounds. *Pediatr. Blood Cancer* 63, 1222–1226. doi: 10.1002/pbc.25952

Smurova, K., and Podbilewicz, B. (2016). RAB-5- and DYNAMIN-1-mediated endocytosis of EFF-1 fusogen controls cell-cell fusion. *Cell Rep.* 14, 1517–1527. doi: 10.1016/j.celrep.2016.01.027

Sobacchi, C., Schulz, A., Coxon, F. P., Villa, A., and Helfrich, M. H. (2013). Osteopetrosis: genetics, treatment and new insights into osteoclast function. *Nat. Rev. Endocrinol.* 9, 522–536. doi: 10.1038/nrendo.2013.137

Stattin, E. L., Henning, P., Klar, J., McDermott, E., Stecksen-Blicks, C., Sandstrom, P. E., et al. (2017). SNX10 gene mutation leading to osteopetrosis with dysfunctional osteoclasts. *Sci. Rep.* 7:3012.

Stein, M., Barnea-Zohar, M., Shalev, M., Arman, E., Brenner, O., Winograd-Katz, S., et al. (2020). Massive osteopetrosis caused by non-functional osteoclasts in R51Q SNX10 mutant mice. *Bone* 136:115360. doi: 10.1016/j.bone.2020.115360

Stepensky, P., Grisariu, S., Avni, B., Zaidman, I., Shadur, B., Elpeleg, O., et al. (2019). Stem cell transplantation for osteopetrosis in patients beyond the age of 5 years. *Blood Adv.* 3, 862–868. doi: 10.1182/bloodadvances.2018025890

Sultana, F., Morse, L. R., Picotto, G., Liu, W., Jha, P. K., Odgren, P. R., et al. (2020). Snx10 and PIKfyve are required for lysosome formation in osteoclasts. *J. Cell Biochem.* 121, 2927–2937. doi: 10.1002/jcb.29534

Sun-Wada, G. H., Tabata, H., Kawamura, N., Aoyama, M., and Wada, Y. (2009). Direct recruitment of H+-ATPase from lysosomes for phagosomal acidification. *J. Cell Sci.* 122(Pt 14), 2504–2513. doi: 10.1242/jcs.050443

Takayanagi, H. (2021). RANKL as the master regulator of osteoclast differentiation. *J. Bone Miner. Metab.* 39, 13–18. doi: 10.1007/s00774-020-01191-1

Teasdale, R. D., and Collins, B. M. (2012). Insights into the PX (phox-homology) domain and SNX (sorting nexin) protein families: structures, functions and roles in disease. *Biochem. J.* 441, 39–59. doi: 10.1042/bj20111226

Teitelbaum, S. L. (2007). Osteoclasts: what do they do and how do they do it? *Am. J. Pathol.* 170, 427–435. doi: 10.2353/ajpath.2007.060834

Teitelbaum, S. L. (2011). The osteoclast and its unique cytoskeleton. *Ann. N.Y. Acad. Sci.* 1240, 14–17. doi: 10.1111/j.1749-6632.2011.06283.x

Tsukasaki, M., Huynh, N. C., Okamoto, K., Muro, R., Terashima, A., Kurikawa, Y., et al. (2020). Stepwise cell fate decision pathways during osteoclastogenesis at single-cell resolution. *Nat. Metab.* 2, 1382–1390. doi: 10.1038/s42255-020-00318-y

Van Wesenbeeck, L., Odgren, P. R., Coxon, F. P., Frattini, A., Moens, P., Perdu, B., et al. (2007). Involvement of PLEKHM1 in osteoclastic vesicular transport and osteopetrosis in incisors absent rats and humans. *J. Clin. Invest.* 117, 919–930. doi: 10.1172/jci30328

Wada, T., Nakashima, T., Hiroshi, N., and Penninger, J. M. (2006). RANKL-RANK signaling in osteoclastogenesis and bone disease. *Trends Mol. Med.* 12, 17–25. doi: 10.1016/j.molmed.2005.11.007

Wallroth, A., and Haucke, V. (2018). Phosphoinositide conversion in endocytosis and the endolysosomal system. *J. Biol. Chem.* 293, 1526–1535. doi: 10.1074/jbc.r117.000629

Wang, K., Li, M., and Hakonarson, H. (2010). ANNOVAR: functional annotation of genetic variants from high-throughput sequencing data. *Nucleic Acids Res.* 38:e164. doi: 10.1093/nar/gkq603

Wartosch, L., Fuhrmann, J. C., Schweizer, M., Stauber, T., and Jentsch, T. J. (2009). Lysosomal degradation of endocytosed proteins depends on the chloride transport protein ClC-7. *FASEB J.* 23, 4056–4068. doi: 10.1096/fj.09-130880

Weinert, S., Jabs, S., Hohensee, S., Chan, W. L., Kornak, U., and Jentsch, T. J. (2014). Transport activity and presence of ClC-7/Ostm1 complex account for different cellular functions. *EMBO Rep.* 15, 784–791. doi: 10.15252/embr.201438553

Weinert, S., Jabs, S., Supanchart, C., Schweizer, M., Gimber, N., Richter, M., et al. (2010). Lysosomal pathology and osteopetrosis upon loss of H+-driven lysosomal Cl- accumulation. *Science* 328, 1401–1403. doi: 10.1126/science.1188072

Willkomm, L., and Bloch, W. (2015). State of the art in cell-cell fusion. *Methods Mol. Biol.* 1313, 1–19. doi: 10.1007/978-1-4939-2703-6_1

Worby, C. A., and Dixon, J. E. (2002). Sorting out the cellular functions of sorting nexins. *Nat. Rev. Mol. Cell Biol.* 3, 919–931. doi: 10.1038/nrm974

Xu, M., Stattin, E. L., Murphy, M., and Barry, F. (2017). Generation of induced pluripotent stem cells (ARO-iPSC1-11) from a patient with autosomal recessive osteopetrosis harboring the c.212+1G>T mutation in SNX10 gene. *Stem Cell Res.* 24, 51–54. doi: 10.1016/j.scr.2017.07.024

Xu, T., Xu, J., Ye, Y., Wang, Q., Shu, X., Pei, D., et al. (2014). Structure of human SNX10 reveals insights into its role in human autosomal recessive osteopetrosis. *Proteins* 82, 3483–3489. doi: 10.1002/prot.24689

Ye, L., Morse, L. R., Zhang, L., Sasaki, H., Mills, J. C., Odgren, P. R., et al. (2015). Osteopetrorickets due to Snx10 deficiency in mice results from both failed osteoclast activity and loss of gastric acid-dependent calcium absorption. *PLoS Genet.* 11:e1005057. doi: 10.1371/journal.pgen.1005057

You, Y., Li, W. Z., Zhang, S., Hu, B., Li, Y. X., Li, H. D., et al. (2018). SNX10 mediates alcohol-induced liver injury and steatosis by regulating the activation of chaperone-mediated autophagy. *J. Hepatol.* 69, 129–141. doi: 10.1016/j.jhep.2018.01.038

Zhang, S., Hu, B., You, Y., Yang, Z., Liu, L., Tang, H., et al. (2018). Sorting nexin 10 acts as a tumor suppressor in tumorigenesis and progression of colorectal cancer through regulating chaperone mediated autophagy degradation of p21(Cip1/WAF1). *Cancer Lett.* 419, 116–127. doi: 10.1016/j.canlet.2018.01.045

Zhang, S., Yang, Z., Bao, W., Liu, L., You, Y., Wang, X., et al. (2020). SNX10 (sorting nexin 10) inhibits colorectal cancer initiation and progression by controlling autophagic degradation of SRC. *Autophagy* 16, 735–749. doi: 10.1080/15548627.2019.1632122

Zhou, C., You, Y., Shen, W., Zhu, Y. Z., Peng, J., Feng, H. T., et al. (2016). Deficiency of sorting nexin 10 prevents bone erosion in collagen-induced mouse arthritis through promoting NFATc1 degradation. *Ann. Rheum Dis.* 75, 1211–1218. doi: 10.1136/annrheumdis-2014-207134

Zhu, C. H., Morse, L. R., and Battaglino, R. A. (2012). SNX10 is required for osteoclast formation and resorption activity. *J. Cell Biochem.* 113, 1608–1615.

Zlotogora, J., and Shalev, S. A. (2014). Marriage patterns and reproductive decision-making in the inhabitants of a single Muslim village during a 50-year period. *Hum. Hered.* 77, 10–15. doi: 10.1159/000357945

Zou, W., and Teitelbaum, S. L. (2015). Absence of Dap12 and the alphavbeta3 integrin causes severe osteopetrosis. *J. Cell Biol.* 208, 125–136. doi: 10.1083/jcb.201410123

**Conflict of Interest:** The authors declare that the research was conducted in the absence of any commercial or financial relationships that could be construed as a potential conflict of interest.

frontiers in Cell and Developmental Biology

METHODS
published: 25 May 2021
doi: 10.3389/fcell.2021.674710

# Quantification of Osteoclasts in Culture, Powered by Machine Learning

*Edo Cohen-Karlik[1†], Zamzam Awida[2†], Ayelet Bergman[1], Shahar Eshed[1], Omer Nestor[1], Michelle Kadashev[2], Sapir Ben Yosef[2], Hussam Saed[2], Yishay Mansour[1], Amir Globerson[1*], Drorit Neumann[2*‡] and Yankel Gabet[3*‡]*

[1] Blavatnik School of Computer Science, Tel Aviv University, Tel Aviv, Israel, [2] Department of Cell and Developmental Biology, Sackler Faculty of Medicine, Tel Aviv University, Tel Aviv, Israel, [3] Department of Anatomy and Anthropology, Sackler Faculty of Medicine, Tel Aviv University, Tel Aviv, Israel

*In vitro* osteoclastogenesis is a central assay in bone biology to study the effect of genetic and pharmacologic cues on the differentiation of bone resorbing osteoclasts. To date, identification of TRAP+ multinucleated cells and measurements of osteoclast number and surface rely on a manual tracing requiring specially trained lab personnel. This task is tedious, time-consuming, and prone to operator bias. Here, we propose to replace this laborious manual task with a completely automatic process using algorithms developed for computer vision. To this end, we manually annotated full cultures by contouring each cell, and trained a machine learning algorithm to detect and classify cells into *preosteoclast* (TRAP+ cells with 1–2 nuclei), *osteoclast type I* (cells with more than 3 nuclei and less than 15 nuclei), and *osteoclast type II* (cells with more than 15 nuclei). The training usually requires thousands of annotated samples and we developed an approach to minimize this requirement. Our novel strategy was to train the algorithm by working at "patch-level" instead of on the full culture, thus amplifying by >20-fold the number of patches to train on. To assess the accuracy of our algorithm, we asked whether our model measures osteoclast number and area at least as well as any two trained human annotators. The results indicated that for osteoclast type I cells, our new model achieves a Pearson correlation (r) of 0.916 to 0.951 with human annotators in the estimation of osteoclast number, and 0.773 to 0.879 for estimating the osteoclast area. Because the correlation between 3 different trained annotators ranged between 0.948 and 0.958 for the cell count and between 0.915 and 0.936 for the area, we can conclude that our trained model is in good agreement with trained lab personnel, with a correlation that is similar to inter-annotator correlation. Automation of osteoclast culture quantification is a useful labor-saving and unbiased technique, and we suggest that a similar machine-learning approach may prove beneficial for other morphometrical analyses.

**Keywords: osteoclasts, automatic quantification of osteoclasts, machine learning, object detection, deep learning, convolutional neural network (CNN), deep neural networks (DNN), artificial intelligence**

OPEN ACCESS

***Edited by:***
*Fernando Antunes, University of Lisbon, Portugal*

***Reviewed by:***
*Helen Knowles, University of Oxford, United Kingdom*
*Teun J. De Vries, VU University Amsterdam, Netherlands*
*Hugo Alexandre Ferreira, University of Lisbon, Portugal*

****Correspondence:***
*Yankel Gabet*
*yankel@tauex.tau.ac.il*
*Drorit Neumann*
*histo6@tauex.tau.ac.il*
*Amir Globerson*
*gamir@tauex.tau.ac.il*

*† These authors have contributed equally to this work and share first authorship*

*‡ These authors have contributed equally to this work and share senior authorship*

***Specialty section:***
*This article was submitted to Cellular Biochemistry, a section of the journal Frontiers in Cell and Developmental Biology*

***Received:*** *01 March 2021*
***Accepted:*** *26 April 2021*
***Published:*** *25 May 2021*

***Citation:***
*Cohen-Karlik E, Awida Z, Bergman A, Eshed S, Nestor O, Kadashev M, Yosef SB, Saed H, Mansour Y, Globerson A, Neumann D and Gabet Y (2021) Quantification of Osteoclasts in Culture, Powered by Machine Learning. Front. Cell Dev. Biol. 9:674710. doi: 10.3389/fcell.2021.674710*

## INTRODUCTION

Bone is a highly dynamic tissue that undergoes continuous remodeling throughout life, in a process involving the concerted actions of monocyte-derived osteoclasts that resorb mineralized tissue, and mesenchymal osteoblasts that deposit new bone (Teitelbaum, 2007; Clarke, 2008; Karsenty et al., 2009).

Bone mass is carefully maintained by a tight coordination of the activity of the bone-resorbing osteoclasts and bone-forming osteoblasts (Boyle et al., 2003; Teitelbaum and Ross, 2003; Takayanagi, 2007; Zaidi, 2007), and an imbalance between their activities results in skeletal pathologies such as osteoporosis (Bruzzaniti and Baron, 2006; Novack and Teitelbaum, 2008). Compounds demonstrating any ability to modulate the balance between osteoclasts and osteoblasts are thus of great interest in treating such diseases.

Osteoclast precursor differentiation to functionally active multinucleated osteoclasts depends on administration of macrophage colony stimulating factor (M-CSF) and receptor activator for nuclear factor kappa B ligand (RANKL) (Teitelbaum, 2000).

This process, called osteoclastogenesis can be examined *in vitro* using a well-established and commonly used assay in which bone marrow derived macrophages are cultured with M-CSF and RANKL (Marino et al., 2014). During differentiation, the cells acquire a higher expression of tartrate-resistant acid phosphatase (TRAP) (Minkin, 1982) and fuse together to become multinucleated cells (Hata et al., 1992). Osteoclasts are commonly defined *in vitro* as TRAP positive (using specific staining) multinucleated cells. This assay is important for the experimental screening of therapeutic candidates targeting osteoclastogenesis and bone resorption.

The current gold standard method for quantifying osteoclast formation in culture is based on manual counting of TRAP-positive, multinucleated ($\geq$3 nuclei) cells visualized under the microscope, which is both a subjective and a time-consuming process of evaluation (Marino et al., 2014). To overcome this significant drawback, we now present an unbiased high-throughput approach that enables fast and accurate measurement of osteoclast number and area for more efficient screening of potential therapeutic agents in bone biology. With the development of machine learning techniques, image classification and object detection applications are becoming more accurate and robust. As a result, machine learning based methods are being applied in a wide range of fields. The use of computer vision algorithms for the analysis of microscopic images has received growing interest in recent years. Such methods have been used for tasks such as detecting cell membranes (Ciresan et al., 2012), detecting cell nuclei (Xue and Ray, 2017), and segmenting cells (Ronneberger et al., 2015). This success motivated us to develop such an approach for osteoclasts. We note that existing tools cannot be directly applied to our setting due to its unique characteristics (see below).

Here, we report the development of an artificial intelligence-based object detection method designed to identify, classify, and quantify osteoclasts in cultures.

To our knowledge, there is no publicly- or commercially available software dedicated to *in vitro* osteoclast detection and evaluation. Previously developed AI-based approaches for cell detection are not applicable for this purpose due to its unique characteristics; the structure of osteoclasts is different from other cells (multinucleated TRAP-stained cells); collecting data for training an AI system dedicated to osteoclasts is time consuming (i.e., annotating a single culture takes several hours to annotate), thus limiting the number of examples that can be obtained in a timely manner. In order to overcome these challenges, we describe a method we developed to train our model on TRAP-stained osteoclast cultures and thereby increase the effective size of the training data.

For the purpose of training and evaluating our algorithm, we manually annotated 11 full osteoclast cultures containing thousands of cells. Osteoclast precursor cultures were treated with M-CSF and RANKL to induce differentiation. Images resulting from the TRAP staining were used to train the system to identify and count multinucleated TRAP+ osteoclasts, and to further validate and generalize the method. The trained model was tested on images that were not included in the training phase.

## MATERIALS AND METHODS

### Materials

Minimum Essential Medium α (Alpha-MEM) and fetal bovine serum (FBS), referred to here as "Standard medium," were purchased from Rhenium (Modiin, Israel), and culture plates were from Corning (New York, NY, United States). As a source of M-CSF, we used supernatant from CMG 14–12 cells, containing 1.3 μg/ml M-CSF (Takeshita et al., 2000). RANKL was purchased from R&D Systems, Minneapolis, MN, United States.

### Animals

Female wild type mice of the inbred strain C57BL/6J-RccHsd, aged 8–12 weeks were purchased from Envigo (Israel) and housed at the Tel-Aviv University animal facility. These mice were used for the generation of bone marrow derived macrophages (BMDM). Animal care and all procedures were in accordance with and with the approval of the Tel Aviv University Institutional Animal Care and Use Committee (Permit number 01-19 -032).

### Cell Culture

Bone marrow cells were harvested from femurs and tibias of 8- to 12-week-old female mice. Cells were seeded on tissue-culture treated plates in standard medium (alpha-MEM supplemented with 10% fetal bovine serum). On the following day, non-adherent cells were seeded in non–tissue culture-treated plates in standard medium supplemented with 100 ng/ml M-CSF, which induces cell proliferation and differentiation into preosteoclasts.

For the osteoclastogenesis assay, preosteoclasts were plated in 96-well plates (8,000 cells per well) with standard medium supplemented with 20 ng/ml M-CSF and 50 ng/ml RANKL, replaced every 2 days. On the 4th day, cells were stained using a TRAP staining kit (Sigma-Aldrich, St. Louis, MO, United States),

and multinucleated (≥3 nuclei) TRAP-positive cells were defined as osteoclasts. Images were acquired at a magnification of ×4 (Evos FLC, Life Technologies, MS, United States) (Hiram-Bab et al., 2015). An open-source graphical image annotation tool was used to measure osteoclast number and surface area from a single operator manual tracing for each well as previously described (Wada, 2016).

## Machine Learning Pipeline

Machine learning algorithms are used in a wide range of domains and underlie many technologies such as speech recognition, image understanding, machine translation, fraud detection, and face recognition.

To understand how machine learning algorithms work, we can consider an image categorization problem where the task of the model is to label an image with the name of the object in the image. Formally, the goal is to map from an input image X to an output label Y. The learning model is then simply a function from X to Y. In order to learn this function, one collects a "training" dataset of X-Y pairs (i.e., images and the corresponding correct label), and the learning process seeks a function that fits this training data well.

A key question is of course what type of functions to use when mapping X to Y. In recent years, functions mimicking neural networks have been found to work particularly well for a wide range of problems (**Figure 1**). This approach is also known as deep learning because it involves a multi-layered computation process.

Arguably, the most striking successes of deep learning to date are in the field of computer vision, where the goal is to develop algorithms that perform a semantic analysis of images, in a manner similar to the human visual system. This field has undergone a revolution since the introduction of the AlexNet architecture (Krizhevsky et al., 2012), and many other more advanced architectures since (Simonyan and Zisserman, 2014; Szegedy et al., 2015; He et al., 2016). AlexNet is an example of a so-called Convolutional Neural Network (CNN) model. These models use specific connectivity patterns between layers to form an architecture that utilizes the spatial structure within images (**Figure 2**).

## Object Detection

Our goal in this study was to automatically evaluate the number and area of osteoclasts in TRAP-stained cultures. To perform this task, we need to detect the cells in an image and then predict the total number of cells and the ratio between the area covered by cells and the size of the culture. This problem is closely related to the machine vision problem of *Object Detection,* which is designed to locate and correctly classify objects in images.

Object detection is a key task in computer vision and has been the focus of much research in recent years (Girshick et al., 2014; Girshick, 2015; Ren et al., 2015). Algorithms developed for this purpose are at the heart of many evolving technologies including autonomous vehicles (Menze and Geiger, 2015) and robotics (Jia et al., 2011). The purpose of object detection pipelines is to locate and correctly classify objects in images (see **Figure 3**). The architecture used for objective detection is a variant of the CNNs described above, but with additional mechanisms for finding multiple objects in an image and providing suitable bounding boxes and visual categories.

This study is based on the Single Shot Detection (SSD) architecture (Liu et al., 2016), which has proven useful for detecting small objects (Lam et al., 2018). SSD consists of two parts: (1) A *backbone* Convolutional Neural Network that extracts features from an input image, and (2) several convolutional layers with detection heads that output bounding boxes and the corresponding class followed by Non-Maximum Suppression (NMS) to filter overlapping bounding boxes (Felzenszwalb et al., 2009; Girshick et al., 2014; Girshick, 2015; **Figure 4**).

The most common use of SSD is for object detection in natural images. As a training set for such SSD models, one uses large datasets of natural images that have been annotated with bounding boxes for visual objects, as well as their visual labels such as the Pascal VOC and MSCOCO datasets (Lin et al., 2014; Everingham et al., 2015).

Here our focus is quite different, as we are interested in detecting images in cell cultures, and thus models trained on natural images are not directly applicable. Instead, the approach we took here is to collect a new dataset of annotated cell images and use this to train a new model. This process will be described in more detail.

## Data Collection

One of the main challenges in utilizing deep learning algorithms in various domains is the need for vast amounts of labeled data for training. Manually labeling data for object detection is a time consuming and expensive process due to the need to annotate each bounding box. In addition, the human annotator may require specific training. In this section we describe the data collection process and considerations.

For data annotation, we used an open-source annotation tool (Wada, 2016) to mark polygons around the cells (**Figure 5**). Marking polygons is more time-consuming than bounding boxes but it allows for a more versatile application such as running algorithms that quantify the contour of cells and segmentation (not tested in the scope of the current study).

We divided the cells into four different types (**Figure 6**): (1) *preosteoclast* – TRAP+ cells with 1–2 nuclei; (2) *osteoclast type I* – cells with more than (≥) 3 nuclei and less than 15 nuclei; (3) *osteoclast type II* – cells with more than (≥) 15 nuclei; (4) *ghost cells* – vanished cells which are distinguishable by their silhouette.

Full cultures may contain over 500 cells (**Figure 5**) and are hard to label accurately. To produce meaningful annotations, we divided each culture into equally sized regions, which are each annotated as separate images. This introduces a trade-off between the annotation speed and the precision of the annotations. We found that dividing each culture well to 16 regions, produced accurate annotations in a reasonable time.

For the annotation process, regions without any cells were discarded; this resulted in 133 regions with an average of 66.4 cells per region from 11 wells. Manually annotating a region took between several minutes for regions with few cells, and over an hour for regions with more than 100 cells (see **Figure 7**). Among

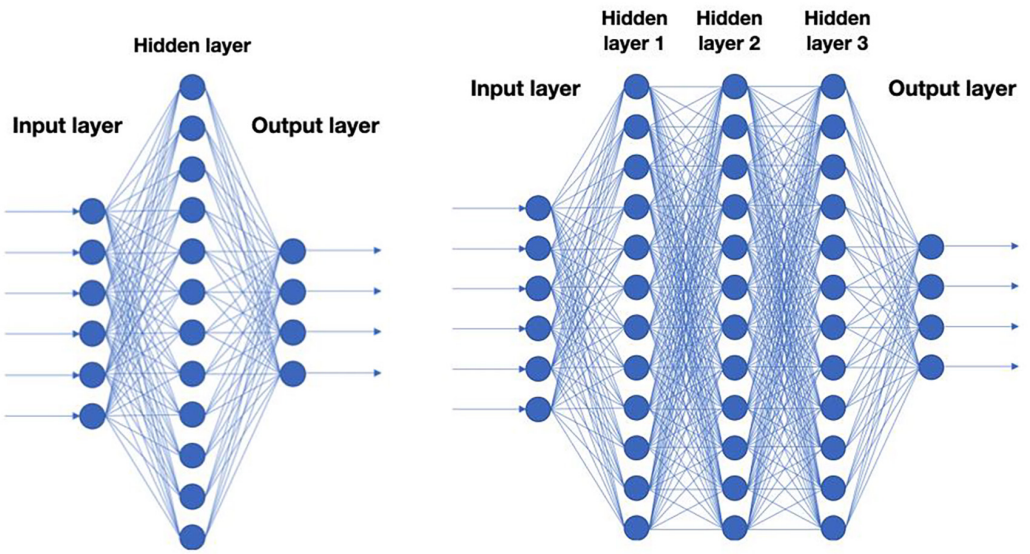


**FIGURE 1 |** Schematic representation of neural nets. Each circle corresponds to a *neuron* in a neural net. A neuron is typically a linear function of the previous layer followed by a non-linearity. Left: A neural net with a single hidden layer. Right: Deep neural net with 3 hidden layers.

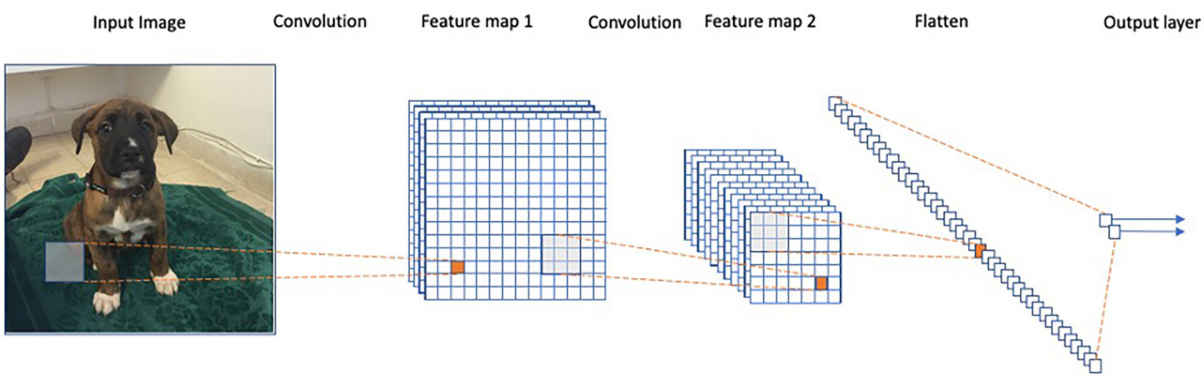


**FIGURE 2 |** Representation of a convolutional neural network. Each convolution operation consists of applying the same filters across the image to obtain a feature map in the following layer. The final iteration produces a fully connected layer similar to a regular neural net.

the 133 regions we annotated, 27 regions had more than 100 cells (**Figure 7** [right]).

## Patch Generation Strategy

Deep learning algorithms typically require a large number of examples for effective training. The considerations and challenges in annotating cell cultures described in the section "Data Collection" restrict the number of fully labeled cultures available. Thus, our main challenge was to train a deep neural network on relatively few training samples. A major advance made here stems from the realization that, in contrast to "images in the wild" where a single object can span most of the image, images of cultured cells can be viewed at a wide range of resolutions and preserve their semantic properties due to the small size of each cell compared to the entire culture. For example, when estimating the number of cells and the area covered by cells, we can restrict ourselves to small sections of the culture at any given point of time and still produce a perfectly annotated culture. This is not true when objects extend over a large section of the image such as in **Figure 3**.

Motivated by this observation, our strategy was to operate in small patch levels of $\frac{1}{8} \times \frac{1}{8}$, which means that each culture comprises 64 non-overlapping patches. This strategy also provides many different options for sampling (overlapping) patches and offers a substantial increase in the number of samples the model can be trained on. Specifically, we sampled a random region of the culture with 10 to 15% of the original width and height. The upper-left coordinate of the region defines the patch location. This process generates an enormous number of options for selecting a patch from a given culture. For example, given an image of a culture of size 1,000 × 1,000, there are more than $850^2 \cdot 50^2$ ($\approx 1.8 \cdot 10^9$) different ways to sample a patch by this

**FIGURE 3 |** Output of SSD trained on Pascal VOC. The algorithm detects and wraps the objects with bounding boxes as well as correctly classifying them into the relevant class (the classification is depicted by the bounding box color: red corresponds to "Person" class, blue to "Dog" class, yellow to "Car" class, and green to "Bicycle" class).

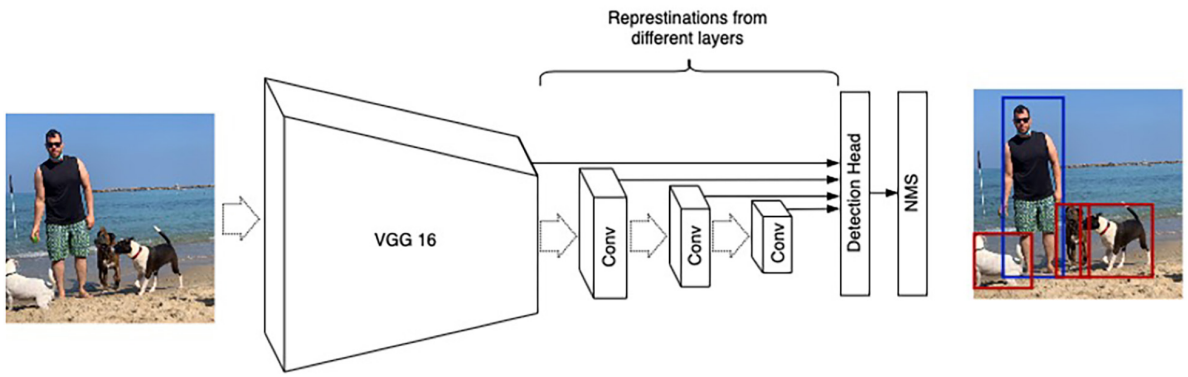


**FIGURE 4 |** SSD architecture illustration. VGG16 (Simonyan and Zisserman, 2014) is used as a base network. Detection heads are connected to numerous convolution layers (denoted as "Conv") to account for different resolutions.

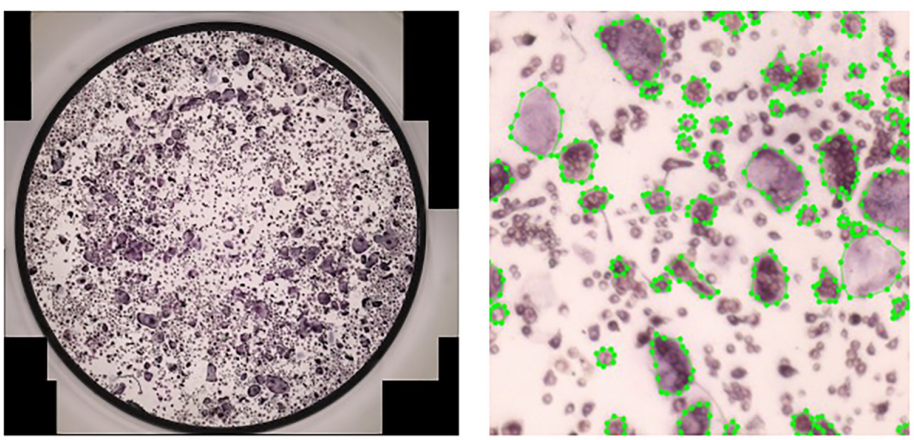

**FIGURE 5 |** Manual annotation of osteoclasts in cultures. Left: A full culture to be annotated. Right: A crop of size $\frac{1}{16} \times \frac{1}{16}$ of a fully annotated culture.

procedure. Here, we sampled 3,600,000 random patches from 10 wells used for training.

Another mechanism for increasing the size of training data, is to apply non-informative transformations to training points. For example, adding a small amount of noise to an image is unlikely to change the semantic content, but provides a new data point for the algorithm to train on. In the deep-learning literature, this is known as "Data Augmentation"

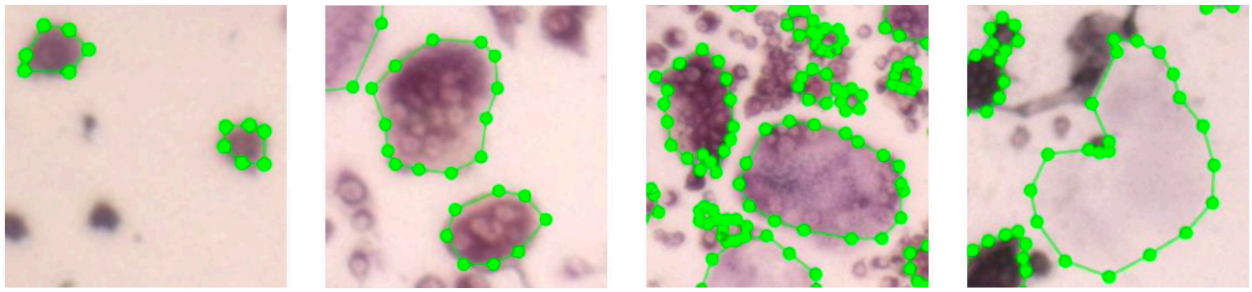

**FIGURE 6 |** Images of the four different cell types. The first three images depict cells with different number of nuclei. The rightmost cell is a ghost cell.

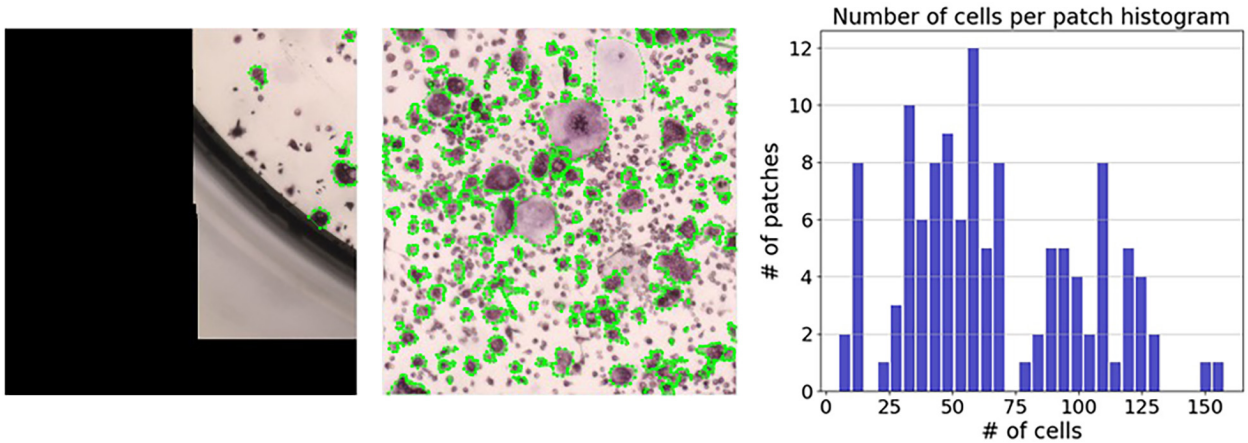


**FIGURE 7 |** Distribution of the number of cells per region. The number of cells per region ranged from 5 annotated cells (left) to 158 annotated cells (middle). The right panel shows a histogram representing the number of cells per region.

(Shorten and Khoshgoftaar, 2019). Here, we augmented the training data by applying a combination of the following transformations: (i) random photometric distortions, affecting brightness, hue, and saturation, (ii) random vertical flips of the patches, and (iii) rotations of the patches by 90°, 180°, and 270°.

Training the model with only 10 images of complete cultures did not allow for meaningful image detection. In contrast, the above procedures for generating random patches significantly increased the size of the training data, and thus improved the learned model.

## Configuration and Hyperparameters

Our implementation was written in PyTorch, a deep learning library (Paszke et al., 2019) written in Python and C++. We used an open-source project as our starting point for SSD[1]. Since object detection pipelines were designed to detect bounding boxes, we transformed each polygon created during the annotation process to the tightest square containing the entire cell (**Figure 8**).

The implementation of SSD contains more than a dozen different hyperparameters, and we adapted some settings to fit our unique data. The main change involves reducing the number of convolution layers from 6 to 4, which removes bounding boxes spanning large sections of an input image. These objects are common in natural data (**Figures 3**, **4**) and less relevant for culture well images (**Figure 8**). The modification of the architecture along with our strategy to operate on patches allows us to detect cells with sizes 51–383 μm.

## Training

Because our scheme for augmentation extracts patches from full cultures, we dedicated 10 cultures for training, and 1 culture for testing. As is common practice for object detection, we utilized VGG16 (Simonyan and Zisserman, 2014), which was previously trained on ImageNet (Russakovsky et al., 2015) as the backbone network, and resumed training from these initial weights. We trained for 120,000 iterations with a batch size of 32 using an Adam optimizer (Kingma and Ba, 2014) with a learning rate of 0.00001.

## Detection in Large Images

As already discussed, our model was trained to detect cells in small patches. We therefore also needed a mechanism that could allow us to apply the model to images that are larger than these small patches. A simple strategy, which we employed here, is to divide the large image into a set of non-overlapping

[1]https://github.com/amdegroot/ssd.pytorch

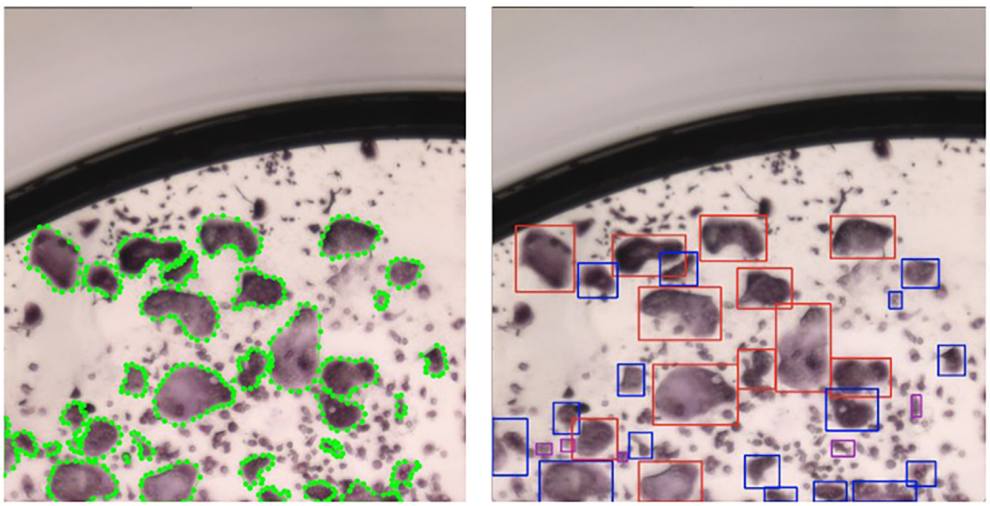

**FIGURE 8 |** SSD implementation using bounding boxes. Left: patch with polygons annotated by a human annotator; Right: patch after transforming the polygons to the tightest square surrounding a polygon. Blue bounding boxes correspond to type I osteoclasts and red bounding boxes correspond to type II osteoclasts.

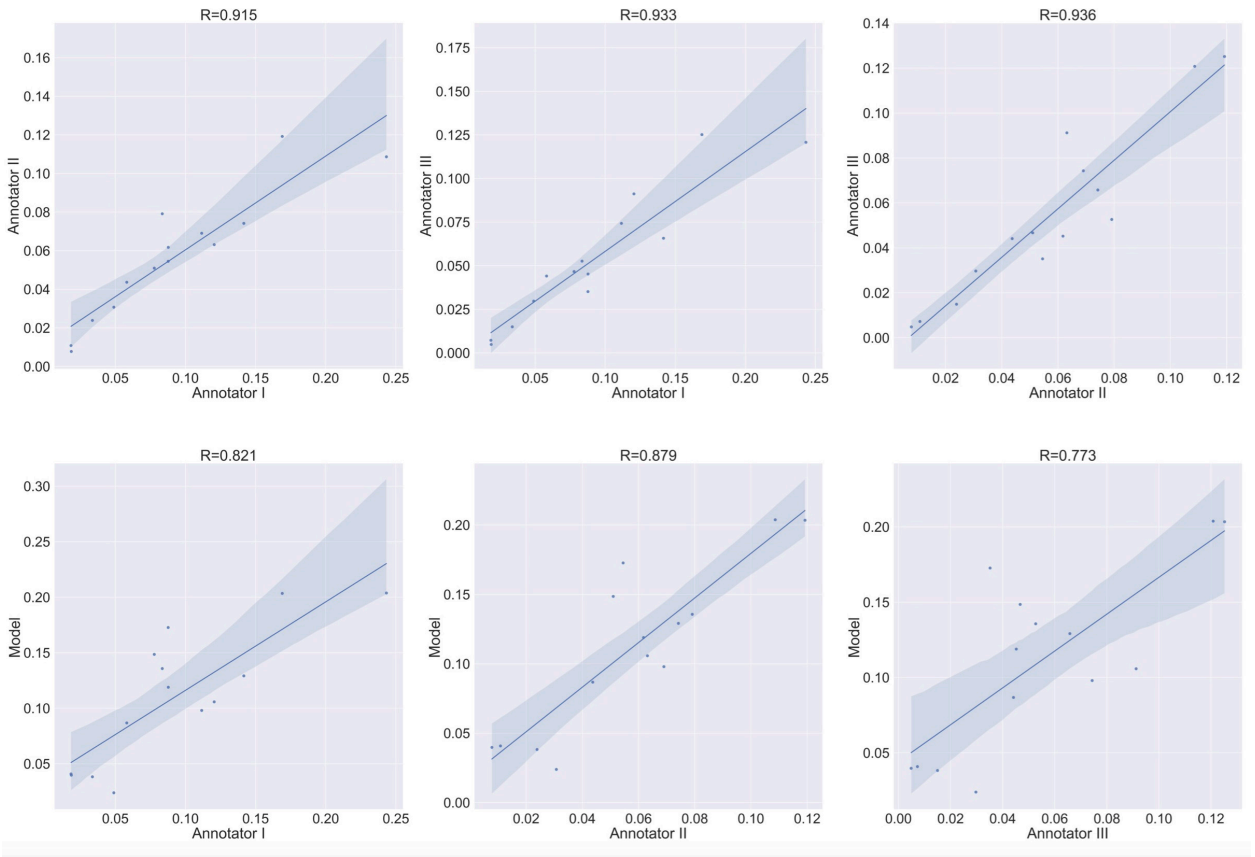


**FIGURE 9 |** Agreement level on the cell counting task of Type 1 osteoclasts. Shaded area represents the variation boundaries. Upper row: correlation between the three annotators for the cell counting task performed on the same set of culture images. Bottom row: correlation between each annotator and the model's prediction for the cell counting task.

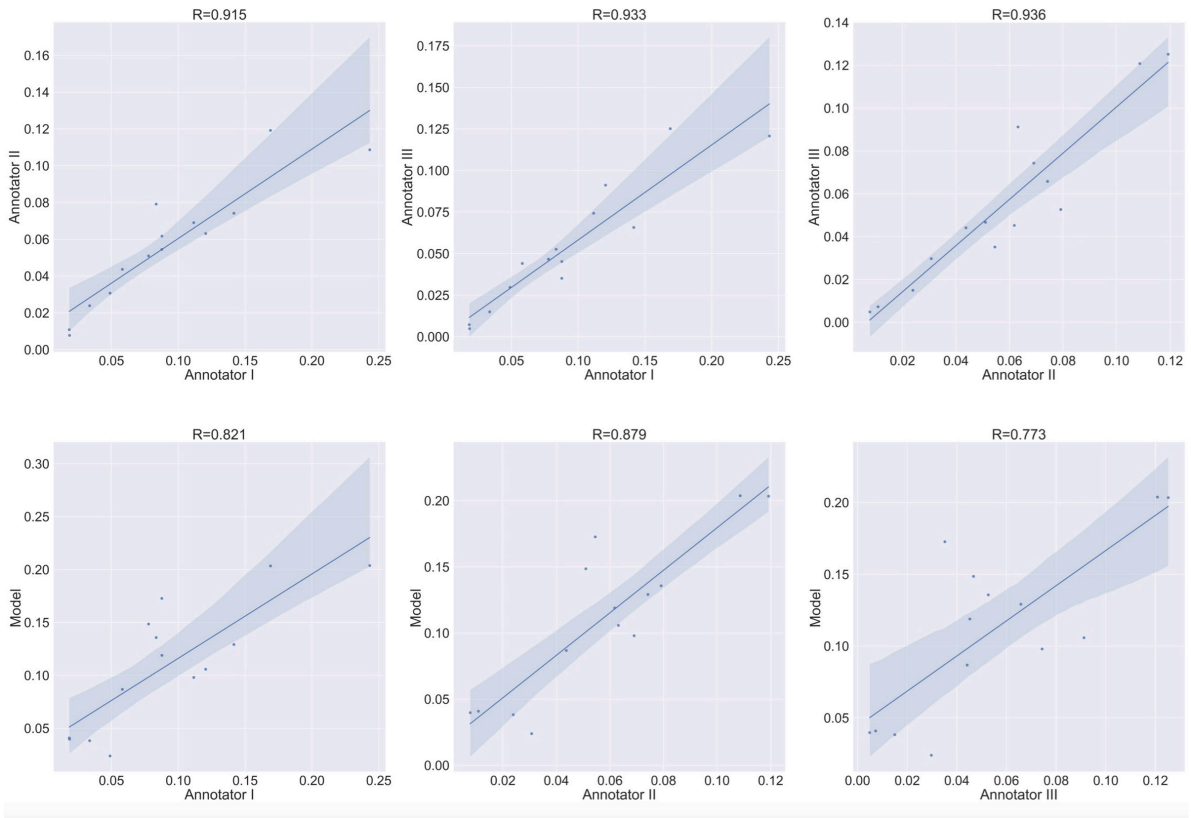


**FIGURE 10 |** Area estimation task for osteoclasts Type 1. Upper row: correlation between each annotator on a single culture and the other two annotators on the area estimation task. Bottom row: correlation between each annotator and the model's prediction on the area estimation task.

**TABLE 1 |** Correlation coefficients between human annotators and the model for cell counting.

| | Annotator II | Annotator III | Model |
|---|---|---|---|
| **Correlation coefficients for preosteoclast numbers** | | | |
| Annotator I | 0.506 | 0.819 | 0.879 |
| Annotator II | | 0.687 | 0.730 |
| Annotator III | | | 0.920 |
| **Correlation coefficients for Type 2 osteoclast numbers** | | | |
| Annotator I | 0.952 | 0.955 | 0.968 |
| Annotator II | | 0.960 | 0.913 |
| Annotator III | | | 0.921 |
| **Correlation coefficients for Ghost cell numbers** | | | |
| Annotator I | 0.597 | 0.287 | 0.269 |
| Annotator II | | 0.781 | 0.410 |
| Annotator III | | | 0.423 |

**TABLE 2 |** Correlation coefficients between human annotators and the model for cell area measurements.

| | Annotator II | Annotator III | Model |
|---|---|---|---|
| **Correlation coefficients for preosteoclasts area** | | | |
| Annotator I | 0.656 | 0.865 | 0.937 |
| Annotator II | | 0.708 | 0.753 |
| Annotator III | | | 0.891 |
| **Correlation coefficients for Type 2 osteoclasts area** | | | |
| Annotator I | 0.980 | 0.978 | 0.995 |
| Annotator II | | 0.991 | 0.978 |
| Annotator III | | | 0.978 |
| **Correlation coefficients for Ghost cells area** | | | |
| Annotator I | 0.326 | −0.007 | 0.590 |
| Annotator II | | 0.917 | 0.300 |
| Annotator III | | | 0.070 |

small patches and apply the model to each one individually. The output is then simply the union of the outputs from the small patches. Since our model was trained on $\frac{1}{8} \times \frac{1}{8}$ images, we had 64 patches per culture. It is true that splitting images into non-overlapping patches may split some cells across multiple patches and may therefore be considered a disadvantage (see "Error Analysis"). However, in practice, we found that the naive approach worked satisfactorily, and more sophisticated schemes were not necessary.

## Evaluation

The main focus in bone cell culture analysis is to quantify the number and area of the cells rather than predicting the location of the cells inside the culture. Thus, the natural metrics for

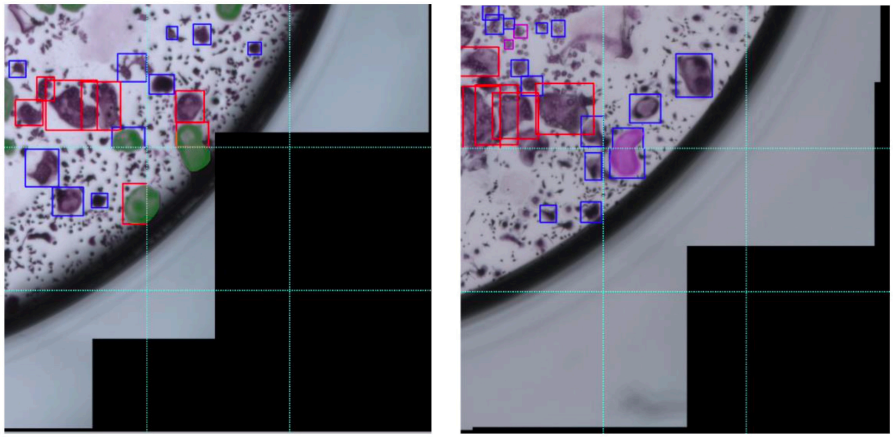

**FIGURE 11 |** Error in annotation due to overlapping of cells over multiple patches. These two cropped images of cultures are divided into 9 smaller patches. Left: Cells that are split across different patches are marked in opaque green. Right: a single cell split across different patches is marked in opaque violet and is covered by two bounding boxes, one in the upper patch and one in the lower one.

evaluation are the number of cells detected and the area covered by cells. Since these are inherently regression tasks, we report the Pearson correlation of (i) the human inter-annotator agreement for both the number and area covered by $TRAP^+$ multinucleated osteoclasts (**Figures 9**, **10** upper rows), and (ii) the agreement between the model-predicted and human annotation for these measurements (**Figures 9**, **10** bottom rows). In these correlation analyses, the residuals were all normally distributed (as calculated using the D'Agostino & Pearson test in Prism 7.0, $\alpha = 0.05$, $p > 0.4$).

# RESULTS

## Inter Annotator Agreement

To verify meaningful annotations, we asked three annotators to annotate a test culture divided into 14 regions (the test culture consists of 16 regions, 2 regions did not contain any cells). We then evaluated the inter annotator agreement for the detection and analysis of preosteoclasts, Type 1 and 2 osteoclasts, and ghost cells (**Figures 9**, **10** upper rows, **Tables 1**, **2**), which is an important measure of the accuracy and reproducibility of the labeling process. Because the most relevant osteoclastic cell type is a TRAP+ osteoclast with 3 to 15 nuclei (Type 1), it was important that our model discriminate between preosteoclasts and Type 1 cells as well as between Type 1 and Type 2 osteoclasts. The correlation between the 3 annotators was near-perfect for Type 1 and Type 2 osteoclast counting and area (>0.915), but more moderate coefficients were obtained for the detection of preosteoclasts (from 0.506 to 0.865). The discrepancies in annotation were mainly due to differences in the exhaustiveness of the labeling, which mostly affects the counting of small cells. Since the contribution of the small cells to the estimated area is low, there is still a high level of agreement for area measurements. Notably, the agreement among the human annotators on the identification of Ghost cells was generally low (0 to 0.917, **Tables 1**, **2**).

## Model vs. Human Annotation Agreement

Next, to assess the prediction accuracy of our model, we evaluated the agreement between our model and the three human annotators on the same set of images. These images were from a test set that was not used for training purposes. Overall, we found a high level of agreement between the model and human annotators (**Figures 9**, **10** bottom row, **Tables 1**, **2**). When running our model on the same images used for the inter-annotator correlation, the model agreed with all 3 annotators with correlation coefficients >0.7 for preosteoclasts and Type 1 and 2 osteoclasts. Notably, the correlation among the three human annotators was similar and sometimes even inferior to the model-to-human correlation. In line with the inter-annotator low level of agreement on the identification of Ghost cells, the model's correlation with the human annotators was also low (**Tables 1**, **2**). For osteoclast (Type 1 and 2) counting, the correlation between the model and the human annotators ranged from 0.913 to 0.968, and for the area between 0.773 and 0.995 (**Figures 9**, **10** bottom row, **Tables 1**, **2**). These correlation coefficients are comparable to the inter-annotator coefficients that ranged from 0.948 to 0.960, and from 0.915 to 0.991, respectively (**Figures 9**, **10** top row, **Tables 1**, **2**).

## Error Analysis

In this section we describe the errors that our model makes. The most common issue is with cells that span multiple patches. This problem is introduced due to the resolution at which the model operates and is most frequently evident in bounding boxes that only partially cover the designated cells, as depicted in **Figure 11** [left]. This type of error has a minor effect on the cell counting task, as most cells are covered by a single bounding box. In the area estimation task, this type of error causes partial

coverage of the cells. In rare cases, a single cell is covered by two bounding boxes (See **Figure 11** [right]), which causes double counting of a cell and has no effect on the area estimation task. A visual inspection of the predictions on the test images resulted in 15 erroneous cells from a total of 896 detected cells, which corresponds to 1.5% of the cells in the entire well. The impact of this type of error is therefore negligible.

## DISCUSSION AND CONCLUSION

We describe a novel method for rapidly and automatically quantifying osteoclast cultures that uses deep learning methods developed for object detection. Previously developed AI-based approaches for cell detection do not recognize the unique characteristics of osteoclasts and do not differentiate between cell types based on their nuclei number. For the training step, we manually annotated the type and location of each cell in 11 full cultures containing thousands of cells. The novelty of our strategy is that we train an SSD by working at "patch-level" instead of on the full culture and thereby generate more data for the algorithm to train on. The results indicate that our trained model is in good agreement with the human annotators, with a correlation that is similar to inter-annotator correlation. Our model performed especially well for the measurement of Type 1 and Type 2 osteoclast numbers and area. Measurements of preosteoclasts were slightly less satisfactory, although the model agreed with the human annotator to a similar degree and sometimes better than human annotators agreed among themselves. The identification of Ghost cells seems to be particularly problematic with little agreement among the human annotators or between the annotators and the model for these cells.

It should be noted that other experimental settings, e.g., using human cells, and different staining protocols, grayscale images, or camera resolutions, may require dedicated training of the algorithm. In such instances, we suggest that the use of the protocol reported here to generate large numbers of training images will provide a customized model that will perform satisfactorily in each specific setting. Using the same approach, the model could be further improved to detect subclasses of osteoclasts, i.e., 3 to 5 nuclei versus 6 to 10 and 11 to 15 nuclei. In theory, the model could also be trained to recognize and measure fluorescence-stained cultures.

In conclusion, we have developed a satisfactory method for the automation of osteoclast culture analysis that can detect and quantify TRAP-positive, multinucleated osteoclasts. This model discriminates between classical osteoclasts (3 to 15 nuclei) and abnormal "giant" cells (>15 nuclei). This model is therefore a useful labor-saving technique and we suggest that a similar approach may prove beneficial in facilitating other image related analysis tasks.

## DATA AVAILABILITY STATEMENT

The raw data supporting the conclusions of this article will be made available by the authors, without undue reservation.

## ETHICS STATEMENT

Written informed consent was obtained from the individual for the publication of any potentially identifiable images or data included in this article.

## AUTHOR CONTRIBUTIONS

EC-K, AB, SE, and ON: algorithm design and development. ZA: experiment design and development. ZA, MK, SBY, and HS: data curation. EC-K, ZA, YG, DN, AG, and YM: data analysis. EC-K, ZA, YG, DN, AG, and YM: writing. YG, DN, AG, and YM: study design and co-direction. All authors contributed to the article and approved the submitted version.

## FUNDING

This work was supported by the Yandex Machine Learning Initiative at Tel Aviv University, an Israel Science Foundation (ISF) Grant No. 1086/17 to YG and Grant No. 343/17 to DN and by a grant from the Dotan Hemato-oncology Fund, the Cancer Biology Research Center, Tel Aviv University to DN and YG.

## ACKNOWLEDGMENTS

This work was carried out in partial fulfillment of the requirements for a Ph.D. degree for ZA and EC-K. The work of AB, SE, and ON was carried out as part of a machine learning workshop, course no. 0368-3300. MK performed an internship with YG and DN in the framework of the "Israel Experience" program and with SBY in the framework of the Sackler Faculty of Medicine's TAU-MED program.

## REFERENCES

Boyle, W. J., Simonet, W. S., and Lacey, D. L. (2003). Osteoclast differentiation and activation. *Nature* 423, 337–342. doi: 10.1038/nature01658

Bruzzaniti, A., and Baron, R. (2006). Molecular regulation of osteoclast activity. *Rev. Endocr. Metab. Disord.* 7, 123–139. doi: 10.1007/s11154-006-9009-x

Ciresan, D., Giusti, A., Gambardella, L., and Schmidhuber, J. (2012). Deep neural networks segment neuronal membranes in electron microscopy images. *Adv. Neural Inf. Process. Syst.* 25, 2843–2851.

Clarke, B. (2008). Normal bone anatomy and physiology. *Clin. J. Am. Soc. Nephrol.* 3(Suppl. 3), S131–S139.

Everingham, M., Eslami, S. A., Van Gool, L., Williams, C. K., Winn, J., and Zisserman, A. (2015). The pascal visual object classes challenge: a retrospective. *Int. J. Comput. Vision* 111, 98–136. doi: 10.1007/s11263-014-0733-5

Felzenszwalb, P. F., Girshick, R. B., McAllester, D., and Ramanan, D. (2009). Object detection with discriminatively trained part-based models. *IEEE Trans. Pattern Anal. Mach. Intell.* 32, 1627–1645. doi: 10.1109/tpami.2009.167

Girshick, R. (2015). "Fast r-cnn," in *Proceedings of the IEEE International Conference on Computer Vision*, (Washington, DC: IEEE).

Girshick, R., Donahue, J., Darrell, T., and Malik, J. (2014). "Rich feature hierarchies for accurate object detection and semantic segmentation," in *Proceedings of the IEEE Conference on Computer Vision and Pattern Recognition*, (Columbus, OH: IEEE).

Hata, K., Kukita, T., Akamine, A., Kukita, A., and Kurisu, K. (1992). Trypsinized osteoclast-like multinucleated cells formed in rat bone marrow cultures efficiently form resorption lacunae on dentine. *Bone* 13, 139–146. doi: 10.1016/8756-3282(92)90003-f

He, K., Zhang, X., Ren, S., and Sun, J. (2016). "Deep residual learning for image recognition," in *Proceedings of the IEEE Conference on Computer Vision and Pattern Recognition*, (Las Vegas, NV: IEEE).

Hiram-Bab, S., Liron, T., Deshet-Unger, N., Mittelman, M., Gassmann, M., Rauner, M., et al. (2015). Erythropoietin directly stimulates osteoclast precursors and induces bone loss. *The FASEB Journal* 29, 1890–1900. doi: 10.1096/fj.14-259085

Jia, Z., Saxena, A., and Chen, T. (2011). "Robotic object detection: Learning to improve the classifiers using sparse graphs for path planning," in *Proceedings of the 22nd International Joint Conference on Artificial Intelligence*, (Barcelona: IJCAI).

Karsenty, G., Kronenberg, H. M., and Settembre, C. (2009). Genetic control of bone formation. *Annu. Rev. Cell Dev.* 25, 629–648. doi: 10.1146/annurev.cellbio.042308.113308

Kingma, D. P., and Ba, J. (2014). Adam: a method for stochastic optimization. *arXiv* [preprint] Available online at: http://arxiv.org/pdf/1412.6980v4.pdf (Accessed March 3, 2015) arXiv:1412.6980,

Krizhevsky, A., Sutskever, I., and Hinton, G. E. (2012). Imagenet classification with deep convolutional neural networks. *Adv. Neural Inf. Process. Syst.* 25, 1097–1105.

Lam, D., Kuzma, R., McGee, K., Dooley, S., Laielli, M., Klaric, M., et al. (2018). xview: objects in context in overhead imagery. *arXiv* [preprint] Available online at: https://arxiv.org/abs/1802.07856 (Accessed February 22, 2018) arXiv:1802.07856,

Lin, T.-Y., Maire, M., Belongie, S., Hays, J., Perona, P., Ramanan, D., et al. (2014). "Microsoft coco: common objects in context," in *Proceedings of the European Conference on Computer Vision*, (New York, NY: Springer).

Liu, W., Anguelov, D., Erhan, D., Szegedy, C., Reed, S., Fu, C.-Y., et al. (2016). "Ssd: Single shot multibox detector," in *Proceedings of the European Conference on Computer Vision*, (New York, NY: Springer).

Marino, S., Logan, J. G., Mellis, D., and Capulli, M. (2014). Generation and culture of osteoclasts. *BoneKEy Rep.* 3:570.

Menze, M., and Geiger, A. (2015). "Object scene flow for autonomous vehicles," in *Proceedings of the IEEE Conference on Computer Vision and Pattern Recognition*, (Boston, MA: IEEE).

Minkin, C. (1982). Bone acid phosphatase: tartrate-resistant acid phosphatase as a marker of osteoclast function. *Calcif. Tissue Int.* 34, 285–290. doi: 10.1007/bf02411252

Novack, D. V., and Teitelbaum, S. L. (2008). The osteoclast: friend or foe? *Annu. Rev. Pathol. Mech. Dis.* 3, 457–484.

Paszke, A., Gross, S., Massa, F., Lerer, A., Bradbury, J., Chanan, G., et al. (2019). Pytorch: an imperative style, high-performance deep learning library. *arXiv* [preprint] arXiv:1912.01703.

Ren, S., He, K., Girshick, R., and Sun, J. (2015). Faster r-cnn: towards real-time object detection with region proposal networks. *arXiv* [preprint] Available online at: https://arxiv.org/abs/1506.01497 (Accessed June 4, 2015) arXiv:1506.01497,

Ronneberger, O., Fischer, P., and Brox, T. (2015). "U-net: convolutional networks for biomedical image segmentation," in *Proceedings of the International Conference on Medical Image Computing and Computer-Assisted Intervention*, (New York, NY: Springer), 234–241.

Russakovsky, O., Deng, J., Su, H., Krause, J., Satheesh, S., Ma, S., et al. (2015). Imagenet large scale visual recognition challenge. *Int. J. Comput. vision* 115, 211–252. doi: 10.1007/s11263-015-0816-y

Shorten, C., and Khoshgoftaar, T. M. (2019). A survey on image data augmentation for deep learning. *J. Big Data* 6, 1–48.

Simonyan, K., and Zisserman, A. (2014). Very deep convolutional networks for large-scale image recognition. *arXiv* [preprint] Available online at: http://arxiv.org/abs/1409.1556 (Accessed September 4, 2014). arXiv:1409.1556,

Szegedy, C., Liu, W., Jia, Y., Sermanet, P., Reed, S., Anguelov, D., et al. (2015). "Going deeper with convolutions," in *Proceedings of the IEEE Conference on Computer Vision and Pattern Recognition*, (Boston, MA: IEEE).

Takayanagi, H. (2007). Osteoimmunology: shared mechanisms and crosstalk between the immune and bone systems. *Nat. Rev. Immunol.* 7, 292–304. doi: 10.1038/nri2062

Takeshita, S., Kaji, K., and Kudo, A. (2000). Identification and characterization of the new osteoclast progenitor with macrophage phenotypes being able to differentiate into mature osteoclasts. *J. Bone Miner. Res.* 15, 1477–1488. doi: 10.1359/jbmr.2000.15.8.1477

Teitelbaum, S. L. (2000). Bone resorption by osteoclasts. *Science* 289, 1504–1508. doi: 10.1126/science.289.5484.1504

Teitelbaum, S. L. (2007). Osteoclasts: what do they do and how do they do it? *Am. J. Pathol.* 170, 427–435. doi: 10.2353/ajpath.2007.060834

Teitelbaum, S. L., and Ross, F. P. (2003). Genetic regulation of osteoclast development and function. *Nat. Rev. Genet.* 4, 638–649. doi: 10.1038/nrg1122

Wada, K. (2016). *Labelme: Image Polygonal Annotation With Python*. GitHub repository Available online at: https://github.com/wkentaro/labelme

Xue, Y., and Ray, N. (2017). Cell Detection in microscopy images with deep convolutional neural network and compressed sensing. *arXiv* [preprint] Available online at: https://arxiv.org/abs/1708.03307 (Accessed February 21, 2018). arXiv:1708.03307,

Zaidi, M. (2007). Skeletal remodeling in health and disease. *Nat. Med.* 13, 791–801. doi: 10.1038/nm1593

**Conflict of Interest:** The authors declare that the research was conducted in the absence of any commercial or financial relationships that could be construed as a potential conflict of interest.

frontiers in Cell and Developmental Biology

REVIEW
published: 18 June 2021
doi: 10.3389/fcell.2021.651161

# Regulation of Osteoclastogenesis and Bone Resorption by miRNAs

*Kazuki Inoue[1,2], Courtney Ng[1], Yuhan Xia[1] and Baohong Zhao[1,2,3]**

*[1] Arthritis and Tissue Degeneration Program, David Z. Rosensweig Genomics Research Center, Hospital for Special Surgery, New York, NY, United States, [2] Department of Medicine, Weill Cornell Medicine, New York, NY, United States, [3] Graduate Program in Cell and Developmental Biology, Weill Cornell Medicine Graduate School of Medical Sciences, New York, NY, United States*

Osteoclasts are specialized bone-resorbing cells that contribute to physiological bone development and remodeling in bone metabolism throughout life. Abnormal production and activation of osteoclasts lead to excessive bone resorption in pathological conditions, such as in osteoporosis and in arthritic diseases with bone destruction. Recent epigenetic studies have shed novel insight into the dogma of the regulation of gene expression. microRNAs belong to a category of epigenetic regulators, which post-transcriptionally regulate and silence target gene expression, and thereby control a variety of biological events. In this review, we discuss miRNA biogenesis, the mechanisms utilized by miRNAs, several miRNAs that play important roles in osteoclast differentiation, function, survival and osteoblast-to-osteoclast communication, and their translational potential and challenges in bone biology and skeletal diseases.

**Keywords: osteoclast, miRNA, bone resorption, rheumatoid arthritis, osteoporosis**

OPEN ACCESS

***Edited by:***
*Natalie A. Sims,*
*University of Melbourne, Australia*

***Reviewed by:***
*Jiake Xu,*
*University of Western Australia, Australia*
*Yankel Gabet,*
*Tel Aviv University, Israel*

****Correspondence:***
*Baohong Zhao*
*zhaob@hss.edu*

***Specialty section:***
*This article was submitted to Cellular Biochemistry, a section of the journal Frontiers in Cell and Developmental Biology*

***Received:*** *08 January 2021*
***Accepted:*** *12 May 2021*
***Published:*** *18 June 2021*

***Citation:***
*Inoue K, Ng C, Xia Y and Zhao B (2021) Regulation of Osteoclastogenesis and Bone Resorption by miRNAs. Front. Cell Dev. Biol. 9:651161. doi: 10.3389/fcell.2021.651161*

## INTRODUCTION

Bone loss related to multiple diseases, such as rheumatoid arthritis (RA), osteoporosis, psoriatic arthritis and periodontitis, is a prevalent cause of disability in patients (Schett and Gravallese, 2012; Goldring et al., 2013). Bone destruction significantly diminishes the quality of life and simultaneously can increase the risk of mortality of these patients. Osteoclasts are giant, multinucleated cells that are derived from monocyte/macrophage lineage and specialize in bone resorption through proteolytic degradation and acid decalcification of the bone matrix. Osteoclast-mediated bone resorption is essential for skeletal development and normal bone remodeling. However, abnormal osteoclast formation and activation in pathological conditions play a crucial role in osteolysis. A broader understanding of the regulatory mechanisms that govern osteoclastogenesis will facilitate development of novel therapeutic strategies for patients subjected to pathological bone resorption.

Myeloid osteoclast precursors first undergo differentiation into mononuclear osteoclasts in response to the master osteoclastogenic cytokine: receptor activator of nuclear factor-κB ligand (RANKL) accompanied by macrophage colony-stimulating factor (M-CSF) and immunoreceptor tyrosine-based activation motif (ITAM)-mediated co-stimulatory signaling pathways. Mononuclear osteoclast precursors then fuse into giant, mature polykaryons driven by the expression of cell-cell fusion genes, such as DC-Stamp, ATP6v0d2 and Gα13 (Yagi et al., 2005; Lee et al., 2006; Nakano et al., 2019). Osteoclastogenesis is delicately regulated and influenced

in order to maintain the balance of osteoclastogenic and anti-osteoclastogenic mechanisms (Zhao and Ivashkiv, 2011). RANKL induces a broad range of signaling cascades including canonical and non-canonical NF-kB pathways, mitogen-activated kinase (MAPK) pathways and calcium signaling. These pathways activate downstream transcription factors to drive osteoclast differentiation, such as c-Fos, nuclear factor of activated T cells c1 (NFATc1), and B lymphocyte-induced maturation protein-1 (Blimp1). On the other hand, negative regulators mediating intrinsic anti-osteoclastogenic mechanisms, such as differentially expressed in FDCP 6 homolog (Def6), interferon regulatory factor (IRF8) and v-maf musculoaponeurotic fibrosarcoma oncogene family protein B (MafB), function as brakes to restrain excessive osteoclast formation and bone resorption (Humphrey et al., 2005; Asagiri and Takayanagi, 2007; Zhao B. et al., 2009; Nakashima and Takayanagi, 2011; Zhao and Ivashkiv, 2011; Xu and Teitelbaum, 2013; Li et al., 2014; Boyce et al., 2015; Binder et al., 2017). Some regulators were identified to preferentially limit pathological osteoclastic bone resorption, such as RBP-J and NF-κB p100 (Yao et al., 2009; Zhao et al., 2012). These regulators and associated mechanisms interact to form regulatory networks that coordinately modulate osteoclastic gene expression to govern osteoclast differentiation and function.

Over the past decade, epigenetic studies have gained rapidly growing research and clinical attention. Epigenetics investigates heritable changes in gene expression and cellular phenotype that do not involve alterations in DNA sequence, which provides a new level and dimension of understanding of gene expression. Major epigenetic mechanisms include DNA methylation, chromatin remodeling, histone posttranslational modifications and non-coding RNAs (ncRNAs) (Zhang and Cao, 2019). These mechanisms often act in concert to play crucial roles in the regulation of gene expression extensively involved in diverse biological and disease settings, such as cell proliferation and differentiation, development, cardiovascular disease, diabetes, autoimmune diseases, and cancer. In human genome, ncRNAs constitute more than 90% of the genome transcripts (Hangauer et al., 2013). ncRNAs consists of multiple classes of RNA that are not translated into proteins, which are classified into two categories by size; long non-coding RNAs (lncRNAs) (>200 nt) and small RNAs (<200 nt). Small RNAs include microRNAs (miRNAs), short interfering RNAs (siRNAs) and Piwi-interacting RNAs (piRNAs) (Kim et al., 2009; Esteller, 2011). Recently, a unique class of ncRNAs transcribed from sequences of enhancer regions, called enhancer RNAs (eRNAs), have been identified (Kim et al., 2010; Lam et al., 2014). Genome-wide cap analysis of gene expression (CAGE) identified eRNA regions at the Nrp2, Dcstamp, and Nfatc1 gene loci in osteoclasts. These eRNAs are necessary for the transcription of these genes that are important for osteoclast differentiation (Sakaguchi et al., 2018). To date, functions of lncRNAs in osteoclastogenesis are largely unknown. The most well-characterized ncRNAs in myeloid cells are miRNAs. In this review, we discuss miRNA biogenesis, several miRNAs that play important roles in osteoclast differentiation, function, survival, osteoblast-to-osteoclast communication, the mechanisms controlled by miRNAs, and their translational potential and challenges in bone biology and skeletal diseases (**Table 1**).

## Post-transcriptional Regulation of Target Gene Expression by miRNAs

MicroRNAs (miRNAs) constitute a class of small single-stranded non-coding RNAs (about 22 nucleotides), that function in diverse regulatory pathways through gene repression of their target mRNAs via post-transcriptional mechanisms (Lagos-Quintana et al., 2001; Bartel, 2004). miRNAs commonly bind to multiple target sequences at the 3′ untranslated region (3′-UTR) of mRNAs, through perfect complementary pairing of nucleotides 2–7 at the 5′ end of the miRNA (the miRNA seed region) (Bartel, 2009). These molecules repress gene expression via mRNA degradation or translational inhibition of their target mRNAs, or a combination of these mechanisms (Ling et al., 2013). A series of processes is required to generate mature miRNAs, beginning with the transcription of long precursor RNAs, called primary miRNAs (pri-miRNAs), by RNA polymerase II (Lee et al., 2004). In the nucleus, long pri-miRNAs are cropped into hairpin structures by the microprocessor complex, which consists of the RNase III enzyme, Drosha and RNA binding protein, DiGeorge syndrome critical region 8 (DGCR8). This process produces the precursor miRNAs (pre-miRNAs) that are approximately 60–70 nucleotides (Lee et al., 2003; Gregory et al., 2004). Pre-miRNAs are then exported from the nucleus by Exportin-5 (Exp5) into the cytoplasm where they are further cleaved by the RNase III enzyme, Dicer (Lund et al., 2004). Upon recognition, Dicer cleaves the pre-miRNA at the double-stranded RNA stem and the terminal loop to generate a mature ∼22 nucleotide miRNA duplex (Park et al., 2011). The miRNA duplex consists of two strands that are often referred to as a guide and a passenger strand. The passenger strand is typically degraded while the guide strand of the mature miRNA is incorporated into the RNA-induced silencing complex (RISC), which comprises Dicer, transactivating response RNA-binding protein (TRBP) and Argonaute proteins (AGO1-4) (Chendrimada et al., 2005; Peters and Meister, 2007). Active RISC is guided by miRNA to complementary target mRNAs and downregulates gene expressing by inducing mRNA degradation, translational repression, or a combination of the two mechanisms. AGO2 was identified to have catalytic slicer activity that can facilitate degradation of specific target mRNA. The target mRNAs sharing the same recognition sequences could compete for miRNA binding and influence the expression of each target gene. A single miRNA can recognize and regulate multiple mRNA targets, and consequently, may have a wide range and substantial effect on gene expression networks. Additionally, within the same cell types, the targets of an miRNA can be variable in response to differential environmental settings. Accordingly, miRNA-targeted gene regulation is both specific and sensitive to environmental changes. Multiple miRNAs can also be involved in the same biological processes, as exemplified by the miRNAs mentioned in this review, which

**TABLE 1 |** Osteoclastogenesis and bone metabolism mediated by miRNAs.

| microRNAs | Targets | miRNA-expressing Cells | *In vitro* effects on osteoclasts | *In vivo* effects (KO,Tg mice, inhibitor, agonist) | Clinical significance |
|---|---|---|---|---|---|
| miR-21 | PDCD4 (Hu et al., 2017)<br>FasL (Sugatani and Hruska, 2013) | Mouse BMMs | Osteoclastogenic promotion (Sugatani and Hruska, 2013; Hu et al., 2017) | miR-21 KO mice: decreased bone resorption and osteoclastogenesis (Hu et al., 2017) | miR-21 expression is increased in osteoporotic human serum and inversely correlated with BMD (Sugatani and Hruska, 2013) |
| miR-31 | RhoA (Mizoguchi et al., 2013) | Mouse BMMs | Osteoclastogenic promotion (Mizoguchi et al., 2013) | NA | NA |
| miR-214 | PTEN (Zhao et al., 2015)<br>TRAF3 (Liu et al., 2017) | RAW264.7 cells<br>Mouse BMMs | Osteoclastogenic promotion (Zhao et al., 2015) | miR-214 transgenic mice: reduced bone mass, increased osteoclastogenesis (Zhao et al., 2015)<br>miR-214 KO mice: the development of osteolytic breast cancer metastasis is prevented (Liu et al., 2017) | miR-214-3p is upregulated in osteolytic bone metastasis of breast cancer (Liu et al., 2017) |
| miR-182 | PKR (Inoue et al., 2018)<br>Foxo3,Maml1 (Miller et al., 2016) | Mouse BMMs<br>Human $CD14^+$ monocytes | Osteoclastogenic promotion (Miller et al., 2016; Inoue et al., 2018) | miR-182 KO mice: increased bone mass, decreased bone resorption and osteoclastogenesis (Inoue et al., 2018)<br>miR-182 transgenic mice: decreased bone mass, increased bone resorption and osteoclastogenesis (Inoue et al., 2018)<br>miR-182 inhibitor: bone loss in OVX and inflammatory arthritis is prevented (Inoue et al., 2018) | miR-182 expression is higher in RA patients, and TNF blockade therapy (TNFi) with Enbrel suppresses miR-182 expression levels in RA (Inoue et al., 2018) |
| miR-183 | HO-1 (Ke et al., 2015) | Mouse BMMs | Osteoclastogenic promotion (Ke et al., 2015) | NA | NA |
| miR-7b | DC-STAMP (Dou et al., 2014) | RAW264.7 cells | Osteoclastogenic inhibition (Dou et al., 2014) | NA | NA |
| miR-124 | Rab27a (Tang et al., 2017) | Mouse BMMs | Osteoclastogenic inhibition (Lee et al., 2013; Tang et al., 2017) | Pre-miR-124 suppresses bone destruction and osteoclast in AIA rats (Nakamachi et al., 2016) | NA |
| miR-141 | Calcr (Ell et al., 2013)<br>EphA2 (Yang S. et al., 2018) | Mouse BMMs | Osteoclastogenic inhibition (Ell et al., 2013; Yang S. et al., 2018) | miR-141 mimic suppresses osteolytic bone metastasis (Ell et al., 2013) and osteoporosis (Yang S. et al., 2018) | miR-141 expression is decreased in osteoporosis patients (Yang S. et al., 2018) |
| miR-503 | RANK (Chen et al., 2014) | Human $CD14^+$ monocytes | Osteoclastogenic inhibition (Chen et al., 2014) | miR-503 mimic suppresses bone resorption and osteoclastogenesis in OVX model (Chen et al., 2014) | miR-503 is downregulated in $CD14^+$ PBMCs of postmenopausal osteoporotic patients (Chen et al., 2014) |
| miR-125b | Prdm1 (Minamizaki et al., 2020) | Osteoblasts | Osteoclastogenic inhibition (Minamizaki et al., 2020) | miR-125 trangenic mice: reduced bone resorption and osteoclastogenesis in OVX model, LPS-induced calvarial bone loss model, and sciatic neurectomy (NX)-induced osteoporosis mouse model (Minamizaki et al., 2020) | NA |
| miR-155 | MITF, SOCS1 (Zhang et al., 2012)<br>TAB2 (Sul et al., 2018) | Mouse BMMs | Dual effects (Zhang et al., 2012; Zhao et al., 2017; Sul et al., 2018) | NA | NA |
| miR-223 | NFI-A (Sugatani and Hruska, 2009; Xie et al., 2015) | RAW264.7 cells | Dual effects (Sugatani and Hruska, 2007, 2009; Kagiya and Nakamura, 2013; Xie et al., 2015) | NA | NA |

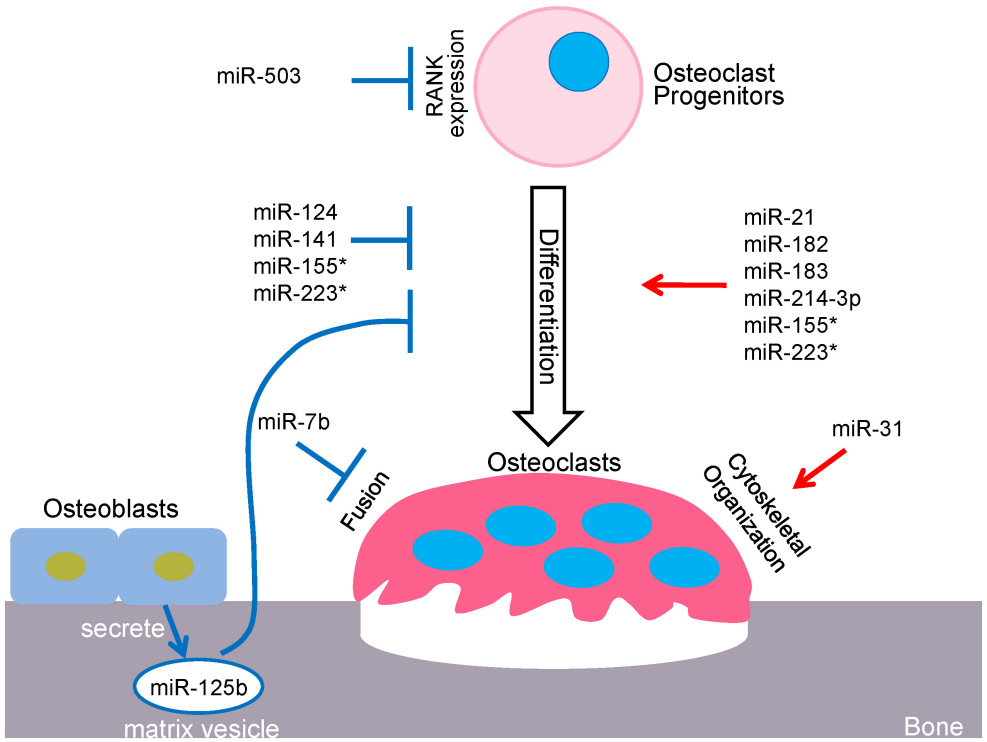


**FIGURE 1 |** miRNA-mediated regulatory network in osteoclastogenesis. *miR-155 and miR223 play dual roles in osteoclastogenesis.

play crucial and exclusive roles in osteoclast differentiation and function (**Figure 1**).

## miRNAs That Positively Regulate Osteoclastogenesis

### miR-21

In mammalian cells, miR-21 is most widely recognized as an oncogenic miRNA and its upregulation is associated to the progression of various cancers (Feng and Tsao, 2016). In addition, miR-21 is induced by inflammatory cytokines and plays regulatory roles in various cells. For example, miR-21 is induced by tumor necrosis factor-α (TNF-α) in endothelial cells (Yang D. et al., 2018), by interleukin-1β (IL-1β) in chondrocytes (Ma et al., 2020) and by interleukin-6 (IL-6) in myeloma cells (Loffler et al., 2007). Recently, miR-21 has gained recognition within the processes of bone metabolism and disease. *In vitro* studies have shown that RANKL induces miR-21 expression and promotes osteoclastogenesis via down-regulation of programmed cell death 4 (PDCD4), which subsequently regulates the c-Fos/NFATc1 axis (Sugatani et al., 2011). The pro-osteoclastic function of miR-21 is further demonstrated *in vivo* using miR-21 knockout mice, in which miR-21 deficiency inhibits bone resorption and osteoclastogenesis via targeting PDCD4 (Hu et al., 2017). miR-21 is found to be downregulated by bisphosphonate in lung cancer patients with osteolytic bone metastasis (Zhao et al., 2020). Another study revealed that estrogen suppresses miR-21 biogenesis, leading to upregulation of Fas Ligand (FasL), which is a target of miR-21 in osteoclasts and induces osteoclast cell death in an autocrine manner (Sugatani and Hruska, 2013). Thus, miR-21 also contributes to osteoclast survival and estrogen-mediated osteoclastogenesis.

### miR-31

miR-31 is induced by RANKL, and positively regulates cytoskeletal organization during osteoclastogenesis and bone resorption activity. It does so by targeting expression of RhoA to optimize actin ring formation in osteoclasts, which is crucial for both cytoskeletal organization and bone resorption (Mizoguchi et al., 2013). In addition, inflammatory cytokines can regulate miR-31 expression. For instance, miR-31 is induced by TNF-α in cord blood mononuclear cells (Kim et al., 2020), by IL-1β in HUVEC endothelial cells (Zhong et al., 2017) and by IL-6 in HuCC-T1 cholangiocarcinoma cell line (Ishigami et al., 2018).

### miR-214

The crosstalk and intercellular interaction between osteoclasts and osteoblasts are necessary for maintaining bone homeostasis and regulating bone remodeling. This communication involves secretory factors or cell-cell contact signaling, such as via RANKL, OPG, TGF-β1, IGF-1, Sema4D, Sema3A, ephrinB2/EphB4, Cthrc1, and Wnt16 (Zhao et al., 2006; Cao, 2011; Negishi-Koga et al., 2011; Hayashi et al., 2012; Takeshita et al., 2013; Moverare-Skrtic et al., 2014), and can be facilitated by bone-derived exosomes (Xie et al., 2017). Extracellular vesicles, or exosomes, are essential in coordinating intercellular

communication through delivery of proteins, lipids, and nucleic acids including DNA, mRNA and miRNA. Moreover, tumor-derived exosomes are crucial in promoting tumor microenvironment and metastasis (Becker et al., 2016). Recent evidence has identified a role of osteoclast-derived exosomal miR-214-3p in mediating inhibition of osteoclast-directed osteoblast formation (Li et al., 2016). Osteoclastic miR-214-3p was found in association with reduced bone formation, and elevated levels of miR-214-3p were found in whole serum, serum exosome and bone tissue from elderly women with fractures and OVX mice. Osteoclast-specific miR-214-3p overexpression mice (OC-miR-214-3p) exhibited elevated exosomal miR-214-3p in serum and reduced bone formation, and this was rescued by injection of antagomiR-214-3p delivered by osteoclast-targeted (D-Asp8)-liposome (Liang et al., 2015). *In vitro* evidence revealed that osteoclastic exosomal miR-214-3p can transfer to osteoblasts and inhibit osteoblast activity. Consistently, *in vivo* osteoclast-targeted inhibition of miR-214-3p was able to enhance bone formation in aging OVX mice. These results highlight the impact of exosomal miR-214-3p as a mediator for bone cell communication on bone disease and related crosstalk. Wang et al. also provided evidence supporting the inhibitory role of miR-214 on bone formation and osteoblast activity via direct targeting of ATF4, an essential transcription factor for osteoblastogenesis and function (Yang et al., 2004; Wang et al., 2013; Li et al., 2016).

Moreover, miR-214-3p was found to be upregulated during osteoclastogenesis and positively regulates the differentiation process through activating PI3K/Akt/NFATc1 pathway by directly targeting phosphatase and tensin homolog (PTEN) (Zhao et al., 2015). Inhibition of miR-214-3p attenuated, while overexpression of miR-214-3p promoted, *in vitro* osteoclastogenesis. OC-miR-214-3p transgenic mice exhibited reduced PTEN expression levels, enhanced osteoclast activity and reduced bone mass, proposing potential as a therapeutic target for osteoporosis. Previous studies have also shown that PTEN is a target of miR-214-3p, which promotes T cell activation and proliferation (Jindra et al., 2010). Upregulation of miR-214-3p was also observed in osteolytic bone metastasis of breast cancer, which was consistently associated with elevated osteoclast activity in nude mice xenografted with human breast cancer cells (Liu et al., 2017). Breast cancer cells are able to induce miR-214-3p expression and interestingly, genetic ablation of osteoclast-specific miR-214-3p prevented the development of osteolytic breast cancer metastasis. This study also revealed that mechanistically, miR-214-3p promotes bone resorption through direct targeting of TNF-α Receptor Associated Factor 3 (TRAF3), and osteoclast-targeted treatment of Traf3 3′UTR plasmid attenuated excessive bone resorption in OC-miR-214-3p mice. In addition, miR-214 is decreased by TNF-α in HT29 colorectal adenocarcinoma cells (Li et al., 2017), induced by IL-1β in primary chondrocytes (Xu et al., 2021) and induced by IL-6 in human colonocytes (Polytarchou et al., 2015). This regulation of miR-214 expression by inflammatory cytokines suggests potential roles for miR-214 in inflammatory bone metabolism. Collectively, these studies strongly support the potential of miR-214-3p as a therapeutic target through regulating both osteoblasts and osteoclasts to treat bone disorders such as osteoporosis and cancer bone metastasis.

### miR-182/miR-183

The miR-183 cluster, an miR family comprised of miR-182, miR-183 and miR-96, is well recognized to be functionally involved in development and also highly expressed and implicated in cancers, neurological disorders, autoimmune diseases (Dambal et al., 2015), and more recently, innate immunity (Singaravelu et al., 2019). miR96 was not detected during osteoclastogenesis (Miller et al., 2016), while miR-183 expression was found to be elevated by RANKL and promoted *in vitro* RANKL-induced osteoclastogenesis via targeting of heme oxygenase-1 (HO-1) (Ke et al., 2015). Recent studies revealed the functions of miR-182 in cell cycle, cell growth, cancer progression, T lymphocyte expansion and Th17 function (Stittrich et al., 2010; Ichiyama et al., 2016; Yao et al., 2019). miR-182 and miR-183 are induced by IL-6 but not IL-1β in Th17 cells and contribute to Th17 cell pathogenicity (Ichiyama et al., 2016).

Through genome-wide miRNA expression profiling via high-throughput miRNA-sequencing, our group identified miR-182 as a TNF-α-induced miRNA in mouse BMMs during inflammatory osteoclastogenesis (Miller et al., 2016). We further elucidated the role of miR-182 in regulating bone metabolism in both physiological and pathological conditions, such as those which occur in osteoporosis and rheumatoid arthritis (RA) (Inoue et al., 2018). Postmenopausal osteoporosis and RA are characterized by pathological bone destruction resulting from osteolysis conducted by osteoclasts. miRNA-based therapeutics for these diseases appear promising, though underdeveloped. Through a series of subsequent studies, we identified miR-182 as a key osteoclastogenic regulator, provided evidence revealing a novel regulatory network mediated by miR-182 in osteoclastogenesis, imparted therapeutic implications of targeting miR-182 to promote osteoprotection, and highlighted significant correlation between miR-182 and RA.

Our findings on miR-182 reveal great significance to the understanding of its role in bone metabolism, and potential impact on therapeutics and drug development for the treatment of bone diseases. Utilizing complementary genetic approaches (myeloid-specific miR-182 KO and Tg mice), miR-182 was identified as a key positive regulator of osteoclastogenesis. OVX-induced osteoporosis, which serves as a model for postmenopausal osteoporosis, and inflammatory arthritis, which mimics RA, were the disease models applied in this study for investigating translational significance. Genetic ablation or pharmacological inhibition of miR-182 prevented pathological bone loss in both models, suggesting a key role for miR-182 in bone protection. To test the efficacy of therapeutically targeting miR-182, chitosan (CH) nanoparticles were utilized to effectively and safely deliver miR-182 inhibitors to bone marrow and specifically target osteoclast lineage. The treatment with miR-182 inhibitors dramatically suppressed excessive osteoclast formation and bone resorption in these models without immune suppression, thus providing proof-of-principle that miR-182 inhibition presents significant clinical value for treating bone destruction. We also revealed and elucidated

the miR-182-PKR-IFN-β axis through the identification of protein kinase double-stranded RNA-dependent (PKR), which is a crucial target of miR-182, and a novel inhibitor of osteoclastogenesis. PKR attenuates osteoclastogenesis by upregulating the endogenous IFN-β-mediated autocrine feedback loop. For the first time, a miR-182-PKR axis is revealed to be responsible for suppressing this IFN-β signaling induced by RANKL to activate osteoclastogenesis, and this network is involved in fine tuning the osteoclastogenic program. In the context of disease, the miR-182-PKR-IFN-β axis exhibits aberrant expression level changes including elevation of miR-182, and downregulation of PKR and IFN-β levels in the PBMCs from RA patients in comparison to healthy donors. Given the role of TNF-α in the pathogenesis of RA, TNF-α blockade therapy (TNFi) with Enbrel suppressed miR-182 expression levels and elevated PKR and IFN-β expression levels, and decreased osteoclastogenesis in RA patients-derived PBMCs. The osteoclastogenic capacity of PBMCs from RA patients is significantly correlated with the expression pattern of the miR-182-PKR-IFN-β axis. Both murine and human data provide strong evidence supporting the role of miR-182 in osteoclastogenesis, and translational promise of targeting miR-182 to treat pathological bone destruction.

## miRNAs That Negatively Regulate Osteoclastogenesis

### miR-7b

miR-7b has been reported to participate in the regulation of B cell receptor (BCR) signaling, which is enhanced in autoreactive B cells from systemic lupus erythematosus (SLE) (Wu et al., 2014). B cell hyper-responsiveness in SLE results from the downregulation of Phosphatase and tensin homolog (PTEN) by upregulated miR-7 (Wu et al., 2014). miR-7b is induced by a cocktail of IL-1β, IFN-γ, and TNF-α in the MIN6 insulinoma cell line (Bravo-Egana et al., 2012), suggesting its involvement in inflammation.

Within the process of osteoclastogenesis, maturation of multi-nucleated osteoclasts requires cell-cell fusion of mononuclear osteoclast precursors. Bone disease, such as osteoporosis can result from deregulated osteoclastic bone-resorbing activity when osteoclast multinucleation is defected. The role of miR-7b was revealed through its direct targeting of dendritic cell-specific transmembrane protein (DC-STAMP), which is a critical mediator of the osteoclast fusion process (Yagi et al., 2005; Dou et al., 2014). Positive regulation of DC-STAMP expression is mediated by NFATc1, c-Fos, and strawberry notch homolog 2 (Sbno2) (Maruyama et al., 2013). At the post-transcriptional level, miR-7b negatively regulates DC-STAMP, resulting in the inhibition of osteoclast fusion. Overexpression of miR-7b represses the expression of other fusogenic genes such as CD47, ATP6v0d2 and OC-STAMP, as well as osteoclast specific genes such as Nfatc1 and OSCAR via DC-STAMP inhibition. These studies characterize the crucial role of miR-7b in osteoclast multinucleation and function.

### miR-124

miR-124 is, notably, abundantly expressed in neuronal cells, promoting cell differentiation (Lagos-Quintana et al., 2002; Makeyev et al., 2007), and also known as a critical regulator of immune function and implicated in inflammatory disorders (Qin et al., 2016). Expression of miR-124 is inversely correlated with activation of microglia during inflammation such as experimental autoimmune encephalomyelitis (EAE) (Ponomarev et al., 2011). Overexpression of miR-124 was found to promote microglia quiescence through directly targeting C/EBP-α and its downstream target, PU.1. This deactivation of macrophages suppresses CNS inflammation and inhibits EAE. In addition, inflammatory cytokines regulate the expression of miR-124. For example, TNF-α in keratinocytes (Yang et al., 2017) or IL-1β in lumbar (Willemen et al., 2012) was reported to decrease miR-124.

In addition to its effect on macrophage phenotypes in the CNS, miR-124 was shown to inhibit osteoclastogenesis in mouse BMMs by suppressing the expression of NFATc1 (Lee et al., 2013). miR-124 is downregulated in BMMs and osteoclasts from OVX mice, resulting in excessive bone resorption and destruction (Tang et al., 2017). This study also revealed a functional target of miR-124, Rab27a, which regulates multinucleation and transport of lysosome-related organelles (Shimada-Sugawara et al., 2015). Furthermore, miR-124 was reported to be downregulated in the ankles of adjuvant-induced arthritis (AIA) rats (Nakamachi et al., 2016). Administration of pre-miR-124 via injection into the ankles of AIA rats strongly suppressed bone destruction and reduced osteoclastogenesis via direct targeting of NFATc1. These findings support the novel role of miR-124 as a suppressor of osteoclastogenesis.

### miR-141

miR-141 is identified as a tumor inhibitor, as well as a significant regulator participating in tumor-induced osteolytic bone metastasis. Conditioned medium (CM) from bone metastatic cell lines such as 4T1.2 and TSU-Pr-B2 cells were shown to be sufficient in inducing osteoclastogenesis, and miRNA microarray analysis revealed significant downregulation of miR-141 in osteoclasts under the treatment (Ell et al., 2013). Overexpression of miR-141 suppressed osteoclast differentiation via targeting of MITF and calcitonin receptor (CALCR), with observed downregulation of osteoclast marker expression such as NFATc1, CtsK, and PU.1. Systemic treatment of miR-141 was able to inhibit osteoclastogenesis and activity *in vivo*, as well as suppress osteolytic activity of breast cancer bone metastasis *in vivo*, accompanied with reduced osteoclast differentiation and activity. Further support of the inhibitory role of miR-141 on osteoclastogenesis and bone resorbing activity was established through the study of aged osteoporotic rhesus monkeys conducted by Yang S. et al. (2018). Both osteoporotic patients and aged rhesus monkeys exhibited downregulated expression of miR-141 in bone tissues. Targeted delivery of miR-141 to osteoclasts using Asp (Aspartic acid) 8-PU (polyurethane) nanoparticles inhibited bone loss, osteoclast differentiation and bone resorption activity *in vivo*, as well as in *in vitro* culture of rhesus monkey osteoclasts. They also demonstrated that miR-141 functionally targets Calcr and ephrin type-A receptor 2 precursor (EphA2) to inhibit osteoclastogenesis. Collectively, these data present the critical role of miR-141 in suppression of

osteoclastogenesis and bone resorption, implicated in aberrant bone loss in bone disease and cancer.

### miR-503

miR-503 has been identified in numerous cancer types via miRNA expression profiling analyses, including human retinoblastoma, glioblastoma, hepatocellular carcinomaand non-small cell lung cancer (NSLC), many of which support a tumor-suppressive role of miR-503 (Zhao J.J. et al., 2009; Zhou and Wang, 2011; Yang et al., 2014; Zhang et al., 2014). It has also been demonstrated that miR-503 can induce G1 cell cycle arrest to promote myogenic differentiation and similarly through promoting cell cycle quiescence, inhibit progression of osteosarcoma and colon cancer cell proliferation (Sarkar et al., 2010; Chong et al., 2014; Chang et al., 2015). In contrast, miR-503 expression has been reported to be upregulated in certain cancers and identified as a tumor-associated miRNA that directly targets Bcl2 apoptosis regulator to promote apoptosis of dendritic cells, indicating a mechanism for tumor immunotolerance (Min et al., 2013).

In the context of bone disorders, miR-503 was identified to be dramatically downregulated in $CD14^+$ PBMCs of postmenopausal osteoporotic patients in comparison to postmenopausal healthy women. Following discontinuation of denosumab (an anti-RANKL antibody) treatment, miR-503 expression is decreased in patients with vertebral fractures (Anastasilakis et al., 2017). These findings suggest a crucial role for miR-503 in bone metabolism (Chen et al., 2014). Overexpression and silencing of miR-503 in $CD14^+$ PBMCs confirmed its inhibitory role on osteoclastogenesis and its direct targeting of RANK, the receptor for RANKL. Treatment with agomiR-503 protected OVX mice from bone loss by inhibiting bone resorption and increased bone mass. Consistently, estrogen upregulated miR-503 expression *in vitro* and *in vivo*, confirming its contribution to the pathogenesis of postmenopausal osteoporosis and potential as a therapeutic target.

### miR-125b

Bone matrix growth factors, such as TGF-β and IGF-1, play essential roles in coupling bone resorption and formation (Tang et al., 2009; Xian et al., 2012). Recently, miR-125b has been identified as a bone matrix-embedded coupling factor that is produced by osteoblasts (Minamizaki et al., 2020). miR-125b is enveloped by matrix vesicles (MVs) and accumulates in bone matrix. The osteoblast-derived MVs containing miR-125b are incorporated into osteoclast precursors and inhibit osteoclastogenesis. Mice overexpressing miR-125b in osteoblasts using human osteocalcin promoter show high bone mass phenotype and reduced number of bone-resorbing osteoclasts, without affecting osteoblasts and bone formation. miR-125b directly targets Prdm1, a key transcriptional factor of osteoclastogenesis, in osteoclast precursors. Overexpression of miR-125b in osteoblasts abrogates bone loss in OVX-induced osteoporosis mouse model, LPS-induced calvarial bone loss model, and sciatic neurectomy (NX)-induced osteoporosis mouse model. The MV containing miR-125b is a novel coupling factor of osteoblast-osteoclast communication. MVs containing miR-125b might be potential therapeutic targets for pathological bone loss.

## miRNAs That Play Dual Roles in Osteoclastogenesis

### miR-155

miR-155 plays crucial roles in cell development and function of various immune cells involved in both innate and adaptive immunity and is implicated in pathological conditions such as cancer (O'Connell et al., 2007, 2009; Thai et al., 2007; Vigorito et al., 2007; Teng et al., 2008). It has been shown that inflammatory cytokines and stimuli, such as TNF-α and lipopolysaccharide (LPS), can activate miR-155 expression, which in turn regulates proliferation, differentiation and function of macrophages and dendritic cells (O'Connell et al., 2007, 2009; Ceppi et al., 2009; Lind et al., 2015).

In addition to its role in immune cells, miR-155 has been revealed to inhibit RANKL-induced osteoclastogenesis through TGF-β1/Smad4 signaling and by mediating the suppressive effect of IFN-β on osteoclast differentiation through targeting microphthalmia-associated transcription factor (MITF), suppressor of cytokine signaling 1 (SOCS1), and PU.1 (Zhang et al., 2012; Zhao et al., 2017). However, in the context of LPS-mediated inflammatory bone loss, it has been recently reported that miR-155 is induced by LPS and enhances autophagy to increase osteoclast differentiation and activity through targeting transforming growth factor β-activated kinase 1-binding protein 2 (TAB2) (Sul et al., 2018). Taken together, miR-155 plays an inhibitory role in RANKL-induced osteoclastogenesis but enhances LPS-mediated inflammatory osteoclastogenesis.

### miR-223

miR-223 was known to be preferentially expressed in hematopoietic cells and identified as a key regulator of myeloid cell differentiation and activation, particularly neutrophils and macrophages, and therefore, a regulator of innate immune response through myeloid cell homeostasis (Fukao et al., 2007; Yuan et al., 2018). Studies have demonstrated that miR-223 has the abilities to promote macrophage polarization to adopt anti-inflammatory phenotype and inhibit activation of macrophages and subsequent inflammatory response through targeting signal transducer and activator of transcription 3 (STAT3) (Chen et al., 2012) and inflammasome sensor-NLRP3 (Bauernfeind et al., 2012). In contrast, miR-223 expression is downregulated under inflammatory conditions activated by Toll-like receptor (TLR) ligands, such as LPS in macrophages (Chen et al., 2012; Zhang et al., 2017). However, elevated expression of miR-223 in $CD68^+$ macrophages, $CD14^+$ monocytes, and $CD4^+$ T cells from synovium of rheumatoid arthritis (RA) patients was reported (Li et al., 2012; Shibuya et al., 2013). miR-223 expression is also induced by TNF-α in MH7A fibroblast-like synoviocyte cell line (Moriya et al., 2017). In osteoclast precursor cells, overexpression of miR-223 was shown to downregulate osteoclastogenesis (Sugatani and Hruska, 2007; Kagiya and Nakamura, 2013). However, conflicting studies have reported that in osteoclast precursor cells, a positive feedback loop exists whereby M-CSF induces transcription factor, PU.1, which

stimulates miR-223 expression, resulting in downregulation of its target, nuclear factor I A (NFIA). The downregulation of NFIA expression allows for upregulation of M-CSF receptor levels and consequently, promotion of osteoclastogenesis (Sugatani and Hruska, 2009; Xie et al., 2015). PU.1, c-Fos, MITF, and NFATc1 levels are upregulated by M-CSF and RANKL during osteoclastogenesis. These results suggest that miR-223 is essential for osteoclast differentiation and function. However, the mechanisms underlying the dual effects of miR-223 on osteoclastogenesis are not well-understood.

## CLOSING REMARK

miRNAs are involved in numerous molecular pathways and cellular events through targeting specific genes. Recent studies have identified competing endogenous RNAs (ceRNAs), which comprise of mRNAs, pseudogenes, long non-coding RNAs (lncRNAs) and circular RNAs (circRNA) (Cesana et al., 2011; Salmena et al., 2011; Tay et al., 2014). These ceRNAs communicate with each other to compete for shared miRNAs, acting as natural miRNA "sponges," to block miRNA binding and repression of its targets. ceRNAs impose a regulatory mechanism upon miRNAs, adding another level of complexity to miRNA-mediated gene regulation. The mechanisms of miRNA-ceRNA networks is another channel to unpack in further exploration and understanding of gene regulation by different RNA species in specific processes, pathways and tissues, which are especially important for understanding their translational implication.

Targeting miRNAs has shown promising therapeutic potential in a few clinical trials, such as in the treatment of diabetes, cancer and hepatitis C (Janssen et al., 2013; Chakraborty et al., 2017; Rupaimoole and Slack, 2017). These inspiring scientific advances highlight the clinical significance of the emerging field of miRNA and miRNA-based therapeutics. The miRNAs discussed in this review strongly support the potential of therapeutic targeting of miRNAs to prevent and treat pathological bone loss, such as that occurring in RA, osteoporosis and bone cancer metastasis. However, further work is needed in elucidating miRNA-mediated gene regulation networks specific to these diseases in order to successfully enhance the development of therapeutic approaches. In addition, generating an ideal miRNA-based drug delivery method presents challenges, such as ensuring stability, specificity and efficacy of targeting, and minimization of toxicities and off-target effects. Future studies and technological developments are expected to address these challenges in the clinical development of miRNA-based drugs.

## AUTHOR CONTRIBUTIONS

BZ designed, wrote, and edited the manuscript. KI wrote and edited the manuscript. CN and YX helped to writing and editing the manuscript. All authors contributed to the article and approved the submitted version.

## FUNDING

This work was supported by grants from the National Institutes of Health (AR062047, AR068970, and AR071463 to BZ) and Tow Foundation (for the David Z. Rosensweig Genomics Center at the Hospital for Special Surgery).

## ACKNOWLEDGMENTS

We apologize to colleagues whose work could not be cited due to space limitation. The content of this manuscript is solely the responsibilities of the authors and does not necessarily represent the official views of the NIH.

## REFERENCES

Anastasilakis, A. D., Yavropoulou, M. P., Makras, P., Sakellariou, G. T., Papadopoulou, F., Gerou, S., et al. (2017). Increased osteoclastogenesis in patients with vertebral fractures following discontinuation of denosumab treatment. *Eur. J. Endocrinol.* 176, 677–683. doi: 10.1530/EJE-16-1027

Asagiri, M., and Takayanagi, H. (2007). The molecular understanding of osteoclast differentiation. *Bone* 40, 251–264. doi: 10.1016/j.bone.2006.09.023

Bartel, D. P. (2004). MicroRNAs: genomics, biogenesis, mechanism, and function. *Cell* 116, 281–297.

Bartel, D. P. (2009). MicroRNAs: target recognition and regulatory functions. *Cell* 136, 215–233. doi: 10.1016/j.cell.2009.01.002

Bauernfeind, F., Rieger, A., Schildberg, F. A., Knolle, P. A., Schmid-Burgk, J. L., and Hornung, V. (2012). NLRP3 inflammasome activity is negatively controlled by miR-223. *J. Immunol.* 189, 4175–4181. doi: 10.4049/jimmunol.1201516

Becker, A., Thakur, B. K., Weiss, J. M., Kim, H. S., Peinado, H., and Lyden, D. (2016). Extracellular vesicles in Cancer: cell-to-cell mediators of metastasis. *Cancer Cell* 30, 836–848. doi: 10.1016/j.ccell.2016.10.009

Binder, N., Miller, C., Yoshida, M., Inoue, K., Nakano, S., Hu, X., et al. (2017). Def6 restrains osteoclastogenesis and inflammatory bone resorption. *J. Immunol.* 198, 3436–3447. doi: 10.4049/jimmunol.1601716

Boyce, B. F., Xiu, Y., Li, J., Xing, L., and Yao, Z. (2015). NF-kappaB-Mediated regulation of osteoclastogenesis. *Endocrinol. Metab.* 30, 35–44. doi: 10.3803/EnM.2015.30.1.35

Bravo-Egana, V., Rosero, S., Klein, D., Jiang, Z., Vargas, N., Tsinoremas, N., et al. (2012). Inflammation-Mediated regulation of MicroRNA expression in transplanted pancreatic islets. *J. Transplant* 2012:723614. doi: 10.1155/2012/723614

Cao, X. (2011). Targeting osteoclast-osteoblast communication. *Nat Med* 17, 1344–1346. doi: 10.1038/nm.2499

Ceppi, M., Pereira, P. M., Dunand-Sauthier, I., Barras, E., Reith, W., Santos, M. A., et al. (2009). MicroRNA-155 modulates the interleukin-1 signaling pathway in activated human monocyte-derived dendritic cells. *Proc. Natl. Acad. Sci. U S A.* 106, 2735–2740. doi: 10.1073/pnas.0811073106

Cesana, M., Cacchiarelli, D., Legnini, I., Santini, T., Sthandier, O., Chinappi, M., et al. (2011). A long noncoding RNA controls muscle differentiation by functioning as a competing endogenous RNA. *Cell* 147, 358–369. doi: 10.1016/j.cell.2011.09.028

Chakraborty, C., Sharma, A. R., Sharma, G., Doss, C. G. P., and Lee, S. S. (2017). Therapeutic miRNA and siRNA: moving from bench to clinic as next generation medicine. *Mol. Ther. Nucleic Acids* 8, 132–143. doi: 10.1016/j.omtn.2017.06.005

Chang, S. W., Yue, J., Wang, B. C., and Zhang, X. L. (2015). miR-503 inhibits cell proliferation and induces apoptosis in colorectal cancer cells by targeting E2F3. *Int. J. Clin. Exp. Pathol.* 8, 12853–12860.

Chen, C., Cheng, P., Xie, H., Zhou, H. D., Wu, X. P., Liao, E. Y., et al. (2014). MiR-503 regulates osteoclastogenesis via targeting RANK. *J. Bone Miner. Res.* 29, 338–347. doi: 10.1002/jbmr.2032

Chen, Q., Wang, H., Liu, Y., Song, Y., Lai, L., Han, Q., et al. (2012). Inducible microRNA-223 down-regulation promotes TLR-triggered IL-6 and IL-1beta production in macrophages by targeting STAT3. *PLoS One* 7:e42971. doi: 10.1371/journal.pone.0042971

Chendrimada, T. P., Gregory, R. I., Kumaraswamy, E., Norman, J., Cooch, N., Nishikura, K., et al. (2005). TRBP recruits the Dicer complex to Ago2 for microRNA processing and gene silencing. *Nature* 436, 740–744. doi: 10.1038/nature03868

Chong, Y., Zhang, J., Guo, X., Li, G., Zhang, S., Li, C., et al. (2014). MicroRNA-503 acts as a tumor suppressor in osteosarcoma by targeting L1CAM. *PLoS One* 9:e114585. doi: 10.1371/journal.pone.0114585

Dambal, S., Shah, M., Mihelich, B., and Nonn, L. (2015). The microRNA-183 cluster: the family that plays together stays together. *Nucleic Acids Res.* 43, 7173–7188. doi: 10.1093/nar/gkv703

Dou, C., Zhang, C., Kang, F., Yang, X., Jiang, H., Bai, Y., et al. (2014). MiR-7b directly targets DC-STAMP causing suppression of NFATc1 and c-Fos signaling during osteoclast fusion and differentiation. *Biochimica et Biophysica Acta* 1839, 1084–1096. doi: 10.1016/j.bbagrm.2014.08.002

Ell, B., Mercatali, L., Ibrahim, T., Campbell, N., Schwarzenbach, H., Pantel, K., et al. (2013). Tumor-Induced osteoclast miRNA changes as regulators and biomarkers of osteolytic bone metastasis. *Cancer Cell* 24, 542–556. doi: 10.1016/j.ccr.2013.09.008

Esteller, M. (2011). Non-coding RNAs in human disease. *Nat. Rev. Genet.* 12, 861–874. doi: 10.1038/nrg3074

Feng, Y. H., and Tsao, C. J. (2016). Emerging role of microRNA-21 in cancer. *Biomed. Rep.* 5, 395–402. doi: 10.3892/br.2016.747

Fukao, T., Fukuda, Y., Kiga, K., Sharif, J., Hino, K., Enomoto, Y., et al. (2007). An evolutionarily conserved mechanism for MicroRNA-223 expression revealed by MicroRNA gene profiling. *Cell* 129, 617–631. doi: 10.1016/j.cell.2007.02.048

Goldring, S. R., Purdue, P. E., Crotti, T. N., Shen, Z., Flannery, M. R., Binder, N. B., et al. (2013). Bone remodelling in inflammatory arthritis. *Annals Rheumatic Dis.* 72(Suppl. 2), ii52–ii55. doi: 10.1136/annrheumdis-2012-202199

Gregory, R. I., Yan, K. P., Amuthan, G., Chendrimada, T., Doratotaj, B., Cooch, N., et al. (2004). The microprocessor complex mediates the genesis of microRNAs. *Nature* 432, 235–240. doi: 10.1038/nature03120

Hangauer, M. J., Vaughn, I. W., and McManus, M. T. (2013). Pervasive transcription of the human genome produces thousands of previously unidentified long intergenic noncoding RNAs. *PLoS Genet.* 9:e1003569. doi: 10.1371/journal.pgen.1003569

Hayashi, M., Nakashima, T., Taniguchi, M., Kodama, T., Kumanogoh, A., and Takayanagi, H. (2012). Osteoprotection by semaphorin 3A. *Nature* 485, 69–74. doi: 10.1038/nature11000

Hu, C. H., Sui, B. D., Du, F. Y., Shuai, Y., Zheng, C. X., Zhao, P., et al. (2017). miR-21 deficiency inhibits osteoclast function and prevents bone loss in mice. *Sci. Rep.* 7:43191. doi: 10.1038/srep43191

Humphrey, M. B., Lanier, L. L., and Nakamura, M. C. (2005). Role of ITAM-containing adapter proteins and their receptors in the immune system and bone. *Immunol. Rev.* 208, 50–65.

Ichiyama, K., Gonzalez-Martin, A., Kim, B. S., Jin, H. Y., Jin, W., Xu, W., et al. (2016). The MicroRNA-183-96-182 cluster promotes T Helper 17 cell pathogenicity by negatively regulating transcription factor foxo1 expression. *Immunity* 44, 1284–1298. doi: 10.1016/j.immuni.2016.05.015

Inoue, K., Deng, Z., Chen, Y., Giannopoulou, E., Xu, R., Gong, S., et al. (2018). Bone protection by inhibition of microRNA-182. *Nat. Commun.* 9:4108. doi: 10.1038/s41467-018-06446-0

Ishigami, K., Nosho, K., Koide, H., Kanno, S., Mitsuhashi, K., Igarashi, H., et al. (2018). MicroRNA-31 reflects IL-6 expression in cancer tissue and is related with poor prognosis in bile duct cancer. *Carcinogenesis* 39, 1127–1134. doi: 10.1093/carcin/bgy075

Janssen, H. L., Reesink, H. W., Lawitz, E. J., Zeuzem, S., Rodriguez-Torres, M., Patel, K., et al. (2013). Treatment of HCV infection by targeting microRNA. *N. Engl. J. Med.* 368, 1685–1694. doi: 10.1056/NEJMoa1209026

Jindra, P. T., Bagley, J., Godwin, J. G., and Iacomini, J. (2010). Costimulation-dependent expression of microRNA-214 increases the ability of T cells to proliferate by targeting Pten. *J. Immunol.* 185, 990–997. doi: 10.4049/jimmunol.1000793

Kagiya, T., and Nakamura, S. (2013). Expression profiling of microRNAs in RAW264.7 cells treated with a combination of tumor necrosis factor alpha and RANKL during osteoclast differentiation. *J. Periodontal Res.* 48, 373–385. doi: 10.1111/jre.12017

Ke, K., Sul, O. J., Rajasekaran, M., and Choi, H. S. (2015). MicroRNA-183 increases osteoclastogenesis by repressing heme oxygenase-1. *Bone* 81, 237–246. doi: 10.1016/j.bone.2015.07.006

Kim, J. H., Kim, J. Y., Park, M., Kim, S., Kim, T., Kim, J., et al. (2020). NF-kappaB-dependent miR-31/155 biogenesis is essential for TNF-alpha-induced impairment of endothelial progenitor cell function. *Exp. Mol. Med.* 52, 1298–1309. doi: 10.1038/s12276-020-0478-x

Kim, T. K., Hemberg, M., Gray, J. M., Costa, A. M., Bear, D. M., Wu, J., et al. (2010). Widespread transcription at neuronal activity-regulated enhancers. *Nature* 465, 182–187. doi: 10.1038/nature09033

Kim, V. N., Han, J., and Siomi, M. C. (2009). Biogenesis of small RNAs in animals. *Nat. Rev. Mol. Cell Biol.* 10, 126–139. doi: 10.1038/nrm2632

Lagos-Quintana, M., Rauhut, R., Lendeckel, W., and Tuschl, T. (2001). Identification of novel genes coding for small expressed RNAs. *Science* 294, 853–858. doi: 10.1126/science.1064921

Lagos-Quintana, M., Rauhut, R., Yalcin, A., Meyer, J., Lendeckel, W., and Tuschl, T. (2002). Identification of tissue-specific microRNAs from mouse. *Curr. Biol.* 12, 735–739. doi: 10.1016/s0960-9822(02)00809-6

Lam, M. T., Li, W., Rosenfeld, M. G., and Glass, C. K. (2014). Enhancer RNAs and regulated transcriptional programs. *Trends Biochem. Sci.* 39, 170–182. doi: 10.1016/j.tibs.2014.02.007

Lee, S. H., Rho, J., Jeong, D., Sul, J. Y., Kim, T., Kim, N., et al. (2006). v-ATPase V0 subunit d2-deficient mice exhibit impaired osteoclast fusion and increased bone formation. *Nat. Med.* 12, 1403–1409. doi: 10.1038/nm1514

Lee, Y., Ahn, C., Han, J., Choi, H., Kim, J., Yim, J., et al. (2003). The nuclear RNase III Drosha initiates microRNA processing. *Nature* 425, 415–419. doi: 10.1038/nature01957

Lee, Y., Kim, H. J., Park, C. K., Kim, Y. G., Lee, H. J., Kim, J. Y., et al. (2013). MicroRNA-124 regulates osteoclast differentiation. *Bone* 56, 383–389. doi: 10.1016/j.bone.2013.07.007

Lee, Y., Kim, M., Han, J., Yeom, K. H., Lee, S., Baek, S. H., et al. (2004). MicroRNA genes are transcribed by RNA polymerase II. *EMBO J.* 23, 4051–4060. doi: 10.1038/sj.emboj.7600385

Li, D., Liu, J., Guo, B., Liang, C., Dang, L., Lu, C., et al. (2016). Osteoclast-derived exosomal miR-214-3p inhibits osteoblastic bone formation. *Nat. Commun.* 7:10872. doi: 10.1038/ncomms10872

Li, J. A., Wang, Y. D., Wang, K., Wang, Z. L., Jia, D. Y., Yang, B. Y., et al. (2017). Downregulation of miR-214-3p may contribute to pathogenesis of ulcerative colitis via targeting STAT6. *Biomed. Res. Int.* 2017:8524972. doi: 10.1155/2017/8524972

Li, S., Miller, C. H., Giannopoulou, E., Hu, X., Ivashkiv, L. B., and Zhao, B. (2014). RBP-J imposes a requirement for ITAM-mediated costimulation of osteoclastogenesis. *J. Clin. Invest.* 124, 5057–5073. doi: 10.1172/JCI71882

Li, Y. T., Chen, S. Y., Wang, C. R., Liu, M. F., Lin, C. C., Jou, I. M., et al. (2012). Amelioration of collagen-induced arthritis in mice by lentivirus-mediated silencing of microRNA-223. *Arthritis Rheumatism*. 64, 3240–3245. doi: 10.1002/art.34550

Liang, C., Guo, B., Wu, H., Shao, N., Li, D., Liu, J., et al. (2015). Aptamer-functionalized lipid nanoparticles targeting osteoblasts as a novel RNA interference-based bone anabolic strategy. *Nat. Med.* 21, 288–294. doi: 10.1038/nm.3791

Lind, E. F., Millar, D. G., Dissanayake, D., Savage, J. C., Grimshaw, N. K., Kerr, W. G., et al. (2015). miR-155 upregulation in dendritic cells is sufficient to break tolerance in vivo by negatively regulating SHIP1. *J. Immunol.* 195, 4632–4640. doi: 10.4049/jimmunol.1302941

Ling, H., Fabbri, M., and Calin, G. A. (2013). MicroRNAs and other non-coding RNAs as targets for anticancer drug development. *Nat. Rev. Drug Discovery* 12, 847–865. doi: 10.1038/nrd4140

Liu, J., Li, D., Dang, L., Liang, C., Guo, B., Lu, C., et al. (2017). Osteoclastic miR-214 targets TRAF3 to contribute to osteolytic bone metastasis of breast cancer. *Sci. Rep.* 7:40487. doi: 10.1038/srep40487

Loffler, D., Brocke-Heidrich, K., Pfeifer, G., Stocsits, C., Hackermuller, J., Kretzschmar, A. K., et al. (2007). Interleukin-6 dependent survival of multiple myeloma cells involves the Stat3-mediated induction of microRNA-21 through a highly conserved enhancer. *Blood* 110, 1330–1333. doi: 10.1182/blood-2007-03-081133

Lund, E., Guttinger, S., Calado, A., Dahlberg, J. E., and Kutay, U. (2004). Nuclear export of microRNA precursors. *Science* 303, 95–98. doi: 10.1126/science.1090599

Ma, S., Zhang, A., Li, X., Zhang, S., Liu, S., Zhao, H., et al. (2020). MiR-21-5p regulates extracellular matrix degradation and angiogenesis in TMJOA by targeting Spry1. *Arthritis Res. Ther.* 22:99. doi: 10.1186/s13075-020-2145-y

Makeyev, E. V., Zhang, J., Carrasco, M. A., and Maniatis, T. (2007). The MicroRNA miR-124 promotes neuronal differentiation by triggering brain-specific alternative pre-mRNA splicing. *Mol. Cell* 27, 435–448. doi: 10.1016/j.molcel.2007.07.015

Maruyama, K., Uematsu, S., Kondo, T., Takeuchi, O., Martino, M. M., Kawasaki, T., et al. (2013). Strawberry notch homologue 2 regulates osteoclast fusion by enhancing the expression of DC-STAMP. *J. Exp. Med.* 210, 1947–1960. doi: 10.1084/jem.20130512

Miller, C. H., Smith, S. M., Elguindy, M., Zhang, T., Xiang, J. Z., Hu, X., et al. (2016). RBP-J-Regulated miR-182 Promotes TNF-alpha-Induced Osteoclastogenesis. *J. Immunol.* 196, 4977–4986. doi: 10.4049/jimmunol.1502044

Min, S., Liang, X., Zhang, M., Zhang, Y., Mei, S., Liu, J., et al. (2013). Multiple tumor-associated microRNAs modulate the survival and longevity of dendritic cells by targeting YWHAZ and Bcl2 signaling pathways. *J. Immunol.* 190, 2437–2446. doi: 10.4049/jimmunol.1202282

Minamizaki, T., Nakao, Y., Irie, Y., Ahmed, F., Itoh, S., Sarmin, N., et al. (2020). The matrix vesicle cargo miR-125b accumulates in the bone matrix, inhibiting bone resorption in mice. *Commun. Biol.* 3:30. doi: 10.1038/s42003-020-0754-2

Mizoguchi, F., Murakami, Y., Saito, T., Miyasaka, N., and Kohsaka, H. (2013). miR-31 controls osteoclast formation and bone resorption by targeting RhoA. *Arthritis Res. Ther.* 15:R102. doi: 10.1186/ar4282

Moriya, N., Shibasaki, S., Karasaki, M., and Iwasaki, T. (2017). The impact of MicroRNA-223-3p on IL-17 receptor d expression in synovial cells. *PLoS One* 12:e0169702. doi: 10.1371/journal.pone.0169702

Moverare-Skrtic, S., Henning, P., Liu, X., Nagano, K., Saito, H., Borjesson, A. E., et al. (2014). Osteoblast-derived WNT16 represses osteoclastogenesis and prevents cortical bone fragility fractures. *Nat. Med.* 20, 1279–1288. doi: 10.1038/nm.3654

Nakamachi, Y., Ohnuma, K., Uto, K., Noguchi, Y., Saegusa, J., and Kawano, S. (2016). MicroRNA-124 inhibits the progression of adjuvant-induced arthritis in rats. *Annals Rheumatic Dis.* 75, 601–608. doi: 10.1136/annrheumdis-2014-206417

Nakano, S., Inoue, K., Xu, C., Deng, Z., Syrovatkina, V., Vitone, G., et al. (2019). G-protein Galpha13 functions as a cytoskeletal and mitochondrial regulator to restrain osteoclast function. *Sci. Rep.* 9:4236. doi: 10.1038/s41598-019-40974-z

Nakashima, T., and Takayanagi, H. (2011). New regulation mechanisms of osteoclast differentiation. *Ann. N. Y. Acad. Sci.* 1240, E13–E18.

Negishi-Koga, T., Shinohara, M., Komatsu, N., Bito, H., Kodama, T., Friedel, R. H., et al. (2011). Suppression of bone formation by osteoclastic expression of semaphorin 4D. *Nat. Med.* 17, 1473–1480. doi: 10.1038/nm.2489

O'Connell, R. M., Chaudhuri, A. A., Rao, D. S., and Baltimore, D. (2009). Inositol phosphatase SHIP1 is a primary target of miR-155. *Proc. Natl. Acad. Sci. U S A.* 106, 7113–7118. doi: 10.1073/pnas.0902636106

O'Connell, R. M., Taganov, K. D., Boldin, M. P., Cheng, G., and Baltimore, D. (2007). MicroRNA-155 is induced during the macrophage inflammatory response. *Proc. Natl. Acad. Sci. U S A.* 104, 1604–1609. doi: 10.1073/pnas.0610731104

Park, J. E., Heo, I., Tian, Y., Simanshu, D. K., Chang, H., Jee, D., et al. (2011). Dicer recognizes the 5′ end of RNA for efficient and accurate processing. *Nature* 475, 201–205. doi: 10.1038/nature10198

Peters, L., and Meister, G. (2007). Argonaute proteins: mediators of RNA silencing. *Mol. Cell* 26, 611–623. doi: 10.1016/j.molcel.2007.05.001

Polytarchou, C., Hommes, D. W., Palumbo, T., Hatziapostolou, M., Koutsioumpa, M., Koukos, G., et al. (2015). MicroRNA214 is associated with progression of ulcerative colitis, and inhibition reduces development of colitis and colitis-associated cancer in mice. *Gastroenterology* 149, 981–992.e11. doi: 10.1053/j.gastro.2015.05.057

Ponomarev, Veremeyko, T., Barteneva, N., Krichevsky, A. M., and Weiner, H. L. (2011). MicroRNA-124 promotes microglia quiescence and suppresses EAE by deactivating macrophages via the C/EBP-alpha-PU.1 pathway. *Nat. Med.* 17, 64–70. doi: 10.1038/nm.2266

Qin, Z., Wang, P. Y., Su, D. F., and Liu, X. (2016). miRNA-124 in immune system and immune disorders. *Front. Immunol.* 7:406. doi: 10.3389/fimmu.2016.00406

Rupaimoole, R., and Slack, F. J. (2017). MicroRNA therapeutics: towards a new era for the management of cancer and other diseases. *Nat. Rev. Drug Discovery* 16, 203–222. doi: 10.1038/nrd.2016.246

Sakaguchi, Y., Nishikawa, K., Seno, S., Matsuda, H., Takayanagi, H., and Ishii, M. (2018). Roles of Enhancer RNAs in RANKL-induced osteoclast differentiation identified by genome-wide cap-analysis of gene expression using CRISPR/Cas9. *Sci. Rep.* 8:7504. doi: 10.1038/s41598-018-25748-3

Salmena, L., Poliseno, L., Tay, Y., Kats, L., and Pandolfi, P. P. (2011). A ceRNA hypothesis: the rosetta stone of a hidden RNA language? *Cell* 146, 353–358. doi: 10.1016/j.cell.2011.07.014

Sarkar, S., Dey, B. K., and Dutta, A. (2010). MiR-322/424 and -503 are induced during muscle differentiation and promote cell cycle quiescence and differentiation by down-regulation of Cdc25A. *Mol. Biol. Cell* 21, 2138–2149. doi: 10.1091/mbc.E10-01-0062

Schett, G., and Gravallese, E. (2012). Bone erosion in rheumatoid arthritis: mechanisms, diagnosis and treatment. *Nat. Rev. Rheumatol.* 8, 656–664. doi: 10.1038/nrrheum.2012.153

Shibuya, H., Nakasa, T., Adachi, N., Nagata, Y., Ishikawa, M., Deie, M., et al. (2013). Overexpression of microRNA-223 in rheumatoid arthritis synovium controls osteoclast differentiation. *Modern Rheumatol.* 23, 674–685. doi: 10.1007/s10165-012-0710-1

Shimada-Sugawara, M., Sakai, E., Okamoto, K., Fukuda, M., Izumi, T., Yoshida, N., et al. (2015). Rab27A regulates transport of cell surface receptors modulating multinucleation and lysosome-related organelles in osteoclasts. *Sci. Rep.* 5:9620. doi: 10.1038/srep09620

Singaravelu, R., Ahmed, N., Quan, C., Srinivasan, P., Ablenas, C. J., Roy, D. G., et al. (2019). A conserved miRNA-183 cluster regulates the innate antiviral response. *J. Biol. Chem.* 294, 19785–19794. doi: 10.1074/jbc.RA119.010858

Stittrich, A. B., Haftmann, C., Sgouroudis, E., Kuhl, A. A., Hegazy, A. N., Panse, I., et al. (2010). The microRNA miR-182 is induced by IL-2 and promotes clonal expansion of activated helper T lymphocytes. *Nat. Immunol.* 11, 1057–1062. doi: 10.1038/ni.1945

Sugatani, T., and Hruska, K. A. (2007). MicroRNA-223 is a key factor in osteoclast differentiation. *J. Cell. Biochem.* 101, 996–999. doi: 10.1002/jcb.21335

Sugatani, T., and Hruska, K. A. (2009). Impaired micro-RNA pathways diminish osteoclast differentiation and function. *J. Biol. Chem.* 284, 4667–4678. doi: 10.1074/jbc.M805777200

Sugatani, T., and Hruska, K. A. (2013). Down-regulation of miR-21 biogenesis by estrogen action contributes to osteoclastic apoptosis. *J. Cell. Biochem.* 114, 1217–1222. doi: 10.1002/jcb.24471

Sugatani, T., Vacher, J., and Hruska, K. A. (2011). A microRNA expression signature of osteoclastogenesis. *Blood* 117, 3648–3657.

Sul, O. J., Sung, Y. B., Rajasekaran, M., Ke, K., Yu, R., Back, S. H., et al. (2018). MicroRNA-155 induces autophagy in osteoclasts by targeting transforming growth factor beta-activated kinase 1-binding protein 2 upon lipopolysaccharide stimulation. *Bone* 116, 279–289. doi: 10.1016/j.bone.2018.08.014

Takeshita, S., Fumoto, T., Matsuoka, K., Park, K. A., Aburatani, H., Kato, S., et al. (2013). Osteoclast-secreted CTHRC1 in the coupling of bone resorption to formation. *J. Clin. Investigation* 123, 3914–3924. doi: 10.1172/JCI69493

Tang, L., Yin, Y., Liu, J., Li, Z., and Lu, X. (2017). MiR-124 attenuates osteoclastogenic differentiation of bone marrow monocytes via targeting Rab27a. *Cell Physiol. Biochem.* 43, 1663–1672. doi: 10.1159/000484027

Tang, Y., Wu, X., Lei, W., Pang, L., Wan, C., Shi, Z., et al. (2009). TGF-beta1-induced migration of bone mesenchymal stem cells couples bone resorption with formation. *Nat. Med.* 15, 757–765. doi: 10.1038/nm.1979

Tay, Y., Rinn, J., and Pandolfi, P. P. (2014). The multilayered complexity of ceRNA crosstalk and competition. *Nature* 505, 344–352. doi: 10.1038/nature12986

Teng, G., Hakimpour, P., Landgraf, P., Rice, A., Tuschl, T., Casellas, R., et al. (2008). MicroRNA-155 is a negative regulator of activation-induced cytidine deaminase. *Immunity* 28, 621–629. doi: 10.1016/j.immuni.2008.03.015

Thai, T.-H., Calado, D. P., Casola, S., Ansel, K. M., Xiao, C., Xue, Y., et al. (2007). Regulation of the germinal center response by MicroRNA-155. *Science* 316, 604–608.

Vigorito, E., Perks, K. L., Abreu-Goodger, C., Bunting, S., Xiang, Z., Kohlhaas, S., et al. (2007). microRNA-155 regulates the generation of immunoglobulin class-switched plasma cells. *Immunity* 27, 847–859. doi: 10.1016/j.immuni.2007.10.009

Wang, X., Guo, B., Li, Q., Peng, J., Yang, Z., Wang, A., et al. (2013). miR-214 targets ATF4 to inhibit bone formation. *Nat. Med.* 19, 93–100. doi: 10.1038/nm.3026

Willemen, H. L., Huo, X. J., Mao-Ying, Q. L., Zijlstra, J., Heijnen, C. J., and Kavelaars, A. (2012). MicroRNA-124 as a novel treatment for persistent hyperalgesia. *J. Neuroinflamm.* 9:143. doi: 10.1186/1742-2094-9-143

Wu, X. N., Ye, Y. X., Niu, J. W., Li, Y., Li, X., You, X., et al. (2014). Defective PTEN regulation contributes to B cell hyperresponsiveness in systemic lupus erythematosus. *Sci. Trans. Med.* 6:246ra99. doi: 10.1126/scitranslmed.3009131

Xian, L., Wu, X., Pang, L., Lou, M., Rosen, C. J., Qiu, T., et al. (2012). Matrix IGF-1 maintains bone mass by activation of mTOR in mesenchymal stem cells. *Nat. Med.* 18, 1095–1101. doi: 10.1038/nm.2793

Xie, Y., Chen, Y., Zhang, L., Ge, W., and Tang, P. (2017). The roles of bone-derived exosomes and exosomal microRNAs in regulating bone remodelling. *J. Cell Mol. Med.* 21, 1033–1041. doi: 10.1111/jcmm.13039

Xie, Y., Zhang, L., Gao, Y., Ge, W., and Tang, P. (2015). The multiple roles of Microrna-223 in regulating bone metabolism. *Molecules* 20, 19433–19448. doi: 10.3390/molecules201019433

Xu, F., and Teitelbaum, S. L. (2013). Osteoclasts: new insights. *Bone Res.* 1, 11–26. doi: 10.4248/BR201301003

Xu, J., Pei, Y., Lu, J., Liang, X., Li, Y., Wang, J., et al. (2021). LncRNA SNHG7 alleviates IL-1beta-induced osteoarthritis by inhibiting miR-214-5p-mediated PPARGC1B signaling pathways. *Int. Immunopharmacol.* 90:107150. doi: 10.1016/j.intimp.2020.107150

Yagi, M., Miyamoto, T., Sawatani, Y., Iwamoto, K., Hosogane, N., Fujita, N., et al. (2005). DC-STAMP is essential for cell-cell fusion in osteoclasts and foreign body giant cells. *J. Exp. Med.* 202, 345–351. doi: 10.1084/jem.20050645

Yang, D., Tan, S., Yang, Z., Jiang, P., Qin, C., Yuan, Q., et al. (2018). Dihydromyricetin attenuates TNF-alpha-Induced endothelial dysfunction through miR-21-Mediated DDAH1/ADMA/NO signal pathway. *Biomed. Res. Int.* 2018:1047810. doi: 10.1155/2018/1047810

Yang, S., Zhang, W., Cai, M., Zhang, Y., Jin, F., Yan, S., et al. (2018). Suppression of bone resorption by miR-141 in aged rhesus monkeys. *J. Bone Miner. Res.* 33, 1799–1812. doi: 10.1002/jbmr.3479

Yang, X., Matsuda, K., Bialek, P., Jacquot, S., Masuoka, H. C., Schinke, T., et al. (2004). ATF4 is a substrate of RSK2 and an essential regulator of osteoblast biology; implication for coffin-lowry syndrome. *Cell* 117, 387–398.

Yang, Y., Liu, L., Zhang, Y., Guan, H., Wu, J., Zhu, X., et al. (2014). MiR-503 targets PI3K p85 and IKK-beta and suppresses progression of non-small cell lung cancer. *Int. J. Cancer* 135, 1531–1542. doi: 10.1002/ijc.28799

Yang, Z., Zeng, B., Wang, C., Wang, H., Huang, P., and Pan, Y. (2017). MicroRNA-124 alleviates chronic skin inflammation in atopic eczema via suppressing innate immune responses in keratinocytes. *Cell Immunol.* 319, 53–60. doi: 10.1016/j.cellimm.2017.08.003

Yao, H., Kong, F., and Zhou, Y. (2019). MiR-182 promotes cell proliferation, migration and invasion by targeting FoxF2 in endometrial carcinoma cells. *Int. J. Clin. Exp. Pathol.* 12, 1248–1259.

Yao, Z., Xing, L., and Boyce, B. F. (2009). NF-kappaB p100 limits TNF-induced bone resorption in mice by a TRAF3-dependent mechanism. *J. Clin. Investigation* 119, 3024–3034. doi: 10.1172/JCI38716

Yuan, X., Berg, N., Lee, J. W., Le, T. T., Neudecker, V., Jing, N., et al. (2018). MicroRNA miR-223 as regulator of innate immunity. *J. Leukoc Biol.* 104, 515–524. doi: 10.1002/JLB.3MR0218-079R

Zhang, J., Zhao, H., Chen, J., Xia, B., Jin, Y., Wei, W., et al. (2012). Interferon-beta-induced miR-155 inhibits osteoclast differentiation by targeting SOCS1 and MITF. *FEBS Lett.* 586, 3255–3262. doi: 10.1016/j.febslet.2012.06.047

Zhang, N., Fu, L., Bu, Y., Yao, Y., and Wang, Y. (2017). Downregulated expression of miR-223 promotes Toll-like receptor-activated inflammatory responses in macrophages by targeting RhoB. *Mol. Immunol.* 91, 42–48. doi: 10.1016/j.molimm.2017.08.026

Zhang, Q., and Cao, X. (2019). Epigenetic regulation of the innate immune response to infection. *Nat. Rev. Immunol.* 19, 417–432. doi: 10.1038/s41577-019-0151-6

Zhang, Y., Chen, X., Lian, H., Liu, J., Zhou, B., Han, S., et al. (2014). MicroRNA-503 acts as a tumor suppressor in glioblastoma for multiple antitumor effects by targeting IGF-1R. *Oncol. Rep.* 31, 1445–1452. doi: 10.3892/or.2013.2951

Zhao, B., Grimes, S. N., Li, S., Hu, X., and Ivashkiv, L. B. (2012). TNF-induced osteoclastogenesis and inflammatory bone resorption are inhibited by transcription factor RBP-J. *J. Exp. Med.* 209, 319–334. doi: 10.1084/jem.20111566

Zhao, B., and Ivashkiv, L. B. (2011). Negative regulation of osteoclastogenesis and bone resorption by cytokines and transcriptional repressors. *Arthritis Res. Therapy* 13:234. doi: 10.1186/ar3379

Zhao, B., Takami, M., Yamada, A., Wang, X., Koga, T., Hu, X., et al. (2009). Interferon regulatory factor-8 regulates bone metabolism by suppressing osteoclastogenesis. *Nat. Med.* 15, 1066–1071.

Zhao, C., Irie, N., Takada, Y., Shimoda, K., Miyamoto, T., Nishiwaki, T., et al. (2006). Bidirectional ephrinB2-EphB4 signaling controls bone homeostasis. *Cell Metab.* 4, 111–121. doi: 10.1016/j.cmet.2006.05.012

Zhao, C., Sun, W., Zhang, P., Ling, S., Li, Y., Zhao, D., et al. (2015). miR-214 promotes osteoclastogenesis by targeting Pten/PI3k/Akt pathway. *RNA Biol.* 12, 343–353. doi: 10.1080/15476286.2015.1017205

Zhao, H., Zhang, J., Shao, H., Liu, J., Jin, M., Chen, J., et al. (2017). Transforming growth factor beta1/Smad4 signaling affects osteoclast differentiation via regulation of miR-155 expression. *Mol. Cells* 40, 211–221. doi: 10.14348/molcells.2017.2303

Zhao, J. J., Yang, J., Lin, J., Yao, N., Zhu, Y., Zheng, J., et al. (2009). Identification of miRNAs associated with tumorigenesis of retinoblastoma by miRNA microarray analysis. *Childs Nerv. Syst.* 25, 13–20. doi: 10.1007/s00381-008-0701-x

Zhao, Q., Liu, C., Xie, Y., Tang, M., Luo, G., Chen, X., et al. (2020). Lung cancer cells derived circulating miR-21 promotes differentiation of monocytes into osteoclasts. *Onco Targets Ther.* 13, 2643–2656. doi: 10.2147/OTT.S232876

Zhong, L., Simoneau, B., Huot, J., and Simard, M. J. (2017). p38 and JNK pathways control E-selectin-dependent extravasation of colon cancer cells by modulating miR-31 transcription. *Oncotarget* 8, 1678–1687. doi: 10.18632/oncotarget.13779

Zhou, J., and Wang, W. (2011). Analysis of microRNA expression profiling identifies microRNA-503 regulates metastatic function in hepatocellular cancer cell. *J. Surg. Oncol.* 104, 278–283. doi: 10.1002/jso.21941

**Conflict of Interest:** The authors declare that the research was conducted in the absence of any commercial or financial relationships that could be construed as a potential conflict of interest.

frontiers in Cell and Developmental Biology

MINI REVIEW
published: 06 July 2021
doi: 10.3389/fcell.2021.648084

# The Effects of Receptor Activator of NF-κB Ligand-Binding Peptides on Bone Resorption and Bone Formation

*Fatma Rashed[1,2], Shingo Kamijyo[1], Yuri Shimizu[1], Yuna Hirohashi[1], Masud Khan[1], Yasutaka Sugamori[3], Ramachandran Murali[4] and Kazuhiro Aoki[1]**

*[1] Graduate School of Medical and Dental Sciences, Institute X, Department of Basic Oral Health Engineering, Tokyo Medical and Dental University, Tokyo, Japan, [2] Department of Oral Biology, Faculty of Dentistry, Damanhour University, El Behera, Egypt, [3] Department of Dentistry and Oral Surgery, Saitama Medical University, Saitama, Japan, [4] Biomedical Sciences, Research Division of Immunology, Samuel Oschin Comprehensive Cancer Institute, Cedars-Sinai Medical Center, Los Angeles, CA, United States*

OPEN ACCESS

**Edited by:**
*Natalie A Sims, St. Vincents Institute of Medical Research, University of Melbourne, Australia*

**Reviewed by:**
*T John Martin, St. Vincents Institute of Medical Research, University of Melbourne, Australia*
*Ulf Holger Lerner, Umeå University, Sweden*

***Correspondence:**
*Kazuhiro Aoki*
*kazu.hpha@tmd.ac.jp*

**Specialty section:**
*This article was submitted to Cellular Biochemistry, a section of the journal Frontiers in Cell and Developmental Biology*

**Received:** *31 December 2020*
**Accepted:** *23 March 2021*
**Published:** *06 July 2021*

**Citation:**
*Rashed F, Kamijyo S, Shimizu Y, Hirohashi Y, Khan M, Sugamori Y, Murali R and Aoki K (2021) The Effects of Receptor Activator of NF-κB Ligand-Binding Peptides on Bone Resorption and Bone Formation. Front. Cell Dev. Biol. 9:648084. doi: 10.3389/fcell.2021.648084*

Receptor activator of NF-κB ligand (RANKL)-binding peptides inhibit bone resorption and were recently shown to activate bone formation. The stimulatory mechanism underlying bone formation associated with these peptides was explained as RANKL-reverse signaling, wherein RANKL molecules on osteoblasts work as receptors to stimulate osteoblast differentiation. However, why RANKL-binding peptides stimulate osteoblast differentiation while osteoprotegerin (OPG), which is well known to bind to RANKL, cannot activate osteoblast differentiation has remained unclear. In this mini-review, we introduce three main issues: (1) The inhibitory effects of two RANKL-binding peptides (W9 and OP3-4) on bone resorption; (2) The stimulatory effects of the RANKL-binding peptides on osteoblast differentiation; and (3) The accumulation and membrane clustering of RANKL molecules at the cell surface of osteoblasts as a potential molecular switch stimulating osteoblast differentiation by RANKL-binding peptides.

**Keywords: RANKL-binding peptide, bone resorption, bone formation, RANKL-reverse signaling, RANKL clustering, osteoprotegerin**

## INTRODUCTION

Several lines of evidence showed that long-term treatment of bisphosphonates, which are bone resorption inhibitors, may cause atypical fracture of the femoral diaphysis due to the building up of micro-cracks induced by the suppression of bone turnover and accumulation of the old bone (Saita et al., 2015). Anti-RANKL antibody is also known to reduce bone formation via the coupling of resorption and formation during bone remodeling (Furuya et al., 2011; Reginster, 2011). While these anti-resorptive drugs have been shown to improve bone mineral density and reduce fracture risks in osteoporotic patients, adding bone formation ability to bone resorption inhibitors may be a useful feature for a novel drug for treating osteoporosis (Lewiecki, 2011). Recently, two anabolic therapies were developed: Intermittent parathyroid hormone (teriparatide) and anti-sclerostin antibody (romosozumab). However, one of their shortcomings is that their treatment period is limited, a maximum of 2 years for parathyroid hormone and 1 year for the anti-sclerostin antibody.

In some cases, teriparatide treatment is shown to increase cortical porosity depending on the time frame and frequency of the treatment. Furthermore, antibody therapy is considered to be a reversible treatment, with short efficacy after therapy discontinuation (Appelman-Dijkstra and Papapoulos, 2018; Lewiecki et al., 2019). Therefore, an alternative bone anabolic reagent with a novel signaling pathway to stimulate bone formation is needed.

We have previously shown that the RANKL-binding peptides WP9QY (W9) and OP3-4 can suppress bone resorption (Cheng et al., 2004; Aoki et al., 2006). For instance, W9 inhibited RANKL-induced osteoclast formation *in vitro* and prevented bone resorption *in vivo* induced by ovariectomy and low dietary calcium. Likewise, OP3-4, a cyclic peptide that was originally designed from the RANKL-binding site on OPG as a template (**Table 1A**), inhibited RANKL-induced osteoclastogenesis and prevented bone resorption in a murine ovariectomized model (**Table 1B**). However, surprisingly, W9 and OP3-4 were also found to exert stimulatory effects on bone formation in addition to inhibiting bone resorption (Kato et al., 2015; Furuya et al., 2013). Herein, we report the effect of these RANKL-binding peptides on bone resorption and bone formation, mainly focusing on the peptides' stimulatory mechanism on bone formation compared with osteoprotegerin (OPG), which cling to RANKL (Simonet et al., 1997; Sone et al., 2019).

## The RANKL-Binding Peptide W9 Inhibits RANK-Downstream Signaling by Inducing Topological Changes in the RANK Structure

W9 is a cyclic peptide composed of nine amino acids, originally designed as a tumor necrosis factor (TNF)-α antagonist (Takasaki et al., 1997). We aligned the amino acid sequence in the cysteine-rich domain of different TNF-receptor-superfamily members, such as TNF type 1 receptor, RANK, and OPG; we found that five amino acids, used to design W9 peptide on TNF type 1 receptor, were homologous with corresponding residues in RANK, but not in OPG (**Table 1C**). Additionally, the soluble RANKL (sRANKL)-induced nuclear translocation of p65, a major component of NF-κB, was blocked by W9 (**Table 1D**). Using surface plasmon resonance (SPR) assay, the peptide-sequence specificity that features RANKL-binding affinity was confirmed. Hereby, changing the tyrosine residue in position 6 (Tyr6) to asparagine (Y6N) of W9 reduced the binding to RANKL by more than 70% at concentrations up to 100μ M.

In general, an antagonist interferes with receptor–ligand interaction separating a ligand and its receptor. OPG is considered an antagonist since it was shown to separate RANK and RANKL and, consequently, prevent trimer formation of RANK, leading to the inactivation of receptor RANK downstream signaling (Lacey et al., 2012). However, a competition assay using SPR showed that W9 was not a typical antagonist since it could not separate receptor RANK and ligand RANKL (**Table 1E**). This left us wondering how this peptide could block the downstream signaling of RANK while maintaining the binding of RANKL with RANK. The molecular modeling revealed that W9 induced conformational changes in the RANK–RANKL complex, especially the trimer formation of RANK (**Table 1F**). These results suggested that the peptide could block the signaling downstream of the receptor RANK by inducing conformational changes of RANK extracellular domain (**Table 1F**). Based on that molecular modeling, our proposed mechanism for W9 to block RANK downstream signaling is shown in **Figure 1**.

## RANKL-Binding Peptides Stimulate Bone Formation in a RANKL-Dependent Manner

In Furuya et al. (2013) first demonstrated the stimulatory effects of W9 on bone formation and osteoblast differentiation, both *in vitro* and *in vivo*, and obtained by subcutaneous injections three times daily for 5 days. OP3-4 treatment did not reduce the inflammatory indices in a murine arthritis model and not only prevented periarticular bone loss at the tibial metaphysis but promoted the bone formation parameters in the secondary spongiosa at the tibial metaphysis in collagen-induced arthritic (CIA) mice (**Table 1G**). The peptide was delivered using subcutaneously implanted osmotic minipumps at a concentration of 9 or 18 mg/kg/day. Furthermore, OP3-4 and W9 had stimulatory effects on osteoblast differentiation *in vitro* and BMP-2-induced bone formation *in vivo* (**Table 1H**). However, the precise mechanism underlying the anabolic effects induced by the RANKL-binding peptides was not clarified by these studies.

Ikebuchi et al. (2018) used vesicles containing RANK secreted from osteoclasts to induce RANKL reverse signaling in osteoblasts. The signaling from an Src family kinase to mammalian target of rapamycin complex 1 (mTORC1) signaling (Saksela et al., 1995; Cuevas et al., 2001) and the signaling from mTORC1 to the activation of alkaline phosphatase activity through runt-related transcription factor 2 (Runx2) (Singha et al., 2008) had already been reported. Ikebuchi et al. (2018) showed the importance of the proline-rich motif in the intracellular domain of the membrane-bound RANKL on osteoblasts, which is a signaling motif, leading to the activation of mTORC1 activity and alkaline phosphatase activity. A mouse model with a one-point mutation of proline to alanine (Pro29Ala) in the RANKL intracellular domain was used to clarify the RANKL-reverse signaling, wherein RANKL works as a receptor on the osteoblast surface. Binding to the membrane-bound RANKL directly activated the intracellular signaling of RANKL in osteoblasts.

The RANKL-binding peptides (OP3-4 and W9) had previously been shown also to activate Akt phosphorylation and S6k1 phosphorylation (upstream and downstream signaling of mTORC1 activity, respectively) (**Table 1I**). Furthermore, the stimulatory effects of RANKL-binding peptide on osteoblast differentiation were blunted in RANKL-deficient osteoblasts (**Table 1J**). These results suggest that the RANKL-binding peptides stimulate osteoblast differentiation in a RANKL-dependent manner, which means that downstream signaling and alkaline phosphatase activity (ALP) activity cannot be

**TABLE 1 |** Evidence supporting the effects of the receptor activator of NF-κB ligand (RANKL)-binding peptides W9 and OP3-4.

| | Subject | Related figures | References |
|---|---|---|---|
| **A** | ***OP3-4 structure:*** OP3-4 was designed based on the RANKL-binding site on OPG as a template. -*Molecular weight:*1448 (**11** amino acid) *YCEIEFCYLIR* | **Figure 1** | Cheng et al., 2004 |
| **B** | ***OP3-4 blocked ovariectomy-induced bone loss.*** | **Figure 5** | Cheng et al., 2004 |
| **C** | ***Alignment of TNF receptor superfamily and WP9QY (W9) peptide:*** W9 is a molecule designed using the TNF-α binding site on the TNF type 1 receptor as a template. It binds to both TNF-α and RANKL. -*Molecular weight:*1226 (**9** amino acids) *YCWSQYLCY* | **Figure 1A** | Aoki et al., 2006 |
| **D** | ***W9 blocks RANKL-induced signaling:*** In the osteoclast precursor RAW 264.7 cell line, W9 inhibited the soluble RANKL-induced translocation of p65, a significant component of NF-κB, to the nucleus. | **Figure 3A** | Aoki et al., 2006 |
| ***E*** | ***W9 cannot separate RANK and RANKL***: A competition assay measuring the binding of RANKL to the soluble RANK-coated surface with W9, compared with an assay using OPG. | **Figures 2B,C** | Aoki et al., 2006 |
| ***F*** | ***Conformational changes of RANK-RANKL complex by W9:*** Molecular modeling revealed the conformational changes in the RANK-RANKL complex induced by W9. | **Figure 1C** | Aoki et al., 2006 |
| ***G*** | ***OP3-4 activated bone formation in the collagen-induced arthritis model:*** The RANKL-binding peptide prevents a reduction in bone formation in the arthritis model. | **Figures 6B,F** | Kato et al., 2015 |
| ***H*** | ***OP3-4 and W9 had similar stimulatory effects on osteoblast differentiation in vitro and on BMP-2-induced bone formation in vivo.*** | **Figures 1–3** | Sugamori et al., 2016 |
| ***I*** | ***OP3-4 and W9 enhanced the upstream and downstream signaling of mTORC1 activity in ST2 cells.*** | **Figure 5** | Sugamori et al., 2016 |
| ***J*** | ***The stimulatory effects of RANKL-binding peptide W9 on osteoblast differentiation were blunted in RANKL-deficient osteoblasts:*** The RANKL-binding peptide enhanced osteoblast differentiation in a RANKL-dependent manner. | **Figure 3A** Extended data | Ikebuchi et al., 2018 |
| ***K*** | ***The RANKL-binding peptide OP3-4 enhanced ALP activity, but the RANKL-binding molecule OPG did not use ST2 cells.*** | **Figure 1D** | Sone et al., 2019 |
| ***L*** | ***The RANKL-binding peptide OP3-4 increased the amount of membrane- RANKL, while OPG did not:*** OP3-4 increased the membrane fraction of RANKL both 6 and 24 h after stimulation of the peptide, but OPG did not. | **Figure 2** | Sone et al., 2019 |
| ***M*** | ***OPG clung to RANKL and disturbed clustering while RANKL-binding peptides did not:*** HS-AFM imaging revealed the formation of clusters of RANKL molecules and highly flexible OPG clinging to RANKL. | **Figure 3** Video S1A_V2 Video S1B_V2 | Sone et al., 2019 |
| ***N*** | ***Artificial induction of molecular clustering of RANKL may lead to the enhancement of osteoblast differentiation, even when OPG is used:*** Inducing pentameric assembly of OPG-Fc-RANKL complex by IgM could lead to osteoblast differentiation and enhancement of RANKL accumulation in ST2 cells. | **Figure 4** | Sone et al., 2019 |
| ***O*** | ***W9 exerted similar or even stronger inhibitory effects on bone destruction than anti-TNF antibody*** | **Figure 5** | Saito et al., 2007 |

activated in the absence of RANKL. **Figure 2A** shows the proposed mechanism underlying the stimulation of osteoblast differentiation by W9 and OP3-4, based on our findings that the proline-rich motif in the RANKL-intracellular domain is important for inducing the RANKL-reverse signaling and stimulating early osteoblast differentiation upon stimulation of RANKL. RANKL (Pro29Ala) mutant mice have an osteopenic phenotype and reduced bone formation activity compared with littermate control mice (Ikebuchi et al., 2018). Generally, bone formation is enhanced after the stimulation of bone resorption due to the coupling mechanism from bone resorption and bone formation; however, bone formation in the mutant mice was not enhanced when bone resorption was activated in the sRANKL-induced osteopenic model. Ikebuchi et al. (2018) further showed that signaling downstream of Src family kinase was reduced in the RANKL mutant mice. The RANKL-binding molecule-induced phosphorylation of Akt and S6k1 was reduced in the osteoblasts derived from the mutant mice compared with the littermate controls. Therefore, the proline-rich motif in the RANKL cytoplasmic tail was proven to be essential for activating the intracellular signal transduction pathway, corresponding to RANKL-reverse signaling (Ikebuchi et al., 2018).

## The Conditions Where the RANKL-Binding Molecules Activate the RANKL-Reverse Signaling

OP3-4 and W9 enhanced alkaline phosphatase activity, but OPG, which also binds to RANKL, did not, indicating that not all RANKL-binding molecules stimulate osteoblast differentiation (**Table 1K**). The high turnover rate of bone remodeling in OPG-deficient mice compared with wild-type mice supports the lack of anabolic effects of OPG on bone formation (Fei et al., 2010). Therefore, we were left wondering about the differences in the effects between RANKL-binding peptides and OPG on RANKL-reverse-signaling activation to stimulate osteoblast differentiation.

We assumed that one condition that can activate the RANKL-reverse signaling is RANKL accumulation at the osteoblasts' plasma membrane, while another condition is RANKL clustering.

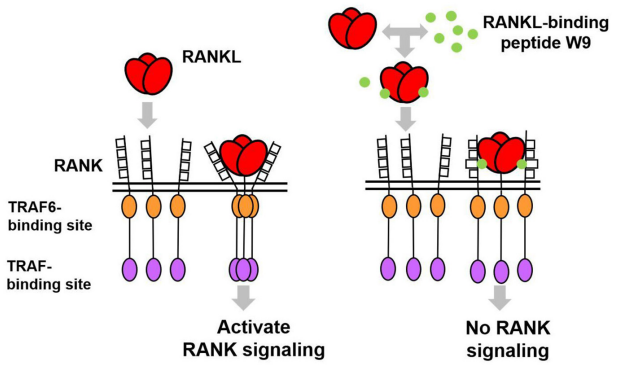


**FIGURE 1 |** A diagram illustrating the proposed mechanism of RANK downstream signaling inhibition, which is induced by the receptor activator of NF-κB ligand (RANKL)-binding peptide. The peptide-induced conformational changes of RANK, especially the region close to the lipid bilayer membrane (shown with double lines), could block the downstream signaling of RANK, thereby allowing RANKL to maintain contact with RANK.

First, the accumulation of RANKL molecules is thought to be necessary to induce RANKL molecule clustering since clustering is unlikely to proceed unless the amount of RANKL on the osteoblast membrane increases. RANKL molecule was shown to translocate from the Golgi apparatus to the plasma membrane and accumulate on the cell surface of ST2 cells, osteoblastic cell line, upon the stimulation of RANK-coated beads (Kariya et al., 2009). In the same way, we found that RANKL molecule accumulated on the plasma membrane on ST2 cells upon the stimulation of RANKL-binding peptide, either OP3-4 or W9 (**Table 1L**). Since OPG did not increase the amount of membrane- RANKL on osteoblasts (**Table 1L**), these results could be evidence to explain the difference between the RANKL-binding peptides and OPG. Second, the clustering of RANKL molecules could be another evidence as described next. It has been shown that the clustering of membrane-bound receptors leads to cell activation (Boger and Goldberg, 2001; Lacey et al., 2012). The distance between the receptors was also found to be crucial for activating the erythropoiesis signal (Erickson-Miller et al., 2005). Furthermore, Kosmides et al. found that inducing artificial clusters of co-stimulatory molecules on the immune cell membrane by magnetic force enhanced T-cells' proliferative activity (Kosmides et al., 2018). Therefore, we hypothesized that clustering of membrane-bound RANKL molecules on osteoblasts would induce a switch to activate osteoblast differentiation in addition to the accumulation of membrane-RANKL.

## OPG Clung to RANKL and Disturbed Clustering While RANKL-Binding Peptides Did Not

Next, we investigated the difference in the molecular features between RANKL molecules with the RANKL-binding peptide and those with OPG in a cell-free system. The RANKL molecules and OPG were observed on mica using a high-speed atomic force microscope (HS-AFM), revealing the characteristic features at the protein's single-molecule level. HS-AFM is a powerful instrument that enables the direct imaging of protein molecules in their dynamic action without disturbing the molecules' function. HS-AFM revealed that the highly flexible OPG clung to the RANKL molecule and disturbed clustering, while the RANKL-binding peptide OP3-4 did not. Furthermore, the molecular features of RANKL itself showed easy clustering, which did not change with the addition of OP3-4. However, OPG appears to move around RANKL while binding to it, suggesting that OPG inhibits the clustering formation of RANKL molecules (**Table 1M**).

## Artificial Induction of Molecular Clustering of RANKL Could Lead to the Enhancement of Osteoblast Differentiation, Even When Osteoprotegerin Was Used

As we mentioned earlier, RANKL-binding peptides increase ALP activity in the cell line and further increase membrane RANKL levels, but OPG does not. Further verification in a cell-free system revealed that the RANKL molecule itself has the property of easily becoming clustered, suggesting that RANKL-binding peptides do not inhibit clustering while OPG does. Therefore, the key to inducing osteoblast differentiation seems to lie in the clustering of RANKL. Artificial cluster induction using IgM to promote pentameric assembly of RANKL–OPG-Fc complex enhances early osteoblast differentiation (**Table 1N**). These results suggest that clustering formation may be a pivotal switch for enhancing osteoblast differentiation by RANKL-binding molecules (**Figure 2B**). Simultaneously, the amount of RANKL on the osteoblast membrane also increased after the induction of pentameric assembly of the RANKL–OPG-Fc complex by IgM (**Table 1N**).

# DISCUSSION

The cyclic peptide W9 was designed to mimic the most critical TNF-α recognition loop on the TNF type 1 receptor, and it prevents interactions of TNF-α with its receptor. Even though the W9 peptide had a weaker inhibitory effect on inflammation than the anti-TNF antibody, W9 exerted similar or even stronger inhibitory effects on bone destruction than the anti-TNF antibody (**Table 1O**). Similarly, the cyclic peptide OP3-4, designed to mimic the binding site of the RANKL molecule on OPG, was shown to cling to RANKL, thereby inhibiting osteoclastogenesis. Kato et al. (2015). further clarified using dynamic histomorphometry that OP3-4 decreased the inhibition of bone formation caused by CIA (**Table 1G**).

While the RANKL-binding peptides have been found to stimulate bone formation, neither OPG nor anti-RANKL antibodies were able to enhance bone formation (Dore et al., 2010). However, a recent paper claimed that anti-RANKL-antibody might also stimulate bone formation using RANKL-reverse signaling (Wang et al., 2020). As anti-RANKL antibody was found to decrease levels of bone formation markers in clinical studies (Cummings et al., 2009; Ominsky et al., 2015), further

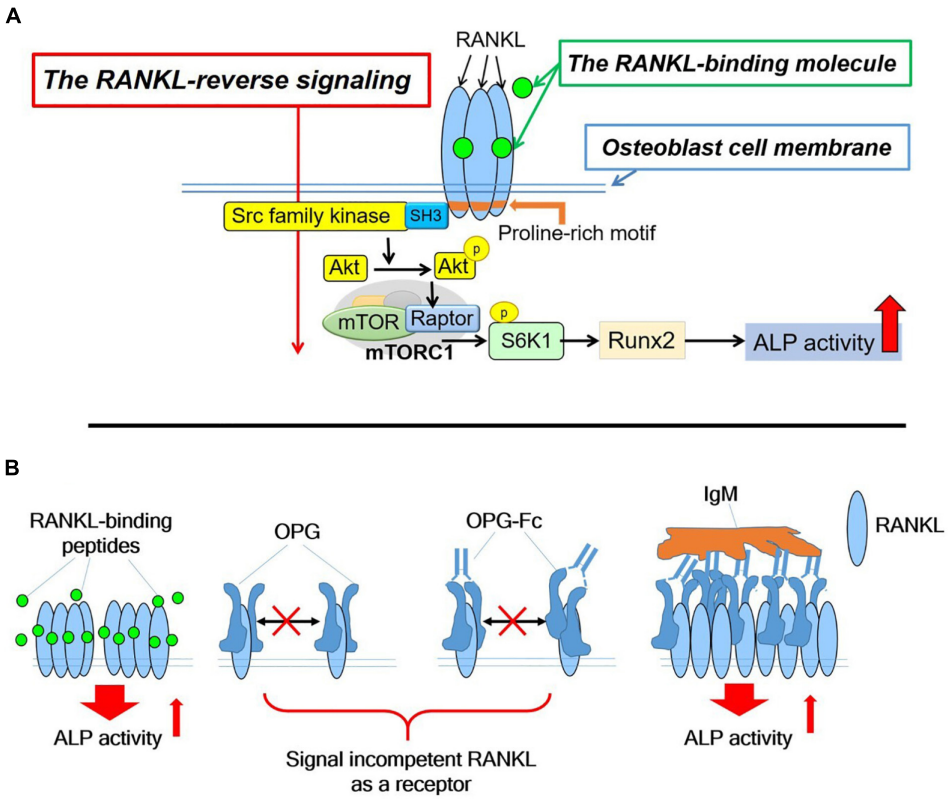


**FIGURE 2 | (A)**. Hypothetical diagram showing the stimulatory mechanism of the OP3-4 and W9 on osteoblast differentiation through RANKL-reverse signaling. SFKs, Src family kinases; mTORC1, the mammalian target of rapamycin complex 1; S6K1, ribosomal protein S6 kinase 1. Although the intracellular domain of RANKL is short, proline-rich motif of the domain is shown to be important to activate the RANKL-reverse signaling, which leads to stimulate early osteoblast differentiation. The proline-rich motif activates a Src-family kinase by associating with SH3 domain followed by Akt and mTORC1 signaling, leading to the activation of runt-related transcription factor 2 (Runx2) and alkaline phosphatase (ALP) activity **(B)**. The RANKL-accumulation and continued clustering of RANKL molecules on the cell- membrane of osteoblasts could be a signaling switch to stimulate the ALP activity. The RANKL molecule itself has the characteristic features of clustering (**Table 1M**). After the peptides bind to membrane-bound RANKL, the accumulation of RANKL molecules takes place without disturbing the characteristic features of the RANKL molecules, thus resulting in the enhancement of the alkaline phosphatase activity leading to early osteoblast differentiation. OPG alone and OPG-Fc alone do not induce RANKL accumulation (**Table 1L**) since they prevent RANKL-clustering (**Table 1M**). However, when IgM induced the pentameric assembly of OPG-Fc, then RANKL accumulation took place. Eventually, both alkaline phosphatase and other early osteoblast differentiation markers were observed to increase (**Table 1N**).

studies are necessary to clarify whether or not anti-RANKL antibody can stimulate bone formation in addition to inhibiting bone resorption. Furthermore, the ideal timing of inducing the accumulation of RANKL molecules and RANKL clustering to activate RANKL-reverse signaling should be investigated.

The pivotal role of RANKL expressed on osteocytes in osteoclast formation was clarified using a cell-specific RANKL-deficient mouse (Nakashima et al., 2011; Xiong et al., 2011), while osteoblasts' RANKL was shown to be involved in a role other than osteoclastogenesis. Ikebuchi et al. (2018) revealed the physiological role of RANKL on osteoblasts, which works as a receptor to stimulate bone formation using RANKL-reverse signaling (**Figure 2A**). The small extracellular vesicles containing RANK secreted from mature osteoclasts (OC-SEVs) were shown to work as a ligand of the acceptor RANKL on osteoblasts. As we described earlier, a coupling phenomenon from bone resorption to bone formation was abolished when RANKL point-mutation mice (Pro29Ala) were used in the RANKL-induced osteopenic model. These results suggest that RANKL on osteoblasts works as a receptor to stimulate bone formation even under pathophysiological conditions. Therefore, RANKL on osteoblasts could be a potential pharmacological target to recover the bone remodeling balance between bone resorption and bone formation. The RANKL-binding molecule could be an effective reagent for the treatment of bone diseases such as postmenopausal osteoporosis. We also expect a RANKL-binding molecule to stimulate local bone formation at the fracture site or the site necessary for bone regeneration. Therefore, RANKL-reverse signaling can be a ground-breaking stone for developing anabolic bone reagent.

The peptides potentiate the effect by bone morphogenetic protein (BMP)-2 as subcutaneous injections of W9 promoted bone mineral density, increased the mineral apposition rate of the femur in mice and accelerated BMP-2-induced ectopic bone formation (Furuya et al., 2013). Of note, W9 promoted BMP-2-induced bone formation by a mechanism other than the antagonism of TNF-α action, as synergistic effects still existed when TNF type 1 receptor-deficient

mice or TNF-α-deficient mice were used to establish a BMP-2-induced subcutaneous bone formation model (Khan et al., 2013). In the same manner, we demonstrated the synergistic effects of RANKL-binding peptides with BMP-2 using a sub-periosteally injected bone formation model of the murine maxilla (Uehara et al., 2016; Keo et al., 2020), a tooth extraction model at the incisor socket (Arai et al., 2016), and a model of standard ectopic bone formation at a calvarial bone defect (Khan et al., 2013; Sugamori et al., 2016). Although W9 peptide stimulation has been shown to enhance the phosphorylation of Smad 1 and 5 (Furuya et al., 2013), further studies are necessary to clarify the cross-talk between BMP-2 signaling and RANKL-reverse signaling.

## CONCLUSION

Induction of accumulation of RANKL molecules and the RANKL clustering at the osteoblast membrane might be a new therapeutic strategy for developing bone anabolic reagents.

## AUTHOR CONTRIBUTIONS

YH and YS drafted the present manuscript. MK and SK contributed to the conceptual idea, performed database search, analyzed data, and wrote the manuscript. FR and KA received a grant for this project, conceived the idea, reviewed the drafts, and supervised this manuscript's writing process and editing. YS and RM gave suggestions and significantly revised and refined the manuscript. All authors read and approved the final manuscript.

## FUNDING

This work was supported in part by the Company of Biologists' grants-Travelling Fellowship-Number: JCSTF1908265 to FR and the Nakatani Foundation for Advancement of Measuring Technologies in Biomedical Engeineering, study in Japan, and the Japan Society for the Promotion of Science (19H01068 to KA).

## ACKNOWLEDGMENTS

We would like to extend our sincere appreciation to Dr. Masashi Honma, Dr. Yuki Ikebuchi at the Department of Pharmacy, The University of Tokyo Hospital, Faculty of Medicine, The University of Tokyo, Dr. Daisuke Noshiro at the Laboratory of Structural Biology, Institute of Microbial Chemistry, and Dr. Eri Sone-Miwa at the Tokyo Medical and Dental University for their collaborative work to investigate the RANKL-reverse signaling. We also thank Dr. Cecile Itzstein at the University of Aberdeen for making a part of a draft of the diagram.

## REFERENCES

Aoki, K., Saito, H., Itzstein, C., Ishiguro, M., Shibata, T., Blanque, R., et al. (2006). A TNF receptor loop peptide mimic blocks RANK ligand-induced signaling, bone resorption, and bone loss. *Journal of Clinical Investigation* 116, 1525–1534. doi: 10.1172/JCI22513

Appelman-Dijkstra, N. M., and Papapoulos, S. E. (2018). Clinical advantages and disadvantages of anabolic bone therapies targeting the WNT pathway. *Nature Reviews Endocrinology* 14, 605–623. doi: 10.1038/s41574-018-0087-0

Arai, Y., Aoki, K., Shimizu, Y., Tabata, Y., Ono, T., Murali, R., et al. (2016). Peptide-induced de novo bone formation after tooth extraction prevents alveolar bone loss in a murine tooth extraction model. *European Journal of Pharmacology* 782, 89–97. doi: 10.1016/j.ejphar.2016.04.049

Boger, D. L., and Goldberg, J. (2001). Cytokine receptor dimerization and activation: Prospects for small molecule agonists. *Bioorganic and Medicinal Chemistry* 9, 557–562. doi: 10.1016/S0968-0896(00)00276-5

Cheng, X., Kinosaki, M., Takami, M., Choi, Y., Zhang, H., and Murali, R. (2004). Disabling of Receptor Activator of Nuclear Factor-κB (RANK) Receptor Complex by Novel Osteoprotegerin-like Peptidomimetics Restores Bone Loss in Vivo. *Journal of Biological Chemistry* 279, 8269–8277. doi: 10.1074/jbc.M309690200

Cuevas, B. D., Lu, Y., Mao, M., Zhang, J., LaPushin, R., Siminovitch, K., et al. (2001). Tyrosine Phosphorylation of p85 Relieves Its Inhibitory Activity on Phosphatidylinositol 3-Kinase. *Journal of Biological Chemistry* 276, 27455–27461. doi: 10.1074/jbc.M100556200

Cummings, S. R., Martin, J. S., McClung, M. R., Siris, E. S., Eastell, R., Reid, I. R., et al. (2009). Denosumab for prevention of fractures in postmenopausal women with osteoporosis. *Obstetrical and Gynecological Survey* 64, 805–807. doi: 10.1097/01.ogx.0000363236.41902.96

Dore, R. K., Cohen, S. B., Lane, N. E., Palmer, W., Shergy, W., Zhou, L., et al. (2010). Effects of denosumab on bone mineral density and bone turnover in patients with rheumatoid arthritis receiving concurrent glucocorticoids or bisphosphonates. *Ann Rheum Dis.* 69, 872–875.

Erickson-Miller, C. L., DeLorme, E., Tian, S. S., Hopson, C. B., Stark, K., Giampa, L., et al. (2005). Discovery and characterization of a selective, nonpeptidyl thrombopoietin receptor agonist. *Experimental Hematology* 33, 85–93. doi: 10.1016/j.exphem.2004.09.006

Fei, Q., Guo, C., Xu, X., Gao, J., Zhang, J., Chen, T., et al. (2010). Osteogenic growth peptide enhances the proliferation of bone marrow mesenchymal stem cells from osteoprotegerin-deficient mice by CDK2/cyclin A. *Acta Biochimica et Biophysica Sinica* 42, 801–806. doi: 10.1093/abbs/gmq086

Furuya, Y., Inagaki, A., Khan, M., Mori, K., Penninger, J. M., Nakamura, M., et al. (2013). Stimulation of bone formation in cortical bone of mice treated with a receptor activator of nuclear Factor-B Ligand (RANKL)-binding peptide that possesses osteoclastogenesis inhibitory activity. *Journal of Biological Chemistry* 288, 5562–5571. doi: 10.1074/jbc.M112.426080

Furuya, Y., Mori, K., Ninomiya, T., Tomimori, Y., Tanaka, S., Takahashi, N., et al. (2011). Increased bone mass in mice after single injection of anti-receptor activator of nuclear factor-κB ligand-neutralizing antibody: Evidence for bone anabolic effect of parathyroid hormone in mice with few osteoclasts. *Journal of Biological Chemistry* 286, 37023–37031. doi: 10.1074/jbc.M111.246280

Ikebuchi, Y., Aoki, S., Honma, M., Hayashi, M., Sugamori, Y., Khan, M., et al. (2018). Coupling of bone resorption and formation by RANKL reverse signalling. *Nature* 561, 195–200. doi: 10.1038/s41586-018-0482-7

Kariya, Y., Honma, M., Aoki, S., Chiba, A., and Suzuki, H. (2009). Vps33a mediates RANKL storage in secretory lysosomes in osteoblastic cells. *Journal of Bone and Mineral Research* 24, 1741–1752. doi: 10.1359/jbmr.090409

Kato, G., Shimizu, Y., Arai, Y., Suzuki, N., Sugamori, Y., Maeda, M., et al. (2015). The inhibitory effects of a RANKL-binding peptide on articular and periarticular bone loss in a murine model of collagen-induced arthritis: A bone histomorphometric study. *Arthritis Research and Therapy* 17, 753–758. doi: 10.1186/s13075-015-0753-8

Keo, P., Matsumoto, Y., Shimizu, Y., Nagahiro, S., Ikeda, M., Aoki, K., et al. (2020). A pilot study to investigate the histomorphometric changes of murine maxillary bone around the site of mini-screw insertion in regenerated bone induced by anabolic reagents. *European Journal of Orthodontics* 2020, 018. doi: 10.1093/ejo/cjaa018

Khan, A. A. M., Alles, N., Soysa, N. S., Mamun, A., Al, Nagano, K., et al. (2013). The local administration of TNF-α and RANKL antagonist peptide promotes BMP-2-induced bone formation. *Journal of Oral Biosciences* 55, 47–54. doi: 10.1016/j.job.2012.12.005

Kosmides, A. K., Necochea, K., Hickey, J. W., and Schneck, J. P. (2018). Separating T Cell Targeting Components onto Magnetically Clustered Nanoparticles Boosts Activation. *Nano Letters* 18, 1916–1924. doi: 10.1021/acs.nanolett.7b05284

Lacey, D. L., Boyle, W. J., Simonet, W. S., Kostenuik, P. J., Dougall, W. C., Sullivan, J. K., et al. (2012). Bench to bedside: Elucidation of the OPG-RANK-RANKL pathway and the development of denosumab. *Nature Reviews Drug Discovery* 11, 401–419. doi: 10.1038/nrd3705

Lewiecki, E. M. (2011). New targets for intervention in the treatment of postmenopausal osteoporosis. *Nature Reviews Rheumatology* 7, 631–638. doi: 10.1038/nrrheum.2011.130

Lewiecki, E. M., Dinavahi, R. V., Lazaretti-Castro, M., Ebeling, P. R., Adachi, J. D., Miyauchi, A., et al. (2019). One Year of Romosozumab Followed by Two Years of Denosumab Maintains Fracture Risk Reductions: Results of the FRAME Extension Study. *Journal of Bone and Mineral Research* 34, 419–428. doi: 10.1002/jbmr.3622

Nakashima, T., Hayashi, M., Fukunaga, T., Kurata, K., Oh-Hora, M., Feng, J. Q., et al. (2011). Evidence for osteocyte regulation of bone homeostasis through RANKL expression. *Nature Medicine* 17, 1231–1234. doi: 10.1038/nm.2452

Ominsky, M. S., Brown, D. L., Van, G., Cordover, D., Pacheco, E., Frazier, E., et al. (2015). Differential temporal effects of sclerostin antibody and parathyroid hormone on cancellous and cortical bone and quantitative differences in effects on the osteoblast lineage in young intact rats. *Bone* 81, 380–391. https://doi.org/10.1016/j.bone.2015.08.007,

Reginster, J.-Y. (2011). Antifracture Efficacy of Currently Available Therapies for Postmenopausal Osteoporosis. *Drugs* 71, 65–78. doi: 10.2165/11536850-000000000-00000

Saita, Y., Kaneko, K., and Ishijima, M. (2015). Atypical femoral fractures and bisphosphonate use: Current evidence and clinical implications. *Therapeutic Advances in Chronic Disease* 6, 185–193. doi: 10.1177/2040622315584114

Saito, H., Kojima, T., Takahashi, M., Horne, W. C., Baron, R., Amagasa, T., et al. (2007). A tumor necrosis factor receptor loop peptide mimic inhibits bone destruction to the same extent as anti-tumor necrosis factor monoclonal antibody in murine collagen-induced arthritis. *Arthritis Rheum.* 56, 1164–1174. doi: 10.1002/art.22495

Saksela, K., Cheng, G., and Baltimore, D. (1995). Proline-rich (PxxP) motifs in HIV-1 Nef bind to SH3 domains of a subset of Src kinases and are required for the enhanced growth of Nef+ viruses but not for down-regulation of CD4. *EMBO Journal* 14, 484–491. doi: 10.1002/j.1460-2075.1995.tb07024.x

Simonet, W. S., Lacey, D. L., Dunstan, C. R., Kelley, M., Chang, M. S., Lüthy, R., et al. (1997). Osteoprotegerin: A novel secreted protein involved in the regulation of bone density. *Cell* 89, 309–319. doi: 10.1016/S0092-8674(00)80209-3

Singha, U. K., Jiang, Y., Yu, S., Luo, M., Lu, Y., Zhang, J., et al. (2008). Rapamycin inhibits osteoblast proliferation and differentiation in MC3T3-E1 cells and primary mouse bone marrow stromal cells. *Journal of Cellular Biochemistry* 103, 434–446. doi: 10.1002/jcb.21411

Sone, E., Noshiro, D., Ikebuchi, Y., Nakagawa, M., Khan, M., Tamura, Y., et al. (2019). The induction of RANKL molecule clustering could stimulate early osteoblast differentiation. *Biochemical and Biophysical Research Communications* 509, 435–440. doi: 10.1016/j.bbrc.2018.12.093

Sugamori, Y., Mise-Omata, S., Maeda, C., Aoki, S., Tabata, Y., Murali, R., et al. (2016). Peptide drugs accelerate BMP-2-induced calvarial bone regeneration and stimulate osteoblast differentiation through mTORC1 signaling. *BioEssays* 38, 717–725. doi: 10.1002/bies.201600104

Takasaki, W., Kajino, Y., Kajino, K., and Murali, R. G. M. (1997). Structure–based design and characterization of exocyclic peptidomimetics that inhibit TNFα binding to its receptor. *Nature Biotechnology* 15, 1266–1270.

Uehara, T., Matsui, M., Tabata, Y., Murali, R., Miyashin, M., and Aoki, K. (2016). Delivery of RANKL-Binding Peptide OP3-4 Promotes BMP-2–Induced Maxillary Bone Regeneration. *Journal of Dental Research* 95, 665–672. doi: 10.1177/0022034516633170

Wang, L., Huang, B., Chen, X., and Su, J. (2020). New insight into unexpected bone formation by denosumab. *Drug Discovery Today* 25, 1919–1922. doi: 10.1016/j.drudis.2020.09.001

Xiong, J., Onal, M., Jilka, R. L., Weinstein, R. S., Manolagas, S. C., and Brien, C. A. O. (2011). Matrix-embedded cells control osteoclast formation. *Nature Medicine* 17, 1235–1242. doi: 10.1038/nm.2448

**Conflict of Interest:** The authors declare that the research was conducted in the absence of any commercial or financial relationships that could be construed as a potential conflict of interest.

frontiers in Cell and Developmental Biology

ORIGINAL RESEARCH
published: 13 July 2021
doi: 10.3389/fcell.2021.657935

# Fluorescence-Based Real-Time Analysis of Osteoclast Development

*Áron Pánczél†, Simon P. Nagy†, János Farkas†, Zoltán Jakus†, Dávid S. Győri† and Attila Mócsai*†*

*Department of Physiology, Semmelweis University School of Medicine, Budapest, Hungary*

Osteoclasts are multinucleated cells of hematopoietic origin which are critically involved in physiological and pathological bone resorption. They develop from myeloid progenitors through characteristic gene expression changes and intercellular fusion. This process is directed by M-CSF and RANKL which are also able to trigger osteoclast development from bone marrow cells *in vitro*. Osteoclasts are conventionally visualized by histochemical staining followed by manual counting, which hinders kinetic studies and automated quantification. Here we describe two fluorescence-based assays for the real-time analysis of myeloid cell to osteoclast development (FRAMCO) in primary mouse bone marrow cell cultures. Both assays rely on red-to-green fluorescence conversion of the membrane-targeted tdTomato/membrane-targeted eGFP (mTmG) transgene by Cre recombinase driven by the osteoclast-specific cathepsin K promoter (Ctsk-Cre). In the first assay (FRAMCO1.1), osteoclast-specific gene expression triggers red-to-green color conversion of cells carrying both the Ctsk-Cre and mTmG transgenes. In the second assay (FRAMCO1.2), red-to-green fluorescence conversion is triggered by fusion of neighboring co-cultured bone marrow cells separately carrying either the Ctsk-Cre or the mTmG transgenes. The two assays were tested using a high-content confocal fluorescence imaging system, followed by automated quantification. The FRAMCO1.1 assay showed robust red-to-green fluorescence conversion of more than 50% of the culture (including mononuclear cells) within 3 days under osteoclastogenic conditions. The FRAMCO1.2 assay showed a less robust but still readily measurable red-to-green color conversion in multinuclear cells within 5 days of differentiation. The assays required both the Ctsk-Cre and the mTmG transgenes and gave no signals in parallel macrophage cultures. The proper functioning of the two assays was also confirmed at the DNA, mRNA and bulk protein level. The assay systems were validated using lisophosphatidylcholine, a previously reported inhibitor of preosteoclast fusion. Taken together, our assays allow high-throughput automated real-time analysis of two critical aspects of osteoclast development, facilitating the screening for novel drug candidates for the pharmacological control of osteoclast-mediated bone resorption.

**Keywords: osteoclasts, cell fusion, fluorescence microscopy, Cre recombinase, myeloid cell differentiation, fluorescent Cre-reporter**

OPEN ACCESS

***Edited by:***
*Natalie A. Sims,*
*University of Melbourne, Australia*

***Reviewed by:***
*Michelle McDonald,*
*Garvan Institute of Medical Research, Australia*
*Kent Søe,*
*University of Southern Denmark, Denmark*

***Correspondence:**
*Attila Mócsai*
*mocsai.attila@med.semmelweis-univ.hu*

**†ORCID:**
*Áron Pánczél*
*orcid.org/0000-0003-1153-4844*
*Simon P. Nagy*
*orcid.org/0000-0001-7196-768X*
*János Farkas*
*orcid.org/0000-0001-6251-8997*
*Zoltán Jakus*
*orcid.org/0000-0002-6304-2369*
*Dávid S. Győri*
*orcid.org/0000-0002-2048-6752*
*Attila Mócsai*
*orcid.org/0000-0002-0512-1157*

***Specialty section:***
*This article was submitted to Cellular Biochemistry, a section of the journal Frontiers in Cell and Developmental Biology*

***Received:*** *24 January 2021*
***Accepted:*** *15 June 2021*
***Published:*** *13 July 2021*

***Citation:***
*Pánczél Á, Nagy SP, Farkas J, Jakus Z, Győri DS and Mócsai A (2021) Fluorescence-Based Real-Time Analysis of Osteoclast Development. Front. Cell Dev. Biol. 9:657935. doi: 10.3389/fcell.2021.657935*

## INTRODUCTION

Osteoclasts are multinucleated cells uniquely capable of degrading bone tissue (Teitelbaum, 2000). They are critically involved in bone resorption required to maintain skeletal homeostasis, as indicated by the increased bone mass in osteopetrosis, a disease caused by inherited defects of osteoclast development or function (Sobacchi et al., 2013). Besides their role in normal bone turnover, osteoclasts also play a critical role in pathological bone loss in diseases, such as osteoporosis, rheumatoid arthritis, and osteolytic bone metastases (Rachner et al., 2011; Kitazawa et al., 2018; Shim et al., 2018; Győri and Mócsai, 2020). The role of osteoclasts in these diseases is also indicated by the therapeutic efficacy of anti-osteoclast therapeutics, such as bisphosphonates, RANKL-inhibiting monoclonal antibodies, or cathepsin K inhibitors (Russell, 2011; Lacey et al., 2012; Duong le et al., 2016).

Osteoclasts develop from the myeloid lineage of the hematopoietic system [either from yolk-sack derived erythromyeloid or bone marrow-derived myeloid progenitors (Jacome-Galarza et al., 2019; Yahara et al., 2020)] and share several characteristics with certain macrophage subsets. The development of osteoclast progenitors into mature osteoclasts is primarily directed by two cytokines, M-CSF, which promotes myeloid cell proliferation and differentiation, and RANKL, which triggers an osteoclast-specific differentiation program. Administration of M-CSF and RANKL to bone marrow cells is able to induce development of mature osteoclast-like cells even in *in vitro* cell culture.

Osteoclast development is characterized by two conceptually different aspects of differentiation: osteoclast-specific gene expression changes and intercellular fusion. During osteoclast-specific transcriptional activity, the primarily osteocyte/osteoblast-derived (Nakashima et al., 2011) RANKL cytokine triggers dramatic upregulation of a number of genes, such as *Acp5* (encoding tartrate-resistant acidic phosphatase or TRAP), *Ctsk* (cathepsin K), or *Nfatc1* (encoding NFATc1, the master regulator of osteoclast development), giving rise to mostly mononuclear preosteoclasts. During intercellular fusion, preosteoclasts fuse to each other to form large multinuclear syncytia (osteoclasts) which are able to spread over and resorb the underlying bone tissue. Though osteoclast-specific gene expression is believed to mostly precede preosteoclast fusion, there is substantial temporal overlap between the two processes.

The standard approach to visualize osteoclasts *in vitro* or *in vivo* is based on the histochemical staining for the TRAP enzyme (Minkin, 1982) and the presence of multiple nuclei in a single cell (**Figure 1A**). In this case, TRAP-positivity correlates with osteoclast-specific gene expression, whereas multinucleation is an indicator of intercellular fusion. However, analysis of osteoclast development based on TRAP staining has a number of shortcomings. Most importantly, the cells need to be fixed prior to staining, therefore it is not possible to follow the same cell culture over a prolonged period of time. In addition, counting TRAP-positive multinuclear cells is a very time-consuming process that is rather difficult to automate.

There has been a number of attempts to overcome the above limitations. Transgenic expression of the red fluorescent tdTomato protein under the control of the *Acp5* promoter allowed the fluorescence-based real-time analysis of TRAP expression as a measure of osteoclast-related gene expression (Kikuta et al., 2013). There have also been several attempts to visualize preosteoclast fusion, based on the analysis of the co-culture of two cell sources labeled by two different chemical stains or expressing two different fluorescent proteins (Levaot et al., 2015; Verma et al., 2018). However, the resources for the live imaging of osteoclast cultures are still rather limited. In addition, some aspects of the above approaches, such as the lack of internal reference for overall cell number or the difficulties of separating accidentally overlapping fluorescence signals from true fusion events, pose significant technical challenges.

The above issues prompted us to develop two separate fluorescence-based assays for the real-time analysis of osteoclast-specific gene expression (FRAMCO1.1) and intercellular fusion of preosteoclasts (FRAMCO1.2). Both assays rely on the conversion of red to green fluorescence by Cre-mediated recombination in *in vitro* osteoclast cultures. This is triggered by *Ctsk* (cathepsin K) expression (FRAMCO1.1) and intercellular fusion (FRAMCO1.2), whereas red fluorescence serves as internal reference for overall cell density. We also provide further non-fluorescence-based evidence of corresponding changes at the DNA, mRNA and protein level. Together with a related recent paper (Li et al., 2018), our experiments may contribute to the improved methodologies of studying osteoclast development in the future.

## MATERIALS AND METHODS

### Animals

Mice carrying the $Gt(ROSA)26Sor^{TM4(ACTB-tdTomato,-EGFP)Luo}$ (referred to as $Rosa26^{mTmG}$ or mTmG) knock-in mutation (Muzumdar et al., 2007) were obtained from the Jackson Laboratory and were maintained in homozygous ($Rosa26^{mTmG/mTmG}$) form. Mice carrying the $Ctsk^{TM1(cre)Ska}$ (referred to as $Ctsk^{Cre}$ or Ctsk-Cre) knock-in allele (Nakamura et al., 2007) were obtained from Shigeaki Kato (University of Tokyo) and were maintained in heterozygous ($Ctsk^{Cre/+}$) form. The two strains were crossed to obtain $Ctsk^{Cre/+}Rosa26^{mTmG/mTmG}$ (referred to as Ctsk-Cre/mTmG) mice. All mice were on the C57BL/6 genetic background. Where indicated, wild-type C57BL/6 mice from our colony (originally obtained from the Jackson Laboratory) were used as controls (referred to as WT). Mice of both sexes were used. The vast majority of animals were between 10 and 16 weeks of age. No obvious difference between sexes or age groups were observed. Animals were kept in individually ventilated cages in a specific pathogen-free facility. All experiments were approved by the Animal Experimentation Review Board of Semmelweis University.

## *In vitro* Osteoclast Cultures

Osteoclasts were generated as previously described (Kertész et al., 2012; Győri et al., 2014; Csete et al., 2019). Long bones from hind limbs of adult mice of the indicated genotypes were dissected, cut open at proximal and distal metaphyses and flushed with sterile PBS. Following erythrocyte lysis with ammonium-chloride-potassium buffer, cells were pelleted and resuspended in α-MEM (Sigma) supplemented with 10% fetal bovine serum (FBS; Euroclone), 2 mM L-glutamine, 10 mM HEPES (pH ≈ 7.3), 100 U/ml penicillin and 100 μg/ml streptomycin (all from Sigma) and cultured in the presence of 10 ng/ml recombinant mouse M-CSF (PeproTech) in a standard $CO_2$ incubator. After two days (referred to as Day 0), non-adherent cells were harvested, diluted to a final density of $10^5$ cells/cm$^2$, supplemented with 50 ng/ml M-CSF only for macrophage, or with 50 ng/ml M-CSF and 50 ng/ml RANKL (PeproTech) for osteoclast cultures, and placed on tissue culture plates (Greiner Bio-One μClear® Cellstar® 655090 for confocal microscopy and Corning Costar 3516 for non-fluorescence-based studies). The cultures were then followed for up to 6 days with the culture medium replaced every 2 days. For representative images, cultures were fixed and stained for tartrate resistant acid phosphatase using the Acid Phosphatase, Leukocyte (TRAP) kit (387A, Sigma). For inhibitor studies, 12:0 lysophosphatidylcholine (1-lauroyl-2-hydroxy-sn-glycero-3-phosphocholine, referred to as LPC) was obtained from Avanti®, dissolved in sterile water and added to the cultures at the indicated final concentrations.

## Fluorescence Microscopy

Cell cultures were imaged with an ImageXpress Micro Confocal High Content Imaging System (Molecular Devices). Filter pairs of 377/50 and 447/60 nm, 474/27 and 525/45 nm or 562/40 and 624/40 nm were used for blue, green and red fluorescence, respectively. For representative images and nucleus-based quantification, a nuclear staining with 0.5 μg/ml Hoechst 33342 dye (Invitrogen) in PBS was applied for 20 min.

For quantitative kinetic analysis, cultures were imaged immediately after plating, then kept in a standard $CO_2$ incubator and taken to the microscope for further imaging at room temperature and atmospheric $CO_2$ concentration at the indicated time-points. Imaging of one 96-well plate took approximately 40 min which the cells seemed to tolerate reasonably well. During image acquisition, six 10× magnified fields of view (each covering 1.96 mm$^2$) were captured from each well and at least four parallel wells were imaged for each condition. Images were quantified with MetaXpress High Content Image Acquisition & Analysis Software to determine the area of objects of interest based on intensity above local background as well as minimal and maximal object sizes. The segmentation workflow used did not attempt to separate touching/overlapping suprathreshold objects, thus only the total area and not the object count was used for further quantitative characterization of the cultures. Detection and quantification of nuclei was likewise performed in the MetaXpress software using a built-in algorithm that determined both the total number of nuclei and the number of nuclei within the objects identified by segmentation of the green channel images.

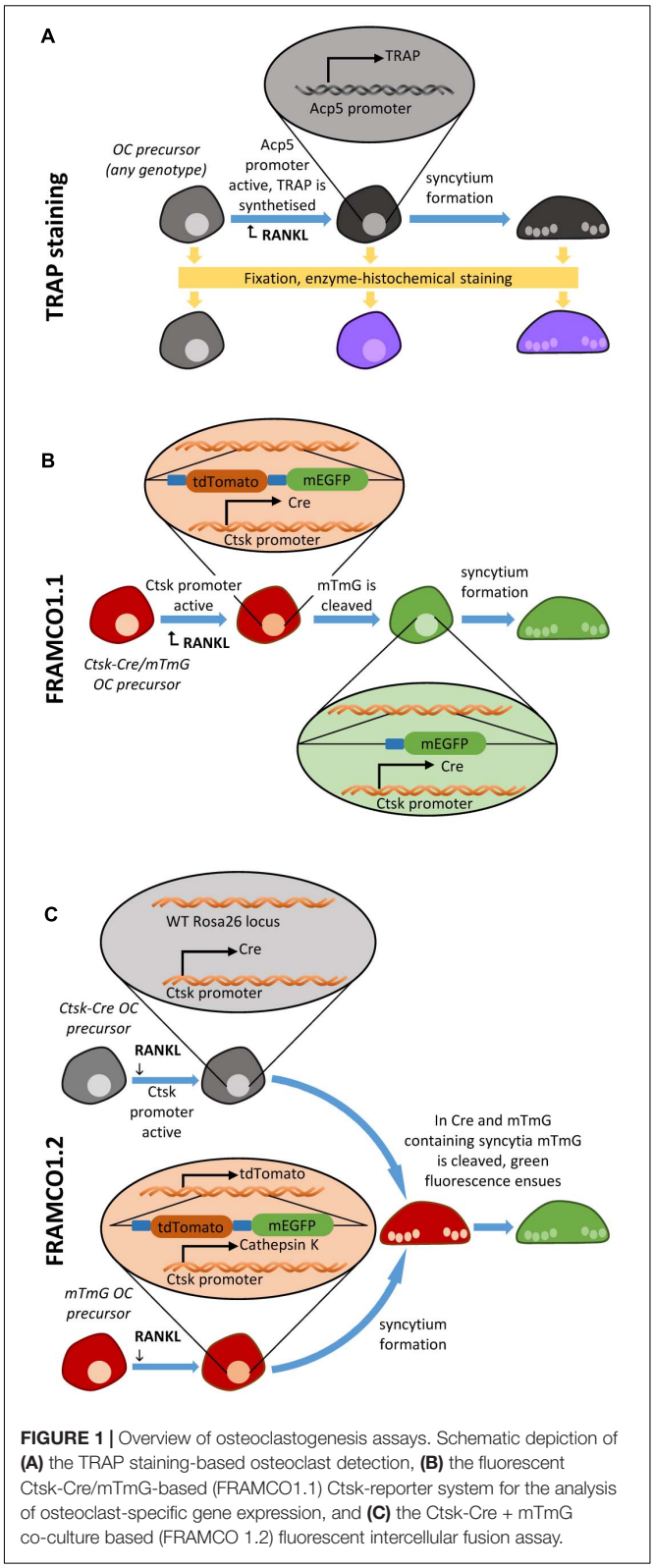


**FIGURE 1 |** Overview of osteoclastogenesis assays. Schematic depiction of **(A)** the TRAP staining-based osteoclast detection, **(B)** the fluorescent Ctsk-Cre/mTmG-based (FRAMCO1.1) Ctsk-reporter system for the analysis of osteoclast-specific gene expression, and **(C)** the Ctsk-Cre + mTmG co-culture based (FRAMCO 1.2) fluorescent intercellular fusion assay.

For real-time time-lapse video microscopy, cell cultures were incubated in a standard $CO_2$ incubator for 48 or 60 h after RANKL addition, then the medium was exchanged, and the culture plate was placed in the ImageXpress system with a sealing ring on top to create a closed space around the wells where a 5% $CO_2$–95% air gas mixture, humidity and a constant temperature of 37°C was provided for the cells using the ImageXpress system's built-in incubation capabilities. Images were taken every 60 min. Videos were processed using ImageJ/Fiji, which involved correction for background bleaching throughout the time-series using the BaSiC plugin (Peng et al., 2017).

## Genomic PCR Analysis

DNA from cultured cells was isolated using an SDS, Tris, EDTA (all from Sigma) and proteinase K (Qiagen) based lysis followed by purification using phenol-chloroform-isoamyl alcohol (Sigma). Cre-mediated recombination was followed by the 5′-CGTGCTGGTTATTGTGCTGTCTC-3′ forward and 5′-CCATTCTCCTGTCCGTTCGCTT-3′ reverse primers yielding a 261 bp product from the recombined (mG) version of the mTmG construct. It should be noted that the design of the mTmG construct does not allow for specific amplification of the recombined allele since any primer binding sites would also be present in the intact mTmG allele. However, the larger (2,674 bp) product amplified from the intact mTmG allele is not expected to interfere with the identification of the mG allele and is therefore not shown in the figures. A different pair of 5′-AATGGGAGCAGTGGTGGAAT-3′ forward and 5′-ATGTTGAGAGTCAGCAGTAGCC-3′ reverse primers was used to amplify a 98 bp segment in the loxP-flanked, tdTomato-encoding portion of the mTmG construct. For loading control, a part of the Rosa26 locus unaffected by the knock-in genetic modification, extending over 689 bp, was amplified using the 5′-GAACACCACCTGACGGGAGA-3′ forward and 5′-AGATGGGCGGGAGTCTTCTG-3′ reverse primers. Reaction products were run on 2% agarose gels and imaged on a Bio-Rad™ Gel Doc XR+ system.

## RT-qPCR Assay

Total RNA was isolated from cultures using the NucleoSpin RNA kit (Macherey-Nagel) and the RNeasy Plus Mini Kit (Qiagen) according to the manufacturer's instructions. Total RNA concentration was determined by a NanoDrop spectrophotometer and cDNA synthesis was performed using the QuantiTect and QuantiNova Reverse Transcription Kits (Qiagen). Reactions were purified using ammonium–acetate-based ethanol precipitation and resuspended in Tris-EDTA buffer. FAM conjugated TaqMan Gene Expression Assays for *Ctsk* (Mm00484039_m1), *Acp5* (Mm00475698_m1), *Nfatc*1 (Mm00479445_m1), *Cre* (custom assay #APRWJMG designed with Thermo Fisher's web application), *Egfp* (Mr04097229_mr), and endogenous control *Gapdh* (Mm99999915_g1) were obtained from Thermo Fisher Scientific. Quantitative PCR was performed using LightCycler 480® Probes Master (Roche) on a Roche LightCycler 480® II instrument. For quantification, the standard-curve based Efficiency Method was applied.

## Immunoblotting

Immunoblotting was performed essentially as described (Győri et al., 2014; Csete et al., 2019). Cells grown on 6-well tissue culture plates were washed with ice-cold PBS and lysed using radioimmunoprecipitation assay buffer (RIPA, containing 1% Triton X, 0.1% SDS, 0.5% sodium deoxycholate, 30 mM HEPES, 5 mM Na-EGTA, 10 mM benzamidine, and 20 mM sodium fluoride in physiological saline) supplemented with sodium-orthovanadate, phosphatase inhibitor cocktails 1 and 2, PMSF and aprotinin (all from Sigma). Cell debris was removed by centrifugation at 16,100 g. Protein concentration was determined using the Micro BCA™ Protein Assay Kit (Thermo Fisher Scientific). Samples then were mixed with 4× reducing sample buffer and boiled for 10 min. Ten micrograms of total protein was run on a 14% SDS-polyacrylamide gel, electroblotted onto nitrocellulose membranes and stained with Ponceau. Membranes were then blocked with 3% dry milk in PBS and 0.1% Tween 20 (PBS-Tween), followed by immunoblotting with primary antibodies against eGFP (1:2,000; clone F56-6A1.2.3; Abcam) or β-actin (1:10,000; Clone AC-74; Sigma) diluted in 3% BSA in PBS-Tween, followed by peroxidase-labeled anti-mouse IgG antibodies (1:5,000; GE Healthcare) diluted in 3% dry milk in PBS-Tween. Signal was developed by ECL (GE Healthcare) and exposed to X-ray film.

## Presentation of the Data

Experiments were performed the indicated number of times. Quantitative results show mean and SEM from all independent experiments performed.

# RESULTS

## Overview of the Osteoclast-Specific Gene Expression Assay

Our first aim was to develop an assay for the fluorescence-based real-time analysis of osteoclast-specific changes of gene expression. To this end, we crossed mice carrying the $Ctsk^{Cre}$ (referred to as Ctsk-Cre) knock-in mutation allowing the expression of the Cre recombinase from the endogenous *Ctsk* locus in an osteoclast-specific manner (Nakamura et al., 2007) with mice carrying the $Rosa26^{mTmG}$ (referred to as mTmG) mutation which leads to the ubiquitous expression of the red fluorescent membrane-targeted tdTomato ("mT") protein but allows switching to ubiquitous expression of the green fluorescent membrane-targeted eGFP ("mG") upon Cre-mediated recombination (Muzumdar et al., 2007). As shown in the schematic representation in **Figure 1B**, presence of both mutations in the same cells (referred to as Ctsk-Cre/mTmG cells) can be considered a Ctsk reporter system which is expected to result in red fluorescence under basal conditions but conversion to green fluorescence upon activation of the *Ctsk* gene during osteoclast differentiation. We have designated this system as FRAMCO1.1, standing for fluorescence-based real-time analysis of myeloid cell to osteoclast differentiation, version 1.1.

## Emergence of Green Fluorescence in Osteoclasts but Not Macrophages

The above approach was tested on *in vitro* cultures of mouse bone marrow-derived myeloid progenitors differentiated toward macrophages in the presence of 50 ng/ml M-CSF or toward osteoclasts in the presence of 50 ng/ml M-CSF and 50 ng/ml RANKL. The cells were cultured for 5 days, stained with Hoechst 33342 dye to label the nuclei, and then imaged using an ImageXpress confocal high-content fluorescence imaging system (**Figure 2**). The cells were fixed and stained for TRAP immediately after capturing the fluorescence images. As shown in **Figure 2**, osteoclast cultures contained large multinucleated TRAP-positive cells (supposedly osteoclasts), whereas neither TRAP-positive nor multinuclear cells were present in macrophage cultures. Ctsk-Cre cells (without the mTmG mutation) showed no substantial red or green fluorescence irrespective of the culture conditions, although cells and nuclei were clearly present in the cultures. In contrast, mTmG cells (in the absence of the Ctsk-Cre mutation) showed a constitutive red fluorescence signal that did not differ between macrophage and osteoclast cultures (except for the different morphologies of the two cell types). Ctsk-Cre/mTmG macrophage cultures were similar to mTmG macrophages. No green fluorescence emerged in any of Ctsk-Cre or mTmG single mutant cultures

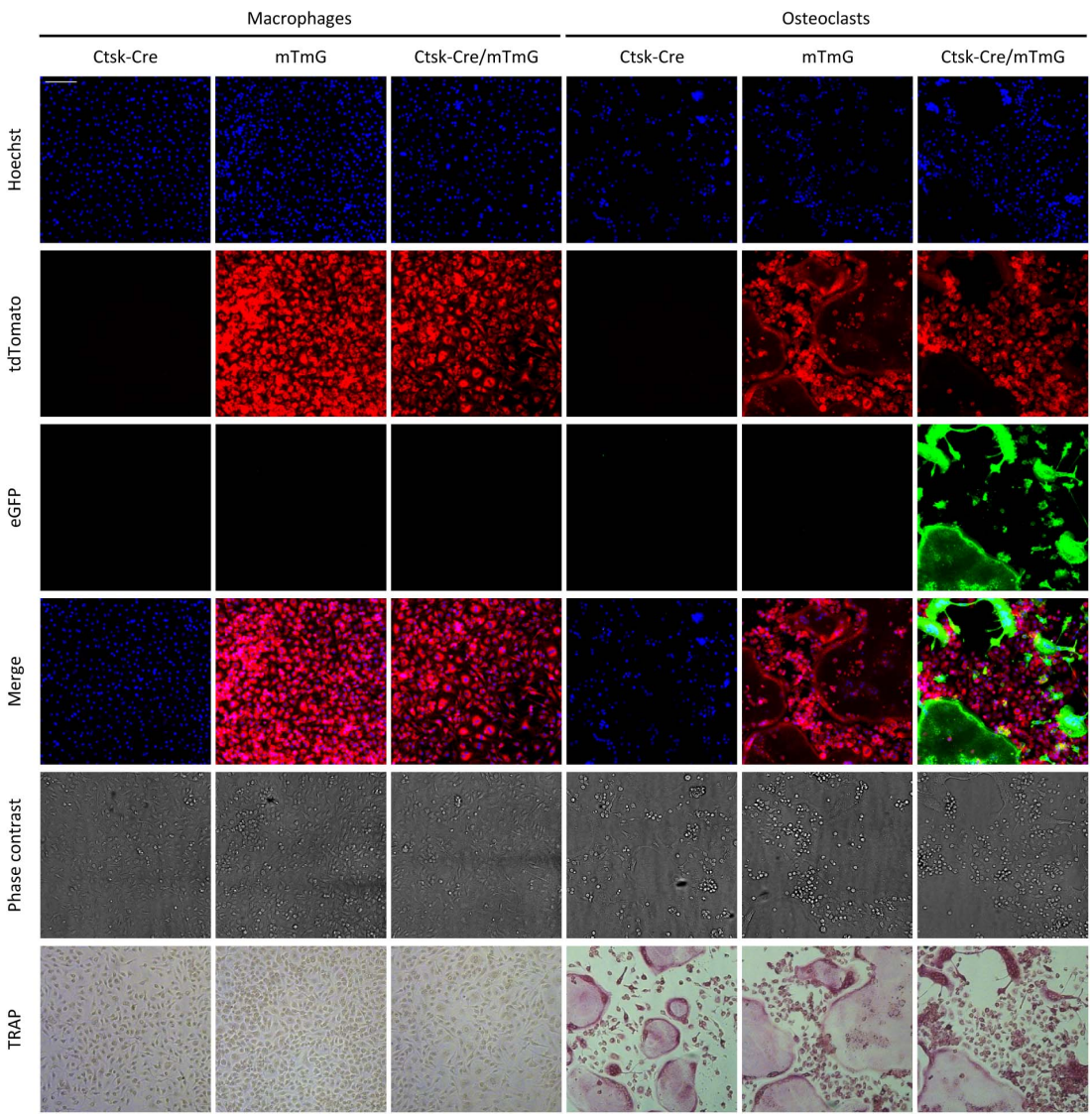


**FIGURE 2 |** Fluorescence and brightfield images of the FRAMCO1.1 assay. Representative images of macrophage and osteoclast cultures taken on Day 5 of differentiation (where Day 0 is defined as the time RANKL is first added to osteoclast cultures). Nuclei were stained with Hoechst dye. The first three rows show images from the blue, red and green fluorescence channels, supposedly corresponding to signals from the indicated fluorophores. The cells were fixed and stained for TRAP after taking fluorescence and phase contrast images. Each column shows images from the same field of view. The scale bar corresponds to 100 μm and applies to all images. Images are representative of 8–10 independent experiments.

or in Ctsk-Cre/mTmG macrophages. Importantly, however, a robust green fluorescence signal could be observed in Ctsk-Cre/mTmG osteoclast cultures. This green fluorescence mostly co-localized with large multinucleated TRAP-positive cells (osteoclasts), though apparently mononuclear green fluorescent cells (supposedly preosteoclasts) could also be observed. Most green fluorescent areas were largely devoid of red fluorescence, indicating a high efficiency of red-to-green color conversion. These snapshot images indicated that the Ctsk-Cre/mTmG mutation (FRAMCO1.1 assay) is capable of identifying cells that have undergone upregulation of osteoclast-specific genes.

## Time-Course of the Appearance of Green Fluorescence

We have also tested the time course of the emergence of green fluorescence signals in the Ctsk-Cre/mTmG cultures, exploiting the possibility of repeated imaging of the same cultures and the same fields of view. As shown in **Figure 3**, only red but not green fluorescence was observed in Ctsk-Cre/mTmG macrophage cultures. In contrast, a substantial number of green fluorescent cells emerged from Day 3 in osteoclast cultures, indicating activation of the osteoclast-specific *Ctsk* gene. These green fluorescent cells became larger by Day 5, supposedly indicating development of large multinucleated osteoclasts. However, both the number and size of green cells were reduced by Day 6, likely reflecting apoptosis of large multinucleated cells. Again, most of the green fluorescent cells showed strongly reduced red fluorescence, indicating effective red-to-green color conversion. We have also generated videos of Ctsk-Cre/mTmG macrophage and osteoclast cultures with higher temporal resolution between Days 2–5 after RANKL addition. One such video is shown as **Supplementary Video 1** to demonstrate the time-lapse capabilities of our FRAMCO1.1 system. Taken together, our Ctsk-Cre/mTmG (FRAMCO1.1) approach allows the fluorescence-based kinetic analysis of osteoclast-specific gene expression during the differentiation of myeloid progenitors toward the osteoclast lineage.

## Quantitative Analysis of the Fluorescence Signals

One of the major advantages of our system is that the emergence of green fluorescence can be readily quantified over a prolonged time during long-term imaging of the same osteoclast cultures. In addition, even eGFP-negative cells can be conveniently detected based on their red fluorescence, allowing the normalization for the total cellular content and therefore the exclusion of effects (e.g., differential proliferation) that are independent of red-to-green color conversion.

Results of the quantification of such experiments are shown in **Figure 4**. Panels A–C show results of macrophage cultures, whereas Panels D–F depict results from osteoclast cultures. All panels derive from analysis of fluorescent objects identified using built-in ImageXpress algorithms which quantify the area of objects showing red or green fluorescence above local background. **Figures 4A,D** show the area of all (red or green, i.e., tdTomato- or eGFP-expressing) fluorescent objects, as an approximation of total cellular area. **Figures 4B,E** show the area of green fluorescent (eGFP-expressing) objects, i.e., where red-to-green color conversion due to activation of the *Ctsk* gene has occurred. The percentage of the area of green fluorescent (eGFP) objects among all fluorescent (tdTomato or eGFP) ones, reflecting the relative extent of red-to-green color conversion, is depicted in **Figures 4C,F**. Besides the Ctsk-Cre/mTmG double-mutant osteoclast cultures, Ctsk-Cre and mTmG single-mutant cultures and parallel macrophage cultures are also shown as reference.

Likely reflecting the proliferation of the cells, the area of all (tdTomato or eGFP) fluorescence gradually increased in Ctsk-Cre/mTmG macrophage cultures (**Figure 4A**), whereas practically no eGFP-positive cells could be detected (**Figure 4B**). Therefore, in agreement with the lack of osteoclast-specific gene expression, the percentage of the area of green fluorescent objects remained practically zero in Ctsk-Cre/mTmG macrophage cultures (**Figure 4C**). Similar changes were also seen in mTmG macrophage cultures, whereas no fluorescence was observed in Ctsk-Cre cultures (**Figures 4A–C**).

The overall level of red or green (tdTomato or eGFP) fluorescence also gradually increased in mTmG and Ctsk-Cre/mTmG osteoclast cultures (**Figure 4D**). Importantly, however, a robust green fluorescence (eGFP) signal was observed in Ctsk-Cre/mTmG osteoclast cultures, whereas no such signals were seen in mTmG ones (**Figure 4E**). As a result, a high percentage of the area of fluorescent objects showed green fluorescence in Ctsk-Cre/mTmG but not in mTmG osteoclast cultures (**Figure 4F**). Further analysis of the Ctsk-Cre/mTmG curve in **Figure 4F** revealed that substantial eGFP expression arose by Day 3 and eGFP-positive area reached its maximum on Day 5 at >50% of the total fluorescent area, followed by a partial decline despite further apparent proliferation of the cells (**Figure 4D**). No fluorescence signal could be observed under any conditions in Ctsk-Cre osteoclast cultures (**Figures 4D–F**).

Taken together, the experiments shown in **Figure 4** indicate that our fluorescence-based Ctsk reporter assay (FRAMCO1.1) is suitable for the long-term follow-up and quantification of osteoclast-specific gene expression. Analysis of control samples, such as single (Ctsk-Cre or mTmG) mutants or macrophages confirm the working principles and specificity of the assay, and the use of red fluorescence readouts provides internal reference for normalization. The >50% color conversion rate also indicates the robustness of our assay.

## Molecular Analysis of Cre-Mediated Recombination and eGFP Expression

Besides fluorescence-based analyses, we also wanted to perform bulk population-based assays on the effects of *Ctsk* promoter-driven Cre expression at the DNA, mRNA, and protein level.

We first designed and utilized allele-specific PCR protocols to distinguish between the intact mTmG transgene and its truncated mG version, generated by Cre-mediated excision of the mT segment. Results of such experiments on genomic DNA are shown in **Figure 5A**. As expected, the intact (mTmG) allele was absent from Ctsk-Cre cultures (without mTmG) but it was readily

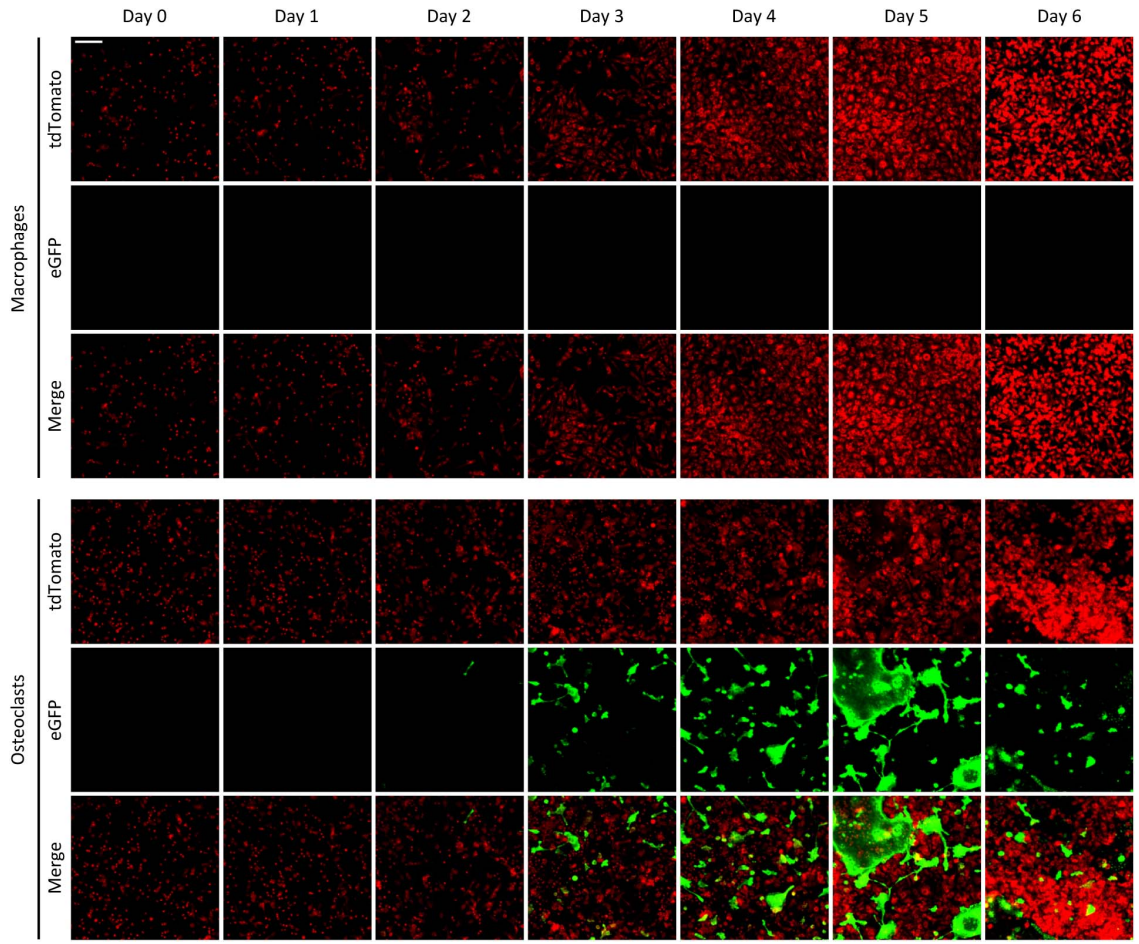


**FIGURE 3 |** The time-course of fluorescence changes in the FRAMCO1.1 assay. Representative images of Ctsk-Cre/mTmG macrophages and osteoclasts captured on the indicated days (Day 0 is the time RANKL was first added to osteoclast cultures). Red and green channels supposedly correspond to the indicated fluorophores. The scale bar corresponds to 100 μm and applies to all images. Images are representative of 8–10 independent experiments.

detected in all mTmG or Ctsk-Cre/mTmG macrophage and osteoclast cultures. In contrast, the mG allele was only present in Ctsk-Cre/mTmG osteoclast cultures but not in other osteoclast or any macrophage samples, confirming the genetic principle of the FRAMCO1.1 system and indicating successful Cre-mediated excision of the mT part of the mTmG transgene only in osteoclasts but not in macrophages. As a reference, we have also performed a PCR assay to detect a downstream Rosa26 sequence. This PCR protocol recognized all samples, although the amplification of the Ctsk-Cre samples was somewhat less robust (the reason for this difference is at present unclear).

Next we performed quantitative RT-PCR-based analysis of the expression of the osteoclast-related *Acp5*, *Ctsk*, and *Nfatc1* genes, as well as of the *Cre* transgene and the *Egfp* reporter. As shown in **Figure 5B**, *Acp5*, *Ctsk*, and *Nfatc1* expression showed robust upregulation in all osteoclast samples compared to parallel macrophage cultures by Day 4. *Cre* was expressed in Ctsk-Cre and Ctsk-Cre/mTmG but not in mTmG osteoclasts, nor in any macrophage cultures. Importantly, *Egfp* was only expressed in Ctsk-Cre/mTmG osteoclast cultures (**Figure 5B**), indicating the strict control of eGFP expression. Further kinetic analysis in Ctsk-Cre/mTmG osteoclast cultures (**Figure 5C**) also revealed substantial upregulation of *Acp5*, *Ctsk*, and *Nfatc1* expression during osteoclastic differentiation. As expected, *Cre* expression mostly followed that of *Ctsk*, and *Egfp* expression showed only a very modest delay compared to *Ctsk* expression.

We have also tested the appearance of the eGFP protein by immunoblotting. As shown in **Figure 5D**, eGFP was present in Ctsk-Cre/mTmG osteoclast cultures but not in osteoclast samples carrying only one of the two mutations, or in any of the macrophage cultures. Kinetic analysis of eGFP protein levels in Ctsk-Cre/mTmG osteoclast cultures (**Figure 5E**) showed the first appearance of eGFP as a faint band on Day 2 and robust eGFP signals on Days 3 and 4. This was in line with the appearance of *Egfp* mRNA (**Figure 5C**).

Taken together, we have been able to document the DNA-level cleavage of the mTmG transgene, as well as the expression of eGFP at the mRNA and protein level in the FRAMCO1.1 system. All these responses required the simultaneous presence of the Ctsk-Cre and mTmG mutations, and were under the strict control of RANKL-induced osteoclastic differentiation,

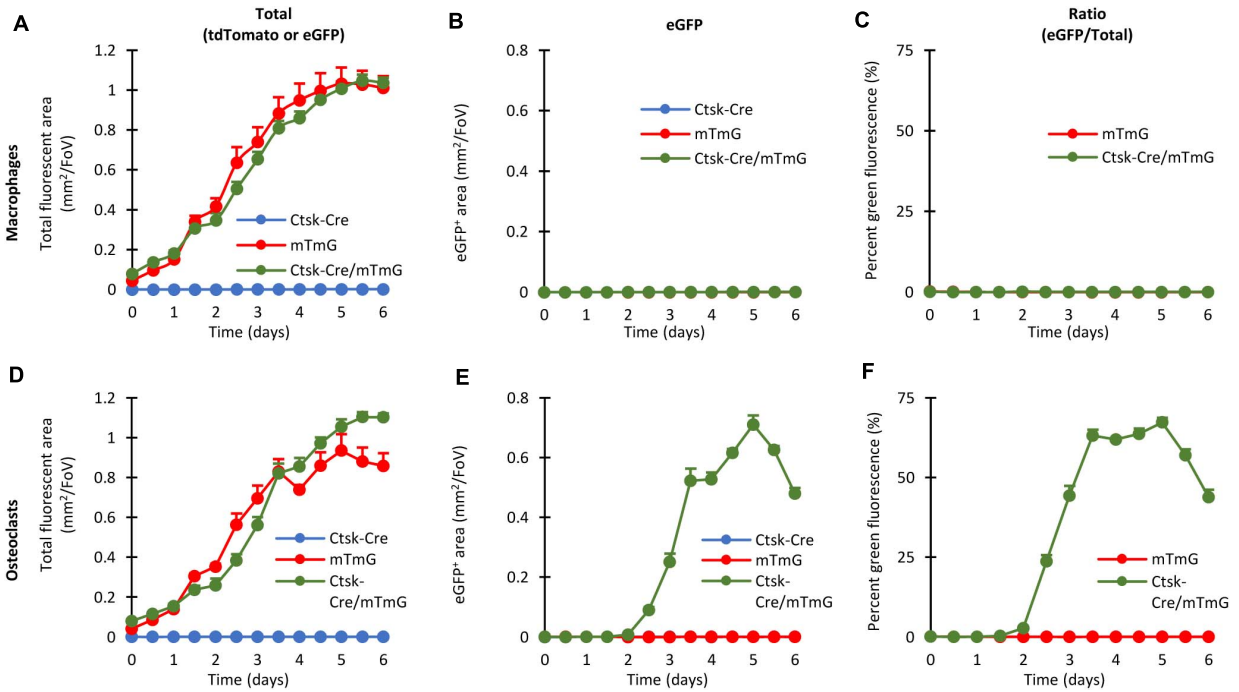


**FIGURE 4 |** Quantitative evaluation of the fluorescent signals in the FRAMCO1.1 assay. Quantification of the fluorescence signals of macrophage **(A–C)** or osteoclast **(D–F)** cultures of the indicated genotypes at the indicated time points. Graphs depict the kinetics of the total (tdTomato, eGFP or both) fluorescent area **(A,D)**, green (eGFP-positive) fluorescent area **(B,E)** and the ratio of the two areas **(C,F)**. All panels depict mean and SEM from 5 to 10 independent experiments.

confirming both the genetic concept and the osteoclast-specific nature of the FRAMCO1.1 assay.

## Overview of the Preosteoclast Fusion Assay

After having established a robust fluorescence-based assay for osteoclast-specific gene expression changes, our next aim was to set up another fluorescence-based assay for the analysis of the fusion of preosteoclasts to large multinucleated cells. We used the same Ctsk-Cre and mTmG mutations for this assay, but in a substantially different manner (**Figure 1C**). The principle of our fusion assay was the co-culture of Ctsk-Cre and mTmG single-mutant cells (referred to as "Ctsk-Cre + mTmG" cultures), where no cells carried both the Ctsk-Cre and mTmG mutations at the beginning of the culture period. Since Cre and its mTmG substrate would be present in different (although possibly neighboring) cells, Cre would not have access to its target and therefore no mTmG cleavage and no eGFP expression would occur. Subjecting these cells to osteoclastogenic conditions would be expected to initiate the fusion of neighboring Ctsk-Cre and mTmG cells and the cleavage of the mTmG transgene to its truncated mG variant, resulting in eGFP expression and emergence of green fluorescence. Therefore, red-to-green fluorescent color conversion in this assay would be the result of the intercellular fusion process. We have designated this system as FRAMCO1.2, standing for fluorescence-based real-time analysis of myeloid cell to osteoclast differentiation, version 1.2.

## Appearance of Green Fluorescence Upon Preosteoclast Fusion

To test the feasibility of the above approach, we mixed bone marrow-derived myeloid progenitors of two different genotypes at a 1:1 ratio and differentiated them toward macrophages or osteoclasts in the presence of 50 ng/ml M-CSF without or with 50 ng/ml RANKL, respectively. Representative fluorescence and phase-contrast images obtained on Day 5 after staining the nuclei with Hoechst 33342 dye, along with concomitant TRAP-stained images of the same fields of view from the same samples are shown in **Figure 6**. TRAP-stained images showed typical morphology of both macrophage (elongated TRAP-negative mononuclear cells) and osteoclast (large multinuclear TRAP-positive cells) cultures. Co-cultures of Ctsk-Cre and wild-type cells (referred to as "Ctsk-Cre + WT" cultures) did not show any red or green fluorescence. Co-cultures of wild-type and mTmG cells (referred to as "WT + mTmG" cultures) resulted in the appearance of a large number of red (tdTomato) but no green (eGFP) fluorescent cells. In line with the expected lack of intercellular fusion, only red but no green fluorescence could be observed in Ctsk-Cre + mTmG macrophage co-cultures. However, a robust green (eGFP) fluorescence signal emerged in Ctsk-Cre + mTmG co-cultures differentiated toward osteoclasts. This green fluorescence was practically entirely localized to large multinucleated osteoclast-like cells, whereas mononuclear cells remained non-fluorescent (supposedly Ctsk-Cre cells) or showed only red fluorescence (supposedly mTmG cells). Green cells also showed reduced red fluorescence, indicating relatively efficient

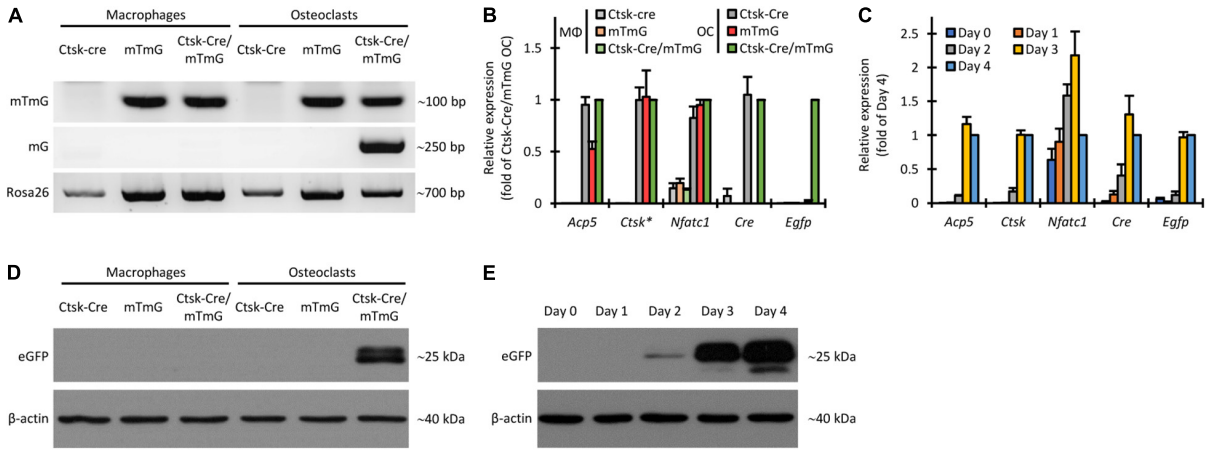


**FIGURE 5 |** Non-fluorescence-based assessment of Cre-mediated recombination in the FRAMCO1.1 assay. **(A)** Genomic PCR analysis of the indicated cultures on Day 4 using primers amplifying a target in the loxP-flanked portion of the intact mTmG construct (upper row), primers yielding an approximately 250 bp product from the Cre-recombined (mG) allele (middle row) or with primers amplifying a portion of the *Rosa26* locus downstream of the mTmG insertion site (lower row). **(B)** RT-qPCR analysis of different transcripts on Day 4 in macrophage (MΦ) or osteoclast (OC) cultures. The asterisk indicates that *Ctsk* expression values for samples carrying the Ctsk-Cre mutation were multiplied by 2 to compensate for the haploinsufficiency of the wild-type *Ctsk* allele. All samples were normalized to Ctsk-Cre/mTmG osteoclast values. **(C)** RT-qPCR analysis of the time course of expression of the indicated genes during differentiation of Ctsk-Cre/mTmG osteoclasts. Data were normalized to Day 4 expression of the respective markers. **(D,E)** Immunoblot experiments detecting eGFP or β-actin as a loading control from whole-cell lysates of the indicated cultures on Day 4 **(D)** or of Ctsk-Cre/mTmG osteoclast cultures at the indicated time points **(E)**. Panels **(A,D,E)** are representative of 3–5 independent experiments. Panels **(B,C)** show mean and SEM from 4 to 7 independent experiments.

red-to-green color conversion. This pattern suggests that the emergence of green fluorescence indeed resulted from the fusion of neighboring Ctsk-Cre and mTmG cells, allowing Cre to access its mTmG target, as expected from the original design of the FRAMCO1.2 system.

## Time-Course of Fusion-Induced Fluorescence

We also followed the same cultures over a prolonged period of time. Representative images of Ctsk-Cre + mTmG co-cultures differentiated toward macrophages or osteoclasts are shown in **Figure 7**. As expected, no green (eGFP) fluorescence could be observed at any time points in macrophage cultures. On the other hand, green fluorescent cells started to emerge in Ctsk-Cre + mTmG osteoclast cultures around Day 4, primarily localized to relatively small but already likely multinuclear cells. Green (eGFP) fluorescence substantially increased by Day 5, primarily through the emergence of very large and spread-out green fluorescent cells, whereas green fluorescence declined again by Day 6, likely reflecting apoptosis of the large eGFP-positive cells. Similar to **Figure 6**, practically no green fluorescence was seen in supposedly mononuclear cells. We have also generated videos of Ctsk-Cre + mTmG osteoclast cultures with higher temporal resolution between Days 2–5 and Days 2.5–6 after RANKL addition. One video for each of the two timespans is shown as **Supplementary Videos 2**, **3** to demonstrate the time-lapse capabilities of our FRAMCO1.2 system. Taken together, these results suggest that the differentiation of Ctsk-Cre + mTmG co-cultures toward osteoclasts in our FRAMCO1.2 assay system is suitable for the kinetic analysis of the intercellular fusion process during osteoclast development.

## Quantification of Preosteoclast Fusion

Quantification of fusion-induced eGFP expression is shown in **Figure 8**. As shown in **Figure 8A**, the area of all (red or green) fluorescent objects increased until Day 4 in Ctsk-Cre + mTmG or WT + mTmG macrophage co-cultures, whereas no fluorescence could be observed in Ctsk-Cre + WT macrophage co-cultures. As expected, practically no green (eGFP) fluorescence could be observed in any of the macrophage cultures (**Figure 8B**) and therefore the percentage green fluorescence (relative to total fluorescence) in Ctsk-Cre + mTmG and WT + mTmG macrophage co-cultures remained close to zero (**Figure 8C**). There was a steady increase in the total fluorescence until the end of the 6-day observation period in Ctsk-Cre + mTmG and WT + mTmG osteoclast co-cultures, whereas no fluorescence could be observed in Ctsk-Cre + WT samples (**Figure 8D**). Importantly, there was a well-measurable emergence of green (eGFP) fluorescence in Ctsk-Cre + mTmG but not in any other osteoclast co-cultures (**Figure 8E**). Accordingly, the percent green fluorescence (ratio of green and total fluorescence) showed a well-measurable increase in Ctsk-Cre + mTmG but not in WT + mTmG co-cultures differentiated toward osteoclasts (**Figure 8F**). This fluorescence signal showed a slower and then accelerated increase until its peak around Day 5, followed by a decline by Day 6 (likely reflecting apoptosis of osteoclasts). Since this signal required the presence of both Ctsk-Cre and mTmG cells and it was not present in macrophage cultures, it is reasonable to assume that this signal reflects the intercellular fusion between neighboring Ctsk-Cre and mTmG cells during osteoclast development, as expected from the original FRAMCO1.2 design.

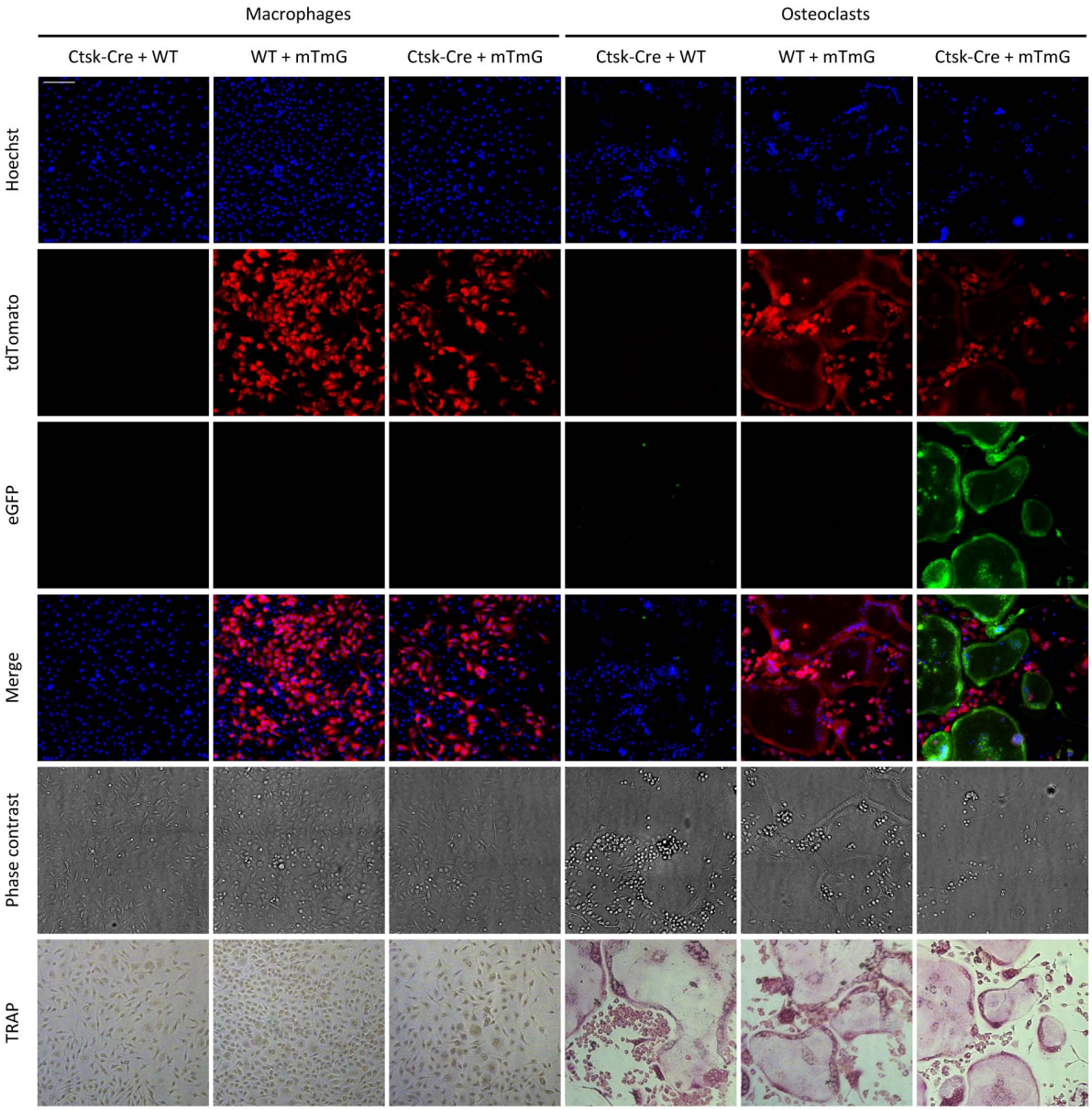


**FIGURE 6 |** Fluorescence and brightfield images of the FRAMCO1.2 (intercellular fusion) assay. Representative images of macrophage and osteoclast co-cultures on Day 5 after RANKL addition. Nuclei were labeled with Hoechst. The first three rows show images from the blue, red, and green fluorescence channels, supposedly corresponding to signals from the indicated fluorophores. The cells were fixed and stained for TRAP after fluorescence imaging. Images in each column show the same field of view. The scale bar corresponds to 100 μm and applies to every image. Images are representative of 8–10 independent experiments.

Taken together, our Ctsk-Cre + mTmG co-culture-based assay (FRAMCO1.2) allows the quantitative fluorescence-based real-time analysis of intercellular fusion during osteoclast development.

## Non-fluorescent Assays to Test Intercellular Fusion

We also performed non-fluorescent assays to demonstrate the fusion-dependent cleavage of the mTmG transgene and the expression of eGFP. First, we tested the presence of the full (mTmG) and truncated (mG) versions of the mTmG transgene by allele-specific PCR from genomic DNA. As shown in **Figure 9A**, the intact mTmG allele could be readily amplified from samples where mTmG cells were present (together with wild-type or Ctsk-Cre cells), whereas no amplification occurred in Ctsk-Cre + WT co-cultures. Importantly, the PCR product corresponding to the truncated (mG) allele could only be amplified from Ctsk-Cre + mTmG osteoclast co-cultures, but not from any other one. It is reasonable to assume that this signal derived from Cre-mediated excision of the mT segment

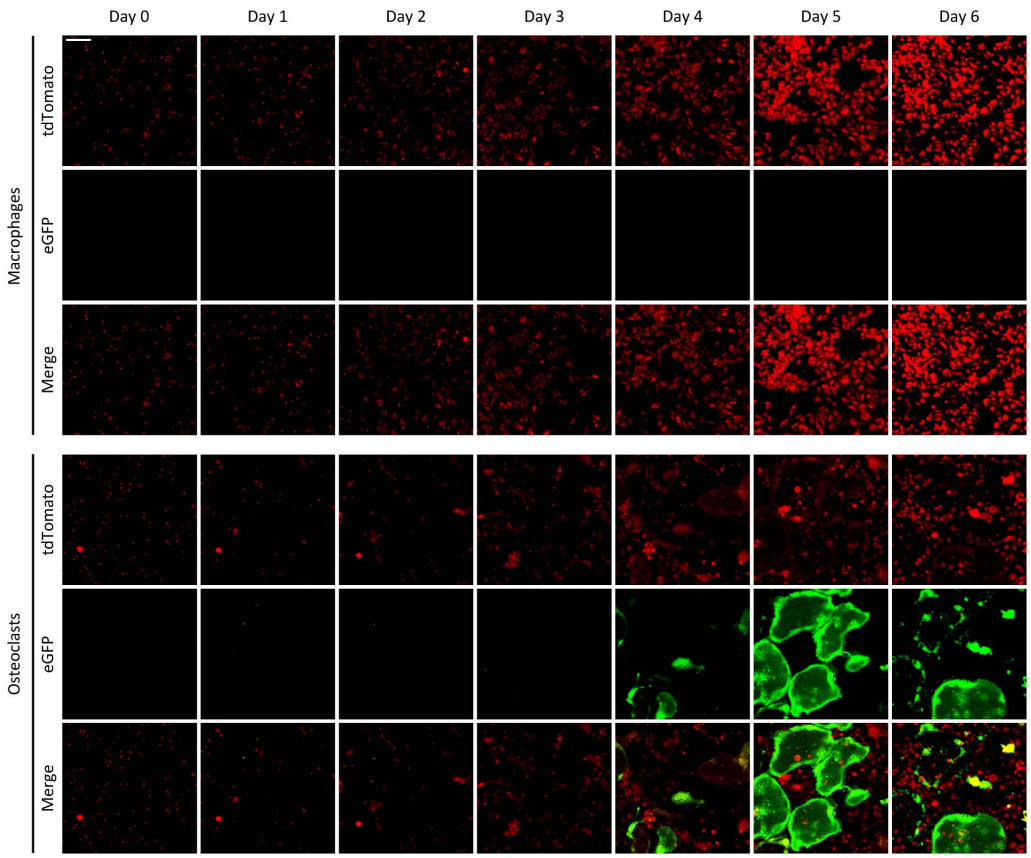


**FIGURE 7 |** The time-course of fluorescence changes in the FRAMCO1.2 assay. Representative images of Ctsk-Cre + mTmG macrophage and osteoclast co-cultures captured on the indicated days after RANKL addition. Red and green channels supposedly correspond to the indicated fluorophores. The scale bar corresponds to 100 μm and applies to all images. Images are representative of 8–10 independent experiments.

from the mTmG transgene as a result of fusion of Ctsk-Cre and mTmG preosteoclasts.

Next we tested expression of *Acp5*, *Ctsk*, *Nfatc1*, *Cre*, and *Egfp* at the mRNA level by quantitative RT-PCR. As shown in **Figure 9B**, *Acp5*, *Ctsk*, and *Nfatc1* were readily expressed in all osteoclast but not in parallel macrophage cultures by Day 4. Cre was expressed in Ctsk-Cre + WT and Ctsk-Cre + mTmG but not in WT + mTmG osteoclasts, nor in any macrophage cultures. Importantly, *Egfp* was only expressed in Ctsk-Cre + mTmG osteoclast cultures (**Figure 9B**), indicating the osteoclast-specificity of red-to-green color conversion. Further kinetic analysis in Ctsk-Cre + mTmG osteoclast cultures (**Figure 9C**) revealed substantial upregulation of *Acp5*, *Ctsk*, and *Nfatc1* expression during osteoclastic differentiation. As expected, *Cre* expression mostly reflected that of *Ctsk*, whereas *Egfp* expression showed a marked delay, possibly indicating a delay between *Ctsk* expression and completion of preosteoclast fusion.

We also tested the appearance of the eGFP protein by immunoblotting. As shown in **Figure 9D**, a measurable signal was seen in Ctsk-Cre + mTmG co-cultures differentiated toward osteoclasts, but not in any other samples. The time-course of this signal (**Figure 9E**) indicated that it began to emerge toward Days 3–4 of the osteoclast cultures. Again, this signal likely reflected fusion of Ctsk-Cre and mTmG cells under osteoclastogenic conditions.

Taken together, experiments testing mTmG cleavage and eGFP expression at the DNA, mRNA, and protein levels confirmed the suitability of the FRAMCO1.2 system to detect intercellular fusion in a strictly osteoclast-specific manner.

## Quantification Based on Nuclear Staining

One of the limitations of the quantification of the FRAMCO1.1 (**Figure 4**) and FRAMCO1.2 (**Figure 8**) systems is that it relies entirely on the area of red and green fluorescence signals without taking into account the number and presence of cell nuclei. To provide a partial solution for that issue, we performed the quantification of Hoechst-stained cultures at a single time point on Day 4 after RANKL addition in both the FRAMCO1.1 and FRAMCO1.2 systems. As shown in **Figure 10A**, the number of nuclei in Ctsk-Cre/mTmG osteoclast cultures (FRAMCO1.1 system) was substantially lower than that in parallel macrophage cultures, possibly indicating less robust proliferation under osteoclastogenic conditions. Nevertheless, a substantial number of nuclei were present within green fluorescent areas in osteoclast cultures, whereas practically no such nuclei were seen in macrophage cultures (**Figure 10B**). As a result, nearly 40% of the

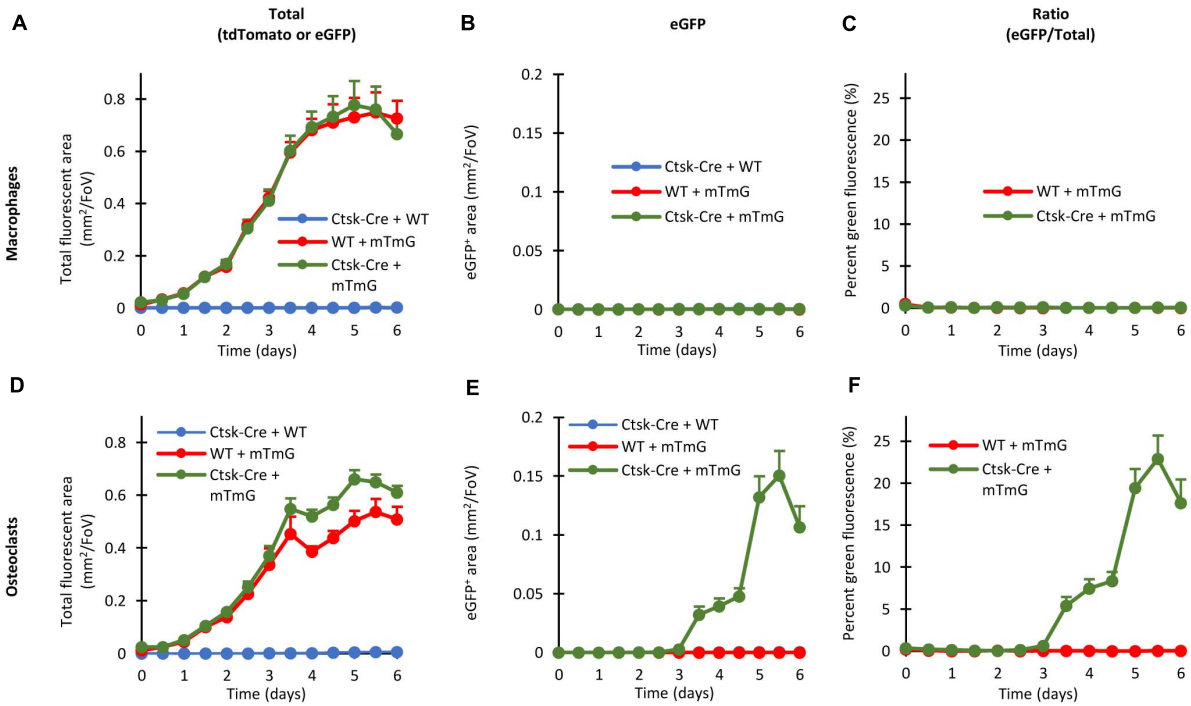


**FIGURE 8 |** Quantitative evaluation of the fluorescent signals in the FRAMCO1.2 assay. Quantitative evaluation of macrophage **(A–C)** and osteoclast **(D–F)** co-cultures of the indicated genotypes either showing the changes in total (tdTomato + eGFP) fluorescent area **(A,D)**, in green (eGFP) fluorescent area **(B,E)** or in the green area as percentage of the total fluorescent area **(C,F)**. All charts depict mean and SEM from 5 to 10 independent experiments.

nuclei in osteoclast cultures, but practically none in macrophage cultures, were within green fluorescent cells/areas (**Figure 10C**). A similar pattern was also seen in Ctsk-Cre + mTmG co-cultures (FRAMCO1.2 system). The overall number of nuclei (**Figure 10D**) was very similar to that seen in the FRAMCO1.1 system (**Figure 10A**). Again, nuclei within green fluorescent areas were practically only seen in osteoclast but not macrophage cultures (**Figure 10E**). This has translated to ∼ 4% of the nuclei being present within green fluorescent areas in osteoclast but none in macrophage cultures (**Figure 10F**), which is in line with the less robust nature of the FRAMCO1.2 compared to the FRAMCO1.1 system (compare **Figures 4**, **8**).

Taken together, determining the percentage of nuclei within green fluorescent areas appears to be a viable alternative quantification strategy for the FRAMCO1.1 and FRAMCO1.2 systems. However, a limitation of this approach is the reported toxicity of Hoechst dyes during long-term fluorescence imaging (Purschke et al., 2010), which was also apparent in our hands (data not shown). We are actively working on solving this issue by introducing genetic nuclear staining into our FRAMCO1.1 and FRAMCO1.2 systems.

## The Effect of Lisophosphatidylcholine on Osteoclast Development

The ultimate aim of our experiments is to establish a framework for highly efficient and internally controlled, readily quantifiable analysis of osteoclast development. This system could be used, among others, for the analysis of the effect of various inhibitors and drug candidates. To validate the usefulness of our system for such purposes, we tested the effect of lysophosphatidylcholine (LPC), a compound previously reported to inhibit preosteoclast fusion (Verma et al., 2018), on our FRAMCO1.1 and FRAMCO1.2 systems.

Quantification of the effect of LPC in our systems is shown in **Figure 11**, whereas snapshot images taken on Day 5 are included in **Supplementary Figure 1**. As shown in **Figure 11A**, 400 μM LPC partially inhibited the growth of total (red and green) fluorescent areas in Ctsk-Cre/mTmG (FRAMCO1.1) osteoclast cultures, possibly reflecting an inhibitory effect on cellular proliferation. The emergence of green fluorescence was inhibited by slightly even more, though eGFP-positive areas still developed (**Figure 11B**). As a result, the percentage of green fluorescence (**Figure 11C**) was only moderately reduced, especially at later time points. A substantially different picture was seen in Ctsk-Cre + mTmG co-cultures (FRAMCO1.2) kept under osteoclastogenic conditions. The partial inhibitory effect of LPC on apparent cell proliferation was also evident under such conditions (**Figure 11D**). However, while eGFP-positive cells readily emerged in control osteoclast cultures, practically no eGFP positivity could be observed in LPC-treated cultures (**Figure 11E**) and this also translated into the abrogation of the increase in percent green fluorescence (**Figure 11F**). The presence of green fluorescence and its confinement to apparently mononuclear cells in the FRAMCO1.1 but not in the FRAMCO1.2 system at 400 μM LPC concentration is also evident

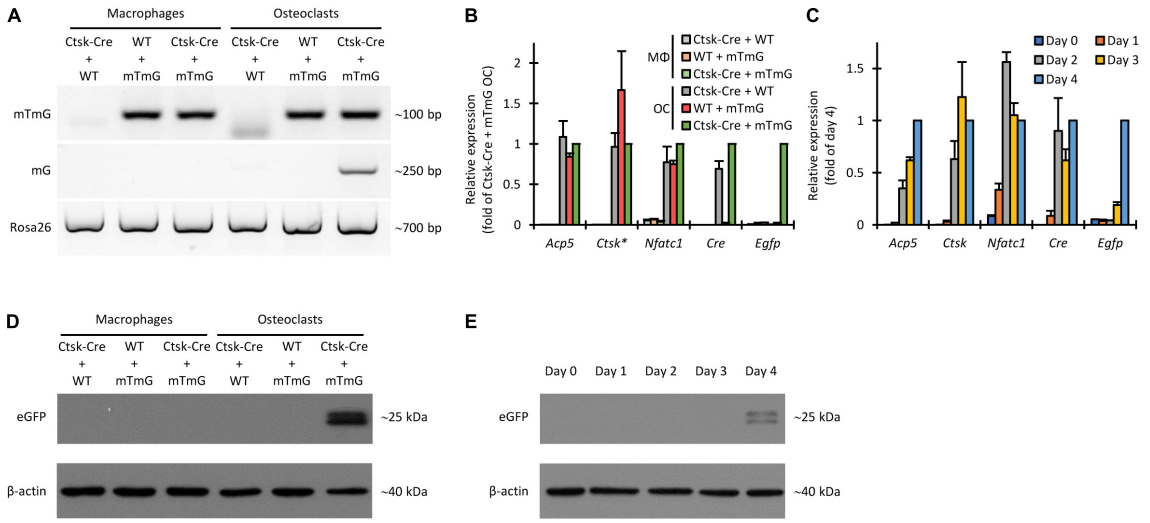


**FIGURE 9 |** Non-fluorescence-based assessment of Cre-mediated recombination in the FRAMCO1.2 assay. **(A)** Genomic PCR analysis of Cre-mediated recombination with primers amplifying a loxP-flanked portion of the mTmG construct (upper row), an ~250 bp region from the recombined (mG) allele (middle row) or a downstream region of the *Rosa26* locus unaffected by the mTmG mutation (lower row). **(B)** RT-qPCR analysis of different transcripts on Day 4 in macrophage (MΦ) or osteoclast (OC) cultures. The asterisk indicates that *Ctsk* expression values for samples with half of the cell-population carrying the Ctsk-Cre mutation were multiplied by 4/3 to compensate for the haploinsufficiency of the wild-type *Ctsk* allele. All samples were normalized to Ctsk-Cre + mTmG osteoclast values. **(C)** RT-qPCR analysis of the time course of expression of the indicated genes during differentiation of Ctsk-Cre + mTmG osteoclast co-cultures relative to *Gapdh*. Data were normalized to Day 4 expression values of the respective transcripts. **(D,E)** Immunoblot experiments detecting eGFP and β-actin as loading control from whole cell lysates of the indicated co-cultures on Day 4 **(D)** or from Ctsk-Cre + mTmG osteoclast co-cultures on the indicated days **(E)**. Panels **(A,D,E)** are representative of 3–6 independent experiments. Panels **(B,C)** show mean and SEM from 4 to 7 independent experiments.

in the snapshot images shown in **Supplementary Figure 1**. We have also performed dose-response analyses in the above systems. As shown in **Figure 11G**, increasing LPC concentrations reduced the total fluorescence signals in both the FRAMCO1.1 and FRAMCO1.2 systems in a mostly parallel manner. Although higher doses of LPC also reduced the emergence of green fluorescence in both systems, this was substantially more pronounced in the FRAMCO1.2 than in the FRAMCO1.1 system (**Figure 11H**), reaching practically complete inhibition in the FRAMCO1.2 system at approximately 400 μM. This can also be seen in the snapshot images shown in **Supplementary Figure 1**. As a result, the percent green fluorescence was only moderately reduced in the FRAMCO1.1 but practically reached zero in the FRAMCO1.2 system (**Figure 11I**) at higher LPC doses.

Taken together, the above experiments confirm an inhibitory effect of LPC on preosteoclast fusion, but they also reveal additional partial inhibitory effects on osteoclast-specific gene expression and, likely, proliferation of precursor cells.

## DISCUSSION

We have developed two separate assays that allow the fluorescence-based real-time analysis of osteoclast-specific gene expression (FRAMCO 1.1; **Figures 2**–**5**) and intercellular fusion of osteoclast-lineage cells (FRAMCO 1.2; **Figures 6**–**9**) during *in vitro* cultures. Both assays rely on red-to-green fluorescence conversion due to the recombination of the mTmG transgene by the Cre recombinase driven by the osteoclast-specific *Ctsk* promoter. The assays allow the prolonged real-time analysis of osteoclast development and are suitable for automated quantification, thereby overcoming the main limitations of the widely used TRAP staining procedure. The two assays also allow the parallel comparison of the osteoclast-specific gene expression and the intercellular fusion components of osteoclast development. Since the assays can be readily performed in multi-well plate formats, they can be adapted to higher-throughput screening of drug candidate molecules. Though we are aware that our methodological study does not provide substantial novel information on osteoclast biology, we hope that the experimental approaches described here will contribute to such discoveries in the future.

We have tested a number of control conditions to ensure that our assays do indeed reflect the transcriptional activity and fusion of osteoclasts. The facts that emergence of green fluorescence required both Cre expression and the mTmG transgene, and that no green fluorescence was observed in parallel macrophage cultures (**Figures 2**, **4**, **6**, **8**), confirmed the suitability of our assay for analysis of osteoclast development. Additional studies on DNA, mRNA and bulk protein level (**Figures 5**, **9**) also confirmed the basic principle of our assays and its reliance on osteoclast-specific gene expression and intercellular fusion.

Our results may also provide some insight into the kinetics of (*in vitro*) osteoclast development. Analysis of the time-course of osteoclast-specific gene expression (**Figure 4F**) revealed that it mainly occurred around Day 3 under osteoclastogenic conditions (though variation between individual cultures was seen). In contrast, the fusion process (**Figure 8F**) mainly occurred around

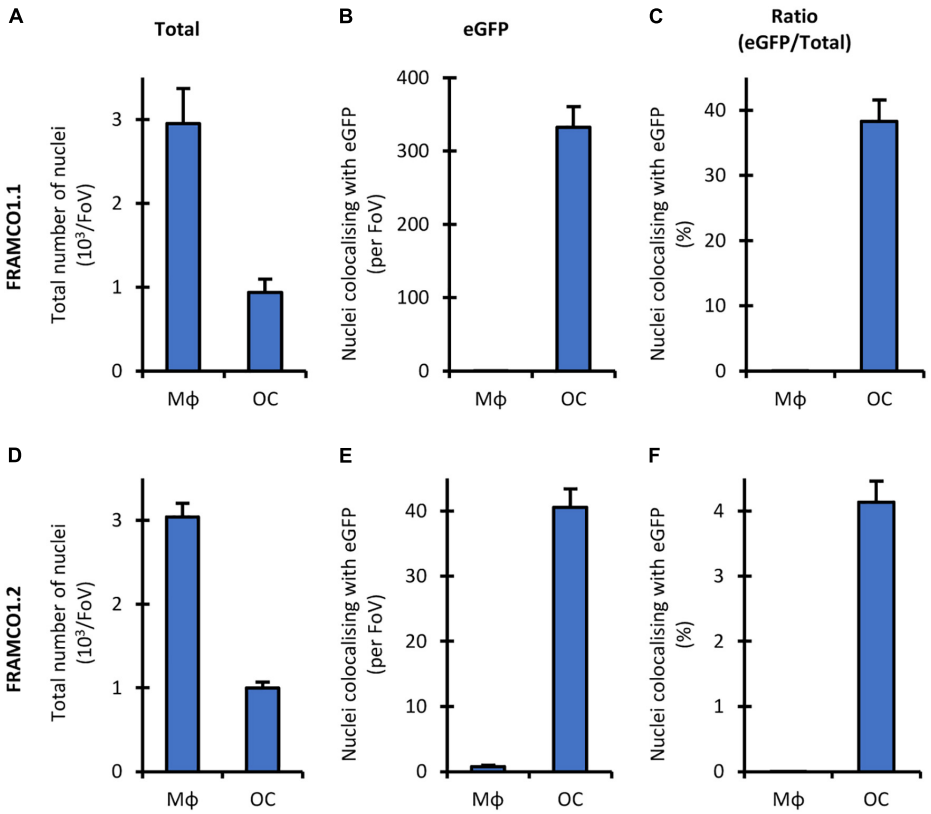


**FIGURE 10 |** Nucleus-based quantification of the FRAMCO1.1 and 1.2 assays. Total number of nuclei **(A,D)**, nuclei localized within above-threshold eGFP$^{+}$ objects **(B,E)** and the latter value as percentage of the former **(C,F)** in Hoechst-stained Ctsk-Cre/mTmG mono- (FRAMCO1.1, **A–C**) or Ctsk-Cre + mTmG co-cultures (FRAMCO1.2, **D–F**) of macrophages (MΦ) or osteoclasts (OC) stained and imaged on Day 4. Mean and SEM of five independent experiments is shown.

Days 4–5. It is also striking that green fluorescence emerged in apparently mononuclear cells (supposedly mononuclear preosteoclasts) in the FRAMCO1.1 system, whereas eGFP expression was confined to larger, supposedly multinuclear cells in FRAMCO1.2. Though care should be taken when interpreting data from the expression of a single gene (*Ctsk* in FRAMCO1.1) and a not yet fully established fusion assay (FRAMCO1.2), our results would be in line with a differentiation pathway where osteoclast-specific gene expression changes mostly precede preosteoclast fusion, at least in *in vitro* assays triggered by recombinant cytokines. It should also be mentioned that the FRAMCO1.2 system is expected not only to detect the first fusion events but also consecutive fusion steps through the inflow of new Cre-expressing (Ctsk-Cre) and red-to-green conversion-capable (mTmG) nuclear material, as well as through the tentatively enhanced spreading of gradually enlarging multinucleated cells. These processes may be responsible for the accelerated increase of green fluorescent areas around Days 4.5–5 in the FRAMCO1.2 system (**Figure 8E**). Nevertheless, the relationship between actual fusion and our area-based quantification is likely not entirely linear. Further steps (such as improved long-term nucleus-based quantification; see below) need to be taken to ensure a more linear quantification of the fusion process. The presence of green fluorescence signals declined by Day 6 in both assays, likely reflecting the apoptosis of primary osteoclasts during prolonged *in vitro* culture.

Further comparison also revealed additional differences between our two assays beyond their different kinetics. Our osteoclast-specific gene expression assay (FRAMCO1.1) was clearly more robust than the fusion assay (FRAMCO1.2). This is indicated by higher level of green fluorescence (compare **Figures 4F** vs. **8F**, **10C** vs. **10F**), higher level of mTmG allele cleavage at the DNA level (compare **Figures 5A**, **9A**), and a much more robust signal in eGFP immunoblots (compare **Figures 5D,E**, **9D,E**). Another obvious difference is that green fluorescence can be observed even in mononuclear cells in FRAMCO1.1 (**Figures 2**, **3**), whereas practically no green fluorescence could be observed in mononuclear cells in the FRAMCO1.2 assay (**Figures 6**, **7**). This observation likely reflects the fact that osteoclast-specific gene expression precedes, and is a prerequisite of, intercellular fusion in osteoclast cultures.

There have been a number of prior approaches to test osteoclast development by fluorescence-based tools. Transgenic expression of tdTomato driven by the *Acp5* (TRAP) promoter (TRAP-tdTomato mutation) (Kikuta et al., 2013) is in principle similar to our fluorescence-based osteoclast-specific gene expression assay. Nevertheless, the two assays use different osteoclast-related promoters (transgenic *Acp5* vs. endogenous

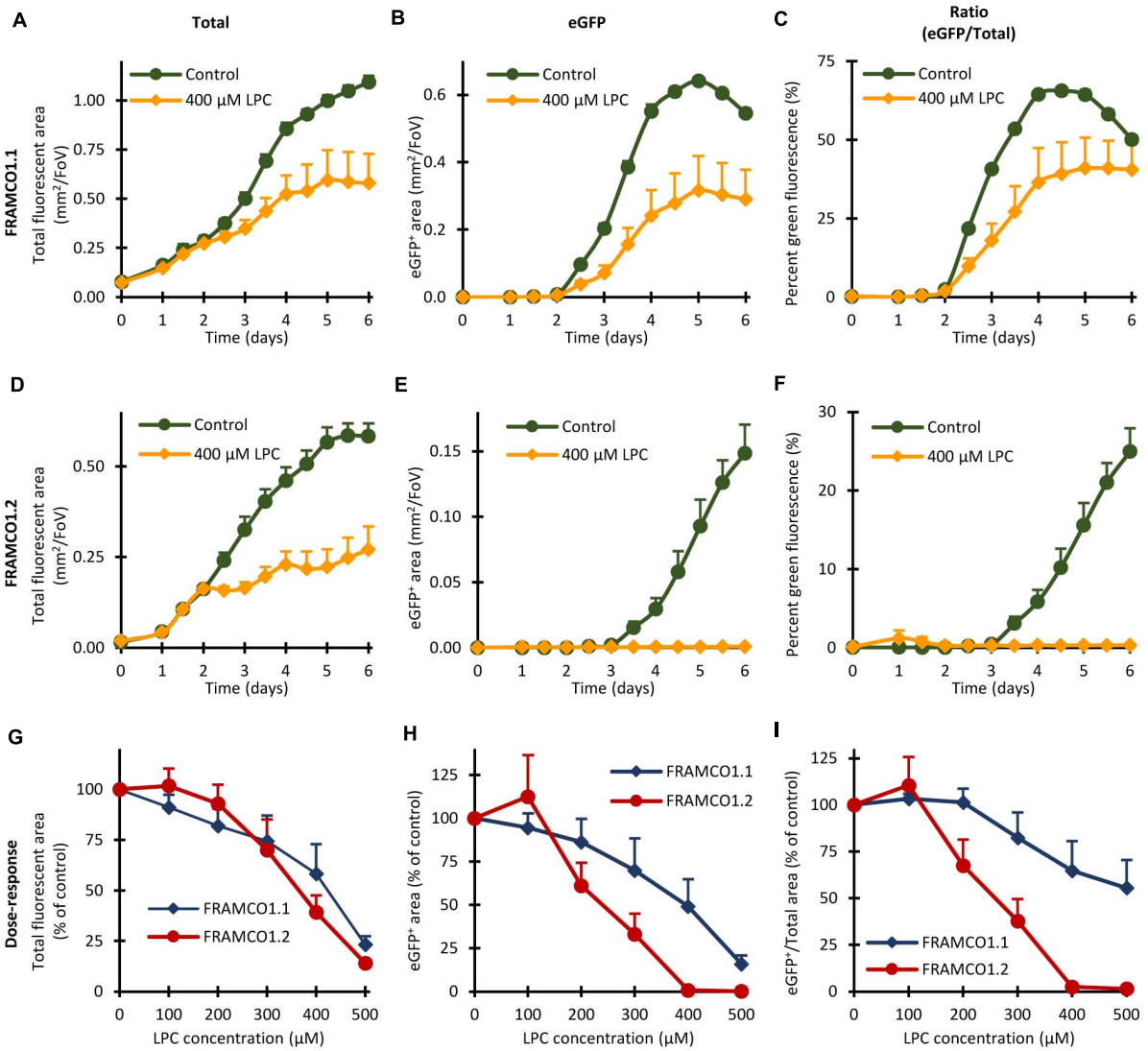


**FIGURE 11 |** Effect of Lysophosphatidylcholine (LPC) in the FRAMCO1.1 and FRAMCO1.2 assays. **(A–F)** Time course of changes in total (tdTomato + eGFP) fluorescent area **(A,D)**, green (eGFP-positive) fluorescent area **(B,E)** or in the green area as percentage of the total fluorescent area **(C,F)** in the absence or presence of 400 µM lysophosphatidylcholine (LPC) as detected in Ctsk-Cre/mTmG (FRAMCO1.1, **A–C**) or Ctsk-Cre + mTmG (FRAMCO1.2, **D–F**) osteoclast cultures. **(G–I)** Dose-response curves of the FRAMCO1.1 and FRAMCO1.2 assays showing total fluorescent area **(G)**, green (eGFP-positive) fluorescent area **(H)** and the latter as percentage of the former **(I)** on Day 5 in the presence of the indicated LPC-concentrations. Values in **(G–I)** are shown as percentage of the controls not treated with LPC. Mean and SEM of six independent experiments is shown.

*Ctsk*) and different labels (tdTomato vs. eGFP) to visualize osteoclasts, and require different (single or double) number of steps to trigger fluorescence, all of which may influence the osteoclast-related signals obtained. In addition, a clear advantage of our system is the basal red fluorescence of cells that have not undergone osteoclast-specific gene expression changes, providing a highly useful internal reference during automated quantification (**Figures 4**, **8**). Regarding fluorescence-based preosteoclast fusion assays, most such assays tested the fusion of two differentially labeled cells, using either chemical (Verma et al., 2018) or genetic (Levaot et al., 2015) labeling tools. Though that approach allows the tracking of the differentially labeled cells during the fusion process, it has substantial limitations, such as the complex computational approaches required to exclude non-fused but overlapping cells, as well as the closely related high background noise, especially when higher cell concentrations are used (which may be required for optimal fusion). In contrast, our fusion assay relies on the emergence of green fluorescence only in cells that have undergone the fusion process, leading to a very good signal-to-noise ratio (**Figure 8**). Therefore we believe that, at least for the overall analysis of intercellular fusion, our assay is superior to those based on the co-localization of labels originating from two differentially labeled cells. It should also be noted that a prior study utilized a two-component retroviral

packaging system to test fusion of osteoclast-related cells (Kondo et al., 2004); however, the complicated readout (viral titer measurement) and the lack of a fluorescence signal did not allow the real-time analysis of the fusion process in that assay.

Our fluorescence-based assays generate a very large amount of detailed high-content imaging information, with related challenges of image data processing. Our main approach was to use area-based calculations, assigning red or green fluorescence to pixels that reach a certain intensity above local background, and performing all further processing steps based on areas calculated from those binary images. Potential disadvantages of this approach are that it does not differentiate between dim and bright fluorescence above the threshold level or that it is also sensitive to changes in cell spreading without changes in overall amount of eGFP. We have not yet been able to solve those potential concerns without generating even more problems. Another possible approach would be to count the number of nuclei and assign red or green fluorescence to each nucleus based on fluorescence in the surrounding area. We have performed such calculation for a single time point in **Figure 10**. However, in agreement with previous reports (Purschke et al., 2010), the Hoechst dye used for those experiments interfered with the long-term cultures in our hands (data not shown) and therefore could not be used to follow osteoclast development during a prolonged culture period. We are actively working on incorporating genetic nuclear staining into our assay systems to allow nucleus-based real-time quantification in future protocols.

Another challenging issue is the acquisition and processing of high temporal resolution time-lapse image series (videos) from cell cultures over prolonged periods (several days). Though there are a few studies reporting such long-term fluorescence-based live cell imaging of osteoclast development (Levaot et al., 2015; Takegahara et al., 2016), such experiments are still scarce in the literature, especially using primary cells in a multiplate format. Since the built-in incubator of our confocal imaging system seemed not to be entirely optimized for prolonged culture of sensitive primary cells or imaging a large number of parallel samples, we performed most of our experiments by keeping the cells in a regular tissue culture incubator and moving them to our imaging station only briefly at the indicated time points. Nevertheless, we have also been able to generate time-lapse videos from a limited number of cultures, demonstrating the usefulness of our system for real-time video microscopy. Taken together, the genetic approach described here places demanding requirements on the imaging system used to record fluorescence changes in such cultures.

One of the potential uses of our assays is the screening of drug libraries on osteoclast cultures. To validate this approach, we have tested the effect of LPC on the FRAMCO1.1 and FRAMCO1.2 systems (**Figure 11**). While our results confirmed prior reports showing an inhibitory effect of LPC on preosteoclast fusion (Verma et al., 2018), it also revealed additional effects of LPC on osteoclast-specific gene expression and, likely, the proliferation of the cells (**Figure 11**). Those results exemplify the depth of details that can be obtained using the FRAMCO1.1 and FRAMCO1.2 systems. Additional questions that may arise in drug screening experiments are the specificity and sensitivity of our approach. The inclusion of parallel macrophage cultures throughout our study and the lack of any sign of eGFP expression in those cultures revealed a very high specificity for osteoclasts. Additional experiments aiming to test the sensitivity of our assays revealed that they are able to detect eGFP signals caused by as low as 1–2 ng/ml RANKL, with an apparently higher sensitivity of the FRAMCO1.1 than the FRAMCO1.2 system (data not shown).

It should also be noted that a parallel study using Ctsk-Cre and mTmG for the visualization of osteoclasts was reported during the course of our experiments (Li et al., 2018). In that complex study, various aspects of osteoclast biology were addressed using Ctsk-Cre and mTmG mutations present either in the same cell or in two different cell populations. Using those approaches, *in vitro* and *in vivo* emergence of cells showing osteoclast-specific gene expression, *in vitro* emergence of fused cells, the effect of PTH and osteoblasts/osteocytes on the fusion process and FACS-based sorting and gene expression of the fused cells was tested. Though our own experiments were initiated before the publication of the aforementioned work, we clearly admit the priority of publication of that study and that our work is based on a conceptually identical approach. Nevertheless, we believe that the more focused nature of our experiments, the clear distinction between the osteoclast-specific gene expression and intercellular fusion assays, the detailed controls used, the careful automated quantification suitable for high-throughput studies, the real-time video microscopy experiments performed and the analysis of non-fluorescence-based readouts provide highly valuable information and tools for the fluorescence-based analysis of osteoclast development. It should also be mentioned that the Li et al. (2018) study suggested the existence of two distinct populations of post-fusion osteoclasts based on the presence or absence of tdTomato-derived red fluorescence. Though we have also observed dual fluorescent (red and green) cells in both of our culture systems, we have not attempted to isolate those cells and therefore cannot speculate whether they represent a unique cell population or merely an intermediate stage in red-to-green conversion.

Though our assays proved to be suitable for the real-time analysis of osteoclast development, there is room for further improvement of our approaches. The relatively weak fusion-induced eGFP fluorescence may be improved by using other (e.g., Vav-Cre, TRAP-Cre, LysM-Cre, or CX3CR1-Cre) mouse strains which begin expressing the Cre recombinase at earlier stages of precursor differentiation or provide a stronger Cre expression, even though care should be taken to maintain the specificity of the assay for osteoclasts. Our assays may be combined with genetic labeling of nuclei, allowing the parallel visualization of nuclei without using the potentially cytotoxic Hoechst dye. Combining the biochemical differentiation and fusion assays into the same single cell cultures would allow the spatiotemporal comparison of the dynamics of the two processes. Applying the osteoclast-specific gene expression and/or the fusion assays to live mice could improve the *in vivo* analysis of osteoclast development.

We believe that the experiments presented in this report represent a major step toward the fluorescence high-content

imaging-based, high-throughput analysis of osteoclast development, as well as a good starting point for further follow-up directions.

## DATA AVAILABILITY STATEMENT

The raw data supporting the conclusions of this article will be made available by the authors, without undue reservation.

## ETHICS STATEMENT

The animal study was reviewed and approved by the Animal Experimentation Review Board of Semmelweis University.

## AUTHOR CONTRIBUTIONS

ÁP, DG, and AM conceived the study. ÁP and AM designed the experiments, analyzed and interpreted the data, and wrote the manuscript. ÁP performed most of the experiments. SN performed preliminary experiments. JF, ZJ, and DG provided intellectual advice. AM supervised the project. All authors contributed to the article and approved the submitted version.

## FUNDING

This work was supported by the Hungarian National Scientific Research Fund (NKFIH-OTKA Grant Nos. K119653 to AM and FK132971 to DG; and NVKP_16-1-2016-0039 to AM).

## ACKNOWLEDGMENTS

We thank Edina Simon and Nikolett Szénási for expert technical assistance and the genomic PCR analyses, Yunjoo (Casey) Lee for help with the experiments and analyses, András Erdélyi and Panna Királyhidi for preliminary experiments, Dániel Csete for helpful suggestions and Shigeaki Kato for the Ctsk-Cre mice.

## SUPPLEMENTARY MATERIAL

The Supplementary Material for this article can be found online at: https://www.frontiersin.org/articles/10.3389/fcell.2021.657935/full#supplementary-material

## REFERENCES

Csete, D., Simon, E., Alatshan, A., Aradi, P., Dobó-Nagy, C., Jakus, Z., et al. (2019). Hematopoietic or osteoclast-specific deletion of Syk leads to increased bone mass in experimental mice. *Front. Immunol.* 10:937. doi: 10.3389/fimmu.2019.00937

Duong le, T., Leung, A. T., and Langdahl, B. (2016). Cathepsin K inhibition: a new mechanism for the treatment of osteoporosis. *Calcif. Tissue Int.* 98, 381–397. doi: 10.1007/s00223-015-0051-0

Győri, D., Csete, D., Benkő, S., Kulkarni, S., Mandl, P., Dobó-Nagy, C., et al. (2014). The phosphoinositide 3-kinase isoform PI3Kβ regulates osteoclast-mediated bone resorption in humans and mice. *Arthritis. Rheumatol.* 66, 2210–2221. doi: 10.1002/art.38660

Győri, D. S., and Mócsai, A. (2020). Osteoclast signal transduction during bone metastasis formation. *Front. Cell Dev. Biol.* 8:507. doi: 10.3389/fcell.2020.00507

Jacome-Galarza, C. E., Percin, G. I., Muller, J. T., Mass, E., Lazarov, T., Eitler, J., et al. (2019). Developmental origin, functional maintenance and genetic rescue of osteoclasts. *Nature* 568, 541–545. doi: 10.1038/s41586-019-1105-7

Kertész, Z., Győri, D., Körmendi, S., Fekete, T., Kis-Tóth, K., Jakus, Z., et al. (2012). Phospholipase Cγ2 is required for basal but not oestrogen deficiency-induced bone resorption. *Eur. J. Clin. Invest.* 42, 49–60. doi: 10.1111/j.1365-2362.2011.02556.x

Kikuta, J., Wada, Y., Kowada, T., Wang, Z., Sun-Wada, G. H., Nishiyama, I., et al. (2013). Dynamic visualization of RANKL and Th17-mediated osteoclast function. *J. Clin. Invest.* 123, 866–873. doi: 10.1172/JCI65054

Kitazawa, R., Haraguchi, R., Fukushima, M., and Kitazawa, S. (2018). Pathologic conditions of hard tissue: role of osteoclasts in osteolytic lesion. *Histochem. Cell Biol.* 149, 405–415. doi: 10.1007/s00418-018-1639-z

Kondo, T., Ikeda, K., and Matsuo, K. (2004). Detection of osteoclastic cell-cell fusion through retroviral vector packaging. *Bone* 35, 1120–1126. doi: 10.1016/j.bone.2004.06.011

Lacey, D. L., Boyle, W. J., Simonet, W. S., Kostenuik, P. J., Dougall, W. C., Sullivan, J. K., et al. (2012). Bench to bedside: elucidation of the OPG-RANK-RANKL pathway and the development of denosumab. *Nat. Rev. Drug Discov.* 11, 401–419. doi: 10.1038/nrd3705

Levaot, N., Ottolenghi, A., Mann, M., Guterman-Ram, G., Kam, Z., and Geiger, B. (2015). Osteoclast fusion is initiated by a small subset of RANKL-stimulated monocyte progenitors, which can fuse to RANKL-unstimulated progenitors. *Bone* 79, 21–28. doi: 10.1016/j.bone.2015.05.021

Li, B., Yu, F., Wu, F., Wang, K., Lou, F., Zhang, D., et al. (2018). Visual osteoclast fusion via A fluorescence method. *Sci. Rep.* 8:10184. doi: 10.1038/s41598-018-28205-3

Minkin, C. (1982). Bone acid phosphatase: tartrate-resistant acid phosphatase as a marker of osteoclast function. *Calcif. Tissue Int.* 34, 285–290. doi: 10.1007/BF02411252

Muzumdar, M. D., Tasic, B., Miyamichi, K., Li, L., and Luo, L. (2007). A global double-fluorescent Cre reporter mouse. *Genesis* 45, 593–605. doi: 10.1002/dvg.20335

Nakamura, T., Imai, Y., Matsumoto, T., Sato, S., Takeuchi, K., Igarashi, K., et al. (2007). Estrogen prevents bone loss via estrogen receptor α and induction of Fas ligand in osteoclasts. *Cell* 130, 811–823. doi: 10.1016/j.cell.2007.07.025

Nakashima, T., Hayashi, M., Fukunaga, T., Kurata, K., Oh-Hora, M., Feng, J. Q., et al. (2011). Evidence for osteocyte regulation of bone homeostasis through RANKL expression. *Nat. Med.* 17, 1231–1234. doi: 10.1038/nm.2452

Peng, T., Thorn, K., Schroeder, T., Wang, L., Theis, F. J., Marr, C., et al. (2017). A BaSiC tool for background and shading correction of optical microscopy images. *Nat. Commun.* 8:14836. doi: 10.1038/ncomms14836

Purschke, M., Rubio, N., Held, K. D., and Redmond, R. W. (2010). Phototoxicity of Hoechst 33342 in time-lapse fluorescence microscopy. *Photochem. Photobiol. Sci.* 9, 1634–1639. doi: 10.1039/c0pp00234h

Rachner, T. D., Khosla, S., and Hofbauer, L. C. (2011). Osteoporosis: now and the future. *Lancet* 377, 1276–1287. doi: 10.1016/S0140-6736(10)62349-5

Russell, R. G. (2011). Bisphosphonates: the first 40 years. *Bone* 49, 2–19. doi: 10.1016/j.bone.2011.04.022

Shim, J. H., Stavre, Z., and Gravallese, E. M. (2018). Bone loss in rheumatoid arthritis: basic mechanisms and clinical implications. *Calcif. Tissue Int.* 102, 533–546. doi: 10.1007/s00223-017-0373-1

Sobacchi, C., Schulz, A., Coxon, F. P., Villa, A., and Helfrich, M. H. (2013). Osteopetrosis: genetics, treatment and new insights into osteoclast function. *Nat. Rev. Endocrinol.* 9, 522–536. doi: 10.1038/nrendo.2013.137

Takegahara, N., Kim, H., Mizuno, H., Sakaue-Sawano, A., Miyawaki, A., Tomura, M., et al. (2016). Involvement of receptor activator of nuclear factor-κB ligand (RANKL)-induced incomplete cytokinesis in the polyploidization

of osteoclasts. *J. Biol. Chem.* 291, 3439–3454. doi: 10.1074/jbc.M115.677427

Teitelbaum, S. L. (2000). Bone resorption by osteoclasts. *Science* 289, 1504–1508. doi: 10.1126/science.289.5484.1504

Verma, S. K., Leikina, E., Melikov, K., Gebert, C., Kram, V., Young, M. F., et al. (2018). Cell-surface phosphatidylserine regulates osteoclast precursor fusion. *J. Biol. Chem.* 293, 254–270. doi: 10.1074/jbc.M117.809681

Yahara, Y., Barrientos, T., Tang, Y. J., Puviindran, V., Nadesan, P., Zhang, H., et al. (2020). Erythromyeloid progenitors give rise to a population of osteoclasts that contribute to bone homeostasis and repair. *Nat. Cell Biol.* 22, 49–59. doi: 10.1038/s41556-019-0437-8

**Conflict of Interest:** The authors declare that the research was conducted in the absence of any commercial or financial relationships that could be construed as a potential conflict of interest.

# Advantages of publishing in Frontiers

**OPEN ACCESS**
Articles are free to read for greatest visibility and readership

**FAST PUBLICATION**
Around 90 days from submission to decision

**HIGH QUALITY PEER-REVIEW**
Rigorous, collaborative, and constructive peer-review

**TRANSPARENT PEER-REVIEW**
Editors and reviewers acknowledged by name on published articles

**Frontiers**
Avenue du Tribunal-Fédéral 34
1005 Lausanne | Switzerland

**Visit us:** www.frontiersin.org
**Contact us:** frontiersin.org/about/contact

**REPRODUCIBILITY OF RESEARCH**
Support open data and methods to enhance research reproducibility

**DIGITAL PUBLISHING**
Articles designed for optimal readership across devices

**FOLLOW US**
@frontiersin

**IMPACT METRICS**
Advanced article metrics track visibility across digital media

**EXTENSIVE PROMOTION**
Marketing and promotion of impactful research

**LOOP RESEARCH NETWORK**
Our network increases your article's readership